PROCEEDINGS OF THE FIFTEENTH WORKSHOP ON GENERAL RELATIVITY AND GRAVITATION in JAPAN

TOKYO INSTITUTE OF TECHNOLOGY, TOKYO, JAPAN
NOVEMBER 28 - DECEMBER 2, 2005

Edited by

Tetsuya Shiromizu, Hirotaka Yoshino, Akio Hosoya,
Takashi Nakamura and Misao Sasaki

Preface

The fifteenth workshop on General Relativity and Gravitation (the 15th JGRG meeting) was held at Tokyo Institute of Technology, from 28 November to 2 December, 2005.

There has been impressive progress in astrophysical/cosmological observations in recent years, including CMB, black holes and gamma-ray bursts. On the theory side, motivated by unified theories of fundamental interactions, especially string theory, physics in higher dimensional spacetimes has been studied intensively. There have been also important developments in various areas of GR, including alternative theories of gravity, quantum gravity, spacetime singularities, etc..

This year, we invited fourteen speakers from various countries, who gave us clear overviews of recent developments and future perspectives. We witnessed active discussions among the participants during the meeting. We would like to thank all the participants for their earnest participation.

This workshop was supported in part by Monbukagaku-sho Grant-in-Aid for Scientific Research Nos. 14047212, 14047214, 13135208 and 17340075.

T. Shiromizu, H. Yoshino, A. Hosoya, T. Nakamura and M. Sasaki 02/02/2006

Organizing Committee

Table of Contents

Invited talks

Oral Presentation

Poster Presentation

Clarifying Slow Roll Inflation and the Quantum Corrections to the Observable Power Spectra

D. Boyanovsky[c,a,1], H. J. de Vega[b,a,2], N. G. Sanchez [a,3]

[a] *Observatoire de Paris, LERMA, Laboratoire Associé au CNRS UMR 8112, 61, Avenue de l'Observatoire, 75014 Paris, France.*

[b] *LPTHE, Laboratoire Associé au CNRS UMR 7589, Université Pierre et Marie Curie (Paris VI) et Denis Diderot (Paris VII), Tour 24, 5 ème. étage, 4, Place Jussieu, 75252 Paris, Cedex 05, France.*

[c] *Department of Physics and Astronomy, University of Pittsburgh, Pittsburgh, Pennsylvania 15260, USA*

Abstract

Slow-roll inflation can be studied as an effective field theory. The form of the inflaton potential consistent with the data is $V(\phi) = N\,M^4\,w\left(\frac{\phi}{\sqrt{N}\,M_{Pl}}\right)$ where ϕ is the inflaton field, M is the inflation energy scale, and $N \sim 50$ is the number of efolds since the cosmologically relevant modes exited the Hubble radius until the end of inflation. The dimensionless function $w(\chi)$ and field χ are generically $\mathcal{O}(1)$. The WMAP value for the amplitude of scalar adiabatic fluctuations yields $M \sim 0.77 \times 10^{16}$GeV. This form of the potential encodes the slow-roll expansion as an expansion in $1/N$. A Ginzburg-Landau (polynomial) realization of $w(\chi)$ reveals that the Hubble parameter, inflaton mass and non-linear couplings are of the see-saw form in terms of the small ratio M/M_{Pl}. The quartic coupling is $\lambda \sim \frac{1}{N}\left(\frac{M}{M_{Pl}}\right)^4$. The smallness of the non-linear couplings is **not** a result of fine tuning but a **natural** consequence of the validity of the effective field theory and slow roll approximation. Our observations suggest that slow-roll inflation may well be described by an almost critical theory, near an infrared stable gaussian fixed point. Quantum corrections to slow roll inflation are computed and turn to be an expansion in powers $(H/M_{Pl})^2$. The corrections to the inflaton effective potential and its equation of motion are computed, as well as the quantum corrections to the observable power spectra. The near scale invariance of the fluctuations introduces a strong infrared behavior naturally regularized by the slow roll parameter $\Delta \equiv \eta_V - \epsilon_V = \frac{1}{2}(n_s - 1) + r/8$. We find the *effective* inflaton potential during slow roll inflation including the contributions from scalar curvature and tensor perturbations as well as from light scalars and Dirac fermions coupled to the inflaton. The scalar and tensor superhorizon contributions feature infrared enhancements regulated by slow roll parameters. Fermions and gravitons do not exhibit infrared enhancement. The subhorizon part is completely specified by the trace anomaly of the fields with different spins and is solely determined by the space-time geometry. This inflationary effective potential is strikingly **different** from the usual Minkowski space-time result. Quantum corrections to the power spectra are expressed in terms of the CMB observables: n_s, r and $dn_s/d\ln k$. Trace anomalies (especially the graviton part) dominate these quantum corrections in a definite direction: they **enhance** the scalar curvature fluctuations and **reduce** the tensor fluctuations.

1 Inflation as an Effective Field Theory

Inflation was originally proposed to solve several outstanding problems of the standard Big Bang model [1] thus becoming an important paradigm in cosmology. At the same time, it provides a natural mechanism for the generation of scalar density fluctuations that seed large scale structure, thus explaining the origin of the temperature anisotropies in the cosmic microwave background (CMB), as well as that of tensor perturbations (primordial gravitational waves). A distinct aspect of inflationary perturbations

[1] E-mail:boyan@pitt.edu

[2] E-mail:devega@lpthe.jussieu.fr

[3] E-mail:Norma.Sanchez@obspm.fr

is that these are generated by quantum fluctuations of the scalar field(s) that drive inflation. Their physical wavelengths grow faster than the Hubble radius and when they cross the horizon they freeze out and decouple. Later on, these fluctuations are amplified and grow, becoming classical and decoupling from causal microphysical processes. Upon re-entering the horizon, during the matter era, these scalar (curvature) perturbations induce temperature anisotropies imprinted on the CMB at the last scattering surface and seed the inhomogeneities which generate structure upon gravitational collapse[2, 3]. Generic inflationary models predict that these fluctuations are adiabatic with an almost scale invariant spectrum. Moreover, they are Gaussian to a very good approximation. These generic predictions are in spectacular agreement with the CMB observations as well as with a variety of large scale structure data [4]. The WMAP data [4] clearly display an anti-correlation peak in the temperature-polarization (TE) angular power spectra at $l \sim 150$, providing one of the most striking confirmations of superhorizon adiabatic fluctuations as predicted by inflation[4].

The robust predictions of inflation (value of the entropy of the universe, solution of the flatness problem, small adiabatic Gaussian density fluctuations explaining the CMB anisotropies, ...) which are common to the available inflationary scenarios, show the predictive power of the inflationary paradigm. While there is a great diversity of inflationary models, they predict fairly generic features: a gaussian, nearly scale invariant spectrum of (mostly) adiabatic scalar and tensor primordial fluctuations. More precisely, the WMAP[4] data can be fit outstandingly well by simple single field slow roll models. These generic predictions of inflationary models make the inflationary paradigm robust. Whatever the microscopic model for the early universe (GUT theory) would be, it should include inflation with the generic features we know today.

Inflationary dynamics is typically studied by treating the inflaton as a homogeneous classical scalar field whose evolution is determined by its classical equation of motion, while the inflaton quantum fluctuations (around the classical value and in the Gaussian approximation) provide the seeds for the scalar density perturbations of the metric. The classical dynamics of the inflaton (a massive scalar field) coupled to a cosmological background clearly shows that inflationary behaviour is an **attractor** [5]. This is a generic and robust feature of inflation.

In quantum field theory, this classical inflaton corresponds to the expectation value of a quantum field operator in a translational invariant state. Important aspects of the inflationary dynamics, as resonant particle production and the nonlinear back-reaction that it generates, require a full quantum treatment of the inflaton for their consistent description. The quantum dynamics of the inflaton in a non-perturbative framework and its consequences on the CMB anisotropy spectrum were treated in refs.[6, 7, 8, 9].

The quantum fluctuations are of two different kinds: (a) Large quantum fluctuations generated at the begining of inflation through spinodal or parametric resonance depending on the inflationary scenario chosen. They have comoving wavenumbers in the range of $10^{13}\text{GeV} \lesssim k \lesssim 10^{15}\text{GeV}$ and they become superhorizon a few efolds after the begining of inflation. Their physical wavenumbers become subsequently very small compared with the inflaton mass. Therefore, the assembly of these modes can be treated as part of the zero mode after $5 - 10$ efolds [6, 7]. That is, the use of an homogeneous classical inflaton is thus justified by the full quantum theory treatment of the inflaton. (b) Small fluctuations of high comoving wavenumbers

$$e^{N_T-60}\, 10^{16}\, GeV < k < e^{N_T-60}\, 10^{20}\, GeV$$

where $N_T \geq 60$ stands for the total number of efolds (see for example Ref. [10]). These are the cosmologically relevant modes that exit the horizon about 50 efolds before the end of inflation and reenter later on (during the matter dominated era) being the source of primordial power for the CMB anisotropies as well as for the structure formation. While modes (b) obey linear evolution equations with great accuracy, modes (a) strongly interact with themselves calling for nonperturbative quantum field theory treatments as in refs.[6, 7]. Notice that particle production is governed by linear unstabilities (parametric or spinodal) only at the begining of inflation. Particle production keeps strong during the nonlinear regime till particles eventually dominate the energy density and inflation stops[6]. The modes (b) correspond to physical scales that were microscopic (even transplanckian) at the begining of inflation, then after they become astronomical and produce the CMB anisotropies as well as the large scale structure of the universe.

The crucial fact is that the excitations can cross the horizon **twice**, coming back and bringing information from the inflationary era. We depict in fig. 1 the physical wavelengths of modes (a) and (b) vs.

the logarithm of the scale factor showing that modes (b) crossed twice the horizon, modes (a) are out of the horizon still today.

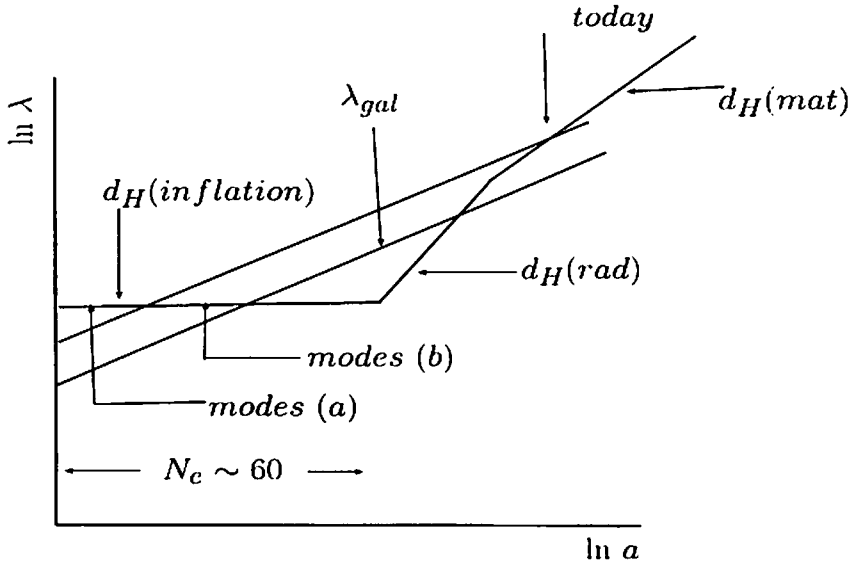

Figure 1: Physical lengths $\lambda = a(t)\ \lambda_{comoving}$ vs. the scale factor $a(t)$ in a log-log plot. The causal horizon d_H is shown for the inflationary (de Sitter), radiation dominated and matter dominated eras. The physical wavelengths (λ) for today's Hubble radius and a typical galactic scale (λ_{gal}) are shown. One sees the modes (b) can cross the horizon **twice** bringing information from extremely short wavelength modes during the inflationary era. Modes (a) which have large amplitudes during inflation and dominated the energy of the universe, have not yet crossed back inside the horizon.

Recently, particle decay in a de Sitter background as well as during slow roll inflation has been studied in ref.[11] together with its implication for the decay of the density fluctuations. Quantum effects during slow roll inflation including quantum corrections to the effective inflaton potential and its equation of motion are derived in ref.[9, 12]. Recent studies of quantum corrections during inflation[9, 11, 12] revealed the robustness of classical single field slow roll inflationary models as a result of the validity of the **effective field theory** description. The reliability of an effective field theory of inflation hinges on a wide separation between the energy scale of inflation, determined by H and that of the underlying microscopic theory which is taken to be the Planck scale M_{Pl}. Inflation as known today should be considered as an **effective theory**, that is, it is not a fundamental theory but a theory of a condensate (the inflaton field) which follows from a more fundamental one (the GUT model). The inflaton field is just an **effective** description while the microscopic description should come from the GUT model in the cosmological spacetime. Such derivation is not yet available.

Bosonic fields do not need to be fundamental fields, for example they may emerge as condensates of fermion-antifermion pairs $< \bar{\Psi}\Psi >$ in a grand unified theory (GUT) in the cosmological background. In order to describe the cosmological evolution is enough to consider the effective dynamics of such condensates. The relation between the low energy effective field theory of inflation and the microscopic fundamental theory is akin to the relation between the effective Ginzburg-Landau theory of superconductivity and the microscopic BCS theory, or like the relation of the $O(4)$ sigma model, an effective low energy theory of pions, photons and chiral condensates with quantum chromodynamics (QCD)[13]. The guiding principle to construct the effective theory is to include the appropriate symmetries[13]. Contrary to the sigma model where the chiral symmetry strongly constraints the model[13], only general covariance can be imposed on the inflaton model.

The inflationary scenarios are usually characterized as small and large fields scenarii. In small fields scenarios the initial classical amplitude of the inflaton is assumed small compared with M_{Pl} while in large field scenarii the inflaton amplitude is initially of the order M_{Pl}. The first type of scenarii is usually

realized with broken symmetric potentials ($m^2 < 0$) while for the second type scenarii ('chaotic inflation') one can just use unbroken potentials with $m^2 > 0$.

Gravity can be treated semiclassically for inflation: the geometry is classical and the metric follows from the Einstein-Friedman equations where the r.h.s. is the expectation value of a quantum operator. Quantum gravity corrections can be neglected during inflation because the energy scale of inflation $M \sim M_{GUT} \sim 10^{-3}\, M_{Planck}$. That is, quantum gravity effects are at most $(M/M_{Planck})^2 \sim 10^{-6}$ and can be neglected in this context. The studies in ref.[11, 12, 14] reveal that quantum corrections in the effective field theory yields an expansion in $\left(\frac{H}{M_{Pl}}\right)^2$ for *general inflaton potentials*. This indicates that the use of the inflaton potential $V(\phi)$ from effective field theory is consistent for

$$\left(\frac{H}{M_{Pl}}\right)^2 \ll 1 \quad \text{and hence} \quad V(\phi) \ll M_{Pl}^4 \,,$$

allowing amplitudes of the inflaton field ϕ well beyond M_{Pl}[14].

1.1 Slow-roll Inflation as an expansion in $1/N_{efolds}$ and no fine tuning

In single field inflation the energy density is dominated by a homogeneous scalar *condensate*, the inflaton, whose dynamics can be described by an *effective* Lagrangian

$$\mathcal{L} = a^3(t)\left[\frac{\dot\phi^2}{2} - \frac{(\nabla\phi)^2}{2\,a^2(t)} - V(\phi)\right] \,, \tag{1}$$

together to the Einstein-Friedman equation

$$\left[\frac{1}{a(t)}\,\frac{da}{dt}\right]^2 = \frac{\rho(t)}{3\,M_{Pl}^2} \,, \tag{2}$$

where the energy density for an homogeneous inflaton is given by

$$\rho(t) = \frac{\dot\phi^2}{2} + V(\phi) \,.$$

The inflaton potential $V(\phi)$ is a slowly varying function of ϕ in order to permit a slow-roll solution for the inflaton field $\phi(t)$. All this in a spatially flat FRW metric

$$ds^2 = dt^2 - a^2(t)\,d\vec{x}^2 = C^2(\eta)\left[(d\eta)^2 - d\vec{x}^2\right] \,, \tag{3}$$

where η is the conformal time and $C(\eta) \equiv a(t(\eta))$.

The inflaton evolution equation takes the form,

$$\ddot\phi + 3\,H\,\dot\phi + V'(\phi) = 0 \,.$$

In the slow-roll approximation $\ddot\phi \ll 3\,H\,\dot\phi$ and $\frac{\dot\phi^2}{2} \ll V(\phi)$, and the inflaton evolution equations become

$$3\,H(t)\,\dot\phi + V'(\phi) = 0 \quad , \quad [H(t)]^2 = \frac{V(\phi)}{3\,M_{Pl}^2} \,, \tag{4}$$

where $H(t) \equiv \frac{1}{a(t)}\,\frac{da}{dt}$ stands for the Hubble parameter. Eq.(4) can be integrated by quadratures with the result

$$\ln a(t) = -\frac{1}{M_{Pl}^2}\int_{\phi(0)}^{\phi(t)} \frac{V(\varphi)}{V'(\phi)}\,d\phi \,.$$

This formula shows that the inflaton field ϕ scales as M_{Pl} and as the square root of the number of efolds [14]. This suggest to introduce the dimensionless field χ and the dimensionless potential $w(\chi)$,

$$\chi \equiv \frac{\phi}{\sqrt{N}\,M_{Pl}} \quad , \quad w(\chi) \equiv \frac{V(\phi)}{N\,M^4} \tag{5}$$

where M stands for the scale of inflation. The dimensionless field χ is *slowly* varying during the stage of slow roll inflation: a large change in the field amplitude ϕ results in a small change in χ amplitude ,

$$\Delta\chi = \frac{1}{\sqrt{N}} \frac{\Delta\phi}{M_{Pl}} , \tag{6}$$

a change in ϕ with $\Delta\phi \sim M_{Pl}$ results in a change $\Delta\chi \sim 1/\sqrt{N}$.

Introducing a *stretched* (slow) dimensionless time variable τ and a rescaled dimensionless Hubble parameter h as follows

$$t = \sqrt{N}\, \frac{M_{Pl}}{M^2}\, \tau \quad , \quad H = \sqrt{N}\, \frac{M^2}{M_{Pl}}\, h , \tag{7}$$

the Einstein-Friedman equation reads

$$h^2(\tau) = \frac{1}{3} \left[\frac{1}{2\,N} \left(\frac{d\chi}{d\tau} \right)^2 + w(\chi) \right] , \tag{8}$$

and the evolution equation for the inflaton field χ is given by

$$\frac{1}{N}\, \frac{d^2\chi}{d\tau^2} + 3\, h\, \frac{d\chi}{d\tau} + w'(\chi) = 0 . \tag{9}$$

The slow-roll approximation follows by neglecting the $\frac{1}{N}$ terms in eqs.(8) and (9). Both $w(\chi)$ and $h(\tau)$ are of order N^0 for large N. Both equations make manifest the slow roll expansion as a **systematic expansion in** $1/N$[14].

Following the spirit of the Ginsburg-Landau theory of phase transitions, the simplest choice is a quartic trinomial for the inflaton potential[15]:

$$w(\chi) = w_0 \pm \frac{1}{2}\, \chi^2 + \frac{G_3}{3}\, \chi^3 + \frac{G_4}{4}\, \chi^4 . \tag{10}$$

where the coefficients w_0, G_3 and G_4 are of order one and the signs $\pm$ correspond to large and small field inflation, respectively. Inserting eq.(10) in eq.(5) yields,

$$V(\phi) = V_0 \pm \frac{m^2}{2}\, \phi^2 + \frac{m\, g}{3}\, \phi^3 + \frac{\lambda}{4}\, \phi^4 . \tag{11}$$

where m, g and λ are given by the following see-saw-like relations,

$$m = \frac{M^2}{M_{Pl}} \quad , \quad g = \frac{G_3}{\sqrt{N}} \left(\frac{M}{M_{Pl}} \right)^2 \quad , \quad \lambda = \frac{G_4}{N} \left(\frac{M}{M_{Pl}} \right)^4 . \tag{12}$$

We can now input the results from WMAP[4] to constrain the scale M. The amplitude of adiabatic scalar perturbations in slow-roll is expressed as

$$|\Delta^{(S)}_{k\,ad}|^2 = \frac{1}{12\,\pi^2\, M^6_{Pl}}\, \frac{V^3}{V'^2} = \frac{N^2}{12\,\pi^2} \left(\frac{M}{M_{Pl}} \right)^4 \frac{w^3(\chi)}{w'^2(\chi)} , \tag{13}$$

Since, $w(\chi)$ and $w'(\chi)$ are of order one, we find

$$\left(\frac{M}{M_{Pl}} \right)^2 \sim \frac{2\sqrt{3}\,\pi}{N}\, |\Delta^{(S)}_{k\,ad}| \simeq 1.02 \times 10^{-5} . \tag{14}$$

where we used $N \simeq 50$ and the WMAP value for $|\Delta^{(S)}_{k\,ad}| = (4.67 \pm 0.27) \times 10^{-5}$ [4]. This fixes the scale of inflation to be

$$M \simeq 3.19 \times 10^{-3}\, M_{PL} \simeq 0.77 \times 10^{16}\, \mathrm{GeV} .$$

This value pinpoints the scale of the potential during inflation to be at the GUT scale suggesting a deep connection between inflation and the physics at the GUT scale in cosmological space-time.

That is, the WMAP data fix the scale of inflation M for single field potentials with the form given by eq.(5). This value for M is below the WMAP upper bound on the inflation scale 3.3 10^{16}GeV [4]. Furthermore, the Hubble scale during (slow roll) inflation and the inflaton mass near the minimum of the potential are thereby determined from eqs.(7) and (12) to be $m = \frac{M^2}{M_{Pl}} = 2.45 \times 10^{13}\,\mathrm{GeV}$, $H = \sqrt{N}\, m\, h \sim 1.0 \times 10^{14}\,\mathrm{GeV} = 4.1\, m$ since $h = \mathcal{O}(1)$. In addition, the order of magnitude of the couplings naturally follows from eq.(12): $g \sim 10^{-6}$. $\lambda \sim 10^{-12}$, since $M/M_{Pl} \sim 3 \times 10^{-3}$.

Since $M/M_{Pl} \sim 3 \times 10^{-3}$, these relations are a **natural** consequence of the validity of the effective field theory and of slow roll and relieve the **fine tuning problem**. We emphasize that the 'see-saw-like' form of the couplings is a natural consequence of the form of the potential eq.(5). While the hierarchy between the Hubble parameter, the inflaton mass and the Planck scale during slow roll inflation is well known, our analysis reveals that small couplings are naturally explained in terms of powers of the ratio between the inflationary and Planck scales *and* integer powers of $1/\sqrt{N}$.

This is one of the main results presented in this lecture: the effective field theory and slow roll descriptions of inflation, both validated by WMAP, lead us to conclude that there is *no fine tuning* problem[14]. The smallness of the inflaton mass and the coupling constants in this trinomial realization of the inflationary potential is a *direct* consequence of the validity of both the effective field theory and the slow roll approximations through a see-saw-like mechanism.

It must be stressed that these order of magnitude estimates follow from the statement that $w(\chi)$ and χ are of order one. They are thus independent of the details of the model. Indeed, model-dependent factors of order one appearing in the observables should allow to exclude or accept a given model by using the observational data.

The WMAP results rule out the purely quartic potential ($m = 0$, $g = 0$). From the point of view of an effective field theory this is not surprising: it is rather *unnatural* to set $m = 0$, since $m = 0$ is a particular point at which the correlation length is infinite and the theory is critical. Indeed the systematic study in ref.[15] shows that the best fit to the WMAP data requires $m^2 \neq 0$.

The general quartic Lagrangian eq.(20) describes a renormalizable theory. However, one can choose in the present context arbitrary high order polynomials for $V(\phi)$. These nonrenormalizable models are also effective theories where M_{Pl} plays the rôle of UV cutoff. However, already a quartic potential is rich enough to describe the full physics and to reproduce accurately the WMAP data [15].

For a general potential $V(\phi)$,

$$V(\phi) = \sum_{n=0}^{\infty} \lambda_n\, \phi^n \quad i.e. \quad w(\chi) = \sum_{n=0}^{\infty} G_n\, \chi^n\,, \tag{15}$$

we find from eq.(5):

$$\lambda_n = \frac{G_n\, m^2}{(N\, M_{Pl}^2)^{\frac{n}{2}-1}}\,, \tag{16}$$

where the dimensionless coefficients G_n are of order one. We find the scaling behavior $\lambda_n \sim 1/N^{\frac{n}{2}-1}$. Eq. (12) displays particular cases of eq.(16) for $n = 3$ and 4.

The slow-roll parameters naturally result of the order $1/N$, $1/N^2$ etc. when expressed in terms of the inflaton potential

$$V(\phi) = N\, M^4\, w(\chi)\,. \tag{17}$$

That is,

$$\epsilon_V = \frac{M_{Pl}^2}{2}\left[\frac{V'(\Phi_0)}{V(\Phi_0)}\right]^2 = \frac{1}{2\,N}\left[\frac{w'(\chi)}{w(\chi)}\right]^2 \quad . \quad \eta_V = M_{Pl}^2\,\frac{V''(\Phi_0)}{V(\Phi_0)} = \frac{1}{N}\,\frac{w''(\chi)}{w(\chi)}\,, \tag{18}$$

The spectral index n_s, its running and the ratio of tensor to scalar fluctuations are expressed as

$$n_s - 1 = -\frac{3}{N}\left[\frac{w'(\chi)}{w(\chi)}\right]^2 + \frac{2}{N}\,\frac{w''(\chi)}{w(\chi)} \quad ,$$

$$\frac{dn_s}{d\ln k} = -\frac{2}{N^2}\,\frac{w'(\chi)\,w'''(\chi)}{w^2(\chi)} - \frac{6}{N^2}\,\frac{[w'(\chi)]^4}{w^4(\chi)} + \frac{8}{N^2}\,\frac{[w'(\chi)]^2\,w''(\chi)}{w^3(\chi)} \quad ,$$

$$r = \frac{8}{N}\left[\frac{w'(\chi)}{w(\chi)}\right]^2 \quad . \tag{19}$$

In eqs.(13), (18) and (19), the field χ is computed at horizon exiting. We choose $N[\chi] = N = 50$. The WMAP results favoured single inflaton models and among them new and hybrid inflation emerge to be preferable than chaotic inflation[15].

The inflationary era ends when the particles produced during inflation dominate the energy density overcoming the vacuum energy. At such stage the universe slows down its expansion to a radiation dominated regime.

1.2 Connection with Supersymmetry

The form of the inflaton potential

$$V(\phi) = N\,M^4\,w(\chi) \tag{20}$$

resembles (besides the factor N) the moduli potential arising from supersymmetry breaking

$$V_{susy}(\phi) = m_{susy}^4\,v\left(\frac{\phi}{M_{Pl}}\right) \,, \tag{21}$$

where m_{susy} stands for the supersymmetry breaking scale. In our context, eq.(21) indicates that $m_{susy} \simeq M \simeq M_{GUT}$. That is, the susy breaking scale m_{susy} turns out to be at the GUT and inflation scales. This may be a *first* observational indication of the presence of supersymmetry. It should be noticed that this supersymmetry scale is unrelated to an eventual existence of supersymmetry at the TeV scale.

Notice that the invariance of the basic interactions (the lagrangian) and the invariance of the physical states (or density matrices) describing the matter are different issues. For example, no thermal state at non-zero temperature can be invariant under supersymmetry since Bose-Einstein and Fermi-Dirac distributions are different. More generally, the inflationary stage is described by a scalar condensate (the inflaton) while fermions cannot condense due to Pauli principle. This makes quite hard to uncover supersymmetric properties of the lagrangian from the physics of the early universe.

1.3 Conjecture: inflation is near a trivial infrared fixed point

There are several remarkable features and consistency checks of the relations (12):

- Note the relation $\lambda \sim g^2$. This is the correct consistency relation in a renormalizable theory because at one loop level there is a renormalization of the quartic coupling (or alternatively a contribution to the four points correlation function) of orders λ^2, g^4 and $\lambda\,g^2$ which are of the same order for $\lambda \sim g^2$. Similarly, at one loop level there is a renormalization of the cubic coupling (alternatively, a contribution to the three point function) of orders g^3 and $\lambda\,g$ which again require $g^2 \sim \lambda$ for consistency.

- In terms of the effective field theory ratio $(H/M_{Pl})^2$ and slow roll parameters, the dimensionless couplings are

$$\frac{m\,g}{H} \sim \frac{1}{N}\,\frac{H}{M_{Pl}} \quad , \quad \lambda \sim \frac{1}{N^2}\left(\frac{H}{M_{Pl}}\right)^2 \,. \tag{22}$$

  These relations agree with those found for the dimensionless couplings in ref.[11, 12] once the slow roll parameters are identified with the expressions (18) in terms of $1/N$. The results of refs. [11, 12] revealed that the loop expansion is indeed an expansion in the effective field theory ratio $(H/M_{Pl})^2$ and the slow roll parameters. The study in ref.[14] allows us to go further in this direction and state that the loop expansion is a consistent double series in the effective field theory ratio $(H/M_{Pl})^2$ *and* in $1/N$. Loops are either powers of g^2 or of λ which implies that for each loop there is a factor $(H/M_{Pl})^2$. The counting of powers of $1/N$ is more subtle: the nearly scale invariant spectrum of fluctuations leads to infrared enhancements of quantum corrections in which the small factor $1/N$

enters as an infrared regulator. Therefore, large denominators that feature the infrared regulator of order $1/N$ cancel out factors $1/N$ in the numerator. The final power of $1/N$ must be computed in detail in each loop contribution.

- We find the relation (12) truly remarkable. Since the scale of inflation M is fixed, presumably by the underlying microscopic (GUT) theory, the scaling of λ with the inverse of the number of e-folds strongly suggests a *renormalization group explanation of the effective field theory* because the number of e-folds is associated with the logarithm of the scale $N = \ln a$. A renormalization group improved scale dependent quartic coupling [16] behaves as $\lambda(K) \propto 1/\ln K$ with K the scale at which the theory is studied. Since in an expanding cosmology the physical scale grows with the scale factor it is natural to expect that a renormalization group resummation yields the renormalized coupling scaling as

$$\lambda \sim 1/\ln a \sim 1/N \; .$$

There are several aspects of slow roll inflation, which when considered together, lead us to conjecture that *the effective field theory of inflation is an almost critical theory near but not at a trivial fixed point of the renormalization group*. These aspects are the following:

- The fluctuations of the inflaton are almost *massless*, this is the statement that the slow roll parameter

$$\eta_V = M_{Pl}^2 \, \frac{V''(\phi)}{V(\phi)} \simeq 3 \, \frac{V''(\phi)}{H^2} \ll 1 \; .$$

  The slow roll relation (18) states that the dimensionless ratio of the inflaton mass and the Hubble scale is $\sim 1/N \sim 1/\ln a$.

- The higher order couplings are suppressed by further powers of $1/N \sim 1/\ln a$ [see eq.(16)]. In the language of critical phenomena, the mass is a relevant operator in the infrared, the quartic coupling λ is marginal, and higher order couplings are irrelevant.

These ingredients taken together strongly suggest that for large $N \sim \ln a$, the effective field theory is reaching a *trivial gaussian infrared fixed point*[14]. The evidence for this is manifest in that:
i) the power spectrum of scalar fluctuations is *nearly scale invariant* (a consequence of $\eta_V \ll 1$),
ii) the coupling constants vanish in the asymptotic limit $N \to \infty$. *If* the number of e-folds were infinite, the theory would be sitting at the trivial fixed point: a massless free field theory.

The physical situation in inflationary cosmology is *not* to be sitting *exactly* at the fixed point, inflation *must* end, and is to be followed by a radiation dominated standard big bang cosmology. Therefore, we conclude that *during the stage of slow roll inflation, the theory is hovering near a trivial gaussian infrared fixed point* but the presence of a small relevant operator, namely the inflaton mass which eventually becomes large at the end of slow roll, drives the theory away from criticality.

Our investigations[14] reveal that it is *not* the ultraviolet behavior of the renormalization group that is responsible for the near criticality of the effective field theory, but rather the infrared, superhorizon physics. That this is the case can be gleaned in eq. (12): the coefficient $(M/M_{Pl})^4$ in front of the term $1/\ln a$ *cannot* be obtained from the usual Minkowski-space renormalization group solution for the running coupling. Furthermore, the true trivial fixed point is obtained in the infrared limit when the scale factor $a \to \infty$, namely infinitely long physical wavelengths.

If this conjecture[14] proves correct, it will have a major fundamental appeal as a description of inflation because field theories near a fixed point feature *universal behavior* independent of the underlying microscopic degrees of freedom. In fact, if the effective field theory of inflation is indeed near (not exactly) an infrared gaussian fixed point, its predictions would be nearly universal, and single field slow roll inflation describes a large *universality class* that features the same robust predictions. Such is the case in critical phenomena described by field theories where widely different systems feature the same behavior near a critical point.

2 Quantum corrections to the equation of motion for the inflaton and its effective potential.

We consider single field inflationary models described by a general self-interacting scalar field theory in a spatially flat Friedmann-Robertson-Walker cosmological space time with scale factor $a(t)$. In comoving coordinates the action is given by

$$S = \int d^3x\, dt\, a^3(t) \left[\frac{1}{2}\,\dot{\phi}^2 - \frac{(\nabla\phi)^2}{2a^2} - V(\phi) \right] . \tag{23}$$

We consider a *generic* potential $V(\phi)$, the only requirement is that its *derivatives* be small in order to justify the slow roll expansion[3, 17]. In order to study the corrections from the quantum fluctuations we separate the classical homogeneous expectation value of the scalar field from the quantum fluctuations by writing

$$\phi(\vec{x},t) = \Phi_0(t) + \varphi(\vec{x},t) , \tag{24}$$

with

$$\Phi_0(t) = \langle \phi(\vec{x},t) \rangle \;\; ; \;\; \langle \varphi(\vec{x},t) \rangle = 0 , \tag{25}$$

where the expectation value is in the non-equilibrium quantum state. Expanding the Lagrangian density and integrating by parts, the action becomes

$$S = \int d^3x\, dt\, a^3(t)\, \mathcal{L}[\Phi_0(t), \varphi(\vec{x},t)] , \tag{26}$$

with

$$\mathcal{L}[\Phi_0(t), \varphi(\vec{x},t)] = \frac{1}{2}\,\dot{\Phi}_0^2 - V(\Phi_0) + \frac{1}{2}\,\dot{\varphi}^2 - \frac{(\nabla\varphi)^2}{2\,a^2} - \frac{1}{2}\,V''(\Phi_0)\,\varphi^2$$

$$-\varphi \left[\ddot{\Phi}_0 + 3\,H\,\dot{\Phi}_0 + V'(\Phi_0) \right] - \frac{1}{6}\,V'''(\Phi_0)\,\varphi^3 - \frac{1}{24}\,V^{(IV)}(\Phi_0)\,\varphi^4 + \text{higher orders in}\,\varphi . \tag{27}$$

We obtain the equation of motion for the homogeneous expectation value of the inflaton field by implementing the tadpole method (see [11] and references therein). This method consists in requiring the condition $\langle \varphi(\vec{x},t) \rangle = 0$ consistently in a perturbative expansion by treating the *linear*, cubic, quartic (and higher order) terms in the Lagrangian density eq.(27) as *perturbations*[11].

Our approach relies on two distinct and fundamentally different expansions: i) the effective field theory (EFT) expansion and ii) the slow-roll expansion.

Quantum corrections to the equations of motion for the inflaton and for the fluctuations are obtained by treating the second line in eq.(27), namely, the *linear* and the non-linear terms in φ, in perturbation theory.

The generating functional of non-equilibrium real time correlation functions requires a path integral along a complex contour in time: the forward branch corresponds to time evolution forward (+) and backward (−) in time as befits the time evolution of a density matrix. Fields along these branches are labeled φ^+ and φ^-, respectively (see refs.[11] and references therein). The tadpole conditions

$$\langle \varphi^{\pm}(\vec{x},t) \rangle = 0 , \tag{28}$$

both lead to the (same) equation of motion for the expectation value $\Phi_0(t)$ by considering the *linear*, *cubic* and higher order terms in the Lagrangian density as interaction vertices. To one loop order we find

$$\ddot{\Phi}_0(t) + 3\,H\,\dot{\Phi}_0(t) + V'(\Phi_0) + g(\Phi_0)\,\langle [\varphi^+(\vec{x},t)]^2 \rangle = 0 . \tag{29}$$

The first three terms in eq.(29) are the familiar ones for the classical equation of motion of the inflaton.

The last term is the one-loop correction to the equations of motion of purely quantum mechanical origin. Another derivation of this quantum correction can be found in[6, 18]. The fact that the tadpole method, which in this case results in a one-loop correction, leads to a covariantly conserved and fully renormalized energy momentum tensor has been established in the most general case in refs.[6, 19, 20].

The coupling g, effective 'mass term' M^2 and the quartic coupling are defined by

$$M^2 \equiv M^2(\Phi_0) = V''(\Phi_0) = 3\,H_0^2\,\eta_V + \mathcal{O}(\frac{1}{N})\;,\; g \equiv g(\Phi_0) = \frac{1}{2}\,V'''(\Phi_0)\;,\; \lambda \equiv \lambda(\Phi_0) = \frac{1}{6}\,V^{(IV)}(\Phi_0)\;. \tag{30}$$

The $\langle\langle(\cdots)\rangle\rangle$ is computed in the free field (Gaussian) theory of the fluctuations φ with an effective 'mass term' M^2, the quantum state will be specified below. Furthermore, it is straightforward to see that $\langle[\varphi^+(\vec{x},t)]^2\rangle = \langle[\varphi^-(\vec{x},t)]^2\rangle = \langle[\varphi(\vec{x},t)]^2\rangle$. In terms of the spatial Fourier transform of the fluctuation field $\varphi(\vec{x},t)$, the one-loop contribution can be written as

$$\langle[\varphi(\vec{x},t)]^2\rangle = \int \frac{d^3k}{(2\pi)^3}\,\langle|\varphi_{\vec{k}}(t)|^2\rangle = \int_0^\infty \frac{dk}{k}\,\mathcal{P}_\varphi(k,t)\,, \tag{31}$$

where $\varphi_{\vec{k}}(t)$ is the spatial Fourier transform of the fluctuation field $\varphi(\vec{x},t)$ and we have introduced the power spectrum of the fluctuation

$$\mathcal{P}_\varphi(k,t) = \frac{k^3}{2\,\pi^2}\,\langle|\varphi_{\vec{k}}(t)|^2\rangle\,. \tag{32}$$

During slow roll inflation the scale factor is quasi de Sitter and to lowest order in slow roll it is given by :

$$C(\eta) = -\frac{1}{H_0\,\eta}\,\frac{1}{1-\epsilon_V} = -\frac{1}{H_0\,\eta}(1+\epsilon_V) + \mathcal{O}(\epsilon_V^2)\,. \tag{33}$$

The spatial Fourier transform of the rescaled free field Heisenberg operators $\chi(\vec{x},\eta) \equiv C(\eta)\varphi(\vec{x},t)$ obey the equation

$$\chi_{\vec{k}}''(\eta) + \left[k^2 + M^2\,C^2(\eta) - \frac{C''(\eta)}{C(\eta)}\right]\chi_{\vec{k}}(\eta) = 0\,. \tag{34}$$

Using the slow roll expressions eqs.(30) and (33), it becomes

$$\chi_{\vec{k}}''(\eta) + \left[k^2 - \frac{\nu^2-\frac{1}{4}}{\eta^2}\right]\chi_{\vec{k}}(\eta) = 0 \tag{35}$$

where the index ν and the quantity Δ are given by

$$\nu = \frac{3}{2} + \epsilon_V - \eta_V + \mathcal{O}(\frac{1}{N^2})\quad,\quad \Delta = \frac{3}{2} - \nu = \eta_V - \epsilon_V + \mathcal{O}(\frac{1}{N^2})\,. \tag{36}$$

The scale invariant case $\nu = \frac{3}{2}$ corresponds to massless inflaton fluctuations in the de Sitter background. Δ measures the departure from scale invariance. In terms of the spectral index of the scalar adiabatic perturbations n_s and the ratio r of tensor to scalar perturbations, Δ takes the form,

$$\Delta = \frac{1}{2}\,(n_s - 1) + \frac{r}{8}\,. \tag{37}$$

The free Heisenberg field operators $\chi_{\vec{k}}(\eta)$ are written in terms of annihilation and creation operators that act on Fock states as

$$\chi_{\vec{k}}(\eta) = a_{\vec{k}}\,S_\nu(k,\eta) + a^\dagger_{-\vec{k}}\,S^*_\nu(k,\eta) \tag{38}$$

where the mode functions $S_\nu(k,\eta)$ are solutions of the eqs. (35). For Bunch-Davis boundary conditions we have

$$S_\nu(k,\eta) = \frac{1}{2}\,\sqrt{-\pi\eta}\;e^{i\frac{\pi}{2}(\nu+\frac{1}{2})}\;H_\nu^{(1)}(-k\eta)\,, \tag{39}$$

this defines the Bunch-Davis vacuum $a_{\vec{k}}|0>_{BD} = 0$.

There is no unique choice of an initial state, and a recent body of work has began to address this issue (see ref.[20] for a discussion and further references). A full study of the *quantum loop* corrections with different initial states must first elucidate the behavior of the propagators for the fluctuations in such states. Here we focus on the standard choice in the literature[3] which allows us to include the quantum corrections into the standard results in the literature. A study of quantum loop corrections with different initial states is an important aspect by itself which we postpone to later work.

The index ν in the mode functions eq.(39) depends on the expectation value of the scalar field, via the slow roll variables, hence it slowly varies in time. Therefore, it is consistent to treat this time dependence of ν as an *adiabatic approximation*. This is well known and standard in the slow roll expansion[3]. Indeed, there are corrections to the mode functions which are higher order in slow roll. However, these mode functions enter in the propagators in loop corrections, therefore they yield higher order contributions in slow roll and we discard them consistently to lowest order in slow roll.

With this choice and to lowest order in slow roll, the power spectrum eq.(32) is given by

$$\mathcal{P}_\varphi(k,t) = \frac{H^2}{8\,\pi}\,(-k\eta)^3\,|H^{(1)}_\nu(-k\eta)|^2\,. \tag{40}$$

For large momenta $|k\eta| \gg 1$ the mode functions behave just like free field modes in Minkowski space-time, namely

$$S_\nu(k,\eta) \stackrel{|k\eta|\gg 1}{=} \frac{1}{\sqrt{2k}}\,e^{-ik\eta} \tag{41}$$

Therefore, the quantum correction to the equation of motion for the inflaton eqs.(29) and (31) determined by the momentum integral of $\mathcal{P}_\varphi(k,t)$ features both quadratic and logarithmic divergences. Since the field theory inflationary dynamics is an *effective field theory* valid below a comoving cutoff Λ of the order of the Planck scale, the one loop correction (31) becomes

$$\int_0^\Lambda \frac{dk}{k}\,\mathcal{P}_\varphi(k,t) = \frac{H^2}{8\,\pi}\int_0^{\Lambda_p}\frac{dz}{z}\,z^3\,\left|H^{(1)}_\nu(z)\right|^2\,, \tag{42}$$

where $\Lambda_p(\eta)$ is the ratio of the cutoff in physical coordinates to the scale of inflation, namely

$$\Lambda_p(\eta) \equiv \frac{\Lambda}{H\,C(\eta)} = -\Lambda\,\eta\,. \tag{43}$$

The integration variable $z = -k\,\eta$ has a simple interpretation at leading order in slow roll

$$z \equiv -k\,\eta = \frac{k}{H_0\,C(\eta)} = \frac{k_p(\eta)}{H_0}\,, \tag{44}$$

where $k_p(\eta) = k/C(\eta)$ is the wavevector in physical coordinates. If the spectrum of scalar fluctuations were strictly scale invariant, (namely for massless inflaton fluctuations in de Sitter space-time), then the index would be $\nu = 3/2$ and the integrand in (42) given by

$$z^3\,\left|H^{(1)}_{\frac{3}{2}}(z)\right|^2 = \frac{2}{\pi}\left[1+z^2\right]\,. \tag{45}$$

In this strictly scale invariant case, the integral of the power spectrum also features an *infrared* logarithmic divergence. While the ultraviolet divergences are absorbed by the renormalization counterterms in the effective field theory, this is not possible for the infrared divergence. Obviously, the origin of this infrared behavior is the **exact** scale invariance of superhorizon fluctuations. However, during slow roll inflation there are small corrections to scale invariance, in particular the index ν is slightly different from 3/2 and this slight departure introduces a natural infrared regularization. In ref.[11] we have introduced an expansion in the parameter $\Delta = 3/2 - \nu = \eta_V - \epsilon_V + \mathcal{O}(\epsilon_V^2, \eta_V^2, \epsilon_V\eta_V)$ which is small during slow roll and we showed in [12] that the infrared divergences featured by the quantum correction manifest as *simple poles* in Δ.

The quantum correction to the equation of motion for the inflaton by isolating the pole in Δ as well as the leading logarithmic divergences were computed in ref.[12] with the result

$$\frac{1}{2}\langle[\varphi(\vec{x},t)]^2\rangle = \left(\frac{H_0}{4\,\pi}\right)^2\left[{\Lambda_p}^2 + \ln\Lambda_p^2 + \frac{1}{\Delta} + 2\,\gamma - 4 + \mathcal{O}(\Delta)\right]\,, \tag{46}$$

where γ is the Euler-Mascheroni constant. While the quadratic and logarithmic *ultraviolet* divergences are regularization scheme dependent, the pole in Δ arises from the infrared behavior and is independent of the regularization scheme. In particular this pole coincides with that found in the expression for $< \phi^2(\vec{x},t) >$ in ref.[21]. The *ultraviolet divergences*, in whichever renormalization scheme, require that the effective field theory be defined to contain *renormalization counterterms* in the bare effective lagrangian, so that these counterterms will systematically cancel the divergences encountered in the calculation of quantum corrections in the (EFT) and slow roll approximations.

2.1 Renormalized effective field theory: renormalization counterterms

The renormalized effective field theory is obtained by writing the potential $V[\phi]$ in the Lagrangian density eq.(23) in the following form

$$V(\phi) = V_R(\phi) + \delta V_R(\phi, \Lambda) , \tag{47}$$

where $V_R(\phi)$ is the renormalized *classical* inflaton potential and $\delta V_R(\phi, \Lambda)$ includes the renormalization counterterms which are found systematically in a slow roll expansion by canceling the ultraviolet divergences. In this manner, the equations of motion and correlation functions in this effective field theory *are cutoff independent*. We find from eqs.(29) and (46)

$$\ddot{\Phi}_0(t) + 3\,H\,\dot{\Phi}_0(t) + V'(\Phi_0) + V'''(\Phi_0)\left(\frac{H_0}{4\,\pi}\right)^2\left[\Lambda_p^2 + \ln\Lambda_p^2 + \frac{1}{\Delta} + 2\,\gamma - 4 + \mathcal{O}(\Delta)\right] = 0 . \tag{48}$$

From this equation it becomes clear that the one-loop ultraviolet divergences can be canceled by choosing appropriate counterterms[12] leading to the final form of the renormalized inflaton equation of motion to leading order in the slow roll expansion

$$\ddot{\Phi}_0(t) + 3\,H_0\,\dot{\Phi}_0(t) + V_R'(\Phi_0) + \left(\frac{H_0}{4\,\pi}\right)^2 \frac{V_R'''(\Phi_0)}{\Delta} = 0 . \tag{49}$$

Although the quantum correction is of order $V_R'''(\Phi_0)$, (second order in slow roll), the strong infrared divergence arising from the quasi scale invariance of inflationary fluctuations brings about a denominator which is of first order in slow roll. Hence the lowest order quantum correction in the slow roll expansion, is actually of the same order as $V_R'(\Phi_0)$. To highlight this observation, it proves convenient to write eq.(49) in terms of the EFT and slow roll parameters,

$$\ddot{\Phi}_0(t) + 3\,H_0\,\dot{\Phi}_0(t) + V_R'(\Phi_0)\left[1 + \left(\frac{H_0}{2\pi\,M_{Pl}}\right)^2 \frac{\xi_V}{2\,\epsilon_V\,\Delta}\right] = 0 . \tag{50}$$

Since $\xi_V \sim \epsilon_V^2$ and $\Delta \sim \epsilon_V$ the leading quantum corrections are of zeroth order in slow roll. This is a consequence of the infrared enhancement resulting from the nearly scale invariance of the power spectrum of scalar fluctuations. The quantum correction is suppressed by an EFT factor $H^2/M_{Pl}^2 \ll 1$.

Restoring the dependence of Δ on Φ_0 through the definitions (18) and (36) we find the equation of motion for the inflaton field to leading order in slow roll and in $(H/M_{Pl})^2$,

$$\ddot{\Phi}_0(t) + 3\,H\,\dot{\Phi}_0(t) + V_R'(\Phi_0) + \frac{1}{24\,(\pi\,M_{Pl})^2}\,\frac{V_R^3(\Phi_0)\,V_R'''(\Phi_0)}{2\,V_R(\Phi_0)V_R''(\Phi_0) - V_R'^2(\Phi_0)} = 0 . \tag{51}$$

2.2 Quantum corrections to the Friedmann equation: the effective potential

The zero temperature effective potential in Minkowski space-time is often used to describe the scalar field dynamics during inflation [3, 22]. However, as we see below the resulting effective potential [see eq.(58)] is remarkably different from the Minkowski one [see Appendix A]. The focus of this Section is to derive the effective potential for slow-roll inflation.

Since the fluctuations of the inflaton field are quantized, the interpretation of the 'scalar condensate' Φ_0 is that of the expectation value of the full quantum field ϕ in a homogeneous coherent quantum state. Consistently with this, the Friedmann equation must necessarily be understood in terms of the *expectation* value of the field energy momentum tensor, namely

$$H^2 = \frac{1}{3\,M_{Pl}^2}\left\langle \frac{1}{2}\,\dot{\phi}^2 + \frac{1}{2}\left(\frac{\nabla\phi}{a(t)}\right)^2 + V[\phi]\right\rangle . \tag{52}$$

Separating the homogeneous condensate from the fluctuations as in eq. (24) and imposing the tadpole equation (25), the Friedmann equation becomes

$$H^2 = \frac{1}{3\,M_{Pl}^2}\left[\frac{1}{2}\,\dot{\Phi}_0^{\,2} + V_R(\Phi_0) + \delta V_R(\Phi_0)\right] + \frac{1}{3\,M_{Pl}^2}\left\langle \frac{1}{2}\,\dot{\varphi}^2 + \frac{1}{2}\left(\frac{\nabla\varphi}{a(t)}\right)^2 + \frac{1}{2}\,V''(\Phi_0)\,\varphi^2 + \cdots\right\rangle \tag{53}$$

The dots inside the angular brackets correspond to terms with higher derivatives of the potential which are smaller in the slow roll expansion. The quadratic term $\langle\varphi^2\rangle$ to leading order in slow roll is given by eq.(46). Calculating the expectation value in eq.(53) in free field theory corresponds to obtaining the corrections to the energy momentum tensor by integrating the fluctuations *up to one loop*[12]. The first two terms of the expectation value in eq.(53) *do not* feature infrared divergences for $\nu = 3/2$ because of the two extra powers of the loop momentum in the integral. These contributions are given by

$$\left\langle \frac{1}{2}\,\dot{\varphi}^2 \right\rangle = \frac{H_0^4}{16\,\pi}\int_0^{\Lambda_P}\frac{dz}{z}\,z^2\left|\frac{d}{dz}\left[z^{\frac{3}{2}}H_\nu^{(1)}(z)\right]\right|^2 = \frac{H_0^4\,\Lambda_P^4}{32\,\pi^2} + \mathcal{O}(H_0^4\Delta)\,, \tag{54}$$

$$\left\langle \frac{1}{2}\left(\frac{\nabla\varphi}{a(t)}\right)^2 \right\rangle = \frac{H_0^4}{16\,\pi}\int_0^{\Lambda_P}\frac{dz}{z}\,z^5\left|H_\nu^{(1)}(z)\right|^2 = \frac{H_0^4\,\Lambda_P^4}{32\,\pi^2} + \frac{H^4\,\Lambda_P^2}{16\,\pi^2} + \mathcal{O}(H_0^4\Delta)\,. \tag{55}$$

The counterterms cancel the ultraviolet divergences arising from the third term in the angular brackets in eq. (53)[12]. Finally, the fully renormalized Friedmann equation to one loop and to lowest order in the slow roll expansion is [12]

$$H^2 = \frac{1}{3\,M_{Pl}^2}\left[\frac{1}{2}\,\dot{\Phi}_0^{\,2} + V_R(\Phi_0) + \left(\frac{H_0}{4\,\pi}\right)^2\frac{V_R''(\Phi_0)}{\Delta} + \text{higher orders in slow roll}\right] \equiv H_0^2 + \delta H^2\,, \tag{56}$$

where H_0 is the Hubble parameter in absence of quantum fluctuations:

$$H_0^2 = \frac{V_R(\Phi_0)}{3\,M_{Pl}^2}\left[1 + \frac{\epsilon_V}{3} + \mathcal{O}(\epsilon_V^2, \epsilon_V\,\eta_V)\right]\,.$$

Using the lowest order slow roll relation eq. (30), the last term in eq.(56) can be written as follows

$$\frac{\delta H^2}{H_0^2} = \left(\frac{H_0}{4\,\pi\,M_{Pl}}\right)^2\frac{\eta_V}{\Delta}\,. \tag{57}$$

This equation defines the back-reaction correction to the scale factor arising from the quantum fluctuations of the inflaton.

Hence, while the ratio η_V/Δ is of order zero in slow roll, the one loop correction to the Friedmann equation is of the order $H_0^2/M_{Pl}^2 \ll 1$ consistently with the EFT expansion. The Friedmann equation suggests the identification of the effective potential

$$V_{eff}(\Phi_0) = V_R(\Phi_0) + \left(\frac{H_0}{4\,\pi}\right)^2\frac{V_R''(\Phi_0)}{\Delta} + \text{higher orders in slow roll} = \tag{58}$$

$$= V_R(\Phi_0)\left[1 + \left(\frac{H_0}{4\,\pi\,M_{Pl}}\right)^2\frac{\eta_V}{\eta_V - \epsilon_V} + \text{higher orders in slow roll}\right]\,. \tag{59}$$

We see that the equation of motion for the inflaton eq.(49) takes the natural form

$$\ddot{\Phi}_0(t) + 3\,H_0\,\dot{\Phi}_0(t) + \frac{\partial V_{eff}}{\partial\Phi_0}(\Phi_0) = 0\,.$$

where the derivative of V_{eff} with respect to Φ_0 is taken at fixed Hubble and slow roll parameters. That is, H_0 and Δ must be considered in the present context as gravitational degrees of freedom and not as matter (inflaton) degrees of freedom.

Eqs.(57) and (58) make manifest the nature of the effective field theory expansion in terms of the ratio $(H_0/M_{Pl})^2$. The coefficients of the powers of this ratio are obtained in the slow roll expansion. To leading order, these coefficients are of $\mathcal{O}(N^0)$ because of the infrared enhancement manifest in the poles in Δ, a consequence of the nearly scale invariant power spectrum of scalar perturbations.

A noteworthy result is the rather different form of the effective potential eq.(58) as compared to the result in Minkowski space time at zero temperature. In the appendix we show explicitly that the same definition of the effective potential as the expectation value of T_{00} in Minkowski space-time at zero temperature is strikingly different from eq.(58) valid for slow roll inflation.

3 Quantum Corrections to the Scalar and Tensor Power. Scalar, Tensor, Fermion and Light Scalar Contributions.

During slow-roll inflation many quantum fields may be coupled to the inflaton (besides itself) and can contribute to the quantum corrections to the equations of motion and to the inflaton effective potential. The scalar curvature and tensor fluctuations are certainly there. We also consider light fermions and scalars coupled to the inflaton. We take the fermions to be Dirac fields with a generic Yukawa-type coupling but it is straightforward to generalize to Weyl or Majorana fermions. The Lagrangian density is taken to be

$$\mathcal{L} = \sqrt{-g}\left\{\frac{1}{2}\,\dot{\varphi}^2 - \left(\frac{\vec{\nabla}\varphi}{2\,a}\right)^2 - V(\varphi) + \frac{1}{2}\,\dot{\sigma}^2 - \left(\frac{\vec{\nabla}\sigma}{2\,a}\right)^2 - \frac{1}{2}\,m_\sigma^2\,\sigma^2 - G(\varphi)\,\sigma^2 + \overline{\Psi}\Big[i\,\gamma^\mu\,\mathcal{D}_\mu\Psi - m_f - Y(\varphi)\Big]\Psi\right\} \tag{60}$$

where $G(\Phi)$ and $Y(\Phi)$ are generic interaction terms between the inflaton and the scalar and fermionic fields. For simplicity we consider one bosonic and one fermionic Dirac field. The γ^μ are the curved space-time Dirac matrices and $\mathcal{D}_\mu$ the fermionic covariant derivative[9, 23]. We will consider that the light scalar field σ has vanishing expectation value at all times, therefore inflationary dynamics is driven by one single scalar field, the inflaton ϕ.

We consider the contributions from the quadratic fluctuations to the energy momentum tensor. There are *four* distinct contributions: i) scalar metric (density) perturbations, ii) tensor (gravitational waves) perturbations, iii) fluctuations of the light bosonic scalar field σ, iv) fluctuations of the light fermionic field Ψ.

Fluctuations in the metric are studied as usual [3, 24]. Writing the metric as

$$g_{\mu\nu} = g^0_{\mu\nu} + \delta^s g_{\mu\nu} + \delta^t g_{\mu\nu}$$

where $g^0_{\mu\nu}$ is the spatially flat FRW background metric eq.(3), $\delta^{s,t}g_{\mu\nu}$ correspond to the scalar and tensor perturbations respectively, and we neglect vector perturbations. In longitudinal gauge

$$\delta^s g_{00} = C^2(\eta)\;2\,\phi \quad , \quad \delta^s g_{ij} = C^2(\eta)\;2\,\psi\,\delta_{ij} \quad , \quad \delta^t g_{ij} = -C^2(\eta)\;h_{ij} \tag{61}$$

where h_{ij} is transverse and traceless and we neglect vector modes since they are not generated in single field inflation[3, 24].

Expanding up to quadratic order in the scalar fields, fermionic fields and metric perturbations the part of the Lagrangian density that is quadratic in these fields is given by

$$\mathcal{L}_Q = \mathcal{L}_s[\delta\varphi^{gi}, \phi^{gi}, \psi^{gi}] + \mathcal{L}_t[h] + \mathcal{L}_\sigma[\sigma] + \mathcal{L}_\Psi[\overline{\Psi}, \Psi]\;,$$

where

$$\mathcal{L}_t[h] = \frac{M_{Pl}^2}{8}\;C^2(\eta)\;\partial_\alpha h^j_i\;\partial_\beta h^i_j\;\eta^{\alpha\beta}\;,$$

$$\mathcal{L}_\sigma[\sigma] = C^4(\eta)\left\{\frac{1}{2}\left(\frac{\sigma'}{C}\right)^2 - \frac{1}{2}\left(\frac{\nabla\sigma}{C}\right)^2 - \frac{1}{2}\,M^2_\sigma[\Phi_0]\,\sigma^2\right\},$$

$$\mathcal{L}_\Psi[\overline{\Psi}, \Psi] = \overline{\Psi}\Big[i\,\gamma^\mu\,\mathcal{D}_\mu\Psi - M_\Psi[\Phi_0]\Big]\Psi\;,$$

here the prime stands for derivatives with respect to conformal time and the labels (gi) refer to gauge invariant quantities[24]. The explicit expression for $\mathcal{L}[\delta\varphi^{gi}, \phi^{gi}, \psi^{gi}]$ is given in eq. (10.68) in ref.[24]. The effective masses for the bosonic and fermionic fields are given by

$$M^2_\sigma[\Phi_0] = m^2_\sigma + G(\Phi_0) \quad , \quad M_\Psi[\Phi_0] = m_f + Y(\Phi_0)\;. \tag{62}$$

We focus on the study of the quantum corrections to the Friedmann equation, for the case in which both the scalar and fermionic fields are light in the sense that during slow roll inflation,

$$M_\sigma[\Phi_0]\;,\; M_\Psi[\Phi_0] \ll H_0\;, \tag{63}$$

at least during the cosmologically relevant stage corresponding to the 60 or so e-folds before the end of inflation.

From the quadratic Lagrangian given above the quadratic quantum fluctuations to the energy momentum tensor can be extracted.

The effective potential is identified with $\langle T_0^0 \rangle$ in a spatially translational invariant state in which the expectation value of the inflaton field is Φ_0. During slow roll inflation the expectation value Φ_0 evolves very slowly in time, the slow roll approximation is indeed an adiabatic approximation, which justifies treating Φ_0 as a constant in order to obtain the effective potential. The time variation of Φ_0 only contributes to higher order corrections in slow-roll. The energy momentum tensor is computed in the FRW inflationary background determined by the *classical* inflationary potential $V(\Phi_0)$, and the slow roll parameters are also explicit functions of Φ_0. Therefore the energy momentum tensor depends *implicitly* on Φ_0 through the background and *explicitly* on the masses for the light bosonic and fermionic fields given above.

We can write the effective potential as

$$V_{eff}(\Phi_0) = V(\Phi_0) + \delta V(\Phi_0) \; , \tag{64}$$

where

$$\delta V(\Phi_0) = \langle T_0^0[\Phi_0] \rangle_s + \langle T_0^0[\Phi_0] \rangle_t + \langle T_0^0[\Phi_0] \rangle_\sigma + \langle T_0^0[\Phi_0] \rangle_\Psi \tag{65}$$

(s, t, σ, Ψ) correspond to the energy momentum tensors of the quadratic fluctuations of the scalar metric, tensor (gravitational waves), light boson field σ and light fermion field Ψ fluctuations respectively. Since these are the expectation values of a quadratic energy momentum tensor, $\delta V(\Phi_0)$ corresponds to the *one loop correction* to the effective potential.

3.1 Light scalar fields

During slow roll inflation the effective mass of the σ field is given by eq. (62), just as for the inflaton fluctuation in sec. 2. It is convenient to introduce a parameter η_σ defined to be

$$\eta_\sigma = \frac{M_\sigma^2[\Phi_0]}{3\, H_0^2} \; . \tag{66}$$

Hence, the sigma field contributions to the inflaton equations of motion and inflaton effective potential can be obtained from sec. 2 just replacing the slow roll parameter η_V by η_σ. In particular, infrared divergences are now regulated by the parameter $\Delta_\sigma \equiv \eta_\sigma - \epsilon_V$.

To leading order in the slow roll expansion and in $\eta_\sigma \ll 1$, the infrared contribution is given by[9],

$$\frac{M_\sigma^2[\Phi_0]}{2} \, \langle \sigma^2(\vec{x}, t) \rangle = \frac{3\, H_0^4}{(4\,\pi)^2} \, \frac{\eta_\sigma}{\eta_\sigma - \epsilon_V} + \text{subleading in slow roll.}$$

The fully renormalized contribution from from the sigma field to T_0^0 to leading order in slow roll takes the form [9],

$$\langle T_0^0 \rangle_\sigma = \frac{3\, H_0^4}{(4\,\pi)^2} \, \frac{\eta_\sigma}{\Delta_\sigma} + \frac{1}{2} \left\langle \dot{\sigma}^2 + \left(\frac{\nabla \sigma}{C(\eta)} \right)^2 \right\rangle_{ren} \tag{67}$$

In calculating here the second term we can set to zero the slow roll parameters ϵ_V, η_V as well as the mass of the light scalar, namely $\eta_\sigma = 0$. Hence, to leading order, the second term is identified with the 00 component of the renormalized energy momentum tensor for a free massless minimally coupled scalar field in exact de Sitter space time. Therefore we can extract this term from refs.[21, 23],

$$\langle T_{\mu\nu} \rangle_{ren} = \frac{g_{\mu\nu}}{(4\,\pi)^2} \left\{ m_\sigma^2 \, H_0^2 \left(1 - \frac{m_\sigma^2}{2\, H_0^2} \right) \left[-\psi\left(\frac{3}{2} + \nu \right) - \psi\left(\frac{3}{2} - \nu \right) + \ln \frac{m_\sigma^2}{H_0^2} \right] + \frac{2}{3} \, m_\sigma^2 \, H_0^2 - \frac{29}{30} \, H_0^4 \right\} , \tag{68}$$

where $\nu \equiv \sqrt{\frac{9}{4} - \frac{m_\sigma^2}{H_0^2}}$ and $\psi(z)$ stands for the digamma function. This expression corrects a factor of two in ref.[23]. In eq. (6.177) in [23] the D'Alambertian acting on $G^1(x, x')$ was neglected. However, in

computing this term, the D'Alambertian must be calculated *before* taking the coincidence limit. Using the equation of motion yields the extra factor 2 and the expression eq.(68).

The pole at $\nu = 3/2$ manifest in eq.(68) coincides with the pole in eq.(67) using that $m_\sigma^2 = 3\,H^2\,\eta_\sigma$ [eq.(66)]. This pole originates in the term $m_\sigma^2 < \sigma^2 >$, which features an infrared divergence in the limit $\nu_\sigma = 3/2$. All the terms with space-time derivatives are infrared finite in this limit. Therefore, we can extract from eq.(68) the renormalized expectation value in the limit $H_0 \gg m_\sigma$,

$$\langle T_0^0 \rangle_\sigma = \frac{H_0^4}{(4\,\pi)^2}\left[\frac{3\,\eta_\sigma}{\eta_\sigma - \epsilon_V} - \frac{29}{30} + \mathcal{O}(\epsilon_V, \eta_\sigma, \eta_V)\right] \tag{69}$$

The second term is completely determined by the **trace anomaly** of the minimally coupled scalar fields[21, 23, 25].

3.2 Quantum Corrections to the Inflaton potential from the Scalar metric perturbations

The gauge invariant energy momentum tensor for quadratic scalar metric fluctuations has been obtained in ref.[26]. In longitudinal gauge and in cosmic time it is given by

$$\begin{aligned}\langle T_0^0 \rangle_s = \quad & M_{Pl}^2\left[12\,H_0\,\langle\phi\dot{\phi}\rangle - 3\,\langle(\dot{\phi})^2\rangle + \frac{9}{C^2(\eta)}\,\langle(\nabla\phi)^2\rangle\right] \\ & + \frac{1}{2}\,\langle(\dot{\delta\varphi})^2\rangle + \frac{\langle(\nabla\delta\varphi)^2\rangle}{2\,C^2(\eta)} + \frac{V''(\Phi_0)}{2}\,\langle(\delta\varphi)^2\rangle + 2\,V'(\Phi_0)\,\langle\phi\,\delta\varphi\rangle\end{aligned} \tag{70}$$

where the dots stand for derivatives with respect to cosmic time. In longitudinal gauge, the equations of motion in cosmic time for the Fourier modes are[3, 24]

$$\begin{aligned}&\ddot{\phi}_{\vec{k}} + \left(H_0 - 2\,\frac{\ddot{\Phi}_0}{\dot{\Phi}_0}\right)\dot{\phi}_{\vec{k}} + \left[2\left(\dot{H}_0 - 2\,H_0\,\frac{\ddot{\Phi}_0}{\dot{\Phi}_0}\right) + \frac{k^2}{C^2(\eta)}\right]\phi_{\vec{k}} = 0 \\ &\ddot{\delta\varphi}_{\vec{k}} + 3\,H\,\dot{\delta\varphi}_{\vec{k}} + \left[V''[\Phi_0] + \frac{k^2}{C^2(\eta)}\right]\delta\varphi_{\vec{k}} + 2\,V'[\Phi_0]\,\phi_{\vec{k}} - 4\,\dot{\Phi}_0\,\dot{\phi}_{\vec{k}} = 0\,,\end{aligned} \tag{71}$$

with the constraint equation

$$\dot{\phi}_{\vec{k}} + H_0\,\phi_{\vec{k}} = \frac{1}{2M_{Pl}}\,\delta\varphi_{\vec{k}}\,\dot{\Phi}_0\,. \tag{72}$$

We split the contributions to the energy momentum tensor as those from superhorizon modes, which yield the infrared enhancement, and the subhorizon modes for which we can set all slow roll parameters to zero. Just as discussed above for the case of the σ field, since spatio-temporal derivatives bring higher powers of the momenta, we can neglect all derivative terms for the contribution from the superhorizon modes and set[26]

$$\langle T_0^0 \rangle_{IR} \approx \frac{1}{2}\,V''[\Phi_0]\,\langle(\delta\varphi(\vec{x},t))^2\rangle + 2\,V'[\Phi_0]\,\langle\phi(\vec{x},t)\,\delta\varphi(\vec{x},t)\rangle\,. \tag{73}$$

The analysis of the solution of eq.(71) for superhorizon wavelengths in ref. [24] shows that in exact de Sitter space time $\phi_{\vec{k}} \sim$ constant, hence it follows that during quasi-de Sitter slow roll inflation for superhorizon modes

$$\dot{\phi}_{\vec{k}} \sim (\text{slow roll}) \times H_0\,\phi_{\vec{k}} \tag{74}$$

Therefore, for superhorizon modes, the constraint equation (72) yields

$$\phi_{\vec{k}} = -\frac{V'(\Phi_0)}{2\,V(\Phi_0)}\,\delta\varphi_{\vec{k}} + \text{higher orders in slow roll}\,. \tag{75}$$

Inserting this relation in eq.(71) and consistently neglecting the term $\dot{\phi}_{\vec{k}}$ according to eq.(74), we find the following equation of motion for the gauge invariant scalar field fluctuation in longitudinal gauge

$$\ddot{\delta\varphi}_{\vec{k}} + 3\,H_0\,\dot{\delta\varphi}_{\vec{k}} + \left[\frac{k^2}{C^2(\eta)} + 3\,H_0^2\,\eta_\delta\right]\delta\varphi_{\vec{k}} = 0\,, \tag{76}$$

where we have used the definition of the slow roll parameters ϵ_V; η_V given in eq.(18), and introduced $\eta_\delta \equiv \eta_V - 2\,\epsilon_V$. This is the equation of motion for a minimally coupled scalar field with mass squared $3\,H_0^2\,\eta_\delta$ and we can use the results obtained in the case of the scalar field σ.

Repeating the analysis presented in the case of the scalar field σ above, we finally find[9]

$$\langle T^0_0\rangle_{IR} = \frac{3\,H_0^4}{(4\,\pi)^2}\,\frac{\eta_V - 4\,\epsilon_V}{\eta_V - 3\,\epsilon_V} + \text{subleading in slow roll} \tag{77}$$

It can be shown that the contribution from subhorizon modes to $\langle T^0_{0s}\rangle$ is given by [9]

$$\langle T^0_{0s}\rangle_{UV} \simeq \frac{1}{2}\langle(\dot{\delta\varphi})^2\rangle + \frac{\langle(\nabla\delta\varphi)^2\rangle}{2\,a^2} \tag{78}$$

where we have also neglected the term with $V''[\Phi_0] \sim 3\,H_0^2\,\eta_V$ since $k^2/a^2 \gg H_0^2$ for subhorizon modes. Therefore, to leading order in slow roll we find the renormalized expectation value of T_{00s} is given by

$$\langle T^0_{0s}\rangle_{ren} \simeq \frac{3H_0^4}{(4\,\pi)^2}\,\frac{\eta_V - 4\,\epsilon_V}{\eta_V - 3\,\epsilon_V} + \frac{1}{2}\left\langle \dot{\delta\varphi}^{\,2} + \left(\frac{\nabla\delta\varphi}{C(\eta)}\right)^2\right\rangle_{ren} \tag{79}$$

To obtain the renormalized expectation value in eq.(79) one can set all slow roll parameters to zero to leading order and simply consider a massless scalar field minimally coupled in de Sitter space time and borrow the result from eq.(69). We find[9]

$$\langle T^0_{0s}\rangle_{ren} = \frac{H_0^4}{(4\,\pi)^2}\left[\frac{\eta_V - 4\,\epsilon_V}{\eta_V - 3\,\epsilon_V} - \frac{29}{30} + \mathcal{O}(\epsilon_V, \eta_\sigma, \eta_V)\right] \tag{80}$$

The last term in eq. (80) is completely determined by the **trace anomaly** of a minimally coupled scalar field in de Sitter space time[21, 23, 25]

3.3 Quantum Corrections to the Inflaton potential from the Tensor perturbations

Tensor perturbations correspond to massless fields with two physical polarizations. The energy momentum tensor for gravitons only depends on derivatives of the field h^i_j therefore its expectation value in the Bunch Davies (BD) vacuum does not feature infrared singularities in the limit $\epsilon_V \to 0$. The absence of infrared singularities in the limit of exact de Sitter space time, entails that we can extract the leading contribution to the effective potential from tensor perturbations by evaluating the expectation value of T_{00} in the BD vacuum in exact de Sitter space time, namely by setting all slow roll parameters to zero. This will yield the leading order in the slow roll expansion.

Because de Sitter space time is maximally symmetric, the expectation value of the energy momentum tensor is given by[23]

$$\langle T_{\mu\nu}\rangle_{BD} = \frac{g_{\mu\nu}}{4}\,\langle T^\alpha_\alpha\rangle_{BD} \tag{81}$$

and T^α_α is a space-time constant, therefore the energy momentum tensor is manifestly covariantly conserved. A large body of work has been devoted to study the trace anomaly in de Sitter space time implementing a variety of powerful covariant regularization methods that preserve the symmetry[25, 23, 21] yielding a renormalized value of $\langle T_{\mu\nu}\rangle_{BD}$ given by eq. (81). Therefore, the full energy momentum tensor is completely determined by the **trace anomaly**. The contribution to the trace anomaly from gravitons has been given in refs.[21, 23, 25], it is

$$\langle T^\alpha_\alpha\rangle_t = -\frac{717}{80\,\pi^2}\,H_0^4 \quad \text{and} \quad \langle T^0_0\rangle_t = -\frac{717}{320\,\pi^2}\,H_0^4\,. \tag{82}$$

3.4 Summary of Quantum Corrections to the Observable Spectra

In summary, we find that the effective potential at one-loop is given by,

$$\delta V(\Phi_0) = \frac{H_0^4}{(4\,\pi)^2}\left[\frac{\eta_V - 4\,\epsilon_V}{\eta_V - 3\,\epsilon_V} + \frac{3\,\eta_\sigma}{\eta_\sigma - \epsilon_V} + \mathcal{T}_\Phi + \mathcal{T}_s + \mathcal{T}_t + \mathcal{T}_\Psi + \mathcal{O}(\epsilon_V, \eta_V, \eta_\sigma, \mathcal{M}^2)\right],$$

where (s, t, σ, Ψ) stand for the contributions of the scalar metric, tensor fluctuations, light boson field σ and light fermion field Ψ, respectively. We have

$$\mathcal{T}_\Phi = \mathcal{T}_s = -\frac{29}{30} \quad , \quad \mathcal{T}_t = -\frac{717}{5} \quad , \quad \mathcal{T}_\Psi = \frac{11}{60} \tag{83}$$

The terms that feature the *ratios* of combinations of slow roll parameters arise from the infrared or superhorizon contribution from the scalar density perturbations and scalar fields σ respectively. The terms $\mathcal{T}_{s,t,\Psi}$ are completely determined by the trace anomalies of scalar, graviton and fermion fields respectively. Writing $H_0^4 = V(\Phi_0)\; H_0^2/[3\; M_{Pl}^2]$ we can finally write the effective potential to leading order in slow roll

$$V_{eff}(\Phi_0) = V(\Phi_0)\left[1 + \frac{H_0^2}{3\,(4\,\pi)^2\,M_{Pl}^2}\left(\frac{\eta_V - 4\,\epsilon_V}{\eta_V - 3\,\epsilon_V} + \frac{3\,\eta_\sigma}{\eta_\sigma - \epsilon_V} - \frac{2903}{20}\right)\right] \tag{84}$$

There are several **remarkable** aspects of this result:

i) the infrared enhancement as a result of the near scale invariance of scalar field fluctuations, both from scalar density perturbations as well as from a light scalar field, yield corrections of *zeroth order in slow roll*. This is a consequence of the fact that during slow roll the particular combination $\Delta_\sigma = \eta_\sigma - \epsilon_V$ of slow roll parameters yield a natural infrared cutoff.

ii) the final one loop contribution to the effective potential displays the effective field theory dimensionless parameter H_0^2/M_{Pl}^2.

iii) the last term is completely determined by the trace anomaly, a purely geometric result of the short distance properties of the theory.

The quantum corrections to the effective potential lead to quantum corrections to the amplitude of scalar and tensor fluctuations with the result[9]

$$|\Delta^{(S)}_{k,eff}|^2 = |\Delta^{(S)}_k|^2\left\{1 + \frac{2}{3}\left(\frac{H_0}{4\,\pi\,M_{Pl}}\right)^2\left[1 + \frac{\frac{3}{8}\,r\,(n_s - 1) + 2\,\frac{dn_s}{d\ln k}}{(n_s - 1)^2} + \frac{2903}{40}\right]\right\}$$

$$|\Delta^{(T)}_{k,eff}|^2 = |\Delta^{(T)}_k|^2\left\{1 - \frac{1}{3}\left(\frac{H_0}{4\,\pi\,M_{Pl}}\right)^2\left[-1 + \frac{1}{8}\,\frac{r}{n_s - 1} + \frac{2903}{20}\right]\right\},$$

$$r_{eff} \equiv \frac{|\Delta^{(T)}_{k,eff}|^2}{|\Delta^{(S)}_{k,eff}|^2} = r\left\{1 - \frac{1}{3}\left(\frac{H_0}{4\,\pi\,M_{Pl}}\right)^2\left[1 + \frac{\frac{3}{8}\,r\,(n_s - 1) + \frac{dn_s}{d\ln k}}{(n_s - 1)^2} + \frac{8709}{20}\right]\right\}. \tag{85}$$

The quantum corrections turn out to **enhance** the scalar curvature fluctuations and to **reduce** the tensor fluctuations as well as their ratio r.

Acknowledgment: H J de V thanks the organizers of JGRG15 for their kind hospitality in Tokyo.

A One loop effective potential and equations of motion in Minkowski space-time: a comparison

In this appendix we establish contact with familiar effective potential both at the level of the equation of motion for the expectation value of the scalar field, as well as the expectation value of T_{00}.

In Minkowski space time the spatial Fourier transform of the field operator is given by

$$\varphi_{\vec{k}}(t) = \frac{1}{\sqrt{2\omega_k}}\left[a_{\vec{k}}\; e^{-i\omega_k\,t} + a^\dagger_{-\vec{k}}\; e^{i\omega_k\,t}\right], \tag{86}$$

where the vacuum state is annihilated by $a_{\vec{k}}$ and the frequency is given by

$$\omega_k = \sqrt{k^2 + V''(\Phi_0)}\,. \tag{87}$$

The one-loop contribution to the equation of motion (29) is given by

$$\frac{V'''(\Phi_0)}{2}\,\langle[\varphi(\vec{x},t)]^2\rangle = \frac{V'''(\Phi_0)}{8\,\pi^2}\int_0^\Lambda \frac{k^2}{\omega_k}\,dk = \frac{d}{d\Phi_0}\left[\frac{1}{4\pi^2}\int_0^\Lambda k^2\,\omega_k\,dk\right]\,. \tag{88}$$

The expectation value of $T_{00} = \mathcal{H}$ (Hamiltonian density) in Minkowski space time is given up to one loop by the following expression

$$\langle T_{00}\rangle = \left\langle \frac{1}{2}\,\dot{\phi}^2 + \frac{1}{2}\,(\nabla\phi)^2 + V(\phi)\right\rangle = \frac{1}{2}\,\dot{\Phi}_0^{\,2} + V(\Phi_0) + \left\langle \frac{1}{2}\,\dot{\varphi}^2 + \frac{1}{2}\,(\nabla\varphi)^2 + \frac{1}{2}\,V''(\Phi_0)\,\varphi^2 + \cdots\right\rangle\,. \tag{89}$$

The expectation value of the fluctuation contribution is given by

$$\left\langle \frac{1}{2}\,\dot{\varphi}^2 + \frac{1}{2}\,(\nabla\varphi)^2 + \frac{1}{2}\,V''(\Phi_0)\,\varphi^2 + \cdots\right\rangle = \frac{1}{4\pi^2}\int_0^\Lambda k^2\,\omega_k\,dk = \frac{\Lambda^4}{16\pi^2} + \frac{V''(\Phi_0)\,\Lambda^2}{16\,\pi^2} - \frac{[V''(\Phi_0)]^2}{64\,\pi^2}\,\ln\frac{4\,\Lambda^2}{V''(\Phi_0)}\,. \tag{90}$$

Renormalization proceeds as usual by writing the bare Lagrangian in terms of the renormalized potential and counterterms. Choosing the counterterms to cancel the quartic, quadratic and logarithmic ultraviolet divergences. we obtain the familiar renormalized one loop effective potential

$$V_{eff}(\Phi_0) = V_R(\Phi_0) + \frac{[V_R''(\Phi_0)]^2}{64\,\pi^2}\,\ln\frac{V_R''(\Phi_0)}{M^2}\,, \tag{91}$$

where M is a renormalization scale. Furthermore from eq. (88) it is clear that the equation of motion for the expectation value is given by

$$\ddot{\Phi}_0 + V_{eff}'(\Phi_0) = 0\,. \tag{92}$$

References

[1] D. Kazanas, ApJ 241, L59 (1980); A. Guth, Phys. Rev. **D23**, 347 (1981); K. Sato, MNRAS, **195**, 467 (1981).

[2] M. S. Turner, Phys. Rev. D48, 3502 (1993). S. Dodelson, W. H. Kinney, E. W. Kolb Phys. Rev. D56, 3207 (1997). S. M. Leach, A. R. Liddle, J. Martin, D. J. Schwarz, Phys. Rev. D66, 023515 (2002). N. Bartolo, S. Matarrese, A. Riotto, Phys. Rev. D64, 083514 (2001). N. Bartolo, E. Komatsu, S. Matarrese, A. Riotto, astro-ph/0406398.

[3] See for example, W. Hu and S. Dodelson, Ann. Rev. Astron. Ap. **40**, 171 (2002); J. Lidsey, A. Liddle, E. Kolb, E. Copeland, T. Barreiro and M. Abney, Rev. of Mod. Phys. **69** 373, (1997). W. Hu, astro-ph/0402060. A. Riotto, hep-ph/0210162, M. Giovannini, astro-ph/0412601 (2004).

[4] C. L. Bennett *et.al.* (WMAP collaboration), Ap.J.Suppl. **148**, 1 (2003). A. Kogut *et.al.* (WMAP collaboration), Ap.J.Suppl. **148**, 161 (2003). D. N. Spergel *et. al.* (WMAP collaboration), Ap. J. Suppl.**148**, 175 (2003). H. V. Peiris *et.al.* (WMAP collaboration), Ap. J. Suppl.**148**, 213 (2003).

[5] V. A. Belinsky, L. P. Grishchuk, Ya. B. Zeldovich, I. M. Khalatnikov, Phys. Lett. **B 155**, 232, (1985), JETP **62**, 195 (1985).

[6] D. Boyanovsky, H. J. de Vega, in the Proceedings of the VIIth. Chalonge School, 'Current Topics in Astrofundamental Physics', p. 37-97, edited by N. G. Sanchez, Kluwer publishers, Series C, vol. 562, (2001), astro-ph/0006446. D. Boyanovsky, D. Cormier, H. J. de Vega, R. Holman, S. P. Kumar, Phys. Rev. **D 57**, 2166 (1998). D. Boyanovsky, H. J. de Vega, R. Holman, Phys. Rev. **D 49**, 2769 (1994). D. Boyanovsky, F. J. Cao and H. J. de Vega, Nucl. Phys. **B 632**, 121 (2002). D. Boyanovsky, D. Cormier, H. J. de Vega, R. Holman, A. Singh, and M. Srednicki, Phys. Rev. **D56**, 1939 (1997); D. Boyanovsky, D. Cormier, H. J. de Vega, R. Holman, Phys. Rev. **D55**, 3373 (1997).

[7] F. J. Cao, H. J. de Vega, N. G. Sanchez, Phys. Rev. **D70**, 083528 (2004).

[8] A. A. Starobinsky and J. Yokoyama, Phys.Rev.**D50**, 6357 (1994).

[9] D. Boyanovsky, H. J. de Vega, N. Sánchez, Phys. Rev. **72**, 103006 (2005).

[10] S. Dodelson, *Modern Cosmology*, Academic Press, 2003.

[11] D. Boyanovsky, H. J. de Vega, Phys. Rev. **D70**, 063508 (2004). D. Boyanovsky, H. J. de Vega, N. Sánchez, Phys. Rev. **D 71**, 023509 (2005).

[12] D. Boyanovsky, H. J. de Vega, N. Sánchez, astro-ph/0503669.

[13] H. Leutwyler, Ann. Phys. 235, 165 (1994), hep-ph/9409423. S. Weinberg, hep-ph/9412326 and 'The Quantum Theory of Fields', vol. 2, Cambridge University Press, Cambridge, 2000.

[14] D. Boyanovsky, H. J. de Vega, N. Sánchez, astro-ph/0507595.

[15] D. Cirigliano, H. J. de Vega, N. G. Sanchez, Phys. Rev. **D 71**, 103518 (2005).

[16] S. Weinberg, *The Quantum Theory of Fields I*, Cambridge University Press,Cambridge, 1995; M. E. Peskin and D. V. Schroeder, *An Introduction to Quantum Field Theory*, Advanced Book Program, Addison Wesley Pub. Co, Reading, Massachusetts, 1995.

[17] A. R. Liddle, P. Parsons , J. D. Barrow, Phys. Rev. **D50**, 7222 (1994).

[18] S. A. Ramsey and B. L. Hu, Phys. Rev. **D56**. 661, (1997); *ibid* 678, (1997).

[19] D. Boyanovsky, D. Cormier, H. J. de Vega, R. Holman and S. P. Kumar, in the Proceedings of the VIth. Erice Chalonge School on Astrofundamental Physics, Eds. N. Sánchez and A. Zichichi, Kluwer, 1998.

[20] P. Anderson, C. Molina-Paris, and E. Mottola, Phys. Rev. D72, 043515(2005).

[21] T. S. Bunch and P. C. W. Davies, Proc. R. Soc. London **A360**, 117 (1978); A. Vilenkin and L. H. Ford, Phys. Rev. **D26**, 1231 (1982). M. A. Castagnino, J. P. Paz and N. Sanchez, Phys. Lett. **B193**, 13 (1987).

[22] D. H. Lyth , A. Riotto, Phys. Rept. **314**, 1 (1999).

[23] N. D. Birrell and P. C. W. Davies, *Quantum fields in curved space*, Cambridge Monographs in Mathematical Physics, Cambridge University Press, Cambridge, 1982.

[24] V. F. Mukhanov, H. A. Feldman , R. H. Brandenberger, Phys. Rept. **215**, 203 (1992).

[25] M. J. Duff, Nucl. Phys. **B125**, 334 (1977); S. M. Christensen and M. J. Duff, Nucl. Phys. **B170**, 480 (1980); Phys. Lett. **B76**, 571 (1978). J. S. Dowker and R. Critchley, Phys. Rev. **D15**, 1484 (1977); *ibid* **D16**, 3390 (1977), **D13**, 224 (1976), **D13**, 3224 (1976). M. V. Fischetti, J. B. Hartle and B. L. Hu, Phys. Rev. **D20**, 1757 (1979). K. Fujikawa, Phys. Rev. **D23**, 2262 (1981).

[26] L. R. Abramo, R. H. Brandenberger and V. F. Mukhanov, Phys. Rev. **D56**, 3248 (1997); L. R. Abramo, Ph. D. Thesis, gr-qc/9709049.

Primordial Black Holes as a Probe of Inflation, Dark Matter and Extra Dimensions

Bernard Carr[1]

Astronomy Unit, Queen Mary, University of London, Mile End Road, London E1 4NS, England
Research Center for the Early Universe, School of Science, University of Tokyo, Tokyo 113-0033

Abstract

Some recent developments in the study of the formation and evaporation of primordial black holes (PBHs) are reviewed. It is still not clear whether PBHs formed but, if they did, they could provide a unique probe of inflation, dark matter and higher dimensions. Inflation is probed because PBHs could be formed from the associated density perturbations. Although PBHs do not form in the simplest "slow-roll" model, they could do so in many other models. PBHs could contribute to the dark matter if they are large enough not to have evaporated by now or if evaporating ones leave stable Planck-mass relicts. However, it is argued that PBHs are unlikely to grow into the supermassive black holes in galactic nuclei through accreting quintessence. If there are large extra dimensions, quantum gravity effects could appear at the TeV scale and small mass black holes may be formed in accelerators. Although such black holes would not themselves be primordial, this would have important implications for PBH formation. It would also mean that one could probe the changing dimensionality of the early universe experimentally.

1 Introduction

Black holes with a wide range of masses could have formed in the early Universe as a result of the great compression associated with the Big Bang [93, 193]. A comparison of the cosmological density at a time t after the Big Bang with the density associated with a black hole of mass M shows that PBHs would have of order the particle horizon mass at their formation epoch:

$$M_H(t) \approx \frac{c^3 t}{G} \approx 10^{15} \left(\frac{t}{10^{-23}\ \mathrm{s}} \right) g. \tag{1}$$

PBHs could thus span an enormous mass range: those formed at the Planck time (10^{-43}s) would have the Planck mass (10^{-5}g), whereas those formed at 1 s would be as large as $10^5 M_\odot$, comparable to the mass of the holes thought to reside in galactic nuclei. By contrast, black holes forming at the present epoch could never be smaller than about $1 M_\odot$.

The realization that PBHs might be small prompted Hawking to study their quantum properties. This led to his famous discovery [94] that black holes radiate thermally with a temperature

$$T = \frac{\hbar c^3}{8\pi G M k} \approx 10^{-7} \left(\frac{M}{M_\odot} \right)^{-1} \mathrm{K}, \tag{2}$$

so they evaporate on a timescale

$$\tau(M) \approx \frac{\hbar c^4}{G^2 M^3} \approx 10^{64} \left(\frac{M}{M_\odot} \right)^3 \mathrm{y}. \tag{3}$$

Only black holes smaller than 10^{15}g would have evaporated by the present epoch, so eqn (1) implies that this effect could be important only for black holes which formed before 10^{-23}s.

Hawking's result was a tremendous conceptual advance, since it linked three previously disparate areas of physics - quantum theory, general relativity and thermodynamics. Even if PBHs never existed,

[1]E-mail: B.J.Carr@qmul.ac.uk

it has been useful to think about them! However, at first sight it was bad news for PBH enthusiasts. For since PBHs with a mass of 10^{15}g would be producing photons with energy of order 100 MeV at the present epoch, the observational limit on the γ-ray background intensity at 100 MeV immediately implied that their density could not exceed 10^{-8} times the critical density [162]. Not only did this render PBHs unlikely dark matter candidates, it also implied that there was little chance of detecting black hole explosions at the present epoch [165]. Nevertheless, it was soon realized that the γ-ray background results did not preclude PBHs playing other important cosmological roles [32] and some of these will be discussed here.

2 How PBHs Form and Why they Are Useful

The high density of the early Universe is a necessary but not sufficient condition for PBH formation. One also needs density fluctuations, so that overdense regions can eventually stop expanding and recollapse. Indeed one reason for studying PBH formation and evaporation is that it imposes important constraints on primordial inhomogeneities. PBHs may also form at various phase transitions expected to occur in the early Universe. In some of these one require pre-existing density fluctuations, but in others the PBHs form spontaneously, even if the Universe starts off perfectly smooth. In the latter case, limits on the number of PBHs constrain any parameters associated with the phase transition. The formation of PBHs from inhomogeneities is discussed in Section 3, but we now briefly review the other mechanisms.

Soft equation of state. Some phase transitions can lead to the equation of state becoming soft for a while. For example, the pressure may be reduced if the Universe's mass is ever channelled into particles which are massive enough to be non-relativistic. In such cases, the effect of pressure in stopping collapse is unimportant and the probability of PBH formation just depends upon the fraction of regions which are sufficiently spherical to undergo collapse [115]. For a given spectrum of primordial fluctuations, this means that there may just be a narrow mass range - associated with the period of the soft equation of state - in which the PBHs form.

Collapse of cosmic loops. In the cosmic string scenario, one expects some strings to self-intersect and form cosmic loops. A typical loop will be larger than its Schwarzschild radius by the factor $(G\mu)^{-1}$, where μ is the string mass per unit length. If strings play a role in generating large-scale structure, $G\mu$ must be of order 10^{-6}. However, as discussed by many authors [29, 71, 96, 142, 164], there is then a small probability that a cosmic loop will get into a configuration in which every dimension lies within its Schwarzschild radius. This probability depends upon both μ and the string correlation scale. Note that the holes form with equal probability at every epoch, so they should have an extended mass spectrum.

Bubble collisions. Bubbles of broken symmetry might arise at any spontaneously broken symmetry epoch and various people have suggested that PBHs could form as a result of bubble collisions [56, 97, 122, 131, 153]. However, this happens only if the bubble formation rate per Hubble volume is finely tuned: if it is much larger than the Hubble rate, the entire Universe undergoes the phase transition immediately and there is not time to form black holes; if it is much less than the Hubble rate, the bubbles are very rare and never collide. The holes should have a mass of order the horizon mass at the phase transition, so PBHs forming at the GUT epoch would have a mass of 10^3g, those forming at the electroweak unification epoch would have a mass of 10^{28}g, and those forming at the QCD (quark-hadron) phase transition would have mass of around $1M_\odot$. There could also be wormhole production at a 1st order phase transition [121, 147]. Recently the production of PBHs from bubble collisons at the end of 1st order inflation has been studied extensively by Khlopov and his colleagues [117, 127].

Collapse of domain walls The collapse of sufficiently large closed domain walls produced at a 2nd order phase transition in the vacuum state of a scalar field, such as might be associated with inflation, could lead to PBH formation [60, 168, 167]. These PBHs would have a small mass for a thermal phase transition with the usual equilibrium conditions. However, they could be much larger if one invoked a non-equlibrium scenario [169]. Indeed Khlopov et al. argue that they could span a wide range of masses, with a fractal structure of smaller PBHs clustered around larger ones [118].

Depending on their mass, the study of PBHs provides a unique probe of four areas of physics: quantum gravity; the early universe; high energy physics; and gravitational collapse. Indeed one can gain insight into these areas even if PBHs never formed.

PBHS as a probe of quantum gravity ($M \sim 10^{-5}g$). Many new factors could come into play when a black hole's mass gets down to the Planck regime, including the effects of extra dimensions and quantum-gravitational spacetime fluctuations. For example, it has been suggested that black hole evaporation could cease at this point, in which case Planck relics could contribute to the dark matter. More radically, it is possible that quantum gravity effects could appear at the TeV scale and this leads to the intriguing possibility that small black holes could be generated in accelerators experiments or cosmic ray events. Although such black holes are not technically "primordial", this would have radical implications for PBHs themselves. These issues are discussed in Section 5.

PBHs as a probe of the early Universe ($M < 10^{15}g$). Many processes in the early universe could be modified by PBH evaporations [160]. For example, recent studies have considered how evaporations could change the details of baryosynthesis [61] and nucleosynthesis [42, 123, 152], provide a source of gravitinos [116] and neutrinos [27], swallow monopoles [107, 180] and remove domain walls by puncturing them [181]. PBHs evaporating at later times could have important astrophysical effects, such as helping to reionize the universe [98]. There has also been interest in whether PBHs could preserve gravitational "memory" if the value of G was different in the early Universes [15, 16, 40, 89, 108]. Other constraints are associated with thermodynamics [133] and the holographic principle [57].

PBHS as a probe of high energy physics ($M \sim 10^{15}g$). PBH evaporating today could contribute to cosmic rays, whose energy distribution would then give significant information about the high energy physics involved in the final explosive phase of black hole evaporation. In particular, PBHs could contribute to the cosmological and Galactic γ-ray backgrounds, the antiprotons and positrons in cosmic rays, gamma-ray bursts, and the annihilation-line radiation coming from centre of the Galaxy. These issues are discussed in Section 6

PBHs as a probe of gravitational collapse ($M > 10^{15}g$). This relates to recent developments in the study of "critical phenomena" and the issue of whether PBHs are viable dark matter candidates. In the latter case, their gravitational effects could lead to distinctive dynamical, lensing and gravitational-wave signatures. They could also influence the development of large-scale structure and the formation of supermassive black holes in galactic nuclei. These issues are discussed in Section 4.

3 PBHs as a Probe of Inhomogeneities and Inflation

One of the most important reasons for studying PBHs is that it enables one to place limits on the spectrum of density fluctuations in the early Universe. This is because, if the PBHs form directly from density perturbations, the fraction of regions undergoing collapse at any epoch is determined by the root-mean-square amplitude ϵ of the fluctuations entering the horizon at that epoch and the equation of state $p = \gamma\rho$ ($0 < \gamma < 1$). One usually expects a radiation equation of state ($\gamma = 1/3$) in the early universe but it may have deviated from this in some periods. As we will see, this in turn places constraints on inflationary scenarios, since all of these generate density fluctuations whose spectrum is determined by the form of the inflaton potential.

3.1 Simplistic Analysis

Early calculations assumed that the overdense region which evolves to a PBH is spherically symmetric and part of a closed Friedmann model. In order to collapse against the pressure, such a region must be larger than the Jeans length at maximum expansion and this is just $\sqrt{\gamma}$ times the horizon size. On the other hand, it cannot be larger than the horizon size, else it would form a separate closed universe and not be part of our Universe [34].

This has two important implications. First, PBHs forming at time t after the Big Bang should have of order the horizon mass, given by eqn (1). Second, for a region destined to collapse to a PBH, one requires the fractional overdensity at the horizon epoch δ to exceed γ. Providing the density fluctuations have a Gaussian distribution and are spherically symmetric, one can infer that the fraction of regions of mass M which collapse is [30]

$$\beta(M) \sim \epsilon(M) \exp\left[-\frac{\gamma^2}{2\epsilon(M)^2}\right] \tag{4}$$

where $\epsilon(M)$ is the value of ϵ when the horizon mass is M. The PBHs can have an extended mass spectrum only if the fluctuations are scale-invariant (i.e. with ϵ independent of M). In this case, the PBH mass distribution is given by [30]

$$dn/dM = (\alpha - 2)(M/M_*)^{-\alpha} M_*^{-2} \Omega_{\rm PBH} \rho_{\rm crit} \tag{5}$$

where $M_* \approx 10^{15}$g is the current lower cut-off in the mass spectrum due to evaporations, Ω_{PBH} is the total density of the PBHs in units of the critical density (which depends on β) and the exponent α is determined by the equation of state:

$$\alpha = \left(\frac{1+3\gamma}{1+\gamma}\right) + 1. \tag{6}$$

$\alpha = 5/2$ if one has a radiation equation of state. This means that the density of PBHs larger than M falls off as $M^{-1/2}$, so most of the PBH density is contained in the smallest ones with mass M_*.

Many scenarios for the cosmological density fluctuations predict that ϵ is at least approximately scale-invariant but the sensitive dependence of β on ϵ means that even tiny deviations from scale-invariance can be important. If $\epsilon(M)$ decreases with increasing M, then the spectrum falls off exponentially and most of the PBH density is contained in the smallest ones. If $\epsilon(M)$ increases with increasing M, the spectrum rises exponentially and - if PBHs were to form at all - they could only do so at large scales. However, the microwave background anisotropies would then be larger than observed, so this is unlikely. It is also possible to enhance PBH formation at particular mass-scales by introducing bumps in $\epsilon(M)$.

The current density parameter $\Omega_{\rm PBH}$ associated with PBHs which form at a redshift z or time t is related to β by [30]

$$\Omega_{\rm PBH} = \beta \Omega_R (1+z) \approx 10^6 \beta \left(\frac{t}{s}\right)^{-1/2} \approx 10^{18} \beta \left(\frac{M}{10^{15} g}\right)^{-1/2} \tag{7}$$

where $\Omega_R \approx 10^{-4}$ is the density parameter of the microwave background and we have used eqn (1). The $(1+z)$ factor arises because the radiation density scales as $(1+z)^4$, whereas the PBH density scales as $(1+z)^3$. Any limit on $\Omega_{\rm PBH}$ therefore places a constraint on $\beta(M)$ and the constraints are summarized in Fig. 1, which is taken from Carr et al. [41]. The constraint for non-evaporating mass ranges above 10^{15}g comes from requiring $\Omega_{\rm PBH} < 1$ but stronger constraints are associated with PBHs smaller than this since they would have evaporated by now. The strongest one is the γ-ray limit associated with the 10^{15}g PBHs evaporating at the present epoch [162]. Other ones are associated with the generation of entropy and modifications to the cosmological production of light elements [160]. The constraints below 10^6g are based on the (uncertain) assumption that evaporating PBHs leave stable Planck mass relics, an issue which is discussed in detail in Section 4.2. Note that the cosmological nucleosynthesis constraints have recently been updated by Carr et al. [42], although their results are not shown in Fig. 1.

The constraints on $\beta(M)$ can be converted into constraints on $\epsilon(M)$ using eqn (4) and these are shown in Fig. 2. Also shown here are the (non-PBH) constraints associated with the spectral distortions in the cosmic microwave background induced by the dissipation of intermediate scale density perturbations and the COBE quadrupole measurement. This shows that one needs the fluctuation amplitude to decrease with increasing scale in order to produce PBHs and the lines corresponding to various slopes in the $\epsilon(M)$ relationship are also shown in Fig. 2

3.2 Refinements of Simplistic Analysis

The simple criterion for PBH formation given above needs to be tested with detailed numerical calculations. The first hydrodynamical studies of PBH formation were carried out by Nadezhin et al. [156]. These roughly confirmed the criterion $\delta > \gamma$ for PBH formation, although the PBHs could be be somewhat smaller than the horizon. In recent years several groups have carried out more detailed hydrodynamical calculations and these have refined the $\delta > \gamma$ criterion, suggesting that one needs $\delta > 0.7$ rather than $\delta > 0.3$ [159, 177]. This in turn affects the estimate for $\beta(M)$ given by eqn (4).

A particularly interesting development has been the application of "critical phenomena" to PBH formation. Studies of the collapse of various types of spherically symmetric matter fields have shown that there is always a critical solution which separates those configurations which form a black hole from those

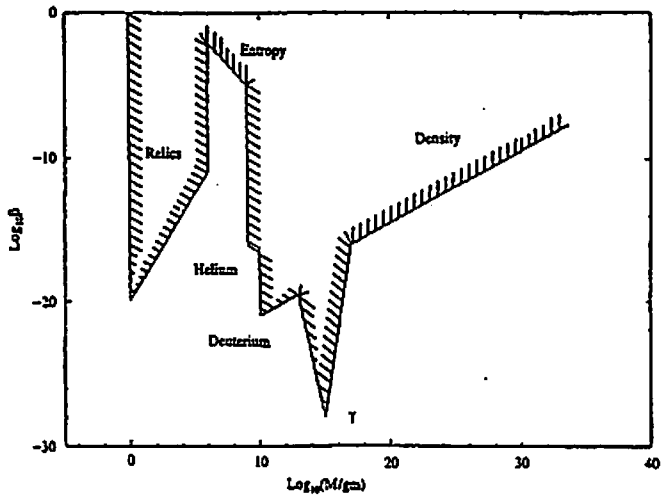

Figure 1: Constraints on $\beta(M)$

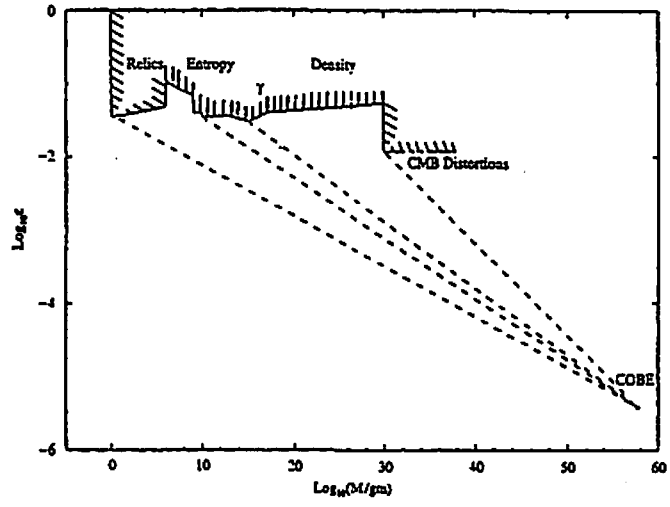

Figure 2: Constraints on $\epsilon(M)$

which disperse to an asymptotically flat state. The configurations are described by some index p and, as the critical index p_c is approached, the black hole mass is found to scale as $(p - p_c)^\eta$ for some exponent η. This effect was first discovered for scalar fields [48] but subsequently demonstrated for radiation [65] and then more general fluids with equation of state $p = \gamma\rho$ [124, 149].

In all these studies the spacetime was assumed to be asymptotically flat. However, Niemeyer & Jedamzik [158] have applied the same idea to study black hole formation in asymptotically Friedmann models and have found similar results. For a variety of initial density perturbation profiles, they find that the relationship between the PBH mass and the the horizon-scale density perturbation has the form

$$M = KM_H(\delta - \delta_c)^\eta \tag{8}$$

where M_H is the horizon mass and the constants are in the range $0.34 < \eta < 0.37$, $2.4 < K < 11.9$ and $0.67 < \delta_c < 0.71$ for the various configurations. More recently, Musco et al. [155] have found that the critical overdensity lies in the lower range $0.43 < \delta_c < 0.47$ if one only allows growing modes at decoupling (which is more plausible if the fluctuations derive from inflation). They also find that the exponent η is modified if there is a cosmological constant. Since $M \to 0$ as $\delta \to \delta_c$, the existence of critical phenomena suggests that PBHs may be much smaller than the particle horizon at formation and this also modifies the mass spectrum [77, 80, 120, 189]. Although Hawke & Stewart [101] claim that the formation of shocks prevents black holes forming on scales below 10^{-4} of the horizon mass, this has been disputed [155].

It should be stressed that the description of fluctuations beyond the horizon is somewhat problematic and it is clearer to use a gauge-invariant description which involves the total energy or metric perturbation [177]. Also the derivation of the mass spectrum given by eqn (5) is based on Press-Schechter theory and it is more satisfactory to use peaks theory. Both these points have been considered by Green et al. [83]. They find that that the critical value for the density contrast is around 0.3, which is close to the value originally advocated 30 years ago!

Another refinement of the simplistic analysis which underlies eqn (4) concerns the assumption that the fluctuations have a Gaussian distribution. Bullock & Primack [28] and Ivanov [105] have pointed out that this may not apply if the fluctuations derive from an inflationary period (discussed in Section 3.3). So long as the fluctuations are small ($\delta\phi/\phi \ll 1$), as certainly applies on a galactic scale, this assumption is valid. However, for PBH formation one requires $\delta\phi/\phi \sim 1$, and, in this case, the coupling of different Fourier modes destroys the Gaussianity. Their analysis suggests that $\beta(M)$ can be very different from the value indicated by eqn (4) but it still depends very sensitively on ϵ. A more detailed analysis of this problem has been carried out by Avelino [8] and Hidalgo & Seery [101].

3.3 PBHs and Inflation

Inflation has two important consequences for PBHs. On the one hand, any PBHs formed before the end of inflation will be diluted to a negligible density. Inflation thus imposes a lower limit on the PBH mass spectrum:

$$M > M_{\rm min} = M_P(T_{RH}/T_{Pl})^{-2} \tag{9}$$

where T_{RH} is the reheat temperature and $T_P \approx 10^{19}$ GeV is the Planck temperature. The CMB quadrupole measurement implies $T_{RH} \approx 10^{16}$GeV, so $M_{\rm min}$ certainly exceeds 1 g. On the other hand, inflation will itself generate fluctuations and these may suffice to produce PBHs after reheating. If the inflaton potential is $V(\phi)$, then the horizon-scale fluctuations for a mass-scale M are

$$\epsilon(M) \approx \left(\frac{V^{3/2}}{M_P^3 V'}\right)_H \tag{10}$$

where a prime denotes $d/d\phi$ and the right-hand side is evaluated for the value of ϕ when the mass-scale M falls within the horizon. In the standard chaotic inflationary scenario, one makes the "slow-roll" and "friction-dominated" assumptions:

$$\xi \equiv (M_P V'/V)^2 \ll 1, \quad \eta \equiv M_P^2 V''/V \ll 1. \tag{11}$$

Usually the exponent n characterizing the power spectrum of the fluctuations, $|\delta_k|^2 \approx k^n$, is very close to but slightly below 1:

$$n = 1 + 4\xi - 2\eta \approx 1. \tag{12}$$

Since ϵ scales as $M^{(1-n)/4}$, this means that the fluctuations are slightly increasing with scale. The normalization required to explain galaxy formation ($\epsilon \approx 10^{-5}$) would then preclude the formation of PBHs on a smaller scale. If PBH formation is to occur, one needs the fluctuations to decrease with increasing mass ($n > 1$) and, from eqn (12), this is only possible if the scalar field is accelerating sufficiently fast that [37]

$$V''/V > (1/2)(V'/V)^2. \tag{13}$$

This condition is certainly satisfied in some scenarios [74] and, if it is, eqn (4) implies that the PBH density will be dominated by the ones forming immediately after reheating. This is because the volume dilution of the PBHs forming shortly before the end of inflation will dominate the enhancement associated with eqn (4). However, it should be stressed that the validity of eqn (10) at the very end of inflation is questionable since the usual assumptions may fail then [125, 137].

Since each value of n corresponds to a straight line in Fig. 3, any particular value for the reheat time t_1 corresponds to an upper limit on n. This limit is indicated in Fig. 3, which is taken from [41], apart from a correction pointed out by Green & Liddle [79]. Similar constraints have been obtained by several other people [24, 119]. The figure also shows how the constraint on n is strengthened if the reheating at the end of inflation is sufficiently slow for there to be a dust-like phase [41, 81]. However, it should be stressed that not all inflationary scenarios predict that the spectral index should be constant. Indeed, Hodges & Blumenthal [102] have pointed out that one can get any spectrum for the fluctuations by suitably choosing the form of $V(\phi)$. For example, eqn (10) suggests that one can get a spike in the spectrum by flattening the potential over some mass range (since the fluctuation diverges when V' goes to 0). This idea was exploited by Ivanov et al. [106], who fine-tuned the position of the spike so that it corresponds to the mass-scale associated with microlensing events observed in the Large Magellanic Cloud [4].

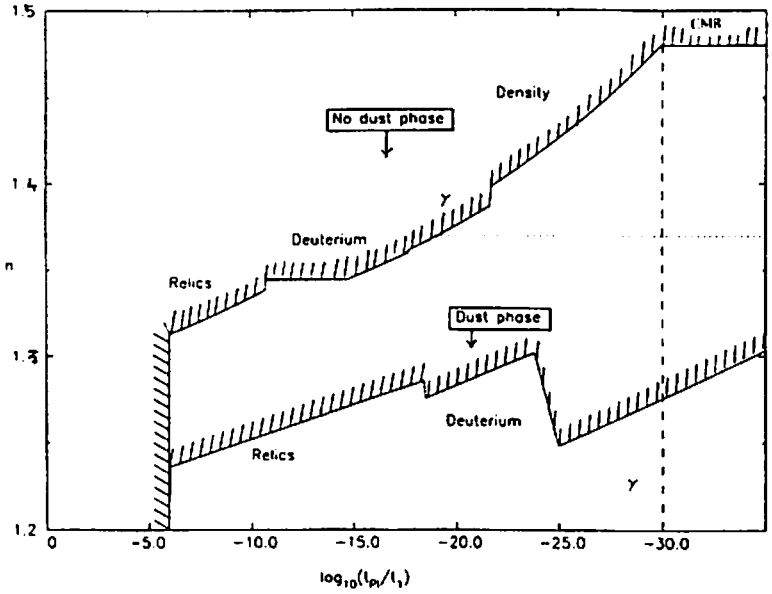

Figure 3: Constraints on spectral index n in terms of reheat time t_1

Even if PBHs never actually formed as a result of inflation, studying them places important constraints on the many types of inflationary scenarios. Besides the chaotic scenario discussed above, there are also the variants of inflation described as designer [102, 106, 190], supernatural [166], supersymmetric [76], hybrid [70, 112], multiple [188], oscillating [183], ghost [154], running mass [132] and saddle [64]. There are also scenarios in which the inflaton serves as dark matter [134]. PBH formation has been studied in all of these models. Note that in the standard scenario inflation ends by the decay of the inflaton into

radiation. However, in the preheating scenario inflation ends more rapidly because of resonant coupling between the inflaton and another scalar field. This generates extra fluctuations, which are not of the form indicated by eqn (10) and these might also produce PBHs [18, 63, 68, 82]. However, a recent analysis by Suyama et al. [182], incorporating a full non-linear lattice simulation for various models, suggests that PBH formation is insignificant. There have also been a variety of other proposals for generating perturbations at the end of inflation [21, 126, 136, 171] and the probability of PBH formation would then again be unrelated to eqn (10).

4 PBHs as a Probe of Dark Matter

Roughly 30% of the total density of the Universe is now thought to be in the form of "cold dark matter". Recently there has been a lot of interest in whether PBHs could provide this, since those larger than 10^{15}g would not have evaporated yet and would certainly be massive enough to be dynamically "cold". It is also possible that the Planck relics of evaporated PBHs could provide the dark matter.

4.1 Constraints on PBHs in the Galactic Halo

There are some mass ranges in which PBHs are already excluded from providing dark matter in galactic halos. For example, femtolensing of gamma-ray bursts by PBHs precludes those in the mass range $10^{17} - 10^{20}$g from having a critical density and microlensing of stars in the Large Magellanic Cloud, while allowing a tenth-critical-density at around a solar mass, excludes $10^{26} - 10^{34}$g PBHs [4]. However, there are no constraints in the intermediate (sublunar) mass range $10^{20} - 10^{26}$g [24]. Note that LISA might detect the gravitational impulse induced by any nearby passing PBH [1, 176]. However, this method would not be feasible below 10^{14}g (because the effect would be hidden by the Moon) or above 10^{20}g (because the encounters would be too rare).

One possibility is that PBHs with a mass of around $1M_\odot$ could have formed at the quark-hadron phase transition at 10^{-5}s because of a temporary softening of the equation of state then. If the QCD phase transition is assumed to be 1st order, then hydrodynamical calculations show that the value of δ required for PBH formation is reduced below the value which pertains in the radiation era [110]. This means that PBH formation will be strongly enhanced at the QCD epoch, with the mass distribution peaking at around the horizon mass then [109, 163, 187]. Such PBHs might be able to explain the MACHO microlensing results [4] and also the claimed microlensing of quasars [92]. Another possibility is that PBHs with a mass of around $10^{-7}M_\odot$ could form in TeV quantum gravity scenarios [103].

One of the interesting implications of these scenarios is the possible existence of a halo population of *binary* black holes [157]. With a full halo of such objects, there could be a huge number of binaries inside 50 kpc and some of these could be coalescing due to gravitational radiation losses at the present epoch [25]. If the associated gravitational waves were detected, it would provide a unique probe of the halo distribution [104]. Gravity waves from binary PBHs would be detectable down to $10^{-5}M_\odot$ using VIRGO, $10^{-7}M_\odot$ using EURO and $10^{-11}M_\odot$ using LISA [103].

4.2 Planck-Mass Relics

Some people have speculated that black hole evaporation could cease once the hole gets close to the Planck mass [26, 54, 146]. For example, in the standard Kaluza-Klein picture, extra dimensions are assumed to be compactified on the scale of the Planck length. This means that the influence of these extra dimensions becomes important at the energy scale of 10^{19}GeV. Such effects could conceivably result in evaporation ceasing at the Planck mass. Various non-quantum-gravitational effects (such as higher order corrections to the gravitational Lagrangian or string effects) could also lead to stable relics [41] but the relic mass is usually close to the Planck scale.

Another possibility, as argued by Chen & Adler [46], is that stable relics could arise if one invokes a "generalized uncertainty principle". This replaces the usual uncertainty principle with one of the form

$$\Delta x > \frac{\hbar}{\Delta p} + l_P^2 \frac{\Delta p}{\hbar}. \tag{14}$$

where the second term is supposed to account for self-gravity effects. This means that the black hole temperature becomes

$$T_{BH} = \frac{Mc^2}{4\pi k}\left(1 - \sqrt{1 - \frac{M_P^2}{M^2}}\right). \tag{15}$$

This reduces to the standard Hawking form for $M \gg M_P$ but it remains finite instead of diverging at the Planck mass itself. Cavaglia and colleagues have extended this argument to higher-dimensional black holes [43] and also included the effects of thermal fluctuations [44].

Whatever the cause of their stability, Planck mass relics would provide a possible cold dark matter candidate [138]. Indeed this leads to the "relics" constraints indicated in Fig.1, Fig.2 and Fig.3. In particular, such relics could derive from inflationary PBHs [17, 24]. If the relics have a mass κM_P, then the requirement that they have less than the critical density implies [41]

$$\beta(M) < 10^{-27}\kappa^{-1}(M/M_P)^{3/2} \tag{16}$$

for the mass range

$$(T_{RH}/T_P)^{-2}M_{Pl} < M < 10^{11}\kappa^{2/5}M_P. \tag{17}$$

The upper mass limit arises because PBHs larger than this dominate the total density before they evaporate. Producing a critical density of relics obviously requires fine-tuning of the index n. Also one needs $n \approx 1.3$, which is barely compatible with the WMAP results [6, 14]. Nevertheless, this is possible in principle. In particular, it has been argued that hybrid inflation could produce relics from 10^5g PBHs formed at 10^{-32}s [45, 184].

4.3 Large-Scale Structure and Supermassive Black Holes

PBHs might also play a role in the formation of large-scale structure [61, 111, 118, 169]. For example, it has been realized for some time that Poisson fluctuations in the number density of PBHs can generate appreciable density perturbations on large scales if the PBHs are big enough [33, 35, 47, 69, 151]. This idea has recently been invoked to explain voids and Lyman-alpha clouds [2]. In such scenarios, it is important to know how much a PBH can grow through accretion and it has been argued that this could be significant even in the period after matter-radiation equality [144].

Several people have suggested that the $10^6 - 10^8 M_\odot$ supermassive black holes thought to reside in galactic nuclei [128] could be of primordial origin. For example, a 1st order phase transition could produce clusters of PBHs, around which a single supermassive black hole might then condense [60]. Alternatively, it has been proposed that inflation could produce closed domain walls, which then collapse to form $10^8 M_\odot$ PBHs [118, 167]. Another scheme invokes more modest mass PBHs of $10^3 M_\odot$, resulting from a feature in the inflaton potential, which then grow to $10^8 M_\odot$ by accretion [62]. In particular, Bean and Magueijo [19] and Custodio and Horvath [58] have suggested that PBHs may accrete from the quintessence field which is invoked to explain the current acceleration of the Universe. On the basis of a semi-Newtonian analysis, they claim that a PBH with size comparable to the cosmological particle horizon scale could grow at the same rate as the particle horizon.

In view of the importance of this claim, we now consider the argument of Bean and Magueijo in more detail. They consider a scalar field in a potential of the form

$$V(\phi) = V_0 e^{-\sqrt{8\pi}\lambda\phi}. \tag{18}$$

By generalizing the analysis of Jacobson [108], which attaches a Schwarzschild solution to a cosmological background in which the field has the asymptotic value ϕ_c, they claim that the energy flux through the event horizon is $\dot{\phi_c}^2$, leading to a black hole accretion rate

$$\frac{dM}{dt} = 16\pi M^2 \dot{\phi_c}^2. \tag{19}$$

They correctly infer that only the kinetic energy of the scalar field is accreted, the scalar potential merely influencing the evolution of the asymptotic background field:

$$\phi_c = \frac{2}{\lambda\sqrt{8\pi}} \log\left(\frac{t}{t_0}\right), \tag{20}$$

where t_0 is a constant of integration. The accretion rate therefore becomes

$$\frac{dM}{dt} = \frac{KM^2}{t^2}, \tag{21}$$

with $K = 8/\lambda^2$, which can be integrated to give

$$M = \frac{M_0}{1 - \frac{KM_0}{t_0}\left(1 - \frac{t_0}{t}\right)} . \tag{22}$$

For $M_0 \ll K^{-1}t_0$, corresponding to an initial black hole mass much less than that of the particle horizon, this implies negligible accretion. However, for $M_0 = K^{-1}t_0$, Eq. (22) predicts a self-similar solution, $M \propto t$, in which the black hole always has the same size relative to the particle horizon. This is the result which Bean and Maguiejo exploit. For $M_0 \gg K^{-1}t_0$, the mass diverges very rapidly.

Eqn (22) suggests that PBHs may accrete surrounding mass very effectively if their initial size is fine-tuned. However, this analysis is questionable since it is semi-Newtonian and neglects the cosmological expansion. Indeed, it is exactly equivalent to an argument presented by Zeldovich and Novikov [193] nearly 30 years ago, which suggested that PBHs could grow self-similarly even in a universe with a radiation equation of state ($p = \epsilon/3$). However, a study of spherically symmetric self-similar PBH solutions in radiation universe [34] demonstrated analytically that there is no self-similar solution which contains a black hole attached to an exact Friedmann background via a sonic point (i.e. in which the black hole forms by purely causal processes). The Newtonian analysis is therefore definitely misleading in this case. There are self-similar solutions which are *asymptotically* Friedmann at large distances from the black hole. However, these correspond to special acausal initial conditions, in which matter is effectively thrown into the black hole at every distance. Similar results were subsequently proved for all perfect fluid systems with equation of state of the form $p = k\epsilon$ with $0 < k < 1$ [22, 31, 36]. Indeed it was shown that the only physical self-similar solution which can be attached to an external Friedmann solution via a sonic point is Friedmann itself; the other solutions either enter a negative mass regime or encounter another sonic point where the pressure gradient diverges.

The stiff fluid case ($k = 1$) is more complicated and requires special consideration. It was originally claimed by Lin et al. [135] that there *could* exist a self-similar solution in this case but a subsequent analysis [23] showed that their argument was flawed. Lin et al. failed to appreciate that the surface which they interpreted as the event horizon is timelike rather than null, with the density going to zero there. The only way of having a black hole would be if the fluid turned into null dust at this timelike surface but this seems unphysical. It therefore appears that there is no self-similar solution containing a black hole in an exact Friedmann background for any value of k in the range [0,1].

In view of the prevalence of scalar fields in the early Universe, it is clearly important to know whether the non-existence of a self-similar solution extends to the scalar field case. One might expect this from the stiff fluid analysis, since a scalar field is equivalent to a stiff fluid provided the gradient is everywhere timelike [145]. This is supported by recent numerical studies of the growth of PBHs in a scalar field system, which - for a variety of initial conditions - give no evidence for self-similar growth [86, 87]. However, it is very difficult to determine through numerical simulations whether self-similar growth is impossible for any specific initial data. Also Bean and Magueijo caution that the Carr-Hawking proof only applies for a perfect fluid and may not be relevant if the scalar field case has a potential. One therefore needs an *analytic* proof that there is no self-similar PBH solution if the cosmological expansion is taken into account. Such a proof has now been provided by Harada et al. [90], even for the case with a potential. We conclude that PBH accretion of quintessence is not as important as Bean and Magueijo claim.

5 PBHs as a Probe of Higher Dimensions

In "brane" versions of Kaluza-Klein theory, some of the extra dimensions can be much larger than the usual Planck length and this means that quantum gravity effects may become important at a much smaller energy scale than usual. If the internal space has n dimensions and a compact volume V_n, then

Newton's constant G_N is related to the higher dimensional gravitational constant G_D and the value of the modified Planck mass M_P is related to the usual 4-dimensional Planck mass M_4 by the order-of-magnitude equations:

$$G_N \sim G_D/V_n. \quad M_P^{n+2} \sim M_4^2/V_n. \tag{23}$$

The same relationship applies if one has an infinite extra dimension but with a "warped" geometry, provided one interprets V_n as the "warped volume". In the standard model, $V_n \sim 1/M_4^n$ and so $M_P \sim M_4$. However, with large extra dimensions, one has $V_n \gg 1/M_4^n$ and so $M_P \ll M_4$.

5.1 Black Hole Production at Accelerators

One exciting implication of these scenarios is that quantum gravitational effects may arise at the experimentally observable TeV scale. If so, this would have profound implications for black hole formation and evaporation since black holes could be generated in accelerator experiments, such as the Large Hadron Collider (LHC) [11, 59, 73, 113, 170, 192]. This is illustrated in Fig. 4, which is taken from ref. [40] and shows how the relationship between the mass and radius of a black hole is modified if the dimensionality changes [2].

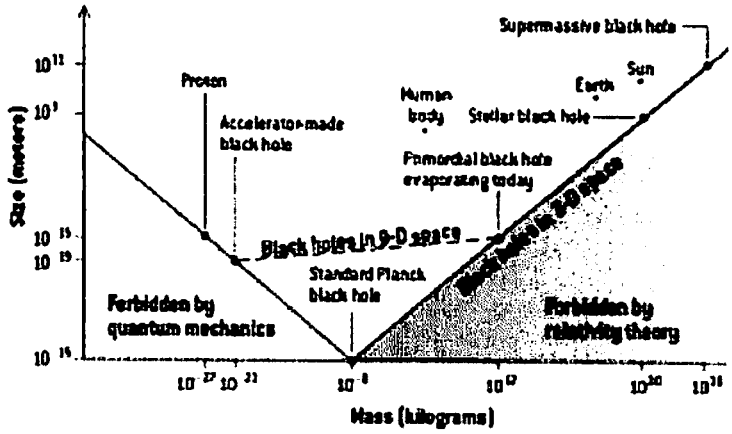

Figure 4: Higher dimensional black holes

Two partons with centre-of-mass energy $\sqrt{s}$ will form a black hole if they come within a distance corresponding to the Schwarzschild radius r_S for a black hole whose mass M_{BH} is equivalent to that energy [73]. Thus the cross-section for black hole production is

$$\sigma_{BH} \approx \pi r_S^2 \Theta(\sqrt{s} - M_{BH}^{min}) \tag{24}$$

where M_{BH}^{min} is the mass below which the semi-classical approximation fails. Here the Schwarzschild radius itself depends upon the number of internal dimensions:

$$r_S \approx \frac{1}{M_P}\left(\frac{M_{BH}}{M_P}\right)^{1/(1+n)}, \tag{25}$$

so that $\sigma_{BH} \propto s^{2/(n+1)}$. This means that the cross-section for black hole production in scattering experiments goes well above the cross-section for the standard model above a certain energy scale and in a way which depends on the number of extra dimensions.

[2] I am very indebted to the conference organizer, Tetsuya Shiromizu, for translating this article into Japanese. This is because I am married to a Japanese lady and, when I presented a copy of the translated paper to her parents, they were very impressed that I could write Japanese so well. Thanks to Tetsuya, they now regard me as a worthy son-in-law!

The evaporation of the black holes produced in this way will produce a characteristic signature [59, 73, 170] because the temperature and lifetime of the black holes depend on the number of internal dimensions:

$$T_{BH} \sim \frac{n+1}{r_S}, \quad \tau_{BH} \sim \frac{1}{M_P}\left(\frac{M_{BH}}{M_P}\right)^{(n+3)/(n+1)}. \tag{26}$$

Thus the temperature is decreased relative to the standard 4-dimensional case and the lifetime is increased. The important qualitative effect is that a large fraction of the beam energy is converted into transverse energy, leading to large-multiplicity events with many more hard jets and leptons than would otherwise be expected. In principle, the formation and evaporation of black holes might be observed by the LHC when it turns on in 2007 and this might also allow one to experimentally probe the number of extra dimensions. On the other hand, this would also mean that scattering processes above the Planck scale could not be probed directly because they would be hidden behind a black hole event horizon [72].

Similar effects could be evident in the interaction between high energy cosmic rays and atmospheric nucleons. Nearly horizontal cosmic ray neutrinos would lead to the production of black holes, whose decays could generate deeply penetrating showers with an electromagnetic component substantially larger than that expected with conventional neutrino interactions. Several authors have studied this in the context of the Pierre Auger experiment, with event rates in excess of one per year being predicted [7, 66, 170]. Indeed there is a small window of opportunity in which Auger might detect such events before the LHC. On the other hand, it must cautioned that these estimates may be overly optimistic. Others have claimed that black hole production in accelerators may be unobservable even if TeV quantum gravity is correct [3].

5.2 PBHs and Brane Cosmology

Although the black holes produced in accelerators should not themselves be described as "primordial", since they do not form in the early Universe, it is clear that these experiments will also have profound implications for PBHs themselves. This is because, at sufficiently early times, the effects of the extra dimensions will be cosmologically important. Indeed Fig. 4 illustrates that one could effectively retrace the changing dimensionality of the early universe by changing the energy of the accelerator.

Brane cosmology modifies the standard PBH formation and evaporation scenario in a number of ways. In particular, in Randall-Sundrum type II scenarios (which have one extra dimension) a ρ^2 term appears in the Friedmann equation and this dominates the usual ρ term for

$$T > 10^{18}(l/l_P)^{-1/4}\mathrm{GeV} \tag{27}$$

where l is the scale of the extra dimension. This exceeds 1 TeV for $l < 0.2$ mm. Black holes which are smaller than l are effectively 5-dimensional. This means that they are cooler and evaporate more slowly than in the standard scenario:

$$T_{BH} \propto M^{-1/2}, \quad \tau \propto M^2. \tag{28}$$

This corresponds to eqn (26) with $n = 1$. The critical mass for PBHs evaporating at the present epoch is now in the range 3×10^9g to 4×10^{14}g. This modifies the standard PBH evaporation constraints [49, 84] and, if some cosmic rays come from PBHs, it means that these could probe the extra dimensions [174, 175]. Another complication is that accretion could dominate evaporation during the era when the ρ^2 term dominates the ρ term in the Friedmann equation [150].

6 Cosmic Rays from PBHs

A black hole of mass M will emit particles like a black-body of temperature [95]

$$T \approx 10^{26}\left(\frac{M}{g}\right)^{-1}\mathrm{K} \approx \left(\frac{M}{10^{13}g}\right)^{-1}\mathrm{GeV}. \tag{29}$$

This assumes that the hole has no charge or angular momentum. This is a reasonable assumption since charge and angular momentum will also be lost through quantum emission but on a shorter timescale

than the mass [161]. This means that it loses mass at a rate

$$\dot{M} = -5 \times 10^{25}(M/g)^{-2} f(M) \text{ g s}^{-1} \tag{30}$$

where the factor $f(M)$ depends on the number of particle species which are light enough to be emitted by a hole of mass M, so the lifetime is

$$\tau(M) = 6 \times 10^{-27} f(M)^{-1}(M/g)^3 \text{ s}. \tag{31}$$

The factor f is normalized to be 1 for holes larger than 10^{17} g and such holes are only able to emit "massless" particles like photons, neutrinos and gravitons. Holes in the mass range 10^{15} g $< M < 10^{17}$ g are also able to emit electrons, while those in the range 10^{14} g $< M < 10^{15}$ g emit muons which subsequently decay into electrons and neutrinos. The latter range includes, in particular, the critical mass for which τ equals the age of the Universe.

Once M falls below 10^{14}g, a black hole can also begin to emit hadrons. However, hadrons are composite particles made up of quarks held together by gluons. For temperatures exceeding the QCD confinement scale of $\Lambda_{QCD} = 250 - 300$ GeV, one would therefore expect these fundamental particles to be emitted rather than composite particles. Only pions would be light enough to be emitted below Λ_{QCD}. Since there are 12 quark degrees of freedom per flavour and 16 gluon degrees of freedom, one would also expect the emission rate (i.e. the value of f) to increase dramatically once the QCD temperature is reached. One can regard the black hole as emitting quark and gluon jets of the kind produced in collider events [139]. The jets will decay into hadrons over a distance which is always much larger than the size of the hole, so gravitational effects can be neglected. The hadrons may then decay into astrophysically stable particles through weak and electomagnetic decays.

To find the final spectra of stable particles emitted from a black hole, one must convolve the Hawking emission spectrum with the jet fragmentation function. In order to determine the present day background spectrum of particles generated by PBH evaporations, one must first integrate over the lifetime of each hole of mass M and then over the PBH mass spectrum [141]. In doing so, one must allow for the fact that smaller holes will evaporate at an earlier cosmological epoch, so the particles they generate will be redshifted in energy by the present epoch.

6.1 Gamma-Rays and Antiprotons from Evaporating PBHs

All the spectra have rather similar shapes: an E^{-3} fall-off for $E > 100$ MeV due to the final phases of evaporation at the present epoch and an E^{-1} tail for $E < 100$ MeV due to the fragmentation of jets produced at the present and earlier epochs. Note that the E^{-1} tail generally masks any effect associated with the mass spectrum of smaller PBHs which evaporated at earlier epochs [32]. The situation is more complicated if the PBHs evaporating at the present epoch are clustered inside our own Galactic halo (as is most likely). In this case, any charged particles emitted after the epoch of galaxy formation (i.e. from PBHs only somewhat smaller than M_*) will have their flux enhanced relative to the photon spectra by a factor ξ which depends upon the halo concentration factor and the time for which particles are trapped inside the halo by the Galactic magnetic field. This time is rather uncertain and also energy-dependent. At 100 MeV one has $\xi \sim 10^3$ for electrons or positrons and $\xi \sim 10^4$ for protons and antiprotons. MacGibbon & Carr [140] first used the observed cosmic ray spectra to constrain Ω_{PBH} but their estimates have been subsequently refined.

EGRET observations [179] of the γ-ray background between 30 MeV and 120 GeV leads to an upper limit $\Omega_{PBH} \leq (5.1 \pm 1.3) \times 10^{-9} h^{-2}$, where h is the Hubble parameter in units of 100 [38]. This is a refinement of the original Page-Hawking limit, but the form of the spectrum suggests that PBHs do not provide the dominant contribution. If PBHs are clustered inside our own Galactic halo, then there should also be a Galactic γ-ray background and, since this would be anisotropic, it should be separable from the extragalactic background. The ratio of the anisotropic to isotropic intensity depends on the Galactic longtitude and latitude, the Galactic core radius and the halo flattening. Wright claims that such a halo background has been detected [186]. His detailed fit to the EGRET data, subtracting various other known components, requires the PBH clustering factor to be $(2 - 12) \times 10^5 h^{-1}$, comparable to that expected.

Since the ratio of antiprotons to protons in cosmic rays is less than 10^{-4} over the energy range 100 MeV – 10 GeV, whereas PBHs should produce them in equal numbers, PBHs could only contribute appreciably to the antiprotons [185]. It is usually assumed that the observed antiproton cosmic rays are secondary particles, produced by spallation of the interstellar medium by primary cosmic rays. However, the spectrum of secondary antiprotons should show a steep cut-off at kinetic energies below 2 GeV, whereas the spectrum of PBH antiprotons should increase with decreasing energy down to 0.2 GeV. Also the antiproton fraction should tend to 0.5 at low energies, so these features provide a distinctive signature [120]. MacGibbon & Carr originally calculated the PBH density required to explain the interstellar antiproton flux at 1 GeV and found a value somewhat larger than the γ-ray limit [140]. More recent data on the antiproton flux below 0.5 GeV come from the BESS balloon experiment [191] and Maki et al. [148] and Barrau et al. [12] have tried to fit this in the PBH scenario. Evaporating PBHs might also be detected by their antideuteron flux [13].

6.2 PBH Explosions

One of the most striking observational consequences of PBH evaporations would be their final explosive phase. However, in the standard particle physics picture, where the number of elementary particle species never exceeds around 100, the likelihood of detecting such explosions is very low. Indeed, in this case, observations only place an upper limit on the explosion rate of $5 \times 10^8 \mathrm{pc}^{-3}\mathrm{y}^{-1}$ [5, 173]. This compares to Wright's γ-ray halo limit of 0.3 $\mathrm{pc}^{-3}\mathrm{y}^{-1}$ [186] and the Maki et al. antiproton limit of 0.02 $\mathrm{pc}^{-3}\mathrm{y}^{-1}$ [148].

However, the physics at the QCD phase transition is still uncertain and the prospects of detecting explosions would be improved in less conventional particle physics models. For example, in a Hagedorn-type picture, where the number of particle species exponentiates at the the quark-hadron temperature, the upper limit is reduced to 0.05 $\mathrm{pc}^{-3}\mathrm{y}^{-1}$ [67]. Cline and colleagues have argued that one might expect the formation of a QCD fireball at this temperature [50, 51] and this might even explain some of the short period γ-ray bursts observed by BATSE. They claim to have found 42 candidates of this kind and the fact that their distribution matches the spiral arms suggests that they are Galactic [52]. Although this proposal is speculative and has been disputed [78], it has the attraction of making testable predictions (eg. the hardness ratio of the burst should increase as the duration decreases). A rather different way of producing a γ-ray burst is to assume that the outgoing charged particles form a plasma due to turbulent magnetic field effects at sufficiently high temperatures [20].

Some people have emphasized the possibility of detecting very high energy cosmic rays from PBHs using air shower techniques [55, 85, 130]. However, this is refuted by the claim of Heckler [99] that QED interactions could produce an optically thick photosphere once the black hole temperature exceeds $T_{crit} = 45$ GeV. In this case, the mean photon energy is reduced to $m_e(T_{BH}/T_{crit})^{1/2}$, which is well below T_{BH}, so the number of high energy photons is much reduced. He has proposed that a similar effect may operate at even lower temperatures due to QCD effects [100]. Several groups have examined the implications of this proposal for PBH emission [53, 114]. However, these arguments should not be regarded as definitive since MacGibbon et al. claim that QED and QCD interactions are never important [143].

7 Conclusions

We have seen that PBHs could be used to study the early Universe, gravitational collapse, high energy physics and quantum gravity. In the "early Universe" context, useful constraints can be placed on inflationary scenarios. In the "gravitational collapse" context, the existence of PBHs could provide a test of critical phenomena and contribute to the dark matter. In the "high energy physics" context, information may come from cosmic ray and even gamma-ray bursts if suitable physics is invoked at the QCD phase transition. In the "quantum gravity" context, the formation and evaporation of small black holes could be observable in cosmic ray events and accelerator experiments if the quantum gravity scale is around a TeV.

References

[1] A.W. Adams and J.S. Bloom (2004), astro-ph/0405266.

[2] N. Afshordi, P. McDonald and D.N. Spergel, Ap.J.Lett. 594 (2003) L71.

[3] E. Ahn, M.Cavaglia and A.V. Olinto. Phys.Rev.D 68 (2003) 043004.

[4] C. Alcock et al., Ap.J. Lett. 550 (2001) L169.

[5] D.E. Alexandreas et al., Phys.Rev.Lett. 71 (1993) 2524.

[6] S.O. Alexeyev, M.V. Sazhin and O.S. Khovanskaya, preprint (2002).

[7] L. Anchordoqui and H. Goldberg, Phys.Rev.D. 65 (2002) 047502.

[8] P.P. Avelino (2005), astro-ph/0510052.

[9] E. Babichev, V. Dokuchaev, Yu. Eroshenko, Phys. Rev. Lett. 93 (2004) 021102.

[10] E. Babichev, V. Dokuchaev, Yu. Eroshenko, J. Exp. Theor. Phys. 100 (2005) 528.

[11] A. Barrau (2003), hep-ph/0311238.

[12] A. Barrau, D. Blais, G. Boudoul and D. Polarski, Phys.Lett.B. 551 (2003) 218.

[13] A.Barrau et al., Astron.Astrophys. 398 (2003) 403.

[14] A. Barrau, D. Blais, G. Boudoul and D. Polarski, Ann.Phys. 13 (2004) 115.

[15] J. D. Barrow, Phys. Rev. D. 46 (1992) R3227.

[16] J. D. Barrow and B. J. Carr, Phys. Rev. D. 54 (1996) 3920.

[17] J.D. Barrow, E.J. Copeland and A.R. Liddle, Phys.Rev.D. 46 (1992) 645.

[18] B.A. Bassett and S. Tsujikawa, Phys.Rev.D. 63 (2001) 123503.

[19] R. Bean and J. Maguiejo, Phys.Rev.D. 66 (2002) 063505.

[20] A.A. Belyanin et al. (1996), MNRAS 283 (1996) 626.

[21] F. Bernardeau, L. Kofman and J.P. Uzan, Phys.Rev.D. 70 (2004) 083004.

[22] G. V. Bicknell and R. N. Henriksen, Ap.J. 225 (1978) 237.

[23] G. V. Bicknell and R. N. Henriksen, Ap.J. 219 (1978) 1043.

[24] D. Blais, C. Kiefer and D. Polarski, Phys.Lett.B. 535 (2002) 11.

[25] J.R. Bond and B.J. Carr, MNRAS 207 (1986) 585.

[26] M.J. Bowick et al., Phys.Rev.Lett. 61 (1988) 2823.

[27] E.V. Bugaev and K.V. Konischev, Phys.Rev.D. 66 (2002) 084004.

[28] J.S. Bullock and J.R. Primack, Phys.Rev.D. 55 (1997) 7423.

[29] R. Caldwell and P. Casper, Phys. Rev.D. 53 (1996) 3002.

[30] B.J. Carr, Ap.J. 201 (1975) 1.

[31] B. J. Carr, Ph.D. thesis, Cambridge University (1976).

[32] B.J. Carr, Ap.J. 206 (1976) 8.

[33] B.J. Carr, Astron.Astr. 56 (1977) 377.

[34] B. J. Carr and S. W. Hawking. MNRAS 168 (1974) 399.

[35] B. J. Carr and J. Silk, Ap.J. 268 (1983) 1.

[36] B.J. Carr and A. Yahil, Astrophys. J. 360 (1990) 330.

[37] B.J. Carr and J.E. Lidsey, Phys.Rev.D., 48 (1993) 543.

[38] B.J. Carr and J.H. MacGibbon, Phys. Rep. 307 (1998) 141.

[39] B.J. Carr and C.A. Goymer, Prog.Theor.Phys. 136 (1999) 321.

[40] B.J. Carr and S. Giddings, Scientific American, May 2005, page 48.

[41] B.J. Carr, J.H. Gilbert and J.E. Lidsey. Phys.Rev.D. 50 (1994) 4853.

[42] B.J. Carr, K. Kohri, Y. Sendouda and J. Yokoyoma, in preparation (2006).

[43] M. Cavaglia and S. Das (2004), astro-ph/0404050.

[44] M. Cavaglia, S. Das and R. Maartens, Class.Quant.Grav. 20 (2003) L205.

[45] P. Chen, astro-ph/0303349; astro-ph/0406514.

[46] P.Chen and R.J. Adler, Nuc.Phys.B. 124 (2003) 103.

[47] J.R. Chisholm (2005), astro-ph/0509141.

[48] M.W. Choptuik, Phys. Rev. Lett. 70 (1993) 9.

[49] D. Clancy, R. Guerdens and A.R. Liddle, Phys.Rev. D. 68 (2003) 023507.

[50] D.B. Cline and W. Hong, Ap.J.Lett. 401 (1992) L57.

[51] D.B.Cline, D.A. Sanders and W. Hong, Ap.J. 486 (1997) 169.

[52] D.B. Cline, C. Matthey and S. Otwinowski, Astropart.Phys. 18 (2003) 531.

[53] J. Cline. M. Mostoslavsky and G. Servant, Phys.Rev.D. 59 (1999) 063009.

[54] S. Coleman, J. Preskill and F. Wilczek, Mod.Phys.Lett.A. 6 (1991) 1631.

[55] D.G. Coyne, C. Sinnis and R. Somerville, in *Proceedings of the Houston Advanced Research Center Conference on Black Holes* (1992).

[56] M. Crawford and D.N. Schramm, Nature 298 (1982) 538.

[57] P.S. Custodio and J.E. Horvath, Class.Quant.Grav. 20 (2003) 827.

[58] P.S. Custodio and J.E. Horvath, Int. J. Mod. Phys. D. 14 (2005) 257.

[59] S. Dimopoulos and G. Landsberg, Phys.Rev.Lett. 87 (2001) 161602.

[60] V.I. Dokuchaev, Yu.N. Eroshenko and S.G. Rubin (2004), astro-ph/0412418.

[61] A.D. Dolgov, P.D. Naselsky and I.D. Novikov (2000), astro-ph/0009407.

[62] N. Duchting, Phys.Rev.D. 70 (2004) 064015.

[63] R. Easther and M. Parry, Phys.Rev.D. 62 (2000) 103503.

[64] R. Easther, J. Khoury and K. Schalm, J.Cos.Astropart.Phys. 6 (2004) 6.

[65] C. R. Evans and J. S. Coleman, Phys. Rev. Lett. 72 (1994) 1782.

[66] J. L. Feng and A. D. Shapere, Phys.Rev.Lett. 88 (2002) 021303.

[67] C.E. Fichtel et al. Ap.J. 1434 (1994) 557.

[68] F. Finelli and S. Khlebnikov, Phys.Lett.B. 504 (2001) 309.

[69] K. Freese, R. Price and D. N. Schramm, Astrophys.J. 275 (1983) 405.

[70] J. Garcia-Bellido, A. Linde and D. Wands, Phys.Rev.D. 54 (1997) 6040.

[71] J. Garriga and M. Sakellariadou, Phys.Rev.D. 48 (1993) 2502.

[72] S. B. Giddings. in *The Future of Theoretical Physics and Cosmology*, ed. G.W. Gibbons et al. (Cambridge 2003), p 278.

[73] S. B. Giddings and S. Thomas, Phys.Rev.D. 65 (2002) 056010.

[74] J. Gilbert, Phys.Rev.D. 52 (1995) 5486.

[75] E. Kolb (2005), private communication.

[76] A.M. Green, Phys. Rev. D. 60 (1999) 063516.

[77] A.M. Green, Ap.J. 537 (2000) 708.

[78] A.M. Green, Phys.Rev.D. 65 (2002) 027301.

[79] A.M. Green and A.R. Liddle, Phys. Rev. D. 56 (1997) 6166.

[80] A.M. Green and A.R. Liddle. Phys. Rev. D. 60 (1999) 063509.

[81] A.M. Green, A.R. Liddle and A. Riotto, Phys. Rev. D. 56 (1997), 7559.

[82] A.M. Green and K.A. Malik, Phys.Rev.D. 64 (2001) 021301.

[83] A.M. Green, A.R. Liddle, K.A. Malik and M. Sasaki, astro-ph/0403181.

[84] R. Guerdens, D. Clancy and A.R. Liddle, Phys.Rev. D. 66 (2002) 04315.

[85] F. Halzen, E. Zas, J. MacGibbon and T.C. Weekes, Nature 298 (1991) 538.

[86] T. Harada and B.J. Carr, Phys.Rev.D. 71 (2005) 10410.

[87] T. Harada and B.J. Carr, Phys. Rev. D. 72 (2005) 044021.

[88] P. R. Brady, Phys. Rev. D**51**, 4168 (1995).

[89] T. Harada, B.J. Carr and C.A. Goymer, Phys.Rev.D 66 (2002) 104023.

[90] T. Harada, H. Maeda and B.J. Carr, in preparation (2006).

[91] I. Hawke and J.M. Stewart, Class.Quant.Grav. 19 (2002) 3687.

[92] M.R.S. Hawkins, Mon.Not.Roy.Astr.Soc. 278 (1996) 787.

[93] S.W. Hawking, MNRAS 152 (1971) 75.

[94] S.W. Hawking, Nature 248 (1974) 30.

[95] S.W. Hawking, Comm.Math.Phys. 43 (1975) 199.

[96] S.W. Hawking, Phys. Lett. B. 231 (1989) 237.

[97] S.W. Hawking, I. Moss and J. Stewart, Phys.Rev.D., 26 (1982) 2681.

[98] P. He and L.Z. Fang, Ap.J.Lett. 568 (2002) L1.

[99] A. Heckler, Phys. Rev.D. 55 (1997) 840.

[100] A. Heckler, Phys. Lett. B. 231 (1997) 3430.

[101] J.C. Hidalgo and D. Seery, in preparation (2006).

[102] H.M. Hodges and G.R. Blumenthal, Phys.Rev.D. 42 (1990) 3329.

[103] K.T. Inoue and T. Tanaka, Phys.Rev.Lett. 91 (2003) 021101.

[104] K. Ioka, T. Tanaka and T. Nakamura et al., Phys. Rev. D. 60 (1999) 083512.

[105] P. Ivanov, Phys. Rev. D. 57 (1998) 7145.

[106] P. Ivanov, P. Naselsky and I. Novikov, Phys.Rev.D. 50 (1994) 7173.

[107] M. Izawa and K. Sato, Prog.Theor.Phys. 72 (1984) 768.

[108] T. Jacobsen, Phys. Rev. Lett. 83 (1999) 2699.

[109] K. Jedamzik, Phys.Rev.D. 55 (1997) R5871; Phys. Rep. 307 (1998) 155.

[110] K. Jedamzik and J. Niemeyer, Phys.Rev.D. 59 (1999) 124014.

[111] S. Kainer and W.K. Rose, AIP Conf. Proc. 666 (2003) 237.

[112] T. Kanazawa, M. Kawasaki and T. Yanagida, Phys.Lett.B. 482 (2000) 174.

[113] P. Kanti (2004), hep-ph/0402168.

[114] J. Kapusta, in *Phase Transitions in the Early Universe: Theory and Observations*, ed. H.J. de Vega et al. (Kluwer 2001), p 471.

[115] M.Yu. Khlopov and A.G. Polnarev, Phys.Lett.B., 97 (1980) 383.

[116] M.Yu. Khlopov and A. Barrau, astro-ph/0406621.

[117] M.Yu.Khlopov, R.V. Konoplich, S.G. Rubin and A.S. Sakharov, Grav.Cos. 2 (1999) 1.

[118] M.Yu.Khlopov, S.G. Rubin and A.S. Sakharov (2004), astro-ph/0401532.

[119] H. Kim, C.H. Lee and J.H. MacGibbon, Phys.Rev.D. 59 (1999) 063004.

[120] P. Kiraly et al., Nature 293 (1981) 120.

[121] H. Kodama, K. Sato, M. Sasaki and K. Maeda, Prog.Theor.Phys. 66 (1981) 2052.

[122] H. Kodama, K. Sato, M. Sasaki, Prog.Theor.Phys. 68 (1982) 1979.

[123] K. Kohri and J. Yokoyama, Phys.Rev.D. 61 (1999) 023501.

[124] T. Koike, T. Hara and S. Adachi, Phys. Rev. D 59 (1999) 104008.

[125] E.W. Kolb (2005), private communication.

[126] E.W. Kolb, A. Riotto and A. Vallinotto, Phys.Rev.D. 71 (2005) 043513.

[127] R.V. Konoplich, S.G. Rubin, A.S. Sakharov and M.Yu. Khlopov, Phys.Atom.Nuc. 62 (1999) 1593.

[128] J. Kormendy and D. Richstone, Ann. Rev. Astron. Astrophys. 33 (1995) 58.

[129] G.D. Kribs, A.K. Leibovich and I.Z. Rothstein, Phys.Rev.D. 60 (1999) 103510.

[130] F. Krennrich, S. Le Bohec and T.C. Weekes, Ap.J. 529 (2000) 506.

[131] D. La and P.J. Steinhardt, Phys.Lett.B. 220 (1989) 375.

[132] S.M. Leach, I.J. Grivell and A.R. Liddle, Phys.Rev.D. 62 (2000) 043516.

[133] H.K. Lee, Phys.Rev.D. 66 (2002) 063001.

[134] J.E. Lidsey, T. Matos and L.A. Urena-Lopez, Phys.Rev.D. 66 (2002) 023514.

[135] D.N.C. Lin, B.J. Carr and S.M. Fall, Mon. Not. R. Astron. Soc. 177 (1976) 51.

[136] D.H. Lyth (2005), astro-ph/0510443.

[137] D.H. Lythe, K.A. Malik, M. Sasaki and I. Zaballa (2005), astro-ph/0510647.

[138] J.H. MacGibbon, Nature 329 (1987) 308.

[139] J.H. MacGibbon, Phys. Rev.D. 44 (1991) 376.

[140] J.H. MacGibbon and B.J. Carr, Ap.J. 371 (1991) 447.

[141] J.H. MacGibbon and B.R. Webber, Phys.Rev.D. 41 (1990) 3052.

[142] J.H. MacGibbon, R.H. Brandenberger and U.F. Wichoski, Phys. Rev. D. 57 (1998) 2158.

[143] J.H. MacGibbon, B.J. Carr and D.N. Page, preprint (2005).

[144] K.J. Mack and J.P. Ostriker, Amer.Astron.Soc. Meeting 205 (2004).

[145] M. S. Madsen Classical Quantum Gravity 5, 627 (1988).

[146] K. Maeda, Class.Quant.Grav. 3 (1986) 233.

[147] K. Maeda, K. Sato, M. Sasaki and H. Kodama, Phys,Lett. 108B (1982) 103.

[148] K. Maki, T. Mitsui and S. Orito, Phys.Rev.Lett. 76 (1996) 3474.

[149] D. Maison, Phys. Lett B 366 (1996) 82.

[150] A.S. Majumdar, Phys.Rev.Lett. 90 (2003), 031303.

[151] P. Meszaros, Astron.Astrophys. 38 (1975) 5.

[152] S. Miyama and K. Sato, Prog.Theor.Phys. 59 (1978) 1012.

[153] I.G. Moss, Phys.Rev.D. 50 (1994) 676.

[154] S. Mukohyama, Phys.Rev.D. 71 (2005) 104019.

[155] I. Musco, J.C. Miller and L. Rezzolla, Class.Quant.Grav. 22 (2005) 1405.

[156] D.K. Nadezhin, I.D. Novikov and A.G. Polnarev, Sov.Astron. 22 (1978) 129.

[157] T. Nakamura, M. Sasaki, T. Tanaka and K. Thorne, Ap.J.Lett. 487 (1997), L139.

[158] J. Niemeyer and K. Jedamzik, Phys.Rev.Lett. 80 (1998) 5481.

[159] J. Niemeyer and K. Jedamzik, Phys.Rev.D. 59 (1999) 124013.

[160] I.D. Novikov, A.G. Polnarev, A.A. Starobinsky and Ya.B. Zeldovich, Astron.Astrophys. 80 (1979) 104.

[161] D.N.Page, Phys.Rev.D. 16 (1977) 2402.

[162] D.N.Page and S.W. Hawking, Ap.J. 206 (1976) 1.

[163] M. Patel and G.M. Fuller (2000), astro-ph/0003062.

[164] A.G. Polnarev and R. Zemboricz, Phys.Rev.D. 43 (1988) 1106.

[165] N.A. Porter and T.C. Weekes, Nature 277 (1979) 199.

[166] L. Randall. M. Soljacic and A.H. Guth, Nuc. Phys. B. 472 (1996) 377.

[167] S.G. Rubin (2005), astro-ph/0511181.

[168] S.G. Rubin, M.Yu. Khlopov and A.S. Sakharov, Grav.Cos. 6 (2001) 1.

[169] S.G. Rubin, A.S. Sakharov and M.Yu. Khlopov, J.Exp.Theor.Phys. 91 (2001) 921.

[170] A. Ringwald and H. Tu, Phys.Lett.B. 525 (2002) 135.

[171] M.P. Salem (2005), astro-ph/0511146.

[172] K. Sato, M. Sasaki, H. Kodama and K. Maeda, Prog.Theor.Phys. 65 (1981) 1443.

[173] D.V. Semikoz, Ap.J. 436 (1994) 254.

[174] Y. Sendouda, S. Nagataki and K. Sato, Phys.Rev.D. 68 (2003) 103510.

[175] Y. Sendouda, K. Kohri, S. Nagataki and K. Sato, Phys.Rev.D. 70 (2004) 063512.

[176] N. Seto and A. Cooray, Phys.Rev.D. 70 (2004) 063512.

[177] M. Shibata and M. Sasaki, Phys.Rev.D. 60 (1999) 084002.

[178] T. Shiromizu

[179] P. Sreekumar et al., Ap.J. 494 (1998) 523.

[180] D. Stoykovic and K. Freese, Phys.Lett. B. 606 (2005) 251.

[181] D. Stoykovic, K. Freese and G.D. Starkman (2005), astro-ph/0505026.

[182] T. Suyama, T. Tanaka, B. Bassett and H. Kudoh, Phys. Rev. D. 71 (2005) 063507.

[183] A. Taruya, Phys.Rev.D. 59 (1999) 103505.

[184] K.A. Thompson, in *22nd Texas Symposium on Relativistic Astrophysics* (2005), astro-ph/0504606.

[185] M.S. Turner, Nature 297 (1982) 379.

[186] E.L. Wright, Ap.J. 459 (1996) 487.

[187] J. Yokoyama, Astron. Astrophys. 318 (1997) 673.

[188] J. Yokoyama, Phys.Rev.D. 58 (1998) 083510.

[189] J. Yokoyama, Phys.Rev.D. 58 (1998) 107502.

[190] J. Yokoyama, Prog.Theor.Phys. Supp. 136 (1999) 338.

[191] K. Yoshimura et al., Phys.Rev.Lett. 75 (1995) 3792.

[192] H. Yoshino, T. Shiromizu and M. Shibata (2005), gr-qc/0508063.

[193] Ya.B. Zeldovich and I.D. Novikov, Sov.Astron.A.J. 10 (1967) 602.

Probing new physics with the LHC

Junichi Tanaka[1]

International Center for Elementary Particle Physics (ICEPP), University of Tokyo, Tokyo 113-0033, Japan

Abstract

We review the discovery potential of new physics at LHC. We expect LHC to give us exciting results thanks to its high energy, which will open a new epoch of the high energy particle physics. This paper is focused on three topics of "new" physics, Standard Model Higgs boson, Supersymmetry and Extra Dimensions.

1 Introduction – LHC

The Large Hadron Collider (LHC) project [1] is the major accelerator program at CERN [2]. It is now under construction using the existing 26.6 km circumference LEP tunnel. 1232 units of 8.3 Tesla superconducting dipole magnet working at 1.9 Kelvin will be arranged in the tunnel. 75% of them have already been assembled and 10% of them have been installed in the tunnel. Protons are accelerated up to 7 TeV and collide with each other at four collision points. The center-of-mass energy of the proton-proton system is 14 TeV. The design luminosity is 10^{34} $cm^{-2}s^{-1}$, which is corresponding to 100 fb^{-1} per year. During the first three or four years, LHC will be operated with the lower luminosity of $1 \cdot 2 \cdot 10^{33}$ $cm^{-2}s^{-1}$. Detectors and front-end electronics are required to be radiation hard for these high luminosities. Furthermore, bunches of proton are separated by only 25 ns, then high speed operations and low dead time of response are strongly demanded on the detectors.

From the point of view of the high energy, we expect the discovery of the standard model Higgs boson, which is the last unobserved particle in the standard model, and the discovery of physics beyond the standard model, such as supersymmetry (SUSY) and extra dimensions. This is the main purpose at the beginning of LHC. From the point of view of the high luminosity, we expect the precise measurement of various parameters, for example, couplings of the Higgs. Table 1 shows event rates for the interesting processes. LHC can produce the large amount of events, which is comparable with the present experiments, with only 10 fb^{-1}. LHC not only is top and b-factory but also can be Higgs and SUSY factory.

The first beam is scheduled in April 2007, and the first physics run will start in summer of 2007. We expect 0.1 fb^{-1} in 2007, a several fb^{-1} in 2008, 10–20 fb^{-1}/year until 2010 and then move to 100 fb^{-1}/year.

In this paper[2], we review the discovery potential of new physics at LHC with ATLAS and CMS detectors. We focus on three topics of new physics, standard model Higgs boson (not so-called "new physics" but unobserved particle), supersymmetry and extra dimensions.

2 Detectors – ATLAS and CMS

Two general purpose experiments exist, ATLAS [3] and CMS [4], at LHC. The ATLAS (A Toroidal LHC Apparatus) detector is illustrated in Fig. 1, and it measures 22 m high, 44 m long and weight 7000 tons. The characteristics of the ATLAS detector are summarized as follows [5]:

- Precision inner tracking system is constituted with pixel, silicon strip and TRT inside a 2 Tesla solenoidal magnet. Good performance is expected on the b-tagging and the γ-conversion tagging.
- Liquid Argon electromagnetic calorimeter has fine granularity for space resolution and longitudinal segmentation for fine angular resolution and particle identifications. It has also good energy resolution of about 1.5% for 100 GeV-e/γ.

[1] E-mail:Junichi.Tanaka@cern.ch

[2] Talk given at JGRG15, The 15th Workshop on General Relativity and Gravitation, Tokyo Institute of Technology, Tokyo, Japan, 28th November – 2nd December, 2005.

Table 1: Event rates at $2 \cdot 10^{33}$ cm^{-2}s^{-1} and event numbers at 10 fb^{-1} per detector of ATLAS and CMS experiments. The expected numbers observed at Tevatron-2 and B-factories until 2007 are listed for the comparison.

Process	Event rate at $2 \cdot 10^{33}$	Event number at 10 fb^{-1}	Comparing to the others
$W^{\pm} \to e^{\pm}\nu$	30 Hz	10^8	10^7 Tevatron-2
$Z^0 \to e^+e^-$	3 Hz	10^7	10^7 Tevatron-2
$t\bar{t}$	1.6 Hz	10^7	10^4 Tevatron-2
$b\bar{b}$ ($p_T > 10$ GeV)	200 kHz	2×10^{12}	
trigger with di-muons (ATLAS)	10 Hz	10^8	10^9 Belle/BaBar
Higgs (130 GeV)	200 events/hour	5×10^5	-
SUSY (1 TeV)	20 events/hour	5×10^4	-

- Large muon spectrometer with air-core toroidal magnet provides a precise measurement on muon momenta (about 2% for 100 GeV-μ) even at the forward direction.
- The tracking system covers the pseudo-rapidity η, $|\eta| < 2.5$ and the calorimeters cover $|\eta| < 4.9$ achieving the good hermeticity.

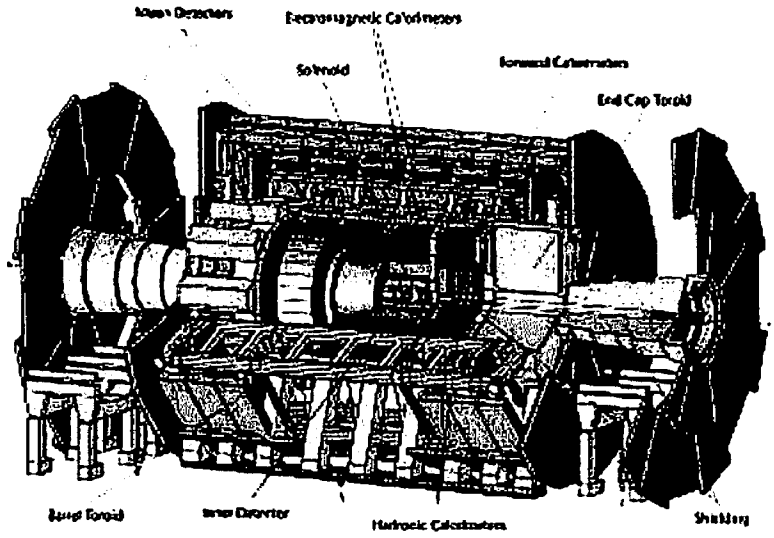

Figure 1: Atlas detector

The CMS (Compact Muon Solenoid) detector measures 15 m high, 21 m long and weight 12500 tons with the following features [6]:

- Precise measurement on high p_T track is performed with strong 4 Tesla solenoidal magnet.
- $PbWO_4$ crystal electromagnetic calorimeter has a good energy resolution.
- High purity identification and precise measurement are expected on μ tracks using compact muon system.

3 Standard Model Higgs

The discovery of the standard model Higgs is one of the most important issues for the elementary particle physics to understand a mechanism of the electroweak symmetry-breaking and an origin of masses. In the standard model, one doublet of a Higgs field is economically assumed, leading to the existence of one neutral scalar particle. A mass of the Higgs boson is no theoretically predicted in the standard model, but the upper-limit is considered to be about 1 TeV, which is obtained from the unitary bound of the W^+W^- scatter. Furthermore, the standard model Higgs is expected to be lighter than about 219 GeV (95% C.L.) with the precition measurements on the standard model processes at LEP [7]. The lower-limit of the Higgs boson mass is 114 GeV obtained directly at LEP-II.

3.1 Production and Decay

There are the following four relevant production processes of the Higgs boson at LHC and Fig. 2 (a) shows the cross-section of each process as a function of the Higgs mass.

- $gg \rightarrow H^0_{\rm SM}$: Gluon fusion process has the leading cross-section and $H^0_{\rm SM}$ is produced via the heavy quark loops. Since there is no characteristic particle associated with $H^0_{\rm SM}$as shown in Fig. 3 ($H^0_{\rm SM} \rightarrow \gamma\gamma$). it is difficult to find out Higgs boson decaying into hadrons due to the huge number of the QCD background. Only $H^0_{\rm SM} \rightarrow \gamma\gamma, ZZ\ (\rightarrow lll)$ and $W^+W^-\ (\rightarrow l\nu l\nu)$ decay modes are promising.

- $qq \rightarrow qqH^0_{\rm SM}$: Vector boson fusion process has also large cross-section in the wide mass range as shown in Fig. 2 (a). Figure 3 shows a diagram of vector boson fusion process with $H^0_{\rm SM} \rightarrow \tau^+\tau^-$. Since W and Z bosons, which are exchanged in t-channel, are heavy, the out-going quarks have larger transverse momenta (p_T) than the QCD background processes. They are observed in a forward region with high p_T. Tagging these forward jets helps us to suppress the background processes. Furthermore, there is no color exchange between two out-going quarks, the Higgs boson is observed in large rapidity gap, where activities of QCD jets are small [8].

- $q\bar{q} \rightarrow W/ZH^0_{\rm SM}$: Higgs boson is associate-produced with a vector boson. It is distinguished from the huge QCD backgrounds, when $W^{\pm}$ (Z^0) decays into leptons.

- $gg, q\bar{q} \rightarrow t\bar{t}H^0_{\rm SM}$: Higgs boson is associate-produced with a top quark pair through a large Yukawa coupling of top quark. Although the production cross-section is relatively small as shown in Fig. 2 (a), the huge QCD background events can be suppressed by tagging the top pair. This channel is mainly used to measure top Yukawa coupling.

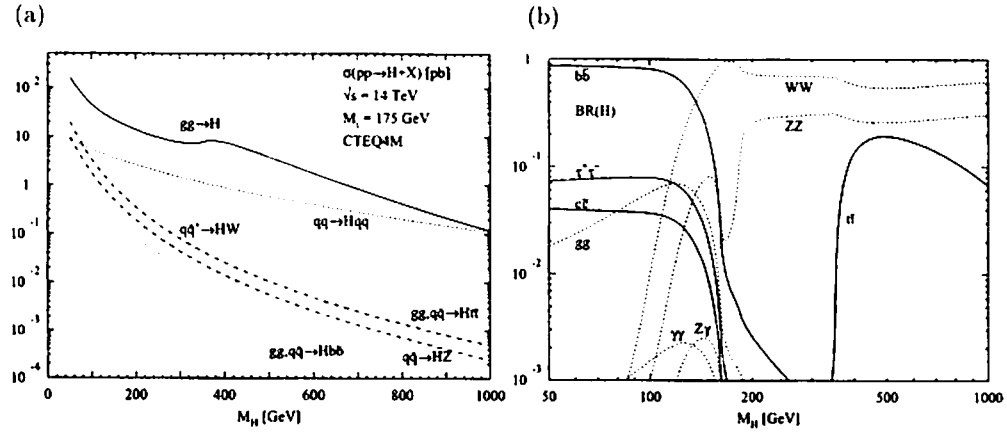

Figure 2: (a) Production cross-section of $H^0_{\rm SM}$ as a function of the mass for various processes. (b) Decay branching fraction of $H^0_{\rm SM}$ as a function of the mass.

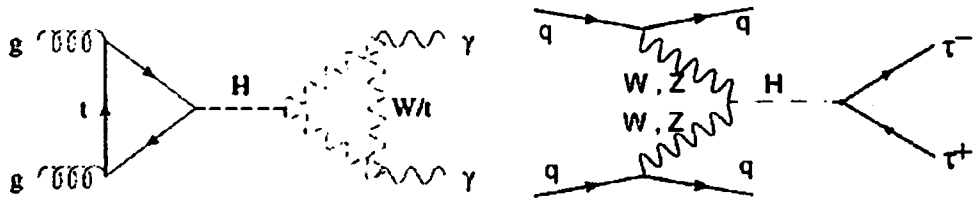

Figure 3: Diagrams of (left) gluon fusion $H^0_{SM} \to \gamma\gamma$ and (right) vector boson fusion $H^0_{SM} \to \tau^+\tau^-$

Figure 2 (b) shows the decay branching fraction of H^0_{SM} as a function of the Higgs mass. H^0_{SM} decays mainly into $b\bar{b}$ and $\tau^+\tau^-$ for the lighter case ($m_{H^0_{SM}} < 130$ GeV). On the other hand, the decays into W^+W^- and ZZ have a large fraction for the heavier case ($m_{H^0_{SM}} > 140$ GeV). Since the Higgs boson mass is expected to be within 114-219 GeV as described before, all the five decay modes ($b\bar{b}$, $\tau^+\tau^-$, $\gamma\gamma$, W^+W^- and ZZ) are important. Moreover, if the Higgs exists in this mass region, we can extract couplings of the Higgs by comparing results of multiple production and decay channels.

3.2 Discovery Channels

We summarize promising channels to discover Higgs and study of the properties at ATLAS in Table 2. We have various channels to discover, and we can also measure mass and couplings of the Higgs boson.

Table 2: Summary of promising channels of the standard model Higgs at ATLAS.

Production	Decay	Mass (GeV)	Discovery?	Measurements
Gluon fusion	$H^0_{SM} \to \gamma\gamma$	110-140	yes	mass
	$H^0_{SM} \to ZZ \to l^+l^-l^+l^-$	140-1000	yes	mass, spin, g_{HZZ}
	$H^0_{SM} \to W^+W^-$	130-170	yes	
Vector boson fusion	$H^0_{SM} \to \tau^+\tau^-$	110-140	yes	mass, g_{HWW}, y_τ
	$H^0_{SM} \to W^+W^-$	130-200	yes	g_{HWW}
	$H^0_{SM} \to \gamma\gamma$	110-140	yes	mass
	$H^0_{SM} \to b\bar{b}$	110-140	-	y_b (still under way)
ttH	$H^0_{SM} \to b\bar{b}$	110-130	-	y_t
	$H^0_{SM} \to \tau^+\tau^-$	110-130	-	y_t
	$H^0_{SM} \to W^+W^-$	130-180	-	y_t
WH	$H^0_{SM} \to W^+W^-$	140-170	yes	g_{HWW}

3.2.1 Gluon fusion : $H^0_{SM} \to ZZ \to \ell^+\ell^-\ell^+\ell^-$

$H^0_{SM} \to ZZ$ and W^+W^- becomes dominant decay channels when the Higgs mass is heavy ($m_{H^0_{SM}} > 200$ GeV). Four lepton channel, $H^0_{SM} \to ZZ \to \ell^+\ell^-\ell^+\ell^-$, is very clean and the gold-plated mode in the bosonic decays. Even if the Higgs mass is light ($m_{H^0_{SM}} < 200$ GeV), this channel is promising for the Higgs discovery as shown in Fig. 4 (a) [9]. Resolutions of invariant mass of four leptons are 1.6 and 2.2 GeV for $m_{H^0_{SM}} = 130$ and 180 GeV, respectively. This channel cover a wide mass range for the Higgs discovery from 140 to 1000 GeV except for 170 GeV. When the Higgs mass is 170 GeV, the branching fraction of $H^0_{SM} \to W^+W^-$ is almost 100% and this case is covered by the analysis of $H^0_{SM} \to W^+W^-$.

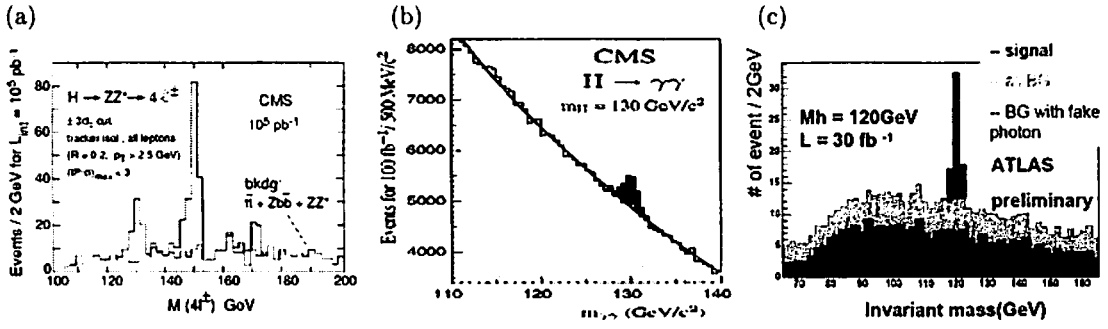

Figure 4: (a) Invariant mass distribution of $\ell^+\ell^-\ell^+\ell^-$ for 100 fb^{-1} at CMS. Open histogram shows the signal with $m_{H^0_{SM}}$=130, 150 and 170 GeV while hatched histogram shows the backgrounds. (b)(c) Invariant mass distributions of $\gamma\gamma$: (b) for gluon fusion with 100 fb^{-1} at CMS and (c) for vector boson fusion with 30 fb^{-1} at ATLAS.

3.2.2 Gluon fusion and Vector boson fusion : $H^0_{SM} \to \gamma\gamma$

The branching fraction of $H^0_{SM} \to \gamma\gamma$ is small. In case of gluon fusion, its production cross-section is large but there are very large backgrounds, such as $q\bar{q}$, $gg \to \gamma\gamma$. But since both ATLAS and CMS electromagnetic calorimeter has the excellent energy and position resolution for photon, a mass resolution of $H^0_{SM} \to \gamma\gamma$ is good enough to distinguish the signal from the backgrounds as shown in Fig. 4 (b) [9]. It is ~1.3 GeV at ATLAS and ~0.6 GeV at CMS with the low luminosity condition. A sharp peak is observed at Higgs boson mass over a huge but smooth distribution of the backgrounds. In case of vector boson fusion, its production cross-section is relatively large and QCD backgrounds are suppressed thanks to the characteristic of the forward jets and the rapidity gap. Figure 4 (c) shows an invariant mass distribution of $\gamma\gamma$ [10]. A sharp peak is also observed with relatively small backgrounds.

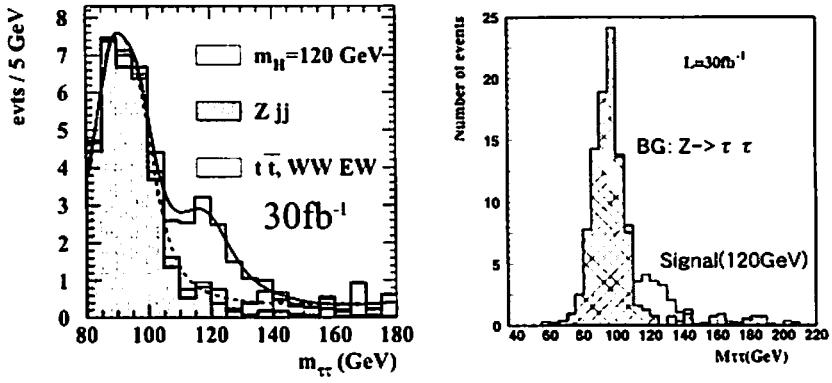

Figure 5: Mass distribution of the reconstructed $\tau^+\tau^-$ (left, lepton-lepton) and (right, lepton-hadron) with an integrated luminosity of 30 fb^{-1} at ATLAS ($m_{H^0_{SM}}$ = 120 GeV). The open histogram shows signal and the hatched histogram shows background.

3.2.3 Vector boson fusion : $H^0_{SM} \to \tau^+\tau^-$

When the mass of H^0_{SM} is relatively small ($115 < m_{H^0_{SM}} < 140$ GeV), a vector boson fusion process with $H^0_{SM} \to \tau^+\tau^-$ plays an important role for this discovery [8, 11]. $H^0_{SM} \to \tau^+\tau^-$ provides a high p_T lepton from a leptonic tau decay and it can be used as a trigger of this event. Momenta carried by

ν's emitted from τ decays can be estimated using the missing transverse energy $\not{E}_T$ information. A Higgs mass can be reconstructed since ν is assumed to be emitted in the same direction as the observed particles (lepton or jet). Figures 5 show invariant mass distributions of the reconstructed $\tau^+\tau^-$, lepton-lepton and lepton-hadron, respectively. The signal can be clearly separated from the background events. Dominant background process is Drell-Yan with two high p_T jets and makes a peak at Z^0 mass in this distribution.

3.3 Discovery Potential

The discovery potential of $H^0_{\rm SM}$ at ATLAS is shown in Fig. 6 as a function of the Higgs mass with an integrated luminosity of 30 fb^{-1} [11]. The vector boson fusion process with $H^0_{\rm SM} \to \tau^+\tau^-$ and $H^0_{\rm SM} \to W^+W^-$ provides an excellent sensitivity in the mass region of 115-140 GeV and 125-190 GeV, respectively. A significance combined with 6 promising channels is larger than 8σ. This corresponds to the fact that we can perform 5σ discovery of the Higgs boson (114-200 GeV) with 10 fb^{-1}. For heavy case ($m_{H^0_{\rm SM}} > 200$ GeV), a decay into ZZ ($\to l^+l^-l^+l^-$) has an excellent performance of much higher than 10σ. To sum up the Higgs discovery, we can discover the standard model Higgs in the region of $m_{H^0_{\rm SM}} > 114$ GeV with 10 fb^{-1}.

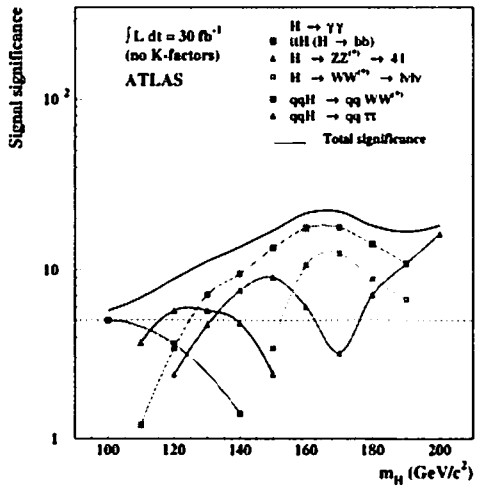

Figure 6: Discovery potential of $H^0_{\rm SM}$ with the integrated luminosity of 30 fb^{-1} at ATLAS. Horizontal axis is the Higgs mass and vertical axis is a significance of the Higgs signal. Horizontal dotted line shows 5σ.

4 Supersymmetry

Supersymmetry (SUSY) is one of the most promising extensions of the standard model (SM) [12] because SUSY can naturally deal with the problem of the quadratic Higgs mass divergence.

There are at least two indirect evidences for us to believe that SUSY can describe the nature. First, SUSY models give a hint of the Grand Unification of gauge couplings around 10^{16} GeV [13]. Figures 7 show coupling strength of three forces as a function of energy scale. In case of SM, they are not unified at any energy scale. On the other hand, in case of SUSY, they are unified around 10^{16} GeV. Second, they provide a candidate for cold dark matter. WMAP measurement of $\Omega_{\rm CDM}h^2 = 0.113^{+0.016}_{-0.018}$ [14, 15] requires sizable amount of cold dark matter. Lightest supersymmetry particle (LSP) in SUSY models is its candidate.

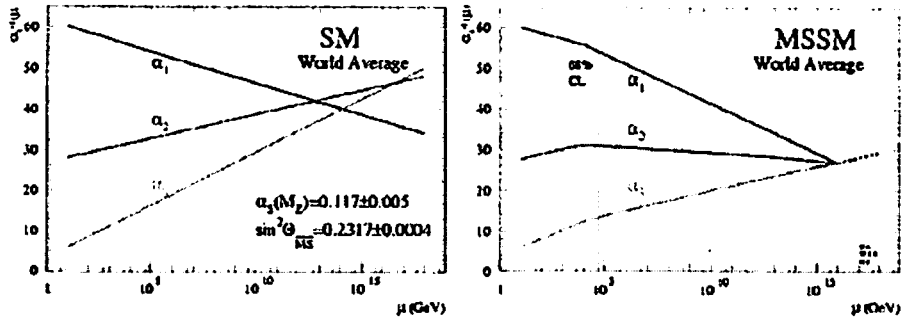

Figure 7: Evolution of the inverse of the three coupling constants in the SM (left) and in the MSSM (right) [13]. In the latter case, the unification is achieved. α_1 is for $U(1)$, α_2 for $SU(2)$ and α_3 for $SU(3)$.

4.1 Introduction

Figure 8 show particles of SM and SUSY. In SUSY models, each elementary particle has a superpartner whose spin differs by 1/2 from that of the SM particle. The fact that we have not observed such particles in nature implies that SUSY is broken by a mechanism which causes sparticles to acquire masses greater than SM particles.

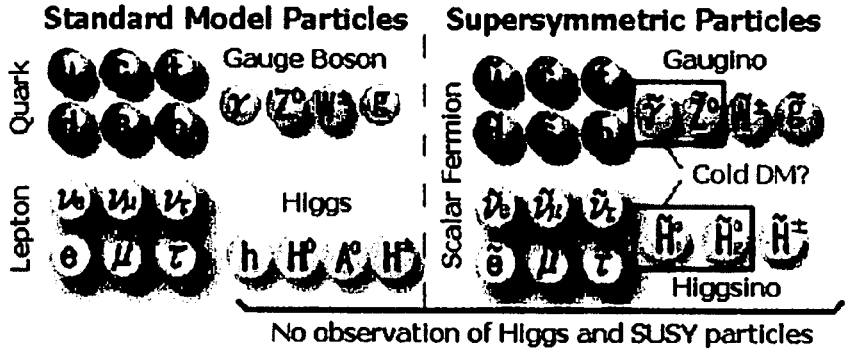

Figure 8: Particles in the standard model and their supersymmetric particles. Higgs and all the SUSY particles have not been observed yet.

In general there are more than 100 free parameters to describe SUSY soft breaking. The following two SUSY models are predictable and promising [12].

- Super-gravity model assumes that gravity is responsible for the mediation of the SUSY breaking and provides a natural candidate for cold dark matter.
- Gauge-mediated model assumes that standard model gauge interactions are responsible for mediation, which naturally solves the Flavor Changing Neutral Current (FCNC) problem.

Many studies have been performed on these and other models. In this paper, we use minimal super-gravity model based on the former.

4.2 Minimal Super-Gravity Model

Minimal super-gravity model (mSUGRA) [16] is a special case of the minimal supersymmetric model (MSSM). In this model, the SUSY soft breaking terms are assumed to be communicated from the SUSY breaking

sector by gravity as described before. Furthermore, these SUSY soft breaking terms are universal at the GUT scale. There are only five parameters after imposing GUTs conditions:

- m_0: Universal mass of all the scalar particles at GUT scale
- $m_{1/2}$: Universal mass of all the gauginos at GUT scale
- A_0: Common trilinear coupling at GUT scale
- $\tan\beta$ $(= v_2/v_1)$: Ratio of vacuum expectation value (VEV) of two Higgs fields at the electroweak scale
- sign(μ): ± 1, sign of Higgsino mass term

We assume that the R-parity is conserved [12]. As a result, the supersymmetry particles are created in pairs and the LSP is stable.

4.2.1 Production and Decay processes

Dominant SUSY production processes at LHC are $\tilde{g}\tilde{g}$, $\tilde{g}\tilde{q}$ and $\tilde{q}\bar{\tilde{q}}$ through the strong interaction. These production cross-sections do not strongly depend on the SUSY parameters except for masses of $\tilde{g}$ and $\tilde{q}$. Figure 9 shows contours of cross-sections in the m_0-$m_{1/2}$ plane. When these masses are 500 GeV, $\tilde{g}\tilde{g}$ is main production process and total cross-section is ~100 pb. It becomes 3 pb for $m_{\tilde{g}} = m_{\tilde{q}} = 1$ TeV. Even when these masses are 2 TeV, sizable production cross-section of ~20 fb is expected.

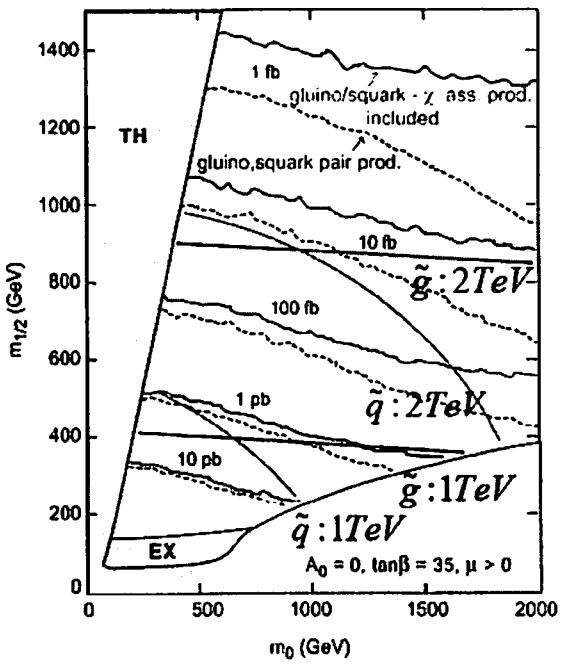

Figure 9: Production cross-section in the m_0-$m_{1/2}$ plane for $\tan\beta$=35. Mass contours for $\tilde{g}$ and $\tilde{q}$ are superimposed.

Decay modes of $\tilde{g}$ and $\tilde{q}$ are determined by the mass-relation between each other and are summarized in Fig 10 (a). If kinematically possible, they decay into 2-body through the strong interaction. Otherwise, they decay into a electroweak gaugino plus quarks. Eigenstates of Bino and Wino become simply mass-eigenstates, that is, $\tilde{B}^0 \sim \tilde{\chi}_1^0, \tilde{W}^0 \sim \tilde{\chi}_2^0$ and $\tilde{W}^\pm \sim \tilde{\chi}_1^\pm$ when m_0 is not too larger than $m_{1/2}$. In this case, Higgsino mass becomes larger than gaugino mass at the electroweak scale, then Higgsino component

decouples from lighter mass-eigenstates. Decay modes of third generation squarks ($\tilde{t}_1$ and $\tilde{b}_1$) are more complicated since they couples to Higgsino due to non-negligible Yukawa couplings.

(a)

	$m(\tilde{g}) < m(\tilde{q})$	$m(\tilde{g}) \approx m(\tilde{q})$	$m(\tilde{g}) > m(\tilde{q})$
$\tilde{g}$	$q\bar{q}\tilde{B}^0(\approx 1)$ $\tilde{g} \to q\bar{q}\tilde{W}^0(\approx 2)$ $q\bar{q}\tilde{W}^{\pm}(\approx 4)$	$\tilde{g} \to \begin{matrix} t\tilde{t}_1 \\ b\bar{b}_1 \end{matrix}$ (3rd is light)	$\tilde{g} \to q\bar{q}$
$\tilde{q}_L$	$\tilde{q}_L \to q\tilde{g}$	$\tilde{q}_L \to \begin{matrix} q\tilde{W}^0(\approx 1) \\ q\tilde{W}^{\pm}(\approx 2) \end{matrix}$	
$\tilde{q}_R$	$\tilde{q}_R \to q\tilde{g}$	$\tilde{q}_R \to q\tilde{B}^0$	

(b)

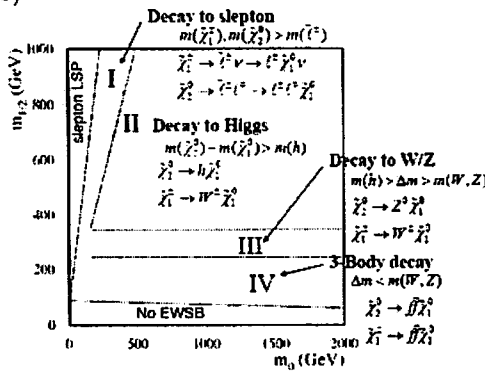

Figure 10: (a) Decay modes of $\tilde{g}$ and $\tilde{q}$ with their mass relation. (b) Decay modes of $\tilde{\chi}_1^{\pm}$ and $\tilde{\chi}_2^0$ in the m_0-$m_{1/2}$ plane.

Decay modes of $\tilde{\chi}_1^{\pm}$ and $\tilde{\chi}_2^0$ are classified into three (I,II+III,IV) for $\tilde{\chi}_1^{\pm}$ and four (I,II,III,IV) regions for $\tilde{\chi}_2^0$ as shown in Fig 10 (b). When the scalar lepton is lighter than $\tilde{\chi}_2^0$, 2-body decay chain $\tilde{\chi}_2^0 \to \tilde{\ell}^{\pm}\ell^{\mp}$ becomes dominant decay mode. Branching fraction of $\tilde{\chi}_2^0 \to \tau\tilde{\tau}_1$ is significant large in the case of $\tan\beta \gg 1$. $\tilde{\chi}_2^0 \to h\tilde{\chi}_1^0$ is dominant mode when the mass difference between $\tilde{\chi}_2^0$ and $\tilde{\chi}_1^0$ is larger then Higgs boson mass. When the mass difference is smaller than m_{Z^0}, three body decay is a main decay process. In the same way, $\tilde{\chi}_1^{\pm}$ has three leading decay modes, $\tilde{\chi}_1^{\pm} \to \tilde{\ell}^{\pm}\nu$, $W^{\pm}\tilde{\chi}_1^0$ and $f\bar{f}\tilde{\chi}_1^0$.

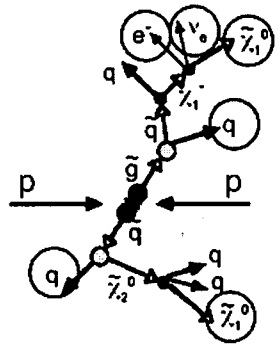

Figure 11: Event topology of SUSY production and decay. Red circles show the origin of $\not{E}_T$, blue circles show high p_T jets and a green circle shows a lepton.

4.2.2 Event Topology and Discovery Potential of mSUGRA

Figure 11 shows a typical event topology of mSUGRA. High p_T jets are emitted from the decays of $\tilde{g}$ and $\tilde{q}$. Each event contains two $\tilde{\chi}_1^0$s in the final state. If R-parity is conserved, $\tilde{\chi}_1^0$ is stable and it is neutral and weakly interacting and escape from the detection. Then missing transverse energy $\not{E}_T$ due to two $\tilde{\chi}_1^0$s plus multiple high p_T jets is the experimental signature of SUSY [17, 18]. Other activities of additional jets, leptons and $b\bar{b}$ are possible coming from the decays of $\tilde{\chi}_2^0$ and $\tilde{\chi}_1^{\pm}$. These additional informations are important to reduce backgrounds, to confirm SUSY signals and to investigate its properties.

SUSY signals is observed as an excess of standard model processes, $W^{\pm}(\to l\nu)$+jets, $Z^0(\to \nu\bar{\nu}, \tau^+\tau^-)$, $t\bar{t}$ and QCD jets. $M_{\rm eff} = \not{E}_T + \sum_{\rm 4jets} p_T$, which is called "effective mass", is a good variable to see

an excess coming from the SUSY signals as shown in Figs 12. Recently we found that the "0-lepton mode" ($M_{\rm eff}$ with no requirement of any lepton) suffers from the standard model backgrounds while "1-lepton mode" [19] has the same discovery potential as the previous study of "0-lepton mode" [17].

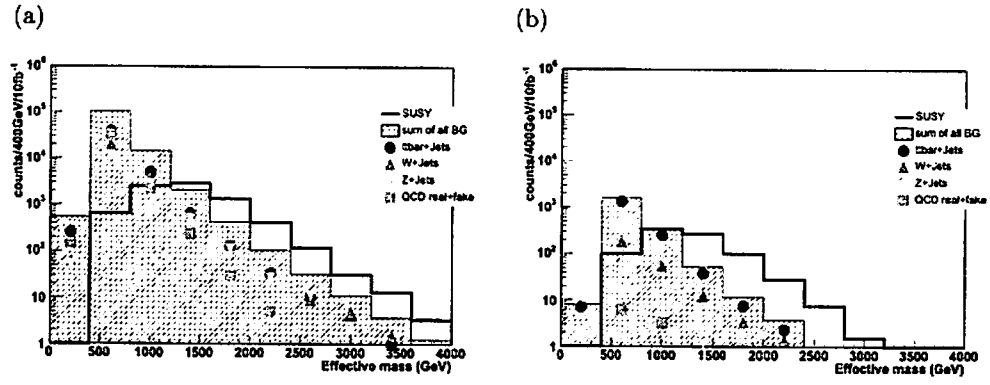

Figure 12: (Preliminary results) Effective mass distributions of (a) 0-lepton mode and (b) 1-lepton mode for the SUSY scale of 1 TeV. The open histogram shows SUSY signal while the hatched histogram shows sum of all the backgrounds ($t\bar{t}$, W + jets, Z + jets and QCD jets).

Figure 13 shows 5σ-discovery potential in the m_0-$m_{1/2}$ plane for $\tan\beta$= 35 using the effective mass with various integrated luminosities [18]. Mass contours for $\tilde{\rm g}$ and $\tilde{\rm q}$ are also superimposed. $\tilde{\rm g}$ and $\tilde{\rm q}$ can be discovered close to 1.5 TeV with a luminosity of 1 fb^{-1}, which is corresponding to just one month run with 10^{33} cm^{-2}s^{-1}. The interesting region for relic density of the dark matter is almost covered with just 1 fb^{-1}. We can discover $\tilde{\rm g}$ and $\tilde{\rm q}$, whose masses are less than $\sim$2 TeV within 10 fb^{-1}.

4.3 Mass Reconstruction

The mass determination of SUSY particles is important after the discovery of the SUSY. In general, we cannot make a distribution of the invariant mass of SUSY particles due to $\tilde{\chi}_1^0$s in the final state. However we can obtain the mass of SUSY particles by using kinematic endpoints of various distributions.

When a $\tilde{\chi}_2^0$ decays to $\tilde{\chi}_1^0\ell^+\ell^-$ (3-body decay), the $\ell^+\ell^-$ mass distribution has an endpoint, that corresponds to $M_{\tilde{\chi}_2^0} - M_{\tilde{\chi}_1^0}$. However the same $\ell^+\ell^-$ distribution from the 2-body decay $\tilde{\chi}_2^0 \to \tilde{\ell}\ell \to \tilde{\chi}_1^0\ell\ell$ has a sharp edge at the endpoint:

$$M_{\ell\ell}^{\rm max} = M_{\tilde{\chi}_2^0}\sqrt{1-\left(\frac{M_{\tilde{\ell}}}{M_{\tilde{\chi}_2^0}}\right)^2}\sqrt{1-\left(\frac{M_{\tilde{\chi}_2^0}}{M_{\tilde{\ell}}}\right)^2}.$$

Figure 14 (a) shows the $\ell^+\ell^-$ mass distribution ($e^+e^- + \mu^+\mu^- - e^\pm\mu^\mp$) at LHC point 5 [17]. The sharp edge is observed and it is fitted to be 108.7 GeV while $M_{\ell\ell}^{\rm max}$ is calculated to be 108.9 GeV.

In general, because the number of constrains (measured endpoints) is smaller than that of unknown parameters (mass of SUSY particles), we need to ask a SUSY model to obtain masses. But when there are three or more 2-body cascade decay chains, we can determine masses model-independently. Figures 14 show four different distributions at LHC point 5, where three 2-body cascade decay chains exist. From these distributions, we can obtain four masses, that is, $M_{\tilde{\rm q}}$, $M_{\tilde{\chi}_2^0}$, $M_{\tilde{\ell}}$ and $M_{\tilde{\chi}_1^0}$.

4.4 mSUGRA with WMAP

WMAP measurement of $\Omega_{\rm CDM}h^2 = 0.113^{+0.016}_{-0.018}$ gave a strong impact on mSUGRA model [14, 15]. It gives a strong constraint on the allowed region in the m_0-$m_{1/2}$ plane as shown in Figs 15. The green regions are in agreement with 95% C.L. of WMAP measurement. We classify it into four regions, 1) bulk region, 2) co-annihilation point, 3) focus point and 4) funnel point [15]. The amount of the LSP should be suppressed to explain the result of WMAP.

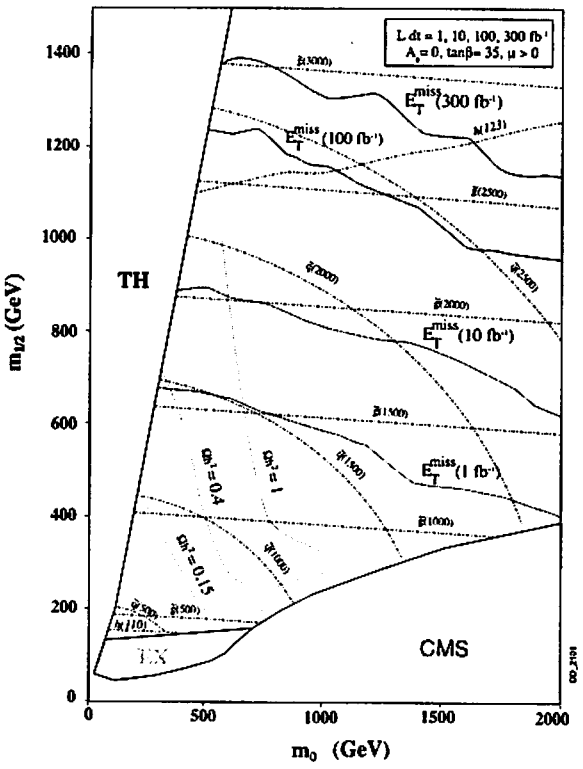

Figure 13: 5σ-discovery region in the m_0-$m_{1/2}$ plane for $\tan\beta$=35 using the $\not{E}_T$+jets channel of 0-lepton mode. Mass contours for $\tilde{g}$ and $\tilde{q}$ are superimposed. Ωh^2 shows relic density of the dark matters. In the "TH" region, $\tilde{\ell}^{\pm}$ becomes the LSP or no electroweak symmetry breaking occurs. The "EX" region is excluded by the present experiment data.

- Bulk region : neutralino pair annihilation occurs via t-channel slepton exchange.
- Co-annihilation point : a neutralino coannihilates with $\tilde{\tau}$.
- Focus point : a neutralino has a significant higgsino component and its pair annihilation to WW and ZZ pairs occurs.
- Funnel point : $\tilde{\chi}_1^0\tilde{\chi}_1^0 \to A \to f\bar{f}$

If we believe that mSUGRA model be correct, studies of the SUSY at LHC could be easy. However, when we look at this result from a different angle, it means that mSUGRA model may be excluded.

5 Extra Dimensions

Extra dimensions models are attractive extensions of the standard model with respect to the hierarchy problem. Arkani-Hamed, Dimopoulos and Davali (ADD) suggested that there is only one fundamental scale in nature, that is, the electroweak scale [20]. Gravity appears much weaker than other forces due to the existence of extra dimensions, where it can propagate but other forces cannot. Furthermore, extra dimensions are also required in string theory, which is expected to be the fundamental theory. The concern with the existence of the extra dimensions has been growing.

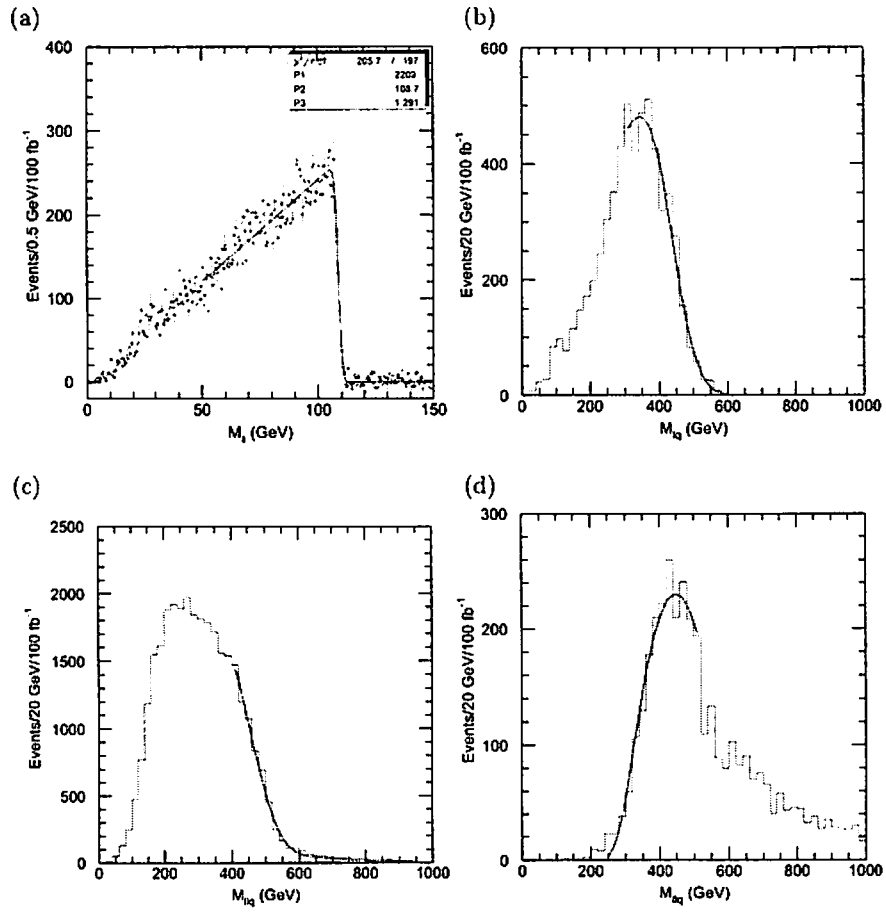

Figure 14: Invariant mass distributions of visible particles for the decay chain of $\tilde{q} \to \tilde{\chi}_2^0 q, \tilde{\chi}_2^0 \to \tilde{\ell}_R \ell$ and $\tilde{\ell}_R \to \tilde{\chi}_1^0 \ell$ (at LHC point 5, m_0=100 GeV, $m_{1/2}$=300 GeV) [17]. (a) $M(\ell^+\ell^-)$, (b) $M(\ell^{\pm}\text{jet})$, (c) $M(\ell\ell\text{jet})^{\min}$, and (d) $M(\ell\ell\text{jet})^{\max}$

5.1 Signals at LHC

We review expected signals from three kinds of extra dimensions at LHC, that is, large extra dimension, TeV^{-1} extra dimension and Randall-Sundrum model.

- Large extra dimension (ADD model) [20] : The observed Planck scale $M_{\rm Pl}$ is related to the fundamental scale of gravity $M_{\rm Pl(4+n)}$ by $M_{\rm Pl}^2 \sim M_{\rm Pl(4+n)}^{2+n} R^n$, where n is the number of extra dimension and R is its size. $M_{\rm Pl(4+n)}$ is set to be near the electroweak scale to solve the hierarchy problem. It this case, R becomes much large for n =1-7, *e.g.*, $R \sim 10^{-15}$ m (>TeV^{-1}) for $n = 7$. Such a model predicts the existence of an infinite number of Kaluza-Klein (KK) excitations of the graviton of very small mass splitting propagating in the extra dimensions. The direct production of the KK gravitons is described in the section 5.1.2. The virtual exchange of KK graviton can lead to deviations of standard model expectation such as Drell-Yan cross-section, where additional diagrams as shown in Figs 16 contribute to diagrams of the standard model.

- TeV^{-1} extra dimension : There are two kinds of extra dimensions in this model. One is large extra dimensions and the other is extra dimensions of TeV^{-1} or smaller size. The standard model fermions propagate only in the usual 4-dimensions while the standard model gauge bosons propagate additionally in the TeV^{-1} scale extra dimensions. Since such a model predicts the existence of KK

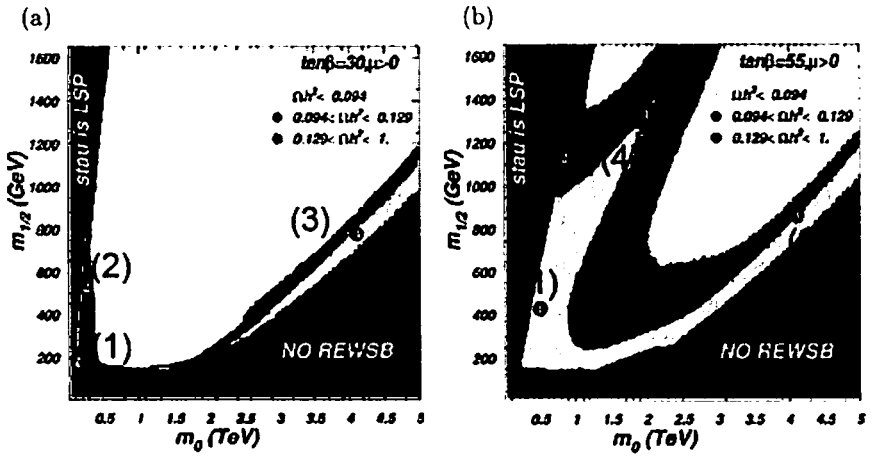

Figure 15: Allowed region of mSUGRA model with the WMAP result in the m_0-$m_{1/2}$ plane for (a) $\tan\beta$=30 and for (b) $\tan\beta$=55.

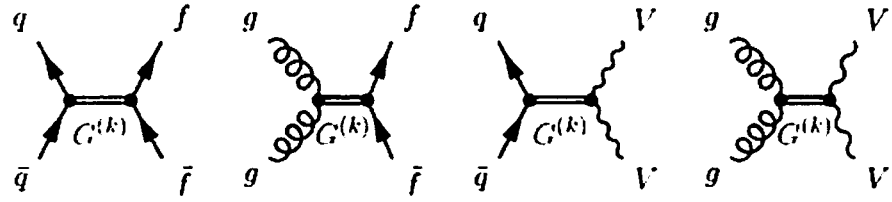

Figure 16: Diagrams of the virtual exchange of KK graviton

excitations of the standard model gauge bosons, we expect a signal of "excited Z^0 boson" Z' via $Z' \to e^+e^-$ at LHC. Moreover, the deviation of electroweak parameters from the standard model expectation is expected.

- Randall-Sundrun model [21] : The universe consists of two branes bounded by a warped 5D bulk in this model, where one of the branes is electroweak scale and the other is Planck scale. The standard model particles are confined in the former brane. This model leads to the existence of KK gravitons. But in this model, their mass splittings are at least of order the electroweak scale. We expect a signal of "excited graviton" G^* via $G^* \to e^+e^-$.

5.1.1 e^+e^- Resonance at a few TeV in the RS Model and TeV^{-1} Extra Dimensions

Observation of e^+e^- resonance at a few TeV is expected in both the RS model and TeV^{-1} extra dimensions. It comes from G^* and Z', respectively. Figure 17 (a) shows a distribution of invariant mass of e^+e^- in the RS model [22]. A clear peak of e^+e^- is observed over the Drell-Yan background. We can observe G^* up to mass of 1.2 TeV with 10 fb^{-1} as shown in Fig 17 (b). Furthermore, angular distribution reveals spin-2 nature of G^* as shown in Fig 17 (c). It has a good separation between G^* (spin-2) and Z/Z' (spin-1).

5.1.2 Direct Production of Graviton in the ADD Model

A KK graviton $G^{(k)}$ is produced via $q\bar{q} \to gG^{(k)}, qg \to qG^{(k)}$, $gg \to gG^{(k)}$ and so on. Since the KK graviton can propagate in the bulk, it is observed as a missing transverse energy $\not{E}_T$ in the 4D. We also observe a mono-jet, that is different from the SUSY case. It means that the main signature is $\not{E}_T$ with a

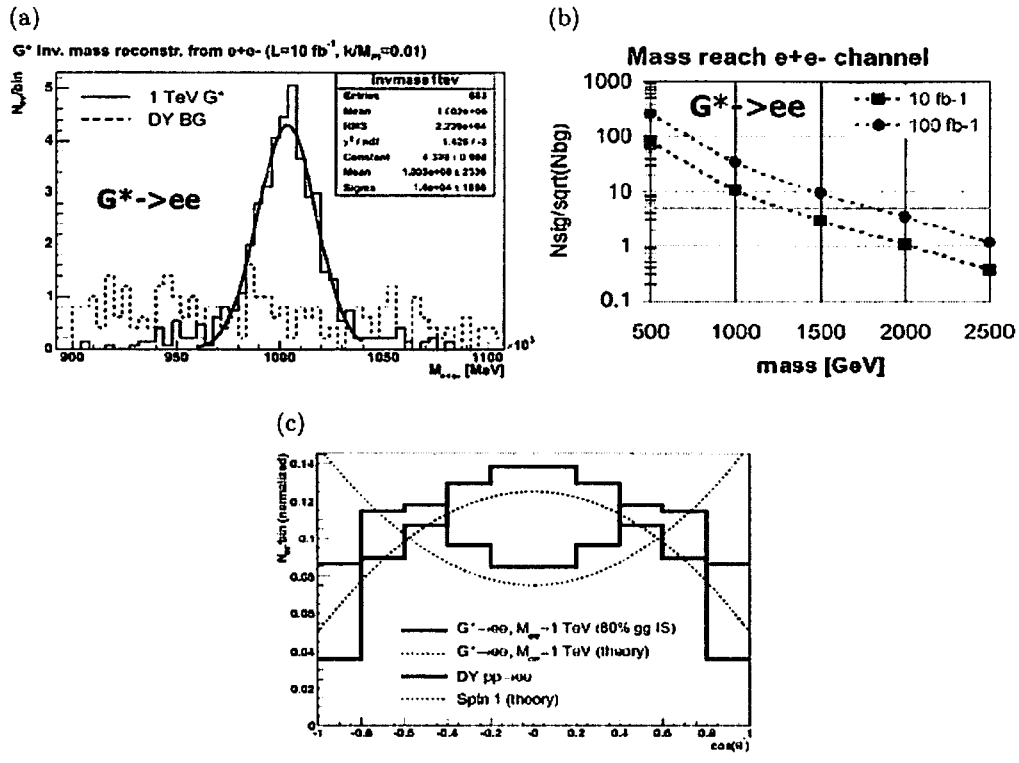

Figure 17: (Preliminary results) (a) Invariant mass of e^+e^- : the solid histogram shows $G^* \to e^+e^-$ and the dotted histogram shows the SM background. (b) Signal significance as a function of G^* mass for 10 fb^{-1} (blue) and 100 fb^{-1} (red). (c) cos(θ^*) distributions. θ^* is a angle between a decay electron and a beam-direction in e^+e^- system [22].

mono-jet as shown in Fig 18. We see an excess in the large $\not{E}_T$ region. For 100 fb^{-1}, the maximum reach in $M_D = (M_{\mathrm{Pl}(4+n)})$ is between 9.1 TeV ($\delta = n = 2$) and 6.0 TeV ($n = 4$) [23].

5.1.3 Black Hole Production in the ADD Model

Black holes (BHs) can be produced at LHC if the fundamental scale is of order a TeV. In classical arguments, when the impact parameter of initial partons is smaller than the Schwarzschild radius ($\sim 10^{-20}$ m), a black hole can be produced. On the other hand, there are many papers of BHs, which cannot be produced or observed at LHC. Needless to say, LHC can give us the answer.

At the present, classical and simple (optimistic) assumptions are used for the simulation [24]. The production cross-section of BHs is large as shown in Fig 19, for example, 20 pb for $M_{\mathrm{Pl}(4+n)} = 3$ TeV (small dependence on n). Figure 19 shows the event display of a BH event. A BH is observed as an energetic and spherical event. An excess of BH events from the standard model backgrounds can be observed for the integrated luminosity of 1 fb^{-1} if $M_{\mathrm{Pl}(4+n)}$ is less than 5 TeV for $n = 2$-7.

6 Other Scenarios

Large number of scenarios are proposed and studied, such as split SUSY [25], universal extra dimension [26], little Higgs [27] and so on. LHC can directly discover them up to mass scale of 5 TeV if they exist. We need to identify a model from which the signal comes after we discover an excess.

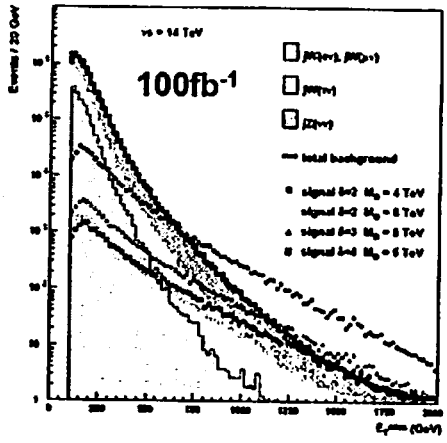

Figure 18: $\not\!\!E_T$ distribution for events with a mono-jet.

7 Conclusions

LHC will start in summer of 2007. LHC accelerator and ATLAS and CMS detectors are constructed on schedule. LHC can give us the exciting physics results, which will open a new epoch of the high energy particle physics. The standard model Higgs can be discovered with 10 fb^{-1}. Discovery of SUSY excess is easy in a few month and signals of extra dimensions are also discovered with 1-100 fb^{-1} (depends on models). LHC has a high discovery potential for any new and unexpected physics up to the mass scale of 5 TeV.

References

[1] http://lhc.web.cern.ch/lhc/

[2] http://www.cern.ch/

[3] ATLAS Technical proposal, CERN/LHCC/94-43.

[4] CMS Technical proposal, CERN/LHCC/94-38.

[5] ATLAS Physics TDR vol.1, CERN/LHCC/99-14

[6] http://cmsdoc.cern.ch/cms/TDR/

[7] http://lepewwg.web.cern.ch/LEPEWWG/

[8] T. Plehn, D. Rainwater and D. Zeppenfeld, Phys. Lett. **B454** (1999) 297

[9] CMS Note-2003/033

[10] M. Kataoka, presented at http://agenda.cern.ch/fullAgenda.php?ida=a053732 (ATLAS)

[11] S. Asai *et al.*, Eur. Phys. J. C32 S2 (2004) 19.

[12] See, for example, S. P. Martin hep-ph/9709356

[13] U. Amaldi, W. de Boer and H. Furstenau, Phys. Lett. **B260** (1991) 447

[14] C. Bennett, Astrophys. J. Suppl. **148** (2003) 1, D. N. Spergel Astrophys. J. Suppl. **148** (2003) 175

[15] A. Belyaev hep-ph/0410385

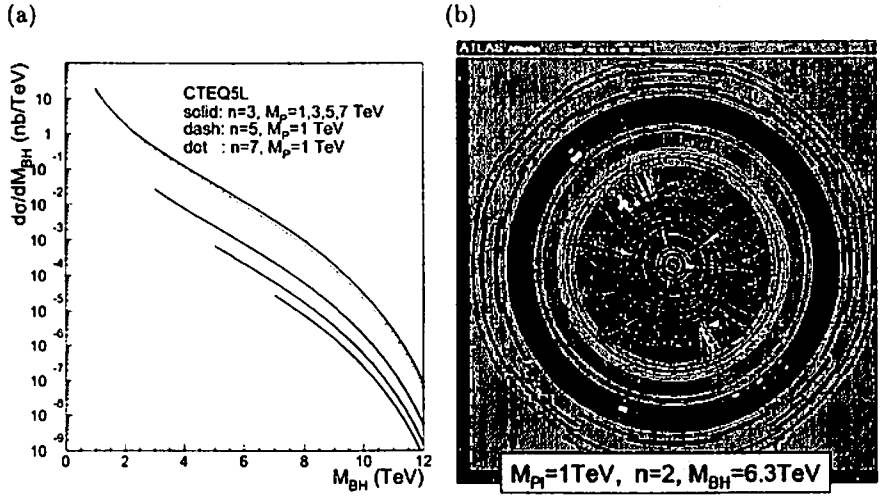

Figure 19: (a) Differential cross section as a function of a black hole mass for each ($M_{\mathrm{Pl}(4+n)}$,n) parameter. (b) Event display of a black hole event at ATLAS.

[16] S. Abel *et al.* hep-ph/0003154

[17] ATLAS Physics TDR vol.2, CERN/LHCC/99-15

[18] S. Abdullin *et al.*, J. Phys. G: Nucl. Part. Phys. **28**, (2002) 469

[19] S. Asai, presented at http://agenda.cern.ch/fullAgenda.php?ida=a044738 (ATLAS)

[20] N. Arkani-Hamed, S. Dimopoulous, and G. Dvali, Phys. Lett. B **429**, 263 (1998)

[21] L. Randall and R. Sundrum Phys. Rev. Lett. **83**, 3370 (1999), L. Randall and R. Sundrum Phys. Rev. Lett. **83**, 4690 (1999)

[22] S. Padhi, presented at http://agenda.cern.ch/fullAgenda.php?ida=a044738 (ATLAS)

[23] L. Vacavant and I. Hinchliffe, J. Phys. G: Nucl. Part. Phys. **27**, (2001) 1839

[24] J. Tanaka, T. Yamamura, S. Asai and J. Kanzaki Eur. Phys. J. C41 (2005) 19, S. Dimopoulous and G. Landsberg Phys. Rev. Lett. **87**, 161602 (2001), S. B. Giddings and S. Thomas Phys. Rev. D **65**, 056010 (2002)

[25] N. Arkani-Hamed and S. Dimopoulos, JHEP 0506 (2005) 073

[26] T. Appelquist, H. -C. Cheng and B. A. Dobrescu, Phys. Rev. D **64**, 035002 (2001), T. G. Rizzo Phys. Rev. D **64**, 095010 (2001)

[27] N. Arkani-Hamed, A. G. Cohen, and H. Georgi, Phys. Lett. **B513** (2001) 232

Recent Discoveries about Gamma-Ray Bursts

Shiho Kobayashi [1]

[1] *Astrophysics Research Institute, Liverpool John Moores University, United Kingdom*

Abstract

Gamma-Ray Bursts (GRBs) are the brightest objects observed. They are also the most relativistic objects known so far. GRBs occur when an ultra-relativistic ejecta is slowed downed by shocks. The successful launch and operation of NASA's Swift Gamma-Ray Burst Explorer open a new era for the multi-wavelength study of the very early afterglow phase of gamma-ray bursts. GRB early afterglow information is essential to explore the unknown physical composition of GRB jets, the link between the prompt gamma-ray emission and the afterglow emission, the central engine activity, as well as its environment. Short GRBs and high redshift bursts have recently been localized. I review some of recent discoveries about GRBs.

1 Introduction

Gamma-Ray Bursts (GRB), short and intense bursts of gamma-ray arriving from random directions in the sky were discovered accidentally more than thirty years ago. During the last decade two satellites, CGRO and BeppoSAX have revolutionized our understanding of GRBs [1, 2, 3]. CGRO has demonstrated that GRBs originate at cosmological distances in the most energetic explosions in the Universe. The discovery of X-ray afterglow by BeppoSAX enabled us to pinpoint the positions of some bursts, locate optical and radio afterglows, identify host galaxies and measure redshifts to some bursts.

With the successful launch of the Swift Gamma-ray Burst Explorer [4], an era of systematic, multi-wavelength observations of GRB early afterglows has been ushered in. There has been widespread expectation that early afterglow observations could answer a series of core questions in GRB studies. Are short duration GRBs different from the long duration GRBs? What is the immediate environment of GRBs, a constant density (ISM) medium or a massive stellar wind? where is the prompt gamma-ray emission emitted, at the external shock just like the afterglows or at an inner radius due to shock or magnetic dissipation? What is the physical composition of the GRB jets, baryonic or magnetic? If they are baryonic, are there free neutrons in the fireball? How does the GRB central engine work? Does it become dormant when the prompt gamma-ray emission is over? Thanks to its capability of promptly slewing the on-board X-Ray Telescope (XRT) and the UV/Optical Telescope (UVOT) to the GRB target, the Swift satellite is an ideal mission to address these questions.

The early X-ray/optical afterglow data would give valuable information on the transition between the prompt gamma-ray emission phase and the afterglow phase. In the optical band, it is expected that the early afterglow emission should include the contribution of a short-lived reverse shock radiation. On the other hand late afterglows are totally dominated by forward shock component and therefore reflect the emission from the circumburst medium. The reverse shock component is very precious since it directly carries the information of the GRB outflow itself, and is valuable to diagnose the physical composition of the fireball jets. Swift has been very fruitful in addressing these problems.

2 Short Burst Afterglow

It is well known that GRBs are divided to two subgroups of long and short according to their duration [5]. Short busts ($T < 2$ sec) are also harder than long ones. Our understanding of long bursts and their association with stellar collapse [6, 7] followed from the discovery of GRB afterglow. However, until recent months no afterglow was detected from any short bursts and those remained as mysterious as ever.

[1] E-mail:sk@astro.livjm.ac.uk

This situation has changed with the detection of X-ray afterglow from several bursts by Swift [8, 9] and by HETEII [10]. This has lead to identification of host galaxies and to redshift measurements. While the current sample is still small, several features emerge. Unlike long GRBs that take place in star-forming galaxies, short busts take place also in elliptical galaxies in which the stellar population is older [11]. The low level of star formation typical for elliptical galaxies makes it unlikely that the bursts originated in a supernova explosion. A supernova origin was also ruled out for a short burst GRB 050709 [12], even though that burst took place in a galaxy with current star formation. The isotropic energy for the short bursts is 2-3 orders of magnitude lower than that for the long bursts. These results therefore strengthen earlier suggestions [13, 14] and provide support for coalescing compact object binaries (neutron star-neutron star or neutron star - black hole binaries) as the progenitors.

3 High Redshift Burst

Long GRBs and their afterglows are expected to occur in sufficient numbers and sufficient brightnesses at very high redshifts ($z > 5$) to eventually replace quasars as the preferred probe of element formation and reionization in the early universe and to be used to characterize the star-formation history of the early universe, perhaps back to when the first stars formed [15, 16, 17].

The event of September 4h, 2005 (GRB 050904) was found to be at redshift $z = 6.3$ [18, 19, 20]. This gave GRB 050904 the distinction of being the most distant cosmic explosion ever observed: the previous record for a GRB was 4.5 [21], the most distant quasar known is at a redshift of 6.4, and the most distance galaxy is at a redshift of ~ 7. The discovery of a gamma-ray burst at such a large redshift implies the presence of massive stars only 700 million years after the Big Bang. A very bright optical flare emitted by GRB 050904 at the time of the prompt gamma-ray event was also detected [22], which is similar to the remarkable optical flash associated with GRB 990123 [23]. These observations suggest the existence of a population of GRBs which have very large isotropic equivalent energies and extremely bright optical counterparts. The luminosity of these GRBs is such that they are easily detectable through the entire universe. GRBs will constitute powerful tools for the exploration of the high redshift Universes.

4 Early X-ray Afterglow

Although early afterglow lightcurves have been extensively modeled in the optical band (mainly driven by the observations and by the theoretical argument that the reverse shock emission component plays an important role in the optical band [24, 25, 26, 27]), possible early X-ray afterglow signatures have been only sparsely studied. In its first several months of operations, Swift XRT has already accumulated a rich collection of early afterglow features in the X-ray band. The XRT can be promptly slewed to GRB targets within 1-2 minutes. It is therefore an ideal instrument to study the transition between the GRB prompt emission and the very early X-ray afterglow. After inspecting a sample of early x-ray afterglow data [28, 29], one can draw a synthetic cartoon X-ray lightcurve [29, 30]. This light curve includes five components I. an early steep decay, II. a follow-up shallower-than-normal decay, III. a normal decay, IV. a jet break, and V. one or more X-ray flares (see Figure 1).

Steep decay. A rapid decay component is evident in the early X-ray lightcurves of the majority of the Swift bursts [31]. In some bursts this component is smoothly connected to the spectrally-extrapolated BAT lightcurve, and it could be generally interpreted as the "tail emission" of the prompt emission due to the so-called "curvature effect" [32]. In some cases, a mismatch between the steep decay and the BAT lightcurve is evident, but it could be well the tail emission of the X-ray flares [33]. The curvature-effect suggests that the temporal decay index α and the spectral index β should satisfy $\alpha = 2 + \beta$ [32]. In order to accommodate the data, additional effects (e.g. shifting the time zero point to the last pulse in the prompt emission or the X-ray flare, subtracting the underlying forward shock component, etc.) are needed [30]. Alternatively, the steep decay may be also a result of the central engine activity [30]. This distinct component suggests that the GRB prompt emission (and the X-ray flare emission) originate from a different location than that of the afterglow, i.e. likely at an internal radius within the deceleration radius [34]. The large contrast between the prompt emission component and the afterglow component (connected with the steep decay component) also suggests a very high gamma-ray emission efficiency [30].

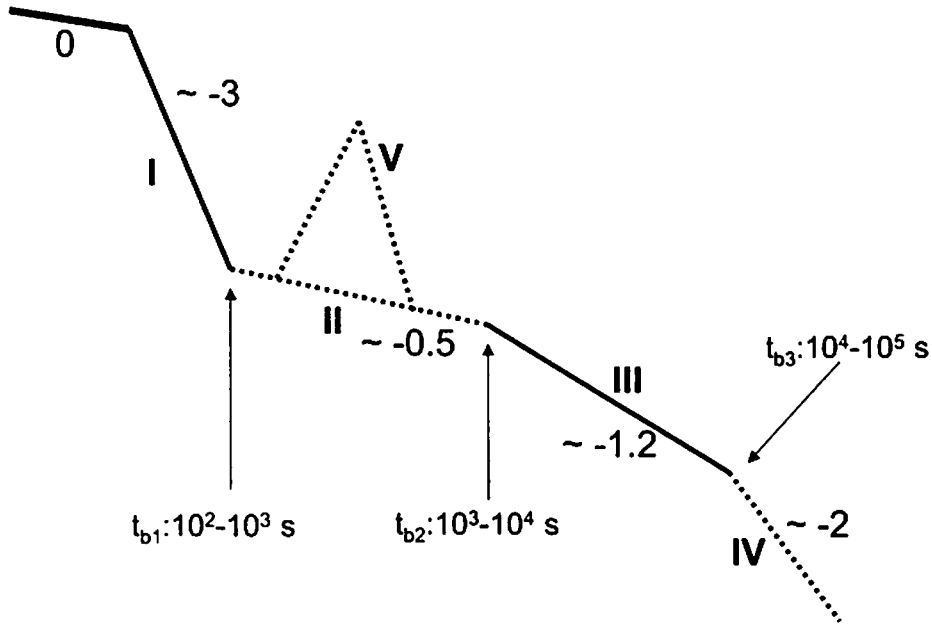

Figure 1: A synthetic cartoon X-ray light-curve based on the observational data from Swift XRT. The phase "0" denotes the prompt emission. Four power law light-curve segments together with a flaring component are identified in the afterglow phase. The segments I and III are most common. Other three components are only observed in a fraction of bursts. Typical temporal indexes in the four segments are indicated in the figure. The spectral indexes remain unchanged for segments II, III and IV. The segment I sometimes has a softer spectrum. From [30].

Shallow-than-normal decay. In a good fraction of the Swift bursts, the decay slope in the afterglow phase after the steep tail emission ends is shallower than what is expected in the standard afterglow model with a constant energy. The total energy in the fireball needs to increase with time, so that the fireball is continuously refreshed for a much longer time than the burst duration [30]. This corresponds to Segment II in Fig.1. There are three physical possibilities that could give rise to such a refreshed shock. 1. The central engine keeps pumping energy with a reduced rate. 2. The energy injection from the central engine is brief but the ejecta have a wide range of Lorentz factors with a power-law distribution. 3. The outflow is Poynting-flux-dominated, so that the magnetic field takes a longer time to be transferred into the medium [35].

X-ray flares. X-ray flares are detected in nearly half of the Swift GRBs [33]. Although a weak flare may be interpreted as the synchrotron self Compton emission in the reverse shock region [36] under well balanced conditions, the general properties of the flares (e.g. the large amplitude in GRB 050502B, rapid rising and falling lightcurves, more than one flares in one burst) strongly suggest that the correct mechanism is the late central engine activity [30, 33]. Even more surprisingly, after the breakthrough of localizing short, hard GRBs and building a close link between the short bursts and the compact star merger models, extensive X-ray flares are discovered in the short burst GRB 050724 [9]. The observed late central engine activity (> few hundred sec) pose great challenge to the merger modelers.

5 Conclusions

With the current abundant early afterglow data collected by Swift and other ground-based optical telescopes, it is now evident that the GRB early afterglow phase is more complicated than what one could imagine in the pre-Swift era. The simplest reverse + forward shock picture, although applicable in the interpretations, is inconclusive. With the current Swift detection rate of one short burst per 2-3 months, the sample will quickly increase and it will enable us to carry out more detailed studies for short burst.

References

[1] T. Piran, Physics Reports 314 (1999) 575.

[2] T. Piran, Physics Reports 333 (2000) 529.

[3] B. Zhang and P. Mészáros, Int. J. Mod. Phys. A 19 (2004) 2385.

[4] N. Gehrels et al., ApJ 611 (2004) 1005

[5] C. Kouveliotou et al., ApJ 413 (1993) L101.

[6] T.J. Galama et al., Nature 395 (1998) 670.

[7] K.Z. Stanek et al., ApJ 591 (2003) L17.

[8] N. Gehrels et al., Nature 437 (2005) 851.

[9] S.D. Barthelmy et al., Nature 438 (2005) 994.

[10] J.S. Villasenor et al.,Nature 437 (2005) 855.

[11] E. Berger et al., Nature 438 (2005) 988.

[12] D. Fox et al., Nature 437 (2005) 845.

[13] Eichler, Livio, Piran and Schramm, Nature 340 (1890) 126.

[14] B. Paczyński, AcA 41 (1991) 257.

[15] T. Totani, ApJ 486 (1997) L71.

[16] D.Q.Lamb and D.E. Reichart, ApJ 536 (2000) 1.

[17] V. Bromm and A. Loeb, ApJ 575 (2002) 111.

[18] N. Kawai et al., submitted to Nature, astro-ph/0512052.

[19] J. Haislip et al., submitted to Nature, astro-ph/0509660.

[20] G. Cusumano et al., submitted to Nature, astro-ph/0509737.

[21] M.I.Andersen et al. A&A 364 (2000) L54.

[22] M.Boer et al. submitted to Nature, astro-ph/0510381.

[23] C.W. Akerlof et al., Nature 398 (1999) 400.

[24] P. Mészáros and M. Rees, ApJ 482 (1997) L29.

[25] R. Sari T. Piran, ApJ 517 (1999) L109.

[26] S. Kobayashi, ApJ 545 (2000) 807.

[27] Zhang, Kobayashi and Mészáros, ApJ 595 (2003) 950.

[28] G. Chincarini et al., submitted to ApJ, astro-ph/0506453.

[29] J. A. Nousek et al., submitted to ApJ, astro-ph/0508332.

[30] B.Zhang et al. 2005. ApJ in press, astro-ph/0508321.

[31] G.Tagliaferri, Nature 436 (2005) 985.

[32] P. Kumar and A. Panaitescu, ApJ 541 (2000) L51.

[33] D.N.Burrows et al. Science 309 (2005) 1833.

[34] M.J. Rees and P. Mészáros, ApJ 430 (1998) L93.

[35] B. Zhang and S. Kobayashi ApJ 628 (2005) 315.

[36] S. Kobayashi et al. submitted to ApJ, astro-ph/0506157.

Verification of some progenitors models of Gamma-Ray Bursts by means of numerical simulations

Miguel A. Aloy[1]

Max-Planck-Institut für Astrophysik, Postfach 1317, D-85741 Garching, Germany
Departamento de Astronomía y Astrofísica, Universidad de Valencia, 46100 Burjassot, Spain

Abstract

In this paper I briefly summarize the observational data which reveals physical properties of the systems that have been postulated as progenitors of both short or long gamma-ray bursts (GRBs). Some of these progenitor models (specifically, collapsars and mergers of compact binary systems) have been verified by means of numerical simulations with different degrees of complexity and physical realism. These simulations provide some quantitative estimates of generic properties of the relativistic outflows leading to GRBs which can (in some cases) be compared with the available observational data. Ideally, from such a comparison it might be possible to disentangle which progenitor models are best suited to reproduce the observed phenomenology.

1 Introduction

After almost 40 years since Gamma-ray bursts (GRBs) were discovered by the Vela military satellites, we still do not have conclusive observations that allow us to settle the fundamental question of what is the origin of these intriguing phenomena. More precisely, observations have not undoubtedly clarified yet which astrophysical systems are the central engines of GRBs. These observations have provided a huge amount of information about the prompt GRB phase and also about the *afterglow* emission that follows the γ-ray emission. A lot of progress has been done in the subgroup of long-soft GRBs (which last more than 2 s and have a soft spectrum). The association of this class of GRBs with supernovae (SN) of type Ib/c has been assumed by the scientific community after the emergence (as theoretically expected) of the spectroscopic signatures of SN 2003dh during the cooling down of the afterglow of GRB 030329 (e.g., [111]). Regarding the progenitors of short GRBs (lasting less than 2 s and having a hard spectrum), much less it is know. The main reasons being that its detection has fallen in the limit of the sensitivity of BATSE and that due to their short duration it was impossible to detect their associated afterglows. Nevertheless, the advent of the satellites HETE-II and Swift has changed this situation. In the last year, afterglows of 5 short GRBs have been followed (GRB 050509b, [37]; GRB 050709, [17]; GRB 050724, [47]; GRB 050813, [99], GRB 051221 [109]).

In this work I review the relevant observational properties that may restrict the nature of the progenitor systems of GRBs (Sect. 2). Furthermore, I will show which are the most widely accepted theoretical models to account for the central engines of GRBs (Sect. 3). Specially emphasis will be made on the numerical verification of some of the previously presented theoretical models (Sect. 4). I will conclude with some general remarks in Sect. 5. The aim of this paper is not to present a detailed review of the properties of these sudden episodes of high energy gamma-radiation which can be found in, e.g., the recent works of Mészáros [59] or Piran [80] and in this proceedings (contribution of S. Kobayashi).

2 What do observations tell about the progenitors of GRBs?

Most of the information provided by observations yields indirect evidence about the nature of the inner engines powering GRBs. While for long GRBs there is a huge amount of very precise observations, for short GRBs the statistics is still too poor to extract firm conclusions. Therefore, in the next sections I will consider separately the cases of long and short GRBs.

[1]E-mail:Miguel.A.Aloy@uv.es

2.1 Progenitors of long GRBs

There is an overwhelming amount of evidence linking long GRBs with star forming regions and also some indications that GRBs follow the star formation rate [80]. These hints suggest that long GRBs are associated with the death of massive stars, i.e., with SN explosions [75]. A necessary (but not sufficient) condition for GRBs to be produced in the course of SN Ib/c explosions (or arising from the same kind of progenitors) is that the intrinsic rate of the latter must be larger or, at least, equal than the intrinsic rate of GRBs. The estimates about intrinsic local rates of SNe and (particularly) of GRBs include rather large uncertainties. For SN Ib/c, the local rate is $\sim 2 \times 10^4\,\mathrm{Gpc^{-3}\,y^{-1}}$ [16]. On the other hand, direct estimates from the sample of GRBs with known redshifts are polluted by observational biases and are insufficient to determine the rate and luminosity functions (see, e.g., [69]). Therefore, alternative procedures based on the assumption that long GRBs follow the star formation history have been developed. For example, Guetta, Piran & Waxman [35] estimate a local rate of long GRBs $\sim 0.16 - 0.44\,\mathrm{Gpc^{-3}\,y^{-1}}$, depending on the star formation rate considered. This value is calculated assuming that burst are isotropic. When beaming is taken into account a *true* rate of $\sim 33 \pm 11\,\mathrm{Gpc^{-3}\,y^{-1}}$ is obtained [35]. By inspection of the two rates it becomes clear that (i) there are about 1000 times more SNe Ib/c than long GRBs and (ii) only an small fraction of all SN Ib/c may yield associated GRBs. This means that those SN I/bc which yield GRBs must have some peculiarities like, e.g., they go off in binary systems, they host specially large magnetic fields, or perhaps they have the appropriate amount of specific angular momentum (e.g., in case of *collapsars*; [122]).

The most direct connection between long GRBs and supernovae are the associations of both events either photometrically or, more convincingly, spectroscopically. Historically, the first observational association was made for the peculiar type Ib/c SN 1998bw located in the nearby ($z = 0.0085$) galaxy ESO184-G82 which was found within the error-box of GRB 980425 and [30]. SN 1998bw was unusually bright, with a kinetic energy ($\sim 2 \times 10^{52}\,\mathrm{erg}$) much larger than any other previously observed supernova [38], and with a radio component expanding at velocities $\sim 0.3c$ ([48]; c begin the speed of light). GRB 980425, with SN 1998bw, showed also unusual properties: an smooth light curve, a lack of high energy component in its spectrum, and a very low isotropic equivalent energy ($\sim 10^{48}\,\mathrm{erg}$). The fact that GRB 980425 and SN 1998bw went off almost simultaneously and at consistent spatial locations (within the instrumental error boxes), was not initially considered as a definitive proof of the SN/GRB association. However, the analysis of the XMM data taken in March 2002 [79] (more precise than that obtained with BeoppoSAX; [78]) and the discovery of other SN/GRB associations in the meantime, have strengthen the case for the validity of the SN 1998bw/GRB 980425 association.

In 2003 was found the first spectroscopic confirmation of the association of a long GRB with a SN. Indeed, the association SN 2003dh/GRB 030329 is considered for most of the scientific community as a conclusive link between SNe and long GRBs. The characteristic spectral signatures of SN 2003dh popped up a few days after the detection of the very bright GRB 030329 ($z = 0.168$) [36, 111]. A number of broad spectral lines (resembling bumps) appeared in the power-law continuum ($F_\nu \propto \nu^{-0.9}$) of the GRB afterglow 9.64 days after the GRB took place. The spectral shapes of SN 2003dh and SN 1998bw are very similar and, according to Matheson et al. [56] or Mazzali et al. [58], at all epochs the best fit to the spectra of SN 2003dh is given by that of SN 1998bw at nearly the same evolutionary epoch. From the delay in the appearance of the SN bump, one can infer that the GRB took place either simultaneously or just before the SN explosion. This evidence argues against a *supranova* interpretation of the phenomenon (see Sect. 3).

In the late (10 to 30 days) lightcurve of detailed afterglow observations a series of late red bumps have been discovered (e.g., [11, 87, 12, 31]). In these red bumps the afterglow re-brightens and the spectrum becomes reader. These features have been interpreted in different ways. Bloom et al. [11] assumes that they are signatures of an underlying supernova. Esin and Blandford [22] suggest that the bumps are produced by light echoes on surrounding dust. Finally, Waxman and Draine [118] considered an alternative explanation based on dust sublimation. However, according to Bloom [14], from the comparison of the upper limit to the magnitude of the bump in the light curve with the maximal magnitudes of type Ib/c SNe, it is rather plausible that SNe could accompany all long GRBs.

Another line of evidence of the association of GRBs with SNe is the appearance of iron X-ray lines. The Fe X-ray lines appear to be emitted by matter at very low velocities and at rather large distances. A supranova model [116] can easily explain them (see Sect. 3) but hardly compatible with SNe being

simultaneous with their accompanying GRBs as suggested by the detection of red bumps in the light curve (see above). A number of alternative interpretations of the Fe X-ray lines which do not need of a supranova model for the inner engine can be found in the references [86, 61, 49].

From the study of the properties of the host galaxies where long GRBs are produced, it is possible to obtain additional hints about the nature of their central engines. It was suggested at the end of the nineties that GRBs follow the star formation rate (e.g., [113, 119, 75]). This suggestions are supported by the fact that both the magnitude and the redshift distribution of GRB host galaxies are typical for normal, faint field galaxies as well as their morphologies (e.g., [71, 19, 13]). However, it is a matter of debate which is the prototype GRB host galaxy. Some researchers have the opinion that GRB hosts are not distinguishable from normal field galaxies with similar magnitudes and redshifts [110, 13], while others claim that they are blue and strongly star-forming galaxies [27]. Le Floc'h [51] also agrees with the latter argument and additionally points out that GRB hosts may be of low metallicity and luminosity. Perhaps, this feature distinguishes GRB host galaxies from typical star-forming galaxies, which are luminous, red, and full of dust starbursts [52]. However, this difference might arise due to an observational bias because the afterglow of GRBs that originate in dust-enshrouded starbursts are obscured (*dark* GRBs).

Observations also tell us that the locus of GRB generation sites within the galaxies follows the light distribution of the hosts [13]. As the light distribution is roughly proportional to the density of star formation, this is another evidence favoring the argument that GRBs follow the star formation rate. Furthermore, using observations in the centimeter and sumillimeter range it turned out that GRB host galaxies have a vigorous star formation rate SFR$\sim 10^3 M_\odot\,y^{-1}$ [8, 24]. Finally, Fynbo et al. [28, 29] found that GRB host galaxies show Lyman-alpha emission, which is in agreement with GRB hosts being active star forming and having moderate metallicity.

2.2 Progenitors of short GRBs

Progenitors of short GRBs are much less well know than those of long GRBs. The most accepted central engines of these kind of events are mergers of two neutron stars (NSs) or a neutron star and a black hole (BH) (e.g., [10, 73, 32, 21, 66]). As for the case of long GRBs the minimum consistency check demands that the rate of this type of mergers must be larger or equal than that of short GRBs. Considering NS+NS mergers alone (the rate of NS+BH mergers is comparable), Kalogera et al. [42] estimate a local rate of $\sim 800\,\mathrm{Gpc^{-3}\,y^{-1}}$. On the other hand, the local rate of short GRBs is $\sim 0.11 - 0.8\,\mathrm{Gpc^{-3}\,y^{-1}}$ [34], assuming that these events release energy isotropically. Including beaming corrections is almost impossible because we lack of sufficiently firm values of the typical opening angle of short GRBs. In case every merger would yield a short GRB, Guetta & Piran [34] estimate that the typical jet opening angle would be $\sim 1.6°$. However, these extremely small values of the opening angle may grow if only a fraction of the mergers, namely, e.g., those having the appropriate magnetic fields, or accretion disk mass, may produce accompanying short GRBs.

Fortunately, during the last year the afterglows of 5 short GRBs have been detected (see § 1). These observations have allowed us to settle that short GRBs are also located at cosmological distances ($z \gtrsim 0.1$) and that have equivalent isotropic energies of about $\gtrsim 10^{49}$erg. Comparing these data with the corresponding to long GRBs, it is clear that short GRBs release about 100 to 1000 times less energy than long ones and that this smaller energetic content can be the reason for not detecting them at average redshifts comparable with those of long GRBs. Furthermore, the discovery of these 5 bursts has provided a (still poor) statistical information about the host galaxies of short GRBs and, in its turn, about the likelihood of some progenitor models. Fox et al. [23] and Prochaska et al. [82] assert that short GRBs take place both in star-forming and in elliptic (old) galaxies, with star formation rates $\sim 0.01 - 0.5 M_\odot\,y^{-1}$, i.e., much smaller than the SFR of long GRBs (§2.1). This fact is roughly consistent with short GRBs being generated by NS+NS/BH mergers if one accepts that there exist *fast* evolutionary tracks to produce mergers [7, 77] and, hence, there may be a broad range of lifetimes ($\sim$several gigayears) for the progenitor systems. Indeed, there are some reliable evidences that some short GRBs are not associated with bright SNe (GRB 050509b, [37]; GRB 050709, [23]; GRB 051221, [109]). Additionally, short GRBs are localized in many cases in the outer regions of their host galaxies. This is specially true when suitable detection error-boxes have been obtained in observations [82]. This suggests that short GRBs do not follow the distribution of light within the galaxy and, therefore, many of them are not associated with massive-star

forming regions. Indeed, the location of short GRBs with respect to their host galaxies is compatible with the kicks delivered to NS binary systems during their birth [23]. So far, the measure of opening angles through the breaks in the afterglow light curve is not sufficiently precise (in my opinion) to make conclusive assessments about the typical opening angles of short GRBs (but see, e.g., [23, 109]). However, there are indications that short GRBs display opening angles of $\sim 10^o$.

2.3 Requested properties of progenitors of GRBs

In the following I will show some of the most likely progenitor systems that have been proposed by theorists. These models have to be consistent with a number of observational restrictions. First, the inner engine has to be able to release $\sim 10^{51}$ erg ($\sim 10^{49}$ erg) in case of long (short) GRBs in the form of thermal energy or Poynting flux. Such energy should be imparted on a mass $\sim 10^{-7}M_\odot$ or $\sim 10^{-5}M_\odot$ in case of progenitors of short or long GRBs, respectively, in order to reach ultrarelativistic speeds, i.e., Lorentz factors $\Gamma \gtrsim 100$. The outflows have to be collimated in angles $1^o < \theta < 20^o$. The progenitor systems should be able of producing GRBs at rates consistent with observations (see § 2.1 and 2.2). In case that the duration of the GRB reflects the time over which the central engine is active, t_a (but see below and [4]), the central energy source should remain active during the typical duration of a GRB. In case of long GRBs, $t_a \sim 2 - 100$ s which requires engines keeping a prolonged activity, while for short GRBs $t_a \sim 0.1 - 2$ s. Finally, the structure produced by the central engine should be able to develop variability down to the millisecond scale (which is a clue linking the progenitors of GRBs with compact objects).

With this properties in mind, the most suggestive theoretical scenario for the generation of GRBs involves the accretion of a massive ($\gtrsim 0.05M_\odot$) disk onto a compact object, most likely a newborn stellar-mass BH. Both the accretion disk and the BH are created simultaneously and there is some consensus on the fact that GRBs are a signature of the formation of a BH. A non-exhaustive classification of different progenitor models is given in the next sections.

3 Theoretical mechanisms powering the central engine of GRB progenitors

All the mechanisms that will be shown here include a central compact object and they are mostly differentiated by whether or not magnetic fields play a fundamental role in the process of generation or acceleration of the outflow or by the necessity of involving accretion as a primary energy source of the engine.

3.1 Hydromagnetic models

Under this classification I consider mechanisms that operate on a thick accretion disk (eventually magnetized) which surrounds a $\sim 1 - 3M_\odot$ BH. Among the possible scenarios which could yield this kind of system we find mergers of binaries like, e.g., NS+NS [73, 32, 21, 66], NS+BH [74] WD-BH [26], BH-He-star [25], as well as models based on *failed supernovae* or *collapsars* [122, 75, 54, 2]. Among these models collapsars and NS+NS/BH mergers are the preferred systems to produce long and short GRBs, respectively. The reason being that the duration of the accretion and its efficiency depends on the size of the disk [68]. NS+NS/BH mergers can host hyper-accreting disks with moderate sizes and masses ($\sim 0.01M_\odot - 0.1M_\odot$ [92, 100]). On the other hand, in order to obtain prolonged episodes of efficient accretion ($\gtrsim 10$ s) the collapsar model proposes the existence of a relatively small disk ($\sim 0.1M_\odot$) which is constantly refilled from the star envelope in which it is embedded.

In the collapsar model devised by Woosley [122] a GRB arises from the collapse to a BH (either directly or during the accretion phase that follows the core collapse) of the iron core of a massive ($\sim 30M_\odot$), rapidly rotating, Wolf-Rayet star which has lost its hydrogen envelope because of the occurrence of a stellar wind or the interaction with a companion. In case there exists an appropriate amount of specific angular momentum, an accretion disk ($\sim 0.1M_\odot$) is formed together with a funnel along the rotation axis. Accretion of the disk onto the BH can last up to few minutes because as the disk is depleted new

stellar matter refills it. The accretion energy, which can be used to power a GRB, is tapped by means of $\nu\bar{\nu}$-annihilation [54] or a hydromagnetic of electrodynamic mechanism (see below). The energy deposited in vicinity of the accretion disk leaks out along the direction of minimum resistance, i.e., the funnel along the rotation axis where the density can be $\sim 10^6$ times smaller than in the disk and the stellar material has relatively little rotational support. The funnel acts as a collimator and the resulting outflow has a jet-like shape with opening angles $\gtrsim 10^o$. An important point of the collapsar model is that one naturally expects a supernova bump on the afterglow light curve. On the other hand, within this model it is difficult to explain how the iron needed for the Fe-X-ray lines reaches the implied large distances from the center.

In the supranova model [116] a GRB takes place when a *supramassive*, NS formed in the course of a SN explosion (which may be more energetic than an average one), collapses to a BH. The collapse can occur if the supramassive NS (i) losses angular momentum via a pulsar wind, (ii) cools down, or (iii) accretes slowly matter from a surrounding accretion disk [117]. In this model the GRB is also fueled by the accretion onto a newborn BH. Whichever is the mechanism of collapse there might be a long time delay between the SN and the GRB, which goes off a few weeks or months afterwards, when the supramassive NS collapses. Such long time delays are incompatible with the detection of SN signatures a few days after the GRB, unless there is a variety of supranova types, with a distribution of time delays between the first collapse to a supramassive NS and the second one to a BH. An additional problem of the supranova model is that the accretion disk should be rather large and, thereby, rather inefficient [68] in order to yield a long lived central engine. In the supranova model the explanation of the Fe-X-ray lines at large distances from the BH is easy because they result from the interaction of the GRB with the SN-shell ejected few weeks or months before.

For short GRBs, the most likely progenitor systems are those arising from the merger of two compact objects, i.e., NS+NS [21, 73, 32, 67, 66, 44, 96, 92] or NS+BH [74, 39, 50]. These mergers also produce a BH – accretion disk system. Mergers take place because of the emission of gravitational radiation during periods of time that vary from 10^5 y to several 10^8 y, depending on the initial distance of the progenitors and the existence of fast evolutionary tracks of the progenitor stars (see § 2.2). Due to the large interval spanned by the life times of this kind of systems the natal kick that is presumably imprinted on the merger [67, 15] may or may not [6] take them outside of their host galaxies. This is relevant to account for the offsets with respect to the galactic center at which short GRBs are detected (§ 2.2).

3.2 Electrodynamic

As an alternative to the BH – accretion disk central engine, one finds purely electrodynamic mechanisms. In such models, the inertia of matter is negligible and the electromagnetic field is able of extracting very efficiently the rotational energy of the BH [9]. This mechanism may operate in any system where a rotating BH is immersed in a monopole magnetosphere. Therefore, it can be at work in collapsars, supranovas or mergers of compact objects. However, some authors [120] claim that this process might not operate and/or other general relativistic processes, like e.g., the Penrose mechanism may be the primary source of high energy, collimated particles fueling GRBs [120]. Nevertheless, this is a matter of on going controversial debate [46] which is beyond the scope to this paper.

3.3 Pulsar-like

Usov [114] proposed that GRBs may be produced during the formation of rapidly rotating, highly magnetized ($B \sim 10^{15}$ G) NSs. In these objects, rotational and/or magnetic energy (a few 10^{51} erg) can be lost in scales of seconds in a pulsar-like mechanism which would produced a Poynting flux dominated flow. Usov [115] and Thompson [112] pointed out that the γ-radiation appears via plasma instabilities when the MHD approximation of the pulsar wind breaks out at distances $\sim 10^{13}$ cm. Other pulsar-like central engines have been discussed by, e.g., Katz [43] or Mészáros and Rees [60].

4 Numerical verification of some theoretical models

Some of the hydromagnetic models summarized in the previous section have been further verified by means of numerical simulations. Such simulations have started to provide preliminary quantitative answers to several key questions in the framework of progenitors of GRBs. In the following, I will focus on the numerical verification of the collapsar model and of the merger model for long and short GRBs, respectively.

MacFadyen and Woosley [54] initiated a series of calculations where the key question to answer was whether or not a collimated relativistic outflow (a jet) could be generated [2, 83, 64, 65] and could be able to penetrate the stellar envelope and produce a GRB [2, 55, 123, 124]. All these works have provided preliminar, partial, positive answers to this fundamental points. However, their degree of realism (regarding the elements included in the simulations) is quite different. On the one hand, the pioneering work of MacFadyen & Woosley included a realistic equation of state (EoS) and the self-gravity of the star but modeled the dynamics with a relatively poor numerical resolution and a Newtonian, axisymmetric, hydrodynamics code. Improving on the same model, Aloy et al. [2] employed a simplified EoS but a more appropriate general relativistic hydrodynamics code [1] where the gravitational support was included by introducing an actual BH in the simulations. Dynamically relevant magnetic fields have been included in the simulations of hydromagnetic generation of jets in collapsars, either assuming Newtonian resistive magnetohydrodynamics (MHD) and a realistic EoS [83] or general relativistic ideal magnetohydrodynamics (GRMHD) and using polytropic EoS [64, 65]. It is important to note that the approaches of Proga et al. and Mizuno et al. differ also in the numerical treatment of the constraint $\nabla \cdot \mathbf{B} = 0$. While Proga et al. [83] uses a constraint transport scheme, the simulations of Mizuno et al. [64, 65] could be handicapped because they do not include any algorithm to control the aforementioned constraint.

Despite of the different degrees of sophistication and physical realism in the numerical modeling, numerical simulations have allowed to verify the collapsar model as well as have pointed out a number of qualitative and quantitative features of the outflows:

- The outflows are highly variable due to Kelvin-Helmholtz [2, 33] or shear-driven instabilities [3]. Despite the presence of instabilities, the outflows are not disrupted even in three-dimensional simulations [124]. These instabilities impose an *extrinsic* (i.e., not produced by the source of energy) variability which can be the source of internal shocks at much larger distances, when the jet becomes transparent. The extrinsic variability might be indistinguishable from the one imposed by the variability of the energy source (*intrinsic*). This makes it very complex to find intrinsic properties of the progenitor by inspection of the variability of the GRB light curve.

- The generated jets show a transverse structure consisting of an ultrarelativistic spine ($\Gamma \sim 50$) endowed by a moderately relativistic, hot shear layer ($\Gamma \sim 5 - 10$; [2]).

- The jet break out through the stellar surface and its interaction with the stellar wind could lead to some thermal precursor activity [123] that has been observed in several GRBs [75].

- The cocoon transports a sizeable fraction of the energy and could yield γ-ray/hard X-ray transients when it is erupted from the star surface [123].

- Jets are initially collimated by the thick accretion disk (they move along the least resistance direction, namely, the funnel along the rotation axis) and afterwards inertially confined by the stellar mantle [2] and break out the star surface with half-opening angles of $\theta_b < 5^o$. This numerical result was also shown analytically to occur by Mészáros & Rees [61]. Zhang et al. [123], additionally, performed a parametric study of the influence of the initiation half-opening angle of the jet and found that even starting with half-opening angles up to $\sim 20^o$ the jet breaks out the star surface with (time varying) half-opening angles of $\sim 5^o$.

- Independent on whether the jet is generated by a thermal energy release [54, 2] or directly induced as a boundary condition [123], jets become rather hot, i.e, most of the jet energy is internal and not kinetic during the initial phases of jet propagation. As the jet escapes, the conversion of its

internal energy into kinetic energy may boost the outflow to terminal Lorentz factors along the axis of ~ 150, as required by the standard fireball paradigm of GRBs.

The numerical study of the merger of 2 NSs as they loose energy due to gravitational radiation is a formidable task that optimally involves three-dimensional GRMHD, detailed neutrino physics (and transport), nuclear reactions (the mergers can have the appropriate conditions to synthesize r-process elements; [21]) and non ideal physics (viscosity, reconnection, resistivity). A number of authors have addressed the merger problem with different degrees of sophistication and focusing on different physical aspects. For example, the earlier simulations of mergers focused on the gravitational wave emission using Newtonian hydrodynamics (HD), a polytropic EoS, including the gravitational radiation back reaction and finite volume methods [72, 102] or SPH techniques [84, 85, 18]. In some of those works different aspects of the problem of generation of GRBs where also discussed, e.g., using a realistic EoS and Newtonian SPH [88, 89, 5, 90] or with finite volume codes including neutrino emission [40, 95, 91, 92, 93, 100, 50]. These simulations performed a number of parametric studies where different initial spin axis and mass rations of the NSs and different estimates of the effects of neutrino cooling where included. In the meantime, the influence of GR effects has also been addressed with several degrees of physical realism, e.g., employing a polytropic EoS, post-Newtonian HD and SPH [5] or finite volume techniques [103], or including special formulations of the full Einstein equations assuming the so called conformal flatness condition (CFC) and finite volume HD [121, 57], SPH and a realistic EoS [70], full GRHD assuming either a polytropic EoS [104, 106, 105, 62, 20] or realistic EoS [107], or even very recently, GRMHD [108]. A common result of most of the mentioned works is that the merger results in a BH - accretion disk system. The mass of the accretion disk is of the order of a few $0.01 M_\odot$ to some $\sim 0.1 M_\odot$ and it depends, on the orientation of the spins, the relative masses of the two neutron stars, the (α-)viscosity included in the disk and the treatment of the GR dynamics (full GRHD simulations seem to yield somewhat smaller disk masses as their Newtonian or post-Newtonian counterparts [107]). The amount of energy the merger is able to release depends on the mechanism of energy extraction. Up to $\sim 5 \times 10^{53}$ erg are released in the form of low energy neutrinos and gravitational waves. The fraction of that energy deposited on the baryons due to $\nu + \bar{\nu} \rightarrow e^+ + e^- \rightarrow \gamma + \gamma$ in the outer layers of the thick accretion torus and in the halo surrounding the merger[2] is rather small $\sim 10^{-3} - 10^{-4}$ [21, 41]. However, some authors pointed out that up to a few 10^{51} erg of energy can be released above the poles of the BH in a region that contains a very small baryonic mass [39]. This amount is enough to power a short GRB according to the recent observational data about the typical energy a short GRB carries along (§ 2.2), even if the efficiency of the process of $\nu\bar{\nu}$-annihilation is as small as calculated by Jaroszynski [41]. Nevertheless, the merger scenario has the problem that the accretion disk is swallowed by the BH at hypercritical rates ($\gtrsim 1 M_\odot\,\mathrm{s}^{-1}$) and, therefore, it may efficiently fuel a GRB up to times of a few 0.1 s, while the longest short GRBs may last up to 2 s.

Most of the aforementioned simulations either did not include a consistent treatment of the microphysics (namely, of the neutrino transport) or, if they did it, the evolution of the system was not followed for sufficiently long time to produce a GRB or general relativistic effects where absent of the model. Aloy et al. [4] try for the first time to validate the merger scenario as potential progenitor of short GRBs by means of GRHD simulations. They assume that the disk is formed after the merger of a system of compact binaries and that there is a thermal energy release in the system (e.g., by $\nu\bar{\nu}$ annihilating preferentially around the axis). The disk is assumed to be a non-selfgravitating relativistic perfect fluid and the gravitational field binding it is provided by a central Schwarzschild BH. The EoS includes a non-degenerate, Boltzman gas of nucleons along with e^+e^--pairs and radiation. The main findings of Aloy et al. [4] can be summarized as follows:

- Releasing energy over the poles of the BH at rates above $\sim 10^{48}\,\mathrm{erg\,s}^{-1}$ with a functional dependence suggested by Janka et al. [39], relativistic ($\Gamma_{\max} \sim 1000$), collimated conical/jet-like, outflows are produced.

- The outflow structure is heterogeneous both in the radial and in the angular directions due to the growth of Kelvin-Helmholtz instabilities. The lateral structure of the outflow displays qualitative resemblances with that produced in relativistic jets penetrating collapsars, namely it shows a ultrarelativistic core ($\Gamma > 100$) surrounded by a relativistic ($10 < \Gamma < 100$), expanding layer.

[2]This halo is produced by matter with a large specific angular momentum which is ejected away from the disk.

- The collimation of the outflow is produced by its interaction with the accretion torus (on the first place) and, in some cases also with the external medium (i.e., with the merger halo). The analytic estimates of Levinson & Eichler [53] for the collimation mechanism yields wrong results. The typical half-opening angles are $\theta \sim 5^o - 20^o$, depending on the model and also slightly on the criterion used to measure the lateral size of the outflow.

- Taking for granted these half-opening angles, an observed rate of $100\,\mathrm{y}^{-1}$ short GRBs needs of $\sim 10^{-5}\,\mathrm{galaxy}^{-1}\,\mathrm{y}^{-1}$ short GRB events, which is smaller than the estimated NS+NS/BH merger rates. This implies that not every merger must necessary produce a short GRB. This assumption is backed up by the fact that from the simulations of Aloy et al. [4] mergers that develop high-density halos won't yield successful GRB events. In such a case, the observational signature may be a thermal UV-flash ($T \sim 5 \times 10^4\,\mathrm{K}$) with very low luminosity ($L \sim 10^{43}\,\mathrm{erg\,s}^{-1}$) and durations of $\sim 1000\,\mathrm{s}$.

- After switching off the energy release the relativistic jet evolves like an expanding conical-shaped shell. This shell stretches radially due to the different velocities of propagation of its front and of its rear edges. As a result of this stretching the duration of the associated GRB event can be substantially larger than the time during which the central engine is active (t_a).

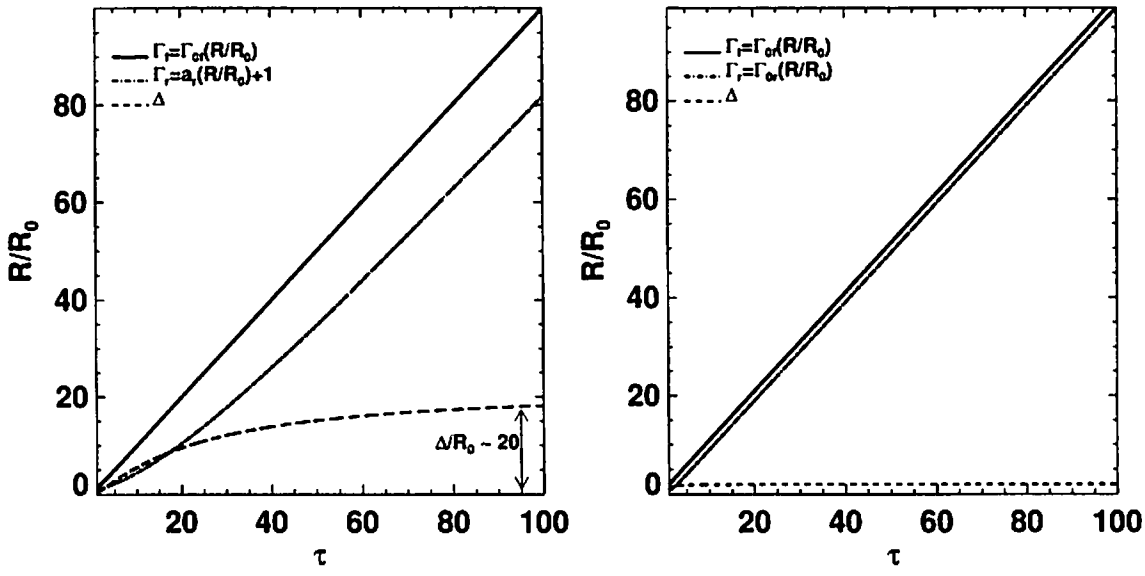

Figure 1: On the left panel: evolution of a relativistic shell that stretches as a result of different acceleration laws of its forward (solid line) and its rear (dashed-dotted line) radial edges as a function of the dimensionless time $\tau = ct/R_0$. We choose $R_0 = \Delta_0$, i.e, the initial shell width as produced by the central engine. The acceleration laws of both edges are shown in the figure legends. We take as an example $\Gamma_{0f} = 1$ but the results are almost independent on this parameter. The value of $a_r = 3.5 \times 10^{-2}$ results from a fit of the Lorentz factor of the rear edge of the shell in the simulations of Aloy et al. [4]. The distance between the position of the forward and backward edges, i.e., the shell width Δ is also shown (dashed line). A few light crossing times of the initial shell width are enough to shrink the shell by a factor ~ 20. The shell width saturates after $\tau \sim 50$. On the right panel: evolution of a relativistic shell that does not stretch because it evolves following the standard acceleration law $\Gamma \propto R$ [101]. For this example we have taken $\Gamma_{0f} = 10$ and $\Gamma_{0r} = 1$. After a couple of light crossing times of the initial shell width the size of the shell saturates and becomes $\Delta \simeq \Delta_0$.

The latter point is of particular relevance because it can naturally explain durations of short GRBs up to a few seconds even if the central engine had only fueled it during $t_a \sim 0.1\,\mathrm{s}$. These result is in contrast with the standard fireball theory [101] and deserves some extra explanation. In the model of

Shemi & Piran [101] an homogeneous shell that accelerates with $\Gamma \propto R$ (R being the distance to the central energy source) yields a shell radial size Δ_c when the Lorentz factor saturates, i.e., at the end of the acceleration phase when the shell starts to coast, which is almost the same as the initial shell size Δ_0. As $\Delta_0 \simeq ct_a$, if the duration of a GRB event is $t_{\rm GRB} \simeq \Delta_c/c$, it follows that $t_{\rm GRB} \simeq t_a$. Therefore, the shell can be treated as a *frozen* pulse [101]. In case there is a spread in the Lorentz factor across the shell $\Delta\Gamma$, Piran, Shemi & Narayan [81] obtained that the shell radial size is

$$\Delta(t) = \Delta_c + \Delta\Gamma(t - t_c)/\bar{\Gamma}_f^3,$$

where t_c is the time at which the coasting takes place and $\bar{\Gamma}_f$ is the average Lorentz factor in the shell. As long as $(t - t_c) < \bar{\Gamma}_f^3/\Delta\Gamma$ (which is the case in the GRB phase), $\Delta(t)$ is constant (i.e., a frozen pulse) and *approximately equal* to the radial size of the shell Δ_c at the coasting time. This situation is illustrated in the right panel of Fig. 1. However, Δ_c can be very different from Δ_0 *if* the acceleration process does not exactly follow the linear acceleration assumption of Shemi & Piran [101]. In the simulations of Aloy et al. [4] the leading front of the shell accelerates according to $\Gamma_f \simeq \Gamma_{0f} R/R_0$, R_0 being a fiducial radius from which we measure the position of the leading front. Because of the presence of a rarefaction that trails the shell structure, the rear edge speeds up following a slightly different law $\Gamma_r \simeq 1 + a_r R/R_0$, with $a_r \simeq 4 \times 10^{-2}$ being some constant used to fit approximately the Lorentz factor of the rear edge of the shell in the simulations of Aloy et al. [4]. With such a difference in the motion of the front and of the rear edges the shell shrinks radially and can multiply its original size by a factor of ~ 20 (Fig. 1 left panel), i.e., $\Delta_c \simeq 20\Delta_0$ (taking $R_0 = \Delta_0$). All this stretching takes place during the initial acceleration phase and the shell width saturates after $\tau \equiv tc/R_0 \sim 50$ or, equivalently, $t \sim 50\Delta_0/c$. Under the assumption that the observed duration of the burst is $t_{\rm obs} = \Delta_c/c$ (which is the standard assumption when internal shocks produce the GRB; see type II model of Sari & Piran [98]), we find that $t_{\rm obs} \gg t_a$. In other words, the observed duration of the burst can be (much) larger than the activity time of the central engine. I explicitly point out that this result is not in contradiction with the conclusions of other authors (e.g., [45]) who claim that the burst duration approximately equals the central engine activity time. The reason being that those authors assume that $\Delta_c \simeq \Delta_0$, which is correct under the assumptions outlined above. However, when $\Delta_c \gg \Delta_0$, the burst duration equals the light crossing time of the shell when the fireball reaches the coasting phase (Δ_c/c), which is not equal to the engine activity time.

5 Summary and conclusions

In this work I have briefly summarized the observational data which reveals physical properties of the systems that have been postulated as progenitors of both short and long GRBs. There is an overwhelming amount of evidence that long GRBs are associated with the death of massive starts (SN associations, red bumps, Fe lines, host galaxies, offsets with respect to the center of the host galaxy, etc.). During this year a convincing case is being made to demonstrate that short GRBs are not produced by the same progenitor systems as long GRBs (differentiated types of host galaxies, lack of SN signature, galactic offsets, redshift distribution). So far, associating short GRBs with NS+NS/BH mergers relies only on circumstantial evidence because we have not detected any signal which is unanimously links a merger progenitor system with its accompanying short GRB. In the future perhaps the detection of high energy neutrinos will help us to solve this mystery but, the most important key will be the measure of the gravitational wave signal associated to the merger itself (preceding the GRB pulse).

Some of the proposed progenitor models (specifically, collapsars and NS+NS/BH mergers mergers) have been verified by means of numerical simulations with different degrees of complexity and physical realism. These simulations provide some quantitative estimates of generic properties of the relativistic outflows leading to GRBs which can (in some cases) be compared with the available observational data. Ideally, from such a comparison it might be possible to disentangle which progenitor models are best suited to reproduce the observed phenomenology. The situation is not ideal yet. Numerical simulations are restricted to relatively small physical domains and the detailed properties of the outflows generated in those progenitors have to be extrapolated by several decades in radius. This is necessary because the γ-ray energy is radiated after the fireball becomes transparent at distances $\sim 10^{13} - 10^{14}$ cm, which are much larger than the typical progenitor sizes. Furthermore, the models linking the magnetohydrodynamic

properties of the fireball and the emitted non-thermal radiation are still very rudimentary. That makes the translation of the properties of the simulated fluids into observable properties very rough. Thereby, we are still not in the position of restricting possible progenitor systems from the comparison of numerical simulations with observations. However, some steps are being done in the direction of developing better models coupling a thermal fluid with a non-thermal particle population embedded into it and responsible for the observed emission (e.g., [63]).

Acknowledgements

Stimulating discussions with H.-T Janka and E. Müller are acknowledged. I kindly acknowledge the invitation of the organizers to give a talk in the JGRG15 meeting and their support. MAA is a Ramón y Cajal Fellow of the Spanish Ministry of Education and Science. MAA acknowledges the partial support of the Spanish Ministry of Education and Science (AYA2004-08067-C03-C01).

References

[1] Aloy, M. A., Ibáñez, J. M., Martí, & Müller, E. 1999, ApJSuppl., 122, 151

[2] Aloy, M. A., Müller, E., Ibáñez, J. M., Martí, J. M., & MacFadyen, A. 2000, ApJ, 531, L119

[3] Aloy, M. A., Ibáñez, J. M., Miralles, J. A., & Urpin, V.. 2002, A&A, 396, 693

[4] Aloy, M.A., Janka, H.-Th., & Müller, E. 2005, A&A, 436 273 (AJM05)

[5] Ayal, S., Piran, T., Oechslin, R., Davies, M. B., & Rosswog, S., 2001, ApJ, 550, 846

[6] Belczyński, K., Bulik, T., & Kalogera, V. 2002, ApJ, 571, L47

[7] Belczyński, K., & Kalogera, V. 2001, ApJ, 550, L183

[8] Berger, E., Kulkarni, S. R. & Frail, D. A. 2001, ApJ, 560, 652

[9] Blandford, R. D. & Znajek, R. L. 1977, MNRAS, 179, 433

[10] Blinnikov, S.I., Novikov, I.D., Perevodchikova, T.V., & Polnarev, A.G. 1984, Sov. Ast. Lett., 10, 177

[11] Bloom, J.S., et al. 1999, Nature, 401, 453

[12] Bloom, J.S., et al. 2002, ApJ, 572, L45

[13] Bloom, J.S., Kulkarni, S. R., & Djorgovski, S. G. 2002, Astron. J., 123, 1111

[14] Bloom, J.S. 2005, in *Cosmic explosions, On the 10th aniversary of SN 1993J.* IAU Colloquium 192, eds., J.M. Marcaide and K.W. Weiler. Springer Proceedings in Physics (Berlin), 99, 411

[15] Bulik, T., Belczyński, K., & Zbijewski, W. 1999, MNRAS, 306, 629

[16] Buonanno, A., Sigl, G., Raffelt, G. G., Janka, H.-Th., & Müller, E. 2005, Phys. Rev. D, 72, 084001

[17] Covino, S., et al., 2005, A&A, submitted (astro-ph/0509144)

[18] Davies, M. B., Wenz, W., Piran, T., & Thielemann, F.K. 1994, ApJ, 431, 742

[19] Djorgovski, S.G., et al. 2001, in *Gamma-ray Bursts in the Afterglow Era*, eds. E. Costa, F. Frontera, and J. Hjorth (Springer-Verlag, Berlin), p. 218

[20] Duez, M. D., Marronetti, P., Shapiro, S. L., & Baumgarte, T. W. 2003, PRD, 67, 024004

[21] Eichler, D., Livio, M., Piran, T., & Schramm, D. N. 1989, Nature, 340, 126

[22] Esin, A.A., & Blandford, R. 2000, ApJ, 534, L151

[23] Fox, D. B., et al. 2005, Nature, 437, 845

[24] Frail, D. A., et al. 2002, ApJ, 565, 829

[25] Fryer, C. L., & Woosley, S. E. 1998, ApJ, 502, L9

[26] Fryer, C. L., Woosley, S. E., Herant, M., & Davies, M. B. 1999, ApJ, 520, 650

[27] Fruchter, A. S., et al. 1999, ApJ, 516, 683

[28] Fynbo, J. P. U., et al. 2002, A&A, 388, 425

[29] Fynbo, J. P. U., et al. 2003, A&A, 406, L63

[30] Galama, T. J., et al. 1998, Nature, 395, 670

[31] Garnavich, P.M., et al. 2003, ApJ, 582, 924

[32] Goodman, J. 1986, ApJ, 308, L47

[33] Gómez, E., & Hardee, P. E. 2004, in *Gamma-ray Bursts: 30 years of discovery: Gamma-ray Burst Symposium*, AIP Conf. Proc., eds. E. E. Fenimore and M. Galassi, (Melville, NY), vol. 727, p. 278

[34] Guetta, D., & Piran, T. 2005, A&A, 435, 421

[35] Guetta, D., Piran, T., & Waxman, E. 2005, ApJ, 619, 412

[36] Hjorth, J., et al. 2003, Nature, 423, 847

[37] Hjorth, J., et al. 2005, ApJL, submitted (`astro-ph/0506123`)

[38] Iwamoto, K. et al. 1998, Nature, 395, 672

[39] Janka, H.-T., Eberl, T., Ruffert. M., & Fryer, C. L. 1999, ApJ, 527, L39

[40] Janka, H.-T. & Ruffert, M. 1996, 307, L33

[41] Jaroszynski M. 1996, 305, 839

[42] Kalogera, V., Kim, C., Lorimer, D. R., et al. 2004, ApJ, 601, L179

[43] Katz, J. I. 1997, ApJ, 490, 633

[44] Katz, J. I., & Canel, L. M. 1996, ApJ, 471, 915

[45] Kobayashi, S., Piran, T., & Sari, R. 1999, ApJ, 513, 669

[46] Komissarov, S. S. 2005, MNRAS, 359, 801

[47] Krimm, H., et al. 2005, GCN Circular N. 3667

[48] Kulkarni, S.R. et al. 1998, Nature, 395, 663

[49] Kumar, P., & Narayan, R. 2003, ApJ, 584, 895

[50] Lee, W.H., Ramirez-Ruiz, E., Page, D. 2004, ApJ, 608, L5

[51] Le Floc'h, E., et al. 2003, A&A, 400, 499

[52] Le Floc'h, E. 2004, New Astron. Rev., 48, 601

[53] Levinson, A. & Eichler, D. 2000, PRL, 85, 236

[54] MacFadyen, A. I., & Woosley, S. E. 1999, ApJ, 523, 262

[55] MacFadyen, A. I., Woosley, S. E., & Heger, A. 2001, ApJ, 550, 410

[56] Matheson, T., et al. 2003, ApJ, 599, 394

[57] Mathews, G. J., & Wilson, J. R 1997, ApJ, 482, 929

[58] Mazzali, P. A., et al. 2003, ApJ, 599, L95

[59] Mészáros, P. 2002, Ann. Rev. Astron. Astroph., 40, 137

[60] Mészáros, P., & Rees, M.J. 1997, ApJ, 482, L29

[61] Mészáros, P., & Rees, M.J. 2001, ApJ, 556, L37

[62] Miller, M., Gressman, P., Suen, W.-M. 2004, PRD, 69, 064026

[63] Mimica, P., Aloy, M.A., Müller, E., & Brinkmann, W. 2004, A&A, 418, 947

[64] Mizuno, Y., Yamada, S., Koide, S., & Shibata, K. 2004a, ApJ, 606, 395

[65] Mizuno, Y., Yamada, S., Koide, S., & Shibata, K. 2004b, ApJ, 615, 389

[66] Mochkovitch, R., Hernanz, M., Isern, J., & Martin, X. 1993, Nature, 361, 236

[67] Narayan, R., Paczyński, B., & Piran, T.. 1992, ApJ, 395, L83

[68] Narayan, R., Piran, T., & Kumar, P. 2001, ApJ, 557, 949

[69] Norris, J. P., Marani, G. F., & Bonnell, J. T. 2000, 534, 248

[70] Oechslin, R., Janka, H.-Th. 2005, astro-ph/0507099

[71] Odewahn, S. C., et al. 1998, ApJ, 509, L5

[72] Oohara, K., & Nakamura, T. 1989, Prog. Theor. Phys, 83, 906

[73] Paczyński, B. 1986, ApJ, 308, L43

[74] Paczyński, B. 1991, Acta Astron., 41, 257

[75] Paczyński, B. 1998, ApJ, 494, L45

[76] Penrose, R. 1969, Nuovo Cimento Rivista, NS1, 252

[77] Perna, R., & Belczynski, K. 2002, ApJ, 570, 252

[78] Pian, E., et al. 2004, ApJ, 536, 778

[79] Pian, E., et al. 2004, AdSpR, 34, 2711

[80] Piran, T. 2005, Rev. Mod. Phys., 76, 1143

[81] Piran, T., Shemi, A., & Narayan, R. 1993, MNRAS, 263, 861

[82] Prochaska, J. X., Bloom, J. S., et al. 2005, astro-ph/0510022

[83] Proga, D., MacFadyen, A. I., Armitage, P. J, & Begelman, M. C., ApJ, 599, L5

[84] Rasio, F. A., & Shapiro, S. L. 1992, ApJ, 401, 226

[85] Rasio, F. A., & Shapiro, S. L. 1995, ApJ, 438, 887

[86] Rees, M. J., & Mészáros, P. 2000, ApJ, 545, L73 L41

[87] Reichart, D. E., 1999, ApJ, 521, L111

[88] Rosswog, S., Liebendörfer, M., Thielemann, F.-K., Davies, M. B., Benz, W., & Piran, T. 1999, A&A, 341, 499

[89] Rosswog, S., Davies, M. B., Thielemann, F.-K., & Piran, T. 2000, A&A, 360, 171

[90] Rosswog, S., & Davies, M. B. 2002, MNRAS, 334, 481

[91] Ruffert, M. & Janka, H.-T. 1998, A&A, 338, 535

[92] Ruffert, M. & Janka, H.-T. 1999, A&A, 344, 573

[93] Ruffert, M. & Janka, H.-T. 2001, A&A, 380, 544

[94] Ruffert, M., Janka, H.-T., & Eberl, T. 1999, Astroph. Lett. and Comm., 38, 189

[95] Ruffert, M., Janka, H.-T., & Schäfer, G. 1995, Ap&SS, 231, 423

[96] Ruffert, M., Janka, H.-T., Takahashi, K., & Schäfer, G. 1997, A&A, 319, 122

[97] Ruffert, M., Janka, H.-T., Takahashi, K., & Schäfer, G. 1995, A&A, 319, 122

[98] Sari, R. & Piran, T. 1997, ApJ, 485, 270

[99] Sato, G., et al. 2005, GCN Circular N. 3793

[100] Setiawan, S., Ruffert, M., & Janka, H.-T. 2004, MNRAS, 352, 753

[101] Shemi, A., & Piran, T. 1990, ApJ, 365, L55

[102] Shibata, M., Nakamura, T., & Oohara, K. 1989, Prog. Theor. Phys, 88, 1079

[103] Shibata, M., Oohara, K., & Nakamura, T. 1997, Prog. Theor. Phys, 98, 1081

[104] Shibata, M., Baumgarte, T. W., & Shapiro, S. L. 2000, PRD, 61, 044012

[105] Shibata, M., & Uryū, K. 2002, Prog. Theor, Phys., 107, 265

[106] Shibata, M., Taniguchi, K., & Uryū, K. 2003, PRD, 68, 084020

[107] Shibata, M., Taniguchi, K., & Uryū, K. 2005, PRD, 71, 084021

[108] Shibata, M., & Sekiguchi, Y.-I 2005, PRD, 72, 044014

[109] Soderberg, A. M., Berger, E., et al. 2005, astro-ph/0601455

[110] Sokolov, V. V., et al. 2001, A&A, 372, 438

[111] Stanek, K. Z., et al. 2003, ApJ, 591, L17

[112] Thompson, C. 1994, MNRAS, 270, 480

[113] Totani, T. 1997, ApJ, 486, L71

[114] Usov, V.V. 1992, Nature, 357, 472

[115] Usov, V.V. 1994, MNRAS, 267, 1035

[116] Vietri. M. & Stella, L. 1998, ApJ, 507, L45

[117] Vietri. M. & Stella, L. 1999, ApJ, 527, L43

[118] Waxman, E., & Draine, B.T. 2000, ApJ, 537, 796

[119] Wijers, R. A. M. J., Bloom, J. S., Bagla, J. S., & Natarajan, P. 1998, MNRAS, 294, L13

[120] Williams, R. K. 2004, ApJ, 611, 952

[121] Wilson, J. R, Mathews, G. J., & Marronetti, P. 1996, PRD, 54, 1317

[122] Woosley, S. E. 1993, ApJ, 405, 273

[123] Zhang, W., Woosley, S. E., & MacFadyen, A. I. 2003, ApJ, 586, 356

[124] Zhang, W., Woosley, S. E., & Heger, A. 2004, ApJ, 608, 365

Eguchi-Hanson Solitons in AdS Spacetime

R. B. Mann[1]

Department of Physics, University of Waterloo,
Waterloo, Ontario N2L 3G1, Canada

Abstract

I describe the construction of a new class solitions that are exact solutions to Einstein's equations in odd-dimensional spacetimes with negative cosmological constant. They are asymptotic to AdS_{d+1}/Z_p, providing an affirmative answer to a previously open question concerning the existence of such solutions. Perturbatively stable, their energy is negative relative to pure AdS. In the limit of zero cosmological constant, equal-time hypersurfaces in 5 dimensions are described by the Eguchi-Hanson metric and in larger numbers of dimensions by a generalization of the Eguchi-Hanson metric.

1 Introduction

Soliton solutions play an important role in furthering our understanding of both gravitational physics and string theory. In recent years attention has turned to the AdS/CFT correspondence conjecture, which implies the existence of extra light states in a gauge theory formulated on a quotient space that can be regarded as the boundary of an asymptotically AdS spacetime. This can be seen as follows. Consider a U(N) gauge theory on a torus of m-dimensions whose typical length is L . One might expect that the states of lowest energy are inversely proportional to the characteristic length scale, and are therefore of order $1/L$. However if N of the fields are arranged to be periodic after traversing one circle N times, then the lowest energy states can actually be of order 1/ (NL). To achieve this one introduces locally flat but globally nontrivial connections. which effectively render the size of the compact space larger by a factor of N. This correspondingly reduces the energy scale of the spectrum of states.

Such low-energy excitations can be understood in the context of string theory to be excitations of one D-brane wrapped N times around a circle, where the U(N) gauge theory describes the low energy excitations of N D-branes wrapped on the torus. The N^2 open strings that connect distinct D-branes in the latter case become N multiply identified open strings on a circle of length NL in the former case. This yields a configuration whose states of lowest energy are of order $1/(NL)$.

One can generalize this construction [1] to quotient spaces $\mathcal{M}/\Gamma$, where Γ is any freely acting discrete group of isometries on the compact Riemannian manifold $\mathcal{M}$. Provided $N = n|\Gamma|$, one can wrap n branes $|\Gamma|$ times around the manifold $\mathcal{M}$, where $|\Gamma|$ is the number of elements in the group. In this way the same U(N) gauge theory is obtained as if one had wrapped N branes once each around $\mathcal{M}/\Gamma$.

The AdS/CFT correspondence conjecture states that string theory on spacetimes that asymptotically approach $AdS_5 \times S^5$ is dual to $\mathcal{N} = 4$ super Yang-Mills U(N) gauge theory. One implication of the correspondence is that the density of low energy states is not affected under identification, i.e. even when the volume of the boundary S^3 is reduced to S^3/Γ. The boundary energy of pure AdS_5 is exactly equal to the Casimir energy of $\mathcal{N} = 4$ super U(N) Yang-Mills on S^3 with radius ℓ. Taking the quotient reduces both the energy and the volume by the same factor, leaving the energy density unchanged. Consequently light states of the type described above must exist. These conclusions would be modified if there existed solutions of the Einstein equations with negative cosmological constant that asymptotically approached AdS_5/Γ but had less energy. If so, then the ground state energy density of the strongly coupled gauge theory on S^3/Γ would be smaller than on S^3.

Recently a set of solutions satsifying this criterion were found [2, 3]. Asymptotic to AdS_n/Z_p (where $p \geq 3$), they yield a non-simply connected background manifold for the CFT boundary theory. Derived from 5-dimensional generalization of the Taub-NUT metric [4], their spatial sections approach that of the

[1]email: rbmann@sciborg.uwaterloo.ca

EH metric for large ℓ, i.e. for a vanishing cosmological constant. For this reason they have been called Eguchi-Hanson solitons. However unlike their four-dimensional Euclidean counterparts, these solutions have Lorentzian signature. In five dimensions their total energy is negative. but bounded from below as anticipated from earlier arguments [1]. These properties are reminiscent of the AdS soliton [5], and indeed the derivation of the solutions has some similarities to this simpler case.

In this article I shall review the construction of these solitons and their basic properties. Details can be found in refs. [2, 3].

2 Construction of EH Solitons

Before constructing the soliton solutions, a brief review of Eguchi-Hanson space [6] will be helpful. The Eguchi-Hanson metric was constructed as an exact solution to the Euclidean Einstein equations that is self-dual in the Riemann curvature tensor. In this sense it is the gravitational analogue of the BPST-instanton of Yang-Mills theory. Its metric is

$$ds^2 = \frac{r^2}{4}\left(1-\frac{a^4}{r^4}\right)[d\psi+\cos(\theta)d\phi]^2 + \frac{dr^2}{1-\frac{a^4}{r^4}} + \frac{r^2}{4}(d\theta^2+\sin(\theta)^2 d\phi^2) \tag{1}$$

where a is a constant of integration.

Setting $a = 0$ yields flat space, where the coordinates (θ, ϕ, ψ) range from zero to respectively $(\pi, 2\pi, 4\pi)$. At any constant value of r the metric is that of S^3. If $a \neq 0$ this is no longer the case because the $\partial/\partial\psi$ isometry has a fixed point at $r = a$. The metric will then have a singularity unless the periodicity $\Delta\psi$ of ψ is appropriately chosen so that

$$\Delta\psi = \frac{4\pi}{p} = \frac{8\pi}{|rf'(r)|_{r=a}} = 2\pi \tag{2}$$

where $f(r) = 1 - \frac{a^4}{r^4}$. The only allowed solution is $p = 2$, implying that the boundary at infinity of the metric (1) is S^3/Z_2.

Construction of EH solitons begins not with the metric (1) but rather with a consideration of the Taub-NUT metric [7, 8]. Intuitively the NUT charge corresponds to a magnetic type of mass. Such solutions are asymptotically locally flat because of the topology of the boundary at infinity. To understand this, consider the Euclidean version of the Schwarzschild solution. Its boundary at infinity is the product manifold $S^2 \times S^1$. In contrast to this, the Euclidean Taub-NUT solution has a twisted S^1 bundle over S^2 as its boundary at infinity. Locally this bundle structure can be untwisted to obtain the form of an asymptotically flat spacetime, but globally this is not possible. A string-like singularity called a Misner singularity (analogous to a 'Dirac string' in electromagnetism) [9] appears in the spacetime, due to the presence of the NUT charge. By an appropriate choice of coordinate patches this singularity can be rendered into removable coordinate singularity. The price paid for this is that the coordinate identifications in the spacetime yield closed timelike curves in certain regions. Extensions of the Taub-NUT solutions setting of nonzero cosmological constant Λ is present have been constructed [10, 11, 12, 13, 14, 15]. For $\Lambda < 0$ these spacetimes are asymptotically locally anti-de Sitter.

In general, the Killing vector that corresponds to the coordinate that parameterizes the fibre S^1 in the Euclidean section can have a fixed point set that either is $(d-2)$-dimensional (referred to as a 'bolt' solution), or is of a smaller dimensionality (referred to as a NUT solution). In four dimensions the bolt solution has a 2 dimensional fixed point set, whereas the NUT solution has a zero-dimensional fixed point set.

The basic idea in constructing the higher-dimensional cases is to regard the Taub-NUT space-time as a $U(1)$ fibration over a $2k$-dimensional base space endowed with an Einstein-Kähler metric g_B; its metric is then

$$F^{-1}(r)dr^2 + (r^2+N^2)g_B - F(r)(dt+A)^2 \tag{3}$$

where t is the coordinate on the fibre S^1 and A has a curvature $F(r) = dA$, which is proportional to some covariantly constant 2-form, where N is the NUT charge. More generally if we can factorize the base space in the form $B = M_1 \times \ldots \times M_k$ where M_i are two dimensional spaces of constant curvature,

then we can then have a NUT charge N_i for every such two-dimensional factor. In the above ansatz this involves replacing $(r^2+N^2)g_B$ with the sum $\sum_i(r^2+N_i^2)g_{M_i}$.

It has recently been shown [4] that an odd-dimensional base space can also be used to construct spacetimes with NUT charge. Here the idea is to construct an S^1 bundle over an even-dimensional Kähler space M that is a factor of the odd dimensional base space, factorized in the form $B = M \times Y$. This leads to the general ansatz

$$F^{-1}(r)dr^2 + (r^2+N^2)g_M + r^2 g_Y - F(r)(dt+A)^2 \tag{4}$$

where g_M is the metric on the even-dimensional space M while g_Y is the metric on the remaining factor space Y.

EH solitons can be derived from these odd-dimensional metrics. In five dimensions the preceding construction yields [4]

$$ds^2 = -\rho^2 dt^2 + 4n^2 F(\rho)\left[d\psi + \cos(\theta)d\phi\right]^2 + \frac{d\rho^2}{F(\rho)} + (\rho^2-n^2)(d\theta^2+\sin(\theta)^2 d\phi^2) \tag{5}$$

which is an exact solution to the Einstein equations with negative cosmological constant $\Lambda = -\frac{6}{\ell^2}$. It can be regarded as the five-dimensional generalization of the Taub-NUT metric in which the $U(1)$-fibration is a partial fibration over a two-dimensional subspace the three dimensional base space. The function $F(\rho)$ is

$$F(\rho) = \frac{\rho^4 + 4m\ell^2 - 2n^2\rho^2}{\ell^2(\rho^2-n^2)} \tag{6}$$

where $n = \frac{\ell}{2}$. By implementing the transformations

$$\rho^2 = r^2 + n^2 \qquad m = \frac{\ell^2}{64} - \frac{a^4}{64\ell^2} \qquad r \to r/2 \qquad t \to 2t/\ell \tag{7}$$

this becomes

$$ds^2 = -g(r)dt^2 + \frac{r^2 f(r)}{4}\left[d\psi + \cos(\theta)d\phi\right]^2 + \frac{dr^2}{f(r)g(r)} + \frac{r^2}{4}(d\theta^2+\sin(\theta)^2 d\phi^2) \tag{8}$$

where

$$g(r) = 1 + \frac{r^2}{\ell^2} \quad , \quad f(r) = 1 - \frac{a^4}{r^4} \tag{9}$$

These metrics are the 5-dimensional Eguchi-Hanson-AdS solitons [2], so named because they resemble the Eguchi-Hanson metric in four dimensions. Indeed, setting $\ell \to \infty$ yields from (8) the Eguchi-Hanson metric

$$ds^2 = \frac{r^2}{4}f(r)\left[d\psi + \cos(\theta)d\phi\right]^2 + \frac{dr^2}{f(r)} + \frac{r^2}{4}(d\theta^2+\sin(\theta)^2 d\phi^2) \tag{10}$$

as a t =constant hypersurface.

As stated in the introduction, the preceding construction is analogous to that used in constructing the AdS soliton. Consider the metric

$$ds^2 = -V(r)dt^2 + \frac{dr^2}{V(r)} + r^2 d\phi^2 + r^2\gamma_{ij}dx^i dx^j \tag{11}$$

where

$$V(r) = \frac{r^2}{\ell^2}\left(1 - \frac{r_0^2}{r^2}\right) \tag{12}$$

ensures that this is a solution to the 5-dimensional Einstein equations with negative cosmological constant, provided the metric γ_{ij} is that of a flat 2-dimensional toroidal space. Under the transformations

$$t \to i\chi \qquad \phi \to i\tau \tag{13}$$

the metric (11) becomes

$$ds^2 = V(r)d\chi^2 + \frac{dr^2}{V(r)} - r^2 d\tau^2 + r^2\gamma_{ij}dx^i dx^j \tag{14}$$

which is the AdS soliton. The transformations (7) play a role in constructing the EH soliton (8) that is analogous to the one played by the transformations (13) in constructing the AdS soliton (14). However the topologies of the two solitons are quite distinct as we shall see.

Generalizations of the metric (8) to any higher odd dimension exist. They are constructed by transforming a class of Einstein metrics on S^{m+2} sphere bundles fibred over $2n$-dimensional Einstein-Kähler spaces [16]. These metrics are given by the expression

$$ds^2 = \frac{2n+m}{2}\left\{\frac{(1-\rho^2)^n d\rho^2}{P(\rho)} + \frac{c^2 P(\rho)}{(1-\rho^2)^n}\left[d\tau - 2A\right]^2 + c(1-\rho^2)d\Sigma_{2n}^2 + \frac{(m-1)\rho^2}{\Lambda_c - 1/c}d\Omega_m^2\right\} \tag{15}$$

with $(d+1) = 2n+m+2$, and A is a 1-form potential for the Kähler form $d\Sigma_{2n}^2$ ($J = dA$). The metric (15) solves the Einstein equations $G_{\mu\nu} + \Lambda_c g_{\mu\nu} = 0$ provided $P(\rho)$ obeys the differential equation

$$\frac{d}{d\rho}\left[\rho^{m-1}P(\rho)\right] = \rho^{m-2}\left[\Lambda_c\left(1-\rho^2\right)^{n+1} - \frac{1}{c}\left(1-\rho^2\right)^n\right] \tag{16}$$

whose solution is given in terms of a linear combination of hypergeometric functions. Setting

$$\rho^2 = 1 + r^2\Lambda_c \qquad \tau = 2\psi \qquad c = \frac{1}{\Lambda_c \nu} \tag{17}$$

yields

$$\begin{aligned} ds^2 &= \frac{2n+m}{2}\left[\frac{(m-1)}{\Lambda_c(1-\nu)}g(r)d\Omega_m^2 + \frac{(-1)^n 4c^2 r^2\Lambda_c^2\tilde{f}(r)}{g(r)^{(m-1)/2}}\left[d\psi - A\right]^2\right. \\ &\left. + \frac{(-1)^n g(r)^{(m-3)/2}dr^2}{\tilde{f}(r)} - cr^2\Lambda_c d\Sigma_{2n}^2\right] \end{aligned} \tag{18}$$

where $g(r) = 1 + r^2\Lambda_c$ and

$$\begin{aligned} \tilde{f}(r) &= \frac{(-1)^{n+1}}{2}\left\{\frac{r^2\Lambda_c}{n+2}{}_2F_1\left(\left[-\frac{(m-3)}{2}, n+2\right], n+3, -r^2\Lambda_c\right)\right. \\ &\left. + \frac{\nu}{(n+1)}\,{}_2F_1\left(\left[-\frac{(m-3)}{2}, n+1\right], n+2, -r^2\Lambda_c\right)\right\} + \frac{\mu}{r^{2n+2}\Lambda_c^{n+2}} \end{aligned} \tag{19}$$

where ${}_2F_1$ denotes the hypergeometric function.

To obtain the d-dimensional EH solitons entails setting $\nu = m = 1$ along with the rescalings

$$\frac{(m-1)}{\Lambda_c(1-\nu)}d\Omega_1 = \frac{(m-1)}{\Lambda_c(1-\nu)}d\varphi = dt \qquad \mu = \frac{(-1)^{n+1}b^{2n+2}\Lambda_c^{n+2}}{2n+2}$$

where $d = 2n+2$ when $m = 1$. Using the further rescalings

$$r \to \frac{r}{\sqrt{d}}, \qquad b = \frac{a}{\sqrt{d}} \qquad \Lambda_c = \frac{2n+2}{\ell^2} \tag{20}$$

yields after a Wick rotation on t

$$ds^2 = -g(r)dt^2 + \left(\frac{2r}{d}\right)^2 f(r)\left[d\psi + \sum_{i=1}^{n}\cos(\theta_i)d\phi_i\right]^2 + \frac{dr^2}{g(r)f(r)} + \frac{r^2}{d}\sum_{i=1}^{n}d\Sigma_{2(i)}^2 \tag{21}$$

where

$$d\Sigma_{2(i)}^2 = d\theta_i^2 + \sin^2(\theta_i)d\phi_i^2 \qquad g(r) = 1 + \frac{r^2}{\ell^2} \quad , \quad f(r) = 1 - \left(\frac{a}{r}\right)^d \tag{22}$$

and the negative cosmological constant is

$$\Lambda = -\frac{d(d-1)}{2\ell^2} \tag{23}$$

The $\ell \to \infty$ limit on any t=constant hypersurface yields the class of metrics

$$ds^2 = \left(\frac{2r}{d}\right)^2 \left(1 - \left(\frac{a}{r}\right)^d\right) \left[d\psi + \sum_{i=1}^{k} \cos(\theta_i) d\phi_i\right]^2 + \frac{dr^2}{1 - \left(\frac{a}{r}\right)^d} + \frac{r^2}{d} \sum_{i=1}^{k} d\Sigma_{2(i)}^2 \tag{24}$$

which can be regarded as d-dimensional generalizations of the Eguchi-Hanson metric.

3 Regularity of the EH Soliton

The conditions for regularity of the spacetimes described by the EH solitons (21) are determined in a manner similar to that of the metric (1). The metrics (21) have an isometry $\partial/\partial\psi$ with a fixed point at $r = a$. To ensure that there are no singularities, regularity in the (r, ψ) section implies that ψ has period $\frac{2\pi}{\sqrt{g(a)}}$ and elimination of string singularities at the north and south poles ($\theta = 0, \pi$) implies that an integer multiple of this quantity must equal 4π. Putting these together implies

$$a^2 = \ell^2 \left(\frac{p^2}{4} - 1\right) \tag{25}$$

where p is an integer with $p \geq 3$, yielding in turn that $a > \ell$. This condition generalizes the relation (2) for the Eguchi-Hanson metric in which $p = 2$, a value recovered in the $\ell \to \infty$ limit. The Ricci and Kretschmann scalars of the the EH soltions (21) are easily seen to be free of singularities over the allowed range of r.

The metrics (21) are therefore asymptotic to AdS_{d+1}/Z_p where $p \geq 3$. Hence the AdS/CFT correspondence conjecture implies the existence of extra light states in a gauge theory formulated on the quotient space that can be regarded as the boundary these spacetimes. This suggests that expected results mentioned in the introduction for $AdS_5 \times S^5$ will carry over to $AdS_{d+1} \times S^{9-d}$, whenever the d-dimensional CFT exists. Generalizing to d dimensions, the conjecture leads one to expect that string theory on spacetimes that asymptotically approach $AdS_{d+1} \times S^m$ is equivalent to a conformal field theory (CFT) on its boundary, whose spatial section is $\left(S^{d-2} \times R\right) \times S^m$. If the CFT contains fermions, these must be antiperiodic in ψ. This breaks supersymmetry, but it has been pointed out that ordinary (i.e., nonsupersymmetric) Yang-Mills gauge theory may be described by compactifying one direction on a circle and requiring antiperiodic boundary conditions for the fermions around it [17]. On the supergravity side this correponds to considering spacetimes that are asymptotically locally AdS. Hence when fermions are present p must be even because going p times along the ψ direction yields a circle that is asymptotically contractible, and the situation (for example in 5 dimensions) is the same as if the asymptotic space were S^3 (and not S^3/Γ). For S^3 the fermions are periodic, and so p must be even when fermions are present in the CFT.

4 5 Dimensional EH Solitons

Restricting attention to the five dimensional soliton (8), one can compute a number of quantities that provide further suggestive evidence in favour of the AdS/CFT correspondence.

Consider first an evaluation of its mass using the (A)dS/CFT-inspired counter-term method. A full description of the method can be found in [18, 19, 20, 21, 22]; here it is sufficient to note that the conjecture posits the a relationship between bulk and boundary quantities. Since the CFT is formulated on the boundary spacetime, counter terms can be added to the divergent gravitational action that are functionals of the boundary metric and its curvature invariants. Writing

$$I = I_B + I_{\partial B} + I_{ct} \tag{26}$$

where I_B and $I_{\partial B}$ are the usual Einstein-Hilbert and Gibbons-Hawking actions, respectively, the counter term action I_{ct}, depending only on quantities intrinsic to the boundary. This ensures that the bulk equations of motion are unchanged. Only a finite number of terms can be nonzero at infinity; a judicious linear combination of these terms serves to cancel the divergences of the first two actions. In five dimensions there are only two such terms, one proportional to the volume of the boundary and the other proportional to its Ricci scalar density.

Variation of the full action (26), yields the boundary stress-tensor, from which finite conserved charges can be calculated using the relationship

$$\mathcal{D}_\xi = \oint_\Sigma d^{d-1} S^a \xi^b T^{\rm eff}_{ab} \tag{27}$$

If ξ is the time-like Killing vector, then one can calculate the conserved mass; if it is a rotational Killing vector, one gets the conserved angular momentum of the spacetime. In this section we investigate the thermodynamic properties of the metric (8) using the (A)dS/CFT-inspired counter-term method.

Computing (27) for $\xi = \partial/\partial t$ yields

$$\mathcal{M} = \frac{\pi(3\ell^4 - 4a^4)}{32G\ell^2 p} < 0 \tag{28}$$

where the latter inequality holds upon application of (25). This is in agreement with the expectations from the AdS/CFT correspondence noted earlier. This result can be compared with that obtained from the field theory on the boundary of the AdS_5/Z_p orbifold in a manner similar to that of the AdS_5 case [23]. The only difference is that the volume of the S^3 is replaced with the volume of S^3/Γ. The parameters of the gravity theory in the bulk are related to those of the CFT on the boundary via

$$\frac{1}{G} = \frac{2N^2}{\pi\ell^3} \tag{29}$$

and the resultant expression [3] for the energy of the field theory on the boundary is

$$\mathcal{E}_{calc} = \frac{3N^2}{16p\ell} \tag{30}$$

which agrees with the Casimir energy from (28) with $a = 0$ once (29) is employed.

5 Stability of the EH Soliton

For any given integer $p \geq 3$ the energy of the soliton is, from (28)

$$\mathcal{E}_{\rm EH-soliton} = -\frac{(p^4 - 8p^2 + 4)N^2}{64\ell p} \tag{31}$$

Since this is negative and lower than that of the AdS_5/Z_p orbifold, this suggests that the soliton could very well be the state of lowest energy in its asymptotic class. This conjecture was made in ref. [2] for both 5D Einstein gravity with negative cosmological constant and in type IIB supergravity in 10 dimensions. Specifically the AdS/CFT correspondence[2] implies that any metric solving the 5D Einstein equations that has the same boundary conditions as the EH soliton will have a greater energy.

This situation is fully analogous to that for the AdS soliton [5]. The perturbative stability properties of the metric (8) can be examined using similar methods. The idea is to calculate the energy density H to second order in the fluctuations $h_{\mu\nu}$ of the metric (8). Writing

$$g_{\mu\nu} = \bar{g}_{\mu\nu} + h_{\mu\nu} \tag{32}$$

where $\bar{g}_{\mu\nu}$ is the EH solition (8) and

$$h_{\mu\nu} = \mathcal{O}\left(r^{-2}\right) \quad h_{\mu r} = \mathcal{O}\left(r^{-4}\right) \quad h_{rr} = \mathcal{O}\left(r^{-6}\right) \quad \mu, \nu \neq r$$

[2] along with the expected stability of the gauge theory

describe the falloff conditions of the perturbation. the Hamiltonian H on a time-symmetric slice to second order in h_{ij} $(i,j \neq t)$ is [24]

$$\mathcal{H} = \bar{N}\left[\frac{1}{\sqrt{\bar{g}}}p^{ij}p_{ij} + \sqrt{\bar{g}}\left(\frac{1}{4}\left(\bar{D}_k h_{ij}\right)^2 + \frac{1}{2}{}^{(4)}\bar{R}^{ijkl}h_{il}h_{jk} - \frac{1}{2}{}^{(4)}\bar{R}^{ij}h_{ik}h_j{}^k\right)\right] \tag{33}$$

where

$$p^t{}_i = 0 = \bar{D}^t h_{ij} \tag{34}$$

are the chosen gauge conditions. Here p_{ij} is the conjugate momentum. The constraint equations to linear order also imply

$$h^t{}_i = 0 = \bar{D}_i p^{ij} \tag{35}$$

Choosing intial conditions $p^{ij} = 0$ so that the nonnegative contribution of the momenta to the energy density vanishes, one needs only calculate the gradient energy density $(\bar{D}_k h_{ij})^2$ and the potential energy density

$$U = \frac{1}{2}\,{}^{(4)}\bar{R}^{ijkl}h_{il}h_{jk} - \frac{1}{2}\,{}^{(4)}\bar{R}^{ij}h_{ik}h_j{}^k$$

The former is always positive, but the latter could be negative. A detailed calculation [3] indicates that for any given set of initial conditions, the total energy is always positive, indicating that the EH soliton is perturbatively stable for all values of p relative to all other metrics with the same boundary conditions. This motivates one to make a set of conjectures that are similar to those for the AdS soliton [5]:

Conjecture 1: All solutions to ten-dimensional IIB supergravity satisfying (32), with $\bar{g}_{\mu\nu}$ given by the metric (8), will have energy greater than this unless $h_{\mu\nu} = 0$.

Conjecture 2: All solutions to Einstein's equation in five dimensions with negative cosmological constant satisfying (32), with $\bar{g}_{\mu\nu}$ given by the metric (8), will have energy greater than this unless $h_{\mu\nu} = 0$.

Conjecture 3: Any nonsingular Riemannian 4-manifold with negative Ricci scalar $R = -\frac{12}{\ell^2}$ satisfying (32), with $\bar{g}_{\mu\nu}$ given by the metric (8), will have energy greater than this unless $h_{\mu\nu} = 0$.

If spacetimes in 10 dimensions that are not direct products with S^5 have higher energy, and if the additional supergravity fields contribute positive energy. then conjecture 1 reduces to conjecture 2. Similarly, if there exists a moment of time symmetry (i.e. there is a surface with zero extrinsic curvature), then conjecture 2 reduces to conjecture 3. The proof of these conjectures remains an interesting open question.

6 Concluding Remarks

The Einstein equations with cosmological constant have been shown to have a new class of soliton solutions. Since they are higher-dimensional version of the Eguchi-Hanson metric on a constant time slice when the cosmological constant vanishes, they have been called Eguchi-Hanson solitons. They furnish an explicit example of solutions that asymptotically approach AdS_{d+1}/Γ but have lower energy, with $\Gamma = Z_p$. The 5-dimensional EH solitons are perturbatively stable, and it is reasonable to conjecture that the AdS EH-soliton is the state of lowest energy in its asymptotic class.

A preliminary study of the Kaluza-Klein reduction of these solitons was recently carried out [25]. Another problem of interest would be to construct a Yang-Mills theory on $R \times S^3/Z_p$ on expects that tachyon condensation should cause orbifold decay into the EH soliton [26]. Solitonic solutions in the asymptotically de Sitter case also exist. Some of their properties have been analyzed in ref. [3]. Further analysis of EH solitons - both asymptotically dS and AdS - should provide some interesting avenues for research.

This work was supported in part by the Natural Sciences and Engineering Research Council of Canada. I would like to thank Richard Clarkson and Cris Stelea for the contributions to this work, and to Tetsuya Shiromizu and Misao Sasaki for their invitation for me to participate in the JGRG15 conference.

References

[1] G. Horowitz and T. Jacobson, *Note on Gauge Theories on M/Gamma and the AdS/CFT Correspondence*, JHEP **0201** 013 (2002) [hep-th/0112131].

[2] R. Clarkson and R.B. Mann, *Soliton solutions to the Einstein equations in five dimensions*, Phys. Rev. Lett. (to appear) [hep-th/0508109].

[3] R. Clarkson and R.B. Mann, *Eguchi-Hanson Solitons in Odd Dimensions*, Class. Quant. Grav. (to appear) [hep-th/0508200].

[4] R.B. Mann and C. Stelea, *Nuttier (A)dS Black Holes in Higher Dimensions*, Class. Quant. Grav. **21** (2004), 2937 [hep-th/0312285].

[5] Gary T. Horowitz, Robert C. Myers, *The AdS/CFT Correspondence and a New Positive Energy Conjecture for General Relativity*, Phys. Rev. **D59**, 026005 (1999).

[6] Tohru Eguchi and Andrew J. Hanson, *Asymptotically Flat Self-Dual Solutions to Euclidean Gravity*, Physics Letters **74B**, Number 3, pg. 249.

[7] A. H. Taub, *Empty Space-times Admitting a Three Parameter Group of Motions*, Ann. Math., **53**, 472 (1951).

[8] E. Newman, L. Tamburino, and T. Unti, *Empty-Space Generalization of the Schwarzschild Metric*, J. Math. Phys. Volume **4**, Number 7, 915 (1963).

[9] C. W. Misner "The Flatter Regions of Newman, Unti and Tamburino's Generalized Schwarzschid Space" J. Math. Phys. **4** (1963) 924

[10] F. A. Bais and P. Batenburg, "A New Class Of Higher Dimensional Kaluza-Klein Monopole And Instanton Solutions," Nucl. Phys. B **253**, 162 (1985).

[11] D. N. Page and C. N. Pope, "Inhomogeneous Einstein Metrics On Complex Line Bundles," Class. Quant. Grav. **4**, 213 (1987)

[12] M. M. Akbar and G. W. Gibbons, "Ricci-flat metrics with U(1) action and the Dirichlet boundary-value problem in Riemannian quantum gravity and isoperimetric inequalities," Class. Quant. Grav. **20**, 1787 (2003) [hep-th/0301026].

[13] M. M. Taylor-Robinson, "Higher dimensional Taub-Bolt solutions and the entropy of non compact manifolds," [hep-th/9809041]

[14] A. Awad and A. Chamblin, "A bestiary of higher dimensional Taub-NUT-AdS spacetimes," Class. Quant. Grav. **19**, 2051 (2002) [hep-th/0012240]

[15] R. Clarkson, L. Fatibene and R.B. Mann, "Thermodynamics of $(d+1)$-dimensional NUT-charged AdS Spacetimes", Nucl. Phys. **B652** 348 (2003) [hep-th/0210280].

[16] H. Lü, Don N. Page and C.N. Pope, *New Inhomogeneouse Einstein Metrics on Sphere Bundles Over Einstein-Kähler Manifolds* [hep-th/0403079].

[17] E. Witten, *Anti-de Sitter Space, Thermal Phase Transition, and Confinement in Gauge Theories*, Adv. Theor. Math. Phys. **2** 505 (1998). [hep-th/9803131]

[18] R. B. Mann, *Misner String Entropy*, Phys. Rev. **D60** 104047 (1999) [hep-th/9903229]

[19] R. B. Mann, *Entropy of Rotating Misner String Spacetimes*, Phys. Rev. **D61** 084013 (2000) [hep-th/9904148]

[20] M. Henningson, K. Skenderis, *The Holographic Weyl Anomaly*, JHEP 9807 (1998) 023; [hep-th/9806087]
S.Y. Hyun, W.T. Kim, J. Lee, *Statistical Entropy and AdS/CFT Correspondence in BTZ Black Holes*, Phys. Rev D 59 (1999) 084020 [hep-th/9811005]

[21] V. Balasubramanian, P. Kraus, *A Stress-Tensor For Anti-de Sitter Gravity*, Commun. Math. Phys. 208 (1999) 413. [hep-th/9902121].

[22] A.M. Ghezelbash, R.B. Mann, *Action, Mass and Entropy of Schwarzschild-de Sitter Black Holes and the de Sitter/CFT Correspondence*, JHEP 0201 (2002) 005 [hep-th/0111217]

[23] Adel M. Awad and Clifford V. Johnson, *Holographic Stress Tensors for Kerr-AdS Black Holes*, Phys.Rev. **D61** (2000) 084025 [hep-th/9910040].

[24] L.F. Abbott and S. Deser, *Stability of Gravity with a Cosmological Constant*, Nucl. Phys. **B195** (1982) 76.

[25] R.B. Mann and C. Stelea, *New Multiply Nutty Spacetimes* [hep-th/0508203]

[26] H. Lin and J. Maldacena, *Fivebranes from gauge theory* [hep-th/0509235]

PBH and DM from cosmic necklaces

Tomohiro Matsuda[1]

[1] *Theoretical Physics Group, Saitama Institute of Technology, Saitama 369-0293, Japan*

Abstract

Cosmic strings in the brane Universe have recently gained a great interest. I think the most interesting story is that future cosmological observations distinguish them from conventional cosmic strings. If the strings are higher-dimensional object that can (at least initially) move along the compactified space and finally settle down to (quasi-)degenerated vacua in the compactified space, kinks should appear on the strings, which interpolate between the degenerated vacua, which become "beads" on the strings. In this case, the strings turn into necklaces. In the case that the compact manifold in not simply connected, a string loop that winds around a non-trivial circle is stable due to the topological reason. Since the existence of the degenerated vacua and the non-trivial circle is a common feature of the brane models, it is important to study cosmological constraints on the cosmic necklaces and their stable winding states.

1 Introduction

In this talk we will explain the cosmological consequences of the production of Dark Matter(DM) and Primordial Black Hole(PBH) from the loops of the cosmic necklaces. To begin with, I think it is fair to explain why necklaces[1] are produced in brane models, since in may papers it is discussed that "only strings are produced in the brane Universe"[2]. Of course I think this claim is not wrong, however somewhat misleading for non-specialists. To explain what is misleading in the "standard scenario", we have a figure in Fig.1. In general, the distance between branes may appear in the four-dimensional effective action as a Higgs field of the effective gauge dynamics. At least in this case, it is natural to consider the defects coming from the spatial variation of the Higgs field, which corresponds to the "deformation" of the branes[3]. Is the spatial variation of the Higgs field unnatural in brane models? The answer is, of course, NO. One can therefore two different kinds of defects in brane models: One is induced by the brane creation that is due to the spatial variation of the tachyon condensation, while the other is induced by the brane deformation that is due to the spatial variation of the brane distance. Along the line of the above arguments, it is possible to construct Q-ball's counterpart in brane models[4], which can be distinguished from the conventional Q-balls by their decay process. We therefore have an expectation that strings can be distinguished from the conventional ones, if one properly considers their characteristic features.

Now let us discuss about the validity of the conventional Kibble mechanism. Of course the Kibble mechanism is an excellent idea that explains the nature of the cosmological defect formation. However, if there is an oscillation of the brane distance that may be induced by the brane inflation or by a later phase transition that changes the brane distance, the four-dimensional counterpart of the brane distance (i.e. the Higgs field) oscillates in the effective action. In the four-dimensional counterpart, defect production induced by such oscillation is already discussed by many authors, including the production of the sphaleron domain walls which otherwise cannot be produced in the Universe[3]. The defect production induced by such oscillation may or may not be explained by the Kibble mechanism, however it should be fair to distinguish it from the "conventional" Kibble mechanism.

Let us summarize the above discussion about the defect production in the brane Universe. Actually, it is possible to produce all kinds of defects in the brane Universe, however it is impossible to produce defects other than the strings **simply as the result of the brane creation that is induced by the conventional Kibble mechanism**. One should therefore be careful about the assumption that is made in the manuscript, which may or may not be explicit. The necklaces are produced as the hybrid

[1] E-mail:matsuda@sit.ac.jp

of the brane creation and the brane deformation. It should be noted that the necklaces that we will discuss in this talk may appear in the four-dimensional gauge dynamics, irrespective of the existence of the branes[5]. The stabilization of the necklace loops is first discussed in Ref.[6] for brane models and in Ref.[5] for necklaces embedded in four-dimensional gauge dynamics.

In order to produce necklaces, their motion in the compactified direction is important. I know that in the "standard scenario" it is sometimes discussed that the position of the strings are fixed by the potential that is induced by the supersymmetry breaking, and the position is a homogeneous parameter of the Universe because all the decay products (Typically, they are F, D, and (p,q) strings) lie along the plane of the original hypersurface on which the tachyon condensation took place. However, in this case one may hit upon the idea that the potential for a string cannot be identical to all other kinds of the strings. One may therefore obtain many kinds of strings that may move independently in different hypersurfaces, with exponentially small intersection ratios. Moreover, I think it is not reasonable(but may not be impossible) to assume that the string motion is utterly restricted by the potential even in the most energetic epoch just after inflation. Please remember that the moving (inflating) brane carries kinetic energy, and the brane annihilation should be an energetic process, although one can admit that there could be exceptional scenarios. I therefore think that the decay products should have kinetic energy, which is enough to climb up the potential hill at least just after brane inflation.

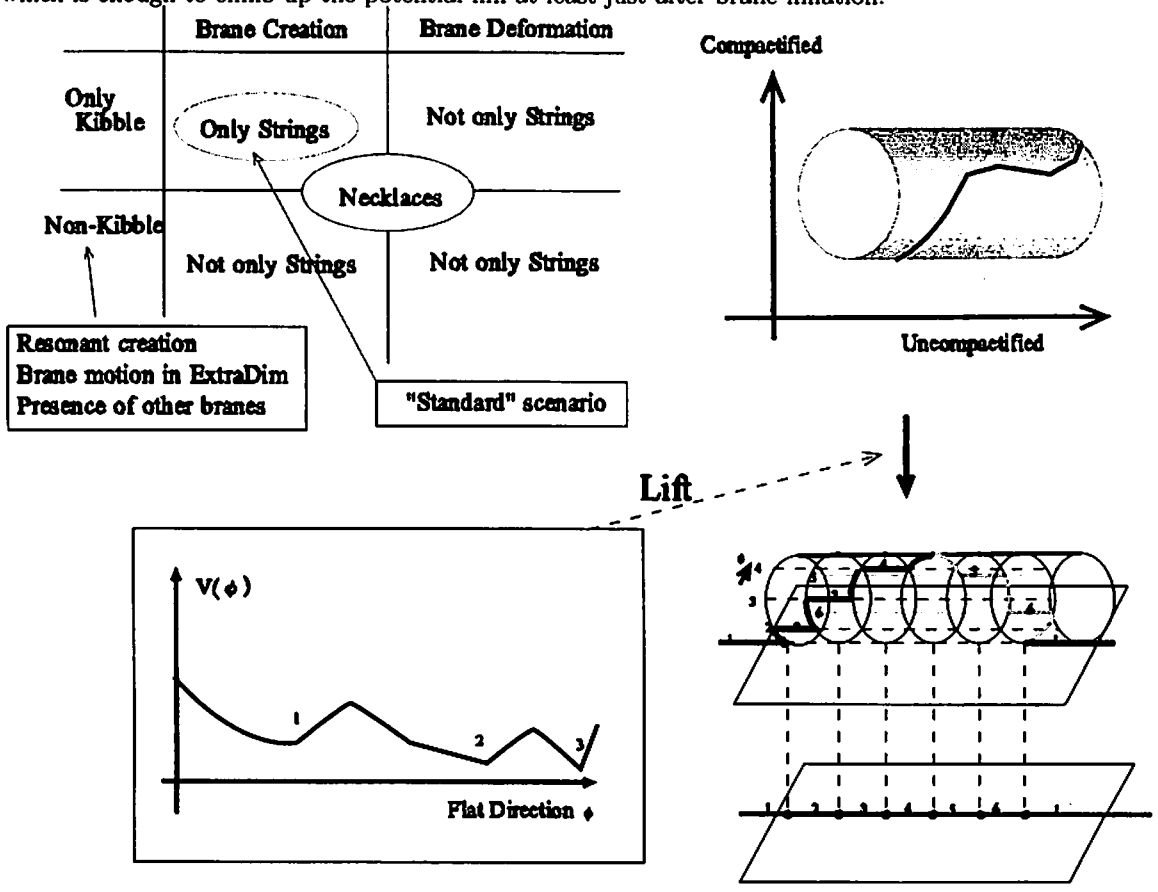

Figure 1: We show how necklaces are produced despite the "standard" arguments.

2 PBH and DM from necklaces

The scenario of the PBH formation from strings is initiated by Hawking[7], who utilizes the huge kinetic energy of the shrinking loops. However, the probability of finding loops that can shrink into their small

Schwarzschild radius is very rare due to their random shape and motion, which weakens the obtained bound for the string tension. In our previous paper hep-ph/0509061[8], we have just extended Hawking's idea to the networks that include monopoles attached to the strings. It should be emphasized that both in the above scenarios, the kinetic energy of the shrinking object plays crucial role.

Now let us discuss about our new idea for producing PBH. The most obvious discrepancy is that in our new scenario we discard the benefit of the kinetic energy. We consider stable relics that can be produced from string loops, whose mass is large enough to turn into black holes, even after they have dissipated their kinetic energy during the loop oscillation. The stability of the loops is due to their windings around the compactified space. Of course the production of PBH is delayed compared to the Hawking's scenario, however the obtained bound is much stronger than the original scenario due to the high (~ 1) production ratio. This new mechanism of PBH production is first advocated in hep-ph/0509062[5].

Let us explain how one can count the winding number of a necklace loop. Please see Fig.2. We introduce $\chi(t)$, which is the step length between each random walk that corresponds to the right or the left movers in the compactified direction. Since the left and the right movers can annihilate on the necklaces, the actual distance between "beads" becomes much larger than $\chi(t)$. We therefore introduce another parameter $d(t)$, which is the typical length between the remaining "beads". Although the annihilation could be efficient, the simple statistical argument shows that the typical number of the beads that remain after annihilation is about $n^{1/2}$, if the initial number of the random walk is given by n. If the strings are in the scaling epoch, the typical length of the loops is initially $l(t) \sim \alpha t$. Then one can obtain the typical mass of the stable relics, $M_{coils} \sim n(t)^{1/2} m \sim [l(t)/\chi(t)]^{1/2} m$, where m is the typical mass of the beads.

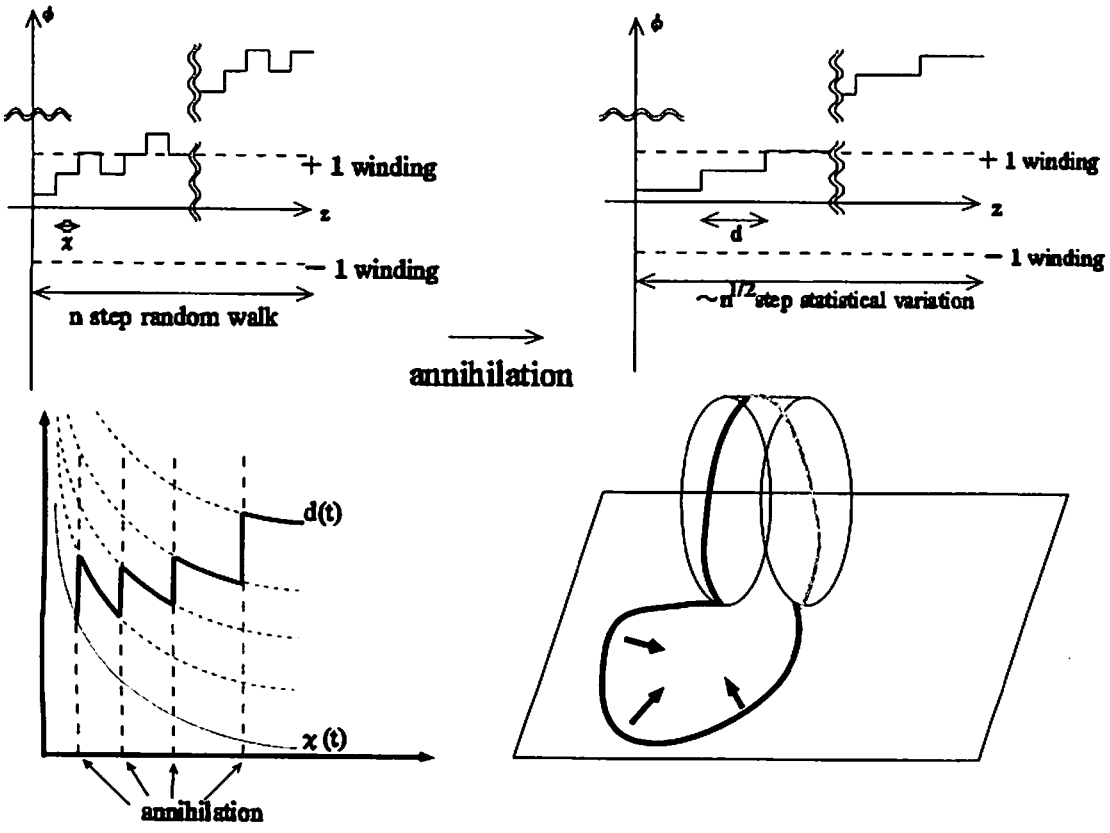

Figure 2: If the windings are stabilized by the topological reason, one can obtain the typical number of the windings from the simple statistical arguments.

Here we should note that disregarding the annihilation, $\chi(t) \propto t^{-1}$ is already obtained in Ref.[9], which means that $d(t)$ should evolve as $d(t) \sim t^{-1}$ at least during the short periods between each annihilation.

Of course $d(t)$ is discontinuous at each annihilation, however the underlying parameter $\chi(t)$ is continuous and depends on time as $\chi(t) \sim t^{-1}$. Using the above ideas, we can calculate the typical mass of the stable relics that are produced from necklace loops. The calculation of the PBH density is straightforward. We have obtained the result

$$G\mu < 10^{-21} \times \left[\frac{p}{10^{-2}}\right]^{4/5} \left[\frac{\gamma}{10^{-2}}\right]^{1/5} \left[\frac{t_n}{M_p/\mu}\right]^{3/5} \left[\frac{d(t_n)}{M_p/\mu}\right]^{3/5} \left[\frac{m}{10^{16}GeV}\right]^{-6/5}, \quad (1)$$

where we have assumed $\alpha \sim \gamma G\mu$, and t_n is the time when necklaces are produced. p is the reconnection ratio that should be ~ 1 for the conventional cosmic strings, but $p \ll 1$ is possible in our case.

The string loops are produced at any time, and the mass of the stable relics depends on the time when they are produced, because the typical length scale of the string network increases with time both in the friction-dominated and in the scaling epoch. Therefore, the relics that are produced in an earlier epoch may be too light to turn into black holes. The "light" relics are the "monopoles" if the cosmic strings are D-branes. However, the "magnetic charge" of the "monopoles" may or may not be identical to the conventional magnetic charge of the electromagnetism. Therefore, they are the candidate of DM, and possibly the origin of the troublesome monopole problem only if they carry the conventional magnetic charge. In our paper hep-ph/0509064[5], we have examined if the DM relics can put significant bound on the tension of the cosmic strings. We have obtained the result for $m \sim M_{GUT} \sim 10^{16}GeV$,

$$G\mu < 10^{-23} \times \left[\frac{p}{10^{-2}}\right]^{9/10} \left[\frac{1}{\beta_s}\right]^{9/10} \left[\frac{10^{-3}}{r}\right]^{9/10} \quad (2)$$

where r is the mass ratio between the string part and the beads on the necklaces, which becomes a constant in the scaling epoch[5].

The difficulty in lowering the typical energy scale is discussed in Ref.[10] for baryogenesis and Ref.[11] for the mechanism to generate density perturbations.

References

[1] A. Vilenkin and E.P.S. Shellard, *Cosmic strings and other cosmological defects, (Cambridge University Press, Cambridge, 2000).*

[2] See *hep-th/0512062* for the most recent tutorial on this matter.

[3] T.Matsuda, *JHEP 0411:039,2004; JHEP 0410:042,2004; JHEP 0309:064,2003.*

[4] T. Matsuda, *JCAP 0410:014,2004.*

[5] T. Matsuda, *hep-ph/0509062; hep-ph/0509064.*

[6] T. Matsuda, *JHEP 0505:015,2005; Phys.Rev.D70(2004)023502.*

[7] S. W. Hawking, *Phys.Lett.B231(1989)237.*

[8] T. Matsuda, *hep-ph/0509061.*

[9] V. Berezinsky and A. Vilenkin, *Rev.Lett.79(1997)5202.*

[10] T. Matsuda, *Phys.Rev.D66(2002)023508; Phys.Rev.D66(2002)047301; Phys.Rev.D65(2002)107302; J.Phys.G27(2001)L103; Phys.Rev.D67(2003)127302; Phys.Rev.D65(2002)103501; Phys.Rev.D65(2002)103502; Phys.Rev.D64(2001)083512.*

[11] T. Matsuda, *Class.Quant.Grav.21(2004)L; hep-ph/0509063; Phys.Rev.D66(2002)107301; Phys.Rev.D68(2003)047702; JCAP 0306:007,2003; Phys.Rev.D67(2003)083519; JCAP 0311:003,2003; Phys.Lett.B423(1998)35; Phys.Rev.D68(2003)127302.*

Super-horizon black hole and its evolution

Tomohiro Harada[1]

Department of Physics, Kyoto University, Kyoto 606-8502, Japan

Abstract

Primordial black holes have important observational implications through Hawking evaporation and gravitational radiation as well as being a candidate for cold dark matter. Those black holes may have formed in the early universe typically with the mass scale contained within the Hubble horizon at the formation epoch and subsequently accreted mass surrounding them. Numerical relativity simulation shows that primordial black holes of different masses do not accrete much, which contrasts with a simplistic Newtonian argument. In particular, we see that primordial black holes larger than the cosmological apparent horizon, i.e. "super-horizon" ones, have decreasing energy and child-universe like struture, suggesting that they might have formed through quantum fluctuations in inflationary cosmology.

1 Introduction

Primordial black holes (PBHs) may have formed in the early universe [1]. Those black holes may contribute to current gamma-ray and cosmic ray backgrounds through Hawking evaporation. They may also contribute to the cosmic density and behave as cold dark matter. They could be a promising target for ground-based interferometric gravitational wave detectors [2, 3]. Thus we can obtain information of the early universe. In particular, we can constrain the probability of PBH formation in the early universe [4]. See [5] for a recent review of theoretical and observational background and development in the studies of PBHs.

PBHs are usually assumed to have formed with the mass scale $M_{\rm h,f} \simeq G^{-1}c^3 t_{\rm f}$ which was contained within the Hubble horizon at the formation epoch, where G, c and $t_{\rm f}$ are the gravitational constant, the light speed and the formation time from big bang, respectively. This is based on the argument of the Jeans scale, gravitational radius and separate universe condition [4, 6]. This picture was subsequently modified after the discovery of critical behaviour in the formation of PBHs [7]. Nevertheless, the typical mass scale of the formed PBHs is still the horizon mass scale at the formation epoch, i.e.,

$$M_{\rm PBH,f} \simeq M_{\rm h,f} \simeq \frac{c^3 t_{\rm f}}{G} \simeq 1 M_\odot \left(\frac{T_{\rm f}}{100\ {\rm MeV}}\right)^{-2} \tag{1}$$

2 Newtonian argument of PBH growth

The accretion onto a PBH could change the mass scale of PBHs in principle. If we assume spherically symmetric and quasi-stationary flow onto a PBH, we can estimate the mass accretion rate of the black hole as

$$\frac{dM}{dt} = 4\pi\alpha r_{\rm A}^2 v_{\rm s} \rho_\infty, \tag{2}$$

where $r_{\rm A} = GM/v_{\rm s}^2$ is the accretion radius, $v_{\rm s}$ is the sound speed, ρ_∞ is the density at infinity and α is a constant of order unity. To apply the above equation for the growth of PBHs in the early universe, we assume that ρ_∞ is given by the density of the background Friedmann universe and $v_{\rm s}$ is the order of the speed of light. Then the above equation is integrated to give [6, 8]

$$M = \frac{At}{1 + \frac{t}{t_{\rm f}}\left(\frac{At_{\rm f}}{M_{\rm f}} - 1\right)}, \tag{3}$$

[1]E-mail:harada@scphys.kyoto-u.ac.jp

where $A \simeq c^3/G$ is a constant and M_f is the PBH mass at the time t_f of formation. Figure 1 shows three categories of solutions expressed by Eq. (3). In this argument, the effects of cosmological expansion are neglected. Therefore, the above analysis for PBHs much smaller than the cosmological horizon scale is expected to be valid. On the other hand, for PBHs as large as or larger than the cosmological horizon, which would be naturally realised just after the formation, the above analysis is suspect.

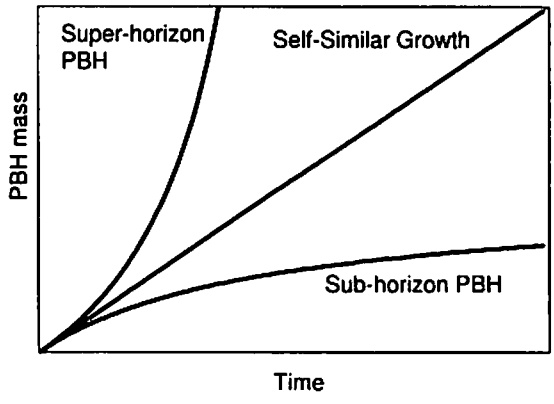

Figure 1: PBH mass growth based on the Newtonian argument. Three categories of solutions, sub-horizon, self-similar and super-horizon, are shown.

3 Numerical relativity in a scalar field universe

One of the dark energy models is a scalar field slowly rolling down on the potential, which is called quintessence. Recently, Bean and Magueijo [9] applied a quasi-Newtonian argument for the accretion of a quintessence field onto a PBH, which leads to solutions given by Eq. (3), and claimed that PBHs of inflation origin could be the seeds for supermassive black holes, based on a quantitative analysis.

To get insight into the growth of horizon-scale PBHs in the context of the quintessence/scalar field cosmology, we implement fully general relativistic numerical simulation of the growth of PBHs in a universe containing a massless scalar field. The line element in spherically symmetric spacetimes is given by

$$ds^2 = -a^2(u,v)dudv + r^2(u,v)(d\theta^2 + \sin^2\theta d\phi^2), \tag{4}$$

in the double-null coordinates and henceforth we use the geometrised units $G = c = 1$. Governing equations in this coordinate system are given in [10] explicitly. For the present problem, this scheme is advantageous because it has no apparent coordinate singularity and it also fits the characteristics of the propagation of the scalar field. The details of the numerical scheme and implementation are described in [10, 11].

In the double null-formulation, it is most natural to provide initial data on the null hypersurfaces $u = u_0$ and $v = v_0$ and solve a diamond region $u_0 < u < u_1$ and $v_0 < v < v_1$. As for initial data we adopt the simplest model, in which the Schwarzschild region is surrounded by the flat Friedmann background. To avoid the discontinuity at the matching surface, we set the smoothing region to retain the numerical accuracy.

Since we have null infinity in the flat Friedmann spacetime, we can define an event horizon. On the other hand, the notion of trapping horizons [12], which is very similar to apparent horizons, is also useful. This is defined as a hypersurface foliated by marginal surfaces and the definition is local. Although the event horizon and the trapping horizon coincide for the Schwarzschild black hole, they are different from each other for general dynamical cases.

4 Numerical results

Here we present the results for three models. See [11, 13] for the details of the chosen parameter values. We define the mass of the black hole using the Misner-Sharp mass [14] on the event horizon. Figure 2 shows the time evolution of the PBH mass and the mass contained within the cosmological apparent

horizon denoted as 'POTH' as the abbreviation of the past outer trapping horizon. We can still see that sub-horizon PBHs do not accrete much, the accretion onto horizon-scale PBHs is suppressed and super-horizon PBHs even decrease their mass.

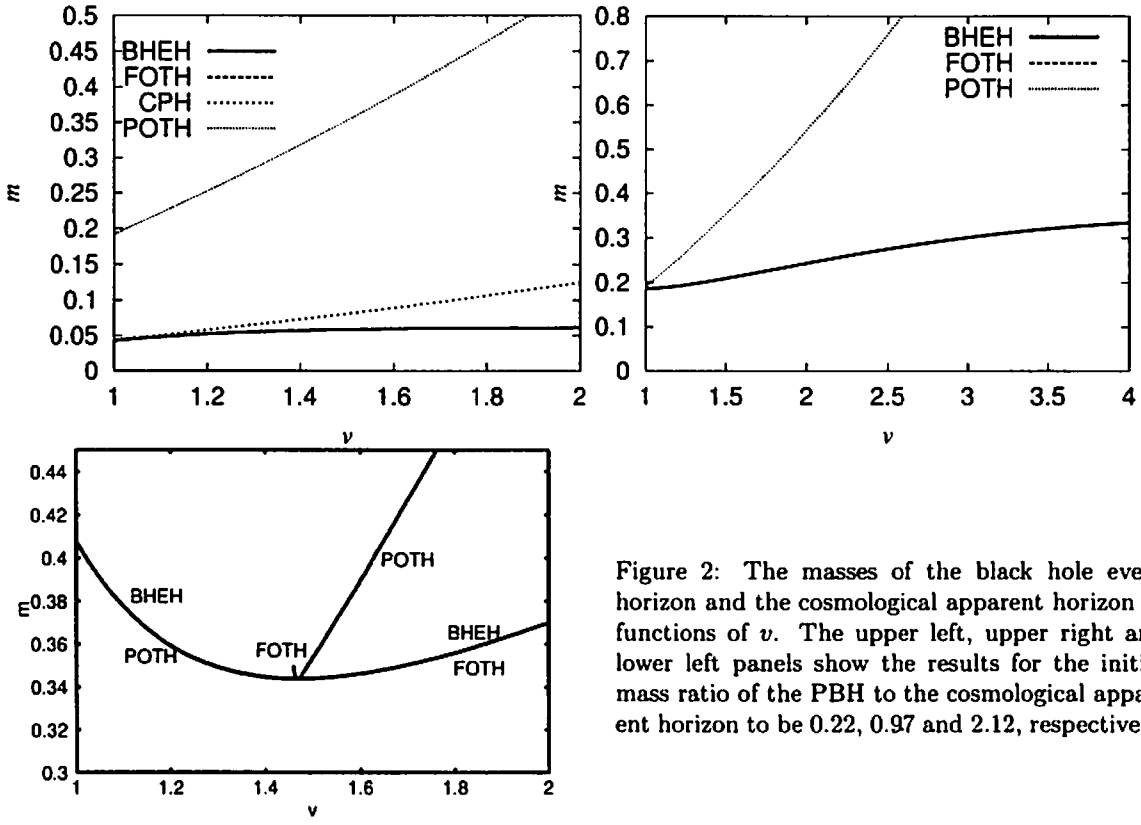

Figure 2: The masses of the black hole event horizon and the cosmological apparent horizon as functions of v. The upper left, upper right and lower left panels show the results for the initial mass ratio of the PBH to the cosmological apparent horizon to be 0.22, 0.97 and 2.12, respectively.

The evolution of PBHs of different masses is understood in terms of the mass accretion equation [11, 13]. The sign of the mass growth rate is governed by $r_{,u}$ on the event horizon. This corresponds to the expansion of ingoing null geodesic congruence on the event horizon. This is negative inside the cosmological horizon, but zero on and positive outside it. Figure 3 schematically summarises the results of general relativistic numerical simulations in contrast to Fig. 1.

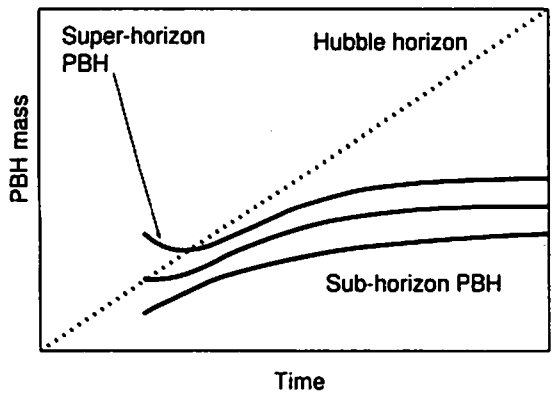

Figure 3: Schematic figure showing the mass growth of PBHs in a universe containing a massless scalar field, based on general relativistic numerical simulations.

For the models where the initial event horizon is past trapped, we can show that both first outgoing null ray $u = u_0$ and ingoing null ray $v = v_0$ reach infinity. This means we have two distinct null infinities but no regular centre and this results cannot be embedded into the standard diagram of the PBH. Figure 4

shows a possible causal struture, which is a very similar structure to the cosmological wormhole [15]. This implies the inflationary origin of super-horizon PBHs.

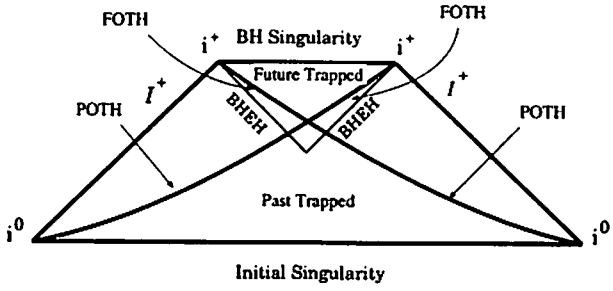

Figure 4: A possible causal struture of a super-horizon PBH in a scalar field universe. The spatial section has a wormhole structure, although it is not traversable.

5 Summary

The cosmic expansion is crucial for the growth of horizon-scale PBHs. The numerical relativity of scalar field PBHs shows that the accretion onto a PBH is significantly suppressed when the PBH is as large as the cosmological apparent horizon. The mass of super-horizon PBHs decreases although it always swallows the scalar field. In any case, PBHs do not accrete very much even during a scalar-field-dominated era. A complementary work is in preparation on the non-existence of PBHs growing self-similarly in a universe containing a scalar field whether massless or with a potential.

References

[1] Hawking S W 1971 *Phys. Rev. Lett.* **26** 1344

[2] Nakamura T, Sasaki M, Tanaka T and Thorne K S 1997 *Astrophys. J.* **487** L139

[3] Abbott B et al 2005 *Phys. Rev.* D**72** 082002

[4] Carr B J 1975 *Astrophys. J.* **201** 1

[5] Carr B J 2005 to appear in *Proceedings of Inflating Horizon of Particle Astrophysics and Cosmology* (Tokyo: Universal Academy Press) (*Preprint* astro-ph/0511743)

[6] Harada T and Carr B J 2005 *Phys. Rev.* D**71** 104009

[7] Niemeyer J C and Jedamzik K 1999 *Phys. Rev.* D**59** 124013

[8] Zel'dovich Y B and Novikov I D 1967 *Sov. Astron.* **10** 602

[9] Bean R and Magueijo J 2002 *Phys. Rev.* D**66** 063505

[10] Hamadé R S and Stewart J M 1996 *Class. Quantum Grav.* **13** 497

[11] Harada T and Carr B J 2005 *Phys. Rev.* D**71** 104010

[12] Hayward S A 1993 *Preprint* gr-qc/9303006

[13] Harada T and Carr B J 2005 *Phys. Rev.* D**72** 044021

[14] Misner C W and Sharp D H 1964 *Phys. Rev.* **136** B571

[15] Sato K, Sasaki S, Kodama H and Maeda K 1981 *Prog. Theor. Phys.* **65** 1443

Correspondence between Loop and Brane Cosmology

Shuntaro Mizuno[1], Edmund J. Copeland[2], James E. Lidsey[3]

[1] *Department of Physics, Waseda University, Okubo 3-4-1, Tokyo 169-8555, Japan*
[2] *School of Physics, University of Nottingham, University Park, Nottingham, NG7 2RD, UK*
[3] *Astronomy Unit, School of Mathematical Sciences, Queen Mary, University of London, Mile End Road, London, E1 4NS, UK*

Abstract

Braneworld scenarios are motivated by string/M-theory and can be characterized by the way in which they modify the conventional Friedmann equations of Einstein gravity. An alternative approach to quantum gravity, however, is the loop quantum cosmology program. In the semi-classical limit, the cosmic dynamics in this scenario can also be described by a set of modified Friedmann equations. We demonstrate that a dynamical correspondence can be established between these two paradigms at the level of the effective field equations. As concrete examples of this correspondence, we illustrate the relationships between different cosmological backgrounds representing scaling solutions.

1 Introduction

The high energy and high curvature regime of the very early universe provides a natural environment for investigating the cosmological consequences of quantum theories of gravity. At present, the two leading contenders for a theory of quantum gravity are string/M-theory and loop quantum gravity (LQG).

Developments in string/M-theory over recent years have led to a new paradigm for early universe cosmology - the braneworld scenario (see [1] for a review). In this picture, our observable, four-dimensional universe is viewed as a co-dimension one brane that is embedded in a five- or higher-dimensional 'bulk' space. Propagation of the brane through the bulk is interpreted as cosmic expansion or contraction by an observer confined to the brane. The brane-bulk dynamics typically results in modifications to the effective four-dimensional Friedmann equations of standard cosmology.

LQG, on the other hand, is a non-perturbative canonical quantization of Einstein gravity [2]. Loop quantum cosmology (LQC) restricts the analysis of LQG to spatially homogeneous models [3]. In the scenario developed by Bojowald [4, 5], there are two critical scales, a_i and a_*. Spacetime has a discrete structure below the scale $a_i \approx \ell_{\rm Pl}$, whereas classical gravity is recovered above a_*. The scale a_* is sensitive to the quantization scheme adopted and can be significantly larger than a_i. In this case, there exists a 'semi-classical' phase in the history of the universe for $a_i < a \ll a_*$, where spacetime may be viewed as a continuum but where non-perturbative quantum effects lead to modifications of the classical Friedmann equations. In particular, the kinetic energy of a scalar field becomes modified in such a way that $T = \dot{\phi}^2/D(a)$, where D is some function of the scale factor that tends to unity for $a \gg a_*$.

To date, the braneworld and LQC scenarios have been investigated along separate lines. However, given that both paradigms are motivated by quantum gravitational considerations, it is of interest to investigate the extent to which they may share any common features. This is the purpose of the present work.

2 Modified Cosmologies

2.1 Braneworld Cosmology

Here, we consider the class of spatially isotropic FRW world-volume metrics, where a canonical scalar field, χ, that self-interacts through a potential, $W(\chi)$, is confined to the brane with energy density

[1] E-mail:shuntaro@gravity.phys.waseda.ac.jp
[2] E-mail:Ed.Copeland@nottingham. ac.uk
[3] E-mail:j.e.lidsey@qmul.ac.uk

$\rho_\chi = \dot{\chi}^2/2 + W(\chi)$, pressure $p_\chi = \dot{\chi}^2/2 - W(\chi)$ and equation of state, $\gamma_B = 2\dot{\chi}^2/(\dot{\chi}^2 + 2W)$.

The dynamics for a wide class of such braneworlds can be described in terms of a generalized Friedmann equation of the form [7]

$$H^2 = \frac{8\pi\ell_{\rm Pl}^2}{3}\rho_\chi L^2(\rho_\chi) - \frac{k}{a^2}, \tag{1}$$

where modifications to conventional cosmology are determined by the form of the function $L(\rho_\chi)$. If there is no transfer of energy–momentum between the brane and bulk dimensions, the standard conservation equation holds:

$$\dot{\rho}_\chi + 3H(\rho_\chi + p_\chi) = 0. \tag{2}$$

Eqs. (1) and (2) are sufficient to completely determine the dynamics once the potential of the scalar field has been specified and may be written in the standard form of the FRW Einstein field equations sourced by a perfect fluid with an effective energy density and pressure:

$$\rho_{\rm B,eff} \equiv \rho_\chi^{n(\rho_\chi)}, \tag{3}$$

$$p_{\rm B,eff} = (\gamma_{\rm B,eff} - 1)\rho_{\rm B,eff}, \tag{4}$$

where the equation of state parameter is defined by

$$\gamma_{\rm B,eff} \equiv -\frac{1}{3}\frac{d(n\ln\rho_\chi)}{d\ln a}, \tag{5}$$

and we have introduced an index n defined as

$$n(\rho_\chi) \equiv 1 + 2\frac{\ln L(\rho_\chi)}{\ln\rho_\chi}. \tag{6}$$

In general, this is a function of the energy density on the brane and its form defines the braneworld model. Eq. (5) follows by differentiating Eq. (3) and substituting in the standard conservation equations. This implies that

$$H_{\rm B,eff}^2 = \frac{8\pi\ell_{\rm Pl}^2}{3}\rho_{\rm B,eff} - \frac{k}{a^2}, \tag{7}$$

$$\dot{\rho}_{\rm B,eff} = -3H(\rho_{\rm B,eff} + p_{\rm B,eff}). \tag{8}$$

2.2 Loop-Inspired Cosmology

The standard FRW equations may be derived by viewing the dynamics as a constrained Hamiltonian system $\mathcal{H} = 0$, where the Hamiltonian is given by

$$\mathcal{H} = -\frac{3}{8\pi\ell_{\rm Pl}^2}\left(\dot{a}^2 + k^2\right)a + \frac{1}{2}a^{-3}p_\varphi^2 + a^3V(\varphi), \tag{9}$$

and $p_\varphi = a^3\dot{\varphi}$ is the momentum canonically conjugate to the scalar field.

An alternative way of considering modified FRW cosmologies is to introduce corrections to the Hamiltonian (9). For example, we may consider the class of modified cosmologies where the inverse volume factor of the momentum of a scalar field, ϕ, is replaced by a function $D(a)$ of the scale factor such that:

$$\mathcal{H}_{\rm mod} = -\frac{3}{8\pi\ell_{\rm Pl}^2}\left(\dot{a}^2 + k^2\right)a + \frac{1}{2}D(a)a^{-3}p_\phi^2 + a^3V = 0, \tag{10}$$

where the conjugate momentum is now given by $p_\phi = D^{-1}(a)a^3\dot{\phi}$.

The primary motivation for considering models of this type comes from LQC. In isotropic LQC, the classical variables are the triad component $|p| = a^2$ and the connection component $c = \frac{1}{2}(k - \gamma\dot{a})$, where $\gamma \approx 0.274$ is the Barbero–Immirzi parameter. The divergent geometrical density, a^{-3}, that is present in the classical Hamiltonian (9) is quantized by employing the classical identity $a^{-3} = [3(8\pi\ell_{\rm Pl}^2 l)^{-1}\{c, |p|^l\}]^{3/(2-2l)}$, where $\{A, B\}$ denotes the Poisson bracket and l is a constant, and replacing the connection with holonomies along curves in space associated with the connection and triad [2]. In this

case, it can be shown that inverse factors of the scale factor are not required if $0 < l < 1$ [2]. Consequently, quantization results in a descrete spectrum of eigenvalues for the geometrical density operator that remains *bounded* as the spatial volume of the universe vanishes. This spectrum is closely approximated by a continuous 'eigenvalue function' of the scale factor $d_{j,l}(a) \equiv D(q)a^{-3}$, where [2, 4]

$$D(q) = \left\{ \frac{3}{2l} q^{1-l} \left[(l+2)^{-1} \left((q+1)^{l+2} - |q-1|^{l+2} \right) - \frac{1}{1+l} q \left((q+1)^{l+1} - \mathrm{sgn}(q-1)|q-1|^{l+1} \right) \right] \right\}^{3/(2-2l)}, \quad (11)$$

and $q = a^2/a_*^2$, $a_*^2 = a_i^2 j/3$, $a_i = \sqrt{\gamma}\ell_{\rm Pl}$. The parameter j must take half-integer (positive) values, but is otherwise arbitrary [8]. It arises because there is an ambiguity in expressing the classical geometrical density in terms of holonomies, since any irreducible SU(2) representation with spin j may be chosen.

The above discussion therefore motivates us to consider cosmological models defined by the effective Hamiltonian (10), where D may be viewed as an unspecified function of the scale factor, in the same way that the potential of the scalar field is regarded as a free function that is ultimately determined by particle physics considerations. We will refer to $D(a)$ as the 'kinetic correction' function. The field equations for this scenario then follow directly from the Hamiltonian constraint $\mathcal{H}_{\rm mod} = 0$ and Hamilton's equations and are given by

$$H^2 = \frac{8\pi l_{Pl}^2}{3} \left[\frac{1}{2D(a)} \dot{\phi}^2 + V \right] - \frac{k}{a^2}, \quad (12)$$

$$\ddot{\phi} + 3H \left(1 - \frac{1}{3} \frac{d\ln D}{d\ln a} \right) \dot{\phi} + D \frac{dV}{d\phi} = 0. \quad (13)$$

Eqs. (12) and (13) may also be expressed in the form of a conventional cosmology by defining an effective energy and pressure [6]:

$$\rho_{\rm L,eff} = \frac{\dot{\phi}^2}{2D} + V, \quad (14)$$

$$p_{\rm L,eff} = \frac{\dot{\phi}^2}{2D} \left(1 - \frac{1}{3} \frac{d\ln D}{d\ln a} \right) - V. \quad (15)$$

It follows that Eqs. (12) and (13) transform to

$$H_{\rm L,eff}^2 = \frac{8\pi \ell_{\rm Pl}^2}{3} \rho_{\rm L,eff} - \frac{k}{a^2}, \quad (16)$$

$$\dot{\rho}_{\rm L,eff} = -3H(\rho_{\rm L,eff} + p_{\rm L,eff}), \quad (17)$$

where the effective equation of state takes the form

$$\gamma_{\rm L,eff} = \frac{2\dot{\phi}^2}{\dot{\phi}^2 + 2DV} \left(1 - \frac{1}{6} \frac{d\ln D}{d\ln a} \right). \quad (18)$$

3 Correspondence between Loop–Inspired and Braneworld Cosmology

The correspondence between the braneworld and loop–inspired descriptions of cosmic dynamics is now established by identifying the effective equations of state for the two scenarios, i.e., $\gamma_{\rm B,eff} = \gamma_{\rm L,eff}$. Equating Eqs. (5) and (18) therefore leads to the constraint equation:

$$\frac{2\dot{\phi}^2}{\dot{\phi}^2 + 2DV} \left(1 - \frac{1}{6} \frac{d\ln D}{d\ln a} \right) = -\frac{1}{3} \frac{d}{d\ln a} (n \ln \rho), \quad (19)$$

where for notational ease we drop the subscript χ on the brane energy density in what follows. Imposing the constraint (19) implies that the two different scenarios lead to cosmologies with identical Hubble parameters, $H_L = H_B = H$, when these are viewed as functions of cosmic time, or equivalently, as

functions of the scale factor. The correspondence is not one–to–one since the loop–inspired description has two free functions – the potential $V(\phi)$ and the function $D(a)$. Thus, a given braneworld model will correspond to a class of loop–inspired cosmologies and vice–versa. More specifically, let us suppose that a particular braneworld scenario has been developed such that the FRW equations (1) and (2) have been solved for a given form of $n(\rho)$ to determine the equation of state for the scalar field, $\gamma_B = \gamma_B(a)$, and therefore the evolution of the energy density $\rho(a)$. Thus, the right–hand side of Eq. (19) is in principle known. A natural way of characterizing the classes of loop–inspired scenarios that lead to such cosmic behaviour is to specify the ratio of the field's potential and kinetic energies as a function of the scale factor: $V/\dot{\phi}^2 \equiv f(a)$. Eq. (19) can then be expressed in the form of a non–linear Bernoulli equation:

$$\frac{dD}{d\ln a} - \left[6 + \frac{d(n\ln\rho)}{d\ln a}\right] D = 2f(a)\frac{d(n\ln\rho)}{d\ln a} D^2, \tag{20}$$

and Eq. (20) may be solved in terms of a single quadrature by defining a new variable $D \equiv G^{-1}$. We find that

$$D^{-1} = \frac{1}{a^6\rho^n}\left[C - 2\int d(\rho^n)\, f(a) a^6\right], \tag{21}$$

where C is an integration constant.

4 Summary

The aim of this paper has been to investigate the extent to which two apparently disparate approaches to early universe cosmology, namely the braneworld scenario and loop quantum cosmology, may share some common features, at least from a dynamical point of view. From a phenomenological perspective, both paradigms are characterized by the way in which they lead to modifications of the standard Friedmann equations of classical cosmology. It has been shown that within the context of a general (spatially curved) FRW background sourced by a scalar field, a dynamical correspondence can be established between a given braneworld model and a class of loop–inspired backgrounds, in the sense that both approaches lead to an identical Hubble expansion if the correction terms arising in the Friedmann equations are related in an appropriate way.

For the applications to the scaling solutions and concrete examples to describe a given braneworld cosmology in terms of a loop-inspiered cosmology, please see Ref. [9].

References

[1] R. Maartens, Liv. Rev. Rel. **7**, 7 (2004).

[2] M. Bojowald, Pramana **63**, 765 (2004).

[3] M. Bojowald, Class. Quantum Grav. **19**, 2717 (2002).

[4] M. Bojowald, Class. Quantum Grav. **19**, 5113 (2002).

[5] M. Bojowald, Phys. Rev. Lett. **89**, 261301 (2002).

[6] J. E. Lidsey, D. J. Mulryne, N. J. Nunes, and R. Tavakol, Phys. Rev. D **70**, 063521 (2004.

[7] E. J. Copeland, S. J. Lee, J. E. Lidsey, and S. Mizuno, Phys. Rev. D **71**, 023526 (2005).

[8] M. Gaul and C. Rovelli, Class. Quantum Grav. **18**, 1593 (2001).

[9] E. J. Copeland, J. E. Lidsey, and S. Mizuno, Phys. Rev. D, to appear in, gr-qc/0510022.

Possibility of realization of a curvaton scenario in a theory with two dilatons coupled to the scalar curvature

Kazuharu Bamba[1], Motohiko Yoshimura[2]

[1] *Department of Earth and Space Science, Graduate School of Science, Osaka University, Toyonaka 560-0043, Japan*

[2] *Department of Physics, Okayama University, Tsushima-naka 3-1-1, Okayama 700-8530, Japan*

Abstract

The possibility of realization of a curvaton scenario is studied in a theory in which two dilatons are introduced along with coupling to the scalar curvature. It is shown that when two dilatons have an approximate O(2) symmetric coupling, a scalar field playing the role of the curvaton may exist in the framework of this theory without introducing any other scalar field for the curvaton. Thus the curvaton scenario can be realized, and in the simple version of the curvaton scenario in which the curvaton potential is quadratic, the curvature perturbation having an enough amplitude and a nearly scale-invariant spectrum suggested by observations obtained from WMAP could be generated.

1 Introduction

The hierarchy problem exists in both particle physics and cosmology: The former is the hierarchy problem between gravity and standard particle physics mass scales. The latter is the presence of a very small, but finite cosmological constant or the dark energy indicated by the analysis of type Ia supernovae observations, whose magnitude is as small as 120 orders less than its theoretically natural value, the Planck or a similar scale; its origin is not well understood yet. There has been no definite convection established in theoretical attempts so far.

Recently one of the present authors has attempted to construct a model [1] which simultaneously solves the above two hierarchy problems by radically changing cosmology in the same spirit of ideas as due to Dirac, [2], Brans and Dicke [3]: In this model, a theory with two dilaton fields coupled to the scalar curvature was considered; the existence of many dilatons is conceivable in the light of higher-dimensional theories. Moreover, it was argued that an effective gravity mass scale (the square root of the inverse of the Newton's constant) increases in the inflationary stage, and that the small cosmological constant or the dark energy density in the present Universe could be dynamically realized in the case that two dilatons have approximately an O(2) symmetry, taking the fundamental mass scale at TeV. In such a TeV scale model where the potential of dilatons is order $(\mathrm{TeV})^4$, however, it is conjectured that a naive estimate of the curvature perturbation gives a magnitude which is much smaller than the recent observational results of the anisotropy of cosmic microwave background (CMB) radiation obtained from Wilkinson microwave background probe (WMAP) [4]. Moreover, as is shown later, the power-law inflation could be realized in this model. In the standard inflation models, however, inflation is driven by the potential energy of a scalar field, called "inflaton", as it slowly rolls down the potential hill. This slow roll over in the quasi-de Sitter stage is practically necessary to account for the nearly scale-invariant spectrum of the primordial curvature perturbation out of the quantum fluctuation of the inflaton, which is also suggested by the observational results obtained from WMAP [4].

On the other hand, in recent years a new mechanism of generating the primordial curvature perturbation has been proposed, where a late-decaying massive scalar field provides the dominant source of the curvature perturbation [5–7]. In this scenario, the dominant part of the curvature perturbation originates from the quantum fluctuation of a new scalar field, called "curvaton", which is different from the inflaton. In contrast with the usual mechanism, inflation need not be of the slow-roll variety. Hence, even in the case of the power-law inflation, the nearly scale-invariant spectrum of the curvature perturbation demanded by the observations can be realized. Instead, it is required that the curvaton potential should be sufficiently flat during inflation.

The purpose of the present paper [8] is to argue that the curvaton scenario may be realized in the above theory, in which two dilatons are introduced along with the coupling to the scalar curvature [1]. In particular, we show that there exists a scalar field corresponding to the curvaton in the framework of this theory without introducing any other scalar field that plays the role of the curvaton, and discuss the case that the curvaton scenario is realized. Throughout the present paper we use units in which $k_B = c = \hbar = 1$ and denote the Newton's constant $G = m_{\rm Pl}{}^{-2}$, where $m_{\rm Pl} = 1.2 \times 10^{19}$GeV is the Planck mass.

2 Model

To begin with, we introduce two scalar fields φ_i $(i = 1, 2)$. Furthermore, we introduce dilatonic coupling of these scalars to the scalar curvature. Our model action is given as follows [1]:

$$S = \int d^4x\sqrt{-g}\left[-f(\varphi_i)R + \frac{1}{2}(\partial\varphi_i)^2 - V[\varphi_i] + \mathcal{L}_{\rm m}\right], \tag{1}$$

$$f(\varphi_i) = \epsilon_1\varphi_1^2 + \epsilon_2\varphi_2^2, \tag{2}$$

$$V[\varphi_i] = V_0\cos\frac{\varphi_{\rm r}}{M} + \Lambda, \tag{3}$$

where R is the scalar curvature arising from the spacetime metric tensor $g_{\mu\nu}$, g is the determinant of $g_{\mu\nu}$, $f(\varphi_i)$ is the coupling between dilaton and the scalar curvature with $\epsilon_i(>0)$ being dimensionless constants, $V[\varphi_i]$ is the potential of the dilaton with $\varphi_{\rm r} = \sqrt{\varphi_1^2 + \varphi_2^2}$ and $V_0 > \Lambda > 0$, M denotes a mass scale. Here we assume that $V_0 \approx \Lambda = O[M^4]$ and take the mass scale M of order TeV. Λ is a collection of all constants in the standard model Lagrangian $\mathcal{L}_{\rm m}$ such that the potential of the standard model Lagrangian vanishes at its minimum. We assume the O(2) symmetry for the potential $V[\varphi_i]$, while we allow its violation by taking $\epsilon_1 \neq \epsilon_2$. Moreover, we have used a simplified notation $(\partial\varphi_i)^2 \equiv g^{\mu\nu}\partial_\mu\varphi_i\partial_\nu\varphi_i$.

Field equations can be derived by taking variations of the above action in Eq. (1) with respect to the metric $g_{\mu\nu}$ and the dilatons φ_i as follows:

$$R_{\mu\nu} - \frac{1}{2}g_{\mu\nu}R = \frac{1}{2f}\left[T^{(\rm m)}_{\mu\nu} + T^{(\varphi_i)}_{\mu\nu}\right] + \frac{1}{f}\left(\nabla_\mu\nabla_\nu f - g_{\mu\nu}\Box f\right), \tag{4}$$

and

$$\Box\varphi_i = -\frac{\partial V}{\partial\varphi_i} - \frac{\partial f}{\partial\varphi_i}R, \tag{5}$$

where ∇_μ is a covariant derivative operator associated with $g_{\mu\nu}$, and $\Box \equiv g^{\mu\nu}\nabla_\mu\nabla_\nu$ is a covariant d'Alembertian for a scalar field. Here $R_{\mu\nu}$ is the Ricci curvature tensor, $T^{(\varphi_i)}_{\mu\nu}$ is contribution to the energy-momentum tensor from the scalars φ_i, while $T^{(\rm m)}_{\mu\nu}$ is the usual contribution of radiation, matter and other fields. Taking the trace of Eq. (4), we obtain

$$-R = \frac{1}{2f}\left[T^{(\rm m)} - (\partial\varphi_i)^2 + 4V(\varphi_i) - 6\Box f\right], \tag{6}$$

where $T^{(\rm m)}$ is the trace of $T^{(\rm m)}_{\mu\nu}$.

We now assume the spatially flat Friedmann-Robertson-Walker (FRW) spacetime with the metric

$$ds^2 = g_{\mu\nu}dx^\mu dx^\nu = dt^2 - a^2(t)d\vec{x}^2, \tag{7}$$

where $a(t)$ is the scale factor. In the FRW metric (7) the equations of motion for the background homogeneous scalar fields read

$$\ddot{\varphi}_i + 3H\dot{\varphi}_i = -\frac{\varphi_i}{\varphi_{\rm r}}V' - 2\epsilon_i\varphi_i R, \tag{8}$$

where a dot denotes a time derivative and a prime denotes a derivative with respect to φ_r. Here H is the Hubble parameter. Using the equations of motion for the dilaton fields (8) with Eq. (6), we find the dynamical equations of time in terms of the following two field variables: $f = \epsilon_1\varphi_1^2 + \epsilon_2\varphi_2^2$ and $\tilde{f} = \epsilon_1\varphi_1^2 - \epsilon_2\varphi_2^2$.

$$\ddot{f} + 3H\dot{f} = 2F^{-1}\left\{(\epsilon_1\dot{\varphi_1}^2 + \epsilon_2\dot{\varphi_2}^2) - \frac{f}{\varphi_r}V' + \frac{\epsilon_1^2\varphi_1^2 + \epsilon_2^2\varphi_2^2}{f}\left[T^{(m)} + 4V - (\dot{\varphi_1}^2 + \dot{\varphi_2}^2)\right]\right\}, \tag{9}$$

$$\ddot{\tilde{f}} + 3H\dot{\tilde{f}} = 2F^{-1}\left\{F(\epsilon_1\dot{\varphi_1}^2 - \epsilon_2\dot{\varphi_2}^2) - \left[\frac{\tilde{f}}{f} - 24\epsilon_1\epsilon_2(\epsilon_1 - \epsilon_2)\left(\frac{\varphi_1\varphi_2}{f}\right)^2\right]\frac{f}{\varphi_r}V'\right.$$
$$\left. + \left(\frac{\epsilon_1^2\varphi_1^2 - \epsilon_2^2\varphi_2^2}{f}\right)\left[T^{(m)} + 4V - (\dot{\varphi_1}^2 + \dot{\varphi_2}^2) - 12(\epsilon_1\dot{\varphi_1}^2 + \epsilon_2\dot{\varphi_2}^2)\right]\right\}, \tag{10}$$

$$F = 1 + 12\frac{\epsilon_1^2\varphi_1^2 + \epsilon_2^2\varphi_2^2}{f}. \tag{11}$$

Furthermore, the gravitational field equations read

$$H^2 = \left(\frac{\dot{a}}{a}\right)^2 = \frac{1}{6f}\left[T_{00}^{(m)} + \frac{1}{2}(\dot{\varphi_1}^2 + \dot{\varphi_2}^2) + V\right] - H\frac{\dot{f}}{f}, \tag{12}$$

$$\dot{H} - 2H\frac{\dot{f}}{f} = -\frac{F^{-1}}{f}\left[\frac{1}{12}\left(4FT_{00}^{(m)} - T^{(m)}\right) + (\epsilon_1\dot{\varphi_1}^2 + \epsilon_2\dot{\varphi_2}^2) + \frac{1}{4}\left(1 + 8\frac{\epsilon_1^2\varphi_1^2 + \epsilon_2^2\varphi_2^2}{f}\right)(\dot{\varphi_1}^2 + \dot{\varphi_2}^2)\right.$$
$$\left. - \frac{f}{\varphi_r}V' + 4\frac{\epsilon_1^2\varphi_1^2 + \epsilon_2^2\varphi_2^2}{f}V\right], \tag{13}$$

where in deriving the expression (13) we have used Eq. (9).

Next, we show that the power-law inflation can be realized in this model. Here we seek solutions with the following ansatz valid for large t:

$$f = At^2, \quad L = Bt, \quad \varphi_r = Ct, \quad a \propto t^\omega, \tag{14}$$

where $L = \varphi_1\dot{\varphi}_2 - \varphi_2\dot{\varphi}_1$ is the angular momentum; the existence of the angular momentum is one of the important feature of this model. We now assume that in the inflationary stage the cosmic energy density is dominated by the dilatons and hence $T_{\mu\nu}^{(m)}$ is negligible. In this model we consider the following case: In the inflationary stage, the field amplitude of the dilatons is given by $\varphi_1 = \gamma_1 M, \varphi_2 = \gamma_2 M$, where γ_1 and γ_2 are dimensionless parameters with time dependence. In addition, we suppose $\gamma_1 \approx \gamma_2 \approx \gamma = \gamma(t)$. In this case, $\varphi_r = \sqrt{\varphi_1^2 + \varphi_2^2} \approx \gamma M$. Hence, if $\gamma(t) \ll 1$ during inflation, we can neglect potential variation and recognize V as to be approximately Λ. Substituting the ansatz (14) into Eqs. (9), (12) and (13) and using the relation $\dot{\varphi_1}^2 + \dot{\varphi_2}^2 = \dot{\varphi_r}^2 + L^2/\varphi_r^2 = C^2 + B^2/C^2$, we find that in the small-value limit $\epsilon_i \ll 1$, ω is approximately expressed as follows:

$$\omega \approx \frac{\epsilon_1 + \epsilon_2}{8(\epsilon_1^2 + \epsilon_2^2)}. \tag{15}$$

In deriving the expression of ω in (15) we have assumed $\varphi_1^2 \approx \varphi_2^2$ and $\dot{\varphi_1}^2 \approx \dot{\varphi_2}^2$. Hence, in the limit $\epsilon_i \ll 1$ the index of the power ω can be much larger than unity, and thus the power-law inflation can be certainly realized.

Furthermore, we shall discuss the fluctuation equation in terms of f and $\tilde{f}$ in order to derive these mass values in the inflationary stage. With the following ansatz:

$$\begin{aligned} f &= f_0 + \delta f, \quad |\delta f| \ll |f_0|, \\ \tilde{f} &= \tilde{f}_0 + \delta\tilde{f}, \quad \left|\delta\tilde{f}\right| \ll \left|\tilde{f}_0\right|, \end{aligned} \tag{16}$$

where f_0 and $\tilde{f}_0$ are the zeroth order quantities and satisfy Eqs. (9) and (10), respectively, the linearized equations follow

$$\begin{pmatrix} \ddot{\delta f} + 3H\dot{\delta f} \\ \ddot{\delta \tilde{f}} + 3H\dot{\delta \tilde{f}} \end{pmatrix} = -\mathcal{M}^2 \begin{pmatrix} \delta f \\ \delta \tilde{f} \end{pmatrix}, \tag{17}$$

where

$$\mathcal{M}^2 \equiv \begin{pmatrix} \mathcal{M}^2{}_{11} & \mathcal{M}^2{}_{12} \\ \mathcal{M}^2{}_{21} & \mathcal{M}^2{}_{22} \end{pmatrix}. \tag{18}$$

In deriving the expression (17) we have taken the terms up to the first order of δf and $\delta \tilde{f}$. Making the diagonalization of the matrix $\mathcal{M}^2$ in (18), we estimate the eigenmasses of f and $\tilde{f}$. For example, for $\epsilon_1 = 3.1 \times 10^{-3}$, $\epsilon_2 = 3.0 \times 10^{-3}$, $\Upsilon = 1.5 \times 10^4$, $\gamma = 3.5 \times 10^{-4}$, and $t^{-1}/M = 3.7 \times 10^2$, the heavier eigenmass m_+ is estimated as $m_+ \approx 4.3H$, while the lighter eigenmass m_- is estimated as $m_- \approx 9.2 \times 10^{-3}H$. In deriving these values we have used the following relation: $H = \omega/t \approx \Upsilon M$, where $\Upsilon \equiv 1/\sqrt{6\alpha\gamma^2}$; this relation is derived from Eq. (12). Moreover, in this case it follows from Eq. (15) that $\omega = 4.1 \times 10^1$. Hence, in this case a huge hierarchy between the eigenmasses of f and $\tilde{f}$ could be realized; in particular, the lighter eigenmass m_- is much smaller than the Hubble parameter in the inflationary stage, so that the scalar field with the lighter eigenmass m_- can effectively correspond to the curvaton.

3 Conclusion

From the above consideration we understand that both two coupling constants between two dilatons and the scalar curvature are much smaller than unity, the power-law inflation in which the power-law exponent is much larger than unity is realized in this model, and that when the difference between the values of the two coupling constants is much smaller than those of them, in other words, two dilatons have an approximate O(2) symmetric coupling, there exists a scalar field corresponding to the curvaton with the mass much smaller than the Hubble parameter in the inflationary stage in this theory without introducing any other scalar field that may play the role of the curvaton. In fact, for $\epsilon_1 = 3.1 \times 10^{-3}$ and $\epsilon_2 = 3.0 \times 10^{-3}$, we have considered the simple version of the curvaton scenario [7] in which the curvaton field σ with mass $m_\sigma \equiv m_- \approx 9.2 \times 10^{-3}H$ has a quadratic potential. As a result, the curvature perturbation with an enough amplitude and a nearly scale-invariant spectrum (the spectral index of which is 0.98) suggested by observations obtained from WMAP [4] could be generated.

References

[1] M. Yoshimura, Phys. Lett. B **608**, 183 (2005).

[2] P.A.M. Dirac, Nature **139**, 323 (1937).

[3] C. Brans and R.H. Dicke, Phys. Rev. **124**, 925 (1961).

[4] D.N. Spergel et al., Astrophys. J., Suppl. Ser. **148**, 175 (2003).

[5] T. Moroi and T. Takahashi, Phys. Lett. B **522**, 215 (2001); Phys. Rev. D **66**, 395 (2002).

[6] K. Enqvist and M.S. Sloth, Nucl. Phys. **B626**, 395 (2002).

[7] D.H. Lyth and D. Wands, Phys. Lett. B **524**, 5 (2002); D.H. Lyth, C. Ungarelli, and D. Wands, Phys. Rev. D **67**, 023503 (2003).

[8] K. Bamba and M. Yoshimura, arXiv:hep-ph/0601047 (to be published in Prog. Theor. Phys. **115**, (2006)).

Black hole phase transition as nonequilibrium dynamics

Hiromi Saida[1]

Department of Physics, Daido Institute of Technology,
Takiharu-cho 10-3, Minami-ku, Nagoya 457-8530, Japan

Abstract

When a black hole evaporates due to the Hawking radiation, there should exist an energy flow from the horizon to the surrounding environment of the black hole. Precisely speaking, the existence of the energy flow means that the thermodynamic state of the whole system which consists of the black hole and the environment never be in any equilibrium state. That is, the Hawking radiation causes some nonequilibrium effect on the black hole evaporation. The aim of this manuscript is to investigate the nonequilibrium effects of the Hawking radiation on the black hole phase transition. And subsequently, a discussion on the information-loss problem is given.

1 Introduction

Consider the system that a black hole is put in a heat bath. It has been well known that the equilibrium state of the whole system which consists of the black hole and the heat bath is unstable for a sufficiently small black hole, and stable for a sufficiently large black hole. Therefore, when one distinguishes the phase of the system by the criterion whether the black hole can exist in equilibrium with the heat bath or not, the phase transition of the system occurs in varying the black hole radius. This is known as the black hole phase transition [1]. [2]

The black hole phase transition may be important in the study of primordial black holes, since the black holes would be formed in the radiation matter in the early universe. And, in relation with the possibility of the black hole formation in particle accelerators in the context of the so-called TeV gravity, the black hole phase transition will be important as well, since the black hole should be formed in the quark-gluon plasma in our brane and in the graviton gas in higher dimensional spacetime. Therefore, the study on the black hole phase transition, which is an old and well studied topic, may give some interesting contribution to the present trend in the study of black hole physics.

Once the instability of the equilibrium state (in four dimensional spacetime) happens, as explained in the next section, the black hole will evaporates out. In this manuscript, we concentrate on the evaporation process of the black hole after the instability of the equilibrium happens. During the black hole evaporation process in a heat bath, there should exist an energy flow from the black hole horizon to the heat bath due to the Hawking radiation. Precisely speaking, the existence of the energy flow means that the thermodynamic state of the whole system which consists of the black hole and the heat bath never be in any equilibrium state. That is, the Hawking radiation causes some nonequilibrium effect on the black hole evaporation. Therefore, we aim to investigate the nonequilibrium effects of the Hawking radiation on the black hole phase transition. And subsequently, we will discuss the information-loss problem at the end of this manuscript.

Throughout this manuscript, we use the Planck unit, $\hbar = c = G = k_B = 1$. Then the Stefan-Boltzmann constant becomes, $\sigma = \pi^2/60$

2 Equilibrium discussion

Before proceeding to the study of the nonequilibrium effects of the Hawking radiation, we briefly review the original discussion of the black hole phase transition [1], which is based only on the equilibrium states of the whole system which consists of a black hole and heat bath.

[1]E-mail:saida@daido-it.ac.jp

[2]The extension of this theoretical phenomenon to AdS black holes is called the Hawking-Page phase transition.

As already been treated in the reference [1], the (Schwarzschild) black hole can be modelled as a spherical black body whose equations of states are as follows,

$$E_g = \frac{1}{8\pi T_g} = \frac{R_g}{2} \quad , \quad S_g = \frac{1}{16\pi T_g} = \pi R_g \,, \tag{1}$$

where R_g, T_g, S_g are respectively the radius, temperature and entropy of the body, and E_g is the internal energy of the body which corresponds to the mass of a black hole. It is obvious from these equations that the radius R_g decreases when the body loses its energy E_g. The black hole evaporation can be represented by the energy-loss of this body. Note that the heat capacity C_g of this body is negative,

$$C_g = \frac{dE_g}{dT_g} = -\frac{1}{8\pi T_g^2} = -2\pi R_g^2 < 0 \,. \tag{2}$$

It should be emphasised here that, although we consider a black body with the equations of states (1), not all effects of the gravity are neglected in our modelling. The negative heat capacity is the peculiar property of self-gravitating systems. That is, the gravitational effects by a black hole is encoded in the forms of the equations of states (1). Hence hereafter, we call the black body the black hole.

Put the black hole into a heat bath of heat capacity $C_h^{(eq)} > 0$, and consider that the whole system which consists of the black hole and the heat bath is isolated from outside environments and in an equilibrium state, in which the temperature of the heat bath T_h equals T_g. The statistical (and/or quantum) fluctuation raises a temperature difference $\delta T = T_g - T_h \neq 0$. What follows the fluctuation is different with respect to the size of the black hole and the signature of δT.

If $|C_g| > C_h^{(eq)}$ and $\delta T > 0$, the energy flows from the black hole to the heat bath, $dE_g < 0$. Further $dT_g > 0$ and $dT_h > 0$ due to $C_g < 0$ and $C_h > 0$. Then, because the whole system is isolated, $dE_g + dE_h = 0$ holds, where E_h is the internal energy of the heat bath. Then we find $dT_g = dE_g/C_g < dE_h/C_h^{(eq)} = dT_h$. This means that $\delta T \to 0$ after a sufficiently long time. The same discussion is true of the case $|C_g| > C_h^{(eq)}$ and $\delta T < 0$. That is, the equilibrium state of the whole system is stable for a sufficiently large black hole for which $|C_g| = 2\pi R_g^2 > C_h^{(eq)}$ holds.

If $|C_g| < C_h^{(eq)}$ and $\delta T > 0$, the energy flows from the black hole to the heat bath, $dE_g < 0$, $dT_g > 0$ and $dT_h > 0$. However, similar calculations as in the previous paragraph result in the inequality, $dT_g > dT_h$. This means that $\delta T \to \infty$ and $R_g \to 0$ after a sufficiently long time, which corresponds to the black hole evaporation. On the other hand, for the case $\delta T < 0$, we obtain $dT_g < 0$, $dT_h < 0$ and $|dT_g| > |dT_h|$. This means that the black hole grows $dR_g > 0$, and finally the heat capacity becomes to satisfy the stable condition $|C_g| > C_h^{(eq)}$. In summary for the case $|C_g| < C_h^{(eq)}$, the whole system transfers to the equilibrium state without black hole (only the heat bath remains) for the fluctuation $\delta T > 0$, or to the equilibrium state with sufficiently large black hole for the fluctuation $\delta T < 0$. Because it seems that the probability of occurrence of the fluctuation $\delta T > 0$ is 1/2, the probability of occurrence of the black hole evaporation for a sufficiently small black hole in a heat bath is 1/2.

3 Nonequilibrium effects

The discussion so far has been based only on the equilibrium state of the whole system which consists of the black hole and the heat bath. As mentioned in the section 1, there should be nonequilibrium region at least near the surface of the black hole due to the energy flow during the evaporation process for a sufficiently small black hole. By the way, the energy exchange between a true black hole and its environment is never carried out by heat conduction but by the exchange of particle fluxes, since the black hole is not composed of matters. The particle flux from the black hole horizon is the Hawking radiation. Hereafter we consider photons as the representative of the particle flux which carries out the energy exchange between the black hole and the heat bath. Hence in our model, we hollow out a spherical (thick) shell region around the black hole from the heat bath as shown in the left panel in the figure 1, then the hollow region is filled up with the radiation fields emitted by the black hole and by the heat bath.

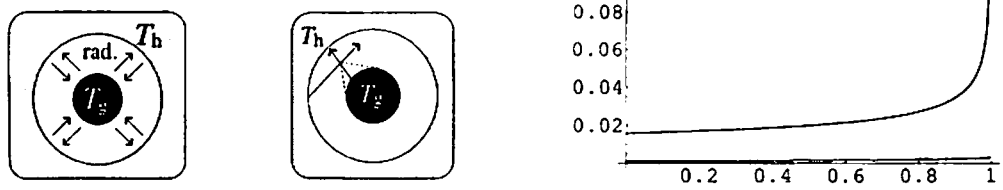

Figure 1: Left and centre are for nonequilibrium modelling. Right is for the temperature evolution. Time is normalised as $t/640\pi R_0^3$, where R_0 is the initial radius of the black hole. The time $630\pi R_0^3$ is the evaporation time of a black hole if it is put in an empty space (without heat bath).

During the evaporation process ($T_g \neq T_h$), the radiation field in the hollow region is in a two-temperature nonequilibrium state. Further, we assume that the evaporation proceeds so slowly that the temperatures T_g and T_h can be approximated as constant during one photon emitted by the black hole flies in the hollow region until absorbed by the heat bath. Therefore the thermodynamic state of the radiation field in the hollow region is a macroscopically stationary nonequilibrium state which we call the *steady state* hereafter. While the thermodynamic states of the black hole and the heat bath change along sequences of equilibrium states in state space during the evaporation process, however the thermodynamic state of the radiation field in the hollow region changes along a sequence of steady states in state space. The thermodynamics of two-temperature steady states for a radiation field has already been established in [2] and already been applied to a black hole evaporation in an empty space (without heat bath) [3].

The total energy of the whole system is $E_{tot} = E_g + E_h + E_{rad}$, where E_g and E_h are respectively the internal energies of the black hole and the heat bath, and E_{rad} is the internal energy of the radiation field in the hollow region which is given by the reference [2],

$$E_{rad} = 4\sigma\left(G_g T_g^4 + G_h T_h^4\right) \quad , \quad G_g = \int_{V_{rad}} dx^3 \gamma_g(x) \quad , \quad G_h = \int_{V_{rad}} dx^3 \gamma_h(x) \, ,$$

where $\gamma_g(x)$ is the solid-angle divided by 4π which is covered with photons emitted by the black hole and comes to a point x (see the centre panel in the figure 1), $\gamma_h(x)$ is defined similarly ($\gamma_g(x) + \gamma_h(x) = 1$), and $V_{rad} = G_g + G_h$ is the volume of the hollow region. The differential of E_{tot} becomes

$$dE_{tot} = C_X dT_g + C_Y dT_h \quad , \quad C_X = C_g + 16\sigma G_g T_g^3 \quad , \quad C_Y = C_h + 16\sigma G_h T_h^3 \, ,$$

where $C_h (> 0)$ is the heat capacity of the heat bath evaluated after the hollow region is removed from the previous heat bath considered in the section 2. From this form of dE_{tot}, we can interpret that the whole system consists of two sub-systems X and Y, where the sub-system X is composed of the black hole and the "out-going" radiation field emitted by the black hole of temperature T_g, and the sub-system Y is composed of the heat bath and the "in-going" radiation field emitted by the heat bath of temperature T_h. The heat capacities of the sub-systems X and Y are respectively C_X and C_Y. Here note that the equation (2) means that the heat capacity C_X of the sub-system X can be positive $C_X > 0$ for a sufficiently small black hole and negative C_Y for a sufficiently large black hole. The positive capacity case $C_X > 0$ is impossible as explained below.

Set $E_{rad}^{(g)} = 4\sigma G_g T_g^4$ and $E_{rad}^{(h)} = 4\sigma G_h T_h^4$, that is $E_{rad} = E_{rad}^{(g)} + E_{rad}^{(h)}$. For the case $T_g > T_h$, we have $dE_g < 0$ and $dE_h > 0$, and consequently $dT_g > 0$ and $dT_h > 0$ due to $C_g < 0$ and $C_h > 0$. Then $dE_{rad}^{(g)} > 0$ and $dE_{rad}^{(h)} > 0$ holds. Further if $C_X > 0$, we find $|dE_g| < dE_{rad}^{(g)}$ due to $dE_X = C_X dT_g > 0$. Hence we obtain $dE_{tot} = dE_g + dE_{rad}^{(g)} + dE_{rad}^{(h)} + dE_h > 0$. This contradicts our assumption that the whole system is isolated $dE_{tot} = 0$. The same discussion holds for the case $T_g < T_h$, and a contradiction results. Therefore we should conclude that $C_X > 0$ is impossible in the framework of our steady state modelling. This indicates that the whole system goes into a highly nonequilibrium state as $T_g \to T_g^* - 0$, where T_g^* is given by $C_X(T_g^*) = 0$. As seen below, the evaporation will proceed in an accelerated fashion as $T_g \to T_g^* - 0$, due to the highly nonequilibrium nature of the system at $T_g = T_g^*$.

Since the energy exchange between the sub-systems X and Y is carried out by radiation, the Stefan-Boltzmann law works well,

$$C_X \frac{dT_g}{dt} = -\sigma \left(T_g^4 - T_h^4\right) \quad , \quad C_Y \frac{dT_h}{dt} = \sigma \left(T_g^4 - T_h^4\right) . \tag{3}$$

The numerical plot of the solutions $T_g(t)$ and $T_h(t)$ for these differential equations is shown in the right panel in the figure 1, and we observe $dT_g/dt \to \infty$ as $T_g \to T_g^* - 0$. This denotes that the black hole goes into a highly nonequilibrium state and proceeds suddenly to the final stage of the evaporation. Further it is also found that the evaporation time t_{ev} which is given by $T_g(t_{ev}) = T_g^*$, is faster than the evaporation time $t_{ev}^{(eq)} (> t_{ev})$ for the case treated in the previous section 2, where the $t_{ev}^{(eq)}$ is calculated by the same way as for t_{ev} using the equations (3) with setting $V_{rad} = 0$. It is concluded that the nonequilibrium effect of the Hawking radiation tends to accelerate the black hole evaporation in comparison with the original consideration done in [1].

Next, for the case $C_X < 0$, the criterion for the instability of the equilibrium of the whole system is given by the similar discussion as in the section 2,

$$|C_X| < C_Y \quad \Rightarrow \quad |C_g| < C_h^{(eq)} + 16\sigma G_g \left(T_g^3 - T_h^3\right) , \tag{4}$$

where $C_h^{(eq)} = C_h + 16\sigma T_h^4 V_{rad}$ is the heat capacity of the heat bath plus the radiation field when it is in the equilibrium state of temperature T_h. Note that the equilibrium discussion given in the previous section 2 can be recovered with setting the radiation field in the hollow region being in an equilibrium with the heat bath. The equation (4) denotes that the nonequilibrium effect makes the whole system more stable for the case $T_g < T_h$ and more unstable for the case $T_g > T_h$ than the equilibrium discussion given in the section 2.

4 Summary and discussions

We have investigated the nonequilibrium effects of the Hawking radiation on the black hole phase transition. It is concluded that, once the black hole evaporation occurs, the evaporation process proceeds more rapidly than the case ignoring the nonequilibrium effects. And the equilibrium state of the whole system is more stable for the fluctuation which causes $T_g < T_h$, and more unstable for the fluctuation which causes $T_g > T_h$.

Finally we estimate the total entropy of the whole system. Using the steady state entropy given in the reference [2] for a radiation field between the black hole and the heat bath, we can obtain the total entropy S_{tot}^* at the time t_{ev} ($T_g = T_g^*$). Next assume that the black hole evaporates out completely and only the equilibrium radiation field is remained after the evaporation, and determine the temperature of the remained radiation by equating its energy with the mass of the black hole at the time t_{ev}. We can calculate the total entropy of the system $S_{tot}^{(eq)}$ which consists of only radiation field. Then it is found that the entropy difference $\Delta S_{tot} = S_{tot}^{(eq)} - S_{tot}^*$ becomes negative. This implies that some remnant should remain after a black hole evaporation, and the remnant possesses the entropy which compensates more than $|\Delta S_{tot}|$.

References

[1] S.W.Hawking, "Black holes and thermodynamics", *Phys.Rev.*D (1976) 191 - 197

[2] H.Saida, "Two-temperature steady state thermodynamics for a radiation field", *Physica* A (2005) 481 - 508

[3] H.Saida, "Black Hole Evaporation and Nonequilibrium Thermodynamics for a Radiation Field", *Proceedings of the 14th Workshop on General Rel. and Grav. in Japan*, gr-qc/0505089

Toward a No-go Theorem for Accelerating Universe by Nonlinear Backreaction

Masumi Kasai[1], Hideki Asada[2], Toshifumi Futamase[3]

[1,2] *Faculty of Science and Technology, Hirosaki University, Hirosaki 036-8561, Japan*
[3] *Astronomical Institute, Tohoku University, Sendai, 980-8578, Japan*

Abstract

Backreaction of nonlinear inhomogeneities to the cosmic expansion is analyzed in the framework of general relativity. In order to pay special attention to the gauge issues, the calculation is done in the Newtonian gauge. By defining the spatially averaged matter energy density as a conserved quantity in the large comoving volume, it is shown that the nonlinear backreaction neither accelerates nor decelerates the cosmic expansion in a matter-dominated universe. The conclusion is consistent with the previous works done in the comoving synchronous gauge. Although our work does not give a complete proof, it strongly suggest the following no-go theorem: no cosmic acceleration occurs due to nonlinear backreaction via averaging.

1 Introduction

The present state of the local universe is neither homogeneous nor isotropic. The density contrast of matter distribution is much larger than unity in smaller scales. The solution of the Einstein equation with an averaged homogeneous matter distribution is not that with realistic matter distribution because of nonlinearity of the Einstein equation. Thus it is naturally expected that the expansion law of the FLRW model may be modified by the local inhomogeneities. In fact there have been such investigations in the past [1, 2, 3, 4, 5, 6, 7, 8, 9, 10] and some modification has been reported with apparent discrepancies among these works (For instance, [3, 8]). It might depend on the choice of the coordinates as well as the definition of the averaging procedure. As a result, it has not been possible to relate such a nonlinear effect clearly with observations. Here we shall settle down this confusion by carefully constructing the averaged FLRW model in the framework of general relativity.

2 post-Newtonian metric

We assume the irrotational dust as a matter in the universe. The energy-momentum tensor is written as

$$T^{\mu\nu} = \rho u^\mu u^\nu, \tag{1}$$

where u^μ is the four velocity of the fluid flow. For simplicity, we assume the Einstein-de Sitter background. It is sufficient to consider the cosmological post-Newtonian metric at the linear order [1, 2, 3, 9]

$$ds^2 = -(1+2\phi(\boldsymbol{x}))\,dt^2 + a^2(1-2\phi(\boldsymbol{x}))\,\delta_{ij}\,dx^i dx^j, \tag{2}$$

where δ_{ij} denotes the Kronecker's delta, because the 00-component of the metric has a second order quantity at the post-Newtonian order but it induces third or higher order corrections in the backreaction and they are thus negligible in our computations. From the Einstein equation at the linear order, we obtain

$$\phi_{,ii} = \frac{3}{2}\dot{a}^2\left(\frac{\rho-\rho_b}{\rho_b} + 2\phi\right), \tag{3}$$

[1]E-mail:kasai@phys.hirosaki-u.ac.jp
[2]E-mail:asada@phys.hirosaki-u.ac.jp
[3]E-mail:tof@astr.tohoku.ac.jp

$$v^i \equiv \frac{u^i}{u^0} = -\frac{2}{3a\dot{a}}\phi_{,i}, \tag{4}$$

where ρ_b is the background density and the contraction is taken by δ_{ij}.

Up to the quadratic order of ϕ, the averaged Einstein equation becomes

$$\left(\frac{\dot{a}}{a}\right)^2 = \frac{8\pi G}{3}\langle T_{00}\rangle + \frac{1}{a^2}\langle\phi_{,i}\phi_{,i}\rangle, \tag{5}$$

$$\frac{\ddot{a}}{a} = \frac{4\pi G}{3}\langle T_{00} + \rho_b a^2 v^2\rangle - \frac{1}{3a^2}\langle\phi_{,i}\phi_{,i}\rangle, \tag{6}$$

where $v^2 = \delta_{ij}v^iv^j$.

Eq. (5) seems to indicate that the nonlinear backreaction expressed by the second term of the R.H.S. might *increase* the expansion rate. However, this is not the case. In order to get a correct answer, we have to clarify what the mean energy density $\bar{\rho}$ of dust matter is. Most of previous works are short of this consideration. The mean density must obey

$$\dot{\bar{\rho}} + 3\frac{\dot{a}}{a}\bar{\rho} = 0. \tag{7}$$

Besides, one could not relate the backreaction properly with a deviation from the Hubble expansion driven by the mean density. Clearly, $\langle T_{00}\rangle$ does not act as $\bar{\rho}$.

In order to guarantee that $\bar{\rho}$ satisfies Eq. (7), we have to define the mean density as

$$\bar{\rho} \equiv \langle T_{00}\rangle + \rho_b a^2\langle v^2\rangle + \frac{1}{4\pi G a^2}\langle\phi_{,i}\phi_{,i}\rangle. \tag{8}$$

Then, Eqs. (5) and (6) are rewritten as

$$\left(\frac{\dot{a}}{a}\right)^2 = \frac{8\pi G}{3}\bar{\rho} - \frac{1}{9a^2}\langle\phi_{,i}\phi_{,i}\rangle, \tag{9}$$

$$\frac{\ddot{a}}{a} = \frac{4\pi G}{3}\bar{\rho}. \tag{10}$$

At this point, we can safely call the second term of the R.H.S. of Eq. (9) the *nonlinear backreaction*.

3 Concluding remarks

Eqs. (9) and (10) show the following things.

- The nonlinear backreaction neither accelerates nor decelerates the cosmic expansion. In other words, the cosmic acceleration $\ddot{a}/a$ is determined merely by the mean density.
- The nonlinear backreaction reduces the expansion rate $\dot{a}/a$.
- The nonlinear backreaction changes as $\propto a^{-2}$ in the averaged Friedmann equation. Hence, it behaves as a (small) positive curvature term in the Friedmann model. This correction might be measure by future space observations such as a Planck mission.

It should be noted that Eqs. (9) and (10) do not rely on averaging procedures, though an explicit form of the mean density does. For instance, one may use simply $\langle A\rangle \equiv V^{-1}\int A d^3x$ [2]. Changes induced by using a different averaging scheme occur simultaneously only inside $\bar{\rho}$ of Eqs. (9) and (10). Furthermore, the nonlinear backreaction term is invariant at the second order for a choice of averaging procedures.

It is worthwhile to mention gauge issues in the backreaction problem. One may ask "what happens under a different gauge condition?" The comoving synchronous (CS) gauge is employed to discuss the influence of the backreaction on the age of the universe [8] based on the relativistic version of the Zeldovich-type approximation [6, 7]. By using the CS gauge, one can obtain equations similar to Eqs. (9) and (10); there is no change in the cosmic acceleration, and the averaged Hubble equation has the positive spatial curvature as a correction. Therefore, it strongly suggests that the above conclusion is valid independent of a gauge choice. In practice, either the post-Newtonian type or the CS gauges is employed in previous studies of the nonlinear backreaction problem as far as the present authors know. In this sense, our conclusion should be considered serious.

References

[1] K. Tomita, Prog. Theor. Phys. **79**, 322 (1988).

[2] T. Futamase, Mon. Not. R. Astron. Soc. **237**, 187 (1989).

[3] T. Futamase, Phys. Rev. D **53**, 681 (1996).

[4] M. Kasai, Phys. Rev. Lett. **69**, 2330 (1992).

[5] M. Kasai, Phys. Rev. D **47**, 3214 (1993).

[6] M. Kasai, Phys. Rev. D **52**, 5605 (1995).

[7] H. Russ, M. Morita, M. Kasai and G. Börner, Phys. Rev. D **53**, 6881 (1996).

[8] H. Russ, M. H. Soffel, M. Kasai and G. Börner, Phys. Rev. D **56**, 2044 (1997).

[9] M. Shibata and H. Asada, Prog. Theor. Phys. **94**, 11 (1995).

[10] H. Asada and M. Kasai, Phys. Rev. D **59**, 0123515 (1999).

Research for the Nature of Dark Matter via the Lensing Effects on High Redshift Type Ia Supernovae Observation

Chul-Moon Yoo[1], Hideki Ishihara[2] and Ken-ichi Nakao[3]

Department of Mathematics and Physics, Graduate School of Science, Osaka City University, Osaka 558-8585, Japan

Abstract

Distance-redshift relation via Type Ia supernovae observations is simulated including effects of gravitational lensing in a clumpy universe. Calculations are carried out in the two cases. In the first case, it is assumed that all of the matter in the universe constitutes randomly distributed spheres each of which has identical mass M_L and uniform mass density. Then we consider the situations in which supernovae can be treated as point sources. In the other case, we assume point mass lenses and consider the situations in which we have to treat the supernovae as extended sources.

1 Introduction

Many cosmological observations suggest that our universe is globally homogeneous and isotropic, or in other word, the time evolution of the global aspect is well approximated by Friedmann-Lemaître (FL) cosmological models. On the other hand, we know that our universe is locally inhomogeneous. Effects of the inhomogeneity to the evolution of our universe or to cosmological observations attract an attention as one of the important issue of the cosmology. However, it is difficult that we directly observe the inhomogeneity with optical observations because most of the matter in our universe is not luminous. One of the useful phenomenon for the investigation into the inhomogeneity is gravitational lensing. Electromagnetic waves receive gravitational lensing effects caused by inhomogeneously distributed matter around their trajectories. Therefore, we may find properties of the inhomogeneity from observational studies of gravitational lensing. For this purpose, theoretical studies about lensing effects in interesting situations are necessary.

There are some candidates for the dark matter such as weakly interacting massive particles (WIMPs) and massive compact halo objects (MACHOs). As far as we know, the configuration of the dark matter is not well constrained by cosmological observations, in other words, one does not know whether the dark matter constitutes smoothly distributed microscopic objects or macroscopic compact objects. Then we assume the clumpy universe model which satisfies following assumptions. Firstly, this model is globally Einstein-de Sitter (EdS) universe. Secondly, all of the matter constitutes spheres (point masses) each of which have the mass M_L. Hereafter, we call this spheres as lenses or dark matter clouds. Finally, the dark matter clouds are uniformly distributed. The concrete description about our clumpy universe model is in Ref. [1]. This study indicate that one may find the typical mass and size (the radius of the sphere) of dark matter clouds in our universe from an observational study about gravitational lensing effects on high redshift supernovae observations.

In this paper, we clarify the effect of gravitational lensing on the distance-redshift relation. There are several works for this purpose [2]. In these works, the main purpose is the suggestion about the method to investigate the fraction of compact objects in the universe using supernovae observations. They have not thought about the situations in which one have to treat the lenses or the sources as extended objects. Here, we consider the following two situations. In the first case, it is assumed that all of the matter in the universe constitutes randomly distributed spheres each of which has identical mass M_L and uniform mass density. Then we consider supernovae as point sources. In the other case, we assume point mass lenses and consider the situations in which we have to treat the supernovae as extended sources.

[1]E-mail:c_m_yoo@sci.osaka-cu.ac.jp
[2]E-mail:ishihara@sci.osaka-cu.ac.jp
[3]E-mail:knakao@sci.osaka-cu.ac.jp

In this paper, we adopt angular diameter distance as cosmological distance. In the clumpy universe, angular diameter distance measured by unlensed light rays is given as the Dyer-Roeder (DR) distance D_{DR} [3]. When a light ray experiences gravitational lensing with magnification μ, the observed angular diameter distance $D_{\rm obs}$ is given as $D_{\rm obs} = D_{DR}/\sqrt{\mu}$.

Hereafter, we adopt the unit of $G = c = 1$.

2 Supernovae as point sources and extended lenses

2.1 Settings and the calculation method

In this section, we treat supernovae as point sources and lenses as extended objects. The above treatment is valid only when the width of a light beam emitted by a supernova is much thiner than the Einstein radius of lens objects. The light beam width is given by the order of the size of supernovae at peak brightness $\sim 10^{15}$cm. The Einstein radius of lens objects is the order of $\sqrt{M_L D}$, where M_L is the mass of the lens and D is typical distance to supernovae given as $\sim$ 1Gpc in high redshift supernova events. Therefore we assume the following inequality:

$$\sqrt{M_L D} \gg 10^{15}\text{cm} \Leftrightarrow M_L \gg 10^{-2} M_\odot.$$

We focus on effects of gravitational lensing on the distance-redshift relation. In the case of point mass lenses, we know that there is large dispersion in the observed distance [4]. On the other hand, if the size of lenses is much larger than the Einstein radius, it may naively be expected that the dispersion in the distance is smaller than the former case and the distance-redshift relation agree with the case in which all of matter is homogeneously distributed. We are also interested in the case $\sqrt{M_L D} \sim L$, where L is the radius of lenses. When the size of the lenses comparable to the Einstein radius, strong lensing, i.e., lensing with multiple images may be important. We assume that the multiple images are can not be separated in observational limit and we can only observe total magnification of the light rays.

In order to take account of multiple images, we use the multiple lensing calculation method proposed by K. P. Rauch [5]. The concrete description about the calculation method is in Ref. [1]. The brief description is follows. 1. The dark matter clouds are put in each redshift uniformly. 2. We ignore clouds far from the ray. 3. Lens mappings are calculated with the multiple lens plane method [6] and the Newton-Raphson method. 4. Summing up magnifications of all images, we obtain total magnification.

2.2 Results

We have calculated distance-redshift relations of 2,000 samples. We have set L/R_E as $L/R_E = 1, 5, 10$ and 20. The results are shown in Fig. 1. The dispersion in the distance decrease with increasing L/R_E and the average of distance vary with the value of L/R_E. This result indicate that we may find the size of dark matter clouds from the dispersion in the distance.

3 Supernovae as extended sources

3.1 Settings and the calculation method

In this section, we treat supernovae as extended sources and lenses as point masses. This treatment is useful in the case $M_L \lesssim 10^{-2} M_\odot$. We focus on the variation of the distance-redshift relation with the value of M_L. In our clumpy universe model, the averaged mass density in the universe is fixed at that of EdS universe. Thus the number density of the lenses are increase with decreasing the mass M_L. When the number density increase, the number of lenses in a light beam increase. Then we can naively expect that the effect of lensing is averaged and the distance-redshift relation might become that of EdS universe.

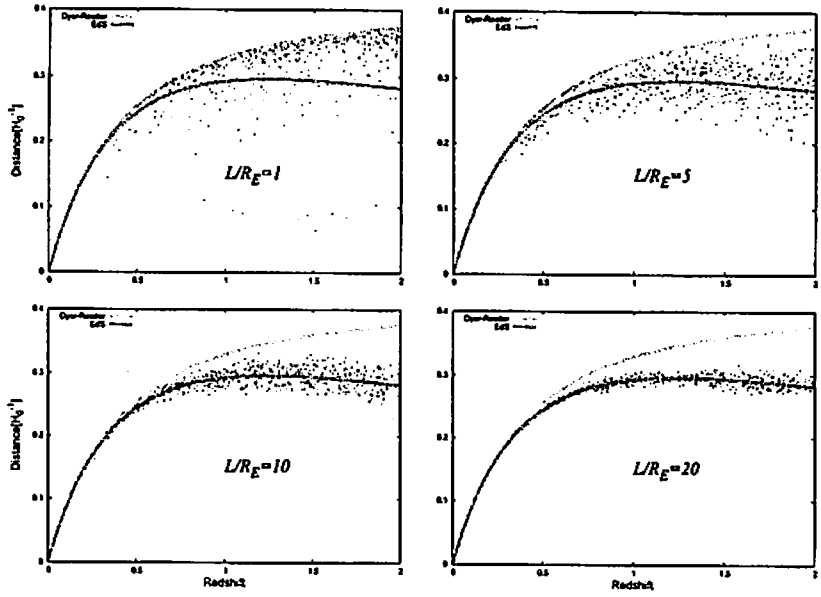

Figure 1: 2,000 samples of distance-redshift relations are depicted in each figure, where $L/R_E = 1, 5, 10$ and 20. The DR distance is represented by the blue line and the conventional distance measured in EdS universe is represented by the green line.

In the calculation, we set sources as spheres whose radius is given as 10^{15}cm. We divide the emitting region into many parts and calculate each magnification with the method stated in Sec. 2.1. Then we average the magnifications given in the above calculations.

3.2 Results

We have calculated distance-redshift relations of 1,000 samples. We have set the lens mass M_L as $M_L = 10^{-5}$ and $10^{-4} M_\odot$. The results are shown in Fig. 2. The dispersion in the distance increase with

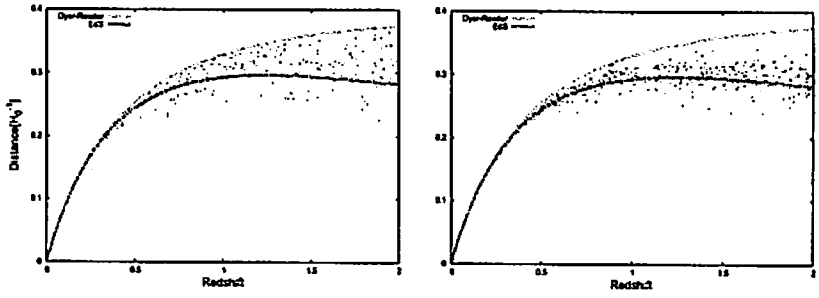

Figure 2: 1,000 samples of distance-redshift relations are depicted in each figure. The lens mass M_L is given as $M_L = 10^{-5}$ and $10^{-4} M_\odot$. The DR distance is represented by the blue line and the conventional distance measured in EdS universe is represented by the green line.

increasing M_L. This result indicate that we may find the typical mass of dark matter clouds via high redshift supernovae observations.

10 samples of the time evolution of the magnification is shown in Fig. 3, where we put $M_L = 10^{-5} M_\odot$. Since supernovae extend with time, the light beam widths become thick with time. Then the number

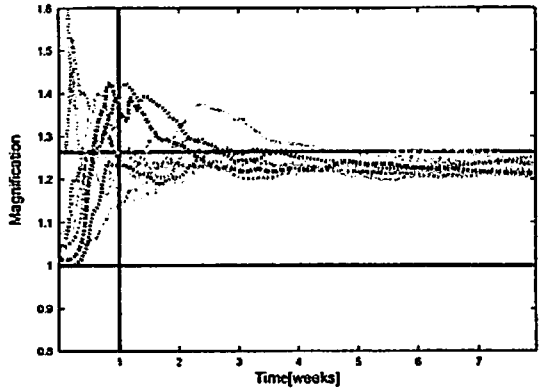

Figure 3: 10 samples of the time evolutions of the magnifications are depicted here. The mass of lenses is put as $M_L = 10^{-5} M_\odot$. The lower horizontal line represents the magnification corresponding to the DR distance. The upper horizontal line represents the magnification corresponding to the distance in EdS universe.

of lenses in the beam increase with time. As a result, dispersion in the magnification is decrease with time and the convergent value of the magnification is nearly equal to the value of the magnification corresponding to the distance in EdS universe. Since the time when the statistical property of the magnifications vary depend on M_L, we may find the typical mass of lenses from the time evolutions of the magnifications.

4 Summary

We have calculated the lensing effects on supernovae observations in the two cases. In the first case, it is assumed that all of the matter in the universe constitutes randomly distributed spheres each of which has identical mass M_L and uniform mass density. Then we consider the situations in which supernovae can be treated as point sources. We have shown that we may find the size of dark matter clouds from the dispersion in the distance measured by high redshift supernovae.

In the other case, we assume point mass lenses and consider the situations in which we have to treat the supernovae as extended sources. We have shown that we may find the mass of dark matter clouds from the dispersion in the distance or time evolutions of the magnifications measured by high redshift supernovae.

References

[1] C. M. Yoo, K. Nakao, H. Kozaki and R. Takahashi, in preparation.

[2] R. B. Metcalf and J. Silk, Astrophys. J. **519**, L1 (1999) [arXiv:astro-ph/9901358]; U. Seljak and D. E. Holz, arXiv:astro-ph/9910482; E. Mörtsell, A. Goobar and L. Bergström, Astrophys. J. **559**, 53 (2001).

[3] C. C. Dyer and R. C. Roeder, Astrophys. J. **180**, 31 (1973).

[4] D. E. Holz and R. M. Wald, Phys. Rev. D **58**, 063501 (1998) [arXiv:astro-ph/9708036].

[5] K. P. Rauch, Astrophys. J. **374**, 83 (1991)

[6] P. Schneider, J. Elers and E. E. Falco, *Gravitational Lenses* (New York : Springer)

The Quintom Model of Dark Energy

Bo Feng[1]

National Astronomical Observatories, Chinese Academy of Sciences, Beijing 100012, P. R. China
Research Center for the Early Universe(RESCEU), Graduate School of Science, The University of Tokyo, Tokyo 113-0033, Japan

Abstract

In this paper I give a brief review on the recently proposed new scenario of dark energy model dubbed *Quintom*. Quintom describes the dynamical dark energy models where the equation of state getting across the cosmological constant boundary during evolutions. I discuss some aspects on the quintom model buildings and the observational consequences.

1 Introduction

The nature of dark energy is among the biggest problems in modern physics and has been studied widely. The simplest candidate of dark energy is the cosmological constant, it suffers from the well-known fine-tuning and coincidence problems [1, 2]. Alternatively, dynamical dark energy models with the rolling scalar fields have also been proposed, such as quintessence[3, 4], the ghost field of phantom [5] and the model of k-essence which has non-canonical kinetic term [6].

Given that currently we know very little on the theoretical aspects of dark energy, the cosmological observations play a crucial role in our understandings. The model of phantom has been proposed in history due to the fact that the observations have shown some mild preference for an equation of state(EOS) smaller than -1[5]. Although in this scenario dark energy violates the weak energy condition(WEC) and leads to the problem of quantum instabilities[7, 8], we need more efforts on this observation-inspired topic.

The Type Ia supernova (SNIa) observations from the HST/GOODS program and the previous supernova data[9], which make the only direct measurements of dark energy, somewhat favor the dynamical dark energy model with an equation of state getting across -1 during the evolutions[10]. If such a kind of dynamical dark energy were verified by future observations, it would be a challenge to the dark energy model buildings. Neither the cosmological constant nor the dynamical scalar fields like quintessence or phantom would be the source driving the current accelerated expansion of the Universe. The model of quintessence has an equation of state which is always no smaller than minus unity while the ghost field of phantom has an EOS always no larger than -1. Basing on these facts we proposed a new model of dark energy dubbed *Quintom*[11], in the sense that the required behavior of the dynamical dark energy combines that of quintessence and phantom. The purpose of this paper is to discuss briefly some aspects on the quintom model buildings and the corresponding observational consequences.

2 The Quintom Model of Dark Energy

Phenomenologically in comparison with quintessence and phantom, the behavior of quintom is more flexible and it can lead to some distinctive pictures in the determinations in the future of our Universe. In Ref.[12] we proposed a scenario of quintom with oscillating equation of state. We find oscillating Quintom can unify the early inflation and current acceleration of the universe, leading to oscillations of the Hubble constant and a recurring universe. Our oscillating Quintom would not lead to a big crunch nor big rip. In Ref.[13] we found interestingly the current observations somewhat favor an oscillating quintom with a much smaller period than that required in the recurrent universe scenario. Note in Refs.[12, 13] they are phenomenological studies only and are not focused on quintom model buildings.

[1] E-mail:fengbo@resceu.s.u-tokyo.ac.jp

At the first sight it seems to be easy for the quintom model buildings, since naively one may consider a model with a non-canonical kinetic term with the following effective Lagrangian[11]:

$$\mathcal{L} = \frac{1}{2} f(T) \partial_\mu Q \partial^\mu Q - V(Q) \,, \tag{1}$$

where $f(T)$ can be a dimensionless function of the temperature or scalar fields. During the evolution of the universe when $f(T)$ crosses the point of zero it gives rise to the crossing of the cosmological constant boundary. However one also needs to consider the dynamics of the $f(T)$ term in reality and this makes it not straightforward for successful quintom model buildings. When we consider realistic quintom models we need also to consider their spatial fluctuations. It is crucial for us to understand its imprints in the cosmological observations. If we simply neglect dark energy perturbations and start from parametrizations of the scale factor $a(t)$, it would be very easy to construct quintom models since this is somewhat like reconstruction of a using $w(t)$.

It turns out that if we consider the usual kessence as the candidate of quintom, at the crossing point it cannot be quantized in a canonical way[15]. Due to the problems on perturbations, we cannot realize quintom with a single fluid or single scalar field in the conventional way. In general one needs to add extra degrees of freedom for successful quintom model buildings. In Ref[11] we considered the simplest case with one quintessence field and the other being the phantom field:

$$\mathcal{L} = \frac{1}{2}\partial_\mu\phi_1\partial^\mu\phi_1 - \frac{1}{2}\partial_\mu\phi_2\partial^\mu\phi_2 - V_0[\exp(-\frac{\lambda}{m_p}\phi_1) + \exp(-\frac{\lambda}{m_p}\phi_2)] \,.$$

Such a two-field model can easily cross the cosmological constant boundary(See also [14]). However for the simplest two-field model we are faced with the problem of ghost instabilities inherited inevitably in the phantom component[7, 8]. Another possibility of introducing the extra degrees of freedom for the realization of quintom was proposed in Ref. [16], where we introduced higher derivative operators to the Lagrangian. Specifically we considered a model with the Lagrangian

$$\mathcal{L} = -\frac{1}{2}\nabla_\mu\phi\nabla^\mu\phi + \frac{c}{2M^2}\Box\phi\Box\phi - V(\phi) \,, \tag{2}$$

where $\Box \equiv \nabla_\mu\nabla^\mu$ is the d'Alembertian operator. The term related to the d'Alembertian operator is absent in the quintessence, phantom and the k-essence model, which is the key to make the model possible for w to cross over -1. We have shown in [16] this Lagrangian is equivalent to an effective two-field model

$$\mathcal{L} = -\frac{1}{2}\nabla_\mu\psi\nabla^\mu\psi + \frac{1}{2}\nabla_\mu\chi\nabla^\mu\chi - V(\psi-\chi) - \frac{M^2}{2c}\chi^2 \,, \tag{3}$$

with

$$\chi \equiv \frac{c}{M^2}\Box\phi \,, \tag{4}$$

$$\psi \equiv \phi + \chi \,. \tag{5}$$

Note that the redefined fields ψ and χ have opposite signs in their kinetic terms. One might be able to derive the higher derivative terms in the effective Lagrangian (2) from fundamental theories. For example it has been shown that this type of operators appears as some quantum corrections or due to the non-local physics in the string theory. In principle as the Lagrangian (2) is equivalent to the two-field model the phantom instabilities still exist. However we can also expect in the two cases their behaviors are different when we consider the possible interactions. In particular, Ref.[18] has shown that in this scenario ghosts arise because of the canonical treatment, where ϕ and $\Box\phi$ are regarded as two independent variables. An alternative quantization based on the path integral seems to be intriguing towards solving the problem of ghosts[18].

The model of quintom was initiated by the SNIa observations, in realistic quintom model buildings we need to consider the imprints in the concordance observational cosmology. In the probe of quintom signatures in cosmic microwave background (CMB) and large scale structure (LSS) we need to consider the effects of dark energy perturbations. When dark energy is not simply the cosmological constant in

general it will cluster on the largest scales, which can leave some imprints on the observations. Ref.[19] has shown that for scalar models of dark energy like quintessence and phantom, the effects of dark energy perturbations are to introduce more degeneracies with the equation of state on CMB. In our simplest two-field quintom case we have found that crossing the cosmological constant boundary would not lead to distinctive effects. On the other hand for models of scalar dynamical dark energy the equation of state is not a constant in general, however the effect on CMB can be almost identically described by a constant EOS:

$$w_{eff} \equiv \frac{\int da\Omega(a)w(a)}{\int da\Omega(a)} \quad , \tag{6}$$

hence it is easily understood when we include the effects of quintom perturbations it will be in more degeneracy with the geometric parameter w. In general when we add geometrical data the degeneracy between a constant w_{eff} and a dynamical w can be somewhat broken, but it still exists due to limits on the precisions of the current SNIa observations.

In the study of quintom perturbations it is straightforward in the two-field case. But cosmologists are sometimes more interested in the inverse study on dark energy through fittings to the cosmological observations. In the fittings one typically parameterizes the equation of state. However when we parameterize quintom-like dark energy the problem arises in the study on the imprints of perturbations. We need to bear in mind what spectrum this kind of dark energy displays: it cannot be a simple one-field scalar or single ideal fluid, the perturbations will diverge for these cases. We introduce a small positive constant c to divide the whole region of the allowed value of the EOS w into three parts[15]: 1) $w > -1 + c$; 2) $-1 + c > w > -1 - c$; and 3) $w < -1 - c$. In Regions 1) and 3) the parameterized dark energy can be described as conventional quintessence and phantom. In Region 2) numerically we have set the derivatives of pressure and density perturbations to be zero at the extremely limited matching point. Through this method our study of parameterized quintom can resemble two-field quintom models and no singularities appear. In Ref.[17] we have made global fittings on the current status of dynamical dark energy including quintessence, phantom and quintom. We have found that a dynamical dark energy with the EOS getting across -1 is favored at 1σ with the combined constraints from WMAP, SDSS and the "gold" dataset of SNIa by Riess *et al*, see Fig.1. In previous investigations due to the problems on quintom perturbations the fittings in the literature typically did not include dark energy perturbations in the probe of dynamical dark energy. We can find this will lead to nontrivial bias. Similarly we can also easily understand quintom perturbation will play a significant role in probing dynamical dark energy using future precise measurements like SNAP and JDEM.

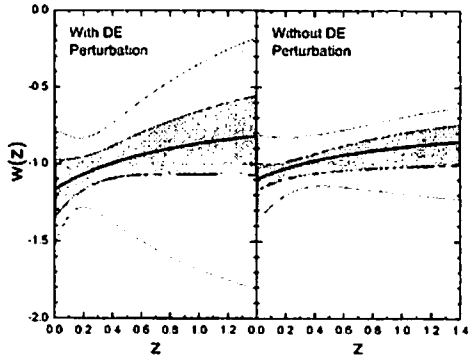

Figure 1: Constrains on w(z) using WMAP + 157 "gold" SNIa data + SDSS with/without DE perturbation[17]. Median(central line), 68%(inner, dark grey) and 95%(outer, light grey) intervals of w(z) using 2 parameter expansion of the EOS: $w(z) = w_0 + w_1 \frac{z}{1+z}$, with z being the redshift.

We should point out currently on the observational aspect a cosmological constant still fits the data quite well. Nevertheless the SNIa observations, which make the only direct detections of dark energy,

somewhat favor a dynamical quintom-like dark energy. Note we need to set several priors before we can get detailed investigations on probing dark energy with SNIa only. On the other we need more thorough understandings on the dynamical mechanism of Type Ia supernova, both the quality and quantity of SNIa are to be improved. Currently there are still various possibilities and alternatives on the model of dark energy[20].

Both theoretical and observational probe of dark energy need still go a long way. If we start always from a ΛCDM model in the probe of our universe we cannot achieve more subtle physics beyond that. This is necessary to bear in mind for us to understand the nature of dark energy with the accumulation of the observational data.

3 Acknowledgments

I thank my collaborators for discussions. I am indebted to Profs. Xuelei Chen and Jun'ichi Yokoyama and without their kind hospitality part of my work cannot be finished.

References

[1] S. Weinberg, Rev. Mod. Phys. **61**, 1 (1989).

[2] I. Zlatev, L.-M. Wang, and P. J. Steinhardt, Phys. Rev. Lett. **82**, 896 (1999).

[3] R. D. Peccei, J. Sola and C. Wetterich, Phys. Lett. B **195**, 183 (1987); C. Wetterich, Nucl. Phys. B **302**, 668 (1988).

[4] B. Ratra and P. J. E. Peebles, Phys. Rev. D **37**, 3406 (1988).

[5] R. R. Caldwell, Phys. Lett. B **545**, 23 (2002).

[6] C. Armendariz-Picon, V. Mukhanov and P. J. Steinhardt, Phys. Rev. Lett. **85**, 4438 (2000); T. Chiba, T. Okabe and M. Yamaguchi, Phys. Rev. D **62** (2000) 023511.

[7] S. W. Hawking, Print-86-0124 (CAMBRIDGE).

[8] S. M. Carroll, M. Hoffman and M. Trodden, Phys. Rev. D **68**, 023509 (2003); J. M. Cline, S.-Y. Jeon and G. D. Moore, Phys. Rev. D **70**, 043543 (2004).

[9] A. G. Riess *et al.* [Supernova Search Team Collaboration], Astrophys. J. **607**, 665 (2004).

[10] e.g. D. Huterer and A. Cooray, Phys. Rev. D **71**, 023506 (2005).

[11] B. Feng, X. L. Wang and X. M. Zhang, Phys. Lett. B **607**, 35 (2005).

[12] B. Feng, M. Li, Y. S. Piao and X. Zhang, arXiv:astro-ph/0407432.

[13] J. Q. Xia, B. Feng and X. M. Zhang, Mod. Phys. Lett. A **20**, 2409 (2005).

[14] Z. K. Guo, Y. S. Piao, X. M. Zhang and Y. Z. Zhang, Phys. Lett. B **608**, 177 (2005); X. F. Zhang, H. Li, Y. S. Piao and X. M. Zhang, arXiv:astro-ph/0501652.

[15] G. B. Zhao, J. Q. Xia, M. Li, B. Feng and X. Zhang, Phys. Rev. D **72**, 123515 (2005).

[16] M. Z. Li, B. Feng and X. M. Zhang, JCAP **0512**, 002 (2005).

[17] J. Q. Xia, G. B. Zhao, B. Feng, H. Li and X. Zhang, arXiv:astro-ph/0511625.

[18] S. W. Hawking and T. Hertog, Phys. Rev. D **65**, 103515 (2002).

[19] J. Weller and A. M. Lewis, Mon. Not. Roy. Astron. Soc. **346**, 987 (2003).

[20] e.g. H. Li, B. Feng, J. Q. Xia and X. Zhang, arXiv:astro-ph/0509272.

Constraining curvature and dark energy from the baryon acoustic peak and supernovae

Kazuhide Ichikawa[1]

Institute for Cosmic Ray Research, University of Tokyo, Chiba 277-8582, Japan

Abstract

We discuss the constraints on the time-varying equation of state for dark energy and the curvature of the universe using observations of type Ia supernovae from Riess et al. and the most recent Supernova Legacy Survey (SNLS), the baryon acoustic oscillation peak detected in the SDSS luminous red galaxy survey and cosmic microwave background. We find degeneracies among the parameters which describe the time dependence of the equation of state and the curvature of the universe, when we use a single observational data, but we show the combination of the above observations yields even if we consider the time-varying equation of state and do not assume a flat universe. Especially, we found that the combined data set favors a flat universe even if we consider the time variation of dark energy equation of state.

1 Introduction

Almost all current cosmological observations indicate that the present universe is accelerating. It can be explained by assuming that the universe is dominated by dark energy today. Although many candidates for dark energy have been proposed so far, we still do not know the nature yet. Many studies have been devoted to investigate dark energy assuming or constructing a specific model and then study its consequences on cosmological observations such as cosmic microwave background (CMB), large scale structure (LSS), type Ia supernovae (SNeIa) and so on. On the other hand, many efforts have also been made to study dark energy in phenomenological way, i.e., as model independent as possible. In such approaches, dark energy can be parameterized with its equation of state and constraints on it can be obtained using cosmological observations. Assuming that the equation of state for dark energy w_X is constant in time, current observations give the constraint as $w_X \sim -1$ [1, 2, 3, 4]. Although one of the most famous models for dark energy is the cosmological constant whose equation of state is $w_X = -1$, most models proposed so far have time-varying equation of state. Thus, when we study dark energy, we should accommodate such time dependence in some way.

Many recent works on dark energy investigate the time dependence of the dark energy equation of state using simple parameterizations such as $w_X = w_0 + w_1(1 - a)$ with a being the scale factor of the universe [5]. Parameterizing the dark energy equation of state in simple ways, the constraints on the time evolution of w_X have been considered (for recent works on this issue, for example, see Ref. [6]). It should be mentioned that, when one studies the equation of state for dark energy, it is usually assumed that the universe is flat. It should be also noted that dark energy is usually assumed to be the cosmological constant when one derives the constraint on the curvature of the universe. However, it has been discussed that, assuming a non-flat universe, the constraints on w_X and the curvature of the universe can be relaxed to some extent even with the time independent w_X from the CMB data alone [7]. Also, even if we assume a flat universe, there are degeneracies among the parameters which describe the evolution of dark energy, i.e., the time dependence of w_X when we consider the constraints on dark energy [8]. Furthermore it has been also discussed that if we remove the prior of a flat universe, the degeneracies becomes much worse [9]. Since it is very important to study the time dependence of w_X to differentiate the models of dark energy and also the curvature of the universe to test the inflationary paradigm, we should investigate how the prior on the curvature of the universe affects the determination of the time-varying equation of state for dark energy and vice versa. Some works along this line have been done using a specific one-parameter parameterization for the time-varying w_X [10].

[1]E-mail:kazuhide@icrr.u-tokyo.ac.jp

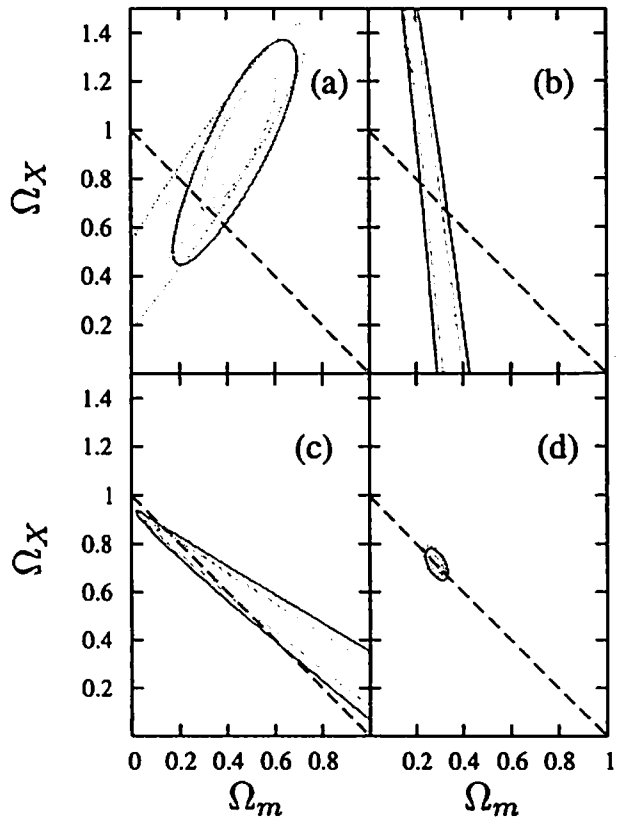

Figure 1: Constraints on Ω_m and Ω_X from SNeIa (a), the baryon acoustic oscillation peak (b), the CMB shift parameter (c) and all data combined (d). For the constraint from SNeIa data and all data combined, we show the contours obtained from the gold set of Ref. [3] and SNLS [4] separately. Contours of 1σ (red solid line) and 2σ (green dashed line) are shown (for SNLS data, 1σ and 2σ contours are shown in blue dash-dotted line and purple dotted line, respectively). We assumed the cosmological constant as dark energy and a flat universe here.

In this study, we investigate this issue, namely the determination of the evolution of dark energy and the curvature of the universe, in some detail using widely used parameterization of the equation of state for dark energy

$$w_X(z) = w_0 + \frac{z}{1+z} w_1 = w_0 + (1-a)w_1, \tag{1}$$

where z is the redshift. . We consider the constraints from observations of SNeIa reported in Refs. [3, 4], the baryon acoustic oscillation detected in the SDSS luminous red galaxy survey [11] and recent CMB observations including WMAP [1]. We refer our full paper Ref.[12] for the details of our analysis method.

2 Constraints

Now we discuss the implication of the dark energy evolution on the determination of the curvature of the universe. For this purpose, we derive the constraints from the observations on the Ω_m vs. Ω_X plane. The results are shown in Figs. 1 and 2.

We see that the constraint on the curvature of the universe is significantly relaxed from a single observation when we allow the time dependence in the dark energy equation of state (see panels (a), (b) and (c) in Figs. 1 and 2). However, it was also shown that, when we use all data sets, the curvature of the universe or the energy density of matter and dark energy are severely constrained to be $\Omega_m \sim 0.3$

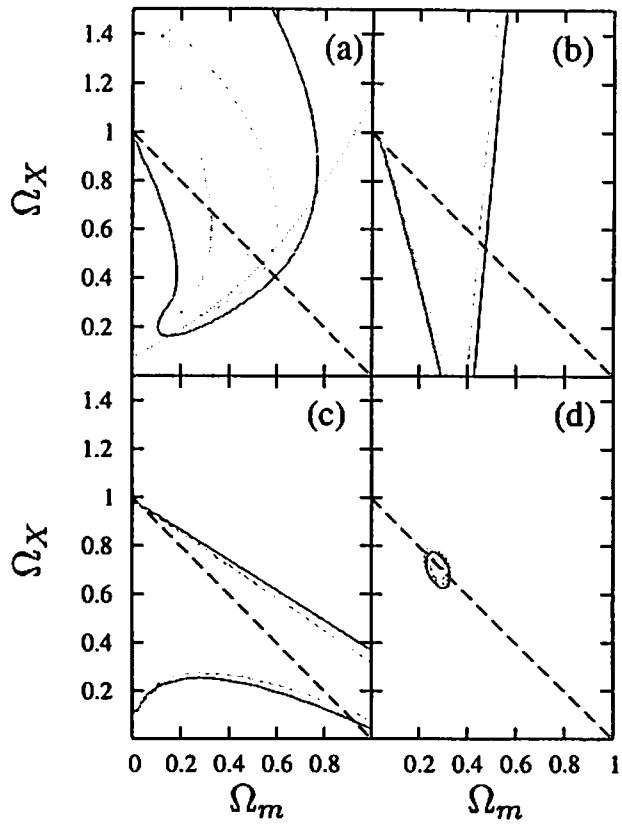

Figure 2: The same as Fig. 1 except that we consider the time dependent equation of state for dark energy and marginalize over w_0 and w_1.

and $\Omega_{\rm tot} \sim 1$ even if we consider the time-varying equation of state for dark energy (see panels (d) in Figs. 1 and 2. The contours in them have almost same size and position on the line which indicates flat universe).

This is understood as follows. Observations we consider here measure some distance scales to certain redshifts which can be determined by the energy density of matter Ω_m, dark energy Ω_X and the equation of state w_X. If we assume a broad range for w_X, the energy density of matter Ω_m and dark energy Ω_X can have more freedom to be consistent with observations since the fit to the data depends on the combinations of these variables. For a single observation, if w_X is allowed to vary more freely, much larger range of values of Ω_m and Ω_X can be consistent with observations. However, when we use all observations, the combinations of Ω_m, Ω_X and w_X consistent with observations become fairly limited. Thus even if the allowed regions become large for each data set, when we combine all the data, we can obtain a severe constraint, which is interestingly almost the same region as that we obtain assuming the cosmological constant as dark energy.

We also investigated the constraint on the time-varying equation of state for dark energy without assuming a flat universe. Similarly to the situation where we constrained the curvature with the time-varying equation of state, the allowed region for w_X becomes larger when we use a single observational data. However, if we use all data sets considered in this paper, we can obtain almost the same constraint as that in the case where a flat universe is assumed. See Ref.[12] for the details. It might be worthwhile to remark here that the Gold set is known to somewhat favor dark energy model which crosses $w_X = -1$ but such tendency is not found for the SNLS data.

3 Conclusion

Finally, we summarize what we found in this study. The combination of the current observations

- favors a flat universe regardless of the prior on the equation of state for dark energy with or without time evolution.
- favors $\Omega_m \sim 0.3$ regardless of the flatness prior and the prior on the equation of state for dark energy with or without time evolution.
- yields constraints on the time evolution of dark energy equation of state regardless of the prior on Ω_m and Ω_k.

In future observations, we can obtain much more stringent constraints on the equation of state for dark energy as well as the curvature of the universe regardless of the prior on other cosmological parameters. Hence we can expect that we will be able to have much insight on the nature of dark energy and also the inflationary paradigm.

References

[1] D. N. Spergel *et al.*, Astrophys. J. Suppl. **148**, 175 (2003).

[2] M. Tegmark *et al.* [SDSS Collaboration], Phys. Rev. D **69**, 103501 (2004); J. L. Tonry *et al.* [Supernova Search Team Collaboration], Astrophys. J. **594**, 1 (2003); C. J. MacTavish *et al.*, arXiv:astro-ph/0507503.

[3] A. G. Riess *et al.* [Supernova Search Team Collaboration], Astrophys. J. **607**, 665 (2004).

[4] P. Astier *et al.*, arXiv:astro-ph/0510447.

[5] M. Chevallier and D. Polarski, Int. J. Mod. Phys. D **10**, 213 (2001); E. V. Linder, Phys. Rev. Lett. **90**, 091301 (2003).

[6] Y. Wang and M. Tegmark, Phys. Rev. Lett. **92** (2004) 241302; B. Feng, X. L. Wang and X. M. Zhang, Phys. Lett. B **607**, 35 (2005); H. K. Jassal, J. S. Bagla and T. Padmanabhan, Mon. Not. Roy. Astron. Soc. **356**, L11 (2005); D. A. Dicus and W. W. Repko, Phys. Rev. D **70**, 083527 (2004); S. Hannestad and E. Mortsell, JCAP **0409**, 001 (2004); U. Seljak *et al.*, Phys. Rev. D **71**, 103515 (2005); F. Giovi, C. Baccigalupi and F. Perrotta, Phys. Rev. D **71**, 103009 (2005); A. Upadhye, M. Ishak and P. J. Steinhardt, Phys. Rev. D **72**, 063501 (2005); H. K. Jassal, J. S. Bagla and T. Padmanabhan, Phys. Rev. D **72**, 103503 (2005); M. Doran, K. Karwan and C. Wetterich, JCAP **0511**, 007 (2005); S. Nesseris and L. Perivolaropoulos, Phys. Rev. D **72**, 123519 (2005); J. Q. Xia, G. B. Zhao, B. Feng, H. Li and X. Zhang, arXiv:astro-ph/0511625.

[7] J. L. Crooks, J. O. Dunn, P. H. Frampton, H. R. Norton and T. Takahashi, Astropart. Phys. **20**, 361 (2003).

[8] I. Maor, R. Brustein and P. J. Steinhardt, Phys. Rev. Lett. **86**, 6 (2001) [Erratum-ibid. **87**, 049901 (2001)]: I. Maor, R. Brustein, J. McMahon and P. J. Steinhardt, Phys. Rev. D **65**, 123003 (2002).

[9] Y. Wang and M. Tegmark, in Ref. [6].

[10] Y. g. Gong and Y. Z. Zhang, Phys. Rev. D **72**, 043518 (2005).

[11] D. J. Eisenstein *et al.*, Astrophys. J. **633**, 560 (2005).

[12] K. Ichikawa and T. Takahashi, arXiv:astro-ph/0511821.

Graviton emission from a higher-dimensional black hole

A. S. Cornell[1], Wade Naylor[2], Misao Sasaki[3]

[1,3] *Yukawa Institute for Theoretical Physics, Kyoto University, Kyoto 606-8502, Japan*
[2] *Department of Physics, Ritsumeikan University, Kusatsu, Shiga 525-8577, Japan*

Abstract

We discuss the graviton absorption probability (greybody factor) and the cross-section of a higher-dimensional Schwarzschild black hole (BH). For simplicity. we investigate the intermediate energy regime for a static Schwarzschild BH. That is, for $(2M)^{1/(n+1)}\omega \sim 1$, where M is the mass of the black hole and ω is the energy of the emitted gravitons in $(2+n)$-dimensions. To find easily tractable solutions we work in the limit $l \gg 1$, where l is the angular momentum quantum number of the graviton.

Introduction

Based on our recent article [1] we study the graviton absorption probability and the cross-section of an $(n+2)$-dimensional Schwarzschild BH. We are motivated by the proposition that the quantum gravity scale can be brought down to as low as a TeV in some higher-dimensional models [2]. Most cases have focused on the low-energy emission of scalar or spinor fields from higher-dimensional Schwarzschild and slowly rotating Kerr BHs, where numerical methods also allow us to evaluate the emission in the full energy range [3]. However, little attention has been paid to the actual emission of gravitons from a BH. Furthermore it is useful to have analytic expressions for the cross-sections etc. not just in the low-energy or high-energy classical regime. In this article we shall discuss BH cross-sections for gravitons in what we shall call the intermediate energy regime for the variable $\varepsilon = 2M\omega^{n+1}$, that is where $\varepsilon \sim 1$. In this regime the energy of the particle is near the peak of the potential barrier in the associated scattering problem. The classical cross-section is reproduced in the high-energy limit, $\varepsilon \gg 1$.

Gravitational perturbations in general separate into scalar, vector and tensor perturbations with respect to the n-sphere. Note that in four-dimensions there is no degree of freedom corresponding to tensor perturbations. For the various perturbations we have[4];

$$-f\frac{d}{dr}\left(f\frac{d\Phi}{dr}\right)+V_P\Phi=\omega^2\Phi\,, \tag{1}$$

where P denotes any one of the three possible perturbations and where, $f(r)=1-\frac{2M}{r^{n+1}}$.

For the scalar perturbations;[4]

$$V_S(r)=\frac{f\,H(r)}{16r^2[m+\frac{1}{2}n(n+1)(1-f)]^2}, \tag{2}$$

where $H(r)$ is defined in reference [4] and in the above $m=l_S(l_S+n-1)-n$ where $l_S=2,3,\ldots$.

For the vector and tensor perturbations;[5]

$$V_{V/T}(r)=\frac{f}{r^2}\left(l(l+n-1)+\frac{n(n-2)}{4}-\frac{\mu_{V/T}}{2}\frac{n^2M}{r^{n+1}}\right) \qquad \begin{matrix} l_V=2,3,\ldots \\ l_T=1,2,\ldots \end{matrix} \tag{3}$$

where $\mu_V=3$ for the vector perturbations, while for the tensor perturbations $\mu_T=-1$. Note that the mode $l=1$ of the vector perturbation, which is absent from the above spectrum, represents a purely rotational mode of the BH.

[1] E-mail:alanc@yukawa.kyoto-u.ac.jp
[2] E-mail:naylor@se.ritsumei.ac.jp
[3] E-mail:misao@yukawa.kyoto-u.ac.jp

[4] Note that for $n=2$ the scalar (polar) perturbation agrees with the Zerilli equation.

[5] The vector (axial) perturbations for $n=2$ reduces to the standard Regge-Wheeler equation.

We shall mainly be interested in evaluating the scattering cross-section, which is related to the absorptions probability, $|\mathcal{A}_l(\omega)|^2$, by;

$$\sigma(\omega) = C\frac{(4\pi)^{(n-1)/2}}{\omega^n}\Gamma\left(\frac{n+1}{2}\right)\sum_l^\infty\sum_P D_{lP}|\mathcal{A}_{lP}(\omega)|^2\,, \tag{4}$$

where D_{lP} is the degeneracy for each respective perturbation, see [1] and the references mentioned therein, for a given angular momentum channel l. In our case we require the absorption probability for the intermediate energy limit $\epsilon \sim 1$, and where C is a normalisation.

To evaluate the absorption probability, and hence the graviton emission rate in the intermediate energy regime, we shall use the WKB approach of Iyer and Will [5]. In the following we shall work to lowest order in the generalised WKB method.

As discussed in reference [6], in order to use the WKB method we must rewrite the perturbations in the $(n+2)$-dimensional tortoise coordinate defined by;

$$\frac{dr_*}{dr} = \frac{1}{f(r)}, \tag{5}$$

thus the perturbation equations reduce to the standard Schrödinger form;

$$\left(\frac{d^2}{dr_*^2} + Q_P(r_*)\right)\Phi = 0\,, \qquad Q_P(r_*) = \omega^2 - V_P(r_*). \tag{6}$$

An adapted form of the WKB method can be employed to find the QNMs or the absorption probability, which we are primarily interested in, when the scattering takes place near the top of the potential barrier. The absorption probability, up to second order in the WKB expansion, is found to be;

$$|\mathcal{A}_{lP}(\omega)|^2 = \left[1 + e^{2i\pi(\nu+1/2)}\right]^{-1}, \tag{7}$$

where $\nu + 1/2$ is defined in reference [5].

Zeroth-order Approximation

To illustrate the method as simply as possible let us work to zeroth order in the WKB expansion for the case of large l. In order to find a difference between the respective perturbations we should consider up to $O(l^0)$ in the potential, which in this case is given by;

$$V_P(r) = \frac{f(r)}{r^2}\left(\tilde{l}^2 + \beta - \frac{\alpha_P}{4}(1-f)\right), \qquad \text{where} \qquad \tilde{l}^2 = l^2 + (n-1)l\,. \tag{8}$$

In the previous equation we have used;

$$\beta_P = \frac{n(n-2)}{4}, \qquad \alpha_S = n(7n-8), \qquad \alpha_V = 3n^2, \qquad \alpha_T = -n^2\,. \tag{9}$$

At this stage it will be convenient to change variables to $z = \omega r$, and by doing so the WKB equation now becomes;

$$\left(\frac{d^2}{dz_*^2} + Q_P(z_*)\right)\Phi = 0\,, \qquad Q_P(z_*) = 1 - V_P(z_*)\,. \tag{10}$$

Hence, from equation (7), we are lead to the result;

$$|\mathcal{A}_{lP}|^2 = \left[1 + e^{\frac{2\pi}{K}\left[f(z_0)(\tilde{l}^2+\beta-\frac{\alpha}{4}\epsilon z_0{}^{1-n}) - z_0^2\right]}\right]^{-1}, \tag{11}$$

where we have expressed $K(\tilde{l}, z_0, \epsilon)$ in our paper [1]. Choosing the appropriate α_P from equation (9) then determines the absorption probability for each respective perturbation mode. The location of the maximum, z_0, for the potential $-Q_P(z_0)$ can also be solved, see reference [1].

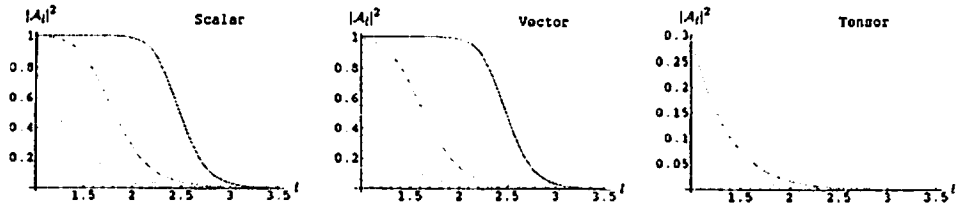

Figure 1: Black hole absorption probability, $|\mathcal{A}_l|^2$, as a function of angular momentum l for $\epsilon = 1$. Blue (solid), red (dashed), green (dot-dashed) and purple (dotted) curves correspond to $n = 2, 3, 4$ and 5 respectively. Note that the scalar and vector perturbations are only valid from $l = 2$ onwards, however, for comparison with the tensor case we start at $l = 1$.

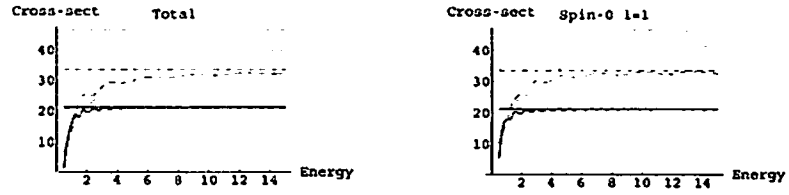

Figure 2: Total BH cross-section as a function of ϵ, in units of $(2M)^{\frac{n}{n-1}}$, for the graviton as compared to that for a spin-0 field with partial wave sum starting from $l = 1$. The horizontal lines correspond to the classical cross-section. Blue (solid), red (dashed) and green (dot-dashed) curves correspond to $n = 2, 3$ and 4 respectively.

Results

We have presented our first set of results in Fig. 1 where we have plotted the absorption probability as a function of l for each of the perturbations. We have also considered scenarios involving different dimensions, n, for $\epsilon \sim 1$. Firstly, the scalar mode has the largest contribution, followed by the vector and then the tensor perturbations; however, this does depend on the value of ϵ. Secondly, we see that the absorption probability is larger for smaller n. In fact numerical plots for different ϵ show that $|\mathcal{A}_{lP}|^2$ saturates to unity for larger and larger l as ϵ increases. This implies that larger l is required in the angular momentum sum for the cross-section, when obtaining the geometric optics limit, see below.

Turning to the cross-section, it should be noted that though we are primarily interested in the intermediate energy regime, $\epsilon \sim 1$, with large angular momentum, $l \gg 1$, equation (4) can also be applied to the case where $l > \epsilon^{1/(n-1)} \sim 1$. Note also that although the next order correction in the WKB expansion becomes larger for $l \sim \mathcal{O}(1)$ we can still extrapolate the results hoping the errors are not too large. In Fig. 2 we plot the total cross-section for the graviton as a function of ϵ and to ensure convergence in the partial wave sums we sum up to $l_{max} \sim 3\epsilon_{max}$. The total cross-section tends to the classical one for large ϵ as we shall soon explain.

Also in Fig. 2 we compare the spin-zero case with that of the total graviton cross-section. Although the classical cross-sections agree in the high-energy limit (asymptotically), at intermediate energies they do not agree due to differences in the partial wave sums. Moreover, at low energy we see that by taking the spin-0 cross-section from $l = 1$ we obtain the best agreement with that for the graviton.

For the classical cross-section, which corresponds to the high-energy limit, $\epsilon^{1/(n-1)} \gg l \gg 1$, it is easy to see that the absorption coefficients are of order unity in this case, see Fig. 1. Furthermore, in this limit the sum over l has a cut-off at $l \approx b\omega$ where b is the critical radius (or impact parameter) at which the BH ceases to absorb radiation. This is given by equation (12) of reference [7], for a massless/relativistic

particle as;

$$b = \left(\frac{n+1}{2}\right)^{\frac{1}{n-1}} \left(\frac{n+1}{n-1}\right)^{\frac{1}{2}} (2M)^{\frac{1}{n-1}} . \tag{12}$$

Given the cut-off in the mode sum one can show that $C\sum_l^{b\omega}\sum_P D_{lP} \sim \sum_l^{b\omega} D_{lS} \approx \frac{2(b\omega)^n}{n!}$, which leads to the classical cross-section. As is well known, the high-energy cross-section is independent of the particle species, and likewise we see that it is independent of the graviton cross-section. These are represented by the horizontal lines in Fig. 2 and we see that our analytic results correctly reproduce the high-energy limit $\varepsilon \gg 1$.

Conclusion

In conclusion we have shown in this paper that the WKB method of Iyer and Will [5] can be applied to the case of graviton emission from a Schwarzschild BH. Indeed our results reproduce the classical cross-section in the high-energy limit. We have also presented new results for the intermediate energy regime.

In the low-energy limit, $M\omega \ll 1$, our method breaks down as can be seen from Fig. 2, where the cross-section starts to diverge. It is well known that the cross-section is proportional to ω^{2l+n} in $(2+n)$-dimensions [3], which essentially corresponds to s-wave scattering for a spin-zero field, as the lowest l modes dominate the cross-section. Indeed it is straightforward to obtain the low-energy cross-section for the vector and tensor perturbations by employing the standard technique of matching the near horizon and far field solutions. Regardless, the focus of this current work has been the intermediate energy regime given that this is where we expect graviton emission to be most interesting for a rapidly rotating BH.

Although in this article we focused on the static Schwarzschild BH, we can also apply our method to the case of spin-zero field emission from a Kerr BH. Note that though the solution to the graviton perturbations for a higher-dimensional Kerr BH have not yet been found, we are encouraged by the fact that there are some similarities between the total graviton and spin-0 cross-sections. As can be seen from Fig. 2, the total cross-section, which is the sum of the perturbations (scalar, vector and tensor) is of the same order of magnitude as the spin-0 case and such an approximation may also be valid for the rotating case.

Acknowledgments

The work of ASC was supported by the Japan Society for the Promotion of Science (JSPS), under fellowship no. P04764. The work of MS was supported in part by Monbukagakusho Grant-in-Aid for Scientific Research(S) No. 14102004 and (B) No. 17340075.

References

[1] A. S. Cornell, W. Naylor and M. Sasaki, arXiv:hep-th/0510009.

[2] S. B. Giddings and S. Thomas, Phys. Rev. D **65** (2002) 056010 [arXiv:hep-ph/0106219]; S. Dimopoulos and G. Landsberg, Phys. Rev. Lett. **87** (2001) 161602 [arXiv:hep-ph/0106295]; S. Hossenfelder, S. Hofmann, M. Bleicher and H. Stoecker, Phys. Rev. D **66** (2002) 101502 [arXiv:hep-ph/0109085].

[3] P. Kanti, Int. J. Mod. Phys. A **19** (2004) 4899 [arXiv:hep-ph/0402168].

[4] H. Kodama and A. Ishibashi, Prog. Theor. Phys. **110** (2003) 701 [arXiv:hep-th/0305147].

[5] S. Iyer and C. M. Will, Phys. Rev. D **35** (1987) 3621.

[6] E. Berti, M. Cavaglia and L. Gualtieri, Phys. Rev. D **69** (2004) 124011 [arXiv:hep-th/0309203].

[7] R. Emparan, G. T. Horowitz and R. C. Myers, Phys. Rev. Lett. **85** (2000) 499 [arXiv:hep-th/0003118].

Close-limit analysis for collision of two black holes in higher dimensions

Hirotaka Yoshino[1], Tetsuya Shiromizu[2], Masaru Shibata[3]

[1,2] *Theoretical Astrophysics Group, Department of Physics, Tokyo Institute of Technology, Tokyo 152-8551, Japan*

[3] *Graduate School of Arts and Sciences, University of Tokyo, Komaba, Meguro, Tokyo 153-8902, Japan*

Abstract

The TeV gravity scenarios predict that the planned accelerators become black hole (BH) factories. One of the necessary studies in this context is the gravitational wave emission during the BH formation in the high-energy particle collision. As an approximation for this system, we consider the head-on collision of two BHs using the Bowen-York method and analyze the evolution adopting the close-slow approximation. Our results indicate that about few% of the system energy would be radiated away in this process. Thus the radiation would not significantly change the previous estimate of the produced BH mass in accelerators.

1 Introduction

It is expected that the black holes (BHs) are produced in the collision of elementary particles with the energy above the Planck scale. It was pointed out that the Planck energy could be O(TeV) if our space is a 3-brane in large extra dimensions and the gauge particles and interactions are confined on the brane. If such TeV gravity scenarios are realized, we would be able to observe the BH phenomena in planned accelerators. The phenomena was discussed from various points of view by many authors, and the review by Carr can be found in this proceeding [1].

If a BH is produced, it would evolve to a stationary state (probably the higher-dimensional Kerr BH) by emitting the gravitational wave. The gravitational radiation determines the mass and angular momentum of the final Kerr BH and it in turn provides the initial condition for the evaporation by the Hawking radiation. Hence, the study of the gravitational wave emission is necessary to predict the phenomena in accelerators.

The most desirable way would be to simulate the collision of high-energy particles by the numerical relativity. However, such method has not been developed yet because this process is not important in astrophysical contexts. Instead, there exist two approximate studies. One is the gravitational emission from the head-on collision of two particles adopting the perturbation from the Minkowski spacetime, and the other is the gravitational emission from a particle falling into the Schwarzschild BH [2], both predicting less than 10% radiation efficiency in higher-dimensional cases. Although they provide the approximate estimate, these studies have some problems: they ignore the non-linearity of the theory or the setup is far from the realistic one.

In order to improve this situation, we would like to adopt another approximate system: the collision of two BHs with momentum using Bowen-York method [3]. If we take the large values of momentum, the system is expected to provide an approximation for the high-energy particle system to a certain extent[4]. As the first step, we analyze the close-slow approximation, in which we treat the distance between the two BHs and the momentum as small parameters. The close-slow analysis can provide the benchmark for the numerical investigation. Moreover, it is well-known that the close-slow approximation provides a good approximation beyond the perturbative regime in the four-dimensional case [4].

[1] E-mail:yoshino@th.phys.titech.ac.jp

[2] E-mail:shiromizu@phys.titech.ac.jp

[3] E-mail:shibata@provence.c.u-tokyo.ac.jp

[4] We should note that the ADM mass $M_{\rm ADM}$ increases as the momentum P is increased in the Bowen-York method, and we cannot take the limit $P \to \infty$ for a fixed value of $M_{\rm ADM}$. This is because the initial data contains a lot of junk energy. We hope that the better method will be developed in future.

In our previous paper [5], we anayzed the evolution of the two BHs which are initially at rest (i.e., $P = 0$) using the close-limit method in D-dimensional spacetime ($4 \leq D \leq 11$). In this paper, we would like to extend this analysis for the system of initially moving BHs. For simplicity, we restrict our attention to the head-on collision case. We will proceed with two kinds of analyses: one is the numerical calculation of the Bowen-York two-BH initial data in higher dimensions and the other is the evolution adopting the close-slow approximation. These two studies are explained in Secs. II and III, respectively.

2 Higher-dimensional Bowen-York initial data

Let us consider the $(D-1)$-dimensional spacelike hypersurface Σ with the metric h_{ab} and the extrinsic curvature K_{ab} and set $n = D-2$. Assuming the conformal flatness $h_{ab} = \Psi^{4/(n-1)}$ and introducing $\hat{K}_{ab} = \Psi^2 K_{ab}$, the Hamiltonian and momentum constraints are written as:

$$\nabla_f^2 \Psi = \frac{n-1}{4n} \hat{K}_{ab} \hat{K}^{ab} \Psi^{-(3n+1)/(n-1)}, \tag{1}$$

$$\nabla_f^a \hat{K}_{ab} = 0, \tag{2}$$

where ∇_f^a denotes the derivative with respect to the Cartesian coordinate (z, x_i). Bowen and York [3] found an analytic solution for the momentum constraint (2) and we extend it for higher-dimensional cases as follows:

$$K_{ab} = \frac{4\pi(n+1)G}{n\Omega_n R^n} \left\{ n_a P_b + n_b P_a + P_c n^c \left[(n-1) n_a n_b - \delta_{ab} \right] \right\}. \tag{3}$$

To setup the two-BH system, we superpose two solutions like

$$\hat{K}_{ab} = \hat{K}_{ab}^{(+)} + \hat{K}_{ab}^{(-)}. \tag{4}$$

Here the centers of $\hat{K}_{ab}^{(\pm)}$ are located at $(z, x_i) = (\pm z_0, 0)$ and $P_a^{(\pm)} = (\mp P, 0)$. We assume that the conformal factor takes the form like

$$\Psi = 1 + [R_h(M_0)]^{n-1} \left(\frac{1/2}{R_+^{n-1}} + \frac{1/2}{R_-^{n-1}} \right) + \psi, \quad R_h(M_0) = \left(\frac{4\pi G M_0}{n\Omega_n} \right)^{1/(n-1)}, \tag{5}$$

and solve ψ numerically using Eq. (1) by imposing appropriate boundary conditions. This solution provides the space with two Einstein-Rosen bridges and three asymptotically flat regions.

Once we generate ψ, we can calculate the ADM mass by the following formula:

$$M_{\rm ADM} = M_0 + \frac{1}{16\pi G} \int_\Sigma \hat{K}_{ab} \hat{K}^{ab} \Psi^{-(3n+1)/(n-1)} d^{n+1}x. \tag{6}$$

The latter term provides the kinetic energy of incoming BHs. Figure 1 shows the behavior of $M_{\rm ADM}$ on the (z_0, P)-plane for $D = 5$ and 6 cases. We also studied the existence of the common apparent horizon (AH) which surrounds both BHs. The region for the AH formation on the (z_0, P)-plane is shown in Figure 2 for $D = 5$ and 6 cases.

3 Close-slow evolution

Now we consider the time evolution adopting the close-slow approximation. In the following, we adopt the gravitational radius of the system $r_h(M_0) = (16\pi GM/n\Omega_n)^{1/(n-1)}$ as the unit of the length. We assume that z_0 and P/M_0 are small and have the same order. The leading order of $\hat{K}_{ab}$ is $O(z_0 P/M_0)$. Then, we can ignore ψ because it is higher order and $M_{\rm ADM} = M_0$. By transforming from the isotropic coordinate to the Schwarzschild-like coordinate $r = R(1 + 1/4R^{n-1})^{2/(n-1)}$, we find that the system is regarded as one Schwarzschild BH plus its perturbation:

$$ds^2 = \left(\frac{\Psi}{\Psi_0} \right)^{4/(n-1)} \left[\frac{dr^2}{1 - 1/r^{n-1}} + r^2 (d\theta^2 + \sin^2\theta d\Omega_{n-1}^2) \right], \tag{7}$$

$$\left(\frac{\Psi}{\Psi_0} \right)^{4/(n-1)} \simeq 1 + \frac{1/(n-1) R^{n-1}}{1 + 1/4R^{n-1}} \left(\frac{z_0}{R} \right)^2 C_2^{[(n-1)/2]}(\cos\theta), \tag{8}$$

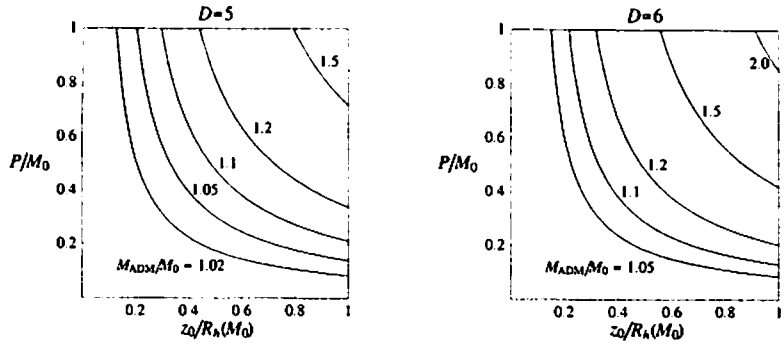

Figure 1: The contour line for $M_{\rm ADM}/M_0$ on the $(z_0/R_{\rm h}(M_0), P/M_0)$-plane.

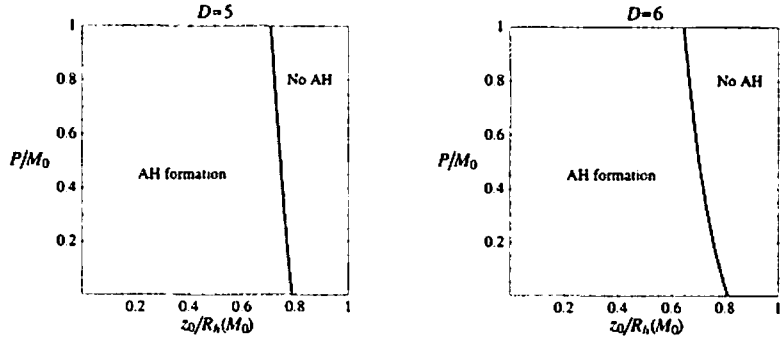

Figure 2: The critical line for the common AH formation on the $(z_0/R_{\rm h}(M_0), P/M_0)$-plane. The AH forms if $z_0/R_{\rm h}(M_0)$ is sufficiently small.

and the order of the perturbation is $O(z_0^2)$. Thus we can evolve this system using Kodama and Ishibashi's gauge-invariant method for the perturbation around the Schwarzschild BH [6]. Their equation is given by

$$\frac{\partial^2\Phi}{\partial t^2} - \frac{\partial^2\Phi}{\partial r_*^2} + V_S\Phi = 0. \tag{9}$$

where Φ is the master variable. The initial value of Φ and $\dot{\Phi}$ are related to the metric perturbation and $\dot{K}_{ab}$, respectively, and hence $\Phi = O(z_0^2)$ and $\dot{\Phi} = O(z_0 P/M_0)$. Thus Φ is decomposed into two parts:

$$\Phi = (z_0^2)\hat{\Phi}_{\rm BL} + (z_0 P/M_0)\,\hat{\Phi}_{\rm BY}. \tag{10}$$

We solved $\hat{\Phi}_{\rm BL}$ and $\hat{\Phi}_{\rm BY}$ numerically using the Lax-Wendoroff scheme. We observed the quasi-normal mode for all dimensions and the power-law tail for four and odd dimensions. The wave form of the $D = 5$ case are shown in Fig. 3.

Once $\hat{\Phi}_{\rm BL}$ and $\hat{\Phi}_{\rm BY}$ are calculated, we obtain the radiated energy of the gravitational wave by the following formula:

$$E_{\rm rad} = \frac{k^2(n-1)(k^2-n)}{32\pi nG}\int \frac{d}{dt}\left[(z_0^2)\dot{\Phi}_{\rm BL} + (z_0 P/M_0)\dot{\Phi}_{\rm BY}\right]^2. \tag{11}$$

Now let us evaluate the radiation efficiency $E_{\rm rad}/M_0$ for some characteristic values of z_0 and P. For this purpose, we draw $P/M_0 = $ const. line on the (z_0, P)-plane recalling Fig. 2. On this line, we can interpret that the Lorentz factor γ of incoming BHs is fixed. The line intersects the critical line for the AH formation and we choose the crossing point. Table 1 shows the values of the radiated energy $E_{\rm rad}$ for $P/M_0 = 0.0, 0.5$ and 1.0 cases (i.e., $\gamma = 0, 1, 2$), respectively. $E_{\rm rad}/M_0$ is few% for $P/M_0 = 0.5$, while $E_{\rm rad}/M_0$ is about 10% for $P/M_0 = 1.0$. However, as we can see from Fig. 1, the difference between M_0 and $M_{\rm ADM}$ is large at $P/M_0 = 1.0$. This indicates that the quadratic term of $z_0 P/M_0$ is large and the

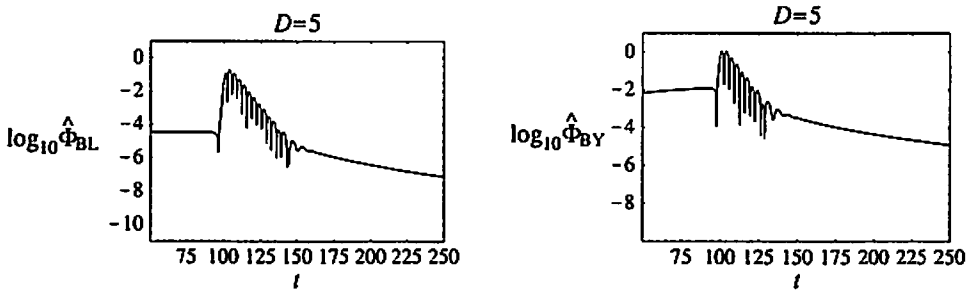

Figure 3: The time evolution of $\hat{\Phi}_{BL}$ and $\hat{\Phi}_{BY}$ in the $D = 5$ case observed at $r_* = 100$.

Table 1: The values of E_{rad}/M_0 evaluated on the AH critical line for $P/M_0 = 0.0, 0.5, 1.0$. The unit is %.

D	4	5	6	7	8	9	10	11
$P/M_0 = 0.0$	0.0034	0.016	0.024	0.024	0.021	0.017	0.014	0.011
$P/M_0 = 0.5$	1.0	2.4	3.2	3.2	2.9	2.6	2.3	2.1
$P/M_0 = 1.0$	5	10	13	13	13	12	11	10

linear approximation breaks down. The non-linear effect naturally suppresses E_{rad}/M_{ADM}, and we expect that the true value of E_{rad}/M_{ADM} would be few% also for $P/M_0 = 1.0$. This leads to the expectation that the radiation efficiency is few% also in the region where both z_0 and P/M_0 are large.

4 Summary

In this paper, we introduced the initial data for the head-on collision of two BHs in D dimensions using the Bowen-York method. We constructed the initial data numerically and calculated the ADM mass. We also clarified the region of the AH formation in the (z_0, P)-plane.

Then we analyzed the gravitational wave emission adopting the close-slow approximation. By regarding the system as the perturbation around one Schwarzschild BH, we could evolve this system using the Kodama-Ishibashi gauge invariant formalism. We obtained the formula for the radiated energy and discussed the difference between D by evaluating it on the critical line of the AH formation for some fixed value of P/M_0. As a result, it indicats that the radiated energy in the high-energy regime would be few% for all dimensions in this system for large values of z_0 and P/M_0. Our result provides the benchmark for the study of this system by numerical relativity.

As an implication of this result, we expect that the radiation efficiency in the high-energy particle collision is similar to the one we have obtained in this paper. The gravitational wave emission would not be so significant for the resultant mass of the produced BHs in accelerators. This study will be completed and submitted soon.

References

[1] B. J. Carr, in this proceeding (2006).

[2] V. Cardoso and J. P. S. Lemos, Phys. Lett. B **538**, 1 (2002) [arXiv:gr-qc/0202019]; E. Berti, M. Cavaglia and L. Gualtieri, Phys. Rev. D **69**, 124011 (2004) [arXiv:hep-th/0309203].

[3] J. M. Bowen and J. W. York, Jr, Phys. Rev. D **21**, 2047 (1980).

[4] R. H. Price and J. Pullin, Phys. Rev. Lett. **72**, 3297 (1994) [arXiv:gr-qc/9402039].

[5] H. Yoshino, T. Shiromizu and M. Shibata, Phys. Rev. D **72**, 084020 (2005) [arXiv:gr-qc/0508063].

[6] H. Kodama and A. Ishibashi, Prog. Theor. Phys. **110**, 701 (2003) [arXiv:hep-th/0305147].

Black holes on and off the wall

Antonino Flachi[1]

Yukawa Institute for Theoretical Physics, Kyoto University, Kyoto 606-8503, Japan

Oriol Pujolàs[2]

Center for Cosmology and Particle Physics, Department of Physics, New York University, 4 Washington Place, New York, NY 10003 US

Misao Sasaki[3]

Yukawa Institute for Theoretical Physics, Kyoto University, Kyoto 606-8503, Japan

Takahiro Tanaka[4]

Department of Physics, Kyoto University, Kyoto 606-8502, Japan

Abstract

We consider the interaction of a small black hole with a brane and study the evolution of such system when the black hole recoils in the extra dimensions. By treating the brane in the Dirac-Nambu-Goto approximation, we find that the black hole tends to escape due to a mechanism of reconnection of the brane. We then test and confirm this result by considering a more involved model where the brane is treated as a domain wall.

Introduction. In recent years extra dimensions have been playing a central role in both particle physics and cosmology. From one hand they have provided a useful tool to parametrise the yet unknown physics beyond the TeV scale, on the other hand, extra dimensions have become a popular ingredient in many cosmological models. However, despite the enormous progress of the theory, the great challenge remains to uncover experimental signatures of their existence. A possibility in this direction has been initially pointed out in [1], where the universe is assumed to have a domain wall structure, *the brane*, where standard model particles are confined. The brane is embedded in a higher dimensional space, where gravity propagates. This scenario, realised in many examples, results in lowering the fundamental (higher dimensional) Planck scale to a few TeVs without conflicting with observations.

One striking prediction of this fact regards the production of small black holes in high energy collisions of particles at energies within the reach of forthcoming experiments: when two particles collide at a center of mass energy $\sqrt{s}$, which exceeds the fundamental Planck scale, and at impact parameter smaller than the Schwarzschild radius associated with $\sqrt{s}$, semiclassical arguments suggest that the system may collapse and form a black hole, whose size is typically much smaller than the characteristic length of the extra dimensions. After formation, the black hole will emit Hawking radiation that can, in principle, be detected at the LHC [4], and this would signal the existence of hidden dimensions.

The radiation of the black hole will partly go into lower dimensional fields (localised on the brane) and partly into higher dimensional modes, which will cause the black hole to recoil into the extra dimensions. The recoil of the black hole in the context described above was first studied in Ref. [5]. In the model of

[1] flachi@yukawa.kyoto-u.ac.jp
[2] pujolas@ccpp.nyu.edu
[3] misao@yukawa.kyoto-u.ac.jp
[4] tama@scphys.kyoto-u.ac.jp

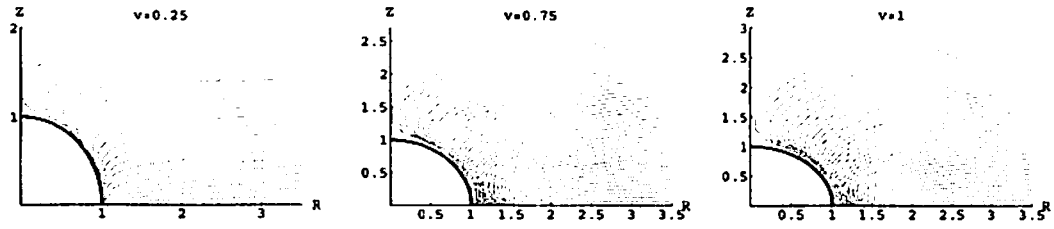

Figure 1: Result of the evolution for a Dirac-Nambu-Goto brane for various different initial recoil velocities v. The plot is in cylindrical coordinates, $R = r\sin\theta$, $Z = -r\cos\theta$. The various slices represent the brane at the various stages of the evolution.

[5] there are two scalar fields: one describes the black hole and the other a possible quanta emitted by the black hole in the process of evaporation; the coupling between them is fixed in such a way that the probability of emission of a scalar quanta from the black hole reproduces the Hawking formula, and a delta function potential is used to mimic the interaction between the black hole and the brane. Within this model and in the approximation that the interaction with the brane is negligibly small, the probability for the black hole to slide off the brane is calculated and the result is that, as soon as a quanta is emitted in the extra dimension, the black hole will leave the brane. This has the important observable effect of a sudden interruption of the radiation on the brane. The model presented in Ref. [5] draws interesting conclusions, but it does not describe how the separation may occur.

To clarify this issue and have further evidence of the conclusions of Ref. [5], we have considered the interaction between mini black holes and branes from the different perspective of studying the dynamics of branes in black hole spacetimes. The results reported here are based on Refs.[6, 7].

Dirac-Nambu-Goto brane. The set-up we consider consists of a $(p+1)-$dimensional brane embedded in a $d-$dimensional spacetime. A black hole, whose gravitational radius is much smaller than the size of the extra dimensions, intersects the brane and this fixes the bulk space to be determined by the black hole. The smallness of the black hole (and the fact the we ignore the self-gravity of the brane) allows us to describe the spacetime by means of asymptotically flat solutions [8, 9]:

$$ds^2 = -f(r)dt^2 + f^{-1}(r)dr^2 + r^2 d\Omega^2_{d-2}\,,$$

where r_H is the horizon radius and $f(r) = 1 - (r_H/r)^{d-3}$.

As a first step, we treated the brane as a Dirac-Nambu-Goto hyper-surface, parametrised by the coordinates ζ^a, whose action is

$$S = -\sigma \int d^{p+1}\zeta\sqrt{\gamma}\,,$$

with σ being the tension and γ_{ij} the induced metric on the hyper-surface. Assuming that the brane is axially symmetric. its trajectory is completely specified by the azimuthal inclination angle $\theta(t,r)$ and this simplifies the action to

$$S = -\sigma\Sigma_{p-1}\int dtdr\,(r\sin\theta)^{p-1}\sqrt{1 + r^2 f(r)\theta_r^2 - r^2 f^{-1}(r)\theta_t^2}\,,$$

which, supplemented by appropriate boundary conditions, describes the evolution of the system. The boundary conditions should describe the recoil of the black hole, and, in the center of mass frame of the black hole, can be implemented by giving some initial asymptotically uniform velocity to the brane, while the intersection between the brane and the black hole is kept fixed. In this way, the system is completely specified and its dynamical evolution can be studied numerically. For brevity we omit the details that can be found in the original reference [6], and simply show the results of the numerical simulation (Fig. 1). The results of the evolution show that the brane tends to wrap around the black hole, suggesting that the black hole might escape in the extra dimensions after two portions of the brane come in contact and reconnect (see Fig. 2). This gives a dynamical mechanism for the creation of baby branes and escape of the black hole.

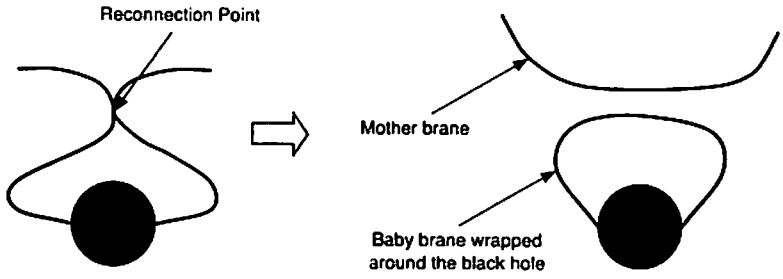

Figure 2: Creation of a baby brane wrapped round the black hole.

Domain Wall. Although the result is suggestive, within the Dirac-Nambu-Goto approximation it is possible to follow the evolution of the brane only until the separation process begins, and therefore it is important to test the robustness of the previous results, possibly within a model that allows us to go beyond such a limitation and follow the evolution also after the separation. This would completely illustrate how the escape of the black hole takes place. For this reason we have considered a more involved construction where the brane is treated as a domain wall within a scalar effective field theory with quartic potential

$$V(\Phi) = \frac{\lambda}{4}(\Phi^2 - \eta^2)^2 \ .$$

Such domain wall solutions would be branes with tension $\sigma \simeq \sqrt{\lambda}\eta^3$ and thickness $\mathrm{t} \simeq 1/\sqrt{\lambda}\eta$. We can now describe the interaction between such 'thick' branes and black holes, as prescribed by the Klein-Gordon equation supplemented with a potential term. The evolution equation can be explicitly written, in the case of an axially symmetric wall, as

$$0 = -f^{-1}(r)\partial_t^2\Phi + \frac{1}{r^{d-2}}\partial_r\left(r^{d-2}f(r)\partial_r\Phi\right) + \frac{1}{r^2\sin^{d-3}\theta}\partial_\theta\left(\sin^{d-3}\theta\partial_\theta\Phi\right) - V'(\Phi) \ .$$

Initial conditions are specified by imposing that, at the initial time, Φ takes a kink profile, which we approximate by the flat space configuration; boundary conditions are imposed at 'infinity' by assuming that Φ reduces to the flat domain wall solution (boosted, in the center of mass frame of the black hole), by requiring regularity at the symmetry axis, and that at horizon $\partial_t\Phi(t, r_H, \theta) = 0$. Solving the previous equation along with the above boundary and initial conditions will describe the evolution of our system. We do so by using a mixed spectral and finite differences scheme: we first decompose the general solution in terms of a complete basis of smooth global functions and reduce the original equation to a system of coupled, 2-dimensional, non-linear partial differential equations, which are then solved by using finite difference methods. Detailed results of the analysis can be found in [7], here, for brevity, we simply present the main result. Fig. 3 illustrates three snapshots of the evolution of energy density of the domain wall confirming the results of the simulation for the Dirac-Nambu-Goto case: the domain wall envelops the black hole, that pinches off completely separating from the mother brane, while the mother brane, after the separation, relaxes into a stable configuration. This gives further evidence in support of the the conclusions of Refs. [5, 6] that suggested that, in the probe brane approximation, a small black hole on a brane may escape once it acquires an initial velocity with respect to the brane.

We would like to conclude by mentioning that the mechanism presented in Refs. [6, 7] and summarised here might find interesting applications in the context of early universe cosmology and primordial black holes, as well as in mini black hole phenomenology. Such studies are in progress and we hope to report on them soon.

Acknowledgements. This article summarises the work of Refs. [6, 7] and is based on talks delivered by A.F. at the JGRG-15, Tokyo University of Science, Tokyo Institute of Technology and Yukawa Institute for Theoretical Physics. We would like to thank Prof. T. Shiromizu, Dr. H. Yoshino, Dr. H. Kudoh for raising interesting questions and for interesting discussions that helped in clarifying many unclear aspects of the problem. A.F. is also grateful to Prof. T. Shiromizu for the kind hospitality extended at Tokyo Institute of Technology after the JGRG-15 meeting.

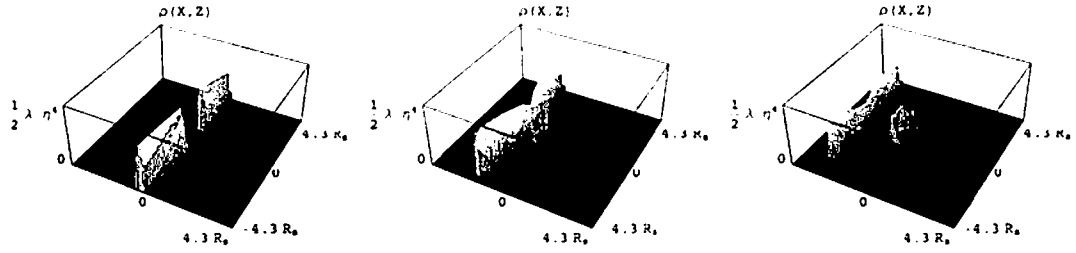

Figure 3: Evolution of the domain wall. The figure shows the energy density of the wall during three stages of the evolution, explicitly illustrating the separation process and escape of the black hole. The reported simulation refers to the five dimensional case, $d = 5$, and a domain wall whose thickness is $1/10$ of the Schwarzschild radius.

References

[1] N. Arkani-Hamed, S. Dimopoulos and G. R. Dvali, Phys. Lett. B **429**, 263 (1998).

[2] S. Dimopoulos and G. Landsberg, Phys. Rev. Lett. **87** (2001) 161602.

[3] S. B. Giddings and S. Thomas, Phys. Rev. **D65** (2002) 056010.

[4] R. Emparan, G. T. Horowitz, R. C. Myers, Phys. Rev. Lett. **85** (2000) 499.

[5] D. Stojkovic, V. Frolov, Phys. Rev. Lett. **89** 151302 (2002).

[6] A. Flachi, T. Tanaka, Phys. Rev. Lett. **95** 161302 (2005).

[7] A. Flachi, O. Pujòlas, M. Sasaki, T. Tanaka, to appear.

[8] F. R. Tangherlini, Nuovo Cim. B **77**, (1963) 636.

[9] R. C. Myers and M. J. Perry, Annals Phys. **172** (1986) 304.

Solitonic generation of 5-dimensional black ring solutions

Hideo Iguchi and Takashi Mishima

Laboratory of Physics, College of Science and Technology, Nihon University, Narashinodai, Funabashi, Chiba 274-8501, Japan

Abstract

Using the solitonic solution-generating technique we rederived the five-dimensional black ring solutions with one rotation found by Emparan and Reall. The technique used in this analysis is explained briefly. The seed solution of the one rotational black ring is presented.

1 Introduction

Recently, the finding exact solutions of higher-dimensional General Relativity has attracted much interest for several reasons, e.g., the string theory, the proposition of the large extradimensions and so on. Emparan and Reall discovered a rotating black ring solution with horizon topology $S^1 \times S^2$ for five-dimensional asymptotically flat solutions [1]. This means that the uniqueness theorem can not be easily generalized to the higher dimensions. Several researchers have tried to search new exact solutions in five dimensions. In this context the present authors showed that the finding some class of five-dimensional solutions can be reduced to the four-dimensional problem [2]. Following this strategy, a one-rotational black ring solution in five dimensions which rotates in the azimuthal direction of S^2 were obtained by solitonic solution-generating technique. Here we show that the black ring solution found by Emparan and Reall also can be derived by this solution-generating technique.

2 Solitonic solution-generating technique

We employ the following Weyl-Papapetrou metric form

$$ds^2 = -e^{2U_0}(dx^0 - \omega d\phi)^2 + e^{2U_1}\rho^2(d\phi)^2 + e^{2U_2}(d\psi)^2 + e^{2(\gamma+U_1)}\left(d\rho^2 + dz^2\right), \tag{1}$$

where U_0, U_1, U_2, ω and γ are functions of ρ and z. Then we introduce new functions $S := 2U_0 + U_2$ and $T := U_2$ so that the metric form (1) is rewritten into

$$ds^2 = e^{-T}\left[-e^{S}(dx^0 - \omega d\phi)^2 + e^{T+2U_1}\rho^2(d\phi)^2 + e^{2(\gamma+U_1)+T}\left(d\rho^2 + dz^2\right)\right] + e^{2T}(d\psi)^2. \tag{2}$$

Using this metric form the Einstein equations are reduced to the following set of equations,

(i) $\nabla^2 T = 0$,

(ii)
$$\begin{cases} \partial_\rho \gamma_T = \dfrac{3}{4}\rho\left[(\partial_\rho T)^2 - (\partial_z T)^2\right] \\ \partial_z \gamma_T = \dfrac{3}{2}\rho\left[\partial_\rho T\, \partial_z T\right]. \end{cases}$$

(iii) $\nabla^2 \mathcal{E}_S = \dfrac{2}{\mathcal{E}_S + \bar{\mathcal{E}}_S}\nabla\mathcal{E}_S \cdot \nabla\mathcal{E}_S$,

(iv)
$$\begin{cases} \partial_\rho \gamma_S = \dfrac{\rho}{2(\mathcal{E}_S + \bar{\mathcal{E}}_S)}\left(\partial_\rho\mathcal{E}_S\partial_\rho\bar{\mathcal{E}}_S - \partial_z\mathcal{E}_S\partial_z\bar{\mathcal{E}}_S\right) \\ \partial_z \gamma_S = \dfrac{\rho}{2(\mathcal{E}_S + \bar{\mathcal{E}}_S)}\left(\partial_\rho\mathcal{E}_S\partial_z\bar{\mathcal{E}}_S + \partial_\rho\mathcal{E}_S\partial_z\bar{\mathcal{E}}_S\right). \end{cases}$$

(v) $(\partial_\rho\Phi,\, \partial_z\Phi) = \rho^{-1}e^{2S}\left(-\partial_z\omega,\, \partial_\rho\omega\right)$,

(vi) $\gamma = \gamma_S + \gamma_T$,

(vii) $U_1 = -\dfrac{S+T}{2}$,

where Φ is defined through the equation (v) and the function $\mathcal{E}_S$ is defined by $\mathcal{E}_S := e^S + i\Phi$. The equation (iii) is exactly the same as the Ernst equation in four dimensions [3], so that we can call $\mathcal{E}_S$ the Ernst potential.

To write down the exact form of the metric functions, we follow the procedure given by Castejon-Amenedo and Manko [4]. In the five-dimensional space time we start from the following form of a seed static metric

$$ds^2 = e^{-T^{(0)}}\left[-e^{S^{(0)}}(dx^0)^2 + e^{-S^{(0)}}\rho^2(d\phi)^2 + e^{2\gamma^{(0)}-S^{(0)}}\left(d\rho^2+dz^2\right)\right] + e^{2T^{(0)}}(d\psi)^2. \tag{3}$$

For this static seed solution, $e^{S^{(0)}}$, of the Ernst equation (iii), a new Ernst potential can be written in the form

$$\mathcal{E}_S = e^{S^{(0)}}\frac{x(1+ab)+iy(b-a)-(1-ia)(1-ib)}{x(1+ab)+iy(b-a)+(1-ia)(1-ib)}, \tag{4}$$

where x and y are the prolate spheroidal coordinates: $\rho = \sigma\sqrt{x^2-1}\sqrt{1-y^2}$, $z=\sigma xy$, with $\sigma > 0$ and the functions a and b satisfy the following simple first-order differential equations

$$\begin{aligned}
(x-y)\partial_x a &= a\left[(xy-1)\partial_x S^{(0)} + (1-y^2)\partial_y S^{(0)}\right],\\
(x-y)\partial_y a &= a\left[-(x^2-1)\partial_x S^{(0)} + (xy-1)\partial_y S^{(0)}\right],\\
(x+y)\partial_x b &= -b\left[(xy+1)\partial_x S^{(0)} + (1-y^2)\partial_y S^{(0)}\right],\\
(x+y)\partial_y b &= -b\left[-(x^2-1)\partial_x S^{(0)} + (xy+1)\partial_y S^{(0)}\right].
\end{aligned} \tag{5}$$

The metric functions for the five-dimensional metric (2) are obtained by using the formulas shown by [4],

$$e^S = e^{S^{(0)}}\frac{A}{B}, \qquad \omega = 2\sigma e^{-S^{(0)}}\frac{C}{A} + C_1, \qquad e^{2\gamma} = C_2(x^2-1)^{-1}Ae^{2\gamma'}, \tag{6}$$

where c_1 and c_2 are constants and A, B and C are given by

$$A := (x^2-1)(1+ab)^2 - (1-y^2)(b-a)^2, \tag{7}$$

$$B := [(x+1)+(x-1)ab]^2 + [(1+y)a+(1-y)b]^2, \tag{8}$$

$$C := (x^2-1)(1+ab)[b-a-y(a+b)] + (1-y^2)(b-a)[1+ab+x(1-ab)]. \tag{9}$$

In addition the γ' in Eq. (6) is a γ function corresponding to the static metric,

$$ds^2 = e^{-T^{(0)}}\left[-e^{2U_0^{(BH)}+S^{(0)}}(dx^0)^2 + e^{-2U_0^{(BH)}-S^{(0)}}\rho^2(d\phi)^2 + e^{2(\gamma'-U_0^{(BH)})-S^{(0)}}\left(d\rho^2+dz^2\right)\right] + e^{2T^{(0)}}(d\psi)^2$$

where $U_0^{(BH)} = \frac{1}{2}\ln\left(\frac{x-1}{x+1}\right)$. And then the function T is equals to $T^{(0)}$ and U_1 is given by the Einstein equation (vii).

3 Generation of one-rotational black ring solution

The seed functions of one-rotational black ring solution are obtained as

$$S^{(0)} = T^{(0)} = \tilde{U}_{\lambda\sigma} + \tilde{U}_{-\eta_1\sigma} - \tilde{U}_{\eta_2\sigma}, \tag{10}$$

where the functions $\tilde{U}_d$ is defined as $\tilde{U}_d := \frac{1}{2}\ln[R_d + (z-d)]$. The parameters λ, η_1 and η_2 should satisfy the following inequalities

$$1 < \lambda, \quad -1 < \eta_1 < 1, \quad -1 < \eta_2 < 1, \quad 0 < \eta_1 + \eta_2. \tag{11}$$

After substitution the seed function (10) for the differential equations (5), we obtain the solutions of these equations as,

$$a = \frac{\alpha}{2}\frac{(x-y+1-\lambda)+\sqrt{(x^2-1)(1-y^2)+(xy-\lambda)^2}}{\left[(xy-\lambda)+\sqrt{(x^2-1)(1-y^2)+(xy-\lambda)^2}\right]^{\frac{1}{2}}}$$

$$\times \frac{(x-y+1+\eta_1)+\sqrt{(x^2-1)(1-y^2)+(xy+\eta_1)^2}}{\left[(xy+\eta_1)+\sqrt{(x^2-1)(1-y^2)+(xy+\eta_1)^2}\right]^{\frac{1}{2}}} \frac{\left[(xy-\eta_2)+\sqrt{(x^2-1)(1-y^2)+(xy-\eta_2)^2}\right]^{\frac{1}{2}}}{(x-y+1-\eta_2)+\sqrt{(x^2-1)(1-y^2)+(xy-\eta_2)^2}},$$

$$b = 2\beta \frac{\left[(xy-\lambda)+\sqrt{(x^2-1)(1-y^2)+(xy-\lambda)^2}\right]^{\frac{1}{2}}}{(x+y-1-\lambda)+\sqrt{(x^2-1)(1-y^2)+(xy-\lambda)^2}}$$

$$\times \frac{\left[(xy+\eta_1)+\sqrt{(x^2-1)(1-y^2)+(xy+\eta_1)^2}\right]^{\frac{1}{2}}}{(x+y-1+\eta_1)+\sqrt{(x^2-1)(1-y^2)+(xy+\eta_1)^2}} \frac{(x+y-1-\eta_2)+\sqrt{(x^2-1)(1-y^2)+(xy-\eta_2)^2}}{\left[(xy-\eta_2)+\sqrt{(x^2-1)(1-y^2)+(xy-\eta_2)^2}\right]^{\frac{1}{2}}},$$

where α and β are integration constants.

Next we reduce the explicit expression for the γ'. Finally the functional form of γ' can be written down as

$$\begin{aligned}
\gamma' &= \frac{1}{2}\left(\tilde{U}_\sigma - \tilde{U}_{-\sigma}\right) + \tilde{U}_{\lambda\sigma} + \tilde{U}_{-\eta_1\sigma} - \tilde{U}_{\eta_2\sigma} \\
&\quad -\frac{1}{4}\left(\ln Y_{\sigma,\sigma} + \ln Y_{-\sigma,-\sigma} + \ln Y_{\lambda\sigma,\lambda\sigma} + \ln Y_{-\eta_1\sigma,-\eta_1\sigma} + \ln Y_{\eta_2\sigma,\eta_2\sigma}\right. \\
&\quad -2\ln Y_{\sigma,-\sigma} + \ln Y_{\sigma,\lambda\sigma} - \ln Y_{-\sigma,\lambda\sigma} + \ln Y_{\sigma,-\eta_1\sigma} - \ln Y_{\sigma,\eta_2\sigma} \\
&\quad \left. - \ln Y_{-\sigma,-\eta_1\sigma} + \ln Y_{-\sigma,\eta_2\sigma} + 2\ln Y_{\lambda\sigma,-\eta_1\sigma} - 2\ln Y_{\lambda\sigma,\eta_2\sigma} - 2\ln Y_{\eta_1\sigma,\eta_2\sigma}\right). \qquad (12)
\end{aligned}$$

Now the functions which is needed to express the full metric are completely obtained. The full metric is expressed as

$$\begin{aligned}
ds^2 &= -\frac{A}{B}\left[dx^0 - \left(2\sigma e^{-S^{(0)}}\frac{C}{A} + C_1\right)d\phi\right]^2 + \frac{B}{A}e^{-2S^{(0)}}\rho^2(d\phi)^2 + e^{2S^{(0)}}(d\psi)^2 \\
&\quad + C_2\sigma^2\frac{x^2-y^2}{x^2-1}Be^{2(\gamma'-S^{(0)})}\left(\frac{dx^2}{x^2-1} + \frac{dy^2}{1-y^2}\right). \qquad (13)
\end{aligned}$$

In the following, the constants C_1 and C_2 are fixed as

$$C_1 = \frac{2\sigma^{1/2}\alpha}{1+\alpha\beta}, \quad C_2 = \frac{1}{\sqrt{2}(1+\alpha\beta)^2}, \qquad (14)$$

to assure that the spacetime asymptotes a five-dimensional Minkowski spacetime globally. This is easily confirmed by taking the asymptotic limit $x \to \infty$.

The metric component $g_{\phi\phi}$ becomes negative around $(x,y) = (1,1)$ and $(1,-1)$. These singular behaviors are cured by setting the parameters α and β as

$$\alpha = \sqrt{\frac{2(1-\eta_2)}{(\lambda-1)(1+\eta_1)}} \quad \text{and} \quad \beta = \sqrt{\frac{(\lambda+1)(1-\eta_1)}{2(1+\eta_2)}}. \qquad (15)$$

The asymptotic form of $\mathcal{E}_S$ near the infinity $\tilde{r} = \infty$ becomes

$$\mathcal{E}_S = \tilde{r}\cos\theta\left[1 - \frac{\sigma}{\tilde{r}^2}\frac{P(\alpha,\beta,\lambda)}{(1+\alpha\beta)^2} + \cdots\right] + 2i\sigma^{1/2}\left[\frac{\alpha}{1+\alpha\beta} - \frac{2\sigma\cos^2\theta}{\tilde{r}^2}\frac{Q(\alpha,\beta,\lambda)}{(1+\alpha\beta)^3} + \cdots\right],$$

where we introduced the new coordinates $\tilde{r}$ and θ through the relations

$$x = \frac{\tilde{r}^2}{2\sigma} + \lambda - \eta_1 - \eta_2, \; y = \cos 2\theta, \qquad (16)$$

and

$$\begin{aligned}
P(\alpha,\beta,\lambda) &= 4(1+\alpha^2-\alpha^2\beta^2) \qquad (17) \\
Q(\alpha,\beta,\lambda) &= \alpha(2\alpha^2 - \eta_1 - \eta_2 + \lambda + 3) - 2\alpha^2\beta^3 \qquad (18) \\
&\quad -\beta\left[2(2\alpha\beta+1)(\alpha^2+1) + (\eta_1+\eta_2-\lambda-1)\alpha^2(\alpha\beta+2)\right]. \qquad (19)
\end{aligned}$$

From the asymptotic behavior of the Ernst potential, we can compute the mass parameter m^2 and rotational parameter $m^2 a_0$ as

$$m^2 = \sigma \frac{P(\alpha,\beta,\lambda)}{(1+\alpha\beta)^2} = \frac{8\sigma(\eta_1+\eta_2)(\lambda-\eta_2)}{(\lambda-1)(1+\eta_1)(1+\eta_2)(1-\alpha\beta)^2}. \tag{20}$$

and

$$m^2 a_0 = 4\sigma^{3/2}\frac{Q(\alpha,\beta,\lambda)}{(1+\alpha\beta)^3} = m^2\frac{\sqrt{\sigma}(\alpha(1+\lambda\eta_1)-2\beta\eta_2)}{1+\alpha\beta}, \tag{21}$$

where we use the Eqs. (15) in the second equalities. When $\eta_1 = \eta_2 = 1$ the solutions becomes static black ring solution.

The periods of ϕ and ψ are defined as

$$\Delta\phi = 2\pi \lim_{\rho\to 0}\sqrt{\frac{\rho^2 g_{\rho\rho}}{g_{\phi\phi}}} \quad \text{and} \quad \Delta\psi = 2\pi \lim_{\rho\to 0}\sqrt{\frac{\rho^2 g_{\rho\rho}}{g_{\psi\psi}}} \tag{22}$$

to avoid a conical singularity. We see that the periods of ϕ and of ψ outside the ring sholud be 2π and

$$\Delta\psi = \frac{2\pi}{1+\alpha\beta}\sqrt{\frac{\lambda+1}{\lambda-1}}\left(\frac{\lambda-\eta_2}{\lambda+\eta_1}\right)\left(1+\alpha\beta\frac{\lambda-1}{\lambda+1}\right) \tag{23}$$

inside the ring. In general there is a conical singularity inside or outside the ring. This conical singularity is cured by setting the parameters λ, η_1 and η_2 satisfy the relation

$$\left(\frac{\lambda-\eta_2}{\lambda+\eta_1}\right)\left(1+\sqrt{\frac{\lambda-1}{\lambda+1}}\sqrt{\frac{(1-\eta_1)(1-\eta_2)}{(1+\eta_1)(1+\eta_2)}}\right) = \sqrt{\frac{\lambda-1}{\lambda+1}}+\sqrt{\frac{(1-\eta_1)(1-\eta_2)}{(1+\eta_1)(1+\eta_2)}}. \tag{24}$$

4 Summary

We have derived the one rotational black ring solution by using the solitonic solution-generating technique. Note that the seed metric of this black ring is not a Minkowski metric, which is the seed of S^2 rotating black ring. The metric function are given in the prolate-spheroidal coordinates. The relation between the expressions of the prolate-spheroidal coordinates and the canonical coordinates obtained by Harmark [5] will be presented elsewhere [6]. The metric form (13) contains some singular solutions which are not contained in the C-metric expression by Emparan and Reall. To exclude these singular solutions we need the condition (15) between the parameters. Also, we have obtained the condition to cure the conical singularity at the end of the previous section. More detailed analysis will be published [6].

Acknowledgments

This work is partially supported by Grant-in-Aid for Young Scientists (B) (No. 17740152) from Japanese Ministry of Education, Science, Sports, and Culture and by Nihon University Individual Research Grant for 2005.

References

[1] R. Emparan and H. S. Reall, Phys. Rev. Lett. **88**, 101101 (2002).

[2] T. Mishima and H. Iguchi, hep-th/0504018.

[3] F. J. Ernst, Phys. Rev. **167**, 1175 (1968).

[4] J. Castejon-Amenedo and V.S. Manko, Phys. Rev. **D 41**, 2018 (1990).

[5] T. Harmark, Phys. Rev. **D 70**, 124002 (2004).

[6] H. Iguchi and T. Mishima, in preparation.

The avoidance of the ghost problem in the DGP brane world
— two-branes model —

Keisuke Izumi[1] and Takahiro Tanaka[2]

Theoretical Astrophysics Group, Department of Physics, Kyoto University, Kyoto 606-8502, Japan

Abstract

We discuss gravitational perturbations of de Sitter brane world in the DGP model. In the original DGP model with a self-accelerating single brane, a ghost-like field appears, which is thought to be problematic. To cure this ghost problem keeping the advantage of the self-acceleration, we propose a two-branes model, which has another boundary brane in the bulk. When the new boundary brane is sufficiently close to the original brane, there is no ghost in this model. Moreover, when the acceleration of the universe is solely due to the modification of gravity without the aid of dark energy, the model is free from ghost irrespective of the position of the new boundary brane.

1 Introduction

Various recent cosmological observations, such as the Type-Ia supernovae, indicate the present-day accelerated expansion of the universe. One approach to this phenomenon is to introduce the dark energy which assists the accelerated expansion of the universe. One can say that this is a modification of the right hand side of the Einstein equations. As an alternative way, we can modify the left hand side of the Einstein equations, which means modification of the theory of gravity. To explain the accelerated expansion of the universe in this scheme, it will be naturally required to introduce the corresponding mass scale into the theory. One interesting possibility is to give a mass to the graviton.

Here we consider the DGP model [2], which is a five-dimensional brane world model with the induced gravity term on the brane. This model admits a solution representing an accelerated expansion of the universe without introducing the dark energy. By studying perturbations around this solution, the mass of graviton is found, in fact, to be non-zero.

In the Minkowski background the form of a covariant mass term is uniquely determined up to the quadratic order in the action by the requirement that the ghost is absent[1]. The action generalized to the case with a general background $g^{(0)}_{\mu\nu}$ is given by

$$S = \int d^4x\sqrt{-g}\left[R - \frac{m^2}{4}(h^{\mu\nu}h_{\mu\nu} - h^2) + O(h^3)\right]. \tag{1}$$

where

$$h_{\mu\nu} = g_{\mu\nu} - g^{(0)}_{\mu\nu}, \tag{2}$$

is the metric perturbation. Basically, the DGP model also takes a similar effective action at the quadratic order.

However, there is an argument that the model defined by the action (1) possesses a ghost-like mode in spin-2 excitations when we adopt de Sitter space as the background spacetime, if the mass of the graviton is small [4]. If we wish to solve the accelerated expansion of the universe by the modification of gravity, it seems that the graviton mass is necessarily as small as the Hubble parameter. If so, the appearance of a ghost seems to be unavoidable. In fact, it was explicitly shown that a similar ghost-like mode appears in the DGP model [3]. Here we consider a variant of the DGP model by introducing another boundary brane, searching for a model coping with both the accelerated expansion of the universe and the ghost-free condition. We will find that such a model can be constructed.

[1]E-mail:ksuke@tap.scphys.kyoto-u.ac.jp
[2]E-mail:tama@scphys.kyoto-u.ac.jp

2 Background spacetime in the DGP model

In this section we consider the unperturbed background of the model[5]. The five dimentional action of the DGP model is given by [2]

$$S = -\frac{1}{2\tilde{\kappa}^2}\int d^5X\sqrt{-\tilde{g}}\,\tilde{R} - \frac{1}{2\kappa^2}\int d^4x\sqrt{-g}\,R + \int d^4x\sqrt{-g}\,L_m + \frac{1}{\tilde{\kappa}^2}\int d^4x\sqrt{-g}\,K, \tag{3}$$

where $\tilde{g}_{\mu\nu}$ and $\tilde{R}$ are the five-dimensional metric and Ricci scalar. $g_{\mu\nu}$, R, $K_{\mu\nu}$ and L_m are all four-dimensional quantity on the brane, and they are the metric, the Ricci scalar, the extrinsic curvature and the matter Lagrangian, respectively. The distinctive feature of this model is the presence of the four-dimensional Einstein-Hilbert term localized on the brane. We assume the Z-2 symmetry across the brane. Then the junction conditions to be imposed at the brane become

$$K_{\mu\nu} = r_c\left[-\kappa^2\left(T_{\mu\nu} - \frac{1}{3}Tg_{\mu\nu}\right) + \left(G_{\mu\nu} - \frac{1}{3}Gg_{\mu\nu}\right)\right], \tag{4}$$

with $r_c \equiv \tilde{\kappa}^2/2\kappa^2$.

Assuming that the three space on the brane is homogeneous and isotropic, the metric takes the form

$$ds^2 = -n^2(\tau, y)d\tau^2 + a^2(\tau, y)\delta_{ij}dx^idx^j + dy^2, \tag{5}$$

where δ_{ij} is Kronecker's delta and the brane is located at y =constant. Under this assumption, one can calculate the Hubble parameter using the five-dimensional Einstein equations and the junction conditions (4) to obtain two solutions

$$H_\pm = \pm\frac{1}{2r_c} + \sqrt{\frac{\kappa^2}{3}\rho + \frac{1}{(2r_c)^2}}. \tag{6}$$

The model with $H = H_+$ is called the "+" branch, while that with $H = H_-$ the "-" branch. In the late time limit ($\rho \to 0$), we have

$$H_+ \to \frac{1}{r_c} = \text{constant}, \qquad H_- \to \frac{1}{6}\rho. \tag{7}$$

Since the Hubble parameter of the "+" branch does not vanish in this limit, this branch can explain the late time accelerated expansion of the universe.

For simplicity, we consider the cases in which the energy-momentum tensor of the four-dimensional matter field is described by a cosmological constant term. Namely, we assume that the Lagrangian of the matter field is given by

$$L_m = -\sigma \text{ (constant)}. \tag{8}$$

Solving the Einstein equations with the junction conditions, we obtain the metric as

$$ds^2 = dy^2 + y^2\left(-d\tau^2 + \exp(2\tau)\delta_{ij}dx^idx^j\right), \tag{9}$$

where the brane is placed at $y = H_\pm^{-1}$, and $H_\pm$ are those given in Eq. (6) with $\rho = \sigma$. By the coordinate translation

$$Y^0 = y\exp(\tau)\left(\frac{r^2}{4} + 1 - \frac{\exp(-2\tau)}{4}\right), \tag{10}$$

$$Y^4 = y\exp(\tau)\left(\frac{r^2}{4} - 1 - \frac{\exp(-2\tau)}{4}\right), \tag{11}$$

$$Y^i = y\exp(\tau)x^i \qquad (i = 1, 2, 3), \tag{12}$$

$$r^2 = \sum_{i=1}^{3}x^i, \tag{13}$$

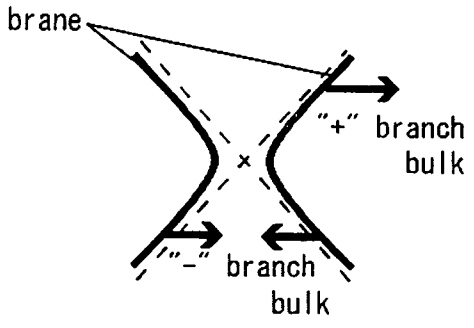

Figure 1: the hyperboloid brane in the 5D Minkowski spacetime

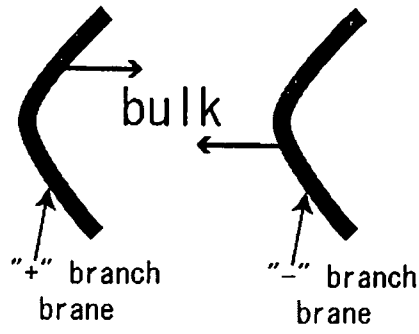

Figure 2: two-brane model

the above metric is transformed into the flat metric as

$$ds^2 = -(dY^0)^2 + (dY^1)^2 + (dY^2)^2 + (dY^3)^2 + (dY^4)^2. \tag{14}$$

In these flat coordinates, the brane exists at

$$\sum_{\mu=1}^{4}(Y^\mu)^2 - (Y^0)^2 = \frac{1}{H^2}. \tag{15}$$

Hence, the brane is a hyperboloid embedded in the 5D Minkowski spacetime. In the "+" ("-") branch the bulk is the outside (inside) of the hyperboloid, $y > H_+^{-1}$ ($y < H_+^{-1}$). (See Fig. 1.)

3 The ghost mode in the DGP brane world

Now we study perturbations around the background obtained in the previous section. When we consider perturbations in the bulk, we can use transverse-traceless gauge. Besides the transverse-traceless conditions, we can choose y-components of the metric kept unperturbed by using the residual gauge degrees of freedom. Then the metric is given by

$$ds^2 = dy^2 + \left(y^2\gamma_{\mu\nu} + h_{\mu\nu}\right)dx^\mu dx^\nu, \qquad \text{with} \quad \nabla^\mu h_{\mu\nu} = 0, \qquad h = 0, \tag{16}$$

where $\gamma_{\mu\nu}$ is the metric of four-dimensional de-Sitter space. In raising and lowering the Greek indices, we use $\gamma_{\mu\nu}$. Since we have fixed the gauge, the brane is not located at a fixed value of y-coordinate any more:

$$y = H^{-1} + \psi(x^\mu). \tag{17}$$

Integrating the action over y-direction, we can obtain four-dimensional effective action. The effective action is divided into three parts, a spin-0 mode, continuous spin-2 modes and a discrete spin-2 mode. The spin-0 part of the effective action becomes[3]

$$S_\psi = C_\psi \int d^4x\sqrt{-g}\psi(\Box + 4)\psi, \qquad C_\psi > 0. \tag{18}$$

Both of the two spin-2 parts take the form

$$S_\chi = C_\chi \int d^4x\sqrt{-g}\ \chi^{\mu\nu}(\Box - 2 - m^2/H^2)\chi_{\mu\nu}, \qquad C_\chi > 0, \tag{19}$$

where the squared masses of the continuous spin-2 modes are larger than $(9/4)H^2$, while the discrete spin-2 mode has a squared mass smaller than $2H^2$. The action for the discrete spin-2 mode is identical to that in the massive gravity theory defined by (1). In massive gravity theory, it is known that a ghost mode appears if m^2 of the spin-2 perturbation is smaller than $2H^2$[4]. Since the same statement applies to the present case, we find that the discrete spin-2 modes in the DGP model have a ghost.

4 Two-branes model

We put a "-" branch brane parallel to the "+" branch brane as shown in Fig. 2. Recalling that in the "+" ("-") branch the bulk is the outside (inside) of the brane, $y > H_+^{-1}$ ($y < H_+^{-1}$), we can place two parallel branes consistently when $H_+ > H_-$. If we move the "-" branch brane to infinity, this model reduces to the single-brane model, which has a ghost. On the other hand, if we move the "-" branch brane toward the "+" branch brane, the model is expected to reduce to the usual four-dimensional model in the coincidence limit. If so, there is no ghost in this limit.

Using the same method as in the case of the single-brane model, we can calculate the perturbations in the two-branes model. The metric takes the same form as before, (16), and the positions of the "+" and "-" branch branes are

$$y = H_+^{-1} + \psi_+(x^\mu), \qquad y = H_-^{-1} + \psi_-(x^\mu). \tag{20}$$

The four-dimensional effective action takes the same form with ψ replaced with $\psi_+ - \psi_-$. However, the wave functions in the y-direction are modified by putting the "-" branch brane. Thus, the mass squared m^2, which corresponds to the eigenvalue of each wave function, also changes. When

$$H_- > H_+ - r_c^{-1}, \tag{21}$$

is satisfied, all spin-2 modes satisfy the condition $m^2 > 2H^2$, which means that there is no ghost.

Let us focus on the most interesting case, i.e., the self acceleration phase ($\rho \to 0$). In this limit, H_+ becomes r_c^{-1}. Then, the no ghost condition reduces to $H_- > 0$, and hence there is no ghost irrespective of the location of the "-" branch brane.

5 Summary and conclusions

As a prescription to cure the ghost problem in the de Sitter phase in the massive gravity theory, we considered a modification of the DGP brane world model. If the mass of the graviton is sufficiently large compared with the Hubble parameter (no-ghost condition), there is no ghost-like spin2 mode. In order to change the mass spectrum, we introduced the second boundary brane, and found that we can arrange the second brane so that no-ghost condition is satisfied. In the case of the self-accelerating brane, in which the universe expands exponentially without the aid of the dark energy, no ghost condition is found to be satisfied irrespective of the position of the the second brane.

The above result looks a bit strange. If there is a ghost mode, pair production occurs explosively at a moment. However, in the self-accelerating phase in the two-branes model, the presence of a ghost mode is controlled by the second brane placed far from the original first brane. Suppose that the boundary condition, i.e., the location of the second brane, is changed at a certain time. An observer living on the brane cannot notice the change of the boundary condition instantaneously due to causality, although the mode analysis will tell that there is a ghost mode. This looks contradictory. We will come back to this issue in a future publication[6].

References

[1] M.Fierz and W.Pauli, Proc. Roy. Soc. **173** (1939) 211.

[2] G.R.Dvali, G.Gabadadze and M.Porrati, Phys. Lett. **B485**(2000) 208.

[3] K.Koyama, phys. Rev. **D72** (2005) 123511.

[4] A.Higuchi, Nucl. Phys. **B282** (1987) 397.

[5] C.Deffayet, Phys. Lett. **B502** (2001) 199.

[6] K.Izumi and T.Tanaka, *in preparation.*

Deformed Horizons and Singularities in Five-dimensional Charged Black Holes

Ken Matsuno[1] and Hideki Ishihara[2]

Department of Mathematics and Physics, Graduate School of Science, Osaka City University, Sumiyoshi-ku, Osaka 558-8585, Japan

Abstract

We investigate global structures of electrically charged static black holes in five-dimensional Einstein-Maxwell system. The geometries can be regarded as five-dimensional black holes with deformed S^3 horizons nearby outer horizon and, in contrast, a twisted S^1 fiber bundle over the four-dimensional Reissner-Nordström black hole far from it. Also we mention some limits of this black hole.

1 Introduction

To consider the higher dimensional spacetime is a play ground of the unification of gravity and other forces. So far the size of spatially extra dimensions has been considered as to be too small to detect, e.g., about the Plank scale. Recently, it is pointed out that the extra dimensions possibly has the more larger scale, such as a sub-millimeter scale. If so, we get the chance to treat the gravity as the TeV scale physics. This idea suggests an interesting experiments : it is possible to make mini-black holes in a large hadron collider. When such black holes are produced, the observers feel these spacetimes as the higher dimensional ones nearby the horizon, while the effectively four-dimensional ones in the distant region from the black hole.

We consider the five-dimensional electrically charged static black holes with the central singularity and asymptotic locally flat, a constant S^1 fiber bundle over the four-dimensional Minkowski spacetime. The geometrical structures are five-dimensionally by the horizon against four-dimensionally at far. The horizons have shape of squashed S^3. These black hole solutions have three parameters, the size of squashed S^3 horizons $r_\pm$ and of the extra dimensional S^1 bundle at spatial infinity r_0. We also point out some limits of these spacetimes.

2 Five-dimensional Charged Black Hole

We start from the five-dimensional Einstein-Maxwell system with the action :

$$S = \frac{1}{16\pi G}\int d^5x\sqrt{-g}\,(R - F_{\mu\nu}F^{\mu\nu}), \tag{1}$$

where G, R and $F_{\mu\nu} = 2\partial_{[\mu}A_{\nu]}$ are the five-dimensional gravitational constant, the Ricci scalar curvature and the electromagnetic field with gauge potential A^μ. From this action, we write down the Einstein equation

$$R_{\mu\nu} - \frac{1}{2}Rg_{\mu\nu} = 2\left(F_{\mu\lambda}F^{\lambda}_{\ \nu} - \frac{1}{4}g_{\mu\nu}F_{\alpha\beta}F^{\alpha\beta}\right), \tag{2}$$

and the Maxwell equation

$$F^{\mu\nu}{}_{;\nu} = 0. \tag{3}$$

We consider the static black hole with SO(3)×U(1) symmetry. The ansatz of metric is

$$ds^2 = -\alpha^2(R)dT^2 + \left(\alpha\beta^2\gamma\right)^2 dR^2 + \beta^2(R)d\Omega^2 + \gamma^2(R)\sigma^2, \tag{4}$$

[1]E-mail: matsuno@sci.osaka-cu.ac.jp
[2]E-mail: ishihara@sci.osaka-cu.ac.jp

with

$$d\Omega^2 = d\theta^2 + \sin^2\theta d\phi^2,\ \sigma = d\psi + \cos\theta d\phi, \tag{5}$$

where α, β, γ are functions depend only on R, and ψ, θ, ϕ are the Euler angles of SU(2) on the three-sphere. The last two terms in (4) denotes the metric on S^3. S^3 is regarded as a twisted S^1 fiber bundle over the round two-sphere S^2, the Hopf fibration.

We assume that the gauge potential one-forms $A = A_\mu dx^\mu$ has only one component A_T and depends only on R,

$$A = A_T(R)dT, \tag{6}$$

i.e., this spacetime has a radial electric field.

In these ansatz, we get a series of general solutions analytically. To select out black hole solutions, we set boundary conditions such that the horizon wraps the central singularity. For the existing of horizon at $R = R_H$ the metric components should satisfy

$$\alpha = 0,\ \alpha' = \text{finite},\ \beta,\ \gamma = \text{finite and } \beta',\ \gamma' = 0, \tag{7}$$

where a prime denotes a derivative with respect to R.

Finally, we do a coordinate transformation $(T, R) \to (t, r)$ and get the electrically charged black hole[1] with the metric

$$ds^2 = -f dt^2 + \frac{k^2}{f}dr^2 + \frac{r^2}{4}\left(k d\Omega^2 + \sigma^2\right), \tag{8}$$

where

$$f(r) = \left(1 - \frac{r_+^2}{r^2}\right)\left(1 - \frac{r_-^2}{r^2}\right),\ k(r) = \frac{\left(r_0^2 - r_+^2\right)\left(r_0^2 - r_-^2\right)}{\left(r_0^2 - r^2\right)^2}, \tag{9}$$

and $r_\pm$, r_0 are constants. The gauge potential (6) is given by

$$A = \pm\frac{\sqrt{3}}{2}\frac{r_+ r_-}{r^2}dt. \tag{10}$$

For an expression of $k(r)$, we set a coordinate r runs from zero to r_0 and parameters $r_\pm$ and r_0 satisfy $0 < r_- \le r_+ < r_0 < \infty$. r_+ and r_- denote the outer horizon and the inner horizon. There is a curvature singularity at $r = 0$ while $r = r_0$ is a coordinate apparent singularity since the Kretschmann scalar

$$R_{\mu\nu\rho\sigma}R^{\mu\nu\rho\sigma} = \left[r^3 k(r)\right]^{-4}\left(\sum_{j=0}^{12} C_j r^{2j}\right),\ C_j = C_j\left(r_\pm,\ r_0\right) = \text{const.}, \tag{11}$$

is finite except $r = 0$.

If we put $r_+ = r_- = 0$ then the metric (8) reduces to the Gross-Perry-Sorkin (GPS) monopole[2] which is regular all around the spacetime. So we can say that this black hole (8) is the black version of the GPS monopole against spherically symmetric black holes are based on the flat Minkowski spacetime.

We can also calculate the surface gravity of horizon r_+ as

$$\kappa = \frac{r_+^2 - r_-^2}{r_+^3}\frac{r_0^2}{r_0^2 - r_-^2}\sqrt{\frac{r_0^2 - r_+^2}{r_0^2 - r_-^2}}. \tag{12}$$

The shape of horizons are represented by the S^3 part of the metric (8) which is foliated by the three-dimensional $r = r_\pm$ surface in the four-dimensional timelike t =const. hypersurface. The explicit form is

$$\frac{r_\pm^2}{4}\left[k(r_\pm)d\Omega^2 + \sigma^2\right],\ k(r_\pm) = \frac{r_0^2 - r_\mp^2}{r_0^2 - r_\pm^2}. \tag{13}$$

Because the squashing parameter $k(r_\pm)$ satisfies $k(r_-) < 1 < k(r_+)$, the outer horizon r_+ is oblate, the base space S^2 is larger than the fiber space S^1, while the inner horizon r_- is prolate, S^2 is smaller than S^1. When $r_+ = r_-$, the horizon becomes round S^3 as same as the five-dimensional Reissner-Nordström black hole (see sec.3).

The function $k(r)$ becomes almost constant in $r_+ < r \ll r_0$ region then observers nearby the outer horizon feel this black hole as the five-dimensional charged black hole. Indeed the central singularity is timelike for the form of metric (8) becomes a similar form to the five-dimensional Reissner-Nordström spacetime near $r = 0$ region.

With introducing new coordinates $\eta = 2\rho_0 t/r_0$, $\rho = \rho_0 r^2/\left(r_0^2 - r^2\right)$ and $\rho_0 = r_0\sqrt{f(r_0)}/2$, the metric (8) is transformed as

$$ds^2 = -Vd\eta^2 + U\left(\frac{d\rho^2}{V} + \rho^2 d\Omega^2\right) + \frac{(\rho_0+\rho_+)(\rho_0+\rho_-)}{U}\sigma^2, \tag{14}$$

where

$$V(\rho) = \left(1 - \frac{\rho_+}{\rho}\right)\left(1 - \frac{\rho_-}{\rho}\right),\ U(\rho) = 1 + \frac{\rho_0}{\rho}, \tag{15}$$

and $\rho_\pm = r_\pm^2\sqrt{\left(r_0^2 - r_\mp^2\right)/\left(r_0^2 - r_\pm^2\right)}/(2r_0)$ correspond to the outer and inner horizons. Because $0 < r < r_0$ implies $0 < \rho < \infty$, this spacetime is asymptotic locally flat, a twisted constant S^1 fiber bundle over the four-dimensional Minkowski spacetime, at $\rho \to \infty$ as $r \to r_0$ and $r_0 = 2\sqrt{(\rho_0+\rho_+)(\rho_0+\rho_-)}$ denotes the size of S^1 bundle at the spatial infinity.

When $\rho_0 \ll \rho_\pm$ then $V(\rho)$ becomes more effectively than $U(\rho)$ and the function $U(\rho)$ is almost constant. Thus distant observers at $\rho_+ < \rho$ feel this black hole as the four-dimensional charged black hole.

3 Limits

We consider four cases of limit for parameters $r_\pm$ and r_0.

3.1 Limit (1) : $r_0 \to \infty$

In this case, a function $k(r)$ goes 1 and the metric becomes

$$ds^2 = -\left(1 - \frac{r_+^2}{r^2}\right)\left(1 - \frac{r_-^2}{r^2}\right)dt^2 + \left(1 - \frac{r_+^2}{r^2}\right)^{-1}\left(1 - \frac{r_-^2}{r^2}\right)^{-1}dr^2 + r^2 d\Omega_3^2, \tag{16}$$

where $d\Omega_3^2$ denotes the metric on an unit three-sphere S^3 with the SO(4) isometry group. This is the five-dimensional Reissner-Nordström black hole[3] which has round S^3 horizons $r_\pm$ and is asymptotically flat at $r \to \infty$. The surface gravity (12) also becomes a similar form, $\kappa = \left(r_+^2 - r_-^2\right)/r_+^3$.

3.2 Limit (2) : $r_- \to 0$

Since the gauge potential (10) becomes zero for this limit, the metric

$$ds^2 = -fdt^2 + \frac{k^2}{f}dr^2 + \frac{r^2}{4}\left(kd\Omega^2 + \sigma^2\right),\ f(r) = 1 - \frac{r_+^2}{r^2},\ k(r) = \frac{r_0^2\left(r_0^2 - r_+^2\right)}{\left(r_0^2 - r^2\right)^2}, \tag{17}$$

denotes a deformed Schwarzschild black hole with an oblete horizon r_+. In other words, because the five-dimensional pure Einstein system corresponds to the four-dimensional Einstein-Maxwell system in the Kaluza-Klein theory, this metric represents a magnetically charged Kaluza-Klein black hole[4].

3.3 Limit (3) : $r_+ = r_-$

The metric of this case represents a deformed extremal Reissner-Nordström black hole with a round S^3 horizon r_+ and, respectively, the surface gravity (12) vanishes as in usual case. Here we use new coordinate $\bar{r}^2 = r^2 - r_+^2$ with $\bar{r}_\infty^2 = r_\infty^2 - r_+^2$, the metric can be rewritten as

$$ds^2 = -H^{-2}dt^2 + Hds_{TN}^2, \tag{18}$$

where

$$H(\bar{r}) = 1 + \frac{r_+^2}{\bar{r}^2}, \tag{19}$$

is a harmonic function of $\bar{r}$ for the four-dimensional Euclidean self-dual Taub-NUT space

$$ds_{TN}^2 = N^2 d\bar{r}^2 + \frac{\bar{r}^2}{4}\left(Nd\Omega^2 + \sigma^2\right), \; N(\bar{r}) = \left(1 - \frac{\bar{r}^2}{\bar{r}_0^2}\right)^{-2}, \tag{20}$$

and the gauge potential (10) becomes

$$A = \pm\frac{\sqrt{3}}{2} H^{-1} dt. \tag{21}$$

This black hole (18) is as same as the one considered in the supersymmetric (SUSY) theory[5]. If we could constract a harmonic solution of $\triangle_{TN} H = 0$ where $\triangle_{TN}$ is the Laplacian on (20) and H depends not only $\bar{r}$ but also the Euler angles then there would be deformed SUSY multi-black holes.

3.4 Limit (4) : $r_+,\ r_- \to r_0$

This special limit keeping with $\rho_\pm$ finite corresponds to $\rho_0 \to 0$ for the metric form (14). The result is

$$ds^2 = -\left(1 - \frac{\rho_+}{\rho}\right)\left(1 - \frac{\rho_-}{\rho}\right) d\eta^2 + \left(1 - \frac{\rho_+}{\rho}\right)^{-1}\left(1 - \frac{\rho_-}{\rho}\right)^{-1} d\rho^2 + \rho^2 d\Omega^2 + \rho_+\rho_-\sigma^2. \tag{22}$$

Now the size of a twisted S^1 fiber bundle takes constant value $\sqrt{\rho_+\rho_-}$. Though we take $\rho_- \to 0$ then above metric (22) goes with a new coordinate $z = \sqrt{\rho_+\rho_-}\psi$,

$$ds^2 = -\left(1 - \frac{\rho_+}{\rho}\right) d\eta^2 + \left(1 - \frac{\rho_+}{\rho}\right)^{-1} d\rho^2 + \rho^2 d\Omega^2 + dz^2. \tag{23}$$

This direct product metric of the four-dimensional Schwarzschild black hole and S^1 gives the neutral black string.

4 Conclusion

We study the series of five-dimensional electrically charged static black holes with squashed S^3 horizons.

These global structures are considered as five-dimensional black holes nearby the horizon region while as effectively four-dimensional black holes with a compactified extra dimension for the distant region.

We also find some limits including spherically symmetric black holes and the neutral black string.

We will consider their stabilities, thermodynamics and constract rotating black hole solutions with angular momentums, inner solutions, more higher dimensional black holes with the cosmological constant.

References

[1] H. Ishihara and K. Matsuno, hep-th/0510094.

[2] D.J. Gross and M.J. Perry, Nucl. Phys. B **226**, 29 (1983);
R. Sorkin, Phys. Rev. Lett. **51**, 87 (1983).

[3] F.R. Tangherlini, Nuov. Cim. **27**, 636 (1963).

[4] P. Dobiasch and D. Maison, Gen. Rel. Grav. **14**, 231 (1982);
G.W. Gibbons and D.L. Wiltshire, Ann. Phys. **167**, 201 (1986).

[5] D. Gaiotto, A. Strominger and X. Yin, hep-th/0503217;
H. Elvang, R. Emparan, D. Mateos and H.S. Reall, JHEP **08**, 042 (2005).

Geometrical Aspects of D-brane
— Black Hole Microstates —

Shunji Matsuura[1], Shinpei Kobayashi[2]

[1] *Theoretical Astrophysics Group, Department of Physics, the University of Tokyo, Tokyo 113-0033, Japan*

[2] *Research Center for the Early Universe, School of Science, the University of Tokyo, Tokyo 113-0033, Japan*

Abstract

We extended the general solution with the symmetry $ISO(1,p) \times SO(D-p-1)$ of Type II supergravity (the three-parameter solution) so as to include traveling waves. Considering the near extremal case, we investigate how the non-extremality works for the fuzzball picture. This work is based on [1].

1 Introduction

Black holes have many puzzles and these are keys to understand self-consistent theory of quantum gravity. It is known that black hole has thermodynamical properties. The entropy, S_{Bek}, of a black hole is proportional to the area of the horizon, $\mathcal{A}$:

$$S_{Bek} = \frac{\mathcal{A}}{4G_d}$$

and the temperature, T, is proportional to the surface gravity at the horizon, κ:

$$T = \frac{\kappa}{2\pi}.$$

These properties suggest that a black hole should have microstates corresponding to its entropy. In classical gravity, it is not clear where these microstates are and thought to be confined near the singularity where classical description breaks down. Another important problem is the information problem. Black hole loses its mass via Hawking radiation. However, because Hawking radiation is thermal, information of what kind of matter fell into the black hole seems to be lost. This is not consistent with the conventional quantum mechanics.

In 1996, Strominger and Vafa[2] showed that in some special system, it is possible to reproduce Bekenstein entropy by counting the number of states of the D-branes which construct the black hole. Recently, Mathur and his collaborators proposed a bold conjecture[3]. The conjecture is

- There is one geometry per microstate.
- The individual state have no horizon, no singularity and no closed timelike curve.
- Coarse-graining gives the notion of entropy.

The conjecture is checked in D1-D5[4] system and some part of D1-D5-P[5] system (see also[6]). Smooth geometries which are thought to be corresponding to the black hole microstates are also found for D1-D5-KK[7] and D1-D5-KK-P[8] system. All these works are in BPS case, but recently Jejjala, Madden, Ross and Titchener found non-BPS smooth geometry[9]. Motivated by these works, we constructed one type of non-BPS D1-D5 geometry. We perform a solution generating method to the three-parameter solution and construct non-BPS NS1-P system which is dual to D1-D5 system.

We first explain the construction of smooth geometry of D1-D5 system in section 2 and construct non-BPS NS1-P geometry in section 3.

[1] E-mail:smatsuura@utap.phys.s.u-tokyo.ac.jp

[2] E-mail:shinpei@resceu.s.u-tokyo.ac.jp

2 Smooth geometry of D1-D5

Consider D1-D5 system compactified on $S^1 \times T^4$. D1 branes are wrapped n_1 times on S^1 and D5 branes are wrapped n_5 times on both S^1 and T^4. Naive geometry of this system is derived as follows. The symmetry of this system is $SO(1,1) \times SO(4) \times SO(4)$. The charges are Q_1' and Q_5', corresponding to n_1 and n_5. The geometry should also be asymptotically flat. The naive geometry can be derived with these assumptions as

$$ds^2 = f_1^{-\frac{3}{4}} f_5^{-\frac{1}{4}}[-dt^2 + dy^2] + f_1^{\frac{1}{4}} f_5^{\frac{3}{4}} dx_i dx_i + f_1^{\frac{1}{4}} f_5^{-\frac{1}{4}} dz_a dz_a$$

where y is S^1 direction, x_i are non-compact directions and z_a are T^4 directions. Functions f_1 and f_5 are given by

$$f_1 = 1 + \frac{Q_1'}{r^2} \tag{1}$$

$$f_5 = 1 + \frac{Q_5'}{r^2}. \tag{2}$$

This geometry has naked singularity at $r = 0$ and $S_{Bek} = 0$. There is a discrepancy between macroscopic entropy S_{Bek} and microscopic entropy S_{micro}, which is non-zero.

So what is the actual geometry? We need the gravity dual of D1-D5 bound states. To see this, it is convenient to move to the dual frame. D1-D5 system is dual to P-NS1. The bound states of P-NS1 system is easy to see; NS1 string has momentum P. This P-NS1 geometry can be constructed by waving the string. We first prepare one long (not winding) string. Using a solution generating method, we can construct the waving string. Because this system is BPS, it is possible to multiwind the string around S^1. It should be emphasized that NS1 can have only transverse waves. So after winding the waving NS1 on S^1, it is not localized at a point but spread to the non-compact directions. The actual metric of P-NS1 is then

$$ds^2 = H^{\frac{3}{4}}(-dudv + Kdv^2 + 2A_i dx_i dv) + H^{-\frac{1}{4}} dx_i dx_i + H^{-\frac{1}{4}} dz_a dz_a$$

with

$$H^{-1} = 1 + \frac{Q_1}{L_T}\int_0^{L_T} \frac{dv}{|\vec{x} - \vec{F}(v)|^2} \tag{3}$$

$$K = \frac{Q_1}{L_T}\int_0^{L_T} \frac{(\dot{F}^2(v))dv}{|\vec{x} - \vec{F}(v)|^2} \tag{4}$$

$$A_i = -\frac{Q_1}{L_T}\int_0^{L_T} \frac{(\dot{F}_i(v))dv}{|\vec{x} - \vec{F}(v)|^2} \tag{5}$$

where $L_T = 2\pi R n_1$, the total range of the y coordinate on the multiwound string, and $F(v)$ represents the shape of waves. If we choose one microstate, there is one corresponding function $F(v)$, which gives one geometry. If we choose another microstate, that gives another different geometry. It is shown that this geometry has no horizon and no singularity. These observations leads to the conjecture, one smooth geometry per microstate.

Translation to D1-D5 system is straightforward by duality.

3 non-BPS NS1-P geometry

The important problem is when and why this conjecture is valid. We extend the above analysis to the non-BPS case. We consider non-BPS P-NS1 system and choose three parameter solution[10] as an original non-BPS string. The action is Three-parameter solution for NS1-string is

$$ds^2 = e^{2A(r)}(-dt^2 + dy^2) + e^{2B(r)}(dr^2 + r^2 d\Omega^2) \tag{6}$$

where

$$A(r) = -\frac{3}{16}c_1 \ln(\frac{f_-}{f_+}) - \frac{3}{8}\ln[\cosh(kh(r)) - c_2 \sinh(kh(r))] \tag{7}$$

$$B(r) = \frac{1}{6}\ln(f_+f_-) + \frac{c_1}{16}\ln(\frac{f_-}{f_+}) + \frac{1}{8}\ln|\cosh(kh(r)) - c_2\sinh(kh(r))| \quad (8)$$

$$f_\pm = 1 \pm \frac{r_0^6}{r^6} \quad (9)$$

$$h(r) = \ln(\frac{f_-}{f_+}) \quad (10)$$

When there is a null, hypersurface orthogonal Killing vector, we can use a solution generating method that has established in [11],[12],[13]. Here we review shortly how the techniques work. Let us consider the action

$$S = \int d^Dx\sqrt{-g}\left[R - \frac{1}{2}(\partial\phi)^2 + \frac{1}{2(p+2)!}e^{c\phi}F^2_{(p+2)}\right] \quad (11)$$

and let $(g_{MN}, \phi, \mathcal{A}_{p+1})$ be a solution of the equations of motion which has a null, hypersurface orthogonal Killing vector k^M. Then there is a scalar Ψ such that

$$\nabla_M k_N = k_{[M}\nabla_{N]}\ln\Psi. \quad (12)$$

Let us define the new metric $\tilde{g}_{MN}$ by

$$\tilde{g}_{MN} \equiv g_{MN} + \Psi\Phi k_M k_N, \quad (13)$$

and let the scalar Φ satisfy

$$k^M\nabla_M\Phi = 0, \quad (14)$$

$$\nabla^M\nabla_M\Phi = 0. \quad (15)$$

We can show that the new solution $(\tilde{g}_{MN}, \phi, \mathcal{A}_{p+1})$ also satisfies the equations of motion (for the details, see [11],[12]).

Applying the above method to our case, we can easily find that

$$\Psi = e^{-2A}. \quad (16)$$

Φ is independent of u, and we assume that it can be written in the form of separation of variables,

$$\Phi = f(v)P(r)Y(\theta_i). \quad (17)$$

All we need is to solve

$$\nabla^M\nabla_M\Phi = 0. \quad (18)$$

Finally we get a new metric of the three-parameter solution with traveling waves as

$$d\tilde{s}^2 = ds^2 + C_1e^{2a}f(v)Y_l(\Omega)(C_2r^{-1}F(\frac{1}{2}, -\frac{l}{6}, \frac{1}{2}-\frac{l}{6}, (\frac{r}{r_0}^{12}))) + C_3r^{6+l}F(\frac{1}{2}, 1+\frac{l}{6}, \frac{3}{2}+\frac{l}{6}, (\frac{r}{r_0})^{12})dv^2 \quad (19)$$

where $f(v)$ is an arbitrary function which depend only on v and l is integer.

Analogous to the BPS case, we choose $l = 1$.

$$P(r) \propto r^7(r \sim 0), P(r) \propto r(r \sim \infty)$$

while in the BPS case

$$P(r) \propto r(r \sim 0). P(r) \propto r(r \sim \infty)$$

4 Summary and Discussion

We derived non-BPS waving string solution which will give some suggestions to fuzzball conjecture. There is still a problem to construct non-BPS multiwound P-NS1 geometry. In the BPS case, no-force condition guarantees the superposition. On the other hand, in the non-BPS case, this condition breaks down and multiwinding is non-trivial. We put this to future works.

References

[1] S. Kobayashi and S. Matsuura, to be appear [hep-th/060****]

[2] A. Strominger and C. Vafa, Phys.Lett. **B379**, 99 (1996).

[3] S. D. Mathur, Fortsch.Phys. **53**, 793 (2005) [hep-th/0502050]; S. D. Mathur, [hep-th/0510180].

[4] O. Lunin and S. D. Mathur, Nucl.Phys. **B610**, 49 (2001) ; O. Lunin and S. D. Mathur, Nucl.Phys. **B623**, 342 (2002).

[5] S. D. Mathur, A. Saxena, and Y. K. Srivastava, Nucl. Phys. **B 680**, 415 (2004) [hep-th/0311092]; S. Giusto, S. D. Mathur and A. Saxena, Nucl. Phys. **B 701**, 357 (2004) [arXiv:hep-th/0405017]; S. Giusto, S. D. Mathur and A. Saxena,[hep-th/0406103]; O. Lunin, JHEP **0404**, 054 (2004) [hep-th/0404006].

[6] J. P. Gauntlett, J. B. Gutowski, C. M. Hull, S. Pakis and H. S. Reall, Class. Quant. Grav. **20**, 4587 (2003) [hep-th/0209114]; J. B. Gutowski, D. Martelli and H. S. Reall, Class. Quant. Grav. **20**, 5049 (2003) [hep-th/0306235]; I. Bena and N. P. Warner, [hep-th/0408106]; J. P. Gauntlett and J. B. Gutowski, Phys. Rev. **D71**, 045002 (2005) [hep-th/0408122].

[7] I. Bena and P. Kraus Phys.Rev. **D72**, 025007 (2005) [hep-th/0503053].

[8] A. Saxena, G. Potvin, S. Giusto and A. W. Peet [hep-th/0509214].

[9] V. Jejjala, O. Madden, S. F. Ross and G. Titchener, Phys.Rev. 71, 124030 (2005)[hep-th/0504181].

[10] B. Zhou and C. J. Zhu, [hep-th/9905146].

[11] D. Garfinkle, Phys. Rev. **D46**, 4286 (1992)[gr-qc/9209002].

[12] D. Garfinkle and T. Vachaspati, Phys. Rev. **D42**, 1960 (1990).

[13] T. Vachaspati, Phys. Lett. **B238**, 41 (1990).

Geometrical Aspects of D-branes
— Boundary States and Gravity Solutions —

Shinpei Kobayashi[1], Shunji Matsuura[2], Tsuguhiko Asakawa[3] and So Matsuura[4]

[1] *Research Center for the Early Universe, The University of Tokyo, Tokyo 113-0033, Japan*
[2] *Department of Physics, The University of Tokyo, Tokyo, 113-0033, Japan*
[3] *Theoretical Physics Laboratory, The Institute of Physical and Chemical Research (RIKEN), Saitama 351-0198, Japan*

Abstract

We investigate the relation between the general solution with the symmetry $SO(p) \times SO(9-p)$ of Type II supergravity (the four-parameter solution) and the boundary states which hold the same symmetry. This solution has a horizon in some parameter regions, different from the $SO(1,p) \times SO(9-p)$-symmetric solution which had been investigated in our previous works [1, 2]. We studied when the solution has a horizon and what kind of the boundary states can reproduce the asymptotic behavior of the solution, which might be useful to interpret the horizons of black holes in the general relativity in terms of the string theory.

1 Introduction

A general classical solution of Type II supergravity with the symmetry $ISO(1,p) \times SO(9-p)$ called as the "three-parameter solution"[3] is thought to be the low energy counterpart of the D$p\bar{\text{D}}p$-brane system with a constant tachyon profile (vacuum expectation value) and this relation has been examined in [1, 2, 4, 5]. This is a rare example of the relation between the non-BPS D-brane systems and the supergravity solution. But this is not enough to interpret the relation between black holes in the general relativity and the stringy objects because the three-parameter solution almost becomes a naked singularity.

On the other hand, it is also known that there exists the $SO(p) \times SO(9-p)$-symmetric supergravity solution called as the "four-parameter solution" It has a horizon in some cases, so it is more similar to the black objects in the general relativity than the three-parameter solution. The four-parameter solution is usually non-extremal, so it can be expected to correspond to non-BPS D-branes.

Here we investigated the relation between the four-parameter solution and non-BPS D-branes. In order to do so, we compared the asymptotic behavior of the supergravity solution and the massless emissions from the deformed boundary state because the non-BPS D-branes can be described by the deformed boundary states as we did in [1, 2]. We also argued the condition for the solution to have a horizon and determined the corresponding deformed boundary states. However, we have not found what kinds of stringy objects can reproduce such boundary states, so we can say that this is a preliminary result.

2 The Four-Parameter Solution

We consider Type II supergravity in the following setting: (1)Assume a fixed, $(p+1)$-dimensional object as a source carrying only RR $(p+1)$-form charge. (2)Spacetime can generally have the symmetry $SO(p) \times SO(9-p)$ and it is asymptotically flat. Note that these ansätze are the same as those for the general black p-brane solution (we will consider the region $0 \leq p \leq 6$ here). Under these conditions, it is sufficient to

[1] E-mail:shinpei@resceu.s.u-tokyo.ac.jp
[2] E-mail:smatsuura@utap.phys.s.u-tokyo.ac.jp
[3] E-mail:t.asakawa@riken.jp
[4] E-mail:matsuso@riken.jp

consider the metric, the dilaton and the RR $(p+1)$-form field. The relevant part of the ten-dimensional action (in the Einstein frame) is given by

$$S = \frac{1}{2\kappa^2}\int d^{10}x\sqrt{-g}\left[R - \frac{1}{2}(\partial\phi)^2 - \frac{1}{2(p+2)!}e^{\frac{3-p}{2}\phi}|F_{p+2}|^2\right], \tag{1}$$

where $F_{(p+2)}$ denotes the $(p+2)$-form field strength which is related to the $(p+1)$-form potential of the RR-field $A^{(p+1)}$ as $F_{(p+2)} = dA_{(p+1)}$. According to the symmetry $SO(p)\times SO(9-p)$, we should impose the following ansatz,

$$\begin{aligned} ds^2 &= e^{2A(r)}\left(-f(r)dt^2 + \delta_{ab}dx^a dx^b\right) + e^{2B(r)}\delta_{ij}dx^i dx^j \\ &= e^{2A(r)}\left(-f(r)dt^2 + \delta_{ab}dx^a dx^b\right) + e^{2B(r)}(dr^2 + r^2 d\Omega^2_{(8-p)}), \\ \phi &= \phi(r), \qquad A^{(p+1)} = e^{A(r)}\, dx^0\wedge dx^1\wedge\cdots\wedge dx^p, \end{aligned} \tag{2}$$

where $a,b = 1,\cdots,p$ are indices of the longitudinal directions of the p-brane, $i,j = p+1,\cdots,9$ express the orthogonal directions, and $r^2 = x^i x_i$.

The authors of [3] gave a general solution of Type II supergravity of this system. As the solution includes four integration constants, it is called as the four-parameter solution, which is given by

$$A(r) = \frac{7-p}{32}\left[\frac{3-p}{2}c_1 + \left(1+\frac{(3-p)^2}{8(7-p)}\right)c_3\right]h(r) - \frac{7-p}{16}\ln\left[\cosh(kh(r)) - c_2\sinh(kh(r))\right], \tag{3}$$

$$B(r) = \frac{1}{7-p}\ln[f_-(r)f_+(r)] - \frac{3-p}{64}\left[(p+1)c_1 - \frac{3-p}{4}c_3\right]h(r) + \frac{p+1}{16}\ln\left[\cosh(kh(r)) - c_2\sinh(kh(r))\right], \tag{4}$$

$$\phi(r) = \frac{7-p}{16}\left[(p+1)c_1 - \frac{3-p}{4}c_3\right]h(r) + \frac{3-p}{4}\ln\left[\cosh(kh(r)) - c_2\sinh(kh(r))\right], \tag{5}$$

$$e^{A(r)} = -\eta(c_2^2-1)^{1/2}\,\frac{\sinh(kh(r))}{\cosh(kh(r)) - c_2\sinh(kh(r))},\quad f(r) = \left(\frac{f_-}{f_+}\right)^{-c_3}, \tag{6}$$

where

$$f_\pm(r) \equiv 1 \pm \frac{r_0^{7-p}}{r^{7-p}},\quad h(r) \equiv \ln\left(\frac{f_-}{f_+}\right),\quad \eta \equiv \pm 1,\quad k^2 \equiv \frac{2(8-p)}{7-p} - c_1^2 + \left(\frac{3-p}{4}c_1 + \frac{7-p}{16}c_3^2\right)^2 - \frac{7}{16}c_3^2, \tag{7}$$

where η denotes the sign of the RR-charge. The four parameters, r_0, c_1, c_2, c_3, are the integration constants that parametrize the solution.

We give the long distance behavior of the four-parameter solution (3)-(6), which is given by the leading term of $1/r$ expansion.

$$\begin{aligned} g_{tt}(r) &= -1 + \frac{7-p}{8}\left\{\sqrt{1+\nu^2} + \frac{3-p}{4}d + \frac{1}{2}\left[1 + \frac{(3-p)^2}{8(7-p)} - \frac{8}{7-p}\right]\lambda\right\}\frac{\mu_0}{r^{7-p}} + \mathcal{O}\left(1/r^{2(7-p)}\right), \\ g_{ab}(r) &= 1 - \frac{7-p}{8}\left\{\sqrt{1+\nu^2} + \frac{3-p}{4}d + \frac{1}{2}\left[1 + \frac{(3-p)^2}{8(7-p)}\right]\lambda\right\}\frac{\mu_0}{r^{7-p}}\delta_{ab} + \mathcal{O}\left(1/r^{2(7-p)}\right), \\ g_{ij} &= 1 + \left\{\sqrt{1+\nu^2} + \frac{3-p}{4}d - \frac{(3-p)^2}{16(p+1)}\lambda\right\}\frac{\mu_0}{r^{7-p}}\delta_{ij} + \mathcal{O}\left(1/r^{2(7-p)}\right), \\ \phi(r) &= \left\{\sqrt{1+\nu^2} - \frac{(7-p)(p+1)}{4(3-p)}d + \frac{7-p}{16}\lambda\right\}\frac{\mu_0}{r^{7-p}} + \mathcal{O}\left(1/r^{2(7-p)}\right),\quad e^{A(r)} = \eta\frac{\mu_0}{r^{7-p}} + \mathcal{O}\left(1/r^{2(7-p)}\right). \end{aligned} \tag{8}$$

Here, for the later convenience, we introduce new parameters (μ_0, ν, d, λ) which are defined as

$$\mu_0 \equiv 2(c_2^2-1)^{1/2}kN_p r_0^{7-p},\quad \nu \equiv (c_2^2-1)^{-1/2},\quad d \equiv c_1\nu/k,\quad \lambda \equiv c_3\nu/k, \tag{9}$$

where $N_p = (8-p)(7-p)\omega_{8-p}V_p/16\kappa^2$. We will compare them with the massless emission from the source in the string theory in the next section. Furthermore, it is known that the four-parameter solution has a horizon if $(c_1, c_3) = ((3-p)/(14-2p), -2)$ (for $p = 1\sim 6$) and if c_1 and c_3 satisfy the condition $c_1 = \frac{3}{4}c_3 + \frac{12}{7}$ (for $p = 0$).

3 Non-BPS Boundary States

It is well known that the extremal black p-brane solutions are the low-energy counterpart of the BPS Dp-branes. This relation was checked by comparing the long distance behavior of the extremal black p-brane solutions with the massless emissions (e.g. graviton, dilaton, $\cdots$) from the BPS Dp-branes. So it is natural that there are also low-energy counterparts of the non-BPS Dp-branes and it had been expected that the three-parameter solution and the four-parameter solution are such objects. The relation between the three-parameter solution and the non-BPS D-branes was investigated in [1, 2, 4, 5]. In particular, in [1, 2], we used the boundary states for the non-BPS D-branes and directly compared the asymptotic behavior of the three-parameter solution and the massless emissions from the boundary states. Here we use this method again.

N BPS Dp-branes are expressed by the ordinary boundary state,

$$|\, Dp\rangle = \mathcal{P}_{\rm GSO}\Big(N\,|\, Bp\rangle_{\rm NS} + N\,|\, Bp\rangle_{\rm RR}\Big), \tag{10}$$

with

$$|\, Bp\rangle_{\rm NS(RR)} = \frac{T_p}{2}\exp\left[-\sum_{n=1}^{\infty}\frac{1}{n}\alpha_{-n}^{M}S_{MN}\tilde{\alpha}_{-n}^{N} + i\sum_{r>0}^{\infty}b_{-r}^{M}S_{MN}\tilde{b}_{-r}^{N}\right]|\, p_\mu = 0, x^i = 0\rangle_{\rm NS(RR)}, \tag{11}$$

where T_p is the tension for a single Dp-brane, $\mu = 0, 1, \cdots, p$ are the directions longitudinal to the worldvolume, $i = p+1, \cdots, 9$ are the directions transverse to the Dp-branes, and α_{-n}^{M} and b_{-r}^{M} ($\tilde{\alpha}_{-n}^{M}$ and $\tilde{b}_{-r}^{M}$) are the creation operators of the modes of the left-moving (right-moving) worldsheet bosons and fermions, respectively. $S_{MN} = \mathrm{diag}\,(\eta_{\mu\nu}, -\delta_{ij})$ gives Neumann (Dirichlet) boundary conditions on the string worldsheet in $\mu(i)$ directions, respectively.

Non-BPS D-branes can be described by the boundary states with boundary interactions as

$$|\, B'p\rangle = e^{-S_{\rm int}}\,|\, Bp\rangle\,. \tag{12}$$

Such a non-BPS boundary state is rewritten as a deformed boundary state as

$$|\, B'_p\rangle_{NS} = CN\frac{T_p}{2}\exp\left[-\sum_{n=1}^{\infty}\frac{1}{n}\alpha_{-n}^{M}S_{MN}^{(n)}\tilde{\alpha}_{-n}^{N} + i\sum_{r>0}b_{-r}^{M}S_{MN}^{(r)}b_{-r}^{N}\right]|\, p_\mu = 0, x^i = 0\rangle_{NS}, \tag{13}$$

where

$$S_{MN}^{(1/2)} = \mathrm{diag}\,(-A_{tt}, A\delta_{ab}, -B\delta_{ij})\,. \tag{14}$$

Here $A^{(n,r)}$, $B^{(n,r)}$ and C are deformation parameters which deform the boundary state without changing its symmetry. When we take $A^{(n,r)} = B^{(n,r)} = C = 1$, the boundary state (11) for the N BPS Dp-branes is reproduced. We also deform the RR-sector of the boundary state (11) as the same manner but $C = 1$ in this case since we fix the RR-charge to be the same as the N Dp-branes. We here note that only the $r = 1/2$ mode contributes the massless mode of closed strings emitted from the boundary state. In other words, the deformations for other modes, $S_{MN}^{(n)}$ and $S_{MN}^{(r\neq 1/2)}$, are arbitrary in our analysis below. However, they should be related among them by other consistency, such as the modular invariance although we do not discuss them at this stage. Third, C denotes the difference of the overall normalization in the NSNS-sector from that in the RR-sector. For example, in the system of $(N + M)$ Dp-branes and M $\bar{\rm D}p$-branes, we take $CN = N + 2M$, the total number of branes, while the RR-sector has a fixed charge proportional to N.

Then, we can calculate the massless emissions with momentum p_M from this deformed state as we

have done in [1, 2]. After the Fourier transformation to the position space, we obtain

$$h_{tt}(r) = -\frac{T_p CN}{2}\frac{2\kappa}{(7-p)\omega_{8-p}r^{7-p}}\frac{1}{8}\left[-7A_{tt}+pA-(7-p)B\right],$$
$$h_{ab}(r) = \frac{T_p CN}{2}\frac{2\kappa}{(7-p)\omega_{8-p}r^{7-p}}\frac{1}{8}\left[-A_{tt}+(8-p)A+(7-p)B\right]\delta_{ab},$$
$$h_{ij}(r) = \frac{T_p CN}{2}\frac{2\kappa}{(7-p)\omega_{8-p}r^{7-p}}\frac{1}{8}\left[-A_{tt}-pA-(p+1)B\right]\delta_{ij},$$
$$\phi(r) = \frac{T_p CN}{2}\frac{2\kappa}{(7-p)\omega_{8-p}r^{7-p}}\frac{1}{4}\left[-A_{tt}+pA-(7-p)B\right],\ e^{\Lambda}(r) = \pm\frac{2\kappa NT_p}{(7-p)\omega_{8-p}}\frac{1}{r^{7-p}}, \qquad (15)$$

where we write $A = A^{(1/2)}$ and $B = B^{(1/2)}$. Comparing these quantities (15) with the long distance behaviors (8), we obtain the relation between the macroscopic quantities and the microscopic ones as

$$\mu_0 = \frac{2\kappa NT_p}{(7-p)\omega_{8-p}},\ \sqrt{1+\nu^2} = \frac{C}{8}\left[A_{tt}+pA+(7-p)B\right],\ d = \frac{C}{8}(A_{tt}+3A-4B),\ \lambda = -\frac{C}{2}(A_{tt}-A). \quad (16)$$

From the conditions which the four-parameter solution has a horizon, we identified a boundary state which can reproduce the asymptotic behavior of the four-parameter solution which has a horizon, but we have not interpreted the physical or stringy meaning of it yet.

4 Summary and Future Works

We discussed the stringy origin of the general solution of Type II supergravity with the symmetry $SO(p)\times SO(9-p)$, which is called as the four-parameter solution. It has a horizon in some cases, so it is more similar to "realistic" black holes than the three-parameter solution which becomes a naked singularity in most cases. We introduce the deformed boundary states and compared the asymptotic behavior of the four-parameter solution with the massless emissions from the boundary states. As a result, we found the deformed boundary states which can reproduce the asymptotic behavior of the four-parameter solution with a horizon. However we have not determined what kinds of stringy objects correspond to such boundary states. So it will be our next step.

References

[1] S. Kobayashi, T. Asakawa and S. Matsuura, "Open String Tachyon in Supergravity Solution," Mod. Phys. Lett. **A15** (2005) 1119 [arXiv:hep-th/0409044].

[2] T. Asakawa, S. Kobayashi and S. Matsuura, "Excited D-branes and Supergravity Solutions", to appear in Int. J. Mod. Phys. A. [arXiv:hep-th/0506221].

[3] B. Zhou and C-J. Zhu, "The complete black brane solutions in D-dimensional coupled gravity system," [arXiv:hep-th/9905146].

[4] P. Brax, G. Mandal and Y. Oz, "Supergravity description of non-BPS branes," Phys. Rev. D **63** (2001) 064008 [arXiv:hep-th/0005242].

[5] J. X. Lu and S. Roy, "Supergravity approach to tachyon condensation on the brane-antibrane system," [arXiv:hep-th/0403147].

[6] K. Ohta and T. Yokono, "Gravitational approach to tachyon matter," Phys. Rev. D **66** (2002) 125009 [arXiv:hep-th/0207004].

Generalized variational principle for stellar dynamics and quasi-equilibrium states in N-body system

Atushi Taruya[1], Masa-aki Sakagami[2], Takashi Okamura[3]

[1] *Research Center for the Early Universe, School of Science, University of Tokyo, Tokyo 113-0033, Japan*
[2] *Graduate School of Human and Environmental Studies, Kyoto University, Kyoto 606-8501, Japan*
[3] *Department of Physics, Kwansei Gakuin University, Sanda, 669-1337, Japan*

Abstract

We present our recent progress on the characterization of self-gravitating N-body system away from the thermal equilibrium. We show that the transient state of out-of-equilibrium system can be approximately described by the stellar polytropic distribution with time-varying polytrope index. The time-scale of quasi-equilibrium states can be analytically estimated by means of the generalized variational method, which reproduces the N-body result quite well.

1 Introduction

Due to the long-range attractivity of the Newton gravity, the long-term evolution of stellar self-gravitating system driven by the two-body encounter shows various peculiar behaviors. In particular, one of the most important consequences is the thermodynamic instability so-called *gravothermal catastrophe*, which has been discovered by Antonov [1] and later investigated by Lynden-Bell and Wood [2]. The presence of thermodynamic instability implies that no stable thermal equilibrium exists for highly dense clusters. Therefore, the stellar self-gravitating system is essentially a non-equilibrium system and thereby the description of out-of-equilibrium state is a central issue in the subject of stellar dynamics. Here, we present a recent progress on the characterization of non-equilibrium states of stellar self-gravitating system.

2 Antonov problem

To discuss the out-of-equilibrium states, we consider the same situation as investigated in classic papers [1, 2], the so-called Antonov problem (see Fig.1). That is, we treat a self-gravitating N-body system confined by the adiabatic wall of a sphere, where the adiabatic wall represents a perfectly reflecting boundary which preserves the total energy of the system. In this setup, Antonov and Lynden-Bell and Wood originally considered the stability of the thermal equilibrium (isothermal state) characterized by the Boltzmann-Gibbs entropy. Since we are especially concerned with the characterization of the evolutionary sequences away from the thermal equilibrium, standard thermostatistical treatment becomes inadequate. Hence, we take the following three approaches: (i) thermostatistical approach by means of the non-extensive entropy [3]; (ii) dynamical approach based on the N-body simulation [4, 5]; (iii) kinetic-theory approach using the Fokker-Planck model for stellar dynamics [6]. In what follows, we mainly focus on the treatment of (ii) and (iii) and present recent results.

3 N-body simulations

Let us first describe the dynamical approach based on N-body simulations. Without loss of generality, we set the units to $G = M = r_e = 1$. All the particles are assumed to have the same mass $m = 1/N$, where N is the total number of the particles. The initial conditions for particle data were whole created

[1] E-mail:ataruya.(at).utap.phys.s.u-tokyo.ac.jp
[2] E-mail:sakagami.(at).phys.h.kyoto-u.ac.jp
[3] E-mail:okamura.(at).ksc.kwansei.ac.jp

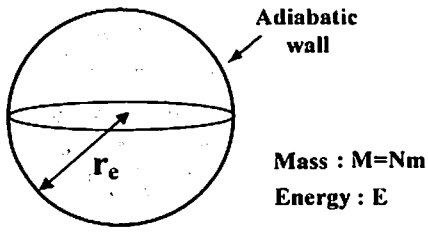

Figure 1: Setup of the Antonov problem.

by a random realization of the stellar models. We deal with the two kinds of the initial stellar models: (a) stellar polytropes, whose distribution functions are characterized by the power-law function, i.e., $f(\varepsilon) = A(\varepsilon_0 - \varepsilon)^{n-3/2}$ with $\varepsilon = v^2/2 + \phi(r)$ and n being polytrope index; (b) the stellar models with cusped density profile, which cannot be described by the power-law distribution. We are specifically concerned with collisional aspects of N-body dynamics, the timescale of which is much longer than the two-body relaxation time. For this purpose, we utilized a special-purpose hardware, GRAPE-6, which is especially designed to accelerate the gravitational force calculations for collisional N-body system. The details of the numerical simulations are described in Ref.[5] (see also Ref.[4]).

The overview of the simulation results is as follows. For the initial conditions (a), the stellar polytropic distribution gradually changes with time on time-scales of two-body relaxation. Focusing on the evolutionary sequence, we found that the transient state starting from the initial stellar polytrope can be remarkably characterized by a sequence of stellar polytropes with time-varying polytrope index n. Interestingly, this is even true for a certain class of the initial conditions (b). That is, even starting from the non-power-law initial distribution, the system soon settles into a stellar polytropic state and follows the equilibrium sequence of stellar polytropes for a long time.

Fig.2 shows the representative result taken from the N-body simulation (run $n3A$, see Table 1 of Ref.[5]). We plot the snapshots of one-particle distribution function $f(\varepsilon)$ starting from the initial conditions (a). To be precise, the initial distribution was chosen as stellar polytropic distribution with index $n = 3$ and the density contrast defined by $D \equiv \rho_{\rm core}/\rho_{\rm edge}$ was set to $D = 10^4$. In this plot, just for illustrative purpose, each output result is artificially shifted to the two-digits below. Only the final output with $t = 30t_{\rm rh,i}$ represents the correct scales. Here, the quantity $t_{\rm rh,i}$ denotes initial half-mass relaxation time [see Eq.(27) of [5]]. Solid lines represents the initial stellar polytrope with $n = 3$ and the other lines indicate the fitting results to the stellar polytrope by varying the polytrope index n.

Clearly, the stellar polytropes quantitatively characterize the evolutionary sequence of the simulation results. The fitting results are remarkably good until $t \simeq 30t_{\rm rh,i}$. Afterwards, the system enters the gravothermally unstable regime and finally undergoes the core-collapse. A closer look at the low-energy part of the distribution function $f(\varepsilon)$ reveals that the simulation results partly resemble the exponential form rather than the power-law function. Nevertheless, it is remarkable that the stellar polytropes as simple power-law distribution globally approximate the simulation results in a quite good accuracy. In Fig.3, the polytrope indices are estimated at each time step and the resultant values are plotted together with the fitting results of $N = 4K$ and $N = 8K$. Apart from the fluctuations, the fitted values of the polytrope index monotonically increase and the growth rates of n normalized by half-mass relaxation time almost coincide with each other, consistent with the fact that the quasi-equilibrium sequence is evolved via two-body relaxation.

4 Characterizing the time-scale of quasi-equilibrium state

The N-body simulations imply that quasi-equilibrium behavior approximately described by the stellar polytropes with time-varying index n may be a unique character of the out-of-equilibrium states in self-gravitating N-body system. We then wish to understand the time-scale of quasi-equilibrium states in an analytical manner. For this purpose, we next focus on the kinetic-theory approach and treat the Fokker-Planck (F-P) model for stellar dynamics

F-P model describes the energy diffusion process driven by the two-body relaxation in phase space. The main assumption in the F-P model is that the orbit of each particle in spherical stellar system is

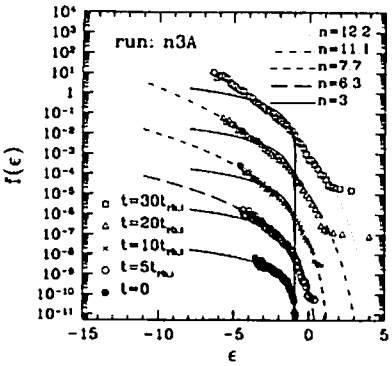

Figure 2: Snapshots of one-particle distribution function as function of specific energy of particle, $\varepsilon = v^2/2+\phi(r)$, taken from the N-body simulation with number of particle $N = 2,048$ (run $n3A$).

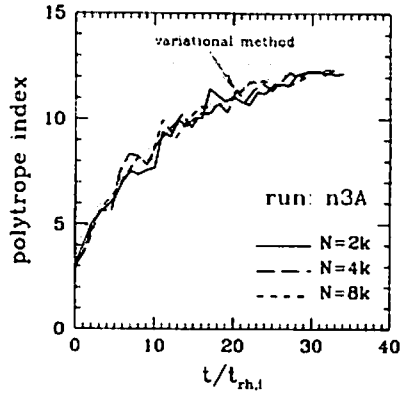

Figure 3: Time evolution of the polytrope index fitted to N-body simulations in the case of run $n3A$: $N = 2,048$ (*solid*); $N = 4,096$ (*long-dashed*); $N = 8,192$ (*short-dashed*).

dominantly affected by the weak encounter. Assuming the isotropy of velocity distribution, the (orbit-averaged) F-P equation can be written as [7]

$$\left(\frac{\partial f}{\partial t}\right)_q = \left(\frac{\partial \Pi}{\partial q}\right)_t \quad : \quad \Pi(q,t) = \Gamma \int f f' \min(q,q') \left(\frac{\partial \ln f}{\partial \varepsilon} - \frac{\partial \ln f'}{\partial \varepsilon'}\right) d\varepsilon' \tag{1}$$

with $\Gamma = (4\pi G m)^2 \ln\Lambda$. Here, q is the volume of phase space where the energy is less than ε, i.e., $q(\varepsilon) = (16\pi^2/3)\int [2\{\varepsilon - \phi(r)\}]^{3/2}\, r^2\, dr$. The function Π represents the flux of stars crossing into the volume q in phase space. Eq.(1) must be solved with Poisson equation self-consistently.

It is important to notice that despite the fact that F-P equation is not self-adjoint, there exists a generalized variational principle to obtain an approximate solution. It is an extension of the classical variational principle to the non-self-adjoint problems and is based on the concept of a *local potential* [8]. Inagaki and Lynden-Bell [7] showed that local potential of F-P equation (1) is given by

$$\Phi(f, f_0) = \int dq \left(\frac{\partial f_0}{\partial t}\right)_q \ln f + \frac{\Gamma}{4} \int\int f_0 f_0 \min(q,q') \left(\frac{\partial \ln f}{\partial \varepsilon} - \frac{\partial \ln f'}{\partial \varepsilon'}\right) d\varepsilon\, d\varepsilon'. \tag{2}$$

Note that the local potential (2) has the following properties: (i) the condition that Φ is minimum with respect to f for fixed f_0, and the subsidiary condition $f = f_0$ lead to the original differential equation; (ii) Φ is absolutely minimum at a solution f_0, i.e., $\Delta\Phi = \Phi(f, f_0) - \Phi(f_0, f_0) > 0$.

Using the local potential, Takahashi and Inagaki [9] have tried to obtain the self-similar solution of F-P equation. Later, Takahashi [10] utilized it to obtain an accurate numerical solution of F-P equation. Here, the generalized variational method is applied to derive the time evolution of polytrope index $n(t)$. To do this, we adopt the polytropic form of the distribution function $f(\varepsilon,t) = A(t)\{\varepsilon_0(t) - \varepsilon\}^{n(t)-3/2}$ as the trial function for f. Substituting this trial function into Eq.(2), we consider the variation of Φ with respect to n with f_0 being held fixed. Note that this variation should be done under keeping the energy and the mass fixed. After that, we set f equal to f_0. The resultant equation to be solved is

$$\left.\frac{\partial \Phi}{\partial n}\right|_{f=f_0} = 0. \quad \Longrightarrow \quad \dot{n}(t) = \mathcal{F}[n(t);\, E,\, M,\, r_e]. \tag{3}$$

The explicit form of the function $\mathcal{F}$ is slightly complicated and includes some integrals (see [6]). Nevertheless, Eq.(3) is nothing but the ordinary differential equation and it can be easily solved by using mathematical software.

As an illustration, the evolution equation for polytrope index n is numerically solved with the same initial condition as in the N-body run $n3A$ (Fig.2) and the result is plotted in Fig. 3 (*dotted* line indicated by arrow). In Fig. 4, we also show another example, whose initial distributions are stellar polytropes

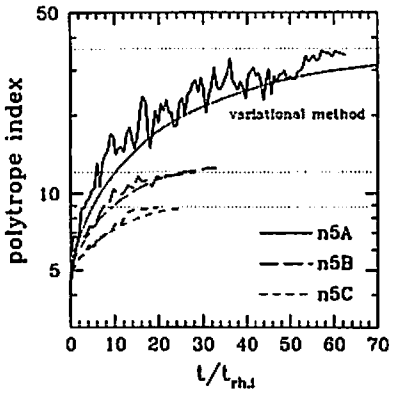

Figure 4: Time evolution of the polytrope index fitted to the N-body simulations labeled as $n5A$(*solid*), $n5B$(*long-dashed*) and $n5C$(*short-dashed*). These N-body results are taken from Ref.[5]. The continuous (blue) lines are the semi-analytic results based on the generalized variational method.

with index $n = 5$ and with various density contrasts, $D = 10^4(n5A)$, $D = 10^3(n5B)$ and $D = 10^2(n5C)$. The time evolution obtained from the variational method successfully reproduces the simulation results quite well until the system enters the gravothermally unstable regime, which is indicated by the marginal stability boundary depicted as the vertical dotted lines. The one remarkable point is that the evolution equation (3) consistently explains the monotonic growth of n. Further, the functional form of Eq.(3) indicates the presence of the slow-down phase before entering the unstable regime, which is clearly seen in Fig. 3. We note that this slow-down phase is intimately related to the marginal stability boundary of the quasi-equilibrium state, characterized by the non-extensive thermostatistics [3]. This may give an interesting suggestion for the physical reality of non-extensive thermostatistics.

5 Summary

We have presented a recent progress on the characterization of self-gravitating N-body system. Particularly focusing on the long-term evolution, we have numerically studied the quasi-equilibrium properties of the N-body systems in the setup of Antonov problem. We have tried to characterize the time-scale of quasi-equilibrium sequences by utilizing the generalized variational principle of F-P equation. Although the present paper did not address the thermostatistical approach by means of the non-extensive entropy, the analysis based on F-P model suggests a possible relationship between the kinetic-theory approach and the thermostatistical approach for the description of the stability boundary of the quasi-equilibrium states. This point will be discussed in details in future publication [6].

References

[1] Antonov V A 1962 *Vest. Leningrad Gros. Univ.* **7** 135

[2] Lynden-Bell D, Wood R 1968 *Mon.Not.R.Astron.Soc.* **138** 495

[3] Taruya A, Sakagami M 2002 *Physica A* **307** 185; 2003 *Physica A* **318** 387; 2003 *Physica A* **322** 285

[4] Taruya A, Sakagami M 2005 *Phys.Rev.Lett.* **90** 181101

[5] Taruya A, Sakagami M 2005 *Mon.Not.R.Astron.Soc.* **364** 990

[6] Taruya A, Sakagami M, Okamura T 2005 in preparation

[7] Inagaki S, Lynden-Bell D 1990 *Mon.Not.R.Astron.Soc.* **244** 254

[8] Glansdorff P, Prigogine I 1971 *Thermodynamic Theory of Structure, Stability and Fluctuations* (London, Wiley-Interscience) Chap.X

[9] Takahashi K, Inagaki S 1992 *Publ.Astron.Soc.Japan* **44** 623

[10] Takahashi K, 1993 *Publ.Astron.Soc.Japan* **45** 233

Analytical study of axi-symmetric shell collapses

Masafumi Seriu[1]

Department of Physics, Faculty of Engineering,
University of Fukui, Bunkyo 3-9-1, Fukui 910-8507, Japan

Abstract

We give detailed analytical investigations on the gravitational dynamics of an axi-symmetric shell model. It is a natural generalization of the cylindrical shell model investigated by the author previously. It turns out that even the slightest z-dependence of the shell-configuration induces a drastic effect on the gravitational dynamics: It is proved that, contrary to the cylindrical case, there always exist the initial conditions which cause the shell collapse, $\rho \longrightarrow 0$ (ρ: the shell-radius). This result, indicating that the final fate of the gravitational contraction is very sensitive to the initial matter configuration as far as the present model is concerned, is of importance in view of the hoop conjecture.

1 Introduction

Analytical study of gravitational collapses is quite different from numerical approaches. At a price of simplification, detailed investigations on, for instance, the relation between initial conditions and the final state of contraction become possible.

In this connection, there is a class of problems related to the hoop conjecture [1], stating that *"black holes are formed when and only when the matter of mass M is contained in a compact region whose circumference C in any direction always satisfies $C \leq 2\pi \cdot \frac{2GM}{c^2}$"*. Roughly speaking, the conjecture claims that compact object is prone to show gravitational collapse, while elongated object is not, suggesting that the final fate seems sensitive to initial matter configuration.

Among analytical models, spherical models and cylindrical models are quite well-investigated. Here we consider the third class, namely an axi-symmetric model which may be placed between these two classes of models, spherical ones and cylindrical ones.

Some spherical models, modeling compact matter configuration, are known to show gravitational collapses [2, 3, 4, 5, 6]. On the other hand, cylindrical models, modeling extremely elongated matter configuration, generally show bouncing back behavior, due to angular momentum effect. For instance, cylindrical thin-shell models investigated so far all show bouncing back behavior [7, 8].

It is of great interest, thus, to study what happens to an axi-symmetric shell model, as a bridge between these two extreme cases: Here ρ, the shell-radius, becomes dependent on z as well as t, $\rho = \rho(t, z)$. Then $\rho_z := \partial\rho/\partial z$ plays the role of a configuration parameter, and when it is large, the model may behave similar to the spherical case, and when it is small, it tends to the cylindrical case, and the intermediate value of ρ_z describes, for instance, spindle-like configuration.

2 The model

The axi-symmetric shell model is a natural generalization of cylindrical shell model [9, 8], which never collapses but bounces back due to rotational pressure effect [8]. The flat inner-spacetime described by

$$ds_-^2 = -dt_-{}^2 + dr_-{}^2 + dz_-{}^2 + r_-{}^2 d\phi_-{}^2 \tag{1}$$

is matched together with the outer axi-symmetric spacetime,

$$ds_+^2 = e^{2\gamma}(-dt_+{}^2 + dr_+{}^2) + dz_+{}^2 + r_+{}^2 d\phi_+{}^2 \ , \tag{2}$$

[1] E-mail:mseriu@edu00.f-edu.fukui-u.ac.jp

which is characterized by a single function γ of $t-r$ and z,

$$\gamma = \gamma(t-r, z) \ .$$

Two spacetimes are matched on the *timelike* 3-surface described by $r = \rho(t, z)$.

The metric function γ should satisfy the "reasonable matter condition", i.e.

$$\gamma > 0 \ , \ \ \gamma' > 0 \ , \tag{3}$$

the former of which guarantees that the energy density of the shell is positive, while the latter comes from the weak energy condition. These conditions are very crucial for getting the final result.

Now the standard junction conditions [10] are imposed across the matching surface. The discrepancy of the extrinsic curvatures across the shell, $\kappa S_{\alpha\beta} := -([K_{\alpha\beta}] - h_{\alpha\beta}[K])$ plays the central role in this analysis. Compared to the cylindrical case [8], the formula for the extrinsic curvatures become very complicated in the axi-symmetric case [11].

Following the previous analysis for the cylindrical case [8, 9], we set $S_{e_z e_z}$, interpreted as the shell pressure in the z-direction (p_z), to be a constant P_0,

$$S_{e_z e_z} = -\frac{1}{\kappa}\left([K_{e_\tau e_\tau}] - [K_{e_\phi e_\phi}]\right) =: p_z = P_0 \ (\text{const}) \ .$$

Then we get an equation of motion for the shell-radius $\rho(t, z)$:

$$\ddot{\rho} = \frac{\xi\Delta - 1}{\Delta - \xi} \cdot \Delta \frac{1-\dot{\rho}^2}{\rho} + \gamma' \frac{\dot{\rho}}{\Delta - \xi}(1-\dot{\rho})[(\Delta - \xi\dot{\rho})\dot{\rho} + \xi] + \frac{\Delta}{\Delta - \xi}(1-\dot{\rho}^2)(1 - \dot{\rho}^2 + e^{2\gamma}\rho_z^2)^{1/2} e^{\gamma} P_0 \ , \tag{4}$$

where

$$\xi := \left(1 - \frac{(e^{2\gamma}-1)(1+e^{-2\gamma}\dot{\rho}^2)}{1-\dot{\rho}^2+e^{2\gamma}\rho_z^2}\rho_z^2\right)^{-1/2}$$

is the **"shell-deformation" function** ($\xi \longrightarrow 1$ as $\rho_z \longrightarrow 0$), and $\Delta := \frac{dt_-}{dt_+} = \left\{e^{2\gamma} - (e^{2\gamma}-1)\dot{\rho}_+^2\right\}^{1/2}$.

Comparing Eq.(4) with the corresponding dynamical equation for the cylindrical case;

$$\ddot{\rho} = \Delta \frac{1-\dot{\rho}^2}{\rho} + \gamma' \frac{\dot{\rho}}{\Delta - 1}(1-\dot{\rho})[(\Delta - \dot{\rho})\dot{\rho} + 1] \ + \frac{\Delta}{\Delta - 1}(1-\dot{\rho}^2)(1 - \dot{\rho}^2 + e^{2\gamma}\rho_z^2)^{1/2} e^{\gamma} P_0 \ , \tag{5}$$

we find that *the sign of the factor $\Delta - \xi$ (compared with $\Delta - 1 > 0$) plays the key role* in the shell-dynamics.

Note that $\Delta \longrightarrow 1$ as $|\dot{\rho}| \longrightarrow 1$ and that $\xi \longrightarrow e^{2\gamma}$ as $|\dot{\rho}| \longrightarrow 1$ with $\rho_z \neq 0$.

Thus $\Delta - \xi$ tends to a negative value, $-(e^{2\gamma}-1)$ as $|\dot{\rho}| \longrightarrow 1$ *as far as ρ_z is non-zero and finite.* We expect in advance that, if $\rho_z \neq 0$ ($\Longleftrightarrow$ the *deformation function* $\xi > 1$), the dynamics would be qualitatively different from the cylindrical case. We also note that this behavior indicates some sort of *universality* in the collapsing phase in the sense that, irrespective of the detailed initial conditions, in particular, irrespective of the detailed z-dependence of ρ, the dynamical behavior in the final phase is universally the same as far as ρ_z is non-zero and finite.

Now let us recall the cylindrical case [8]. Let $[[1]]_{cyl}$, $[[2]]_{cyl}$ and $[[3]]_{cyl}$ be the three terms on the R.H.S. (right-hand side) of Eq.(5) (in order of appearance). Then Eq.(5) is written as

$$\ddot{\rho} = [[1]]_{cyl} + [[2]]_{cyl} + [[3]]_{cyl} \ .$$

The term $[[1]]_{cyl} \sim$ *centrifugal force* and always **repulsive** (> 0), while the term $[[2]]_{cyl} \sim$ *Newtonian gravity* when $|\dot{\rho}| \ll 1$, turns to repulsive when $|\dot{\rho}| \to 1$. (It turns out that the term $[[3]]_{cyl}$ is not important in the dynamics.) Thus $\ddot{\rho}$ becomes positive when $|\dot{\rho}| \to 1$, resulting in the bouncing behavior with no singularity formation.

The dynamics of the present axi-symmetric case, on the other hand, is qualitatively different. Let $[[1]]$, $[[2]]$ and $[[3]]$ be the three terms on the R.H.S. of Eq.(4) (in order of appearance). Then Eq.(4) is written as

$$\ddot{\rho} = [[1]] + [[2]] + [[3]] \ .$$

Note that $[[1]], [[2]] \propto (\Delta - \xi)^{-1}$, so that these two terms would behave as strongly **attractive** forces when $|\dot{\rho}| \sim 1$, implying the possibility of the gravitational collapse. (It turns out that the term $[[3]]$ is not important in the dynamics.)

At this point, it is useful to define the **critical velocity** for a fixed ρ_z :

$$|\dot{\rho}_{cr}| = V_{cr} = \left\{ \frac{1 + e^{2\gamma}\rho_z^2 - |\rho_z|\sqrt{e^{4\gamma}\rho_z^2 + \{2e^{2\gamma} - (1 - e^{-2\gamma})\}}}{1 + (1 - e^{-2\gamma})\rho_z^2} \right\}^{1/2} . \tag{6}$$

The factor $\Delta - \xi$ is negative (positive) when $|\dot{\rho}|$ is greater (smaller) than V_{cr}. (Conversely, one can also define the **critical shell-curvature** for a fixed $\dot{\rho}$, $|\rho_{z_{cr}}| = \frac{e^{\gamma}(1-\dot{\rho}^2)}{\{e^{4\gamma} - (e^{2\gamma}-1)\dot{\rho}^2\}^{1/2}|\dot{\rho}|}$. The factor $\Delta - \xi$ is negative (positive) when $|\rho_z|$ is greater (smaller) than $\rho_{z_{cr}}$.)

With the help of the following further Ansatz, one can do detailed investigations on the relation between the initial shell configuration and the final fate of the gravitational contraction:

$$\rho(t, z) = \sigma(t) f(z) \ . \tag{7}$$

Now one can prove [11],

Theorem 1
If $V < V_{cr}$ initially, the shell never collapses.

Theorem 2
There always exist initial conditions causing the shell-collapse, $\rho \longrightarrow 0$.

In other words, contrary to the cylindrical case, there always exist the initial conditions which cause the shell collapse, $\rho \longrightarrow 0$.

Finally, we show some typical numerical results in Figure 1 and Figure 2. Figure 1 shows the bouncing behavior because the initial conditions satisfy the criterion $|\dot{\rho}_+(0)| < V_{cr}$. On the other hand, Figure 2 shows the collapsing behavior on account of the initial conditions satisfying $|\dot{\rho}_+(0)| > V_{cr}$.

3 Summary and Discussions

In this paper, we have investigated the dynamics of an axi-symmetric shell in the axi-symmetric spacetime, as a natural generalization of the cylindrical shell model investigated previously [8]. The present model is interesting in that it plays the role of a bridge between two extreme classes of models, spherical ones and cylindrical ones. It has turned out that , contrary to the cylindrical case, there always exist the initial conditions which cause the shell collapse, $\rho \longrightarrow 0$. This result implies a kind of "instability" of cylindrical models: The shell-collapsing solutions are strictly forbidden in the case of the cylindrical shell models, while the present axi-symmetric shell model, i.e. the slightest perturbation of the cylindrical shell model, opens a window of the shell-collapse. We need further investigations on, e.g., the property of singularities, generality and implications to the hoop conjecture.

This work has been supported by the Japan Ministry of Education, Culture, Sports, Science and Technology with the grant #14740162.

References

[1] K. S. Thorne, in *Magic Without Magic: John Archibald Wheeler* (J. Klauder (ed.), Freeman, San Francisco, 1972), p.1.

[2] For spherical models, see P.S. Joshi, *Global Aspects in Gravitation and Cosmology* (Clarendon, Oxford, 1993).

[3] See also L. D. Landau and E. M. Lifshitz, *The Classical Theory of Fields* (Fourth revised English edition) (Reed Educational and Professional Publishing, Oxford, 1975), Chapter 12.

[4] R. C. Tolman, Proc. Natl. Acad Sci USA **20**, 169 (1934).

[5] J. R. Oppenheimer and H. Snyder, Physical Review **56**, 455 (1939).

[6] H. Bondi, Mon. Not. Astron. Soc. **107**, 400 (1948).

[7] T. A. Apostolatos and K. S. Thorne, Physical Review **D46**, 2435 (1992).

[8] M. Seriu, Physical Review **D69** #124030 (2004).

[9] P. R. C. T. Pereira and A. Wang, Physical Review **D62**, #124001 (2000); *ibid.* **D67**, #129902(E) (2003).

[10] W. Israel, Il Nuovo Cimento **B44**, 1 (1966); **B48**, 463(E) (1967).

[11] M. Seriu, submitted for publication.

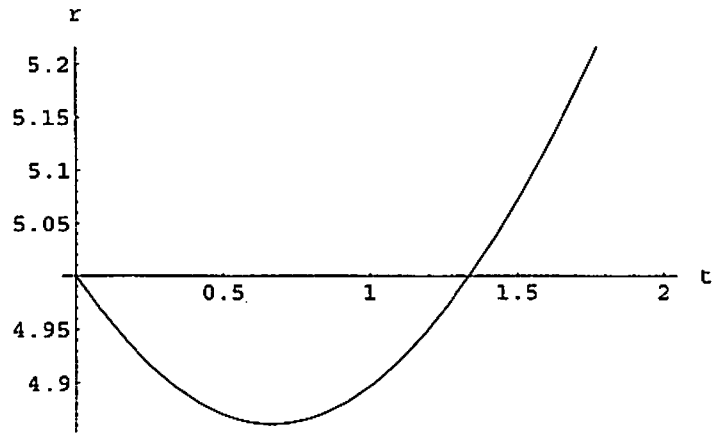

Figure 1: Typical evolution of the shell-radius showing bouncing behavior. It is set $\gamma_+(r_+ - t_+) = \frac{1}{10^6}(r_+ - t_+ + 100)^3$ $f(z) = e^{-0.01\frac{z^2}{2}}$, so that $\rho(t,z) = e^{-0.01\frac{z^2}{2}}\sigma(t)$. Initial conditions are $\rho_0 = 5$ and $\dot{\rho}_+(0) = -0.4$. The observation point is at $z = 1$.

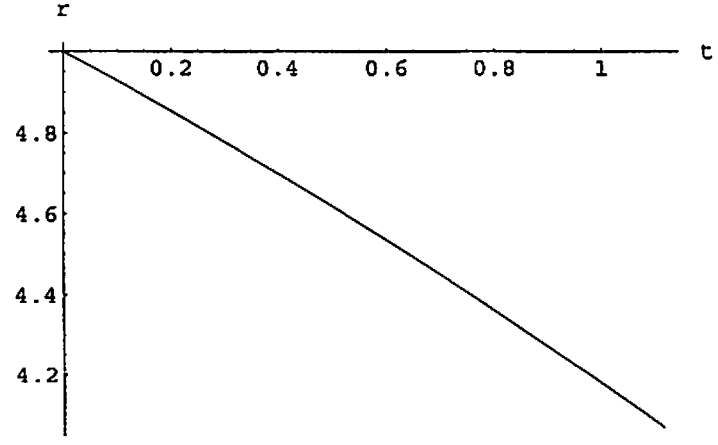

Figure 2: Typical evolution of the shell-radius showing collapsing behavior. The same model as the one shown in *Figure 1* except for the initial velocity $\dot{\rho} = -0.7$.

Gravitational Radiation from Stationary Rotating Cosmic Strings

Kouji Ogawa[1], Hideki Ishihara[2], Hiroshi Kozaki[3], Hiroyuki Nakano[4], Izumi Tanaka[5]

Department of Mathematics and Physics, Graduate School of Science, Osaka City University, Osaka 558-8585, Japan

Abstract

Rigidly and uniformly rotating cosmic strings are studied. We call this type of strings, 'stationary rotating strings.' Analytic solutions of stationary rotating strings, governed by ordinary differential equations, are derived and these solutions are characterized by two parameters. Using these solutions, the gravitational waveforms from stationary rotating strings and the adiabatic evolutions of the strings by gravitational wave radiations are discussed.

1 Introduction

Topological defects were necessarily produced due to spontaneous symmetry breakdowns in the early universe, then topologically stable ones must exist in the present universe [1]. As one type of topological defects, cosmic strings are considered. It is seems that an object in the universe becomes to stationary rotating state naturally, on the analogy of the uniqueness of the Kerr black hole, here we treat "stationary rotating cosmic strings." A possible way to confirm the existence of cosmic strings is gravitational wave experiments. Damour and Vilenkin mentioned the formulation of cosmic strings how to emit gravitational waves [2]. The desirable purpose is what are like the waveforms of gravitational waves which are emitted from stationary rotating strings.

Previously, Frolov et al. analytically obtained the solutions of stationary rotating string in stationary spacetime [3]. We obtained the analytic solutions of stationary rotating strings by alternative parametrization on the world sheet and clarified the solutions are characterized by two parameters.

It is prepared to obtain the waveform of gravitational waves from stationary rotating strings. However, it is doubtful whether the string configurations are stable, because of the loss of energy and angular momentum of the strings due to the gravitational radiation of ones. It is necessary to confirm whether the evolutions of the strings are adiabatically.

2 Analytic Solutions of Stationary Rotating Strings

If you neglect the gravitational effects and assume its thickness is zero, then the string configuration is described as a timelike minimal surface which corresponds to an extremum of the Nambu-Goto action [1]. We consider a stationary rotating stringwith an angular velocity Ω in Minkowski spacetime, where the line element is $ds^2 = -dt^2 + d\rho^2 + \rho^2 d\varphi^2 + dz^2$. A stationary rotating string corresponds to the string, the world sheet of which is tangent to the timelike Killing vector field $\xi^a = \partial_t + \Omega\partial_\varphi$. We use the property that a equation of motion for the Nambu-Goto stationary string is reduced to a geodesic equation [3] [4].

[1]E-mail:kouji@sci.osaka-cu.ac.jp
[2]E-mail:ishihara@sci.osaka-cu.ac.jp
[3]E-mail:furusaki@sci.osaka-cu.ac.jp
[4]E-mail:denden@sci.osaka-cu.ac.jp
[5]E-mail:itanaka@sci.osaka-cu.ac.jp

The solutions of the equations of motion are analytically obtained as

$$
\begin{aligned}
t(\tau) &= \tau, \quad \rho(\sigma) = \frac{1}{|\Omega|}\sqrt{\frac{1}{2}\left\{\alpha - \beta \sin\left(\frac{2\Omega\sigma}{p}\right)\right\}}, \\
\varphi(\tau,\sigma) &= \Omega\tau + \bar{\varphi}(\sigma), \quad z(\sigma) = \sigma, \qquad (1) \\
&\bar{\varphi}(\sigma) := -\frac{\ell}{p}\Omega\sigma - \tan^{-1}\left\{\frac{\beta - \alpha\tan(\Omega\sigma/p)}{2\ell}\right\} + \frac{\ell}{|\ell|}\pi\,\Theta\left(\frac{\Omega\sigma}{\pi p} + \frac{1}{2}\right) + \tan^{-1}\left(\frac{\beta}{2\ell}\right), \\
&\alpha := 1 + \ell^2 - p^2, \quad \beta := \sqrt{(1+\ell^2-p^2)^2 - 4\ell^2}, \\
&\Theta(x) := n \ \ (= 0, \pm 1, \pm 2, \cdots), \ \text{ if } \ n \le x < n+1,
\end{aligned}
$$

where two parameters ℓ and p satisfy $|\ell| + |p| \le 1$, $p \neq 0$. These parameters characterize string's configuration, e.g. for typical cases; "straight" ($\ell = 0, p = \pm 1$), "helical" ($|\ell| + |p| = 1$), "planar" ($\ell = 0$), "triangle" ($|\ell| = 1/3$), and so on (See the FIG. 1).

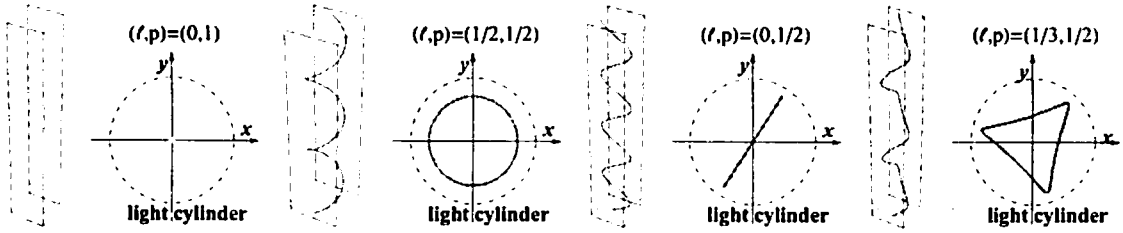

Figure 1: Configurations of stationary rotating strings

3 Gravitational Radiation from Stationary Rotating Strings

3.1 Waveforms of Gravitational waves

Using the solutions (1), we can obtain waveforms from the stationary rotating strings, by solving the linearized Einstein equations: $\nabla^\alpha\nabla_\alpha \bar{h}_{\mu\nu} = -16\pi T^{(\mathrm{st})}_{\mu\nu}$, under the Lorenz gauge condition, $\nabla^\nu \bar{h}_{\mu\nu} = 0$, where $\bar{h}_{\mu\nu} := h_{\mu\nu} - \frac{1}{2}g_{\mu\nu}h_\alpha{}^\alpha$, and $T^{(\mathrm{st})}_{\mu\nu}$ is the energy momentum tensor of the string. Using the periodicities of the solutions $x^\mu = x^\mu(\tau,\sigma)$ with respect to t, φ and z directions, we treat Fourier expansions of the metric perturbation $\bar{h}_{\mu\nu}$:

$$
\bar{h}_{\mu\nu}(t,\rho,\varphi,z) = \sum_{\substack{n=-\infty \\ (n\neq 0)}}^{\infty}\sum_{m=-\infty}^{\infty}\sum_{s=-\infty}^{\infty} e^{-i\omega_n t}\, e^{im\varphi}\, e^{ik_s z}\, \tilde{\bar{h}}^{(nms)}_{\mu\nu}(\rho), \qquad (2)
$$

where ω_n is an angular frequency and k_s is a wave number with respect to the z direction and we also treat $\tilde{T}^{(nms)}_{\mu\nu}(\rho)$, that are the Fourier expansions of $T_{\mu\nu}(x^\alpha)$. The ordinary differential equations for each Fourier coefficient $\tilde{\bar{h}}^{(nms)}_{\mu\nu}(\rho)$ are solved by using the one-dimensional Green's function method:

$$
\tilde{\bar{h}}^{(nms)}_{\mu\nu}(\rho) = \int d\rho' \overset{(nms)}{G}{}_{\mu\nu}{}^{\alpha\beta}(\rho,\rho')\tilde{T}^{(nms)}_{\alpha\beta}(\rho'), \qquad (3)
$$

where ρ means the distance between the string and an observer and $\overset{(nms)}{G}{}_{\mu\nu}{}^{\alpha\beta}(\rho,\rho')$ denotes Green's function with appropriate boundary conditions. The amplitudes $\left|\tilde{\bar{h}}^{(nms)}_{\mu\nu}(\rho)\right|$ is proportional to the value $\mu/\sqrt{\Omega\rho}$ as long as $\rho \gg 1/\Omega$ and where μ denotes the tension of a string so we treat the normalized value: $\hat{\bar{h}}_{\mu\nu}(x^\alpha) := \frac{\sqrt{\Omega\rho}}{\mu}\bar{h}_{\mu\nu}(x^\alpha)$. Here, TT(Transverse Traceless) gauge fixed components, i.e., the plus-mode and cross-mode, denoted as $\hat{h}_+(x^\alpha)$ and $\hat{h}_\times(x^\alpha)$, are considered.

It is found that the Fourier modes that $n \neq m$ are zero, then we consider the waveform constituted by the superposition of only (n,s)-modes, that is $\tilde{\bar{h}}^{(nns)}_{\mu\nu}(\rho)$. It is noticed that any $s=0$ modes, i.e., the modes in ρ-direction, are proportional to $e^{-i\omega_n(t-\rho)}/\sqrt{\rho}$, but $s \neq 0$ modes have the different exponential factors from each other, then the superposition of all (n,s)-modes, except for that of only $s=0$ modes, is dissipated with respect to choice of ρ. It is found that $s \neq 0$ modes are non-negligible in comparison with $s=0$ modes, then as the typical gravitational waves from the stationary rotating strings, we describe the waveforms constituted by only $s=0$ modes in the FIG. 2, Here we consider only planar and triangle cases as the typical configurations, because the other configurations have same qualitative properties as that of the triangle case.

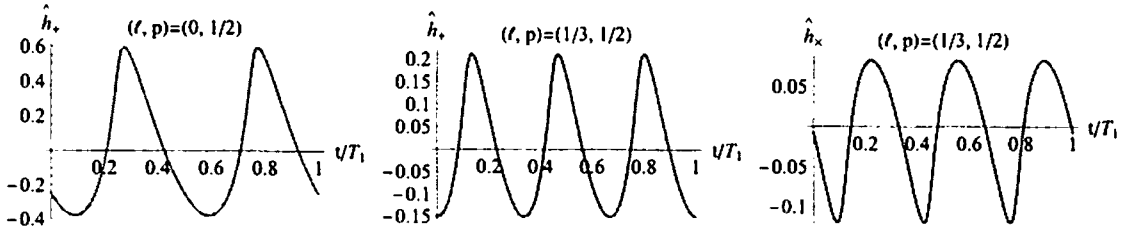

Figure 2: Waveforms
From left to right, the waveforms of a plus-mode $\hat{h}_+$ in planar case, a plus mode $\hat{h}_+$ and cross mode $\hat{h}_\times$ in triangle case, respectively. Because of the comment in the text, these waves are only phase-shifted with respect to choice of x^μ but do not change these waveforms. T_1 is the period of one-rotation time, i.e., $T_1 = 2\pi/\Omega$. It is found that there are no cross-modes $h_\times$ from planar strings ($\ell = 0$).

3.2 Adiabatic Evolutions of Stationary Rotating Strings

We confirm whether the evolutions of stationary rotating strings are adiabatically. Due to the numerical calculation, it is found that;

$$\frac{1}{\Omega}\frac{\dot{E}_{(\mathrm{GW})}}{E_{(\mathrm{st})}} \leq \mathcal{O}(1)\mu, \quad \frac{1}{\Omega}\frac{\dot{J}_{(\mathrm{GW})}}{J_{(\mathrm{st})}} \leq \mathcal{O}(1)\mu, \tag{4}$$

where $\dot{E}_{(\mathrm{GW})}$ and $\dot{J}_{(\mathrm{GW})}$ denote the rates of energy and angular momentum loss of the string by gravitational radiation and $E_{(\mathrm{st})}$ and $J_{(\mathrm{st})}$ denote the energy and angular momentum of the string. Due to the CMB data by WMAP, the tension of cosmic strings are constrained as $\mu < 6.1 \times 10^{-7}$ [5]. Because of the numerical results (4) and the constraint, it is found that the evolutions of stationary rotating strings are adiabatically.

Using the adiabatic approximation, we consider the adiabatic evolution of the string configuration, in consideration of the evolution of p and Ω;

$$\dot{E}_{(\mathrm{GW})} = \dot{p}\partial_p E_{(\mathrm{st})} + \dot{\Omega}\partial_\Omega E_{(\mathrm{st})}, \quad \dot{J}_{(\mathrm{GW})} = \dot{p}\partial_p J_{(\mathrm{st})} + \dot{\Omega}\partial_\Omega J_{(\mathrm{st})}, \tag{5}$$

where the dots means differentiation by t. In this case, we do not consider the evolution of the parameter ℓ, because gravitational waves are never emited as long as ℓ is an irrational number, so it is expected that there are no evolutions of ℓ, at least due to the gravitational radiation.

Because of the solutions (1), assuming $p = 1 - \ell$, the configuration of the string is helical, except for the case $(\ell, p) = (0, 1)$(See the FIG. 1), at the same time, assuming the limit; $\Omega \to \infty$, the configuration becomes to straight, independent of the choice of (ℓ, p). Assuming that $\ell = 0$ (in planar case) or $1/3$ (in triangle case), the numerical results of adiabatic evolutions of p and Ω are shown in the left two figure in FIG. 3, where the inclination of arrows means $d\Omega/dp$. It seems that all arrows trend in the direction of higher Ω and higher p; $p = 1$ (planar) or $2/3$ (triangle), and higher Ω, except for the arrows which trend in the direction of lower Ω, where we do not discuss the flowing. By looking at the leftest figure in FIG. 3, in planar case, the ultimate states of all trajectories of solution flows means straight configurations. In

the rightest figure in FIG. 3, in triangle case, it precisely shows the value $d\Omega/dp$ near $p = 2/3$ region. It seems that $d\Omega/dp$ approaches finite value closer to $p = 2/3$, that means, there exist the trajectories that the ultimate states are $(p, \Omega) = (2/3, \text{finite})$, i.e., helical.

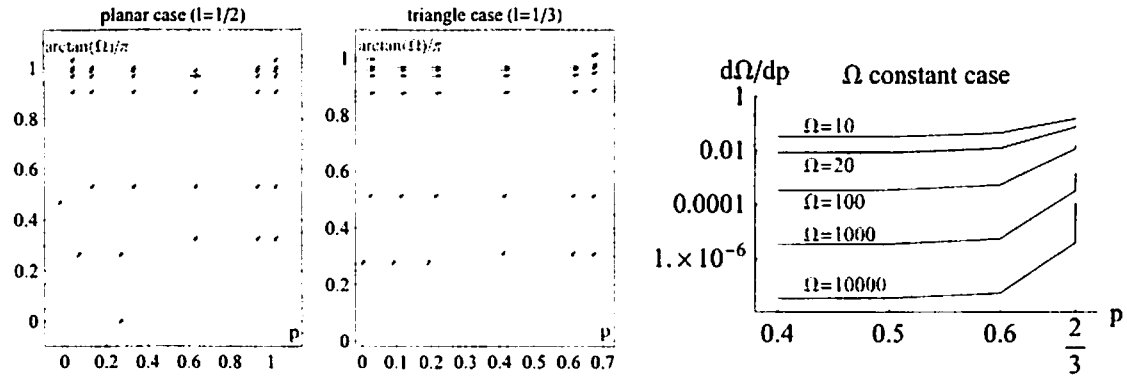

Figure 3: Left two figures describe the adiabatic evolutions of p and Ω in planar and triangle cases, where the inclination of arrows means $d\Omega/dp$. The rightest figure describe the log plot p vs $d\Omega/dp$ near the region $p = 2/3$ in triangle case.

4 Summary

1. The analytic solutions of stationary rotating strings in Minkowski spacetime are obtained.
   Stationary rotating strings are determined by only two parameters (ℓ, p).

2. The waveforms of gravitational waves from stationary rotating strings are studied.
   Some characteristic properties are found;
   The "helical" strings do not emit gravitational waves.
   The amplitudes of gravitational waves from the strings are proportional to the value $\mu/\sqrt{\Omega\rho}$, as long as $\Omega\rho \gg 1$.
   It is found that the only waveforms which is constituted by the $s = 0$ modes are meaningful.
   The "planar" strings do not emit cross-modes $h_\times$ (considering only $s = 0$ modes) but emit plus-modes h_+.

3. We confirm that the configurations of the stationary rotating strings evolute adiabatically.
   By using the adiabatic property, We estimate the evolutions of the stationary rotating strings, in typical case; planar and triangle case.
   It seems that all planar strings become to straight, and the other shapes, e.g., There exist "triangle" strings which become to helical. But the results are preliminary, because the present numerical results are obtained in consideration of only $= 0$ modes. It is needed to consider how contribute the Fourier components that $s \neq 0$ to the results.

References

[1] A. Vilenkin and E. P. S. Shellard, *Cosmic Strings and Other Topological Defects* (Cambridge University Press, 1994).

[2] T. Damour and A. Vilenkin, Phys. Rev. D **64**, 064008 (2001) [arXiv:gr-qc/0104026].

[3] V. P. Frolov, S. Hendy and J. P. De Villiers, Class. Quant. Grav. **14**, 1099 (1997)

[4] H. Ishihara and H. Kozaki, Phys. Rev. D **72**, 061701 (2005)

[5] L. Pogosian, M. C. Wyman and I. Wasserman, arXiv:astro-ph/0403268.

Wave effects in gravitational lensing by a cosmic string

Teruaki Suyama[1], Takahiro Tanaka[2], Ryuichi Takahashi[3]

[1,2] *Department of Physics, Kyoto University, Kyoto 606-8502, Japan*
[3] *Division of Theoretical Astrophysics, National Astronomical Observatory of Japan, Mitaka, Tokyo 181-8588,Japan*

Abstract

We present exact solutions of the massless Klein-Gordon equation in a spacetime in which an infinite straight cosmic string resides. The first solution represents a plane wave entering perpendicular to the string direction. We also present and analyze a solution with a static point-like source. In the short wavelength limit these solutions approach the results obtained by using the geometrical optics approximation: magnification occurs if the observer lies in front of the string within a strip of angular width $8\pi G\mu$, where μ is the string tension. We find that when the distance from the observer to the string is less than $10^{-3}(G\mu)^{-2}\lambda \sim 150\mathrm{Mpc}(\lambda/\mathrm{AU})(G\mu/10^{-8})^{-2}$, where λ is the wave length, the magnification is significantly reduced compared with the estimate based on the geometrical optics due to the diffraction effect.

1 Introduction

Typical wavelength of gravitational waves from astrophysical compact objects such as BH(black hole)-BH binaries is in some cases very long so that wave optics must be used instead of geometrical optics when we discuss gravitational lensing. In most of the works which studied gravitational lensing phenomenon in the framework of wave optics, isolated and normal astronomical objects such as galaxies are concerned as lens objects [1, 2, 3, 4, 5, 6, 8, 9, 10].

Recently Yamamoto and Tsunoda[7] studied wave effects in gravitational lensing by an infinite straight cosmic string. The metric around a cosmic string is completely different from that around a usual massive object.

We study in detail wave effects in the gravitational lensing by an infinite straight cosmic string. In Ref. [7], wave propagation around a cosmic string was studied but they put the waveform around the string by hand. Their prescription is correct only in the limit of geometrical optics, which breaks down when the wavelength becomes longer than a certain characteristic length. In this paper, we present exact solutions of the (scalar) wave equation in a spacetime with a cosmic string. We analytically show that our solutions reduce to the results of the geometrical optics in the short wavelength limit. We derive a simple analytic formula of the leading order corrections to the geometrical optics due to the finite wavelength effects and also an expression for the long wavelength limit. Interference caused by the lensing remains due to the diffraction effects even when only a single image can be seen in the geometrical optics. This fact increases the lensing probability by cosmic strings.

2 A solution of the wave equation around an infinite straight cosmic string

A solution of Einstein equations around an infinite straight cosmic string to first order in $G\mu$ is given by [11]

$$d^2s = -dt^2 + dr^2 + (1-\Delta)^2 r^2 d\theta^2 + dz^2, \tag{1}$$

where (r, z, θ) is a cylindrical coordinate($0 \leq \theta < 2\pi$) and $2\pi\Delta \approx 8\pi G\mu$ is the deficit angle around the cosmic string.

[1] E-mail:suyama@tap.scphys.kyoto-u.ac.jp
[2] E-mail:tama@tap.scphys.kyoto-u.ac.jp
[3] E-mail:takahasi@th.nao.ac.jp

Here we consider waves of a massless scalar field ϕ instead of gravitational waves for simplicity, but the wave equations are essentially the same in these two cases. An extension to the cosmological setup is straightforwardly done by adding an overall scale factor. In that case the time coordinate t is to be understood as the conformal time. The wave equation remains unchanged if we consider a conformally coupled field, but it is modified for the other cases due to curvature scattering. The correction due to curvature scattering of the Friedmann universe is suppressed by the square of the ratio between the wavelength and the Hubble length, which can be neglected in any situations of our interest.

We find that a solution of the wave equation which corresponds to a plane wave injected perpendicularly to and scattered by the cosmic string is

$$\phi(r,\theta) = \frac{1}{1-\Delta}\sum_{m=0}^{\infty} \epsilon_m i^m e^{-\frac{i\pi m\Delta}{2(1-\Delta)}} J_{\nu_m}(\omega r)\cos m\theta. \tag{2}$$

3 Limiting behaviors of the solution

3.1 Approximate waveform in the wave zone

The solution (2) describes the waveform propagating around a cosmic string. But it is not easy to understand the behavior of the solution because it is given by a series. In fact, it takes much time to perform the summation in Eq. (2) numerically for a realistic value of tension of the string, say, $G\mu \lesssim 10^{-6}$ because of slow convergence of the series. In particular it is not manifest whether the amplification of the solution in the short wavelength limit coincides with the one which is obtained by the geometrical optics approximation. Therefore it will be quite useful if one can derive a simpler analytic expression. Here we reduce the formula by assuming that the distance between the string and the observer is much larger than the wave length,

$$\xi \equiv \omega r \gg 1. \tag{3}$$

which is valid in almost all interesting cases.

Here we only quote the final result which keeps terms up to $O(1/\sqrt{\xi})$,

$$\begin{aligned}\psi(\xi,\theta) \approx\ & \exp\left(i\xi\cos\frac{\alpha(\theta)}{\sqrt{\xi}}\right)\Theta(\alpha(\theta)) - \frac{\sigma(\theta)}{\sqrt{\pi}}\exp\left(i\xi + \frac{i\alpha(\theta)}{(1-\Delta)\sqrt{\xi}} - \frac{i}{2}\tilde{\alpha}^2(\theta)\right)\mathrm{Erfc}\left(\sigma(\theta)\frac{\tilde{\alpha}(\theta)}{\sqrt{2}}e^{-i\pi/4}\right) \\ & + \frac{1}{\sqrt{2\pi\xi}}\frac{1}{1-\Delta}\frac{e^{-i\xi+i\pi/4}}{1-e^{\frac{1}{1-\Delta}(\pi-\alpha(\theta)/\sqrt{\xi})}}.\end{aligned} \tag{4}$$

where

$$\tilde{\alpha}(\theta) := i(1-\Delta)\sqrt{\xi}\left[1-\exp\left(i\frac{\alpha(\theta)}{(1-\Delta)\sqrt{\xi}}\right)\right], \tag{5}$$

$$\sigma(\theta) := \mathrm{sign}(\alpha(\theta)), \tag{6}$$

and

$$\mathrm{Erfc}(x) := \int_x^{+\infty} dt\, e^{-t^2}. \tag{7}$$

3.2 Geometrical optics limit

Geometrical optics limit corresponds to the limit $\xi \to \infty$ with Δ and θ fixed. In this limit $\alpha(\theta)$ also goes to $+\infty$, and hence the error function in Eq. (4) vanishes. Hence the waveform in the geometrical optics limit, which we denote as $\phi_{\rm go}$, becomes

$$\begin{aligned}\phi_{\rm go}(\xi,\theta) =\ & e^{i\xi\cos(\pi\Delta+\varphi)}\Theta(\pi\Delta+\varphi) \\ & + e^{i\xi\cos(\pi\Delta-\varphi)}\Theta(\pi\Delta-\varphi),\end{aligned} \tag{8}$$

where φ is defined as $\varphi \equiv (1-\Delta)\theta$.

For $\varphi > \pi\Delta$, we have

$$\phi_{\rm go}(\xi,\theta) = e^{i\xi\cos(\varphi+\pi\Delta)}. \tag{9}$$

This is a plane wave whose traveling direction is $\varphi = -\pi\Delta$.

For $|\varphi| < \pi\Delta$, $\phi_{\rm go}$ is

$$\phi_{\rm go}(\xi,\theta) = e^{i\xi\cos(\varphi-\pi\Delta)} + e^{i\xi\cos(\varphi+\pi\Delta)}. \tag{10}$$

This is the superposition of two plane waves whose traveling directions are different by the deficit angle $2\pi\Delta$. Hence amplification of the images and interference occur for $|\varphi| < \pi\Delta$, which coincides with the one derived under the geometrical optics.

3.3 Quasi-geometical optics approximation

Here we expand the waveform (4) to the lowest order in $1/\alpha(\pm\theta)$. This includes the leading order corrections to the geometrical optics approximationdue to the finite wavelength effects.

Using the asymptotic formula for the error function, the leading order correction due to the finite wavelength, which we denote as $\delta\phi_{\rm qgo}$, is obtained as

$$\delta\phi_{\rm qgo}(\xi,\theta) = -\frac{e^{i\xi+i\pi/4}}{\sqrt{2\pi}}\left(\frac{1}{\alpha(\theta)}+\frac{1}{\alpha(-\theta)}\right). \tag{11}$$

As is expected, the correction blows up for $|\varphi| \approx \pi\Delta$, where $\alpha(\theta)$ or $\alpha(-\theta)$ vanishes, irrespectively of the value of ξ. In such cases, we have to evaluate the error function directly, going back to Eq. (4).

The expression on the first line in Eq.(11) manifestly depends only on $\alpha(\pm\theta)$ aside from the common phase factor $e^{i\xi}$. Except for this unimportant overall phase, the waveform is completely determined by $\alpha(\pm\theta)$.

The geometrical meaning of these parameters $\alpha(\pm\theta)$ is the ratio of two length scales defined on the lens plane. To explain this, let us take the picture that a wave is composed of a superposition of waves which go through various points on the lens plane. In the geometrical optics limit the pathes passing through stationary points of $T(\vec{x})$, which we call the image points, contribute to the waveform. The first length scale is $r_s = |\alpha(\pm\theta)|/\sqrt{\xi} \times r$ which is defined as the separation between an image point and the string on the lens plane. In this picture we expect that pathes whose pathlength is longer or shorter than the value at an image point by about one wavelength will not give a significant contribution because of the phase cancellation. Namely, only the pathes which pass within a certain radius from an image point need to be taken into account. Then such a radius will be given by $r_F = \sqrt{\lambda r}$, which we call Fresnel radius. Namely, a wave with a finite wavelength can be recognized as an extended beam whose transverse size is given by r_F. The ratio of these two scales gives $\alpha(\pm\theta)$:

$$|\alpha(\pm\theta)| = \frac{\sqrt{2\pi}r_s}{r_F}.$$

When $r_s \gg r_F$, i.e., $\alpha(\pm\theta) \gg 1$, the beam width is smaller than the separation. In this case the beam image is not shadowed by the string, and therefore the geometrical optics becomes a good approximation. When $r_s \lesssim r_F$, i.e.,

$$\alpha(\pm\theta) \lesssim 1, \tag{12}$$

we cannot see the whole image of the beam, truncated at the location of the string. Then the diffraction effect becomes important. The ratio of the beam image eclipsed by the string determines the phase shift and the amplification of the wave coming from each image. If we substitute $|\varphi| \approx 0$ as a typical value, we obtain a rough criterion that the diffraction effect becomes important when

$$\lambda \gtrsim 2\pi(\pi\Delta)^2 r, \tag{13}$$

or $\xi \lesssim (\pi\Delta)^{-2}$ in terms of ξ.

Interestingly, the absolute value of the amplification factor deviates from unity even for $\varphi \gtrsim \pi\Delta$ which is not observed in the geometrical optics limit. This is a consequence of diffraction of waves, the amplitude of oscillation of the interference pattern becomes smaller as θ becomes larger, which is a typical

diffraction pattern formed when a wave passes through a single slit. The broadening of the interference pattern due to the diffraction effect means that the observers even in the region $|\varphi| > \pi\Delta$ can detect signatures of the presense of a cosmic string.

So far, we have considered the stringy source rather than a point source. Extension to a point source can be done in a similar manner to the case of the stringy source [12].

4 Summary

We have constructed a solution of the Klein-Gordon equation for a massless scalar field in the flat spacetime with a deficit angle $2\pi\Delta \approx 8\pi G\mu$ caused by an infinite straight cosmic string. We showed analytically that the solution in the short wavelength limit reduces to the geometrical optics limit. We have also derived the correction to the amplification factor obtained in the geometrical optics approximation due to the finite wavelength effect and the expression in the long wavelength limit.

The waveform is characterized by a ratio of two different length scales. One length scale r_s is defined as the separation between the image position on the lens plane in the geometrical optics and the string. We have two r_s since there are two images corresponding to which side of the string the ray travels. (When the image cannot be seen directly, we asign a negative number to r_s.) The other length scale r_F, which is called Fresnel radius, is the geometrical mean of the wavelength and the typical separation among the source, the lens and the observer. The waveform is characterized by the ratios between r_s and r_F. If $r_F > r_s$, the diffraction effect becomes important and the interference patterns are formed. Even when the image in the geometrical optics is not directly seen by the observer, the interference patterns remain. In contrast, in the geometrical optics magnification and interference occur only when the observer can see two images which travel both sides of the string. Namely, the angular range where lensing signals exist is broadened by the diffraction effect.

T.S. thanks Kunihito Ioka, Takashi Nakamura and for useful comments.

References

[1] R. Takahashi and T. Nakamura, Astrophys. J. **595**, 1039 (2003) [arXiv:astro-ph/0305055].

[2] N. Seto, Phys. Rev. D **69**, 022002 (2004) [arXiv:astro-ph/0305605].

[3] T. T. Nakamura, Phys. Rev. Lett. **80**, 1138 (1998).

[4] K. Yamamoto, arXiv:astro-ph/0309696.

[5] C. Baraldo, A. Hosoya and T. T. Nakamura, D **59**, 083001 (1999).

[6] T. T. Nakamura and S. Deguchi Prog. Theor. Phys. Suppl. **133**, 137 (1999).

[7] K. Yamamoto and K. Tsunoda, Phys. Rev. D **68**, 041302 (2003) [arXiv:astro-ph/0309694].

[8] T. Suyama, R. Takahashi and S. Michikoshi, arXiv:astro-ph/0505023.

[9] R. Takahashi, T. Suyama and S. Michikoshi, Astron. Astrophys. **438**, L5 (2005) [arXiv:astro-ph/0503343].

[10] R. Takahashi, Astron. Astrophys. **423**, 787 (2004) [arXiv:astro-ph/0402165].

[11] A. Vilenkin, Phys. Rev. D **23**, 852 (1981).

[12] T. Suyama, T. Tanaka and R. Takahashi, arXiv:astro-ph/0512089.

The verification of tidal effects in the relativistic treatment

Kentaro Takami[1] and Yasufumi Kojima[2]

Theoretical Astrophysics Group, Department of Physics,
Hiroshima University, Higashi-Hiroshima 739-8526, Japan

Abstract

We examine the gyration motion of a charged particle viewed from a reference observer falling along Z axis into a Schwarzschild black hole. The magnetic field is assumed to be constant and uniform along Z axis. The motion far from the gravitational source is circular in X-Y plane. Fate of the circular orbit is calculated as the reference observer approaches the black hole. The circular orbit is eventually disrupted due to tidal force. The final plunging velocity increases in the non-relativistic treatment. On the other hand, the plunging velocity decreases, if initial circular velocity exceeds a critical value $\sim 0.7c$. In this way, we verified the peculiar property in the relativistic regime, previously reported by Chicone and Mashhoon.

1 Introduction

Gravity can be removed in one point of the spacetime but cannot be removed in more than two points at the same time. Therefore, the difference of the gravitational force between two points, i,e, tidal force represents 'true' gravity, which is discriminated from uniform acceleration. Tidal effect is well known in Newtonian gravity.

Recently, Chicone and Mashhoon [1] point out a very interesting aspect of the tidal force. When ultra relativistic velocity is taking into account, the tidal force exhibits unexpected property contrary to non-relativistic dynamics. Suppose an object of a finite size falling into a black hole along Z axis. The object is stretched along Z axis and is squeezed along X and Y axes under the Newtonian tidal force. The tidal force therefore causes anisotropic acceleration/deceleration in particle dynamics occurred near a freely falling observer. That is, from the viewpoint of the observer, particles out-going along Z axis are accelerated, whereas those ones out-going along X axis, or Y axis are decelerated. This is non-relativistic expectation. Chicone and Mashhoon show that the property changes when the particle velocity exceeds a critical value $c/\sqrt{2} \sim 0.7c$. That is, relativistic particles moving outward along Z axis are decelerated, but those moving along X axis, or Y axis are accelerated. In their one dimensional model, the relativistic particles instantaneously escape away from valid region of the local observer frame.

In this study, we present another concrete model to study the tidal effects on relativistic motion. Motion of a charged particle in a magnetic field is considered. The magnetic field is assumed to be weak, and the spacetime is described by Schwarzschild metric. Fermi normal coordinates are constructed around the reference observer falling into a black hole. The magnetic field is assumed to be uniform along Z axis in this frame. The orbit is circular on X-Y plane, when the tidal force is negligible in far region from the gravitational source. As the reference frame approaches a black hole along Z axis, the tidal force becomes important. How is the circular motion disturbed? In particular, how does the relativistic rotating velocity affect the result? The spatial orbit of the particle is always bound, so that it is possible to pursue the long term evolution in Fermi system. This toy problem would deepen our understanding of the tidal force.

2 Equation of motion

We consider a reference observer whose world line is a geodesic. Fermi normal coordinates, (cT, X^k) in a neighborhood of the observer are constructed in such a way that the world line of the observer is

[1]E-mail:takami@theo.phys.sci.hiroshima-u.ac.jp
[2]E-mail:kojima@theo.phys.sci.hiroshima-u.ac.jp

given by observer's proper time T and $X^k = 0$. We consider the dynamics of a particle with mass m and charge q, which is labeled by $(X(T), Y(T), Z(T))$ in the Fermi system. We assume for simplicity that the electric field is zero and that the magnetic field B is constant and uniform along Z direction in the reference observer system. In this case, equation of motion is

$$\ddot{X} + KX\left(1 - 2\dot{X}^2 + \frac{4}{3}\dot{Y}^2 - \frac{2}{3}\dot{Z}^2\right) - \frac{2}{3}K\dot{X}\left(5Y\dot{Y} - 7Z\dot{Z}\right) = +\frac{\omega}{c\Gamma}\dot{Y}, \tag{1}$$

$$\ddot{Y} + KY\left(1 - 2\dot{Y}^2 + \frac{4}{3}\dot{X}^2 - \frac{2}{3}\dot{Z}^2\right) - \frac{2}{3}K\dot{Y}\left(5X\dot{X} - 7Z\dot{Z}\right) = -\frac{\omega}{c\Gamma}\dot{X}, \tag{2}$$

$$\ddot{Z} - 2KZ\left(1 - 2\dot{Z}^2 + \frac{1}{3}\dot{X}^2 + \frac{1}{3}\dot{Y}^2\right) - \frac{4}{3}K\dot{Z}\left(X\dot{X} + Y\dot{Y}\right) = 0, \tag{3}$$

where an overdot denotes differentiation with respect to time cT and K is expressed by Schwarzschild radial coordinate r, gravitational constant G and mass M:

$$K = \frac{GM}{c^2 r^3}, \tag{4}$$

$$\Gamma^{-2} = 1 - \left(\dot{X}^2 + \dot{Y}^2\right) + \frac{2}{9T^2}\left(X^2 + Y^2\right) + \frac{4}{27T^2}\left(X^2\dot{Y}^2 - 2XY\dot{X}\dot{Y} + \dot{X}^2Y^2\right) \tag{5}$$

and

$$\omega = qB/(mc). \tag{6}$$

The spatial range valid for the coordinate system is limited by a radius $\mathcal{R}^{-1/2}$, where $\mathcal{R}$ is a typical component of curvature tensor evaluated at observer's world line. As one simple limit in our problem, the condition may be taken as

$$X^2 + Y^2 < \frac{3}{2K} = \frac{27}{4}(cT)^2. \tag{7}$$

Outside this region, the spatial metric in X-Y plane changes the sign.

3 Numerical results

Numerical results are given for the motion with initial circular velocity $v = 0.1c$ from large $|T|$, as far as the condition (7) is satisfied. The trajectories are shown for the gyro-center $(r_c/2, 0)$ in the left panel and for $(3r_c/2, 0)$ in the right panel of figure 1, where r_c is the circular radius of initial gyration motion. The condition (7) is no longer satisfied at the end of each curve, which corresponds to different time T. The final phase is therefore masked because the particle eventually escapes outside of valid Fermi coordinate system. This behavior seems to be general, because the particle motion is slow compared with the shrinkage of valid spatial range, which is proportional to the time $|T|$ as shown in eq.(7). The locally measured value of the velocity v at the particle position is given by $v = c(-g_{ij}\dot{X}^i\dot{X}^j/g_{00})^{1/2}$, which is reduced to $c(\dot{X}^2 + \dot{Y}^2)^{1/2}$ in flat spacetime. The time evolution of v normalized by the initial velocity $v = 0.1c$ is shown in figure 2. Like the non-relativistic cases, the velocity increases with ωT from the transition time $\omega T_* \approx -1$. However, the final behavior, i.e, divergence of velocity appeared in non-relativistic case can not be treated in this system, because the particle position is outside the valid coordinate system. Sudden drop of the velocity in the right panel of figure 2 corresponds to the kink in the orbit shown in figure 1. In that case, the tidal acceleration almost reverses the direction of particle orbit.

We show the results for initial circular velocity, $v = 0.9c$. The orbits are shown for gyro-center $(r_c/2, 0)$ in the left panel and for $(3r_c/2, 0)$ in right panel of figure 3. The spiral of the orbits is much tight due to larger circular velocity. In their final phase, the particles always escape from the valid coordinate system like in figure 1, so that the subsequent evolution can not be followed. This termination may

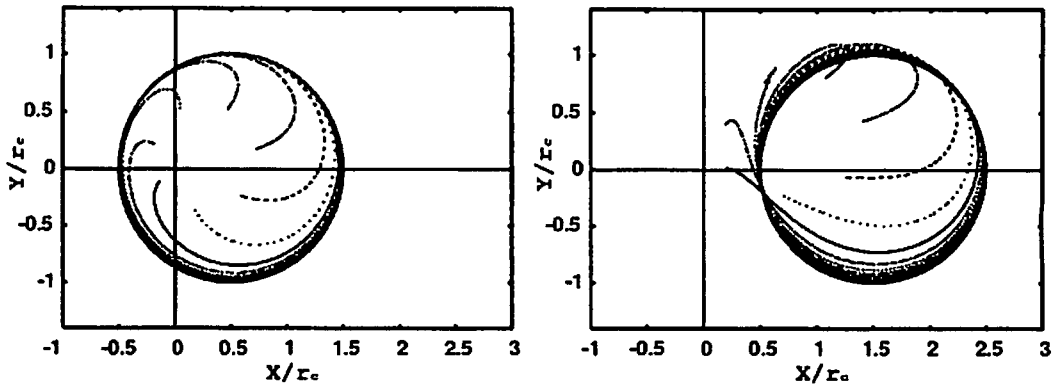

Figure 1: The initial circular velocity is 0.1c.

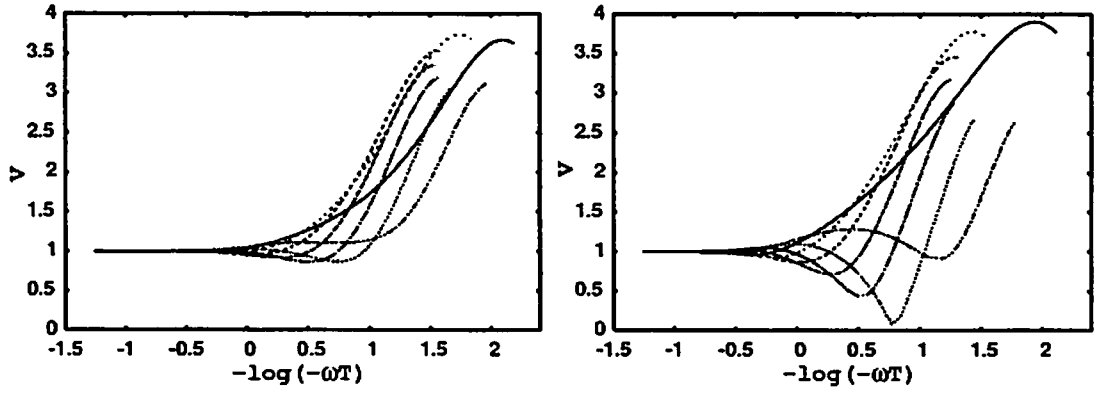

Figure 2: The initial circular velocity is 0.1c.

artificially cause these orbits converge to $(0.5r_c, 0.2r_c)$ in the left panel and $(1.5r_c, 0.5r_c)$ in the right panel. Each position suggested from the figure is not a true convergent position because the end points do not correspond to the same coordinate time. Curves stopped at early time have larger $(X^2+Y^2)^{1/2}$ due to eq.(7). Time evolution of velocity $v = c(-g_{ij}\dot{X}^i\dot{X}^j/g_{00})^{1/2}$ is shown in figure 4. It is normalized by the initial velocity $v = 0.9c$. Remarkable result is that the velocity never increases, but decreases. In this case, tidal force acts as deceleration, contrary to our intuition. The physical mechanism is not easily understood, but the mathematical reason is simple. The tidal acceleration terms coupled with velocity in eqs.(1) and (2) possibly change the sign for large velocity $\dot{X} \sim \dot{Y} \sim \mathcal{O}(1)$. Beyond a critical value, the tidal force becomes repulsive contrary to attractive one in the non-relativistic dynamics. This property is analogous to that found in Chicone and Mashhoon [1]. We have calculated evolution for various values of the initial circular velocity in order to determine whether the tidal force acts as acceleration or deceleration. It is found that the critical initial velocity is approximately given by $\sim 0.7c$. Above this value, the velocity decreases.

4 Conclusion

In this study, we have examined tidal effect on a charged particle orbiting in uniform magnetic field. From this simple toy model, we found that the tidal force changes the property for the relativistic velocity, as shown by Chicone and Mashhoon [1]. In our model, the gyration velocity on the X-Y plane changes due to the tidal force coupled to the velocity, as the particle falls into a black hole along Z axis. The

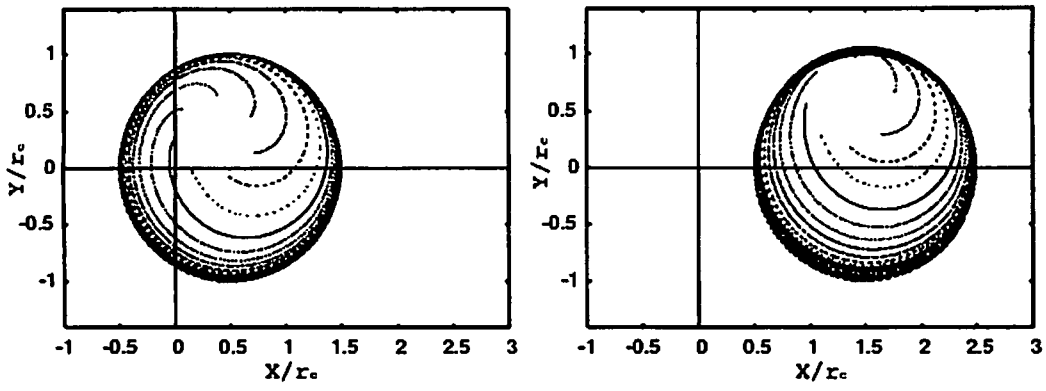

Figure 3: The initial circular velocity is 0.9c.

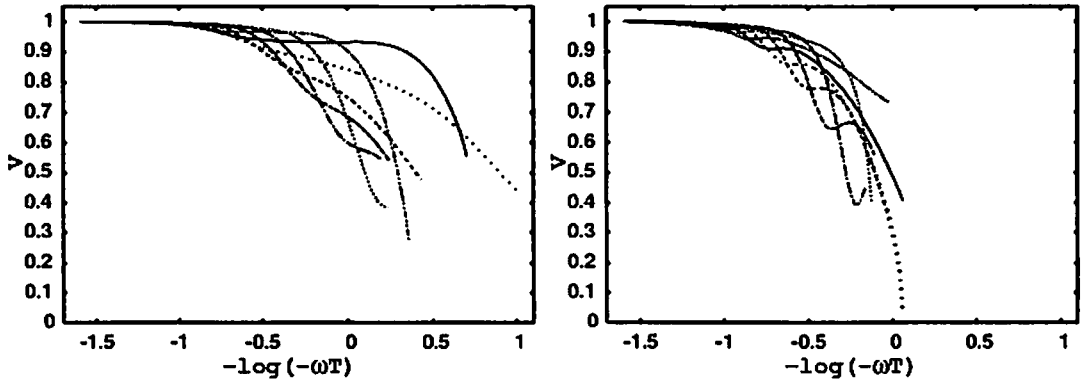

Figure 4: The initial circular velocity is 0.9c.

velocity at the final plunging phase increases, when the initial velocity is less than the critical value. On the other hand, the velocity decreases, when it is larger than the critical value. The critical velocity to discriminate between acceleration and deceleration is of order $0.7c$ in our model. However, the value would depend on situation of the process.

The details of this work will appear in [2].

References

[1] Chicone C and Mashhoon B 2004 *Class. Quant. Grav.* **21** L139;
Chicone C and Mashhoon B 2005 *Class. Quant. Grav.* **22** 195;
Chicone C and Mashhoon B 2005 *Astron. Astrophys.* **437** L39;
Chicone C and Mashhoon B 2005 *Annalen Phys.***14** 290

[2] Yasufumi K and Kentaro T 2006 *Class. Quant. Grav.* **23** 609-616

Accurate Evolution of Orbiting Binary Black Holes

Peter Diener[1,2], Frank Herrmann[3,4], Denis Pollney[3], Erik Schnetter[1,3], Edward Seidel[1,2,3], Ryoji Takahashi[1], Jonathan Thornburg[3], Jason Ventrellai[1]

[1] *Center for Computation & Technology, Louisiana State University, Baton Rouge, LA 70803, USA*
[2] *Department of Physics and Astronomy Louisiana State University, Baton Rouge, LA 70803, USA*
[3] *Max-Planck-Institut für Gravitationsphysik, Albert-Einstein-Institut, Am Mühlenberg 1, 14476 Golm, Germany*
[4] *Center for Gravitational Physics & Geometry, Penn State University, University Park, PA 16802*
[5] *Max-Planck-Institut für Gravitationsphysik, Albert-Einstein-Institut, Am Mühlenberg 1, 14476 Golm, Germany*

Abstract

We present a detailed analysis of binary black hole evolutions in the last orbit, and demonstrate consistent and convergent results for the trajectories of the individual bodies. The gauge choice can significantly affect the overall accuracy of the evolution. It is possible to reconcile certain gauge dependent discrepancies by examining the convergence limit. We illustrate these results using an initial data set recently evolved by Brügmann *et al.* (*Phys. Rev. Lett.* **92**, 211101). For our highest resolution and most accurate gauge, we estimate the duration of this data set's last orbit to be approximately $59M_{\rm ADM}$.

1 Introduction

Over the course of the next decade, instruments capable of detecting gravitational radiation (such as LIGO, VIRGO, TAMA, GEO600) are expected to open a new observational window on the universe. The collision of binary compact objects such as black holes (BHs) is one of the most promising sources for first generation gravitational wave observatories. The theoretical framework for modelling binary BH systems is the complete set of nonlinear Einstein equations. Intensive efforts to develop numerical codes able to solve these equations using supercomputers, have shown that it is now possible to evolve BHs for periods of an orbit [1, 2, 3]. If these simulations are to produce waveforms useful for detector searches, high demands are placed on their accuracy [4].

The near-zone dynamics of binary BH systems are notoriously difficult to simulate, and to analyse. Using the BSSN formulation and a particular set of gauges, a series of BBH configurations, corresponding to initial data in quasi-circular orbit at successively larger separations [5], were all found to coalesce in slightly more than a half orbit [2]. A similar BSSN evolution carried out using somewhat different gauges and numerical methods for another data set, slightly further out along the orbital sequence, was found to evolve for much more than the estimated orbital timescale $114M_{\rm ADM}$ without finding a common apparent horizon (AH) [1]. In fact, no common horizon was found long after the BHs would reasonably be expected to have merged.

In this paper, we carry out an evolution of the same data set and show that it does indeed carry out a complete orbit before a common AH forms. As the BH separation decreases, a local measure of the angular velocity Ω increases, so that the duration of the final orbit is approximately $59M$. The trajectories are convergent for a range of resolutions and within a class of gauge conditions.

However, we do find that very high resolutions are required in order to obtain evolutions close to the continuum limit. The resolutions we have applied here are significantly higher than those used in analogous BH evolutions to date, except for [3] where similar resolutions were used. With insufficient resolution, we show that it is possible to substantially under- or over-predict the orbital period. We also find that apparently small deviations in the chosen coordinate conditions (gauge), based on choice of parameters within a particular family, can have a strong influence on the discretisation error within the subsequent evolution.

2 Methods

Initial data for the evolutions discussed in this paper correspond to Brandt-Brügmann "punctures" [6]. The particular orbital parameters are chosen to be identical to those first evolved in [1], namely initial separation $L/M = 9.32M$, bare masses $m = 0.47656M$ of each BH, and equal and opposite linear momenta, $p = \pm 0.13808$. These parameters are chosen to approximate a BH pair in quasi-circular orbit. The angular velocity $\Omega_0 = 0.054988$ suggests an orbital timescale of $114M$ for a perfectly circular orbit. The initial geometry is determined by numerically solving the constraint equations using the solver of Ansorg et al. [7].

The binary BH evolution is carried out using the "BSSN" formulation of the Einstein equations [8, 9, 10], with an implementation described explicitly in [11]. We use a version of the "1+log" lapse and Γ-driver shifts, given by Eqs. (33) (with $f(\alpha) = 2\Psi_{BL}^m/\alpha$) and (46) (with $F(\alpha) = 3/4\,\alpha^p/\Psi_{BL}^n$) of [11]. We generalise the parameter η to a lapse-dependent coefficient $\alpha^q\eta$, where typically $q \in [0,4]$. This is helpful for long-term evolution of BHs from large initial separations through merger, and will be discussed in detail elsewhere.

We also dynamically adapt our gauges to the horizon location so as to approximate co-motion. Individual horizons are located often during the evolution using the finder described in [12]. From the motion of the horizon centroid, the angular and radial positions and velocities are determined. Using a damped harmonic oscillator equation, the acceleration needed to bring the horizon centroid back to the initial position is determined by $\ddot{\lambda} = -[2TQ\dot{\lambda} + (\lambda - \lambda^0)]/T^2$. Here λ stands for either the current azimuthal angle ϕ or radius $r = \sqrt{x^2+y^2}$ in the orbital plane, and λ^0 for its initial value. T and Q are constants determining the timescale and damping factor of the harmonic oscillator. The correction is added to the time derivative of the shift vector as $\Delta\dot{\beta}^i = (-y,x,0)^i\,\ddot{\theta} - (x,y,0)^i\,\ddot{r}/r^0$. The punctures are excised using an extension of the "simple excision" techniques which have proven successful in evolving single BH spacetimes [13, 14]. In particular, we apply the boundary condition to an embedded boundary whose shape is determined by the horizon location, as described in [15, 2].

Spatial differentiation is performed via straightforward finite-differencing, incorporating nested mesh-refined grids with the highest resolution concentrated in the neighbourhood of the individual horizons. The mesh refinement is implemented via the Carpet driver [16] for Cactus. The evolutions carried out in this paper made use of 8 levels of fixed 2:1 refinement. We fix the regions of increased resolution around the initial BH locations. Because we are making use of a BH-adapted gauge, the individual horizons remain on the fine grids throughout the evolution without requiring moving grids or excised regions. We have used finest grid resolutions of $h = 0.025M, 0.02M, 0.018M, 0.015M$ and $0.0125M$, with an outer boundary at $96M$ in all cases. Our overall finite differencing accuracy is second order in space and time.

3 Results and Conclusions

Evolutions were carried out for a number of resolutions and gauge parameters. A first observation, important in interpreting the results of [2, 1], is that the infall coordinate trajectory at a given resolution depends crucially on the gauge choice. The first, which we label "$GC1$", sets $(m,n,p,q,\eta,T,Q) = (0,2,1,1,4,5,1)$. The second gauge choice, "$GC2$", sets parameters to $(4,2,1,4,2,5,1)$. The third gauge choice, "$GC3$", is described below.

We note that for the $GC1$ evolutions at a grid spacing of $h = 0.025M$, the BHs fall together rather rapidly. By coordinate time $t = 75M$, the proper distance between the AHs is down to $L/M = 4.5$. Increasing the resolution to $h = 0.020M$, $h = 0.018M$, and $h = 0.015M$ there is a trend towards longer evolution times before reaching the same separation, though the convergence is slow. For the highest resolution which we have evolved, $h = 0.0125$, the infall to the same separation is delayed to only $t = 88M$.

The evolutions resulting from gauge choice $GC2$ have an entirely different character. At the lowest resolution, with $h = 0.025M$, we find that not only does the system evolve well beyond an orbital time period before a common AH appears, the orbit appears to be elliptical, with proper separation first increasing with time, and then falling back, reaching a separation $L/M = 4.5$ only after $t = 119M$. This behaviour is qualitatively similar to what was reported for the same initial data set in [1]. Increasing the resolution as above, however, we find a faster coalescence as resolution is increased, and the apparent elliptical nature of the orbit disappears.

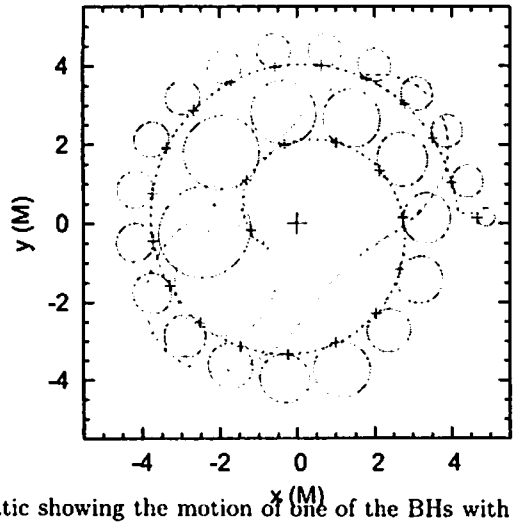

Figure 1: Schematic showing the motion of one of the BHs with time, for the $GC3$ gauge choice at the highest resolution $h = 0.015M$. At intervals of $t = 5M$, the AH cross-sections in the xy plane are plotted by transforming the co-rotating coordinate system by the specified angle and distance. The apparent growth of the AHs with time is a non-physical coordinate effect. The first appearance of a common AH at $t = 124M$, and corresponding final single AH. are shown superposed on the figure as dotted lines.

Importantly, the two families of evolutions corresponding to $GC1$ and $GC2$ do show a tendency towards each other as resolution is increased. In fact, a 3-term Richardson extrapolation (eliminating 2nd and 3rd order error terms) of the computed trajectories show that the two families converge to a common result in the continuum limit.

The differences between $GC1$ and $GC2$ results may at first seem to be the expected result of the variation in slicing condition between the two classes of evolutions. However, the fact that the results converge to the same coordinate trajectory in the continuum limit suggests a somewhat different explanation, namely that the finite difference error inherent in the evolution (particularly in the lapse) can be strongly influenced by the gauge choice.

The Richardson extrapolation provides an indication of the accuracy of the evolutions at a given resolution, or conversely, the resolution required to obtain a result of a given accuracy. The Richardson-extrapolated coordinate trajectory seems robust, but we note that the highest resolution (h=0.0125M) $GC2$ simulations which we have carried out still represent a 22% error in separation at $t = 100M$ compared to the extrapolated result. The sensitive dependence of accuracy on gauge suggests that "ideal" gauge conditions may be able to improve the accuracy greatly at a given resolution.

Based on results of the previous experiments, a third gauge choice parameters was found to demonstrate this point. Under the label $GC3$, evolutions of the same data were carried out using gauge parameters (4,2,1,4,2,5,2.6), i.e. the same as for $GC2$ except for the drift-correction damping parameter.

Fig. 1 plots the overall motions of the AHs for the $GC3$ case. The individual horizon shapes are shown at intervals of $5M$, transformed according to the radial and angular motion determined above. The initial rapid dip in separation can now be seen to be largely a result of the initial coordinate expansion of the individual horizons, due to our choice of zero radial shift in the initial data.

A common AH is first detected at $t = 124M$, by which time an angular displacement of 10.2 radians, or 1.6 revolutions, has taken place. The common horizon is found via the method of pre-tracking, in which a family of surfaces with smallest possible generalised expansion is followed to provide an estimate which converges on the first common AH [17]. The listed time is expected to correspond to the first genuine appearance of a common AH, independent of the search algorithm. Counting backwards from the appearance of the common horizon, the duration of the last orbit is approximately $59M$.

Given the demonstrated resolution dependence of these results, it is likely that these results will be subject to some modification as more accurate evolutions become available. It should also be recalled that a merged event horizon within the slice will have formed earlier than the common AH. Experience

with closely separated binaries suggests this is typically not more than about $5M$ before the appearance of the first common AH, but studies of the event horizon evolution for these spacetimes will need to be the subject of future studies. We also note that the notion of an "orbit" for closely separated BHs is an intrinsically gauge-dependent quantity - for example, a sufficiently small lapse in the region of the horizons could be used to indefinitely delay merger. The slicings used here are quite similar in profile to maximal slices, and thus not atypical for numerical relativity simulations.

The most accurate estimate of the duration of the last complete orbit before formation of the first common AH was $59M$. As might be expected for bodies falling towards each other, this orbital period is considerably less than is predicted by the initial angular velocity, $114M$. The results have been carried out at resolutions much higher than similar studies to date, and exhibit good numerical consistency under a range of resolutions and for a variety of gauge parameter choices.

These evolutions required extremely high resolution to attain good accuracy. Insufficient resolution can result in very different predictions for the orbital trajectories and the period of the final orbit. This period directly influences the phase of asymptotically observed wave forms at their strongest point, and thus is crucial to reproduce accurately.

Acknowledgments. We thank B. Brügmann for many discussions and for sharing details of his codes, M. Ansorg for providing the initial data solver, and L. Rezzolla and M. Alcubierre for many discussions and suggestions. We have used computing time allocations at the AEI, CCT, LRZ, NCSA, NERSC, PSC and RZG. We use the Cactus code infrastructure with a number of locally developed thorns. This work was supported in part by DFG grant SFB TR/7 "Gravitational Wave Astronomy", by the Center for Computation & Technology at LSU, and the Center for Gravitational Wave Physics at PSU.

References

[1] B. Brügmann, W. Tichy, and N. Jansen, Phys. Rev. Lett. **92**, 211101 (2004).

[2] M. Alcubierre *et al.*, Phys. Rev. D **72**, 044004 (2005).

[3] F. Pretorius, Phys. Rev. Lett. **95**, 121101 (2005).

[4] M. Miller, Phys. Rev. D **71**, 104016 (2005).

[5] G. B. Cook, Phys. Rev. D **50**, 5025 (1994).

[6] S. Brandt and B. Brügmann, Phys. Rev. Lett. **78**, 3606 (1997).

[7] M. Ansorg, B. Brügmann, and W. Tichy, Phys. Rev. D **70**, 064011 (2004).

[8] T. Nakamura, K. Oohara, and Y. Kojima, Prog. Theor. Phys. Suppl. **90**, 1 (1987).

[9] M. Shibata and T. Nakamura, Phys. Rev. D **52**, 5428 (1995).

[10] T. W. Baumgarte and S. L. Shapiro, Phys. Rev. D **59**, 024007 (1999).

[11] M. Alcubierre *et al.*, Phys. Rev. D **67**, 084023 (2003).

[12] J. Thornburg, Class. Quantum Grav. **21**, 743 (2004).

[13] M. Alcubierre and B. Brügmann, Phys. Rev. D **63**, 104006 (2001).

[14] M. Alcubierre *et al.*, Phys. Rev. D **64**, 061501(R) (2001).

[15] M. Alcubierre *et al.* (unpublished).

[16] E. Schnetter, S. H. Hawley, and I. Hawke, Class. Quantum Grav. **21**, 1465 (2004).

[17] E. Schnetter, F. Herrmann, and D. Pollney, Phys. Rev. D **71**, 044033 (2005).

Gravitational wave from realistic stellar collapse : odd parity perturbation

Kenta Kiuchi[1], Ken-ichiro Nakazato[2] , Kei Kotake,[3] Kohsuke Sumiyoshi,[4] Shoichi Yamada[5]

[1]*Department of Physics, Waseda University, Okubo, 3-4-1, Shinjuku-ku, Tokyo 169-8555, Japan*
[2]*Science and Engineering, Waseda University, Okubo, 3-4-1, Shinjuku, Tokyo 169-8555, Japan*
[3]*Numazu College of Technology, Ooka 3600, Numazu, Shizuoka 410-8501, Japan*
[4]*Science and Engineering, Waseda University, Okubo, 3-4-1, Shinjuku, Tokyo 169-8555, Japan*
[5]*Science and Engineering, Waseda University, Okubo, 3-4-1, Shinjuku, Tokyo 169-8555, Japan*

Abstract

We study gravitational wave from massive stellar core collapse with the spherical symmetry. We choose a perfect fluid with the realistic equation of state as a matter. The gauge-invariant approach is adopted to estimate the gravitational wave. Performing the numerical simulation, the waveform and the frequency for $l = 2$ are obtained. Analyzing the result of the simulation, we find that the gravitaional wave is produced at the core bounce. The frequency is about 1Hz.

1 Introduction

For a future gravitational wave (G.W.) astronomy, it is very important to make theoretical templates of G.Ws. from any kinds of relativistic dynamical system. In this work, we focus on G.W. from a massive stellar core collapse. In many previous works in which the G.Ws from such a kind of source have been studied, it is standard scenario that rotation of stellar core breaks down the spherical symmetry and produce the G.W. as a result. Some works adapted the rapidly rotating core collapse model. But the recent work reported by Heger et al. show that the rotation of the star is not so rapid [1]. Taking account of this result, we consider that there is a possibility that the spherical symmetry preserves under gravitational core collapses. This implies that the linear perturbation approach is efficient to estimate G.Ws. from stellar core collapses. On the other hand, there are many intensive works using this perturbation approach under the dynamical background [2]-[4]. But one cannot say that the templates for detection have been made completely, because the stellar models have been simplified in these works, e.g., dust ball or polytropic EOS. Therefore, our purpose is to analyze G.Ws. from realistic stellar collapses by using the perturbation approach. For simplicity, we only consider the odd parity mode for perturbation. Throughout this paper, we use the geometrical unit $c = G = 1$.

2 Basic equations

We simply write down set of the basic equations. The details are shown in [5, 6] and references therein. The background spacetime is specified by

$$ds^2 = -e^{2\phi}d\tau^2 + e^{2\lambda}d\mu^2 + r^2 d\Omega^2, \quad (interior\ \ metric) \tag{1}$$

$$ds^2 = -\left(1 - \frac{2M}{R}\right)dT^2 + \left(1 - \frac{2M}{R}\right)^{-1} dR^2 + R^2 d\Omega^2, \quad (exterior\ \ metric) \tag{2}$$

$$T_{\mu\nu} = (\rho_b(1+e) + P)u_\mu u_\nu + P g_{\mu\nu}, \quad (interior\ \ matter) \tag{3}$$

$$u^\mu = (u^\tau, 0, 0, 0), \quad (comoving\ \ coordinate) \tag{4}$$

$$4\pi\rho_b r^2 e^\lambda = 1 \quad (mass\ \ coordinate) \tag{5}$$

[1]E-mail:kiuchi@gravity.phys.waseda.ac.jp
[2]E-mail:nakazato@heap.phys.waseda.ac.jp
[3]E-mail:kkotake@heap.phys.waseda.ac.jp
[4]E-mail:sumi@numazu-ct.ac.jp
[5]E-mail:shoichi@heap.phys.waseda.ac.jp

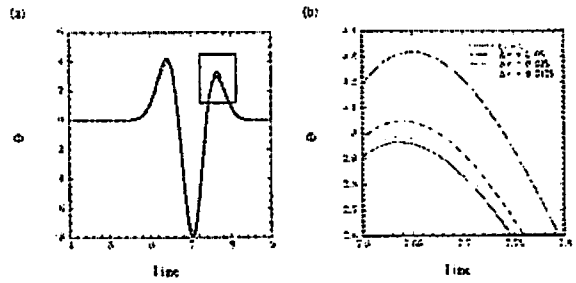

Figure 1: Linear gravitational waveforms for $l = 2$ in the Minkowski spacetime extracted at r = 5. Three levels of the grid resolutions as Δr = 0.05, 0.025, and 0.0125. (b) is the magnification of the region encompassed by the square in (a).

where $d\Omega^2 = \sin^2\theta^2 d\theta^2 + d\phi^2$, ρ_b, e, P and u^μ are the rest-mass density, the specific internal energy, the pressure and the fluid four-velocity, respectively. We use the equation of state developed by Shen et al. [7]. This EOS is based on the relativistic mean field theory. The detail of the hydrodynamic calculation is shown in [8].
The perturbation equations and some conditions for the odd parity are given as follow:
(a) Interior field equation

$$-(\frac{e^{-\phi+\lambda}}{r^2}(r^4\Pi)_{,r})_{,r} + (\frac{e^{\phi-\lambda}}{r^2}(r^4\Pi)_{,\mu})_{,\mu} - (l-1)(l+2)e^{\phi+\lambda}\Pi = -16\pi[e^{\phi}\beta(\rho_b(1+e)+P)]_{,\mu}, \quad (6)$$

where $\Pi(\tau,\mu)$ and $\beta(\tau,\mu)$ are a gravitational perturbation and fluid velocity one for odd parity, respectively.
(b) Conserved quantity

$$4\pi j(\mu) = -h(\tau,\mu)\beta(\tau,\mu), \quad (7)$$

where $h \equiv 1 + e + P/\rho_b$ is the relativistic enthalpy.
(c) Exterior field equation

$$-\Phi_{,TT} + \Phi_{,R_*R_*} - \left(1 - \frac{2M}{R}\right)\left(\frac{l(l+1)}{R^2} - \frac{6M}{R^3}\right)\Phi = 0, \quad (8)$$

where Φ is the Regge-Wheeler variable [9].
(d) Matching condition on the surface

$$\Pi = R^3\Phi, \quad (9)$$

$$e^{-\lambda}\Pi_{,\mu} + 16\pi R^{-2}\beta(\rho_b(1+e)+P) = U/(1-2M/R)\Phi_{,T} + \Gamma\Phi_{,R}, \quad (10)$$

where $U \equiv e^{-\phi}R_{,\tau}$ and $\Gamma \equiv e^{-\lambda}R_{,\mu}$.
(e) Regularity condition at the origin

$$\Pi = r^{l-2}\bar{\Pi}, \quad (11)$$

$$\beta = r^{l+1}\bar{\beta}, \quad (12)$$

where $\bar{\Pi}$ and $\bar{\beta}$ are regular function at the origin.

3 Code Test

To check the accuracy of our code, we perform the two kinds of test simulations. The first check is the linear gravitational wave propagating in the Minkowski space time. This is analytic solution of Eq. (6) for $l = 2$, which is the regular at the origin [10]. This solution is given by

$$\Pi = 3\frac{I(t-r) - I(t+r)}{r^5} + 3\frac{I'(t-r) + I'(t+r)}{r^4} + \frac{I''(t-r) - I''(t+r)}{r^3}, \quad (13)$$

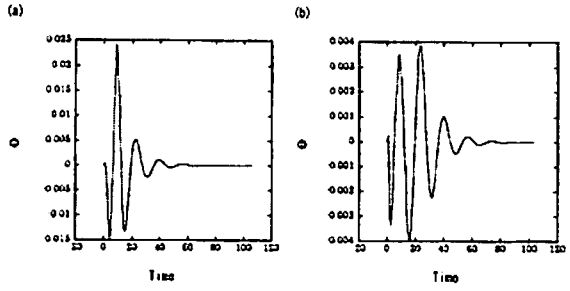

Figure 2: Gravitational wave for l = 2 from the Oppenheimer-Snyder dust collapse with initial radius $R = 4M$. We set the momentarily static initial date with (a)$\tilde{\beta}_{int} = \exp[-(R/R_c)^2]$ and (b)$\tilde{\beta}_{int}$ =const., the radius R_c is chosen to be one-third of the initial radius of the dust ball.

where I is an arbitray function, and I' its derivative. Here, we choose

$$I(x) = \exp[-4(x-2)^2]. \tag{14}$$

In Fig. 1 we show the numerical results with the exact solution for the waveforms observed at r = 5. To demonstrate the convergence of the numerical solutions, we performed the simulations with three levels of the grid resolution as $\Delta r = 0.05, 0.025, 0.0125$. Figure 1 shows that numerical results converge at second order to the exact solution.

Next we computed the propagation of gravitational waves in the collapse of a homogeneous dust ball. Following [4], we give the two kinds of matter perturbation, (a) $\tilde{\beta}_{int} = \exp[-(R/R_c)^2]$ and (b)$\tilde{\beta}_{int}$ =const.. We also set the momentarily static initial condition. Fig. 2 shows the waveforms for l = 2 from a collapsing dust ball with initial radius $R = 4M$. Gravitational waves are extracted at $R = 40M$. As found in [2], the quasinormal mode ringing oscillation characterize the gravitational waveforms. The complex frequency of the fundamental quasinormal mode was calculated to be $2M\omega = 0.74734 + 0.17792i$. On the other hand, our numerical results show that the real part of the frequency is given by $\mathrm{Re}(2M\omega) = 0.751$. Thus, the numerical results agree with the theoretical value within 1% error for the frequency.

4 Numerical Result

We choose two kinds of stellar collapse as the background. One is the core which has 1.5 solar mass and this model occurs the core bounce. This is the model of supernova explosion. The other core has 13.5 solar mass, which collapses to the black hole, and models population III star. For both models, we set the momentarily static condition on the initial surface and the matter perturbation as $\tilde{\beta}_{int} = \exp[-(R/R_c)^2]$, Rs is the same as before. In this work, we only give one kind of matter perturbation for simplicity.

4.1 Model A : type II supernova explosion

We show the numerical results in Fig. 3. Fig. 3(a) shows the gravitational waveform. This waveform is similar to the typical waveform, which is emitted at the core bounce of massive core collapse. We also estimate a frequency of this burst-type gravitational wave. The frequency is about 1 Hz. This value is within the frequency bands of the ground-base detectors, e.g., TAMA, LIGO. Next, we analyze what generates the gravitational wave. Fig. 3(b) shows the trajectories of the mass shell and represents that the core bounce occurred around 0.32s. Fig. 3(c) is the time variation of the lapse function. From this figure, we confirm that the lapse function becomes small at the core bounce, that is the magnitude of the gravity becomes larger. As a result, the gravitational wave generates.

4.2 Model B : Pop III Star

In the Model B, the background calculation stopped before the gravitational wave reach to the observer because of black hole formation. One of method to avoid this problem is the single null formulation [4].

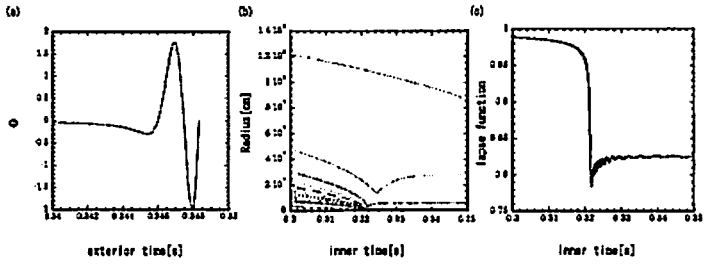

Figure 3: (a) Gravitational wave for $l = 2$ from the realistic stellar core collapse. We set the momentarily static initial date with $\bar{\beta}_{int} = \exp[-(R/R_c)^2]$, the radius R_c is chosen to be one-third of the initial radius of the core, (b) the trajectories of the mass shell, and (c) the lapse function.

Using this formulation, one can perform the hydrodynamic simulation just before black hole forms. But our hydrodynamic code is made to solve the Boltzman equation for neutrino transfer under the metric (1). Therefore, it is a not simple problem to restructure the code for single null formulation. In stead of this method, we plane to perform black hole excision.

5 Conclusion

In this work, we estimate gravitational waves emitted from general relativistic and realistic stellar collapse. To calculate the wave form, we use the gauge-invariant approach. The results are that in the Model A, the gravitational wave is generated at the core bounce and its frequency is about 1 Hz and in the Model B, black hole formation prevents performing the long-time numerical calculation. Therefore we cannot see the G.W. reaching to the observer.
The future works are following :
1. Black hole excision
2. The dependence of G.W. for the matter perturbation (initial condition).
3. The dependence of G.W. for initial stellar model.
4. Including the neutrino effect.

References

[1] A. Heger, S. E. Woosley and H. C. Spruit, Astrophys. J. **626**, 350 (2005) [arXiv:astro-ph/0409422].

[2] C. T. Cunningham, R. H. Price and V. Moncrief, Astrophys. J. **224**, 643 (1978); **230**, 870 (1979); **236**, 674 (1979).

[3] E. Seidel and T. Moore, Phys. Rev. D **35**, 2287 (1987); **38**, 2349 (1988); **42**, 1884 (1990).

[4] T. Harada, H. Iguchi and M. Shibata, Phys. Rev. D **68**, 024002 (2003)

[5] U. H. Gerlach and U. K. Sengupta, D **19**, 2268 (1979).

[6] J. M. Martin-Garcia and C. Gundlach, Phys. Rev. D **61**, 084024 (2000); **64**, 024012 (2001)

[7] H. Shen, H. Toki, K. Oyamatsu and K. Sumiyoshi, Nucl. Phys. A **637** (1998) 435

[8] K. Nakazato, K. Sumiyoshi and S. Yamada, arXiv:astro-ph/0509868.

[9] T. Regge, Phys. Rev. **108**, 1063 (1957).

[10] S. A. Teukolsky, Phys. Rev. D **26**, 745 (1982).

The Evolution of the 'Constants' of Motion in the Kerr Background

Katsuhiko Ganz[1], Wataru Hikida[2], Norichika Sago[3], Hiroyuki Nakano[4], and Takahiro Tanaka[5]

[1,5] *Department of Physics, Graduate School of Science, Kyoto University, Kyoto 606-8502, Japan*
[2] *Yukawa Institute for Theoretical Physics, Kyoto University, Kyoto 606-8502, Japan*
[3] *Department of Earth and Space Science, Graduate School of Science, Osaka University, Toyonaka 560-0043, Japan*
[4] *Department of Mathematics and Physics, Graduate School of Science, Osaka City University, Osaka 558-8585, Japan*

Abstract

The orbit of a particle (mass μ) around the Kerr black hole (mass M) is approximately geodesic in the zeroth order of μ/M, and is characterized by three 'constants' of motion, the energy, angular momentum, and Carter constant. In the next order, the orbit deviates from geodesic by the effect of radiation reation. We give the change rates of these 'constants' of motion in the addiabatic approximation analytically.

1 Introduction

A binary system composed of a supermassive black hole (SMBH) and a compact object (CO) is one of the most important gravitational wave target for space based interferometers such as LISA[1], DECIGO[2]/ BBO[3]. This system provides us with an opportunity for testing general relativity in the strong gravity region. However, to extract physical information from signal, we have to prepare accurate theoretical wave templates.

Wave forms are constructed by means of blackhole perturbation method. The background is the Kerr spacetime, and we treat CO as a point particle. The orbit of CO is approximately geodesic in the zeroth order of μ/M, M is the mass of SMBH, and μ is that of CO. But in the next order, the orbit deviates from geodesic because of the gravitational radiation reaction effect.

If the SMBH is the Schwarzchild black hole, the orbit of CO is characterized by two parameters, the energy E, and angular momentum L. In this case, we can describe the deviation from the geodesic as the evolution of E and L. Fortunately, we can calculate the change rates of E and L by the assymptotic amplitude of gravitaional waves, since the change rates of E and L of CO should balance with the energy and angular momentum fluxes of gravitational waves in the assymptotic region.

But, in the case of the Kerr backgrond, it is not so easy. The geodesic orbit in the Kerr background is characterized by three parameters. We need the Carter constant Q besides E, and L. The evolution of the Carter constant is not obtained from the amplitude of gravitaional waves because there is no conserved current correspond to Q for gravitational waves. Therefore we have to investigate the radiation reaction force, and directly to calculate the change rate of the Carter constant.

The radiation reaction force is calculated from the self field of the CO. However, this self field diverges at the location of CO. Thus we have to regularize the self field. But if we use the adiabatic approximation, we can calculate the change rate of the Carter constant without regularization [4], and in this paper, we calculate for general orbits under the conditions that the eccentricity $e \ll 1$, and the radius of orbit r is $r \gg M$.

2 Geodesic Motion

The Kerr background spacetime is

$$ds^2 = -\left(1 - \frac{2Mr}{\Sigma}\right)dt^2 - \frac{4Mar\sin^2\theta}{\Sigma}dtd\varphi + \frac{\Sigma}{\Delta}dr^2 + \Sigma\, d\theta^2 + \left(r^2 + a^2 + \frac{2Ma^2r\sin^2\theta}{\Sigma}\right)\sin^2\theta d\varphi^2, \quad (1)$$

[1] E-mail:ganz@tap.scphys.kyoto-u.ac.jp

with $\Delta \equiv r^2 - 2Mr + a^2$ and $\Sigma \equiv r^2 + a^2\cos^2\theta$. The geodesic motion of the CO is characterized by three constants of motion,

$$\begin{aligned} E/\mu &\equiv -u^\alpha \xi^{(t)}_\alpha = \left(1 - \frac{2Mr}{\Sigma}\right) u^t + \frac{2Mar\sin^2\theta}{\Sigma} u^\varphi, \\ L/\mu &\equiv u^\alpha \xi^{(\varphi)}_\alpha = -\frac{2Mar\sin^2\theta}{\Sigma} u^t + \frac{(r^2+a^2)^2 - \Delta a^2\sin^2\theta}{\Sigma}\sin^2\theta u^\varphi, \\ Q/\mu^2 &\equiv K_{\alpha\beta}u^\alpha u^\beta = \frac{(L - aE\sin^2\theta)^2}{\sin^2\theta} + a^2\cos^2\theta + \Sigma^2 (u^\theta)^2, \end{aligned} \tag{2}$$

where u^α is four velocity of the CO. $\xi^{(t)}_\alpha$ and $\xi^{(\varphi)}_\alpha$ are the timelike and azimuthal Killing vectors, and $K_{\alpha\beta} \equiv 2\Sigma \ell_{(\alpha} n_{\beta)} + r^2 g_{\alpha\beta}$ is the Killing tensor. $\ell^\alpha \equiv ((r^2+a^2), \Delta, 0, a)/\Delta$ and $n^\alpha \equiv ((r^2+a^2), -\Delta, 0, a)/(2\Sigma)$, are the Newman-Penrose null vectors.

Using these constants of motion, we have

$$\begin{aligned} &\left(\frac{dr}{d\lambda}\right)^2 = R(r), \quad \left(\frac{d\cos\theta}{d\lambda}\right)^2 = \Theta(\cos\theta), \\ &\frac{dt}{d\lambda} = -a(aE\sin^2\theta - L) + \frac{r^2+a^2}{\Delta}P(r), \quad \frac{d\varphi}{d\lambda} = -aE + \frac{L}{\sin^2\theta} + \frac{a}{\Delta}P(r), \end{aligned} \tag{3}$$

$$\begin{aligned} &P(r) = E(r^2+a^2) - aL, \quad R(r) = [P(r)]^2 - \Delta[r^2 + Q], \\ &\Theta(\cos\theta) = C - (C + a^2(1-E^2) + L^2)\cos^2\theta + a^2(1-E^2)\cos^4\theta. \end{aligned} \tag{4}$$

λ is related to the proper time τ by $d\lambda = d\tau/\Sigma$. C is also called the Carter constant and the relation between C and Q is $C \equiv Q - (aE - L)^2$. Apparently, orbits in the equatorial plane ($\cos\theta = 0$) satisfy $C = 0$. We note that the right hand side of the equation of $dr/d\lambda$ does not depend on $\cos\theta$, t, φ. Similarly, that of $d\cos\theta/d\lambda$ also does not contain r, t, φ. Therefore for bound orbits, r and $\cos\theta$ oscillate independently with frequencies Ω_r and Ω_θ. In the case of t and φ, the right hand sides are separated into r-dependent terms, and $\cos\theta$-dependent terms. So, each of t and φ is expressed as a linear combination of a r-oscillation term, a θ-oscillation term, and a term proportional to λ.

3 Adiabatic Approximation

The adiabatic approximation requires two conditions. 1) The orbit of CO is approximately a geodesic in the background metric. 2) The radiation reaction time scale is long enough. The first condition will be satisfied for $\mu/M \ll 1$ because the deviation from geodesic is μ/M effect. The validity of the second condition is not so obvious. But as far as the secular changes of E,L, and Q are concerned, it is sufficient to calculate averaged effect because the periodic deviation cancels out after the long time average.

The averaged change rate of the energy is evaluated as:

$$\left\langle \frac{dE}{d\lambda} \right\rangle = \lim_{T\to\infty} \frac{-\mu}{2T} \int_{-T}^{T} d\lambda \Sigma \xi^{(t)}_\alpha f^\alpha, \tag{5}$$

where f^α is the self force of the CO constructed by the regularized self field $h^{\rm ret.}$,

$$f^\alpha[h] = -\frac{1}{2}(g^{\alpha\beta} + u^\alpha u^\beta)(h^{\rm ret.}_{\beta\gamma;\delta} + h^{\rm ret.}_{\beta\delta;\gamma} - h^{\rm ret.}_{\gamma\delta;\beta})u^\gamma u^\delta. \tag{6}$$

where "ret." means "retarded". In the same manner, we have

$$\begin{aligned} \left\langle \frac{dL}{d\lambda} \right\rangle &= \lim_{T\to\infty} \frac{\mu}{2T} \int_{-T}^{T} d\lambda \Sigma \xi^{(\varphi)}_\alpha f^\alpha, \\ \left\langle \frac{dQ}{d\lambda} \right\rangle &= \lim_{T\to\infty} \frac{\mu^2}{2T} \int_{-T}^{T} d\lambda\, 2\Sigma K_{\alpha\beta} u^\alpha f^\beta. \end{aligned} \tag{7}$$

In Ref. [5], it was shown that we can use the radiative field, $h^{\rm rad.} \equiv (h^{\rm ret.} - h^{\rm adv.})/2$, in place of the regularized retarded field ("adv." means "advanced"). The most important point is that this radiative field does not contain singularity at the location of CO. Therefore we do not have to worry about regularization.

Gal'tsov [6] showed that the above $< dE/dt >$ and $< dL/dt >$ can be expressed as,

$$\left\langle \frac{dE}{dt} \right\rangle = -\mu^2 \sum_{\ell m n_r n_\theta} \frac{1}{4\pi\omega^2_{mn_rn_\theta}} \left(|Z^{\infty}_{\ell m n_r n_\theta}|^2 + \frac{\omega_{mn_rn_\theta}}{k_{mn_rn_\theta}} |Z^{\rm hor.}_{\ell m n_r n_\theta}|^2 \right), \tag{8}$$

$$\left\langle \frac{dL}{dt} \right\rangle = -\mu^2 \sum_{\ell m n_r n_\theta} \frac{m}{4\pi\omega^3_{mn_rn_\theta}} \left(|Z^{\infty}_{\ell m n_r n_\theta}|^2 + \frac{\omega_{mn_rn_\theta}}{k_{mn_rn_\theta}} |Z^{\rm hor.}_{\ell m n_r n_\theta}|^2 \right). \tag{9}$$

$Z^{\infty/\rm hor.}$ is the partial wave amplitude of the Teukolsky variable at the infinity/horizon. $\omega_{mn_rn_\theta}$ is

$$\omega_{mn_rn_\theta} \equiv \left\langle \frac{dt}{d\lambda} \right\rangle^{-1} \left(m \left\langle \frac{d\varphi}{d\lambda} \right\rangle + n_r\Omega_r + n_\theta\Omega_\theta \right), \tag{10}$$

where n_r and n_θ are the indices of the overtone with respect to r-oscillation and θ-oscillation. Apparently, these formulas are identical to the energy and angular momentum fluxes of gravitational waves.

In the case of the Carter constant [4], analogous reduction has been done recently:

$$\begin{aligned} \left\langle \frac{dQ}{dt} \right\rangle = {} & 2\mu \left\langle \frac{(r^2+a^2)P}{\Delta} \right\rangle \left\langle \frac{dE}{dt} \right\rangle - 2\mu \left\langle \frac{aP}{\Delta} \right\rangle \left\langle \frac{dL}{dt} \right\rangle \\ & + \mu^3 \sum_{\ell m n_r n_\theta} \frac{n_r\Omega_r}{2\pi\omega^3_{mn_r,n_\theta}} \left(|Z^{\infty}_{\ell m n_r n_\theta}|^2 + \frac{\omega_{mn_rn_\theta}}{k_{mn_rn_\theta}} |Z^{\rm hor.}_{\ell m n_r n_\theta}|^2 \right). \end{aligned} \tag{11}$$

4 Analytic Approach

We apply these formulas (8), (9) and (11) to CO orbit. In this paper, we ignore the abdorption into the horizon.

There are two approaches to obtain the change rates of the 'constants' of motion: numerical approach and analytic approach. In the numerical approach, we can obtain the change rates without any approximarions. But numerical computation needs calculation for each orbit(not for general orbit). On the other hand, in the analytic approach, we can obtain the change rates for general orbits simulutaneously. Moreover, if we have analytic formulas of the time evolution of orbits, it is easy to apply it to analyse of the observational data. Therefore, we consider an the analytic approach here.

For a bounded orbit, dr/d vanishes at the perihelion and aphelion. Thus, we define the eccentricity e as

$$R\left(\frac{r_0}{1+e}\right) = 0, \quad R\left(\frac{r_0}{1-e}\right) = 0. \tag{12}$$

We call r_0 the semimajor axis of the CO orbit.

Here, we use two expansions. (1) Post-Newton expansion: $v^2 \equiv M/r_0 \ll 1$. (2) Small eccentricity expansion: $e \ll 1$. With these expansions, the differential equation of r is solved as a finite fourier sum whose period is Ω_r. With regard to the incliation angle, we define new variable $Y = (C + L^2)/L^2$. Orbits with $Y = 1$ are in the equatorial plane, and orbits with $Y = \infty$ cross z-axis. Using Y, and previous two expansions, $\cos\theta$ is also expressed as a finite fourier sum whose period is Ω_θ.

After calculating geodesic orbits, we solve the Teukolsky equation. Once we obtain the homogeneous solution of the Teukolsky equation, we can calculate the amplitude of gravitational wave by means of Green function method. There is analytical mathod to construct the homogeneous solution of the Teukolsky equation: Mano-Suzuki-Takasugi method [7, 8]. Finally, using (8), (9) and (11), we evaluate the change rate of E, L, and C.

5 Result

The change rates of the 'constants' of motion are as follows:

$$
\begin{aligned}
\left\langle \frac{dE}{dt} \right\rangle &= -\frac{32\mu^2}{5M^2} v^{10} (1-e^2)^{3/2} \left[\left(1 + \frac{73}{24} e^2\right) - \left(\frac{1247}{336} + \frac{9181}{672} e^2\right) v^2 - \left(\frac{73}{12Y} + \frac{823}{24Y} e^2\right) qv^3 \right. \\
&\quad \left. + \left(4 + \frac{1375}{48} e^2\right) \pi v^3 - \left(\frac{44711}{9072} + \frac{172157}{2592} e^2\right) v^4 - \left(\frac{329}{96} - \frac{527}{96Y^2} + \left\{\frac{4379}{192} - \frac{6533}{192Y^2}\right\} e^2\right) q^2 v^4 \right], \\
\left\langle \frac{dL}{dt} \right\rangle &= -\frac{32\mu^2}{5M} v^7 (1-e^2)^{3/2} \left[\left(\frac{1}{Y} + \frac{7}{8Y} e^2\right) - \left(\frac{1247}{336Y} + \frac{425}{336Y} e^2\right) v^2 + \left(\frac{61}{24} - \frac{61}{8Y^2} + \left\{\frac{63}{8} - \frac{91}{4Y^2}\right\} e^2\right) qv^3 \right. \\
&\quad \left. + \left(\frac{4}{Y} + \frac{97}{8Y} e^2\right) \pi v^3 - \left(\frac{44711}{9072Y} + \frac{302893}{6048Y} e^2\right) v^4 - \left(\frac{57}{16Y} - \frac{45}{8Y^3} + \left\{\frac{201}{16Y} - \frac{37}{2Y^3}\right\} e^2\right) q^2 v^4 \right], \\
\left\langle \frac{dC}{dt} \right\rangle &= -\frac{64\mu^3}{5} v^6 (1-e^2)^{3/2} \left(\frac{Y^2-1}{Y^2}\right) \left[\left(1 + \frac{7}{8} e^2\right) - \left(\frac{743}{336} - \frac{23}{42} e^2\right) v^2 - \left(\frac{85}{8Y} + \frac{211}{8Y} e^2\right) qv^3 \right. \\
&\quad \left. + \left(4 + \frac{97}{8} e^2\right) \pi v^3 - \left(\frac{129193}{18144} + \frac{84035}{1728} e^2\right) v^4 - \left(\frac{329}{96} - \frac{53}{8Y^2} + \left\{\frac{929}{96} - \frac{163}{8Y^2}\right\} e^2\right) q^2 v^4 \right], \qquad (13)
\end{aligned}
$$

where $q = a/M$. These results are factorized by $(1-e^2)^{3/2}$ to ease compare with the well-known Peters and Mathews flux. As there is one-to-one relation between $\{E, L, Q\}$ and $\{e, v, Y\}$, so we can write the evolution of $\{e, v, Y\}$ as

$$
\begin{aligned}
\frac{dv}{dt} &= \frac{32}{5} \left(\frac{\mu}{M^2}\right) v^9 (1-e^2)^{3/2} \left[\left(1 + \frac{7}{8} e^2\right) - \left(\frac{743}{336} + \frac{55}{21} e^2\right) v^2 - \left(\frac{133}{12Y} + \frac{379}{24Y} e^2\right) qv^3 \right. \\
&\quad \left. + \left(4 + \frac{97}{8} e^2\right) \pi v^3 + \left(\frac{34103}{18144} - \frac{526955}{12096} e^2\right) v^4 - \left(\frac{329}{96} - \frac{815}{96Y^2} + \left\{\frac{929}{96} - \frac{477}{32Y^2}\right\} e^2\right) q^2 v^4 \right], \\
\frac{de}{dt} &= -\frac{304}{15} \left(\frac{\mu}{M^2}\right) v^8 e (1-e^2)^{3/2} \left[\left(1 + \frac{121}{304} e^2\right) - \left(\frac{6849}{2128} + \frac{4509}{2128} e^2\right) v^2 - \left(\frac{879}{76Y} + \frac{515}{76Y} e^2\right) qv^3 \right. \\
&\quad \left. + \left(\frac{985}{152} + \frac{5969}{608} e^2\right) \pi v^3 - \left(\frac{286397}{38304} + \frac{2064415}{51072} e^2\right) v^4 - \left(\frac{3179}{608} - \frac{5869}{608Y^2} + \left\{\frac{8925}{1216} - \frac{10747}{1216Y^2}\right\} e^2\right) q^2 v^4 \right], \\
\frac{dY}{dt} &= \frac{244}{15} \left(\frac{\mu}{M^2}\right) v^8 (1-e^2)^{3/2} (Y^2-1) \\
&\quad \times \left[\left(1 + \frac{189}{61} e^2\right) qv^3 - \left(\frac{13}{244Y} + \frac{277}{244Y} e^2\right) q^2 v^4 - \left(\frac{10461}{1708} + \frac{83723}{3416} e^2\right) qv^5 \right]. \qquad (14)
\end{aligned}
$$

If the orbit is initially in the equatorial plane ($Y = 1$), the orbit is always in it. But if the orbit has initial inclination, it increases (decreases) for a corotating (counterrotating) orbit. Finally, we note that the evolution timescale of the inclination is $\mathcal{O}(v^3)$ higher than those of e, v. Therefore we expect that the inclination angle changes little by the radiation reaction.

References

[1] LISA web page: http://lisa.jpl.nasa.gov/

[2] N. Seto, S. Kawamura and T. Nakamura, Phys. Rev. Lett. **87**, 221103 (2001).

[3] BBO web page: http://universe.gsfc.nasa.gov/program/bbo.html

[4] N. Sago, T Tanaka, W. Hikida, and H. Nakano, Prog. Theor. Phys. **114**, 509 (2005).

[5] Y. Mino, Phys. Rev. D **67**, 084027 (2003).

[6] D. V. Gal'tsov, J. Phys. A **15**, 3737 (1982).

[7] S. Mano, H. Suzuki and E. Takasugi, Prog. Theor. Phys. **95**, 1079 (1996).

[8] S. Mano and E. Takasugi, Prog. Theor. Phys. **97**, 213 (1997).

Progress in observational two-body problem

Hideki Asada[1]

Faculty of Science and Technology, Hirosaki University, 036-8561, Japan

Abstract

The orbit determination for a Newtonian binary is solved exactly and completely by Asada, Akasaka and Kasai. Here, this solution is extended to a case of a realistic observational data. Furthermore, it is generalized to a parabolic or hyperbolic orbit.

1 Introduction

The two-body problem was raised when Kepler found the laws for motion of celestial objects. It was solved by Newton in his gravity theory.

The inclination of the orbital plane with respect to the line of slight causes an observational problem: How do we determine a orbit and mass from observation ?

In a body in our solar system, the method was given by Gauss and improved later by Laplace and many people. These are all historical issues. Thus one may think that there were nothing to do any more in this subject. However, it is not true of a two-body system outside the solar system. Namely, the observational two-body problem has been solved very partly because only for a visual binary, in which both stars can be observed, the exact method was found by Thiele-Innes in 1886. In the twentieth century, we have recognized widely an astrometric binary, which consists of a visible star and an unseen object such as a black hole, neutron star. The exact method for orbit determination of the astrometric binary system was not known. At last, Asada, Akasaka and Kasai have found the exact solution [1].

In practice, the least square method needs numerical calculations. One may thus ask a question: Is AAK formula practically useful?

The answer is yes. I will show it briefly in the following.

2 Extending the AAK formula

First, we summarize the AAK formula [1]. Observations at five epochs determine a position of the primary star at $(\bar{x}_i, \bar{y}_i)$ for $i = 1, \cdots, 5$. The five points are located on an ellipse written as

$$\frac{x^2}{a^2} + \frac{y^2}{b^2} = 1. \tag{1}$$

We take four points at time t_i $(i = 1, \cdots, 4)$ $\mathbf{P}_i = (x_i, y_i) = (a\cos u_i, b\sin u_i)$. To avoid Kepler equation, we use the time interval as $t_{ij} \equiv t_i - t_j$. The original Keplerian orbit is specified by a_K, e_K, T.

An important quantity is the position of the projected common center of mass (COM) denoted by (x_e, y_e). Even after the projection, the areal velocity is constant, where the area is swept around the projected COM.

This fact allows us to determine (x_e, y_e) in the form as

$$x_e = -a\frac{A_2B_3 - A_3B_2}{A_1B_2 - A_2B_1}, \tag{2}$$

$$y_e = b\frac{A_3B_1 - A_1B_3}{A_1B_2 - A_2B_1}. \tag{3}$$

The remaining quantities are obtained geometrically or algebraically.

$$e_K = \sqrt{\frac{x_e^2}{a^2} + \frac{y_e^2}{b^2}}. \tag{4}$$

[1]E-mail:asada@phys.hirosaki-u.ac.jp

$$a_K = \sqrt{\frac{C^2 + D^2}{1 + \cos^2 i}}, \tag{5}$$

$$\cos 2\omega = \frac{C^2 - D^2}{a_K^2 \sin^2 i}, \tag{6}$$

where

$$C = \frac{1}{e_K}\sqrt{x_e^2 + y_e^2}, \tag{7}$$

$$D = \frac{1}{abe_K}\sqrt{\frac{a^4 y_e^2 + b^4 x_e^2}{1 - e_K^2}}, \tag{8}$$

$$\xi = \frac{(C^2 + D^2)\sqrt{1 - e_K^2}}{ab}. \tag{9}$$

The extended solution to a realistic case assuming a Gaussian random error and the arbitrary number of observations denoted by n is given in the form of [2]

$$x_e = -\frac{a}{{}_nC_4}\sum_j \frac{F_jG_{j+1} - G_jF_{j+1}}{E_jF_{j+1} - F_jE_{j+1}}. \tag{10}$$

$$y_e = \frac{b}{{}_nC_4}\sum_j \frac{G_jE_{j+1} - E_jG_{j+1}}{E_jF_{j+1} - F_jE_{j+1}}. \tag{11}$$

e_K, $\cos i$, a_K, $\cos 2\omega$ take the same form.

3 Conclusion

The complete exact solution to the observational two-body problem has been found [1]. It has been extended to a realistic observational data [2]. Furthermore, it has been generalized to a parabolic or hyperbolic orbit [3].

References

[1] Asada H., Akasaka T., Kasai M., PASJ., 56, L35 (2004)

[2] Asada H., Akasaka T., Kudoh K., submitted to Cel. Mech.

[3] Asada H., submitted to Cel. Mech.

Operator geometry and algebraic quantum gravity

Masaru Siino[1]

Department of Physics, Tokyo Institute of Technology,
Oh-Okayama 1-12-1, Megro-ku, Tokyo 152-8550, Japan

Abstract

An algebraic formulation of general relativity is proposed. The formulation is available to quantum gravity and noncommutative space. To investigate the quantum gravity we develop the canonical formalism of operator geometry, after reconstructing an abstract canonical formulation on analytical mechanics. The remarkable fact is that the constraint equation of the gravitational system is algebraically solvable. From the discussion of regularization we find the quantum correction of the semi-classical gravity is same as that already known in graviton one-loop calculus.

1 Introduction

There is no doubt that the essence of quantum theory is the noncommutativity of operator algebra for physical variables. Usually, this noncommutativity reflects the ordering of quantum observations. In quantum gravity, how can we understand the noncommutativity? One standard is the framework of field theory where the gravity is decomposed into a fluctuation of potential and background geometry. As long as the gravity is sufficiently weak, that will promise to treat spacetime geometry.

Since general relativity is remarkably non-linear theory, however, we are afraid that strong gravity drastically changes background geometry. Indeed, the topological instanton of quantum gravity implies the microscopic nontriviality of topology for spacetime. In this sense one should care the topological structure as a physical variable. Then one see such a topological variable, for example, a representation by Wilson loop or moduli parameter. If we complete the topological variable, one might treat the open neighborhoods of spacetime points, whose set and coordinate transformation yields a concept of manifold. Roughly speaking, considering all open neighborhoods as physical variable is similar to regarding their own spacetime points as physical variables by themselves. This will realize any noncommutativity through quantization of spacetime dynamics. Of course, though such an idea is an imaginary picture without mathematical background, in the context of noncommutative geometry, algebraic consideration, that is given by abstraction of geometry, will realize the concept of noncommutativity of spacetime points! Then we hope the investigation of the noncommutative geometry sheds light on the dark side of quantum gravity.

In a sense, noncommutative geometry is a kind of movement in the mathematical community to change ordinary multiplication which appears in many aspects of analytical geometry into noncommutative multiplication. The most successful framework to study the noncommutative space has been established by A. Connes and is well known by his textbook. In the study of the noncommutative geometry, the most important concept is abstraction of conventional commutative geometry. While ordinary commutative geometry is constructed on a space with any mathematical structure, noncommutative geometry should be developed on an operator algebra which acts on a Hilbert space. So we will require abstraction of gravity theory when we concern noncommutative gravity theory. We will have corresponding algebraic objects instead of the conventional objects with which we realize geometry, that is, topological space, differentiable manifold and Riemannian manifold. The counter part of them are a set of continuous function, pseudodifferential operators and a Dirac operator; and are defined in the framework of a commutative operator algebra. Now that the things have come to such pass, the operator algebra naturally extends from commutative to noncommutative.

Here it should be emphasized that by the noncommutative extension, space may lose its continuity or differentiability. The most terrible thing might be missing of reasonable measure which is indispensable

[1]E-mail:msiino@th.phys.titech.ac.jp

to develop physics theory there. Nevertheless the framework of the spectral geometry established by Connes provide the substantial structure that is appropriate trace of operators. So the terribleness becomes rather interest in the extension of the concept of space, which is what we imagine as the world of quantum gravity.

Of course we convince that our world is commutative as far as our eye can reach. In the sense that relativists studies spacetime dynamics, however, there are two motivations to consider noncommutative space. One is interest about the characteristic of real noncommutative space. For example, the noncommutative torus or the space of irreducible Penrose tiling is a famous model of noncommutative space. The noncommutative torus of irrotational ring is known as not Lebesgue measurable space. The set of the Penrose tiling is an equivalence class of Cantor set. We want to investigate the dynamics of such pathological structures, so that we reach the answer why our world is not so pathological, for instance, why our spacetime dimension is integer (with n-dimensional Lebesgue measurable), why we live in a locally compact space, and why our macroscopic world is commutative.

The other is virtual interest that on considering quantum gravity, not only commutative spacetime but also noncommutative spacetime should be included in the contour of path integral as fluctuation of spacetime. Recently many authors study the quantum space, in the standpoint that in quantum scale spacetime should be noncommutative. The same is expected by the calculation of string theory. The most valid way, however, to include the noncommutative quantum space might be to formulate the gravity in an algebraic manner. In the present mission, we want to apply the algebraic consideration to general relativity with the aid of elegant works by Connes and other authorized mathematicians.

In the study of quantum theory of gravitation, the string theory is paid the most attention and it seems there have been much progress. In exchange of that, the string theory force us uncomfortable changes of our outlook on the world, for example extra dimensional spacetime, infinite number of vacuum state, and so on. On the other hand, the outlook of the world in the loop gravity theory might be easier to accept than that of the string theory but it is still hard to understand the whole of quantum gravity. Of course, as quantum mechanics is, not only one formulation of quantum gravity would be available. It is rather complementary and cooperative to develop various formulations. We expect the noncommutative study becomes a lost puzzle-peace of quantum gravity.

In those viewpoints, it is promising to develop the quantum gravity in the context of noncommutative geometry. The main purpose of the present article is reformulate general relativity with the tools of operator algebra. One will get a new equations of gravitation as the algebraic equation of bounded operators on a Hilbert space. Then we advance toward quantum geometry through the canonical theory of that and will find that constraint equation is formally solved. Moreover from a semi-classical effect on such algebraic gravity we rephrase the quantum correction of graviton one-loop. Though the full quantization is postponed until forthcoming works, it is possible to discuss the ability of the algebraic formulation in study of quantum gravity.

1.1 topological notion and Connes' axioms

To develop the noncommutative geometry, the abstraction of topological notion is fundamental. That is based on the following Gel'fand-Naĭmark's two theorems.

Theorem 1 (Gel'fand-Naĭmark 1). *If $\mathcal{A}$ is a commutative C^*-algebra, the Gel'fand transformation is an isometric $*$-isomorphism of $\mathcal{A}$ onto $C_0(M(\mathcal{A}))$.*

There $M(\mathcal{A})$ is the spectrum space which is a set of all characters μ (the unitarily equivalence class of irreducible representation) with Gel'fand topology. Gel'fand transformation of $a \in \mathcal{A}$ is the function $\hat{a} : M(\mathcal{A}) \mapsto \mathbf{C}$ given by

$$\hat{a}(\mu) := \mu(a). \tag{1}$$

If $\mathcal{A}$ is unital, M is compact. For instance, the convolution algebra $\mathcal{A} = L^1(\mathbb{R})$ of Lebesgue-integrable functions of $\mathbb{R}$ is a nonunital algebra whose characters are the integrals $f \mapsto \int_{\mathbf{R}} e^{-itx} f(x)$ for any $t \in \mathbb{R}$ then $\hat{f}$ is the Fourier transform of f, and the Gel'fand transformation is the Fourier transformation that takes $L^1(\mathbb{R})$ into $C_0(\mathbb{R})$.

This theorem insist that $C_0(M)$ can work instead of topological space M. All topological information about M is algebraically stored within $C_0(M)$. We do gain the insight to go beyond conventional topology by regarding a noncommutative C^*-algebra as a kind of function algebra for a virtual of noncommutative topological space this viewpoint also allows one to study the topology of non-Hausdorff space such as arise in probing a continuum where points are unresolved.

The second theorem of Gel'fand-Naĭmark states that any C^*-algebra can be embedded as a norm-closed subalgebra of a full algebra of operators for a large enough Hilbert space $\mathcal{H}$;

Theorem 2 (Gel'fand-Naĭmark 2). *Any C^*-algebra has an isometric representation as a closed subalgebra of the algebra $\mathcal{L}(\mathcal{H})$ of bounded operators on some Hilbert space.*

Thus all C^*-algebras are fairly concrete. Indeed, $C(M)$ may be embedded in $\mathcal{L}(\mathcal{H})$, the algebra of bounded operators on the Hilbert space $\mathcal{H}$ with a countable orthonormal basis, in many ways: if M is infinite but separable, take ν to be any finite regular Borel measure on M, and identify $\mathcal{H}$ with $L^2(M, d\nu)$; then $f \in C(M) \subset L^\infty(M, d\nu)$ can be identified with the multiplication operator $h \mapsto fh$ on $L^2(M, d\nu)$.

It is in the spirit of noncommutative geometry to relax closure conditions as much as possible when defining our algebras; for instance, if M is a compact differential manifold, we would like to use the algebra of smooth functions $\mathcal{A} = C^\infty(M)$, which is a dense subalgebra of $C(M)$. Of course, we are able to consider noncommutative algebra instead. Then corresponding space is no longer than locally compact or continuous. These possibilities are not discussed in detail in the present article.

To take an extension of general relativity to such noncommutative spacetime, so called noncommutative gravity models provide a good guidance. At least three gravity models are possible approaches. They are 'gravity à la Connes-Dixmier-Wodzicki', 'spectral gravity', and 'linear connections'. Former two are essentially same but with different spirit. In the spirit of spectral gravity, the eigenvalues of the Dirac operator, which are diffeomorphic invariant functions of the geometry and therefore true observable in general relativity, have been taken as a set of variables for an invariant description of the dynamics of the gravitational field.

In the present article, we develop the algebraic formulation of general relativity in the sense of gravity à la Connes-Dixmier-Wodzicki. Similar trial was carried by Hawkins, but in his formulation spacetime concept is not included since only the spacelike section is noncommutative there. As one can see later, the noncommutativity in the direction of evolution is the essence of the present work. That is closely related to the quantum theory of geometry. Our purpose is to establish a algebraically formulated dynamics of geometry. To do so, we develop the dynamical equation of fundamental operator that is Dirac operator.

The scheme to construct gravity models in noncommutative geometry, and in fact to reconstruct the full geometry out of the algebra $C^\infty(M)$, is based on the Dirac operator (a spectral triple) and the use of the Dixmier trace and Wodzicki residue. That is Connes' axioms of noncommutative gravity presented as

Connes' axioms 1. *Suppose we have a smooth compact manifold M without boundary and of dimension n. Let $\mathcal{A} = C^\infty(M)$ and $\mathcal{D}$ just a 'symbol' for the time being. Let $(\mathcal{A}_\pi, \mathcal{D}_\pi)$ be a unitary representation of the couple $(\mathcal{A}, \mathcal{D})$ as operators on an Hilbert space $\mathcal{H}_\pi$ such that $(\mathcal{A}_\pi, \mathcal{D}_\pi, \mathcal{H}_\pi)$ satisfy axioms of a spectral triple (also called an unbounded K-cycle). Then*

1. *There is a unique Riemann metric $g = g(\mathcal{D})$ on M, whose geodesic distance between any two points on M is given by*

$$d_g(p, q) = \sup\{|f(p) - f(q)| : ||[\mathcal{D}, f]|| \leq 1, f \in C^\infty(M)\}, \quad \forall p, q \in M \tag{2}$$

2. *The metric g depends only on the unitary equivalence class of the representations to metrics form a finite collection of affine spaces $\mathcal{A}_\sigma$ parametrized by the spin structures σ on M.*

3. *The action functional given by the Wodzicki residue*

$$S(\mathcal{D}) \sim \mathrm{Wres}(\mathcal{D}^{2-n}) \tag{3}$$

is a positive quadratic form with a unique minimum π_σ on each $\mathcal{A}_\pi$. The minimum π_σ is the representation of $(\mathcal{A}, \mathcal{D})$ on the Hilbert space of square integrable spinors $L^2(M, S_\sigma)$; $\mathcal{A}_\sigma$ acts by multiplicative operators and $\mathcal{D}_\sigma$ is the Dirac operator of the Levi-Civita connection.

4. *At the minimum π_σ, the values of $S(\mathcal{D})$ coincides with the Wodzicki residue of $\mathcal{D}_\sigma^{n-2}$ and is proportional to the Einstein-Hilbert action of general relativity*

$$S(\mathcal{D}_\sigma) = \mathrm{Wres}(\mathcal{D}_\sigma^{2-n}) = c_n \int_M R dv \tag{4}$$

According to this Connes' axioms, we develop the formulation of gravity by operator algebra ('operator geometry') and its canonical dynamics. We will find that the constraint equation of gravitational system is algebraically solvable. Though we do not plunge into the construction of full quantum theory in the present article, in the semi-classical discussion of regularization, it is clarified that quantum correction of the gravitational action is given by the heat kernel expansion, that is same as the already well-known one in the quantum field theory of curved space.

In section 2, we briefly introduce some elements of noncommutative geometry as an fundamental concepts and express fundamental frameworks of spectral calculus developed by Connes and other authors. The Connes' axioms will have been developed in this section. In section 3, we develop the canonical formulation of algebraically formulated gravitation based on the section 2, after giving an abstraction of analytical mechanics. The relation between operator geometry and classical gravity is investigated in section 4. Furthermore we discuss the quantum effects there. The final section is devoted to conclusion and discussions.

The notation related to the noncommutative geometry is according to the Reference.

2 conclusion and discussions

We have developed a new formulation of gravity ('operator geometry') which is expressed in the context of operator algebra. The geometrical values of the operator geometry are expressed by a Dirac operator algebraically defined as a spectral triple. A newly established abstract analytical mechanics gives the dynamics of the operator geometry. Then a Hamiltonian formalism is given. Remarkably it is found that the constraint equation is formally solved under quantum assumption of regularity.

Finally we have argued that the classical equation which is the continuous limit of discrete system by the quantum assumption and the semi-classical effect as a correction of the continuous (large dimensional Hilbert space) limit. We have found the semi-classical action agrees with just known result of one-loop correction of graviton. To understand the discretized or truncated aspects of gravitation the noncommutativity of operators arises. From that one may realize that the eigenstate of position loses its privileged classical meaning in quantum scale. Then pure states will take place as a component of quantum space. A full quantization of the operator geometry is postponed to the forthcoming work.

Along with the present work we have some possibilities of noncommutative space to study. For example, a commutative algebra on a quotient space has the same spectral space as that of another algebra by crossed product in the noncommutative geometry. Sometimes the quotient space suffers topological irregularity; a famous example is Lebesgue non-measurability of a irrational rotation ring, which is isomorphic to noncommutative torus. Even with such an irregularity, the present formulation would work; at least in the above example, noncommutative geometry is well established.

Moreover we expect the formulation is also applicable to other singular spacetime. At first sight, this seems probable for the singularity allowing a self-adjoint extension since we have a sound Dirac operator there without knowing the topological structure of the singularity. After we understand the problem algebraically, K-theory may help to understand that in topologically.

To include matter field, some idea are succeeding. The simplest step is to include the cosmological constant. Since $V = \int dv \propto \mathrm{Tr}^+|D|^{-n}$ from the Connes theorem, the contribution of cosmological constant would be $\Lambda \mathrm{Tr}|D|^{-n}$. It is easy to extend the geometry to fiber bundle which is determined as an idempotent algebraically. in order to have gauge boson. Furthermore considering discrete geometry the Higgs sector is able to be contained. The interaction with fermions, which has the right hypercharge assignment, is obtained directly from $< \psi, D\psi >$ (with $D + A + JAJ^{-1}$ instead of D), and is thus also of spectral nature being invariant under the full unitary group of operators in Hilbert space. Along that the standard model is proposed by Connes and Chamseddine. Hybrid of the model and the present formulation may be possible to study for further progress.

Classification of cohomogeneity-one membranes

Hiroshi Kozaki[1] and Hideki Ishihara[2]

Department of Mathematics and Physics, Graduate School of Science, Osaka City University, Sugimoto, Sumiyoshi-ku, Osaka, 558-8585, Japan

Abstract

We define the cohomogeneity-one membrane as its world surface is foliated by two-dimensional orbits of an isometry group of a target space. We classify pairs and triplets of the Killing vectors which constitute Lie algebra by an equivalence relation using isometries of the target space. We find that i) triplets of the Killing vectors which span two-dimensional spaces with non-degenerate metric are fallen into five classes, ii) pairs of the Killing vectors which span two-dimensional spaces with non-degenerate metric are classified into infinite number of equivalence classes which are partitioned into one isolated class, one two-parameter families and seven one-parameter families, iii) triplets of the Killing vectors which span two-dimensional spaces with degenerate metric have only one equivalence class and iv) there is no pairs of the Killing vectors which spans two-dimensional spaces with degenerate metric. It is clarified that there are as many classes of cohomogeneity-one membranes as the pairs and triplets of the Killing vectors listed above.

The brane universe models have gathered much attention for several years. A matter of main interest is the embedding of a symmetric brane in a bulk spacetime. The effective Einstein equations induced on the brane have an additional term which comes from the Weyl curvature of the bulk spacetime [1]. In the context of brane world cosmology, this term will appear in the evolution equations of the universe. Therefore, there will be differences between the conventional cosmology and the brane world cosmology. These differences can be prospective testing of the brane world scenarios.

A simple model of a FRW brane has been found so far [2]. In this model, the FRW brane is embedded in the five-dimensional analog of the Schwarzschild-anti-de Sitter (Sch-AdS) spacetime, and the analog of the Friedmann equation also has been derived. The modified Friedmann equation has an additional term which comes from the Weyl curvature of the bulk spacetime and behaves as radiation. This behavior may be characteristic to the Sch-AdS bulk spacetime. If the FRW brane is embedded in another bulk spacetime, behavior of this term may be different. Therefore, embedding of the FRW brane in another bulk spacetime should be pursued.

The conventional approach to find a consistent embedding is not to fix the bulk geometry, but to take ansatz for the bulk metric which equips desired symmetry to embed a symmetric brane. Then, we solve the Einstein equations. However, the Einstein equations have still complicated form and cannot be solved exactly except for some special cases which include the Sch-AdS spacetime.

We propose another approach to find an embedding of a symmetric brane. First, we fix the bulk to a highly symmetric spacetime, such as AdS^5. And then, we find an isometry subgroup whose orbits span three-dimensional constant curvature spaces. If there are two isometry subgroups whose orbits span the same constant curvature spaces with different extrinsic curvatures, two kind of embeddings of brane universe with the same intrinsic symmetry will be possible. If it is possible, there are two FRW branes with the same curvature but different evolution in the same bulk spacetime.

As a preliminary investigation of the brane universe models, we consider the cohomogeneity-one membranes in the four-dimensional Minkowski spacetime. The world surface of the cohomogeneity-one membrane is foliated by orbits of an isometry subgroup which span two-dimensional spaces. In the scope of the FRW brane, i.e., a brane with spatial homogeneity and isotropy, the orbit must span two-dimensional constant curvature space.

On the other hand, general cohomogeneity-one membranes are important in the context of domain wall dynamics. Due to the symmetry on the world surface, the equations of motion are reduced to

[1]E-mail:furusaki@sci.osaka-cu.ac.jp
[2]E-mail:ishihara@sci.osaka-cu.ac.jp

ordinary differential equations. Then, we can easily analyze the dynamics. Several authors investigated stationary membranes which are the special cases of cohomogeneity-one membranes, and clarified rich properties [3, 4].

In this paper, we clarify how many cohomogeneity-one membranes exist in the four-dimensional Minkowski spacetime upto the action of isometry. In order to do so, we find out every isometry subgroup whose orbits span two-dimensional space, and then, we classify them by an equivalence relation using the isometry of the target space.

The world surface of the cohomogeneity-one membrane is a three-dimensional submanifold which is foliated by orbits of an isometry subgroup, say H. Since the restricted action of H on its orbit is also isometry with respect to the induced metric on it, the dimension of H is restricted upto 3. Therefore, $\dim H = 2, 3$. Considering infinitesimal transformation of H on the orbit, the Killing vectors which generate H are tangent to the orbit. We denote the Lie algebra of the Killing vectors as h. Corresponding to $\dim H = 2, 3$, we have $\dim h = 2, 3$.

In the case of $\dim h = 3$ and orbits with nondegenerate metrics, the orbit spans a two-dimensional constant curvature space(time). Then, h is isomorphic to the Lie algebra of the Killing vectors in the constant curvature space(time). In terms of the Bianchi classification of three-dimensional Lie algebras, h must be isomorphic to one of the Lie algebras of the Bianchi type VI_0, VII_0, VIII and IX.

In case of $\dim h = 2$ and orbits with nondegenerate metrics, the orbit also spans two-dimensional constant curvature space(time) by the Fubini theorem. In terms of the intrinsic geometry on the orbit, there are three independent Killing vector on it. However, only two of three Killing vectors can be Killing vectors of the target space, and they constitute h. Therefore, h must be included in the Lie algebras of the Killing vectors of constant curvature space(time) as a subalgebra. It is easily shown that soluble algebras cannot be included as a subalgebra. Then, h must be a commutative Lie algebra.

Now, we introduce the equivalence relation. Let us consider a pair of three-dimensional world surface, Σ_A and Σ_B, embedded in a symmetric target space $(\mathcal{M}, g_{ab})$ with an isometry group G. The world surfaces Σ_A and Σ_B are geometrically equivalent if there is an isometry $\phi \in G$ which maps Σ_A onto Σ_B:

$$\phi : \Sigma_A \to \Sigma_B. \tag{1}$$

Next, let Σ_A be a cohomogeneity-one world surface which is tangent to linearly independent Killing vectors ξ_i ($i = 1, 2, 3$ or $1, 2$). The isometry ϕ which maps Σ_A onto Σ_B pushes forward the Killing vector fields ξ_i to vector fields, say ξ'_i:

$$\phi^* : \xi_i \to \xi'_i. \tag{2}$$

It is evident that ξ'_i are also Killing vector fields and Σ_B is tangent to them, i.e., Σ_B is a cohomogeneity-one world surface tangent to the Killing vectors ξ'_i. Note that ξ_i and ξ'_i satisfy the same commutation relation, since a push-forward of an isometry preserves a commutation relation.

The above observations suggest an equivalence relation, $\sim$, among the pairs or the triplets of the Killing vectors which constitute Lie algebra. Let h_A and h_B be the Lie algebras of the pairs or triplets of the Killing vectors $\{\xi_i^{(A)}\}$ and $\{\xi_i^{(B)}\}$. $\{\xi_i^{(A)}\}$ and $\{\xi_i^{(B)}\}$ are equivalent if there is an isometry ϕ of the target space $(\mathcal{M}, g_{ab})$ such that its push forward ϕ^* is an isomorphism between h_A and h_B:

$$\phi^* : h_A \to h_B. \tag{3}$$

We classify two-dimensional commutative subalgebras and three-dimensional Bianchi type VI_0, VII_0, VIII, IX subalgebras of Killing vectors in the Minkowski spacetime based on the equivalence relation introduced above. In the Minkowski spacetime with the metric

$$ds^2 = -dt^2 + dx^2 + dy^2 + dz^2, \tag{4}$$

there are ten independent Killing vectors:

P_a $(a = t, x, y, z)$,	translation along a-direction,	(5)
K_i $(i = x, y, z)$,	Lorentz boost along i-direction,	(6)
L_i $(i = x, y, z)$,	spatial rotation around i-axis.	(7)

	Bianchi type	basis	orbits	isometric to
1	I	—	—	—
2	II	$\{P_t - P_x, K_z - L_y, -P_z\}$	$t + x, y = \text{const.}$	—
3	VI_0	$\{P_t, P_x, K_x\}$	$y, z = \text{const.}$	Minkowski
4	VII_0	$\{P_x, P_y, L_z\}$	$t, z = \text{const.}$	Euclid
5	VII_0	$\{K_x + L_y, K_y - L_x, L_z\}$	$\eta, \zeta = \text{const.}$	Euclid
6	VIII	$\{K_x, K_y, L_z\}$	$-t^2 + x^2 + y^2 = -a^2$	Hyperbolic
			$-t^2 + x^2 + y^2 = a^2$	dS spacetime
7	IX	$\{L_x, L_y, L_z\}$	$x^2 + y^2 + z^2 = a^2$	S^2

Table 1: Equivalence classes of three-dimensional Lie algebras Representatives of three-dimensional Lie algebras of Killing vectors. Basis of the Killing vectors and the corresponding orbits are listed. Lie algebras of the Killing of the constant curvature space(time)s are those of type 3 to 7. The type 1 and type 2 are added in order to complete the comparison with the G_3A of the Bianchi classification. The type 1 include three-dimensional commutative Lie algebras. Hence, they do not span two-dimensional orbits. The type 2 class of algebras or orbits are found as null orbits spanned by three independent Killing vectors.

An arbitrary Killing vector can be written as their linear combination.

The strategy is as follows: First, we find every subalgebra of Killing vectors in the Minkowski spacetime satisfying the conditions noted above. In this process, we make use of the result of the classification of the Killing vectors [5], in which the Killing vectors of the Minkowski spacetime are classified into seven families upto actions of isometries. We can generally take one of the Killing vectors in the seven families as ξ_1 since ξ_1 is always reduced to one of the element in the seven families by an isometries. Then, we find the counterparts in the pairs or the triplets of the Killing vectors. Next, we classify the subalgebras, or the pairs and the triplets of the Killing vectors, based on the equivalence relation introduced above and list inequivalent representatives of equivalence classes.

In the case of $\dim h = 3$, we find that there are five equivalence classes of three Killing vectors which form a subalgebra and span two-dimensional tangent space. In Table 1, we list the representatives of the equivalence classes and corresponding orbits.

The equivalence classes 3, 4, 5, 6 and 7 include the constant curvature spaces spanned by orbits with non-degenerate metrics. Among them, classes 3, 4, 6 and 7 consist only of the trivial orbits which have been expected before the classifications. The equivalence class 5 is the new finding. Although the intrinsic geometries of type 5 orbits are identical to that of the type 4, i.e., two-dimensional Minkowski spacetime, the extrinsic geometries differ.

There are not any orbits isometric to AdS^2. AdS^2 is originally defined as a hyperboloid in a three-dimensional flat spacetime with unusual signature $(-,-,+)$, i.e., two timelike directions are needed to embed AdS^2. Then, orbits isometric to AdS^2 cannot be realized in the Minkowski spacetime whose signature is $(-,+,+,+)$.

In the case of $\dim h = 2$, we find that there are infinite number of equivalence classes. However, the set of all equivalence classes are partitioned into one isolated equivalence class whose representative is

$$\{K_x, L_x\}, \tag{8}$$

one two-parameter family whose representatives are written by two-parameter a and b as follows:

$$\{(K_y + L_z) + aP_z + bP_y, (K_z - L_y) + aP_y - bP_z, \} \tag{9}$$

and five one-parameter families listed in Table 2. In the table, we have introduced a notation, $\boxplus$, such that

$$\{P_t, P_x \boxplus L_x\} := \left\{ \{P_t, aP_x + bL_x\} \middle| a \geq 0, b \geq 0, a^2 + b^2 = 1 \right\}. \tag{10}$$

The constraints on a and b are for eliminating the total scaling of Killing vectors or basis of the Lie algebra and redundancy under space and time reflections.

	basis	$\det \gamma_{ab}$
T1	$\{P_t, P_x \boxplus L_x\}$	$-a^2 - b^2(y^2 + z^2)$
S1	$\{P_x, P_t \boxplus L_x\}$	$-a^2 + b^2(y^2 + z^2)$
S2	$\{P_x, P_y \boxplus K_z\}$	$a^2 + b^2(t^2 - z^2)$
S3	$\{P_x, (P_t + P_y) \boxplus (K_z + L_x)\}$	$-4abz + b^2(t + y)^2$
N1	$\{P_t + P_x, P_z \boxplus (K_y - L_z)\}$	0
N2	$\{P_t + P_x, P_x \boxplus L_x\}$	$-a^2$
N3	$\{P_t + P_x, P_x \boxplus (K_y - L_z)\}$	$-a^2$

Table 2: Representatives of one-parameter families of equivalence classes of subalgebras of two-dimensions. a and b are non-negative constants satisfying $a^2 + b^2 = 1$. Determinants of the induced metric γ_{ab} on the orbits spanned by the basis are shown.

Finally, we consider the case that the orbits span spaces with degenerate metrics. In this case, the structure of the Lie algebra h has not been clarified systematically. Then, we enumerate pairs or triplets of the Killing vectors which constitute Lie algebras of another structure listed above.

In the case of $\dim h = 3$, we enumerate triplets of the Killing vectors which satisfy the commutation relations of the remaining Bianchi types:type II, III, IV, V, VI_h and VII_h and check whether they span two-dimensional spaces with degenerate metric. After the classification upto the action of isometries, we find that there is only one equivalence class of the Bianchi type II. This is the equivalence class 2 in Table 1. Including null orbits, we find that there are two-dimensional orbits which span constant curvature spaces corresponding to three-dimensional Lie algebras of the Bianchi class $G_3\mathrm{A}$ except for the type I. Type I is the commutative Lie algebra, then the orbits are necessarily three-dimensions. In the case of $\dim h = 2$, we find that there is no orbits.

References

[1] T. Shiromizu, K. i. Maeda and M. Sasaki, Phys. Rev. D **62**, 024012 (2000) [arXiv:gr-qc/9910076].

[2] D. Ida, JHEP **0009**, 014 (2000) [arXiv:gr-qc/9912002].

[3] M. Christensen, V. P. Frolov and A. L. Larsen, Phys. Rev. D **58**, 085008 (1998)

[4] V. P. Frolov, A. L. Larsen and M. Christensen, Phys. Rev. D **59**, 125008 (1999)

[5] H. Ishihara and H. Kozaki, Phys. Rev. D **72**, 061701 (2005)

Cosmology with Warped String Compactification

Shinji Mukohyama[1]

Department of Physics and Research Center for the Early Universe, The University of Tokyo, Tokyo 113-0033, Japan

Abstract

It is pointed out that in the warped string compactification, motion of $\bar{D}$-branes near the bottom of a throat behaves like dark matter. Several scenarios for production of the dark matter are suggested, including one based on the $D/\bar{D}$ interaction at the late stage of $D/\bar{D}$ inflation.

1 Introduction

M/string theory is considered as a strong candidate for a unified theory of fundamental physics. Its mathematical consistency and beauty have been attracting interest of many physicists. On the other hand, one of the drawbacks is lack of direct experimental or observational evidence of such a structure at high energies. Having this situation, it seems rather natural to turn our eyes to cosmology and look for cosmological implication of M/string theory since the universe is supposed to have experienced a high energy epoch at its early stage.

Considering the success of inflation as a scenario of the early universe and the observational evidences for accelerating expansion of the present universe, one of the important steps toward establishment of M/string cosmology would be construction of de Sitter or quasi-de Sitter universe. However, for a long time it seemed rather difficult to construct 4-dimensional de Sitter universe in M/string theory, especially if we seriously take account of the moduli stabilization. Indeed, the no-go theorem of [1] says that in a large class of supergravity theories, there is no no-singular (warped) compactification to 4-dimensional de Sitter space with a finite 4-dimensional Newton's constant.

There are several proposals to evade the no-go theorem by inclusion of additional sources such as stringy corrections to the supergravity theories in the g_s or α' expansion and extended sources, i.e. branes. The recent proposal by Kachru, Kallosh, Linde and Trivedi (KKLT) [2] utilizes various ingredients of string theory including warped geometry, fluxes, D-branes, $\bar{D}$-branes, instanton corrections to moduli potential in order to construct a meta-stable de Sitter vacua in string theory. In the KKLT setup $\bar{D}3$-branes play an essential role. Inclusion of $\bar{D}3$-branes at the bottom of a warped throat uplifts stable AdS vacua with negative cosmological constant to meta-stable de Sitter vacua with positive cosmological constant in a theoretically controllable way. Without $\bar{D}3$-branes, we would end up with a negative cosmological constant, which is inconsistent with observations.

The purpose of this paper is to point out that motion of the $\bar{D}3$-branes near the bottom of a warped throat behaves like dark matter [3].

2 $\bar{D}3$-brane in Klebanov-Strassler geometry

In the KKLT setup [2] a throat region is described by the warped deformed conifold solution of Klebanov and Strassler [4]. To be precise, the warped deformed conifold geometry is compactified by additional fluxes as described by Giddings, Kachru and Polchinski [5]. Hence, the geometry in the UV region of the throat significantly deviates from the Klebanov-Strassler solution, but the geometry near the bottom of the throat, i.e. in the IR region, is approximated by the Klebanov-Strassler solution.

When $g_s M$ is sufficiently large, we can treat a $\bar{D}3$-brane as a probe brane [6]. Here, g_s is the string coupling and M is an integer representing the number of R-R flux. In the non-relativistic limit the action

[1]E-mail: mukoyama@phys.s.u-tokyo.ac.jp

for the probe $\bar{D}3$-brane is

$$S_{\bar{D}3} = T_3 \int d^4\xi \left[-\frac{1}{2}\gamma_{mn}\eta^{\alpha\beta}\frac{\partial\psi^m}{\partial\xi^\alpha}\frac{\partial\psi^n}{\partial\xi^\beta} - 2h^{-1} \right]. \tag{1}$$

where T_3 is the brane tension, $\gamma_{mn}d\psi^m d\psi^n$ is the metric of the deformed conifold [7] (whose explicit form in an appropriate limit will be given below) and

$$h(\tau) = 2^{2/3}\cdot(g_s M\alpha')^2\epsilon^{-8/3}\int_\tau^\infty dx \frac{x\coth x - 1}{\sinh^2 x}(\sinh(2x) - 2x)^{1/3}. \tag{2}$$

Hereafter, ϵ is a parameter associated with the large hierarchy stabilized by NS-NS flux.

Let us now consider cosmological implication of this effective action. With moduli stabilization, the 4-dimensional Einstein gravity should be recovered [2]. In cosmological situations, we still expect that the KS geometry is a good approximation to the geometry of extra dimensions in the throat region as far as the energy scale associated with the 4-dimensional physics is sufficiently lower than the stabilization scale. Hence, we promote the action formulated in the flat 4-dimensional spacetime to a curved background $ds_4^2 = g^{(4)}_{\alpha\beta}d\xi^\alpha d\xi^\beta$ as

$$S_{\bar{D}3} = T_3 \int \sqrt{-g^{(4)}}d^4\xi \left[-\frac{1}{2}\gamma_{mn}g^{(4)\alpha\beta}\frac{\partial\psi^m}{\partial\xi^\alpha}\frac{\partial\psi^n}{\partial\xi^\beta} - 2h^{-1} \right]. \tag{3}$$

We expect that this action describes the dynamics of the brane at energy scales sufficiently lower than the stabilization scale. In general, stabilization of the volume modulus introduces corrections to the effective action, in particular to the mass of the fields. However, as far as the mass of the field of interest is much larger than the Hubble expansion rate H, the corrections due to the modulus stabilization should be ignorable.

With the FRW ansatz

$$ds_4^2 = -dt^2 + a(t)^2 d\mathbf{x}^2, \quad \psi^m = \psi^m(t), \tag{4}$$

the equation of motion of ψ^m is

$$\dot{\pi}_m + 3H\pi_m + \frac{\partial}{\partial\psi^m}\rho(\psi,\pi) = 0, \quad \pi_m \equiv T_3\gamma_{mn}\dot{\psi}^n, \tag{5}$$

where a dot denotes the time derivative and

$$\rho(\psi,\pi) \equiv \frac{1}{2T_3}\gamma^{mn}\pi_m\pi_n + 2T_3h^{-1} \tag{6}$$

is the energy density written in terms of ψ^m and π_m.

Hereafter, we consider the $\bar{D}3$-brane near the bottom of the throat $\tau = 0$. Thus, we take the small τ limit of the deformed conifold metric:

$$\gamma_{mn}d\psi^m d\psi^n = \frac{\epsilon^{4/3}}{2}\left(\frac{2}{3}\right)^{1/3}\left\{\frac{1}{2}d\tau^2 + \left[\frac{1}{2}\left(g^5\right)^2 + \left(g^3\right)^2 + \left(g^4\right)^2\right] + \frac{1}{4}\tau^2\left[\left(g^1\right)^2 + \left(g^2\right)^2\right]\right\}, \tag{7}$$

where the first square bracket represents the regular S^3 at the bottom of the throat and the second square bracket represents the shrinking S^2. With this form of the deformed conifold metric, it is shown by using the equations of motion that there are constants of motion J_3^2 and J_2^2 related to the angular momenta along the S^3 and the S^2, respectively. For later convenience the constants of motion J_3^2 and J_2^2 are normalized as

$$\begin{aligned}
\left(\frac{2}{\epsilon^{4/3}T_3}\right)^2\left(\frac{3}{2}\right)^{1/3}\frac{J_3^2}{2a^6} &\equiv \frac{1}{2}\left(g^5(\partial_t)\right)^2 + \left(g^3(\partial_t)\right)^2 + \left(g^4(\partial_t)\right)^2, \\
\left(\frac{8}{\epsilon^{4/3}T_3}\right)^2\left(\frac{3}{2}\right)^{2/3}\frac{J_2^2}{2a^6\tau^4} &\equiv \left(g^1(\partial_t)\right)^2 + \left(g^2(\partial_t)\right)^2.
\end{aligned} \tag{8}$$

[2]Evidence can be seen for the recovery of the 4-dimensional Einstein gravity in a simplified setup of warped flux compactification [8].

It is shown that $a^3\pi_{\phi_1}$ and $a^3\pi_{\phi_2}$ are also constants of motion, but they do not appear in the following discussions. The equation of motion for τ and the energy density ρ are written in terms of J_3^2 and J_2^2 as

$$\ddot{\varphi} + 3H\dot{\varphi} + \left(\frac{\partial V}{\partial \varphi}\right)_a = 0, \quad \rho = \frac{1}{2}\dot{\varphi}^2 + V + \rho_6 + \rho_0, \tag{9}$$

where

$$\begin{aligned} \varphi &\equiv \frac{\sqrt{\epsilon^{4/3}T_3}}{2}\left(\frac{2}{3}\right)^{1/6}\tau, \quad V(\varphi, a) = \frac{1}{2}m^2\varphi^2 + \frac{J_2^2}{2a^6\varphi^2}, \\ \rho_6 &= \frac{1}{\epsilon^{4/3}T_3}\frac{J_3^2}{2a^6}, \quad \rho_0 = 2T_3\, h^{-1}|_{\tau=0}, \end{aligned} \tag{10}$$

and

$$m^2 = \frac{8}{\epsilon^{4/3}}\left(\frac{3}{2}\right)^{1/3}\frac{d^2}{d\tau^2}h^{-1}\Big|_{\tau=0} = \frac{4\cdot 2^{2/3}}{3I_0^2}\frac{\epsilon^{4/3}}{(g_s M\alpha')^2}. \tag{11}$$

Here, $I_0 \simeq 0.71805$.

For $J_2 \neq 0$, the potential V is minimized if φ evolves as

$$\varphi = \sqrt{\left|\frac{J_2}{m}\right|}\frac{1}{a^{3/2}}. \tag{12}$$

Actually, this is a solution to the equation of motion if the FRW universe evolves as $H \propto a^{-3/2}$. (We shall confirm this cosmological evolution below.) With this solution, the energy density ρ is

$$\rho = \left(1 + \frac{9H^2}{8m^2}\right)\rho_3 + \rho_6 + \rho_0, \quad \rho_3 = \frac{|mJ_2|}{a^3}. \tag{13}$$

At low energy we can safely neglect $9H^2/8m^2$ compared to 1. The term ρ_6 can also be neglected since it decays faster than other terms as the universe expands. Therefore, we obtain

$$\rho \simeq \rho_3 + \rho_0. \tag{14}$$

The first term behaves like dark matter while the second term contributes to the cosmological constant. In this paper we shall not try to solve the cosmological constant problem and simply assume that ρ_0 is (almost) canceled by other contributions to the cosmological constant (eg. stabilization of the volume modulus, tension of other branes, etc.). With this assumption, the cosmological energy density is dominated by ρ_3 and it is confirmed that the cosmological evolution is $H \propto a^{3/2}$ as assumed, provided that the Friedmann equation is recovered at low energy. Now let us consider a small perturbation around the solution (12) for $J_2 \neq 0$:

$$\varphi = \sqrt{\left|\frac{J_2}{m}\right|}\frac{1}{a^{3/2}} + \delta\varphi(t). \tag{15}$$

The linearized equation of motion implies that the perturbation $\delta\varphi$ behaves like a massive scalar field with mass $2m$,

$$\delta\ddot{\varphi} + 3H\delta\dot{\varphi} + (2m)^2\delta\varphi = 0, \tag{16}$$

and that the solution (12) is indeed stable. At low energy $H \ll m$, the stress energy tensor due to $\delta\varphi$ behaves like a pressure-less dust ($\propto a^{-3}$) if it is averaged over a timescale sufficiently longer than m^{-1} and sufficiently shorter than H^{-1}.

For $J_2 = 0$, φ behaves as a massive scalar field with mass m and at low energy $H \ll m$, its energy density behaves like a pressure-less dust ($\propto a^{-3}$) if it is averaged over a timescale sufficiently longer than m^{-1} and sufficiently shorter than H^{-1}.

3 Summary

In summary we have shown that the stress energy tensor due to the motion of a $\bar{D}3$-brane near the bottom of a warped throat region behaves like dark matter $\rho \propto a^{-3}$. It is of course possible to consider motion of more than one $\bar{D}3$-branes as multi-component dark matter.

In ref. [3] several scenarios were suggested for the dark matter production. One of them is based on the $D/\bar{D}$ interaction at the late stage of $D/\bar{D}$ inflation. Suppose that inflation in our 4-dimensional universe is driven by the modulus representing the position of a mobile D-brane relative to $\bar{D}$-branes near the bottom of a throat. As argued in ref. [9], a successful inflation in this setup is possible although fine-tuning is required to ensure the flatness of the inflaton potential. The rolling of the inflaton is due to an attractive force between the branes, and the same force inevitably generates the motion of $\bar{D}$-branes as well. Since the $\bar{D}$-brane potential has the minimum at the bottom of the throat, the $\bar{D}$-branes should start moving around the bottom. When the inter-brane distance becomes sufficiently short, the inflation ends and a pair of D- and $\bar{D}$-branes annihilates. The 4-dimensional universe should be reheated by the energy released in the annihilation process. After the annihilation of a $D/\bar{D}$ pair and the reheating of the universe, the remaining $\bar{D}$-branes are still moving around the bottom. As we have shown in this paper, the $\bar{D}$-brane motion around the bottom behaves like dark matter in the 4-dimensional universe.

In order for this scenario to work, it must be made sure that the amount of produced dark matter is not too much. Otherwise, the energy density of the dark matter ($\propto a^{-3}$) would start dominating the radiation energy density ($\propto a^{-4}$) too soon. In the above example, the production is due to the $D/\bar{D}$ interaction and the interaction is very weak by definition: the enough inflation requires a flat potential and the flat potential implies the weak interaction between branes. From this consideration, it is expected that the amount of dark matter (i.e. the amplitude of $\bar{D}$-brane motion) after inflation should be tiny. Very importantly, this expectation seems compatible with the fine-tuning required for successful inflation since both the smallness of the production rate and the flatness of the inflaton potential are related to the weakness of the inter-brane interaction. It is certainly worthwhile quantifying how much fine-tuning this requires.

It is also interesting to investigate motion of various branes and their cosmological consequences, such as inflation [10].

References

[1] B. de Wit, D. J. Smit and N. D. Hari Dass Nucl. Phys. **B283**, 165 (1987); J. M. Maldacena and C. Nunez, Int. J. Mod. Phys. **A16**, 822 (2001) [hep-th/0007018].

[2] S. Kachru, R. Kallosh, A. Linde and S. P. Trivedi, Phys. Rev. **D68**, 046005 (2003) [hep-th/0301240].

[3] S. Mukohyama, Phys. Rev. **D72**, 061901 (2005) [hep-th/0505042].

[4] I. R. Klebanov and M. J. Strassler, JHEP **0008**, 052 (2000) [hep-th/0007191].

[5] S. B. Giddings, S. Kachru, J. Polchinski, Phys. Rev. **D66**, 106006 (2002) [hep-th/0105097].

[6] S. Kachru and L. McAllister, JHEP **0303**, 018 (2003) [hep-th/0205209].

[7] P. Candelas and X. de la Ossa, "Comments on Conifolds," Nucl. Phys. **B342** (1990) 246; R. Minasian and D. Tsimpis, "On the Geometry of Non-trivially Embedded Branes,"hep-th/9911042.

[8] S. Mukohyama, Y. Sendouda, H. Yoshiguchi and S. Kinoshita, JCAP **0507**, 013 (2005) [hep-th/0506050]; H. Yoshiguchi, S. Mukohyama, Y. Sendouda and S. Kinoshita, "Dynamical Stability of Six-dimensional Warped Flux Compactification", hep-th/0512212.

[9] S. Kachru, R. Kallosh, A. Linde, J. Maldacena, L. McAllister, S. P. Trivedi, JCAP **0310**, 013 (2003) [hep-th/0308055].

[10] R. Kallosh, L. Kofman, A. Linde and S. Mukohyama, in preparation.

The spectrum of gravitational waves in Randall-Sundrum braneworld cosmology

Tsutomu Kobayashi[1], Takahiro Tanaka[2]

[1,2]*Department of Physics, Kyoto University, Kyoto 606-8502, Japan*

Abstract

We study the generation and evolution of gravitational waves (tensor perturbations) in the context of Randall-Sundrum braneworld cosmology. We assume that the initial and final stages of the background cosmological model are given by de Sitter and Minkowski phases, respectively, and they are connected smoothly by a radiation-dominated phase. Using the Wronskian formulation, we numerically compute the power spectrum of gravitational waves, and find that the effect of initial vacuum fluctuations in the Kaluza-Klein modes is subdominant, contributing not more than 10% of the total power spectrum. Thus it is confirmed that the damping due to the Kaluza-Klein mode generation and the enhancement due to the modification of the background Friedmann equation are the two dominant effects, but they cancel each other, leading to the same spectral tilt as the standard four-dimensional result.

1 Introduction

Cosmological inflation predicts the gravitational wave background arising due to quantum fluctuations in the graviton field. Gravitational wave fluctuations are stretched beyond the horizon radius by rapid expansion during inflation, and at a later stage they come back inside the horizon possibly with rich information on the early universe and hence on high energy physics. Though yet undetected, gravitational waves will provide us with a powerful tool to probe fundamental physics in near future. Motivated by string theory, recently braneworld scenarios have attached much attention, in which our four-dimensional universe is realized as a brane embedded in a higher dimensional bulk spacetime. In order to reveal five-dimensional effects particular to the braneworld scenario, we have to focus on the scales smaller than the bulk curvature scale ℓ. This is our motivation to study gravitational waves from inflation on the brane.

In the Randall-Sundrum braneworld, at least in the low energy regime ($\ell H \ll 1$) corrections to the evolution of gravitational waves are shown to be small [1]. To understand the evolution of gravitational waves in a much more general and interesting case, i.e., in the high energy ($\ell H \gg 1$) radiation-dominated phase, numerical studies have been done by Hiramatsu *et al.* [2] and by Ichiki and Nakamura [3]. Their results give us a lot of implications, for example, on the damping nature of the gravitational wave amplitude due to the Kaluza-Klein mode generation, but the initial condition they adopt is naive, neglecting initial quantum fluctuations in the Kaluza-Klein modes. Hence, its validity is open to question.

The goal of the present paper is to clarify the late time power spectrum of gravitational waves in the Randall-Sundrum brane cosmology, evolving through the radiation-dominated stage after their generation during inflation. We closely follow the same line as our previous work [4], in which, using the Wronskian formulation, we have formulated a numerical scheme for the braneworld cosmological perturbations. The initial condition in our analysis is imposed quantum-mechanically, and therefore we will be able to obtain a true picture of the generation and evolution of gravitational perturbations in the braneworld. A detailed discussion is done in a much longer paper [5].

[1]E-mail:tsutomu@tap.scphys.kyoto-u.ac.jp
[2]E-mail:tama@scphys.kyoto-u.ac.jp

2 Preliminaries

2.1 The background model

Now we describe a model for the background. We shall work in the cosmological setting of the Randall-Sundrum braneworld, and so the bulk is given by a five-dimensional AdS spacetime. The AdS metric in the Poincoré coordinates is $ds^2 = (\ell/z)^2(-dt^2 + \delta_{ij}dx^i dx^j + dz^2)$, where ℓ is the bulk curvature scale. A cosmological brane moves in this static bulk, the trajectory of which is given by $z = z(t)$. The scale factor of the universe is related to the position of the brane as $a(t) = \ell/z(t)$.

We consider the following cosmological model on the brane. The initial stage of the model is given by de Sitter inflation with a constant Hubble parameter $H = H_i$, which is smoothly connected to the radiation-dominated phase. In the radiation stage the scale factor evolves subject to the modified Friedmann equation $H^2 = (\rho_r/3M_{\rm Pl}^2)(1 + \rho_r/2\sigma)$, where ρ_r is the radiation energy density and $\sigma = 6M_{\rm Pl}^2/\ell^2$ is the tension of the brane. After a period of time the energy scale of the universe becomes sufficiently low, and the radiation-dominated phase is then smoothly connected to the Minkowski phase.

2.2 Minkowski and de Sitter braneworlds

Let us consider tensor perturbations in AdS spacetime bounded by a brane. We can decompose the graviton field into a zero mode and Kaluza-Klein (KK) modes without ambiguity when the brane is maximally symmetric. This is the reason why the initial and final stages of the background model are given by the de Sitter and Minkowski phases, respectively.

As usual we decompose tensor perturbations h_{ij} into the spatial Fourier modes as $h_{ij} = \sqrt{2}/(2\pi M_5)^{3/2}$. $\int d^3k\ \phi_{\mathbf{k}} e^{i\mathbf{k}\cdot\mathbf{x}} e_{ij}$. Here M_5 is the fundamental mass scale which is related to the four-dimensional Planck mass $M_{\rm Pl}$ by $\ell(M_5)^3 = M_{\rm Pl}^2$.

For the analysis of perturbations from the Minkowski brane, the above Poincaré coordinate system will be best suited. It is easy to find mode solutions. Going to quantum theory, the graviton field can be expanded in terms of the zero mode and KK modes as

$$\phi = \hat{A}_0\varphi_0 + \hat{A}_0^\dagger\varphi_0^* + \int_0^\infty dm \left(\hat{A}_m\varphi_m + \hat{A}_m^\dagger\varphi_m^*\right), \tag{1}$$

where $\hat{A}_n$ and $\hat{A}_n^\dagger$ $(n = 0, m)$ are the annihilation and creation operators, respectively, of their corresponding modes. The mode functions form a complete orthonormal basis with respect to the Wronskian. In the de Sitter braneworld we introduce another set of coordinates (η, ξ), which is related to (t, z) as $t = \eta\cosh\xi + t_0$, and $z = -\eta\sinh\xi$, where t_0 is an arbitrary constant. In (η, ξ) frame the de Sitter brane is located at a fixed coordinate position $\xi = \xi_b$ = constant, and the perturbation equation again has a separable form. Treating ϕ as an operator, the graviton field can be expanded as

$$\phi = \hat{a}_0\phi_0 + \hat{a}_0^\dagger\phi_0^* + \int_0^\infty d\nu \left(\hat{a}_\nu\phi_\nu + \hat{a}_\nu^\dagger\phi_\nu^*\right), \tag{2}$$

where $\hat{a}_n$ and $\hat{a}_n^\dagger$ $(n = 0, \nu)$ are the annihilation and creation operators of each mode. These mode functions also form a complete orthonormal basis with respect to the Wronskian.

3 Wronskian formulation

Due to the presence of an infinite tower of Kaluza-Klein modes, cosmological perturbations in the braneworld have infinite degrees of freedom. Instead of solving an initial value problem for such a system, it would be better to use the Wronskian formulation in order to take necessary degrees of freedom out of infinite information. In the present case, we would like to know the final amplitude of the zero mode, and therefore in fact what we need to do is solving the (backward) evolution of a single degree of freedom.

In the double null coordinates $u = t - z$ and $v = t + z$, which will be convenient for numerical calculations, the trajectory of the brane can be specified arbitrarily by $v = q(u)$. By a further coordinate transformation $U = u$ and $q(V) = v$, the bulk metric can be rewritten as $ds^2 =$

$[2\ell/(q(V)-U)]^2[-q'(V)dUdV+\delta_{ij}dx^idx^j]$. Now in the new coordinates the position of the brane is simply given by $U=V$. We will use this coordinate system for actual numerical calculations.

The Klein-Gordon-type equation for a gravitational wave perturbation ϕ in the (U,V) coordinates reduces to

$$\left[4\partial_U\partial_V+\frac{6}{q(V)-U}(\partial_V-q'(V)\,\partial_U)+q'(V)\,k^2\right]\phi=0, \tag{3}$$

supplemented by the boundary condition $[\partial_U-\partial_V]\phi|_{U=V}=0$. The expression for the Wronskian evaluated on a constant V hypersurface is given by

$$(X\cdot Y)=2i\int_{-\infty}^{V}dU\left[\frac{2\ell}{q(V)-U}\right]^3(X\partial_UY^*-Y^*\partial_UX), \tag{4}$$

which is independent of the choice of the hypersurface.

In the initial de Sitter phase, the graviton field can be expanded as Eq. (2), while in the final Minkowski phase it can be expanded as Eq. (1). We assume that initially the gravitons are in the de Sitter invariant vacuum state annihilated by $\hat{a}_0$ and $\hat{a}_\nu$. $\hat{a}_0|0\rangle=\hat{a}_\nu|0\rangle=0$. The final power spectrum is given by

$$\mathcal{P}(k) \;:=\; \frac{4\pi k^3}{(2\pi)^3}\frac{2}{(M_5)^3}\cdot\frac{1}{k\ell}N_f, \tag{5}$$

where $N_f:=\langle 0|\hat{A}_0^\dagger\hat{A}_0|0\rangle$ is the number of created zero mode gravitons. The operator $\hat{A}_0$ can be projected out by making use of the Wronskian relations, and noting that the Wronskian is constant in time we have

$$\hat{A}_0=(\phi\cdot\varphi_0)_f=(\phi\cdot\Phi)=(\phi_0\cdot\Phi)_i\hat{a}_0+\int d\nu(\phi_\nu\cdot\Phi)_i\hat{a}_\nu+\text{ h.c.}, \tag{6}$$

where Φ is a solution of the Klein-Gordon equation (3) whose final configuration is the zero mode function φ_0 in the Minkowski phase, and subscript f and i denote the quantities evaluated on the final and initial hypersurfaces, respectively. Thus we clearly see that final zero mode gravitons are created from the vacuum fluctuations both in the initial zero mode and in the KK modes: $N_f=|(\phi_0^*\cdot\Phi)_i|^2+\int d\nu|(\phi_\nu^*\cdot\Phi)_i|^2$. Correspondingly, the power spectrum (5) can be written as a sum of the two contributions:

$$\mathcal{P}=\mathcal{P}_0+\mathcal{P}_{\rm KK}, \tag{7}$$

where $\mathcal{P}_0:=(k^2/\pi^2M_{\rm Pl}^2)|(\phi_0^*\cdot\Phi)_i|^2$ and $\mathcal{P}_{\rm KK}:=(k^2/\pi^2M_{\rm Pl}^2)\int d\nu|(\phi_\nu^*\cdot\Phi)_i|^2$.

4 Spectrum of gravitational waves

De Sitter inflation on the brane predicts the flat primordial spectrum $\delta_T^2:=[2C^2(\ell H_i)/M_{\rm Pl}^2](H_i/2\pi)^2$ [6]. During inflation the gravitational wave perturbations stretched to super-horizon scales, and then they stays constant until horizon reentry, with their amplitude given by δ_T.

For long wavelength modes with $k\ll k_*$, where $k_*:=a_*H_*=a_*/\ell$ labels the mode that reenters the horizon when $\ell H=1$, the amplitude will decay as $h_{\mu\nu}\propto a^{-1}$ after horizon reentry, because gravity on the brane is basically described by four-dimensional general relativity in the low energy regime ($\ell H\ll 1$). In fact, it is explicitly shown that leading order corrections to the cosmological evolution of gravitational waves are suppressed by ℓ^2 and $\ell^2\ln\ell$ at low energies [1]. In particular, modes with $k<k_0$, where $k_0:=a_0H_0=H_0$, and H_0 is the Hubble parameter evaluated at the end of the radiation-dominated phase (i.e., just before the Minkowski phase), reenter the "horizon" in the final Minkowski phase, and then they begin to oscillate (but their amplitude will not decay). As a result, the mean-square vacuum fluctuations of such modes become half of the initial value, leading to $\mathcal{P}=\delta_T^2/2$ for $k<k_0$. For the reason mentioned above, modes with $k_0<k\ll k_*$ have the standard spectrum $\mathcal{P}=(\delta_T^2/2)(k/k_0)^{-2}$.

Something nontrivial may happen to gravitational waves with $k\gtrsim k_*$. If the effects of mode mixing are neglected, only the modification of the background expansion rate alters the spectrum for these short wavelength modes to $\tilde{\mathcal{P}}\simeq(\delta_T^2/2)(k/k_*)^{-2/3}(k_*/k_0)^{-2}$. However, this evaluation will not be correct because mode mixing is expected to be efficient at high energies.

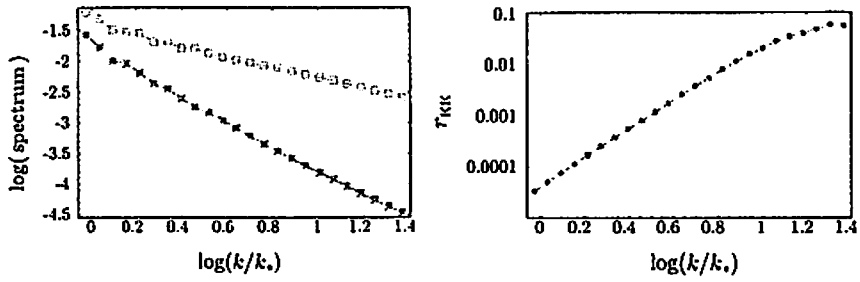

Figure 1: (left) Power spectrum of gravitational waves from inflation with $\ell H = 100$, normalized by $\delta_T^2/2$. The total power spectrum is shown by red circles, while blue crosses represent the contribution only from the initial zero mode. Green squires indicate results from basically four-dimensional calculations, only including the effect of the modification of the background expansion rate. (right) Contribution from initial Kaluza-Klein fluctuations.

Our procedure to obtain a correct power spectrum is as follows. We solve the perturbation equation (3) with its boundary condition set to be $\Phi(U, V_f) = \varphi_0$ on the final hypersurface. The numerical backward evolution scheme we use here is the same as that used in our previous work [4], and the detailed description of the scheme is found there. After obtaining the configuration on the initial hypersurface we evaluate the Wronskian to get the power spectrum.

We performed numerical calculations for the inflationary Hubble parameter $\ell H_i = 100$. The radiation-dominated phase is terminated when the Hubble parameter decreases down to $H \simeq 0.03/\ell =: H_0$, and then it is connected smoothly to the Minkowski phase, so that we can see the amplitude of the well-defined zero mode. The power spectra of gravitational waves are shown in the left figure of Fig. 1. We find that irrespective of the inflationary energy scale, the power spectrum is approximately given by

$$\mathcal{P} \simeq \frac{\delta_T^2}{2}\left(\frac{k}{k_0}\right)^{-2}, \tag{8}$$

Namely, we have the same spectrum as the standard one even for short wavelength modes with $k \gtrsim k_*$. As is shown in the right figure of Fig. 1, the contribution of the vacuum fluctuations in the initial KK modes to the final spectrum, $r_{\rm KK}(k) := \mathcal{P}_{\rm KK}/(\mathcal{P}_0 + \mathcal{P}_{\rm KK})$, never exceeds 10% so far as the present calculations are concerned, and hence it gives a subdominant effect. On the other hand, the excitation of KK modes suppress the amplitude of the gravitational waves relative to $\tilde{\mathcal{P}}$, and our result implies that the effect of the modification of the background Friedmann equation compensate this suppression, leading to approximately the same spectral tilt as that in conventional four-dimensional cosmology.

References

[1] T. Kobayashi and T. Tanaka, JCAP 0410, 015 (2004).

[2] T. Hiramatsu, K. Koyama and A. Taruya, Phys. Lett. B 609, 133 (2005).

[3] K. Ichiki and K. Nakamura, arXiv:astro-ph/0406606.

[4] T. Kobayashi and T. Tanaka, Phys. Rev. D 71, 124028 (2005).

[5] T. Kobayashi and T. Tanaka, arXiv:hep-th/0511186.

[6] D. Langlois, R. Maartens and D. Wands, Phys. Lett. B 489, 259 (2000).

Effective Action Approach to String Gas Compactification

Sugumi Kanno[1], Jiro Soda[2]

Department of Physics, Kyoto University, Kyoto 606-8501, Japan

Abstract

We investigate the stability of $T_2 \otimes T_2 \otimes T_2$ compactification in the context of massless string gas cosmology. By constructing the 4-dimensional effective action with T-duality invariance, we found that the volume moduli, the shape moduli, and the flux moduli are stabilized at the self dual point in the moduli space. Thus, it is proved that this simple compactification model is stable.

1 Introduction

Brandenberger and Vafa proposed an interesting cosmological scenario [1]. They argued the avoidance of the cosmological singularity due to T-duality and proposed a mechanism how only 3 spatial dimensions become large through the annihilation of winding modes. Recent developments of D-brane physics stimulates the study of string gas or brane gas scenario [2].

The stability of internal dimensions in string gas compactification has been studied. However, previous works on the subject have focused on the volume modulus for the compact space. It is important to check if the stabilization mechanism works for shape and flux moduli. In this paper, we focus on the compactification manifold $T_2 \otimes T_2 \otimes T_2$ and argue that a gas of winding and momentum strings can stabilize the volume, flux and shape moduli. We also show that the dilaton is marginally stable. Moreover, we will clarify the role of T-duality in the string gas compactification [3].

2 T-duality in Cosmology

Here, we would like to review T-duality in string theory with focusing on its relation to cosmology. In the low energy effective action of string theory, there exists the $O(6,6,\mathbf{R})$ symmetry which includes the T-duality symmetry $O(6,6,\mathbf{Z})$ as a special case. In the full string theory, $O(6,6,\mathbf{R})$ symmetry cease to exist. However, the T-duality symmetry $O(6,6,\mathbf{Z})$ remains. Here, we treat the gas of strings as test objects and take the metric in a self-consistent manner.

2.1 T-duality in Low Energy Effective Action

The bosonic part of the low energy effective action of the superstring theory takes the following form

$$S = \frac{1}{2\kappa^2}\int d^{10}x\sqrt{-G}e^{-2\phi}\left[\overset{(10)}{R} + 4(\nabla\phi)^2 - \frac{1}{12}H^2\right] , \tag{1}$$

where G_{AB} and ϕ denote the 10-dimensional metric with $A, B = 0, 1, \cdots, 9$ and the dilaton, respectively. Here, we used the notation $(\nabla\phi)^2 = \partial^A\phi\partial_A\phi$ and $H = dB$ is the field strength of the anti-symmetric tensor field B_{AB}. We also defined the 10-dimensional gravitational coupling constant κ.

We assume the 4-dimensions are selected by the Brandenberger-Vafa mechanism. Hence, we consider the cosmological ansatz for the metric:

$$ds^2 = g_{\mu\nu}(x^\mu)dx^\mu dx^\nu + \gamma_{ab}(x^\mu)dy^a dy^b ,$$

where $g_{\mu\nu}$ is the metric of 4-dimensional external spacetime and γ_{ab} is the metric of the internal 6-dimensional compact space. Here, both metric are assumed to depend only on 4-dimensional coordinates

[1]E-mail:sugumi@tap.scphys.kyoto-u.ac.jp
[2]E-mail:jiro@tap.scphys.kyoto-u.ac.jp

x^μ. This means the internal space is flat with respect to y^a . It is convenient to define shifted dilaton $\tilde{\phi}$ by $\sqrt{\gamma}e^{-2\phi} \equiv e^{-2\tilde{\phi}}$. Now, we define the 6×6 matrix $(\Gamma)_{ab} = \gamma_{ab}$ in terms of the internal space components of the metric. We assume the anti-symmetric field B_{AB} exists only in the internal space defined by the 6×6 matrix, $(B)_{ab} = B_{ab}$ depending only on 4-dimensional coordinate x^μ. Then the action can be set into a more compact form by using the 12 × 12 matrix Q:

$$Q = \begin{pmatrix} \Gamma^{-1} & -\Gamma^{-1}B \\ B\Gamma^{-1} & \Gamma - B\Gamma^{-1}B \end{pmatrix} \tag{2}$$

which satisfies a symmetric matrix element of the pseudo- orthogonal $O(6,6,\mathbf{R})$ group, since $Q^T\eta Q = \eta$, $Q^T = Q$, for any B and Γ. Here, η consists of the unit 6-dimensional matrix I, $\eta = \begin{pmatrix} 0 & I \\ I & 0 \end{pmatrix}$. Using the metric ansatz, shifted dilaton, and the variables (2), the action can be written as

$$S = \frac{V_6}{2\kappa^2}\int d^4x e^{-2\tilde{\phi}}\left[R + 4(\partial\tilde{\phi})^2 + \frac{1}{8}\mathrm{Tr}\partial^\mu Q\partial_\mu Q^{-1}\right] , \tag{3}$$

where V_6 is the coordinate volume of the internal space and R is the 4-dimensional scalar curvature. Here, $(\partial\tilde{\phi})^2$ represents $\partial^\mu\tilde{\phi}\partial_\mu\tilde{\phi}$ and Tr denotes the trace of the matrix. One can see the action is invariant under $O(6,6,\mathbf{R})$ transformation $Q \to \tilde{Q} = \Lambda^T Q\Lambda$, where Λ is the 12 × 12 matrix satisfying $\Lambda^T\eta\Lambda = \eta$. Note that the shifted dilaton is invariant under this $O(6,6,\mathbf{R})$ transformation $\tilde{\phi} \to \tilde{\phi}$. The special $O(6,6,\mathbf{R})$ transformation represented by $\Lambda = \eta$ belongs to T-duality transformation. More explicitly the transformation of the matrix Q gives,

$$\tilde{\Gamma} = \left(\Gamma - B\gamma^{-1}B\right)^{-1} , \quad \tilde{B} = -\Gamma^{-1}B\left(\Gamma - B\Gamma^{-1}B\right)^{-1} . \tag{4}$$

When we set $B = 0$, this corresponds to an inversion of the internal space matrix, $\tilde{\Gamma} = \Gamma^{-1}$. So far, we have seen only the kinetic part. It is interesting to see if the potential energy for the moduli can be induced by the string gas. If yes, because of T-duality, one can expect the moduli in the internal space are stabilized at the self-dual point, $\tilde{\Gamma} = \Gamma$ and $\tilde{B} = B$. This is the subject of the next subsection.

2.2 T-duality Invariant String Gas

Let us consider a closed string in the constant background field $g_{\mu\nu}, \gamma_{ab}, B_{ab}$. Using the vector $Z = \begin{pmatrix} p_a \\ w^b \end{pmatrix}$, where p_a and w^b are the momentum of the center of mass and the winding for the compact internal dimensions, the mass spectrum and the level matching condition can be written as

$$M^2(Q) = Z^TQZ + 2(N + \tilde{N} - 2) , \quad N - \tilde{N} = \frac{1}{2}Z^T\eta Z . \tag{5}$$

One can see the mass spectrum and the level matching condition are invariant under $O(6,6,\mathbf{Z})$ transformation $Q \to \tilde{Q} = \Lambda^T Q\Lambda$, $Z \to \tilde{Z} = \Lambda^{-1}Z$ where $\Lambda \in O(6,6,\mathbf{Z})$ is the integer valued 12 × 12 matrix satisfying $\Lambda^T\eta\Lambda = \eta$. As Z is an integer valued vector, $O(6,6,\mathbf{R})$ symmetry does not exist.

The basic assumption made in string gas cosmology is the adiabaticity in the following sense. We assume the matter action can be represented by the action of the modes of the string theory on the torus with constant G_{AB} and B_{AB} replaced by functions of 4-dimensional coordinates as $G_{AB}(x^\mu)$ and $B_{AB}(x^\mu)$. The resulting action will be invariant under the T-duality transformation. Let us imagine a gas of string consists of modes which become massless at the self-dual point. This is legitimate at low energy. The energy of a string can be written as $\sqrt{g^{ij}p_ip_j + M^2(Q)}$ where p_i is the 3-dimensional external momentum. Thus, the action for the string gas is given by

$$S_{gas} = -\int d^4x\sqrt{-g}\rho , \qquad \rho = \frac{\mu_4}{\sqrt{g_s}}\sqrt{g^{ij}p_ip_j + M^2(Q)} , \tag{6}$$

where ρ is the energy density of the gas, μ_4 is the comoving number density of a string gas in 4-dimensions, and g_s denotes the determinant of the spatial part of the 4-dimensional metric.

2.3 T-duality invariant effective action

In order to see the stability of the moduli, we need to move on to the Einstein frame. Performing the conformal transformation, $g_{\mu\nu} = e^{2\bar{\phi}}\bar{g}_{\mu\nu}$, to the action (3), we obtain

$$S = \frac{V_6}{2\kappa^2}\int d^4x\sqrt{-\bar{g}}\left[\bar{R} - 2(\partial\bar{\phi})^2 + \frac{1}{8}\mathrm{Tr}\partial^\mu Q\partial_\mu Q^{-1}\right] . \tag{7}$$

Thus, the shifted dilaton $\bar{\phi}$ and the matrix Q are separated. The action for the string gas is transformed to

$$S_{gas} = -\int d^4x\sqrt{-\bar{g}}\bar{\rho} , \qquad \bar{\rho} = \frac{\mu_4}{\sqrt{\bar{g}_s}}\sqrt{\bar{g}^{ij}p_ip_j + e^{2\bar{\phi}}M^2(Q)} \equiv V_{\rm eff}(\bar{g}_{ij},\bar{\phi},Q) . \tag{8}$$

which can be interpreted as the effective potential. Notice that the effective potential $V_{\rm eff}$ depends on the shifted dilaton only through $e^{2\bar{\phi}}$.

Suppose the moduli Q are stabilized at the self-dual point. As the mass of a string $M^2(Q)$ vanishes at the self-dual point by assumption, the potential of the shifted dilaton disappears. As there exists no potential, the hubble expansion prevents the shifted dilaton from running along the flat direction. Thus, the shifted dilaton is marginally stable. Then, the question is if the moduli Q are really stabilized or not. To investigate this issue, we need to specify the concrete compactification model. This is discussed in the next section.

3 Stability of $T_2 \otimes T_2 \otimes T_2$ Compactification

We would like to analyze the stability of $T_2\otimes T_2\otimes T_2$ compacification. Fortunately, as the internal space is the direct product of torus, it is enough to investigate the simple 6-dimensional spacetime with one torus as the internal space. Now, we shall take the metric and the anti-symmetric tensor field in 2-dimensions

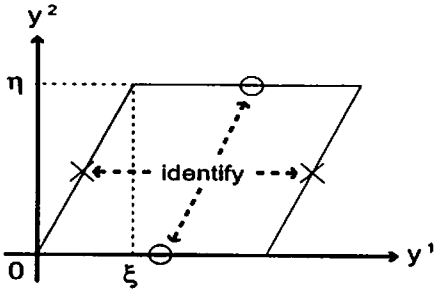

Figure 1: The shape of the torus is specified by ξ and η. Both ends are understood to be identified.

as

$$\Gamma = \frac{b^2}{\eta}\begin{pmatrix} 1 & \xi \\ \xi & \xi^2+\eta^2 \end{pmatrix} , \qquad B = \begin{pmatrix} 0 & \beta \\ -\beta & 0 \end{pmatrix} , \tag{9}$$

where b represents the scale factor of the torus, i.e. volume moduli and ξ, η denote the shape moduli. We call β the flux moduli, hereafter. The 4-dimensional effective action in the Einstein frame becomes

$$\begin{aligned} S &= \frac{V_6}{2\kappa^2}\int d^4x\sqrt{-\bar{g}}\left[\bar{R} - 2(\partial\bar{\phi})^2 - 2(\partial\log b)^2 - \frac{1}{2\eta^2}\left\{(\partial\eta)^2 + (\partial\xi)^2\right\} - \frac{1}{2b^4}(\partial\beta)^2\right] \\ &\quad -\mu_4\int d^4x\sqrt{-\bar{g}_{00}}\sqrt{\bar{g}^{ij}p_ip_j + e^{2\bar{\phi}}M^2(\beta,b,\eta,\xi)} , \end{aligned} \tag{10}$$

where the mass is given by the formula (5). We see the above action has the T-duality symmetry (4) and it is easy to find the self-dual point $b = 1$, $\eta = 1$, $\xi = 0$, $\beta = 0$.

One may expect this self-dual point is a stable minimum of the effective potential. In order to verify this, we should examine where is the minimum of $M^2(\beta, b, \eta, \xi)$ in the potential in the action (10). First, let us consider the string gas consisting of modes $N = 1, p_1 = w^1 = 1, p_2 = w^2 = 0$ which becomes massless at the self-dual point. For this gas, we have $M_1^2 = \frac{1}{\eta b^2}(\xi - \beta)^2 + \frac{\eta}{b^2} + \frac{b^2}{\eta} - 2$. In this case, there exists flat directions $b^2 = \eta$, $\xi = \beta$ in contrast to the naive expectation. However, we only considered one kind of string gas which winds around one specific cycle. Apparently, we have the other cycle for the torus. Hence, we consider another string gas consisting of modes $N = 1, p_1 = w^1 = 0, p_2 = w^2 = 1$ which becomes massless at the self-dual point. In this case, we obtain $M_2^2 = \frac{1}{\eta b^2}(1 + \beta\xi)^2 + \frac{\eta\beta^2}{b^2} + \frac{b^2\xi^2}{\eta} + \eta b^2 - 2$. Now, we also have flat directions $\beta^2 = \frac{b^4\xi^2}{\eta^2}$, $1 + \beta\xi = \eta b^2$. We find these two flat directions intersect at the self-dual point $b = 1$, $\eta = 1$, $\xi = 0, \beta = 0$. Hence, by taking into account both type of string gas, the self-dual point would be stable minimum. The stability can be explicitly verified by expanding the potential around this extrema as

$$V = \mu_4 \sqrt{\frac{\bar{g}^{ij} p_i p_j}{g_s}} + \frac{1}{2} \frac{\mu_4 e^{2\tilde{\phi}}}{\sqrt{g_s}\sqrt{\bar{g}^{ij} p_i p_j}} M^2(\beta, b, \eta, \xi) \tag{11}$$

where we have used the fact that $M^2 \approx 0$ near the self-dual point. Let us linearize the scale factor b and the modulus η as $b = 1 + \delta b$ and $\eta = 1 + \delta\eta$. Other variables ξ and β are already linear because the background values of these variables are zero. By adding up both contributions, we get

$$\delta M^2 = \delta M_1^2 + \delta M_2^2 = 2\xi^2 + 2\beta^2 + 2\delta\eta^2 + 8\delta b^2 \tag{12}$$

where flat directions disappear. Thus, we have proved the stability of all of the moduli of the torus. The dilaton is also stabilized due to the reason explained in the previous section. This concludes the stability of $T_2 \otimes T_2 \otimes T_2$ compacification as we expected.

4 Conclusion

We have analyzed the stability of $T_2 \otimes T_2 \otimes T_2$ compactification in the context of massless string gas cosmology. We emphasized the importance of the T-duality and massless modes in a string. We have constructed the 4-dimensional effective action by taking into account the T-duality. It turned out that the dilaton is marginally stable. We performed the stability analysis of the volume moduli, the shape moduli and the flux moduli. We have found that all of these moduli are stabilized at the self dual point in the moduli space.

Of course, what we have shown is the stability of moduli during the string gas dominated stage. After the string gas dominated stage, the ordinally matter come to dominate the universe. Then, the dilaton will start to run. Therefore, we need to find a mechanism to stabilize the dilaton in these periods.

This work was supported in part by Grant-in-Aid for Scientific Research Fund of the Ministry of Education, Science and Culture of Japan No. 155476 (SK), No.14540258 and No.17340075 (JS).

References

[1] R. H. Brandenberger and C. Vafa, Nucl. Phys. B **316**, 391 (1989).

[2] R. H. Brandenberger, arXiv:hep-th/0509099.

[3] S. Kanno and J. Soda, Phys. Rev. D **72**, 104023 (2005) [arXiv:hep-th/0509074].

Black hole entropy in loop quantum gravity

Takashi Tamaki[1], Hidefumi Nomura[2]

[1]*Department of Physics, Kyoto University, 606-8501, Japan*
[2]*Department of Physics, Waseda University, 3-4-1 Okubo, Shinjuku, Tokyo 169-8555, Japan*

Abstract

We reexmine some proposals of black hole entropy in loop quantum gravity and consider a new possible choice of the Immirzi parameter.

1 Introduction

Loop quantum gravity (LQG) has attracted much attention because of its background independent formulation, account for microscopic origin of black hole entropy [1], singularity avoidance in the universe. The spin network has played a key role in the development of this theory [2]. Basic ingredients of the spin network are edges and vertices. In Fig. 1, edges are expressed by lines lebeled by $j = 0, 1/2, 1, 3/2, \ldots$ reflecting the SU(2) nature of the gauge group. A vertex is an intersection between edges. For three edges having spin j_1, j_2, and j_3 that merges at an arbitrary vertex, we have

$$j_1 + j_2 + j_3 \in N\ , \qquad j_i \leq j_j + j_k,\ \ (i,j,k \ \text{different from each other.}) \tag{1}$$

to garantee the gauge invariance of the spin network. This is also displayed in Fig. 1.

Using this, expressions for the spectrum of the area can be derived as [3] $A = 8\pi\gamma\sum\sqrt{j_i(j_i+1)}$, where γ is the Immirzi parameter. The sum is added up all intersections between a surface and edges as shown in Fig. 1. The number of states that determines the black hole entropy was first estimated as [1]

$$S = \frac{A\ln(2j_{\min}+1)}{8\pi\gamma\sqrt{j_{\min}(j_{\min}+1)}}\ , \tag{2}$$

where A and $j_{\min}$ are the horizon area and the lowest nontrivial representation usually taken to be $1/2$ because of SU(2), respectively. In this case, the Immirzi parameter is determined as $\gamma = \ln 2/(\pi\sqrt{3})$ to produce the Bekenstein-Hawking entropy formula $S = A/4$.

However, the formula (2) was corrected as [4, 5] $S = \frac{\gamma_M A}{4\gamma}$, where γ_M is the solution of

$$1 = \sum_{j=Z/2}^{\infty} 2\exp(-2\pi\gamma_M\sqrt{j(j+1)})\ , \tag{3}$$

where j takes all the positive half-integer. In this case, γ_M is numerically obtained as $\gamma_M = 0.23753\cdots$. Interestingly, another possibility has also been argued. It is to determine γ_M as the solution of [6, 7]

$$1 = \sum_{j=Z/2}^{\infty} (2j+1)\exp(-2\pi\gamma_M\sqrt{j(j+1)})\ . \tag{4}$$

In this case, $\gamma_M = 0.27398\cdots$.

These provide us with the following question: that is, which is the best choice for the Immirzi parameter? Therefore, we reanalyze these possibilities. This is important in the following reasons.

(i) In string theory, number counting for microscopic states of black holes has been considered, and it has reproduced the Bekenstein-Hawking formula $S = A/4$. In future, it is desirable for us to have a connection with the number counting in string theory. Probably, we will need to proceed many steps toward this purpose.

[1]E-mail:tamaki@tap.scphys.kyoto-u.ac.jp
[2]E-mail:nomura@gravity.phys.waseda.ac.jp

However, there is a subject which can be attacked soon. This is (ii) the possible relation to the quasinormal mode which has been argued as another consistency check of the Immirzi parameter in the area spectrum. Using (2), an encounter between LQG and the quasinormal mode was considered first in Ref. [8]. This means that if we have $j_{\min} = 1$, we can determine γ as $\ln 3/(2\pi\sqrt{2})$ which gives $A = 4\ln 3$. This coincides the area spectrum determined by quasinormal mode using Bohr's correspondence [9]. Moreover, the quasinormal mode analysis that originally performed in Schwarzschild black hole [10] has been extended to single-horizon black holes [11]. Thus, we also want to know which is the best choice for the Immirzi parameter in this view point.

This paper is organized as follows. In Sec. 2, we summarize the framework [1] (which we call the ABCK framework.). In Sec. 3, we argue various possibilities that determine the number of state. In Sec. 4, we summarize our results and discuss their meaning. For details, see [12].

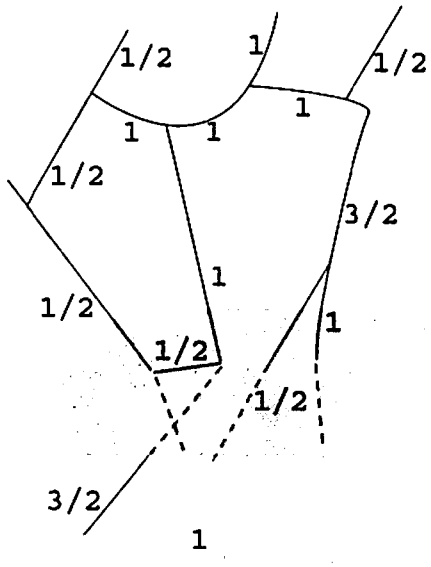

Figure 1: Spin network and a surface.

2 Summary of the ABCK framework

First, we introduce the isolated horizon (IH) where we can reduce the SU(2) connection to the U(1) connection. Next, we imagine that spin network pierces the IH. By eliminating the edge tangential to the isolated horizon, we can decompose the Hilbert space as the tensor product of that at the IH H_{IH} and that in the bulk H_Σ, i.e., $H_{IH} \otimes H_\Sigma$. If we specify the points that are intersections of edges having spin $(j_1, j_2, \cdots, j_n)$ and the IH, we can write H_Σ as the orthogonal sum $H_\Sigma = \bigoplus_{j_i,m_i} H_\Sigma^{j_i,m_i}$, where m_i takes the value $-j_i$, $-j_i+1$, $\cdots$, j_i. This is related to the flux operator eigenvalue $e_{s'}^{m_i} := 8\pi\gamma m_i$ that is normal to the IH (s' is the part of the IH that have only one intersection between the edge with spin j_i.). Since we eliminate the edge tangential to the IH, we have $m_i \neq 0$. The horizon Hilbert space can be written as the orthogonal by eigenstates Ψ_b of the holonomy operator $\hat{h}_i$, i.e., $\hat{h}_i\Psi_b = e^{\frac{2\pi i b_i}{k}}\Psi_b$.

Next, we consider the constraints in the bulk and at the IH, respectively. In the bulk, the Gauss constraint is already satisfied and the diffeomorphism constraint means that the place to which the edges stick the IH is not relavant. It is assumed that the bulk scalar constraint does not affect (j, m). At the IH, we do not consider the scalar constraint since the lapse function disappears. If we require that the horizon should be invariant under the diffeomorphism and the U(1) gauge transformation, The horizon area A is fixed as $A = 4\pi\gamma k$, where k is natural number and it is the level of the Chern-Simons theory. In addition, it is required that we should fix an ordering $(b_1, b_2, \cdots, b_n)$. The area operator eigenvalue A_j should

satisfy (i) $A_j = 8\pi\gamma \sum \sqrt{j_i(j_i+1)} \leq A$. From the quantum Gauss-Bonnet theorem, (ii) $\sum_{i=1}^{n} b_i = 0$. From the boundary condition between the IH and the bulk, (iii) $b_i = -2m_i \mod k$. All we need to consider in number counting are (i)(ii)(iii).

3 Number counting

If we use (ii) and (iii), we obtain $(ii)'$ $\sum_{i=1}^{n} m_i = n'\frac{k}{2}$. In [5], it was shown that this condition is irrelevant in number counting. Thus, we perform number counting only concentrating on (i) below.

For this purpose, there are two different points of view. The one adopted in the original paper [1. 4, 5] counts the *surface* freedom $(b_1, b_2, \cdots, b_n)$. The second counts the freedom for both j and b [6, 7].

We first consider the second possibility since (we suppose) it is easier to understand. To simplify the problem, we first consider the set M_k by following [4], that is

$$M_k := \left\{ (j_1, \cdots, j_n) | 0 \neq j_i \in \frac{Z}{2}, \sum_i j_i \leq \frac{k}{2} \right\} . \tag{5}$$

Let N_k be the number of elements of M_k plus 1. Certainly, $N(a) \leq N_k$, where $N(a)$ ($a := \frac{A}{8\pi\gamma}$) is the number of states which account for the entropy. Note that if $(j_1, \cdots, j_n) \in M_{k-1}$, then $(j_1, \cdots, j_n, \frac{1}{2}) \in M_k$. In the same way, for natural $0 < s \leq k$,

$$(j_1, \cdots, j_n) \in M_{k-s} \Rightarrow (j_1, \cdots, j_n, \frac{s}{2}) \in M_k . \tag{6}$$

Then, if we consider all $0 < s \leq k$ and all the sequence $(j_1, \cdots, j_n) \in M_{k-s}$, we found that $(j_1, \cdots, j_n, \frac{s}{2})$ form the entire set M_k. Moreover, for $s \neq s'$, $(j_1, \cdots, j_n, \frac{s}{2}) \neq (j_1, \cdots, j_n, \frac{s'}{2}) \in M_k$. The important point to remember is that we should include the condition $m_i \neq 0$ (or equibalently $b_i \neq 0$). Thus, each j_i has freedom $2j_i$ for the j_i integer and the $2j_i + 1$ way for the j_i half-integer. They are summarized as $2[\frac{2j+1}{2}]$ where $[\cdots]$ is the integer parts. For this reason, the recursion relation is

$$N_k = \sum_{s=1} 2[\frac{s+1}{2}](N_{k-s} - 1) + 1 . \tag{7}$$

This is the point which has not been examined out so far.

As a stright forward extension of this, we can consider $N(a)$, which is

$$N(a) := \left\{ (j_1, \cdots, j_n) | 0 \neq j_i \in \frac{Z}{2}, \sum_i \sqrt{j_i(j_i+1)} \leq \frac{k}{2} = a \right\} . \tag{8}$$

In this case, we obtain the recursion relation

$$N(a) = 2N(a - \sqrt{3}/2) + 2N(a - \sqrt{2}) + \cdots + 2[\frac{2j+1}{2}]N(a - \sqrt{j_i(j_i+1)}) + \cdots + [\sqrt{4a^2+1} - 1] . \tag{9}$$

If we notice that the solution of $\sqrt{j_i(j_i+1)} = a$ is $j_i = (\sqrt{4a^2+1} - 1)/2$, meaning of $[\sqrt{4a^2+1} - 1]$ is obvious. If we use the relation $N(a) = Ce^{\frac{A\gamma_M}{4\gamma}}$, where C is a constant, that was obtained in [5], we obtain

$$1 = \sum_{j=Z/2} 2[\frac{2j+1}{2}] \exp(-2\pi\gamma_M \sqrt{j(j+1)}) , \tag{10}$$

by taking the limit $A \to \infty$. Then if we require $S = A/4$, we have $\gamma = \gamma_M$. In this case, $\gamma_M = 0.26196\cdots$.

Next, we consider the first possibility that counts only the surface freedom. This means that even if $(j_1, j_2, \cdots, j_n)$ is different, it is regareded as the *same* surface state if the horizon area and $(b_1, b_2, \cdots, b_n)$ are same. For example, $(j_1, j_2) = (3/2, 1/2)$ and $(1/2, 3/2)$ both give the possibility $(b_1, b_2) = (-1, -1)$.

Then, it should *not* be distinguished in this description. This following is the method taken in [4], i.e., we rewrite (i) as $(i)'$ $8\pi\gamma\sum_i \sqrt{|m_i|(|m_i|+1)} \leq A$. Let us compare (6) with

$$(m_1, \cdots, m_n) \in M_{k-s} \Rightarrow (m_1, \cdots, m_n, \pm\frac{s}{2}) \in M_k \ . \tag{11}$$

At first glance, it might seem that we abondon the freedom $m_{n+1} = -\frac{s}{2}+1, \cdots \frac{s}{2}-1$. However, it is not the case since we obtain that freedom from M_{k-s+2}, M_{k-s+4}, $\cdots$. It is the crucial difference from (6) where the freedom of j is counted. In this way, we have the relation

$$N_k = \sum_{s=1} 2(N_{k-s}-1)+1 \ . \tag{12}$$

Therefore, we obtain (3).

4 Conclusions and discussion

We have considered two possibilities for the number of states of black holes in the ABCK framework. One of them gives a new value for the Immirzi parameter. From these results, we consider whether or not there is a consistency between the area spectrum in LQG and the area spectrum in the quasinormal mode. Since the area spectrum obtained from the quasinormal mode is $dA = 4\ln 3$, it is obvious that we do not have the same consistency if we adopt the Immirzi parameter determined by (3) or (10). This means that if we take the consistency to the quasinormal mode seriously, we will need new considerations. Finally, we want to consider which of the two candidates is the better choice. The reason why only surface degree was counted in [1, 4, 5] is to separate surface degree from the bulk freedom. If we admit j as an independent variable, it is difficult to separate it from other bulk freedoms since that in the bulk can communicate with infinity. However, as pointed out in [7], it is j that determines area eigenvalue and other bulk variables are irrelevant. Moreover, since quantum horizons would fluctuate, it may be a problem to consider the IH as a sharp boundary. For these reasons, it is too early to choose the candidate. Of course, it is also important to consider the other method in the calculating the number of freedom. We also want to examine these possibilities in future.

References

[1] A. Ashtekar, J. Baez, A. Corichi, and K. Krasnov, Phys. Rev. Lett. **80**, 904 (1998); A. Ashtekar, J. Baez, and K. Krasnov, Adv. Theor. Math. Phys. **4**, 1 (2000).

[2] C. Rovelli and L. Smolin, Phys. Rev. D **52**, 5743 (1995).

[3] C. Rovelli and L. Smolin, Nucl. Phys. B **442**, 593 (1995); Erratum, *ibid.*, **456**, 753 (1995).

[4] M. Domagala and J. Lewandowski, Class. Quant. Grav. **21**, 5233 (2004).

[5] K. A. Meissner, Class. Quant. Grav. **21**, 5245 (2004).

[6] I.B. Khriplovich, gr-qc/0409031; gr-qc/0411109.

[7] A. Ghosh and P. Mitra, Phys. Lett. B **616**, 114 (2005).

[8] O. Dreyer, Phys. Rev. Lett. **90**, 081301 (2003).

[9] S. Hod, Phys. Rev. Lett. **81**, 4293 (1998).

[10] L. Motl, Adv. Theor. Math. Phys. **6**, 1135 (2003); L. Motl and A. Neitzke, *ibid.*, **7**, 307 (2003).

[11] T. Tamaki and H. Nomura, Phys. Rev. D **70**, 044041 (2004).

[12] T. Tamaki and H. Nomura, Phys. Rev. D **72**, 107501 (2005).

Scalar Field Contribution to Rotating Black Hole Entropy
— Euclidean Path Integral Method —

Masakatsu Kenmoku[1]

Department of Physics, Nara Women's University, Nara 630-8506, Japan

Abstract

Scalar field contribution to rotating black hole entropy is studied using Euclidean path integral method. The area law is obtained by imposing the minimal set of conditions on the metrics. Single parameter rotating case is treated in this report, which is based on the paper [1].

1 Introduction

Recently there are lots of Rotating Black Holes (BH) are observed and they are described by Kerr metric in good approximation [2]. As black holes are thermal objects [3], statistical study of the quantum field contributions to rotating black holes is interesting.

However there are some problems on scalar field contribution: additional divergences appear, no rotating limit cannot be taken and the result depends on calculation methods [4].

Our strategy is to study the rotating entropy problem in a general treatment: not assuming explicit expression on black hole solutions and minimal requirement to metric form in arbitraly D dimensional spacetime. We adopted two methods: Euclidean path integral method [5] and semiclassical method with brick wall scheme [6]. As a conclusion, area law of black hole entropy is obtained in general.

2 Scalar Field Contribution to Rotating BH Entropy

The rotating BH entropy is studied in Euclidean path integral method using the heat kernel scheme with asymptotic expansion in an arbitraly D dimension.

2.1 Entropy Formula under Rotating BH Spacetime

Euclidean polar coordinate and the line element are defined:

$$\begin{aligned} x^a &= (x^1, x^2, x^3, \cdots, x^D) = (r, \phi, \theta^3, \cdots, \theta^{D-1}, \tau) \ , \\ ds^2 &= g_{\tau\tau} d\tau^2 + g_{rr} dr^2 + g_{\phi\phi} d\phi^2 + 2 g_{\tau\phi} d\tau d\phi + \sum_{a=3}^{D-1} g_{aa} (d\theta^a)^2 \ . \end{aligned}$$

The action and Lagrangian density of scalar field with mass μ areexpressed:

$$I_{\rm scalar} = \int d^D x \sqrt{g_E}\, \mathcal{L} \quad , \quad \mathcal{L} = - \sum_{a,b=1}^{D} \frac{1}{2} (g^{ab} \partial_a \Phi \partial_b \Phi + \mu^2 \Phi^2) \ .$$

Then canonical momentum conjugate to scalar field is defined as

$$\Pi := i \frac{\partial \mathcal{L}}{\partial \dot{\Phi}} = -i (g^{\tau\tau} \dot{\Phi} + g^{\tau\phi} \partial_\phi \Phi) \ ,$$

and the quantization condition is imposed:

$$[\Phi(\tau, x), \Pi(\tau, y)] = i \frac{\delta^{D-1}(x - y)}{\sqrt{g_E}} \ .$$

[1] E-mail:kenmoku@asuka.phys.nara-wu.ac.jp

Here the metric does not depend on t, ϕ, and two Killing vectors exist: $\xi_\tau = \partial_\tau$, $\xi_\phi = \partial_\phi$, which induce conservations of total energy and angular momentum:

$$H = \int d^{D-1}x\sqrt{g_E}\left(\Pi\dot{\Phi} - \mathcal{L}\right) \ , \ P_\phi = -\int d^{D-1}x\sqrt{g_E}\,\Pi\,\partial_\phi\Phi \ .$$

A future directed null Killing vector $\eta := \xi_t + \xi_\phi\Omega_H$ is introduced with the angular velocity on the horizon r_H : $\Omega_H := g^{t\phi}/g^{tt}\big|_{r_H}$, which induces the restriction on the allowed range of scalar energy: $P\cdot\eta := -H + \Omega_H P_\phi \leq 0$.

This combination defines the new Hamiltonian density $\mathcal{H}'$:

$$H - \Omega_H P_\phi =: \int d^{D-1}x\sqrt{g_E}\mathcal{H}' \ ,$$

with

$$\begin{aligned}\mathcal{H}' &= \frac{1}{2g^{\tau\tau}}\Pi^2 + \sum_{a=1}^{D-1}\frac{1}{2g_{aa}}(\partial_a\Phi)^2 + (\Omega_H + \frac{g_{\tau\phi}}{g_{\phi\phi}})\Pi\partial_\phi\Phi + \frac{\mu^2}{2}\Phi^2 \\ &\simeq \frac{1}{2g^{\tau\tau}}\Pi^2 + \sum_{a=1}^{D-1}\frac{1}{2g_{aa}}(\partial_a\Phi)^2 + \frac{\mu^2}{2}\Phi^2 \ ,\end{aligned}$$

which is diagonal and non-negative near the horizon. The partition function of inverse temperature β is expressed as

$$Z = \int [D\Phi\, D\Pi\, g_E^{1/2}] \exp\left(\int d^Dx\,\sqrt{g_E}\,(\Pi\dot{\Phi} - \mathcal{H}')\right) \ ,$$

where the Boltzmann factor is understood to take account of rotation effect [7].

After the path integration over Π and Φ, the free energy $F = -\log Z/\beta$ is obtained using the heat kernel expression evaluated by asymptotic expansion as

$$F = -\int_0^\infty \frac{ds}{s}\frac{1}{(4\pi s)^{D/2}}\sum_{n=1}^\infty \exp(-\frac{\beta^2n^2}{4s})\bar{B}_0\exp(-\frac{\mu^2 s}{g^{\tau\tau}}) \ ,$$

where the lowest contribution $\bar{B}_0$ is the volume in the optical space:

$$\bar{B}_0 = \int d^{D-1}x(g^{\tau\tau})^{(D-1)/2}(g_{rr}g_{\phi\phi}g_{33}\cdots g_{D-1\,D-1})^{1/2} \ .$$

As the massless case $\mu = 0$ is interesting, the free energy and the entropy are obtained:

$$F = -\frac{\zeta(D)\Gamma(D/2)}{\pi^{D/2}\beta^D}\,\bar{B}_0 \ , \ S = \beta^2\frac{\partial F}{\partial\beta} = \frac{\zeta(D)D\Gamma(D/2)}{\pi^{D/2}\beta^{D-1}}\bar{B}_0 \ .$$

It is worthwhile to note that: (i) The rotation effects are included in $\bar{B}_0$ and β, (ii)Non-rotating limit can be taken smoothly and the resultant free energy and entropy agree with the known non-rotating results.

2.2 Area Law under Rotating Black Hole Spacetime

The area law is obtained from the generalized entropy formula by performing the real space integration in $\bar{B}_0$ under the conditions:

1. Simple zeros are required for $1/g^{\tau\tau}$ and $1/g_{rr}$ at horizon position r_H:

$$1/g^{\tau\tau} \simeq C_\tau(\theta)(r - r_H) \ , \ 1/g_{rr} \simeq C_r(\theta)(r - r_H) \ ,$$

where

$$C_\tau(\theta) := \partial_r 1/g^{\tau\tau}\big|_{r_H} \ , \ C_r(\theta) := \partial_r 1/g_{rr}\big|_{r_H} \ .$$

2. Temperature is defined by "no conical singularity in the Rindler space", which should not depend on zenithsal angle variables:

$$\frac{2\pi}{\beta_H} = \left.\frac{\partial_r(1/g^{\tau\tau})}{2\sqrt{g_{rr}/g^{\tau\tau}}}\right|_{r_H} = \frac{1}{2}\left(C_\tau(\theta)C_r(\theta)\right)^{1/2} = \text{independent on } \theta \ .$$

Under these conditions radial integration in $\bar{B}_0$ is performed with the short and large distance cutoff parameters ϵ and L :

$$\int_{r_H+\epsilon}^{L} dr\,(g^{\tau\tau})^{D/2-1/2}(g_{rr})^{1/2} \simeq C_\tau(\theta)^{-D/2+1/2}C_r(\theta)^{-1/2}\frac{\epsilon^{-D/2+1}}{D/2-1} \ .$$

Changing the idea from θ independent cutoff ϵ to θ dependent cutoff $\epsilon(\theta)$:

$$\epsilon_{\rm inv} := \int_{r_H}^{r_H+\epsilon(\theta)} dr\sqrt{g_{rr}} \quad \text{or} \quad \epsilon(\theta) \simeq C_r(\theta)\epsilon_{\rm inv}^2/4 \ ,$$

the entropy can be expressed as

$$S = \frac{\zeta(D)D\Gamma(D/2-1)}{2^D\pi^{3D/2-1}}\frac{A}{(\epsilon_{\rm inv})^{D-2}} \ ,$$

where A is the surface area of the rotating BH on the horizon

$$A := \int d\phi d\theta^3 \cdots d\theta^{D-1}(g_{\phi\phi}g_{33}\cdots g_{D-1D-1})^{1/2}\Big|_{r_H} \ .$$

Note that the generalized area law is derived without using any explicit expression for the metric but using two conditions; Horizon and Temperature Condition.

3 Application to Kerr-Newman Black Hole

The general entropy formula is applied to Kerr-Newman black hole solution in (3+1)-dimension. The line element is given as

$$ds^2 = g_{\tau\tau}d\tau^2 + g_{rr}dr^2 + g_{\phi\phi}d\phi^2 + 2g_{\tau\phi}d\tau d\phi + g_{\theta\theta}d\theta^2 \ ,$$

with the metric

$$\begin{aligned} g_{\tau\tau} &= \frac{\Delta - a^2\sin^2\theta}{\Sigma} \ , \ g_{\tau\phi} = \frac{a\sin^2\theta(r^2+a^2-\Delta)}{\Sigma} \ , \\ g_{\phi\phi} &= \frac{(r^2+a^2)^2 - \Delta a^2\sin^2\theta}{\Sigma}\sin^2\theta \ , \ g_{\theta\theta} = \Sigma \ , \\ g_{rr} &= \frac{\Sigma}{\Delta} \ , \end{aligned}$$

where

$$\Sigma(r,\theta) := r^2 + a^2\cos^2\theta \ , \ \Delta(r) := r^2 - 2Mr + a^2 + e^2 \ .$$

Here the three hairs of BH are mass M, angular momentum per mass a and sharge e. The horizon is given by the outer zeros of $1/g^{\tau\tau}$ and $1/g_{rr}$, or $\Delta = 0$ as $r_H = M + (M^2 - a^2 - e^2)^{1/2}$, $(a^2+e^2 \le M^2)$. Using the temperature on the horizon

$$\frac{2\pi}{\beta_H} = \frac{r_H - r_-}{2(r_H^2+a^2)} \ ,$$

the θ dependent cutoff parameter

$$\epsilon(\theta) = \frac{(r_H - r_-)^2}{4(r_H^2 + a^2\cos^2\theta)}\epsilon_{\rm inv}^2 \ ,$$

and the area of the Kerr-Newman BH $A = 4\pi(r_H^2 + a^2)$, the area law is obtained

$$S = A/(360\pi{\epsilon_{\rm inv}}^2)$$

The final form is the same form as the non-rotating BH cases, but the rotating effects are included in A and in $\epsilon_{\rm inv}$ through $\epsilon(\theta)$ paremeter.

4 Another Derivation: Semiclassical Method

Semiclassical method with brick wall regularization scheme by 't Hooft [6] is also studied and the consistent result is obtained [1].

5 Summary

(1) The entropy formula and area law are derived for the rotating BH in arbitrary D dimensional spacetime.
(2) One of the key point is the introduction of angle dependent parameter $\epsilon(\theta)$, which leads to the area law in a compact form.
(3) The area law is applied to the Kerr-Newman BH in (3+1) demension. (4) Non-rotating limit can be taken smoothly.

The consistency between our result and the superradiant instabilities in quainormal modes for Kerr BH remains our future problem [8].

References

[1] M. Kenmoku, K, Ishimoto, K. Shigemoto and K.K. Nandi, gr-qc/051012 ;M. Kenmoku, in preparetion.

[2] G.W. Gibbons, H. Lii. D.N. Page and C.N. Pope, hep-th/0404008 ; G.W. Gibbons, M.J. Perry and C.N. Pope, Class. Qunatum Grav. **22**(2005)1503.

[3] J.D. Bekenstein, Phys. Rev. **D7** (1973) 2333.; S.W. Hawking, Commun. Math. Phys. **43** (1975) 199.

[4] See, for example, M-H. Lee and J.K. Kim, Phys. Rev. **D54** (1996) 3904; V. Frolov and V. Fursaev, Phys. Rev. **D61** (2000) 024007; I. Ichinose and Y. Satoh, Nucl. Phys. **B447** (1995) 340.

[5] S.P. de Alwis and N. Ohta, Phys. Rev. **D52** (1995) 3529.

[6] G. 't Hooft, Nucl. Phys. **B256** (1985) 727.

[7] J.B. Hartle and S.W. Hawking, Phys. Rev. **D13** (1976) 2188.

[8] See, for example, V. Cardoso, O.J.C. Dias, J.P.S. Lemos and S. Yoshida, hep-th/0404096; S. Mukohyama, Phys. Rev. **D61** (2000) 124021.

Universal property from local geometry of Killing horizon

Jun-ichirou Koga[1]

[1] *Advanced Research Institute for Science and Engineering, Waseda University, Shinjuku-ku, Tokyo 169-8555, Japan*

Abstract

We first define a local geometric structure universal to arbitrary Killing horizons, which we call an asymptotic Killing horizon. By computing the acceleration of the timelike orbits associated with asymptotic Killing horizons, we then show that the behavior of the acceleration is consistent with the discrepancy on the entropy of an extreme black hole between string theory and the Euclidean approach to black hole thermodynamics. We thus argue that it is fascinating to speculate that the microscopic states responsible for black hole thermodynamics are described by asymptotic Killing horizons, at least at the classical level.

1 Introduction

Black hole thermodynamics will play an important role in constructing a quantum theory of gravity. Actually, various progresses have been made in the candidates of quantum gravity for special classes of black holes, but the statistical physics of an *arbitrary* black hole has not been uncovered yet.

From a classical point of view, it is argued by Jacobson that the thermodynamic property is possessed by not only black hole horizons, but also arbitrary causal horizons [1]. This indicates that the thermodynamic property arises from (quasi-)local geometric structures of a horizon, which is universal to arbitrary horizons. The effort by Carlip to derive the Bekenstein–Hawking formula from the asymptotic symmetries on a black hole horizon also is based on local geometry of the horizon [2], while this idea has not been completed. On the other hand, in the Euclidean approach to black hole thermodynamics [3], the partition function, which correctly gives the Bekenstein–Hawking formula, is evaluated only with a classical solution. These facts seem to suggest that the microscopic states responsible for black hole thermodynamics are described by a classical geometric language, whereas a quantum theory of gravity will be necessary ultimately in order to understand the physics of these microscopic states completely. It is then interesting to consider local geometric structures that are universal to arbitrary horizons.

As the first step, it is reasonable to start with equilibrium states of a horizon, i.e., a stationary horizon. By recalling the fact that the zeroth and the first laws of black hole, which govern equilibrium states of a horizon, are established based on the properties of a Killing horizon, we will thus consider a local geometric structure that respects the essential features of a Killing horizon, and investigate whether the universal properties of a horizon associated with such a local geometric structure are related with the microscopic states responsible for black hole thermodynamics.

2 Asymptotic Killing horizon

We first define a local geometric structure of a horizon, which we call an asymptotic Killing horizon, based on the essential features of a Killing horizon. To do so, we recall that we need to use a Killing vector to specify a Killing horizon, and a Killing vector should satisfy the Killing equation globally in the spacetime. Since our interest here is a local structure of a horizon, it is reasonable to weaken the condition that the Killing equation is satisfied globally. We emphasize also that local structures of a horizon cannot be defined by simply specifying a null hypersurface and the metric near that hypersurface. We thus define an asymptotic Killing horizon, by extending the previous perturbative definition [4], as follows.

[1] E-mail:koga@gravity.phys.waseda.ac.jp

Definition 1 *Let H be a null hypersurface in a spacetime $(\mathcal{M}, g_{ab})$. The pair (H, ξ^a) of H and a vector ξ^a, which is not identically vanishing on H, is defined to be an asymptotic Killing horizon, and ξ^a is called the generator of the asymptotic Killing horizon (H, ξ^a), if there exists a neighborhood of H, in which*

1. *there exists a smooth scalar u, such that $u = 0$ and $\nabla_a u \neq 0$ on H.*
2. *ξ^a satisfies the following three conditions:*

$$\mathcal{L}_\xi g_{ab} = O(u), \tag{1}$$
$$g_{ab}\,\xi^a \xi^b = O(u), \tag{2}$$
$$\xi^a \nabla_a u = O(u). \tag{3}$$

The scalar u in the first condition in Definition 1 is introduced to specify the null hypersurface H in a non-degenerate manner. We thus note that u plays a role much similar to the conformal factor in the conformal completion of an asymptotically flat or (anti-)de Sitter spacetime. Eqs. (2) and (3) in Definition 1 imply that the generator ξ^a of an asymptotic Killing horizon (H, ξ^a) is null on H and tangent to H, respectively, as in the case of a Killing horizon. The essential point in Definition 1 is Eq. (1), which states that the generator ξ^a of an asymptotic Killing horizon (H, ξ^a) behaves like a Killing vector only on H, but may not away from H. This is contrasted with a Killing horizon. A Killing horizon is defined by a Killing vector, for which the right-hand side of Eq. (1) vanishes globally. We note also that an asymptotic Killing horizon is defined without depending on the choice of u.

Now we introduce the scalar λ defined by

$$\xi^a = \nabla^a \lambda + O(u), \tag{4}$$

and $\lambda = 0$ on H. According to Eq. (4), we call λ the potential of ξ^a. It is not difficult to show that λ exists for an arbitrary asymptotic Killing horizon, and that λ is uniquely determined up to $O(u^2)$. Once there exists an asymptotic Killing horizon (H, ξ^a), it is then easy to see that the vectors ξ'^a given by

$$\xi'^a = \omega \xi^a - \lambda \nabla^a \omega + O(u^2), \tag{5}$$

generate another asymptotic Killing horizons, i.e., (H, ξ'^a) also are asymptotic Killing horizons, where u is an arbitrary smooth scalar such that $u = 0$ and $\nabla_a u \neq 0$ on H, ω denotes arbitrary smooth functions, and λ is the potential of ξ^a. This fact implies that infinitely many asymptotic Killing horizons reside on the same null hypersurface H. In particular, a single Killing horizon is accompanied by infinitely many asymptotic Killing horizons. Since an arbitrary Killing horizon is an asymptotic Killing horizon, this feature is possessed universally by arbitrary Killing horizons. We thus have the degeneracy of asymptotic Killing horizons, in the sense that they all possess the same local geometric structure.

3 Acceleration

Similarly to the surface gravity of a Killing horizon, we define the surface gravity κ of an asymptotic Killing horizon (H, ξ^a) as a *function* on H, which is given by

$$\xi^c \nabla_c \xi^a = \kappa \xi^a + O(u). \tag{6}$$

By using Eqs. (4) and (6), it is possible to show that κ is related with $N^2 \equiv -\xi^a \xi_a$ as

$$N^2 = 2\kappa\lambda + O(u^2), \tag{7}$$

where λ is the potential of ξ^a. We note here that the surface gravity of an asymptotic Killing horizon is not necessarily constant on H, even along ξ^a. Also, there are no *a priori* reasons to expect that the surface gravity of an asymptotic Killing horizon is related with any notion of temperature.

Then, rather than the surface gravity, it is reasonable to consider the notion of acceleration of timelike orbits associated with asymptotic Killing horizons, because the acceleration is related with the quantum

effect measured by the particle detectors running along the timelike orbits. Since the sign of λ is set as $\lambda > 0$ in the region under consideration, e.g., the exterior region of a black hole, by choosing the direction of the generator ξ^a, we see from Eq. (7) that if $\kappa > 0$, the orbits of ξ^a are timelike near H in that region. These timelike orbits asymptotically approach the null hypersurface H of asymptotic Killing horizons (H, ξ^a), and hence H acts as a causal boundary for these timelike orbits, much like a Killing horizon.

By focusing on the asymptotic Killing horizons with $\kappa > 0$, the magnitude a of the acceleration of the orbit of the generator ξ^a of an asymptotic Killing horizon (H, ξ^a) is computed as

$$a = \frac{1}{N}\left[\kappa - \frac{1}{2}\xi^c \nabla_c \ln \kappa + O(u)\right]. \tag{8}$$

Eq. (8) reduces to the standard relation between the acceleration a and the surface gravity κ of a Killing horizon, when κ is constant. However, for general asymptotic Killing horizons, the acceleration a receives the correction described by the second term in the bracket.

In order to understand the behavior of the acceleration a, it is meaningful to consider the most interesting case, where the asymptotic Killing horizons (H, ξ^a) reside on the same null hypersurface H as a Killing horizon generated by the Killing vector ξ_0^a does. Thus, by recalling Eq. (5), we express ξ^a as

$$\xi^a = \omega \xi_0^a - \lambda_0 \nabla^a \omega + O(u^2), \tag{9}$$

where λ_0 is the potential of ξ_0^a defined by

$$\xi_0^a = \nabla^a \lambda_0 + O(u). \tag{10}$$

Since the Killing horizon is translationally invariant along its generator ξ_0^a, it is reasonable to expand the arbitrary function ω in Eq. (9) into the Fourier modes as

$$\omega = n_p e^{ipV} f_p, \tag{11}$$

by defining the scalar V as

$$\xi_0^c \equiv \left(\frac{\partial}{\partial V}\right)^c \tag{12}$$

on H, where p is the wave number, n_p is an arbitrary normalization constant, and f_p is an arbitrary function that does not depend on V, i.e., $\xi_0^c \nabla_c f_p = 0$. By denoting the surface gravity of the Killing horizon by κ_0, the acceleration a is then calculated as

$$a = \frac{1}{\sqrt{2\lambda_0}\,(\kappa_0 + ip)^{1/2}}\left[\left(\kappa_0 + i\frac{p}{2}\right) + O(u)\right]. \tag{13}$$

In the case of $\kappa_0 \neq 0$, we find that the acceleration a diverges as $u^{-1/2}$ as the orbit approaches the null hypersurface H, as it does in the case of a non-extreme Killing horizon. In this case, Eq. (13) reduces in the limit of $p \to 0$ to the standard relation for a Killing horizon. Even when $\kappa_0 = 0$, i.e., when the Killing horizon is extreme, the acceleration a diverges as $u^{-1/2}$, as long as $p \neq 0$. However, the acceleration for an extreme Killing horizon is shown to converge to a finite value. Therefore, we see that the acceleration for the asymptotic Killing horizons on an extreme Killing horizon is discontinuous in the limit $p \to 0$. An extreme Killing horizon is thus isolated from the asymptotic Killing horizons that reside on itself. In this sense, an extreme Killing horizon is clearly distinguished from a non-extreme Killing horizon.

In contrast, in the limit of $p \to \infty$, the behavior of the acceleration a of asymptotic Killing horizons on an extreme Killing horizon approaches that on a non-extreme Killing horizon. Thus, the asymptotic Killing horizons on an extreme Killing horizon and those on a non-extreme Killing horizon behave similarly in the high-energy regime. This indicates that a non-extreme Killing horizon and an extreme Killing horizon will not be distinguishable in a high-energy theory, such as quantum gravity, which is capable to probe the regime $p \to \infty$.

4 Discussion

Since the acceleration of a timelike orbit is closely related with the quantum effect perceived by a particle detector running along the orbit, it is expected that we can prospect the quantum feature of an asymptotic Killing horizon from the behavior of the acceleration of the orbit of the generator of an asymptotic Killing horizon. We found from the divergent behavior of the acceleration that the difference between an extreme Killing horizon and a non-extreme Killing horizon is manifest when the wave number p is small, e.g., in the Euclidean approach to black hole thermodynamics, where one takes into account only a single classical configuration with the geometric structure of the Killing horizon being respected. On the other hand, the behavior of the asymptotic Killing horizons on an extreme Killing horizon approaches that of the asymptotic Killing horizons on a non-extreme Killing horizon as the wave number increases. These properties of the acceleration are consistent with the discrepancy on the entropy of an extreme black hole between string theory [5] and the Euclidean approach [6], if the asymptotic Killing horizons correspond to the microscopic states responsible for black hole thermodynamics. It then may be possible that the quantum physics of asymptotic Killing horizons fills this unresolved gap between string theory and the Euclidean approach.

It is thus fascinating to speculate that the microscopic states responsible for black hole thermodynamics are described by asymptotic Killing horizons, at least at the classical level. In order to count the number of independent asymptotic Killing horizons precisely, we have to know the "spectrum" of asymptotic Killing horizons, and hence a complete theory of quantum gravity will be necessary ultimately. As we mentioned in Introduction, however, these microscopic states may possibly be described in a classical and geometric language. Since asymptotic Killing horizons are universal, classical, and geometric objects, and the acceleration associated with asymptotic Killing horizons shows the remarkable behavior mentioned above, it is interesting to investigate further the quantum features of asymptotic Killing horizons.

References

[1] T. Jacobson, in *General Relativity And Relativistic Astrophysics: Eighth Canadian Conference*, AIP Conference Proceedings 493, eds. C.P. Burgess and R.C. Myers (AIP Press, 1999) 85; T. Jacobson and R. Parentani, Found. Phys. **33** (2003) 323.

[2] S. Carlip, Phys. Rev. Lett. **82** (1999) 2828; Class. Quantum Grav. **16** (1999) 3327.

[3] G. W. Gibbons and S. W. Hawking, Phys. Rev. D **15** (1977) 2752.

[4] J. Koga, Phys. Rev. D **64** (2001) 124012.

[5] A. Strominger and C. Vafa, Phys. Lett. **B379** (1996) 99; see, for review, G. T. Horowitz, preprint gr-qc/9604051.

[6] S. W. Hawking, G. T. Horowitz and S. F. Ross, Phys. Rev. D **51** (1995) 4302; C. Teitelboim, Phys. Rev. D **51** (1995) 4315.

Moduli Instability in Warped Compactification

Hideo Kodama[1] and Kunihito Uzawa[2]

Yukawa Institute for Theoretical Physics, Kyoto University, Kyoto 606-8502, Japan

Abstract

We derive four-dimensional effective theories for warped compactification of the ten-dimensional IIB supergravity. We show that these effective theories allow a much wider class of solutions than the original higher-dimensional theories. This result indicates that the effective four-dimensional theories should be used with caution, if one regards the higher-dimensional theories more fundamental.

1 Introduction

Recently, a new class of dynamical solutions describing a size-modulus instability in the ten-dimensional type IIB supergravity model have been discovered by Gibbons et al. [1] and the authors [2]. These solutions can be always obtained by replacing the constant modulus h_0 in the warp factor $h = h_0 + h_1(y)$ for supersymmetric solutions by a linear function $h_0(x)$ of the four-dimensional coordinates x^μ. Such extensions exist for many of the well-known solutions compactified with flux on a conifold, resolved conifold, deformed conifold and compact Calabi-Yau manifold [2].

In most of the literature, the dynamics of the internal space, namely the moduli, in a higher-dimensional theory is investigated by utilising a four-dimensional effective theory. In particular, effective four-dimensional theories are used in essential ways in recent important work on the moduli stabilisation problem and the cosmological constant/inflation problem in the IIB sugra framework [3]. Hence, it is desirable to find the relation between the above dynamical solutions in the higher-dimensional theories and solutions in the effective four-dimensional theory.

In the conventional approach where the non-trivial warp factor does not exist or is neglected, an effective four-dimensional theory is derived from the original theory assuming the "product-type" ansatz for field variables. This ansatz requires that each basic field of the theory is expressed as the sum of terms of the form $f(x)\omega(y)$, where $f(x)$ is an unknown function of the four-dimensional coordinates x^μ, and $\omega(y)$ is a known harmonic tensor on the internal space. Further, it is assumed that the higher-dimensional metric takes the form $ds^2 = ds^2(\mathrm{X}_4) + h_0^3(x)ds^2(\mathrm{Y})$, where $ds^2(\mathrm{X}_4) = g_{\mu\nu}(x)dx^\mu dx^\nu$ is an unknown four-dimensional metric, $h_0(x)$ is the size modulus for the internal space depending only on the x-coordinates, and $ds^2(\mathrm{Y}) = \gamma_{pq}dy^p dy^q$ is a (Calabi-Yau) metric of the internal space that depends on the x-coordinates only through moduli parameters. Under this ansatz, the four-dimensional effective action is obtained by integrating out the known dependence on y^p in the higher-dimensional action.

The dynamical solutions in the warped compactification mentioned at the beginning, however, do not satisfy this ansatz. Hence, in order to incorporate such solutions to the effective theory, we have to modify the ansatz. Taking account of the structure of the supersymmetric solution, the most natural modification of the ansatz is to introduce the non-trivial warp factor h into the metric as $ds^2 = h^\alpha ds^2(\mathrm{X}_4) + h^\beta ds^2(\mathrm{Y})$ and assume that h depends on the four-dimensional coordinates x^μ only through the modulus parameter of the supersymmetric solution as in the case of the internal moduli degrees of freedom. This leads to the form $h = h_0(x) + h_1(y)$ for the IIB models, which is consistent with the structure of the dynamical solutions in the ten-dimensional theory.

In the present work, starting from this modified ansatz, we study the dynamics of the four-dimensional effective theory and its relation to the original higher-dimensional theory for warped compactification of the ten-dimensional type IIB supergravity For simplicity, we assume that the moduli parameters other than the size parameter are frozen.

[1] E-mail:kodama@yukawa.kyoto-u.ac.jp
[2] E-mail:uzawa@yukawa.kyoto-u.ac.jp

2 Ten-dimensional solutions

In our previous work [2], we derived a general dynamical solution for warped compactification with fluxes in the ten-dimensional type IIB supergravity. In that work, we imposed $d*(B_2 \wedge H_3) = 0$, which led to a slightly strong constraint on the free data for the solution, especially in the case of a compact internal space. Afterward, we have noticed that this condition is not necessary to solve the field equations, and without that condition, we can find a more general class of solutions. Because we take this class as the starting point of our argument, we first briefly explain how to get a general solution without that condition. We omit the details of calculations because they are essentially contained in our previous paper [2].

We assume that the ten-dimensional spacetime metric takes the form

$$ds^2(\mathrm{X}_{10}) = h^{-1/2}(x,y)ds^2(\mathrm{X}_4) + h^{1/2}(x,y)ds^2(\mathrm{Y}_6), \tag{1}$$

where X_4 is the four-dimensional spacetime with coordinates x^μ, and Y_6 is the six-dimensional internal space. We further require that the dilaton and the form fields satisfy the following conditions:

$$\tau \equiv C_0 + i e^{-\Phi} = i g_s^{-1} (= \mathrm{const}), \qquad G_3 \equiv i g_s^{-1} H_3 - F_3 = \frac{1}{3!} G_{pqr}(y)\, dy^p \wedge dy^q \wedge dy^r,$$
$$*_{\mathrm{Y}} G_3 = \epsilon i G_3 \quad (\epsilon = \pm 1), \qquad \tilde{F}_5 = dC_4 + B_2 \wedge F_3 = (1 \pm *) V_p dy^p \wedge \Omega(\mathrm{X}_4), \tag{2}$$

where g_s is a constant representing the string coupling constant, and $*$ and $*_{\mathrm{Y}}$ are the Hodge duals with respect to the ten-dimensional metric $ds^2(\mathrm{X}_{10})$ and the six-dimensional metric $ds^2(\mathrm{Y}_6)$, respectively.

Under these assumptions, we obtain the following expressions from the field equations for form fields [4]:

$$\tilde{F}_5 = \pm\epsilon(1 \pm *) d(h^{-1}) \wedge \Omega(\mathrm{X}_4), \qquad \triangle_{\mathrm{Y}} h = -\frac{g_s}{2}(G_3 \cdot \bar{G}_3)_{\mathrm{Y}}. \tag{3}$$

Next, by using the equations (2) and (3), the ten-dimensional Einstein equations can be written

$$h R_{\mu\nu}(\mathrm{X}_4) - D_\mu D_\nu h + \frac{1}{4} g_{\mu\nu}(\mathrm{X}_4) \triangle_{\mathrm{X}} h = 0, \qquad \partial_\mu \partial_p h = 0, \qquad R_{pq}(\mathrm{Y}_6) - \frac{1}{4} g_{pq}(\mathrm{Y}_6) \triangle_{\mathrm{X}} h = 0. \tag{4}$$

From the second of these equations, we immediately see that the warp factor h can be expressed as $h(x,y) = h_0(x) + h_1(y)$. Further, if we require that $d_y h \neq 0$, the rest of the equations can be reduced to

$$R_{\mu\nu}(\mathrm{X}_4) = 0, \qquad D_\mu D_\nu h_0 = \lambda g_{\mu\nu}(\mathrm{X}_4), \qquad R_{pq}(\mathrm{Y}_6) = \lambda g_{pq}(\mathrm{Y}_6). \tag{5}$$

Thus, we have found that the most general solutions satisfying the conditions (1) and (2) are specified by a Ricci flat spacetime X_4, an Einstein space Y_6, a closed imaginary-self-dual (ISD) 3-form G_3 on Y_6, and the function $h(x,y)$ that is the sum of $h_0(x)$ satisfying the second of the equations (5) and $h_1(x)$ satisfying the second of the equations (3). The additional constraint on G_3, $d_y[h^{-2}(B_2 \cdot dB_2)_{\mathrm{Y}}] = 0$, in Ref. [2] does not appear. Further, closed ISD 3-forms on Y_6 are in one-to-one correspondence with real harmonic 3-forms on Y_6. Hence, this class of dynamical solutions exist even for a generic compact Calabi-Yau internal space, if we allow $h_1(y)$ to be a singular function. This singular feature of h in the compact case with flux arises because h is a solution to the Poisson equation (3) and has nothing to do with the dynamical nature of the solution. It is shared by the other flux compactification models.

Here, note that the Ricci flatness of X_4 is required from the Einstein equations. This should be contrasted with no-warp case [4]. This point is quite important in the effective theory issue, as we see soon. Moreover, one can show that the Ricci flatness of X_4 and the second in the equations (5) are consistent only when X_4 is locally flat if $(Dh_0)^2 \neq 0$.

3 Four-dimensional effective theory

Now we study the four-dimensional effective theory that incorporates the dynamical solutions obtained in the previous section. For simplicity, we do not consider the internal moduli degrees of freedom of the metric of Y_6 or of the solution $h_1(y)$ in the present work. Then, in its x-independent subclass with $\lambda = 0$,

we have only one free parameter h_0. When we rescale $ds^2(\mathrm{Y}_6)$ by a constant ℓ as $\ell^2 ds^2(\mathrm{Y}_6) \to ds^2(\mathrm{Y}_6)$, we have to rescale h as $h/\ell^4 \to h$. We can easily see that the corresponding rescaled h_1 satisfies (3) again with the same G_3 as that before the rescaling. We can also confirm that the D3 brane charges associated with the 5-form flux do not change by this scaling. In contrast, h_0 changes its value by this rescaling. Therefore, h_0 represents the size modulus of the Calabi-Yau space Y_6.

On the basis of this observation, we construct the four-dimensional effective theory for the class of ten-dimensional configurations specified as follows. First, we assume that X_{10} has the metric

$$ds^2(\mathrm{X}_{10}) = h^{-1/2}(x,y)\, ds^2(\mathrm{X}_4) + h^{1/2}(x,y)\, ds^2(\mathrm{Y}_6), \tag{6}$$

where $h = h_0(x) + h_1(y)$ and $ds^2(\mathrm{Y}_6)$ is a fixed Einstein metric on Y_6 satisfying the third of the equations (5), while $ds^2(\mathrm{X}_4)$ is an arbitrary metric on X_4. Further, we assume that the dilaton is frozen as in (2), G_3 is given by a fixed closed ISD 3-form on Y_6, $h_1(y)$ is a fixed solution to the second of the equations (3), and $\tilde{F}_5$ is given by the first of the equations (3). Hence, the metric of X_4 and the function h_0 on it are the only dynamical variables in the effective theory.

The four-dimensional effective action for these variables can be obtained by evaluating the ten-dimensional action of the IIB theory

$$S_{\mathrm{IIB}} = \frac{1}{2\tilde{\kappa}^2}\int_{\mathrm{X}_{10}} d\Omega(\mathrm{X}_{10})\left[R(\mathrm{X}_{10}) - \frac{\nabla_M \bar{\tau}\nabla^M \tau}{2(\mathrm{Im}\tau)^2} - \frac{G_3\cdot\bar{G}_3}{2\,\mathrm{Im}\tau} - \frac{1}{4}\tilde{F}_5^2\right] \pm \frac{i}{8\tilde{\kappa}^2}\int_{\mathrm{X}_{10}} \frac{C_4\wedge G_3\wedge \bar{G}_3}{\mathrm{Im}\tau}, \tag{7}$$

for the class of configurations specified above. In general, there is a subtlety concerning the action of the type IIB supergravity, because the correct field equations can be obtained by imposing the self-duality condition $*\tilde{F}_5 = \pm\tilde{F}_5$ after taking variation of the action in general. In the present case, however, since we are only considering configurations (3) satisfying the self-duality condition, this problem does not affect our argument. We can obtain the "correct" effective action by simply inserting (3) into the above ten-dimensional action.

Inserting the expressions (3) and the third of the equations (5) into (7), we get [4]

$$S_{\mathrm{IIB}} = \frac{1}{2\kappa^2}\int_{\mathrm{X}_4} d\Omega(\mathrm{X}_4)\left[HR(\mathrm{X}_4) + 6\lambda\right], \tag{8}$$

where we have dropped the surface term coming from $\Delta_{\mathrm{X}} h_0$ and neglected the boundary term in the Chern-Simons term, $\kappa = (V_6)^{-1/2}\tilde{\kappa}$, and $H(x)$ is defined by

$$H(x) = h_0(x) + c; \quad c := V_6^{-1}\int_{\mathrm{Y}_6} d\Omega(\mathrm{Y}_6) h_1. \tag{9}$$

This effective action has the same form as the case of vanishing flux [4]. Hence, it gives the four-dimensional field equations of the same form as in the no-flux case:

$$R_{\mu\nu}(\mathrm{X}_4) = H^{-1}\left[D_\mu D_\nu H - \lambda g_{\mu\nu}(\mathrm{X}_4)\right], \qquad \Delta_{\mathrm{X}} H = 4\lambda. \tag{10}$$

If the four-dimensional spacetime is Ricci flat, these equations reproduce the correct equation for $h_0(x) = H - c$ obtained from the ten-dimensional theory [4]. However, the Ricci flatness of X_4 is not required in the effective theory unlike in the ten-dimensional theory. Hence, the class of solutions allowed in the four-dimensional effective theory is much larger than the original ten-dimensional theory.

In particular, the effective theory has a modular invariance similar to that found in the no-flux Calabi-Yau case with $\lambda = 0$. In fact, by the conformal transformation $ds^2(\mathrm{X}_4) = H^{-1} ds^2(\bar{\mathrm{X}}_4)$, (8) is expressed in terms of the variables in the Einstein frame as

$$S_{\mathrm{IIB}} = \frac{1}{2\kappa^2}\int_{\bar{\mathrm{X}}_4} d\Omega(\bar{\mathrm{X}}_4)\left[R(\bar{\mathrm{X}}_4) - \frac{3}{2}(\bar{D}\ln H)^2 + 6\lambda H^{-2}\right], \tag{11}$$

where $R(\bar{\mathrm{X}}_4)$ and $\bar{D}_\mu$ are the scalar curvature and the covariant derivative with respect to the metric $ds^2(\bar{\mathrm{X}}_4)$. The corresponding four-dimensional Einstein equations in the Einstein frame and the field equation for H are given by

$$R_{\mu\nu}(\bar{\mathrm{X}}_4) = \frac{3}{2}\bar{D}_\mu \ln H\, \bar{D}_\nu \ln H - 3\lambda H^{-2} g_{\mu\nu}(\bar{\mathrm{X}}_4), \qquad \Delta_{\bar{\mathrm{X}}} \ln H = 4\lambda H^{-2}, \tag{12}$$

where $\Delta_{\bar{X}}$ is the Laplacian with respect to the metric $ds^2(\bar{X}_4)$. It is clear that for $\lambda = 0$, this action and the equations of motion are invariant under the transformation $H \to k/H$, where k is an arbitrary positive constant.

This transformation corresponds to the following transformation in the original ten-dimensional metric. Let us denote the new metric of X_4 and the function h obtained by this transformation by $ds'^2(X_4)$ and h', respectively. Then, since the transformation preserves the four-dimensional metric in the Einstein frame, $ds'^2(X_4)$ is related to $ds^2(X_4)$ as $ds'^2(X_4) = (H^2/k)ds^2(X_4)$. In the meanwhile, from $H' = k/H = h'_0 + c$, h' is expressed in terms of the original h_0 as

$$h' = \frac{k}{h_0(x) + c} - c + h_1(y). \tag{13}$$

The corresponding ten-dimensional metric is written

$$ds^2 = k^{-1}H^2(h')^{-1/2}ds^2(X_4) + (h')^{1/2}ds^2(Y_6). \tag{14}$$

It is clear that this metric and h' do not satisfy the original ten-dimensional field equations. Hence, the modular-type invariance of the four-dimensional effective theory is not the invariance of the original ten-dimensional theory.

4 Summary

In the present work, we have derived four-dimensional effective theories for the spacetime metric and the size modulus of the internal space for warped compactification with flux in the ten-dimensional type IIB supergravity. The basic idea was to consider field configurations in higher dimensions that are obtained by replacing the constant size modulus in supersymmetric solutions for warped compactifications, by a field on the four-dimensional spacetime. The effective action for this moduli field and the four-dimensional metric has been determined by evaluating the higher-dimensional action for such configurations. In all cases, the dynamical solutions in the ten-dimensional theories found by Gibbons et al. [1], Kodama and Uzawa [2] were reproduced in the four-dimensional effective theories [4].

In addition to this, we have found that these four-dimensional effective theories have some unexpected features. First, the effective actions of both theories are exactly identical to the four-dimensional effective action for direct-product type compactifications with no flux in ten-dimensional supergravities. In particular, the corresponding effective theory has a kind of modular invariance with respect to the size modulus field in the Einstein frame. This implies that if there is a solution in which the internal space expands with the cosmic expansion, there is always a conjugate solution in which the internal space shrinks with the cosmic expansion.

Second, the four-dimensional effective theory for warped compactification allows solutions that cannot be obtained from solutions in the original higher-dimensional theories. The modular invariance in the four-dimensional theory mentioned above is not respected in the original higher-dimensional theory either. The same results hold for the heterotic M-theory[4]. This situation should be contrasted with the no-warp case in which the four-dimensional effective theory and the original higher-dimensional theory are equivalent under the product-type ansatz for the metric structure. This result implies that we have to be careful when we use a four-dimensional effective theory to analyse the moduli stabilisation problem and the cosmological problems in the framework of warped compactification of supergravity or M-theory.

References

[1] G. W. Gibbons, H. Lü and C. N. Pope, Phys. Rev. Lett. **94** (2005) 131602 [arXiv:hep-th/0501117].

[2] H. Kodama and K. Uzawa, JHEP **0507** (2005) 061 [arXiv:hep-th/0504193].

[3] S. Kachru, R. Kallosh, A. Linde and S. P. Trivedi, Phys. Rev. D **68** (2003) 046005 [arXiv:hep-th/0301240].

[4] H. Kodama and K. Uzawa, arXiv:hep-th/0512104.

Inner Structure of Kaluza-Klein Black Holes

Hideki Ishihara[1] and Ken Matsuno[2]

Department of Mathematics and Physics, Graduate School of Science, Osaka City University, Sumiyoshi-ku Osaka 558-8585, Japan

Abstract

We study static charged Kaluza-Klein black hole solutions in the five-dimensional Einstein-Maxwell system. The solution has horizons of squashed three-sphere, and the asymptotic structure is four-dimensional flat with a compact S^1 bundle. It is shown that the singularity is point-like when the charge is small in comparison to the size of S^1 at infinity, and is spindle-like when the charge is large.

1 Introduction

The studies on higher dimensional black holes have started from the pioneering works [1, 2, 3] in the context of unified theories of gravity with other forces [4]. Almost higher dimensional black holes are obtained with the boundary condition of asymptotic flatness in all dimensions. If the size of black hole is much smaller than the size of extra dimension, such a solution is approximately valid in the vicinity of the hole, However, in far away from the hole its geometry should be four-dimensional, effectively[5].

We study the geometry of static charged black holes in the five-dimensional Einstein-Maxwell theory[6]. Horizons of the black hole are in the shape of squashed S^3, and the spacetime is asymptotically locally flat, i.e., asymptotes to a twisted S^1 bundle over four-dimensional Minkowski spacetime.

The solutions are characterized by three parameters: size of inner and outer horizons and size of S^1 fiber at infinity. The singularity of the present static solution is hidden in the horizons that is deformed owing to the non-trivial asymptotic structure. We show that two types of singularity are possible depending on the ratio of charge to size of extra dimension at infinity.

2 Static solution with horizon

The action we consider is

$$S = \frac{1}{16\pi G}\int d^5x\sqrt{-g}\,(R - F_{\mu\nu}F^{\mu\nu})\,, \tag{1}$$

where R is the scalar curvature and F is the Maxwell field strength 2-form and G denotes the five-dimensional Newton's constant. The equations of motion derived from (1) are

$$d\,{}^*F = 0, \quad dF = 0, \tag{2}$$

and

$$R_{\mu\nu} - \frac{1}{2}Rg_{\mu\nu} = 2\left(F_{\mu\lambda}F^{\lambda}_{\nu} - \frac{1}{4}g_{\mu\nu}F_{\alpha\beta}F^{\alpha\beta}\right). \tag{3}$$

We assume a five-dimensional static spacetime with SO(3)× U(1) symmetry. The metric has the form

$$ds^2 = -h^2(x)dt^2 + N^2(x)dx^2 + a^2(x)\sigma_1^2 + b^2(x)(\sigma_2^2 + \sigma_3^2), \tag{4}$$

where a, b, and f are function of x and σ_i $(i = 1, 2, 3)$ satisfy the relation

$$d\sigma^i = \frac{1}{2}C^i_{jk}\sigma^j \wedge \sigma^k, \quad C^1_{23} = C^2_{31} = C^3_{12} = 1.$$

[1]E-mail:ishihara@sci.osaka-cu.ac.jp
[2]E-mail:matsuno@sci.osaka-cu.ac.jp

The 2-form

$$F = \frac{u}{ab^2}(hdt) \wedge (Ndx) \tag{5}$$

solves the Maxwell equations (2), where u is a constant. When we take a coordinate condition

$$N = hab^2 \tag{6}$$

the Einstein equations (3) are represented as

$$2\left(2\frac{a'}{a} + \frac{b'}{b}\right)\frac{b'}{b} + 2\left(\frac{a'}{a} + 2\frac{b'}{b}\right)\frac{h'}{h} - (2b^2 - \frac{1}{2}a^2)a^2h^2 = -\frac{3}{2}u^2h^2, \tag{7}$$

$$\left(\frac{a'}{a}\right)' - \frac{1}{2}a^4h^2 = -\frac{1}{2}u^2h^2, \tag{8}$$

$$\left(\frac{b'}{b}\right)' - (b^2 - \frac{1}{2}a^2)a^2h^2 = -\frac{1}{2}u^2h^2, \tag{9}$$

$$\left(\frac{h'}{h}\right)' = u^2h^2. \tag{10}$$

where the prime denotes the derivative with respect to x.

If the metric (4) has a horizon, the temporal component h vanishes on the horizon while a and b take finite values there. Then, we take the solution to (10) in the form

$$h = \frac{\alpha}{u\sinh\alpha x}, \tag{11}$$

where α is an arbitrary constant. It is possible to assume $\alpha \geq 0$ without loss of generality. Since $h \to 0$ as $x \to \infty$ then we should require that

$$a \to finite, \quad b \to finite. \quad \text{as} \quad x \to \infty. \tag{12}$$

We obtain the solutions satisfying (12) in the form

$$a^2 = \frac{|u|\sinh\alpha x}{\sinh\alpha(x - x_a)}, \qquad b^2 = \frac{|u|\sinh\alpha x \sinh\alpha(x - x_a)}{\sinh^2\alpha(x - x_b)}, \tag{13}$$

where x_a, x_b are arbitrary constants. The set of solutions (11) and (13) surely satisfy the constraint equation (7).

3 Properties of Solutions

It would be easy to see the geometrical structure of the spacetime in a new coordinate system. Introducing the radial coordinate by $r^2/4 = a^2(x)$, we have the metric in the form

$$ds^2 = -fdt^2 + \frac{k^2}{f}dr^2 + \frac{r^2}{4}\left[k(\sigma_1^2 + \sigma_2^2) + \sigma_3^2\right], \tag{14}$$

where

$$f(r) := \frac{(r^2 - r_+^2)(r^2 - r_-^2)}{r^4}, \quad k(r) := \frac{(r_\infty^2 - r_+^2)(r_\infty^2 - r_-^2)}{(r_\infty^2 - r^2)^2}, \tag{15}$$

and

$$r_\pm^2 := 4ue^{\pm\alpha x_a}, \quad r_\infty^2 := \frac{4|u|\sinh\alpha x_b}{\sinh\alpha(x_b - x_a)}. \tag{16}$$

In the expression (14), we rescaling of time coordinate has been done. Here, we assume the positivity of k so that $r_\pm < r_\infty$ or $r_\pm > r_\infty$ to keep Lorentzian signature of the metric.

Each $r = const.$ surface on a time-slice in (14) has S^3 topology which is squashed geometrically by the function $k(r)$. It is clear that there are horizons at $r_\pm$, where they are squashed in their shapes[6]. There exist curvature singularities at $r = 0$ and $r = \infty$. The singularity at $r = 0$ is 'point-like' because $r = const.$ surfaces shrink to a point as $r \to 0$. On the other hand, the singularity at $r = \infty$ is 'spindle-like' because the squashing function $k(r)$ goes to zero as $r \to \infty$, i.e., two directions of S^3 shrink but one direction diverges.

The apparent singularity at $r = r_\infty$ of the metric (14) is spatial infinity. To observe this we introduce a new radial coordinate ρ as

$$\rho = \rho_0 \frac{r^2}{r_\infty^2 - r^2}. \tag{17}$$

where

$$\rho_0^2 = \frac{(r_\infty^2 - r_+^2)(r_\infty^2 - r_-^2)}{4r_\infty^2}. \tag{18}$$

We take positive sign of ρ_0 for the case $r_\infty^2 > r^2$ and negative sign for $r_\infty^2 < r^2$. The new coordinate ρ varies $0 \to \infty$ as r does $0 \to r_\infty$, and ρ varies $\infty \to |\rho_0|$ as r does $r_\infty \to \infty$. Two regions in r coordinate, $0 < r < r_\infty$ and $r_\infty < r < \infty$, are described separately in ρ coordinate with the parameter $\rho_0 > 0$ and $\rho_0 < 0$, respectively.

The metric (14) can be rewritten by ρ and $T = \sqrt{f_\infty}\, t$ as

$$ds^2 = -V dT^2 + \frac{K^2}{V} d\rho^2 + R^2 d\Omega_{S^2}^2 + W^2 \chi^2, \tag{19}$$

where V, K, R and W are functions of ρ in the form

$$\begin{aligned} &V = \frac{(\rho - \rho_+)(\rho - \rho_-)}{\rho^2}, \quad K^2 = \frac{\rho + \rho_0}{\rho}, \quad R^2 = \rho^2 K^2, \\ &W^2 = \frac{r_\infty^2}{4} K^{-2} = (\rho_+ + \rho_0)(\rho_- + \rho_0)\, K^{-2}, \quad \rho_\pm = \rho_0 \frac{r_\pm^2}{r_\infty^2 - r_\pm^2}. \end{aligned} \tag{20}$$

and

$$d\Omega_{S^2}^2 = d\theta^2 + \sin^2\theta d\phi^2, \quad \chi = \sigma^3 = d\psi + \cos\theta d\phi. \tag{21}$$

It should be noted that each surface $r = const.$ on a time-slice, topologically S^3, is regarded as the Hopf bundle, S^1 fiber over S^2 base space. Then, we use an angular coordinate in (21).

When $\rho \to \infty$, i.e., $r \to r_\infty$, the metric (19) with (20) approaches

$$ds^2 = -dT^2 + d\rho^2 + \rho^2 d\Omega_{S^2}^2 + \frac{r_\infty^2}{4} \chi^2. \tag{22}$$

Therefore, $\rho \to \infty$, equivalently $r \to r_\infty$, means spatial infinity, and the spacetime is locally asymptotically flat, i.e., topologically not a direct product but twisted S^1 fiber bundle over four-dimensional Minkowski spacetime. The value r_∞ means the size of S^1 fiber at the infinity. Therefore, metric (14) describes a couple of spacetimes, $0 < r < r_\infty$ and $r_\infty < r < \infty$, attached at r_∞. From the geometrical point of view, these are disconnected because $r = r_\infty$ is spatial infinity.

When Mass and charge of the black holes are defined by the integral over the three-dimensional topological sphere at spatial infinity as

$$M = -\frac{3}{32\pi G} \int_\infty dS_{\mu\nu} \nabla^\mu (\partial_T)^\nu, \quad Q = \frac{1}{8\pi G} \int_\infty dS_{\mu\nu} F^{\mu\nu}, \tag{23}$$

we have

$$\begin{aligned} &M = \frac{3\pi}{4} \frac{r_\infty}{G} (\rho_+ + \rho_-), \\ &Q = \frac{\sqrt{3}\pi}{G} r_\infty \sqrt{\rho_+ \rho_-} = \frac{\sqrt{3}\pi}{2G} r_\infty^2 \sqrt{\frac{1}{(1 + \rho_0/\rho_+)(1 + \rho_0/\rho_-)}}. \end{aligned} \tag{24}$$

4 Point-like and Spindle-like Singularities

From (19) with (20), the metric with the parameter $\rho_0 > 0$ has the point-like singularity at $\rho = 0$ ($r = 0$), and metric with $\rho_0 < 0$ has spindle-like singularity at $\rho = |\rho_0|$ ($r = \infty$). If $\rho_\pm > 0$ the spacetime has horizons at $\rho = \rho_\pm$ which conceal the singularity behind them, while if $\rho_\pm < 0$ naked singularities appear. The variation of solutions are summarized in the following table.

	Point-like Singularity	Spindle-like Singularity
Black Hole	$\rho_0 > 0,\ \rho_\pm > 0$	$\rho_0 < 0,\ \rho_\pm > 0$
Naked Singularity	$\rho_0 > 0,\ \rho_\pm < 0$	$\rho_0 < 0,\ \rho_\pm < 0$

We see, from (24), that $\frac{2G}{\sqrt{3}\pi} Q/r_\infty^2 < 1$ for $\rho_0 > 0$ case, and $\frac{2G}{\sqrt{3}\pi} Q/r_\infty^2 > 1$ for $\rho_0 < 0$. Then, we can say that the black hole has point-like singularity when the ratio of charge to size of S^1 at infinity is smaller than unity, and the black hole has spindle-like singularity when the ratio is samller than unity.

In the limiting case of $\rho_0 = 0$, i.e., $Q = \frac{\sqrt{3}\pi}{2G} r_\infty^2 = \frac{2\sqrt{3}\pi}{G} \rho_+ \rho_-$, the metric becomes

$$ds^2 = -\frac{(\rho - \rho_+)(\rho - \rho_-)}{\rho^2} dT^2 + \frac{\rho^2 d\rho^2}{(\rho - \rho_+)(\rho - \rho_-)} + \rho^2 d\Omega_{S^2}^2 + \rho_+ \rho_- \chi^2. \tag{25}$$

The metric is S^1 bundle over the four-dimensional Reissner-Nordström metric, where the size of S^1 bundle is constant which is determined by the charge, everywhere. The singularity is 'ring-like' with the size $\sqrt{\frac{2G}{\sqrt{3}\pi} Q}$.

We can take another limit $\rho_+ = \rho_-$, equivalently $M = \frac{\sqrt{3}}{2} Q$. In this limit, the metric becomes a squashed version of the extremal Reissner-Nordström solution with a degenerate horizon. This is a supersymmetric solution for five-dimensional Einstein-Maxwell-Chern-Simon system, which is the bosonic part of five-dimensional supergravity[7]. It is interesting that there are three types of supersymmetric black hole solutions: the extremal black hole with the point-like singularity, the spindle-like singularity, and the ring-like singularity.

References

[1] F.R. Tangherlini, Nuov. Cim. **27**, 636 (1963).

[2] P.Dobiasch and D.Maison, Gen. Relativ. Grav. **14**, 231 (1982);
G.W.Gibbons and D.L.Wiltshire, Ann. Phys. **167**, 201 (1986).

[3] R. C. Myers and M. J. Perry, Annals Phys. **172**, 304 (1986).

[4] M. Cvetic and D. Youm, Nucl. Phys. B **476**, 118 (1996);
D. Klemm and W. A. Sabra, JHEP **0102**, 031 (2001);
J. P. Gauntlett, J. B. Gutowski, C. M. Hull, S. Pakis, H. S. Reall, Class. Quant. Grav. **20** 4587, (2003);
M. Cvetic, H. Lu and C. N. Pope, Phys. Lett. B **598**, 273 (2004);
J. B. Gutowski and H. S. Reall, JHEP **0404**, 048 (2004).

[5] R. C. Myers, Phys. Rev. **D 35**, 455 (1987).

[6] H.Ishihara and K.Matsuno, hep-th/0510094;
See also report by K.Matsuno in this volume.

[7] D. Gaiotto, A. Strominger, X. Yin, hep-th/0503217;
H.Elvang, R. Emparan D.Mateos and H.S.Reall, JHEP **08**, 042 (2005).

Stationary Spacetime from Intersecting M-branes

Kei-ichi Maeda[1,2,3] [1], Makoto Tanabe[1] [2]

[1] *Department of Physics, Waseda University, 3-4-1 Okubo, Shinjuku, Tokyo 169-8555, Japan*

[2] *Advanced Research Institute for Science and Engineering, Waseda University, Shinjuku, Tokyo 169-8555, Japan*

[3] *Waseda Institute for Astrophysics, Waseda University, Shinjuku, Tokyo 169-8555, Japan*

Abstract

We study a stationary "black" brane in M/superstring theory. Assuming BPS-type relations between the first-order derivatives of metric functions, we present general stationary black brane solutions with a traveling wave for the Einstein equations in D-dimensions. The solutions are given by a few independent harmonic equations (and plus the Poisson equation). General solutions are constructed by superposition of a complete set of those harmonic functions. Using the hyperspherical coordinate system, we explicitly give the solutions in 11-dimensional M theory for the case with M2⊥M5 intersecting branes and a traveling wave. Compactifying these solutions into five dimensions, we show that these solutions include the BMPV black hole and the Brinkmann wave solution. We also find new solutions similar to the Brinkmann wave. We prove that the solutions preserve the 1/8 supersymmetry if the gravi-electromagnetic field $\mathcal{F}_{ij}$, which is a rotational part of gravity, is self-dual. We also discuss non-spherical "black" objects (e.g., a ring topology and an elliptical shape) by use of other curvilinear coordinates.

1 Introduction

Black holes are now one of the most important subjects in string theory. The Beckenstein-Hawking black hole entropy of an extreme black hole is obtained in string theory by statistical counting of the corresponding microscopic states [1]. While, we have found several interesting black hole solutions in supergravity theories [2], which are obtained as an effective theory of a superstring model in a low energy limit. We also know black hole solutions in a higher-dimensional spacetime [3, 4], which play a key role in a unified theory such as string theory. In higher dimensions, because there is no uniqueness theorem of black holes [5, 6, 7], we have a variety of "black" objects such as a black brane [8]. One of the most remarkable solutions is a black ring, which horizon has a topology of $S^1 \times S^2$ [9].

Among such "black" objects, supersymmetric ones are very important. The black hole solutions in a supergravity include the higher-order effects of a string coupling constant, although these are solutions in a low energy limit. On the other hand, the counting of states of corresponding branes is performed at the lowest order of a string coupling. The results of these two calculations need not coincide each other. However, if there is supersymmetry, these should be the same because the numbers of dynamical freedom cannot be different in these BPS representations. Therefore, supersymmetric black hole (or black ring) solutions are often discussed in many literature [10].

The classification of supersymmetric solutions in minimal $\mathcal{N} = 2$ supergravity in $D = 4$ was first performed by a time-like or null Killing spinor [15]. Recently, solutions in minimal $\mathcal{N} = 1$ supergravity in $D = 5$ have been classified into two classes by use of G-structures analysis [16, 17, 18, 19, 20]. The six-dimensional minimal supergravity has also been discussed [21].

However, the fundamental theory is constructed in either ten or eleven dimensions. When we discuss the entropy of black holes, we have to show the relation between those supersymmetric black holes and more fundamental "black" branes in either $D = 10$ or 11, from which we obtain "black" holes (or rings)

[1] e-mail address:maeda@gravity.phys.waseda.ac.jp
[2] e-mail address:tanabe@gravity.phys.waseda.ac.jp

via compactification. The entropy is microscopically described by the charges of branes [22, 23]. A supersymmetric rotating solution is obtained by compactification from M or type II supergravity [24, 25]. The supersymmetric rotating black ring solution is found [26, 27. 28, 29, 30]. Such solutions are obtained also in lower dimensions. These solutions are in fact new classes of rotating solutions in four- or five-dimensional supergravity. The existence of such solutions suggests that the uniqueness theorem of black holes is no longer valid even in supersymmetric spacetime if the dimension is five or higher [31]. Thus we may need to construct more generic "black" brane solutions in the fundamental theory and the black holes by some compactification. M-theory is the best candidate for such a unified theory. Since its low energy limit coincides with the eleven-dimensional supergravity, it provides a natural framework to study "black" brane or BPS brane solutions.

In this paper we study a class of intersecting brane solutions in D-dimensions with a $(d-1)$-dimensional transverse conformally flat space. We start with a generic form of the metric and solve the field equations of the supergravity (the Einstein equations and the equations for form fields). Assuming the intersection rule for the intersecting branes, which is the same as that derived in a spherically symmetric case [32, 33, 34], we derive the equations for each metric. We find that most metric components are described by harmonic functions. which are independent. One metric component f. which corresponds to a traveling wave, is usually given by the Poisson equation, which source term is given by the quadratic form of the "gravi-electromagnetic" field $\mathcal{F}_{ij}$. In some configuration of branes, e.g., for two intersecting charged branes (M2⊥M5), the source term vanishes. As a result, we find only independent harmonic functions. Hence, we can easily construct arbitrary solution by superposing those harmonics. In order to preserve 1/8 supersymmetry, we have to impose that $\mathcal{F}_{ij}$ is self-dual.

2 A Stationary Spacetime with Branes

We first present the basic equations for a stationary spacetime with intersecting branes and describe how to construct generic solutions. We consider the following bosonic sector of a low energy effective action of superstring theory or M-theory in D dimensions ($D \leq 11$):

$$S = \frac{1}{16\pi G_D}\int d^D X\sqrt{-g}\left[\mathcal{R} - \frac{1}{2}(\nabla\varphi)^2 - \sum_A \frac{1}{2\cdot n_A!}e^{a_A\varphi}F^2_{\mathbf{n_A}}\right], \tag{1}$$

where $\mathcal{R}$ is the Ricci scalar of a spacetime metric $g_{\mu\nu}$, $F_{\mathbf{n_A}}$ is the field strength of an arbitrary form with a degree $n_A(\leq D/2)$, and a_A is its coupling constant with a dilaton field φ. Each index A describes a different type of brane. Although we leave the spacetime dimension D free, the present action is most suitable for describing the bosonic part of $D = 10$ or $D = 11$ supergravity.

As for a metric form for a spacetime with intersecting branes, we assume the following metric form [25]:

$$ds^2 = 2\theta^{\hat{u}}\theta^{\hat{v}} + \sum_{i=1}^{d-1}(\theta^{\hat{i}})^2 + \sum_{\alpha=2}^{p}(\theta^{\hat{\alpha}})^2, \tag{2}$$

where $D = d + p$ and the dual basis $\theta^{\hat{A}}$ are given by

$$\theta^{\hat{u}} = e^{\xi}du, \quad \theta^{\hat{v}} = e^{\xi}\left(dv + fdu + \frac{\mathcal{A}}{\sqrt{2}}\right), \quad \theta^{\hat{i}} = e^{\eta}dx^i, \quad \theta^{\hat{\alpha}} = e^{\zeta_\alpha}dy^\alpha. \tag{3}$$

Here we have used light-cone coordinates: $u = -(t - y_1)/\sqrt{2}$ and $v = (t + y_1)/\sqrt{2}$. This metric form includes rotation of spacetime and a traveling wave. Since we are interested in a stationary solution, we assume that the metric components f, $\mathcal{A} = \mathcal{A}_i dx^i$, ξ, η and ζ_α depend only on the spatial coordinates x^i in d-dimensions, which coordinates are given by $\{t, x^i(i = 1, 2, \cdots, d-1)\}$. In this setting, we set each brane A in a submanifold of p-spatial dimensions, which coordinates are given by $\{y_\alpha(\alpha = 1, 2. \cdots, p)\}$. Note that the solution in this metric form is invariant under the gauge transformation, $\mathcal{A} \to \mathcal{A} + d\Lambda$, $v \to v - \Lambda/\sqrt{2}$.

As for the n_A-form field with a q_A-brane, we assume that the source brane exists in the coordinates $\{y_1, y_{\alpha_2}, \cdots, y_{\alpha_{q_A}}\}$. The form field generated by an "electric" charge is given by the following form:

$$F_{\mathbf{n_A}} = \partial_j E_A dx^j \wedge du \wedge dv \wedge dy_2 \wedge \cdots \wedge dy_{q_A} + \frac{1}{\sqrt{2}} \partial_i B_j^A dx^i \wedge dx^j \wedge du \wedge dy_2 \wedge \cdots \wedge dy_{q_A}, \quad (4)$$

where $n_A = q_A + 2$ and E_A and B_j^A are scalar and vector potentials. This setting automatically guarantees the Bianchi identity.

We can also discuss the form field generated by a "magnetic" charge by use of a dual ${}^*n_A$-field with ${}^*q_A$-brane, which is obtained by a dual transformation of the n_A-field with a q_A-brane (${}^*n_A \equiv D - n_A, {}^*q_A \equiv {}^*n_A - 2$). In other words, the field components of $F_{\mathbf{n_A}}$ generated by a "magnetic" charge are described by the same form of (4) of the dual field ${}^*F_{\mathbf{n_A}} = F_{{}^*\mathbf{n_A}}$. We then treat $F_{{}^*\mathbf{n_A}}$, which is generated by a "magnetic" charge, as another independent form field with a different brane from $F_{\mathbf{n_A}}$, which is generated by an "electric" charge, when we sum up by the types of branes A.

The solution obtained in this section is summarized as follows:

$$ds^2 = \prod_A H_A^{2\frac{\gamma_{AA}+1}{\Delta_A}} \left[2 \prod_B H_B^{-2\frac{D-2}{\Delta_B}} du \left(dv + f du + \frac{\mathcal{A}}{\sqrt{2}} \right) + \sum_{\alpha=2}^{p} \prod_B H_B^{-2\frac{\gamma_{\alpha B}}{\Delta_B}} dy_\alpha^2 + \sum_{i=1}^{d-1} dx_i^2 \right],$$
$$\varphi = (D-2) \sum_A \frac{\epsilon_A a_A}{\Delta_A} \ln H_A, \quad (5)$$

where

$$\Delta_A = (q_A + 1)(D - q_A - 3) + \frac{D-2}{2} a_A^2,$$
$$\gamma_{\alpha A} = \delta_{\alpha A} + q_A + 1 = \begin{cases} D-2 & \alpha = \alpha_2, \cdots, \alpha_{q_A} \\ 0 & \text{otherwise} \end{cases}. \quad (6)$$

H_A for each q_A-brane and $\mathcal{A} = \mathcal{A}_i dx^i$ are arbitrary harmonic functions, while the vector potential B_i^A can be chosen either as $B_i^A \propto \mathcal{A}_i / H_A$ (when $H_A \neq 1$), or an arbitrary harmonic function (when $H_A = 1$). The "wave" metric f usually satisfies the Poisson equation

$$\partial^2 f = \frac{1}{2} \left[1 - \sum_A \frac{D-2}{\Delta_A} \right] \prod_B H_B^{-\frac{2(D-2)}{\Delta_A}} (\partial_{[j} \mathcal{A}_{i]})^2, \quad (7)$$

with some source term originated by the "rotation"-induced metric $\mathcal{A}_i$, although it can be also an arbitrary harmonic function for some specific configuration of branes.

It is worth noticing that we have independent Laplace equations for H_A and $\mathcal{A}_i$. This makes the construction of solutions very easy. The superposition of any solutions also provides us an exact solution. Hence we can construct an infinite number of solutions. We can also show that a part of supersymmetry is preserved if $\mathcal{F}_{ij}$ is self-dual.

We consider solutions in five-dimensions. There are two branes (M2 and M5). In the ten-dimensional type IIB case, we find the exactly the same as what we show below, when we replace M2 and M5 with D1 and D5 (the indices $A = 2, 5$ with the indices $A = 1, 5$).

The metric in five-dimensions is written by

$$d\bar{s}_5^2 = -\Xi^2 \left(dt + \frac{\mathcal{A}}{2} \right)^2 + \Xi^{-1} ds_{\mathbf{E}^4}^2, \quad (8)$$

where $\Xi = [H_2 H_5 (1+f)]^{-1/3}$. The unknown functions $H_A (A = 2, 5)$, $\mathcal{A}_i$ and f satisfy the following equations:

$$\partial^2 H_A = 0 \quad (A = 2, 5) \quad (9)$$
$$\partial_j \mathcal{F}^{ij} = 0 \quad (10)$$
$$\partial^2 f = 0, \quad (11)$$

where $\mathcal{F}_{ij} = \partial_i \mathcal{A}_j - \partial_j \mathcal{A}_i$.

References

[1] A. Strominger and C. Vafa, Phys. Lett. B 379 (1996) 99, hep-th/9601029.

[2] G.W. Gibbons, Nucl. Phys. B 207 (1982) 337.

[3] F. R. Tangherlini, Nuovo Cim. 27 (1963) 636.

[4] R.C. Myers and M.J. Perry, Ann. Phys. 172 (1986) 304.

[5] G. W. Gibbons, D. Ida and T. Shiromizu, Phys. Rev. Lett. 89 (2002) 041101, hep-th/0206136.

[6] H. S. Reall, Phys. Rev. D 68 (2003) 024024, hep-th/0211290.

[7] H. Elvang, R. Emparan JHEP 0311 (2003) 035, hep-th/0310008.

[8] R. R. Khuri, and R. C. Myers, Fields Inst. Comm. 15 (1997) 273, hep-th/9512137.

[9] R. Emparan and H.R. Reall, Phys. Rev. Lett. 88 (2000) 101101, hep-th/0110260.

[10] R. Kallosh, Phys. Lett. B 282 (1992) 80, hep-th/9201029.

[11] K. P. Tod, Phys. Lett. B 121 (1983) 241.

[12] W. A. Sabra, Mod. Phys. Lett. A 13 (1997) 239, hep-th/9708103.

[13] J.P. Gauntlett, R.C. Myers, and P.K. Townsend, Class. Quantum Grav. 16 (1999) 1, hep-th/9809065.

[14] J.P. Gauntlett, J. B. Gutowski, C. M. Hull, S. Pakis and S. Reall, Class. Quant. Grav. 20 (2003) 4587, hep-th/0209114.

[15] J. P. Gauntlett, Fortsch. Phys. 53 (2005) 468, hep-th/0501229.

[16] J. P. Gauntlett and S. Pakis, Commun. Math. Phys. 247 (2004) 421, hep-th/0212008.

[17] J. B. Gutowski, D. Martelli and H. S. Reall, Class. Quant. Grav. 20 (2003) 5049, hep-th/0306235.

[18] S. R. Das, hep-th/9602172.

[19] M. Cvetic, and C. M. Hull, Nucl. Phys. B 519 (1988) 141, hep-th/9709033.

[20] J. C. Breckenridge, R. C. Myers, A. W. Peet and C. Vafa, Phys. Lett. B 391 (1993) 93, hep-th/9602065.

[21] C. A. R. Herdeiro, Nucl. Phys. B 582 (2000) 363, hep-th/0003063.

[22] H. Elvang, R. Emparan, D. Mateos, H.S. Reall, Phys.Rev.Lett. 93 (2004) 211302, hep-th/0407065.

[23] H. Elvang, R.Emparan, D. Mateos, H.S. Reall, Phys.Rev. D 71 (2005) 024033, hep-th/0408120.

[24] I. Bena and P. Kraus, JHEP 0412 (2004) 070, hep-th/0408186.

[25] P. Kraus and F. Larsen, hep-th/0503219.

[26] H. Elvang, R. Emparan, D. Mateos, H.S. Reall, JHEP 0508 (2005) 042, hep-th/0504125.

[27] J. B. Gutowski, H. S. Reall, JHEP 0402 (2004) 006, hep-th/0401042.

[28] N. Ohta, Phys. Lett. B 403 (1997) 218, hep-th/9702164.

[29] N. Ohta, K. L. Panigrahi and Sanjay, Nucl.Phys. B 674 (2003) 306, hep-th/0306186.

[30] Y.-G. Miao and N. Ohta, Phys. Lett. B 594 (2004) 218, hep-th/0404082.

Is there a stable phase of non-uniform black branes?

Umpei Miyamoto [1], Hideaki Kudoh [2]

[1] *Department of Physics, Waseda University, Okubo 3-4-1, Tokyo 169-8555, Japan*
[2] *Department of Physics, The University of Tokyo, Tokyo 113-0033, Japan*

Abstract

The final fate of dynamical (Gregory-Laflamme) instability of black objects with a translational invariance is an open problem in general relativity and string theory. In this article, we investigate the stability and thermodynamical properties of charged black strings wrapped over a transverse circle by constructing perturbatively inhomogeneous solutions. A surprising result is that there exist thermodynamically favored inhomogeneous non-extremal states even in sensibly low spacetime dimensions ($5 \leq D \leq 13$), which was known only for high dimensions ($D \geq 14$) in vacuum spacetime. We argue that the final fate of Gregory-Laflamme instability highly depends on charge even when the homogeneous branes are sufficiently non-extremal.

1 Introduction

It is known that the black objects with translational symmetries such as black branes and black strings suffer from a dynamical instability to distribute their mass breaking the translational symmetries, which is called Gregory-Laflamme (GL) instability [1]. Naive expectation is that they decay into individual black holes, having larger entropy via certain topological changing. Horowitz and Maeda [2] showed, however, that inhomogeneous black strings do not "pinch off" in finite proper time under certain assumption, forbidding a naked singularity. It is fare to say that the final fate of GL instability is still an open problem.

In vacuum, static black strings (branes) would not avoid the dynamical instability without compactification in the direction of translational symmetries. The GL mode is marginally stable static mode, and an interesting point here is that the non-uniform black string branch emerging from the critical point continues to be static beyond linear regime. By using this fact, Gubser developed a method to construct perturbative non-uniform solutions up to an arbitrary order, in principle [3]. He performed the static perturbation up to third order to show the phase transition from uniform to non-uniform strings is first order in 5 dimension, e.g., the entropy of the non-uniform black string is smaller than the uniform solution for same mass. The generalization of his analysis to higher dimensions reveals the existence of critical dimension above which the phase transition is higher order [4, 5]. Recently, it was shown by non-perturbative numerical calculation that branches of static black hole and black string merge at a certain topological changing solution in a phase diagram [6].

For the instability of charged black objects with translational symmetry, which of course contains the vacuum as a special case, there is an interesting conjecture called Correlated-Stability Conjecture (CSC), which is called also Gubser-Mitra conjecture [7]. CSC asserts that the GL instability of black objects with a non-compact translational invariance occurs if and only if they are (locally) thermodynamically unstable. Although this conjecture has been verified for several cases in string-theory setting [8], a possible counterexample was proposed and possible sophistication of original CSC was discussed in [9] very recently. Although one can believe that charges (, angular momenta, dilaton and so on) play crucial roles, our understanding for stability and phase structure of charged black objects are highly restricted.

For the purpose of understanding the final fate of GL instability, we perform static perturbations of charged (non-dilatonic) black strings, and investigate their thermodynamical properties. As the main result, we discover new thermodynamically favored non-uniform black strings over the uniform ones with same mass and charge (and also with same temperature and charge), which were not known for sensibly low spacetime dimensions in neutral spacetime.

[1] E-mail: umpei at gravity.phys.waseda.ac.jp
[2] E-mail: kudoh at utap.phys.s.u-tokyo.ac.jp

2 Perturbative construction of inhomogeneous black strings

2.1 Background solution and its thermodynamical stability

We consider the following $(d+1)$-dimensional action $(d \geq 4)$:

$$I_{d+1} = \frac{1}{16\pi G_{d+1}} \int d^{d+1}x\sqrt{-g}\left[R - \frac{2}{(d-2)!}F^2\right], \tag{1}$$

where F is a $(d-2)$-form field. We would like to construct non-uniform black string solutions in this system. Metric ansatz is

$$\begin{aligned} ds^2_{d+1} &= -e^{2a(r,z)}f_+dt^2 + \frac{e^{2b(r,z)}}{f_+f_-}dr^2 + e^{2b(r,z)}f_-dz^2 + e^{2c(r,z)}r^2d\Omega^2_{d-2}, \\ f_\pm(r) &= 1 - \left(\frac{r_\pm}{r}\right)^{d-3}. \end{aligned} \tag{2}$$

Settling $a = b = c = 0$, we recover the well-known black string solution obtained by Horowitz and Strominger [10]. $r = r_+$ corresponds to event horizon. For parameter region of $0 < r_- \leq r_+$, there exist a curvature singularity at $r = r_-$. Under this ansatz, we can obtain general solution for the magnetic part of form fields: $F = Q\varepsilon_{d-2}$, where Q is a magnetic charge and ε_{d-2} is the volume element of a unit sphere.

The thermodynamical stability of the uniform black string solution is equivalent to the positivity of heat capacity, given by

$$\left(\frac{\partial M}{\partial T}\right)_Q \propto \frac{\sqrt{1-q^{d-3}}[(d-2)-q^{d-3}]}{(d-2)q^{d-3}-1}, \quad q \equiv \frac{r_-}{r_+} \quad (0 \leq q < 1). \tag{3}$$

We can see that there is a critical value of q, given by $q_c = (d-2)^{1/(3-d)}$, below (above) which the heat capacity (3) is negative (positive). CSC asserts that GL instability exists if and only if $q < q_c$.

2.2 Perturbation scheme

Under the metric ansatz, we construct non-uniform black strings by static perturbation around the uniform solution $(a = b = c = 0)$. First of all, we normalize coordinates by horizon radius

$$y \equiv \frac{r}{r_+}, \quad x \equiv \frac{z}{r_+}. \tag{4}$$

According to Gubser [3], we expand the metric functions $X(x,y)$ $(X = a, b, c)$ as follows:

$$\begin{aligned} X(x,y) &= \sum_{n=0}^{\infty} \epsilon^n X_n(y)\cos(nKx), \\ X_n(y) &= \sum_{p=0}^{\infty} \epsilon^{2p} X_{n,p}(y), \quad K = \sum_{q=0}^{\infty} \epsilon^{2q} k_q, \end{aligned} \tag{5}$$

where ϵ is a small expansion parameter and $X_{0,0} = 0$ is imposed. K is the GL critical wave number and $L = 2\pi/K$ gives the asymptotic length of the compactified x-direction.

At each order of ϵ, we obtain ODEs for $X_{n,p}(y)$ $(n, p \in \{0\} \cup \mathbf{N})$, which appears at $O(\epsilon^{n+2p})$. At first order $O(\epsilon)$, we have ODEs for KK mode $X_{1,0}$. Solving them by shooting method, we can specify the GL critical wave number k_0. The dependence of k_0 on charge Q, which is a certain function of q, is shown in Fig. 1. As expected from CSC, we can see that the GL mode disappears at $q = q_c$ above which the background solutions becomes thermodynamically stable.

3 Higher-order perturbations and thermodynamics

At $O(\epsilon^2)$, we have second-order KK mode $X_{2,0}$ and lowest-order zero $X_{0,1}$ mode, which contributes to correction of asymptotic quantities such as mass, charge and so on. It is known that one have to solve perturbations up to third order $O(\epsilon^3)$ to estimate physically meaningful thermodynamical quantities being invariant under rigid rescalings of solutions. We solve perturbation equations for $X_{1,1}$, which contain the next order correction of critical wave number, k_1.

Anyway, we can discuss thermodynamics of non-uniform black string by solving perturbative equations up to third order. What we are most interested in is whether the non-uniform black string solution is favored over the uniform black string in suitable ensembles, such as microcanonical and canonical ensembles. The entropy difference between uniform and non-uniform black string for same mass and charge can be written as

$$\frac{S_{\rm NU} - S_{\rm U}}{S_{\rm NU}} = \sigma_1 \epsilon^2 + \sigma_2 \epsilon^4 + O(\epsilon^6). \tag{6}$$

From the first law of black hole thermodynamics, we can show $\sigma_1 = 0$, which is seen also by numerical results. In fact, we use this vanishing of σ_1 as a code test. Therefore, the leading order is $O(\epsilon^4)$. In a similar way, the comparison of (Helmholtz) free energy between uniform and non-uniform black strings for same temperature and charge can be written as

$$\frac{F_{\rm NU} - F_{\rm U}}{F_{\rm NU}} = \rho_1 \epsilon^2 + \rho_2 \epsilon^4 + O(\epsilon^6), \tag{7}$$

where $\rho_1 = 0$ vanishes from the first law.

We present the dependence of σ_2 and ρ_2 on charge in Fig. 2 for $D \equiv d + 1 = 6$. It is interesting that there exist regions where non-uniform black strings are thermodynamically favored, i.e., regions where $\sigma_2 > 0$ and/or $\rho_2 < 0$. It should be noted that in vacuum case, dimensions at which non-uniform black strings are entropically favored are restricted to $D \geq 14$ [4], and for free-energy restricted to $D \geq 13$ [5]. We have observed that the appearance of regions where $\sigma_2 > 0$ and $\rho_2 < 0$ is generic in a large range of spacetime dimensions, $6 \leq D \leq 14$.

4 Conclusion

In this article, we have constructed charged non-uniform black strings by static perturbations, and then investigated their thermodynamical properties. As the result, we have found that there exists sufficiently non-extremal inhomogeneous black strings which are thermodynamically favored over the uniform black strings. It should be noted that inhomogeneous neutral black strings have larger entropy (lower free-energy) than homogeneous ones *only* for large spacetime dimensions, $D \geq 14$ [4] ($D \geq 13$ [5]). We have seen that inhomogeneous thermodynamically favored black strings (therefore also branes) are generic and ubiquitous in that they exist for generic spacetime dimensions $6 \leq D \leq 14$ (it would be the case for $D = 5$ and $D \geq 15$ although we have not confirmed yet), and for non-zero measure parameter regions. The results suggest that the phase transition from uniform to non-uniform black strings can be smooth even in lower dimensions, $D < 14$.

There is a discussion by Horowitz and Maeda [11] that there exist near extremal non-uniform black strings which have larger entropy than the uniform counterpart. They argued that non-uniform black strings are not necessarily result of dynamical instability. Although their argument is similar to ours, the non-uniform solutions obtained in this paper are very on a branch of solutions emerging from the GL static points, and therefore would be related to GL instability. The point is that solutions obtained in this paper is sufficiently non-extremal.

For simplicity, we have considered non-dilatonic, KK compactified, and asymptotically flat solutions. For example, a dilaton, however, is known to drastically change stability structure of black branes even at linear level [8]. Therefore, taking into consideration of dilation, other compactification and another asymptotics, such as AdS, will be interesting applications of this analysis.

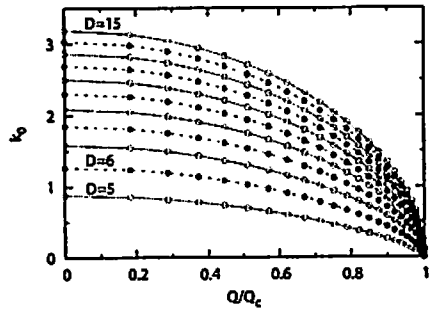

Figure 1: Dependence of GL critical wave number, k_0 (normalized by the inverse of horizon radius), on magnetic charge for various spacetime dimensions $D = d + 1 = 5 \sim 15$. Q_c represents the magnetic charge of background solution at which the sign of heat capacity changes. As far as authors know, these are the clearest evidence of Correlated-Stability Conjecture (Gubser-Mitra conjecture).

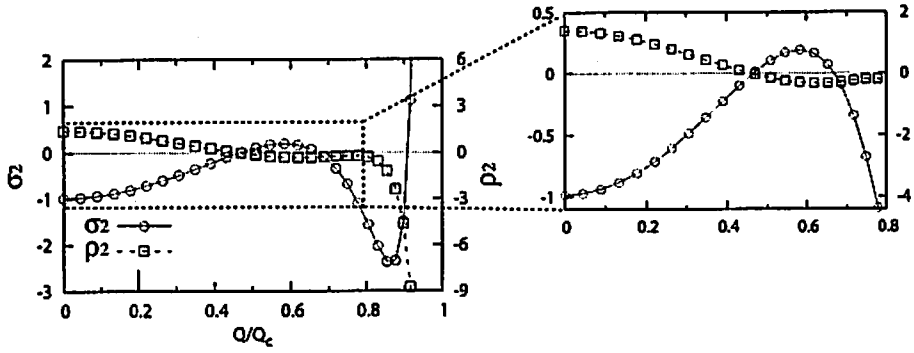

Figure 2: The comparison of entropy (free-energy) between uniform and non-uniform black strings for same mass (temperature) and charge for $D = 6$. σ_2 and ρ_2 are defined by Eqs. (6) and (7). We can see that there exist charge regions where non-uniform black strings are thermodynamically favored, i.e., $\sigma_2 > 0$ and/or $\rho_2 < 0$.

References

[1] R. Gregory and R. Laflamme, Phys. Rev. Lett. **70**, 2837 (1993).

[2] G. T. Horowitz and K. Maeda, Phys. Rev. Lett. **87**, 131301 (2001).

[3] S. S. Gubser, Class. Quant. Grav. **19**, 4825 (2002).

[4] E. Sorkin, Phys. Rev. Lett. **93**, 031601 (2004).

[5] H. Kudoh and U. Miyamoto, Class. Quant. Grav. **22**, 3853 (2005).

[6] H. Kudoh and T. Wiseman, Phys. Rev. Lett. **94**, 161102 (2005).

[7] S. S. Gubser and I. Mitra, arXiv:hep-th/0009126; JHEP **0108**, 018 (2001).

[8] T. Hirayama, G. Kang and Y. Lee, Phys. Rev. D **67**, 024007 (2003).

[9] J. J. Friess, S. S. Gubser and I. Mitra, Phys. Rev. D **72**, 104019 (2005).

[10] G. T. Horowitz and A. Strominger, Nucl. Phys. B **360**, 197 (1991).

[11] G. T. Horowitz and K. Maeda, Phys. Rev. D **65**, 104028 (2002).

Fractional spacelike branes on a timelike orbifold
— A string toy model of initial singularity —

Shinsuke Kawai[1]

Yukawa Institute for Theoretical Physics, Kyoto University, Kyoto 606-8502, Japan

Abstract

A new type of space-like brane solution is constructed in the rolling tachyon picture. The solution describes nucleation and decay of an unstable brane at a fixed point of a spacetime orbifold, $\mathbb{R}^{1,d}/\mathbb{Z}_2$, which is obtained from the Minkowski spacetime by a $\mathbb{Z}_2$ identification. The unstable brane at the orbifold fixed point may be considered as a string theoretical initial condition of the brane gas cosmology since it cascades into closed strings.

1 Introduction

In observational cosmology a number of experimental projects are now yielding copious high-precision data on the cosmological microwave background as well as the large scale structure, and there are also new projects, such as gravitational wave detectors, which are expected to yield exciting and important results in the coming decade. Today string theory on time-dependent backgrounds is an active area of theoretical study. This is partially motivated by the developments of cosmology; it is natural for string theorists to consider the Universe as a sort of laboratory in which various ideas and possible models may be tested.

From a string theory perspective physics near the initial singularity is of particular interest since there the general relativity breaks down and purely stringy effects are expected to play some rôle. Our knowledge of cosmological singularities in string theory is still quite limited, apart from a few concrete toy models that allow explicit computations. Such toy models[1, 2, 3] are normally obtained from a known exact background (Minkowski, say) using an orbifold identification, so that the resulting spacetime contains a spacelike orbifold singularity. This of course is somewhat different from the Big Bang singularity of the Friedmann-Robertson-Walker spacetime and may seem odd from an eye of a cosmologist, but the idea here is that the priority is on being an exact string theory target space, since general relativity as a low energy effective theory cannot be trusted near singularities.

The topic of this talk is on a construction of soliton-like extended objects, which we call fractional S(pacelike)-branes, on one of such toy models namely a spacetime orbifold[3]. There are mainly three motivations for considering such objects: (i) in string-inspired cosmological scenarios such as the Pre-Big Bang, Ekpyrotic and Cyclic models, it is usually assumed that by some resolution mechanism the time continues beyond the Big Bang singularity (the singularity thus corresponding to the reheating stage of the standard inflationary cosmology). As the resolution of the singularity is not established and the concept of time itself breaks down at the singularity, one may instead consider a model which has finite past, i.e. one could speculate that the arrow of time starts from a single point. On such a background branes are natural objects. In particular, one could hope that introducing S-branes may give rise to the origin of matter as well as imposing a controllable initial condition of the spacetime. (ii) resolution mechanism of *static* orbifold singularities is well understood in string theory. As twisted strings and fractional branes are known to be essential in such resolution, if an analogous mechanism exist for a spacelike singularity the fractional S-branes may be essential in the physics near the singularity. (iii) the original prototype model of rolling tachyon (the full S-brane solution) [4, 5] describes a creation and decay process of an unstable brane. Its variant, the half S-brane solution[6], describes decay of an unstable brane that starts at past infinity and continues to future infinity. Our fractional S-brane scenario is a sort of hybrid of those two basic models, keeping merits of both: it has the virtue of having a parameter of time scale as does the full S-brane, and it is free from fine-tuned creation phase like the half S-brane.

This talk is based on our recent work[7]. Below we shall sketch the main ideas.

[1] E-mail:skawai@yukawa.kyoto-u.ac.jp

2 Spacetime orbifold: the background geometry

The spacetime orbifold, on which we shall construct S-branes, is obtained from the Minkowski space by folding in temporal as well as spacial d directions with a $\mathbb{Z}_2$ identification:

$$(X^0, X^1, \cdots, X^d) \to (-X^0, -X^1, \cdots, -X^d). \tag{1}$$

The resulting spacetime is $(\mathbb{R}^{1,d}/\mathbb{Z}_2) \otimes \mathbb{R}^{25-d}$ for bosonic and $(\mathbb{R}^{1,d}/\mathbb{Z}_2) \otimes \mathbb{R}^{9-d}$ for superstring theory. Such a spacetime is bounded in past, is not (globally) time-orientable and contains a fixed point of the $\mathbb{Z}_2$ reflection. Quantum field theory and string theory on this orbifold have been studied in [3, 8]. There are some issues that are specific to the orbifold theory. For example, the time function needs to be chosen appropriately, and the Hilbert space has to be doubled and then symmetrised. It has been found that (i) the no-ghost theorem holds (ii) closed string tachyons are absent in the superstring theory (iii) one may choose the time function so that closed causal curves are absent (iv) S-matrices are locally well-defined. The spacetime orbifold is hence almost as well-behaved as the Minkowski space. On the initial spacelike hypersurface the energy-momentum tensor diverges and the spacetime is singular. We note that the initial hypersurface is nevertheless well defined in the dual open string picture.

3 Rolling tachyon on the spacetime orbifold

Let us recall the full and half S-brane solutions in the standard unorbifolded spacetime. The full S-brane is associated with tachyon profile of the form, $T(X^0) = \lambda \cosh(X^0/\sqrt{\alpha'})$, which describe a tachyon field that rolls up the potential hill, reaches the maximum point at $X^0 = 0$ and then rolls back to the original position at large X^0. The target space interpretation of this is an unstable brane temporally localised around $X^0 = 0$, generated by incoming radiation at $X^0 < 0$ and decaying into closed strings at $X^0 > 0$. The parameter λ determines the lifetime of the S-brane, $\Delta X^0 \sim 2 \ln \sin \pi\lambda$. This profile is symmetric under time reflection $X^0 \leftrightarrow -X^0$. The second type of solution, the half S-brane[6], is generated by the boundary tachyon of the profile $T(X^0) = \lambda \exp(X^0/\sqrt{\alpha'})$. In this solution the tachyon is infinitesimally displaced from the top of the potential at $X^0 = -\infty$ and rolls down the hill as time evolves (the side being determined by the sign of λ). The half S-brane solution does not have a formation phase; the unstable brane only decays. In this solution the absolute value of λ does not have a physical meaning as it can be absorbed into redefinition of X^0. In both full and half S-brane solutions the profile of the tachyon has been chosen so that upon Wick rotation it becomes exactly marginal and that the conformal invariance is unspoiled by the boundary perturbation.

Finding an S-brane solution on the spacetime orbifold background amounts to studying the moduli space of orbifold D-branes in particular direction of deformation that corresponds to boundary tachyon profile of interest. Without deformation, on $S^1/\mathbb{Z}_2$ orbifold of generic compactification radius R we know that there are two possible boundary conditions, Dirichlet and Neumann, which may be imposed. These boundary conditions correspond to boundary states. Away from the fixed points they are $\mathbb{Z}_2$ projected superposition of covering space images[9],

$$|D(x_0)\rangle\!\rangle^{orb}_{bulk} = \frac{1}{\sqrt{2}}(|D(x_0)\rangle_U + |D(-x_0)\rangle_U), \qquad |N(\tilde{x}_0)\rangle\!\rangle^{orb}_{bulk} = \frac{1}{\sqrt{2}}(|N(\tilde{x}_0)\rangle_U + |N(-\tilde{x}_0)\rangle_U), \tag{2}$$

where x_0 ($0 < x_0 < \pi R$) and $\tilde{x}_0$ ($0 < \tilde{x}_0 < \pi\alpha'/R$) are respectively the position of the D-brane and the value of Wilson line on the Neumann boundary. The subscript U means the *untwisted* sector. At the orbifold fixed points $\xi = 0, \pi R$ and $\tilde{\xi} = 0, \pi\alpha'/R$, the states $D(x_0)$ and $N(\tilde{x}_0)$ above do not belong to irreducible representations of the CFT and one needs to introduce the fractional states that involve the twisted sector[9],

$$|D(\xi, \pm)\rangle\!\rangle^{orb}_{frac} = \frac{1}{\sqrt{2}}|D(\xi)\rangle_U \pm \frac{1}{\sqrt[4]{2}}|D(\xi)\rangle_T, \qquad |N(\tilde{\xi}, \pm)\rangle\!\rangle^{orb}_{frac} = \frac{1}{\sqrt{2}}|N(\tilde{\xi})\rangle_U \pm \frac{1}{\sqrt[4]{2}}|N(\tilde{\xi})\rangle_T. \tag{3}$$

Here, T stands for the *twisted* sector, i.e. states which are periodic only up to $\mathbb{Z}_2$. We consider the $S^1/\mathbb{Z}_2$ as the compactified time direction, such that $x_0 = 0$ as the beginning and $x_0 = \pi R$ as the end of time (after suitable Wick rotation).

It is important to notice that among the three directions of deformation in the unorbifolded theory (corresponding to the three generators of $SU(2)$) only one associated with the full S-brane tachyon profile survives the $\mathbb{Z}_2$ projection (recall that $\cosh(X^0/\sqrt{\alpha'})$ is symmetric under $X^0 \leftrightarrow -X^0$). We are interested in the dynamics of the fractional branes (3) in the spacetime orbifold so shall consider their deformation by $\mathbb{Z}_2$-projected full S-brane tachyon profile. We have analysed the moduli space of boundary in this model following various approaches. One way of doing this is to use the equivalence of two CFTs, the $S^1/\mathbb{Z}_2$ orbifold theory at $R = \sqrt{\alpha'}$ and S^1 compactified theory at $R = \frac{1}{2}\sqrt{\alpha'}$, which is explained in [10]. It can be shown that the generator $J_1^{orb} = \cos(2X/\sqrt{\alpha'})$ of the orbifold theory (which becomes the full S-brane tachyon profile after Wick rotation) corresponds to $J_3^{circ} = i\partial X$ of the S^1 theory. Since the latter is the operator which shifts the position of D-branes along the compactified S^1 direction, we see that the moduli space of D-branes in the orbifold theory is S^1 in the direction of J_1^{orb}. This correspondence can be made more precise by comparing partition functions (the overlaps of boundary states) of the two theories. It turns out that the eight fractional boundary states are transformed into one anther as the deformation parameter λ is varied; they are eight evenly spaced points on S^1, as shown in Figure 1 below. This picture is valid only when $R = \sqrt{\alpha'}$. As we are interested in a macroscopic spacetime whose scale is much larger than the string length $\sqrt{\alpha'}$ we need to take the decompactified limit $R \to \infty$. Within the boundary state formalism the boundary deformation for more general radii may be considered by introducing suitable projection operators analogous to the S^1 case of [11]. Here we have taken a more direct approach by moving over to the open string formalism. The key idea is to use the fermionisation of [12] to convert the system into free fermions with masses localised on worldsheet boundaries. Once the fermionisation has been accomplished one can move on to arbitrary, at least rational, value of orbifold radius since the system has been converted into free fermions which interact only indirectly with the boundary through mass terms. In the decompactified limit, we can see that one of the fixed points which has been sent to infinity decouples from the system so the deformation of the fractional branes becomes

$$D(0,\pm) \to N(0,\pm). \tag{4}$$

Dynamics of the fractional S-branes can be seen from an overlap, $\langle V|B\rangle$, between a closed string state V and the fractional S-brane boundary state, $|B\rangle = N_p|B\rangle_{X^0}|B\rangle_{sp}|B\rangle_{gh}$, where sp and gh stand for the spatial and ghost parts. In the open string picture the overlap may be obtained by factorisation of the 1-loop amplitude, $\langle B'|\Delta|B\rangle \sim \sum_j \langle B'|V_j\rangle\langle V_j|B\rangle$, where Δ is a probagator. We have computed an overlap between the fractional S-brane and the untwisted sector ground state, yielding a result similar to the standard unorbifolded case[13, 14]. There are some technical issues specific to the orbifold; in the spacetime orbifold it is natural to take the prescription of [13] for computing the number density and energy density of emitted closed strings. Since X^0 is now on a complex half plane with no past direction in real time, integration must be performed along the (double) Hartle-Hawking contour. The result, in the fundamental domain, may then be interpreted as a nucleation of an unstable fractional S-brane at $X^0 = 0$ which subsequently decays into closed strings. Interpretation of the twisted sector is more subtle; there are very few physical states in this sector, and they are localised at the initial spacelike hypersurface $X^0 = 0$. Although we do not have a clear conceptual understanding of the twisted sector of this model at the moment, it may be speculated that, analogously to the Euclidean orbifolds, that the twisted sector may play some rôle in smoothing the spacelike singularity. Actually in a model of boost orbifold that has a spacelike singularity some mechanism of resolution has been proposed[1]. Such a possibility clearly deserves further investigation.

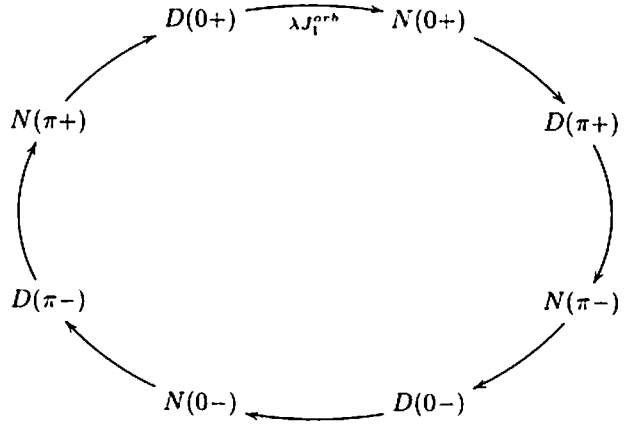

Figure 1. J_1^{orb}-deformation of the fractional boundary states on the $\mathbb{Z}_2$ orbifold at the self-dual radius $R = \sqrt{\alpha'} \equiv 1$. The 8 states are evenly spaced 8 points on S^1.

4 Summary and concluding remarks

We have presented our construction of a new type of rolling tachyon solution which we call fractional S-branes. This solution describes nucleation and decay of an unstable brane in the spacetime orbifold background. We conclude this talk by listing some directions of study that we think is of interest: (i) the spacetime orbifold is, while it is extremely simple, an interesting and useful toy model of a spacetime that is bounded in past. The fractional S-brane sets a natural boundary condition of the spacetime orbifold and, as it cascades into closed strings, it may be used to explain the origin of matter in such a spacetime. In particular, it might be regarded as a initial condition of the string gas cosmology[15]. (ii) as is mentioned previously it would be intriguing to study a possible resolution of a spacelike singularity in the spacetime orbifold, and investigate the resolved geometry using the fractional S-branes. (iii) if there exists a correspondence between a supergravity theory in $D+1$-dimensional de Sitter space and a gauge theory in D dimensions the fractional S-branes that we have discussed here would be instrumental in studying such a correspondence.

Acknowledgements

I thank Esko Keski-Vakkuri, Rob Leigh and Sean Nowling for enjoyable collaboration. Support from JSPS (Research Fellowships for Young Scientists) is acknowledged.

References

[1] B. Durin and B. Pioline, arXiv:hep-th/0501145.

[2] B. Craps, S. Sethi and E. P. Verlinde, JHEP **0510** (2005) 005 [arXiv:hep-th/0506180].

[3] V. Balasubramanian, S. F. Hassan, E. Keski-Vakkuri and A. Naqvi, Phys. Rev. D **67** (2003) 026003.

[4] A. Sen, JHEP **0204** (2002) 048.

[5] M. Gutperle and A. Strominger, JHEP **0204** (2002) 018.

[6] F. Larsen, A. Naqvi and S. Terashima, JHEP **0302** (2003) 039.

[7] S. Kawai, E. Keski-Vakkuri, R. G. Leigh and S. Nowling, Phys. Rev. Lett. **96** (2006) 031301.

[8] R. Biswas, E. Keski-Vakkuri, R. G. Leigh, S. Nowling and E. Sharpe, JHEP **0401** (2004) 064.

[9] M. Oshikawa and I. Affleck, Nucl. Phys. B **495** (1997) 533.

[10] A. Recknagel and V. Schomerus, Nucl. Phys. B **545** (1999) 233.

[11] M. R. Gaberdiel and A. Recknagel, JHEP **0111** (2001) 016.

[12] J. Polchinski and L. Thorlacius, Phys. Rev. D **50** (1994) 622.

[13] N. Lambert, H. Liu and J. Maldacena, arXiv:hep-th/0303139.

[14] D. Gaiotto, N. Itzhaki and L. Rastelli, Nucl. Phys. B **688** (2004) 70.

[15] R. H. Brandenberger and C. Vafa, Nucl. Phys. B **316** (1989) 391.

A variational formulation for the Einstein-Maxwell equations

Sumio Yamada[1]

Mathematical Institute, Tohoku University
Sendai, Japan

Abstract

We construct a time-symmetric asymptotically flat initial date set to the Einstein-Maxwell equations which satisfies the inequality

$$m < \frac{1}{2}\left(R + \frac{Q^2}{R}\right)$$

where m is the ADM mass, $R := \sqrt{\frac{A}{4\pi}}$ is the area radius of the outer-most horizon, and Q is the total charge. This yields a counter-example to a natural generalization of the Penrose Inequality $m \geq R/2$ to charged black holes.

1 Introduction

The aim of this article is to present an overview of a result proven in [7] by the author together with Gilbert Weinstein.

As an attempt to understand the properties of the ADM mass, there has been much interest in inequalities bounding the total mass of initial data sets from below in terms of other geometrical quantities.

The first such inequality is the Positive Mass Theorem [6, 8]. The Riemannian version of this result, that is, when the second fundamental form of the initial data set vanishes identically, can be formulated as:

Among all time-symmetric asymptotically flat initial data sets for Einstein-Vacuum Equations, flat Euclidean 3-space is the unique minimizer of the total mass.

Thus the total mass satisfies $m \geq 0$ with equality if and only if the data set is isometric to $\mathbb{R}^3$ with the flat metric.

A stronger result is the Riemannian version of the Penrose Inequality [1, 3], which can be stated in a similar variational vein:

Among all time-symmetric asymptotically flat initial data sets for the Einstein-Vacuum Equations with an outermost minimal surface of area A, the Schwarzschild slice is the unique minimizer of the total mass.

In other words, $m \geq R/2$ where $R = \sqrt{A/4\pi}$ is the area radius of the outermost horizon, and equality occurs if and only if the data is isometric to the *Schwarzschild slice*:

$$g_{ij} = \left(1 + \frac{m}{2r}\right)^4 \delta_{ij}.$$

defined on $\mathbb{R}^3 \backslash \{0\}$.

When these results are phrased in this fashion, a natural question is whether similar variational characterizations of the other known stationary solutions of the Einstein Equations hold. In particular, one could ask whether among all asymptotically flat axisymmetric maximal gauge initial data sets for

[1]E-mail:yamada@math.tohoku.ac.jp

the Einstein-Vacuum Equations with an outermost minimal surface of area A and angular momentum J, the Kerr slice is the unique minimizer of the mass. Such a statement would imply that:

$$m \geq \frac{1}{2}\left(R^2 + \frac{4J^2}{R^2}\right)^{1/2}. \tag{1}$$

with equality if and only if the data is isometric to the *Kerr slice*. Since it is not known how to define the angular momentum of a finite surface, it is necessary to assume the axisymmetry of the data set. With that hypothesis, if X is the generator of the axisymmetry, then the Komar integral:

$$J(S) = \frac{1}{8\pi}\int_S k_{ij}X^i n^j \, dA$$

gives a quantity which depends only on the homological type of S and tends to the total angular momentum, as S tends to the sphere at infinity.

A similar question can be asked with charge replacing angular momentum:

Is the Reissner-Nordström slice the unique minimizer of the mass among all asymptotically flat time-symmetric initial data set for the Einstein-Maxwell Equations?

Recall here that A time-symmetric initial data set (M, g, E, B) for the Einstein-Maxwell Equations consists of a Riemannian manifold (M, g), and two vector fields E and B on M such that:

$$R_g = 2\left(|E|_g^2 + |B|_g^2\right),\ \mathrm{div}_g E = \mathrm{div}_g B = 0,\ E \times B = 0,\ \int_S g(B, n_g)\, dA = 0,$$

where R_g is the scalar curvature of g, and $S \subset M$ is an arbitrary closed surface with normal n_g of unit length in g. The question posed above is equivalent to asking whether the following inequality holds for any initial data set:

$$m \geq \frac{1}{2}\left(R + \frac{Q^2}{R}\right), \tag{2}$$

where Q is the total charge, with equality if and only if the data is a Reissner-Nordström slice. As above, the charge:

$$Q(S) = \frac{1}{4\pi}\int_S E_i n^i \, dA$$

depends only on the homological type of S.

When the horizon is connected, inequality (2) can be proved by using the Inverse Mean Curvature flow [3, 5]. Indeed, the argument in [5] relies simply on Geroch montonicity of the Hawking mass — which still holds for the weak flow introduced by Huisken and Ilmanen in [3] — while keeping track of the scalar curvature term $R = 2\left(|E|^2 + |B|^2\right)$. However, when the horizon has several components the same argument yields only the following inequality:

$$m \geq \frac{1}{2}\max_i\left(R_i + \frac{\left(\min\sum_i \varepsilon_i Q_i\right)^2}{R_i}\right),$$

where R_i and Q_i are the area radii and charges of the components of the horizon $i = 1, \ldots, N$, $\varepsilon_i = 0$ or 1, and the minimum is taken over all possible combinations.

In [7] we prove that (2) does not hold:

Main Theorem *There is a strongly asymptotically flat time-symmetric initial data set $(M, g, E, 0)$ for the Einstein-Maxwell Equations such that:*

$$m - \frac{1}{2}\left(R + \frac{Q^2}{R}\right) < 0. \tag{3}$$

In 1984, Gibbons [2] conjectured an inequality similar to (2). However, in his conjecture, the right hand side of (2) is taken to be additive over connected components of the horizon. Thus, Gibbons's conjecture states that:

$$m \geq \frac{1}{2} \sum_i \left(R_i + \frac{Q_i^2}{R_i} \right). \tag{4}$$

In particular, when there is no electromagnetic field this inequality reduces to:

$$m \geq \frac{1}{2} \sum_i R_i, \tag{5}$$

which is stronger than the usual Riemannian Penrose inequality;

$$m \geq \frac{1}{2} \left(\sum_i R_i^2 \right)^{1/2}.$$

It is not known whether (5) holds, but two Schwarzschild slices a large distance apart would seem to violate this inequality. Gibbons further conjectured that equality occurs in (4) if and only if the data is Majumdar-Papapetrou; see the next section for a description of these metrics. We note that these metrics do not actually have horizons and are not asymptotically flat. Instead, they have one asymptotically flat end and N asymptotically cylindrical ends which we will call *necks*. The cross-sections of these necks are spheres with mean curvature tending to zero as the surfaces goes further down the end.

Our construction of the counterexample to (2) is based on the fact that the Majumdar-Papapetrou metrics 'violate' (2). Choose $N > 0$, $m_k > 0$, and $p_k \in \mathbb{R}^3$ for $k = 1, \ldots, N$, and let r_k denote the Euclidean distance in $\mathbb{R}^3$ to p_k. The *Majumdar-Papapetrou* solutions are given by:

$$u = \left(1 + \sum_{k=1}^{N} \frac{m_k}{r_k} \right)^{1/2}, \qquad g_{ij} = u^4 \delta_{ij}, \qquad E_i = 2\nabla_i \log u, \qquad B_i = 0. \tag{6}$$

When $N = 1$, this is simply the extreme case $m = |Q|$ of the Reissner-Nordström data set. Note that if we take $E_- = -2\nabla \log u$ instead of $E = 2\nabla \log u$, we get another solution with charges of opposite sign. We consider a particular situation with $N = 2$, and $m_1 = m_2$. The metric $-u^{-4}dt^2 + g$ is a static solution of the Einstein-Maxwell equations. Let r denote the Euclidean distance from the origin. We denote by $B_i(\rho) = \{r_i < \rho\}$ the Euclidean ball of radius ρ centered at p_i, and by $B_0(\rho) = \{r < \rho\}$ the Euclidean ball of radius ρ centered at the origin. Note that for R large enough $N = \mathbb{R}^3 \setminus B_0(R)$ equipped with the metric g is a strongly aymptotically flat end, and the necks $B_i(\rho) \setminus \{p_i\}$ are asymptotically cylindrical. It is easy to check that the total mass μ of N is $2m$, the total charge $Q = \int_S g(E, n)\, dA$ is $2m$, while the total cross sectional area A of both necks is asymptotically $8\pi m^2$, i.e., $R = \sqrt{2}m$. Thus, we get:

$$\mu - \frac{1}{2} \left(R + \frac{Q^2}{R} \right) = 2m - \frac{1}{2}(\sqrt{2}m + 2\sqrt{2}m) = m \left(2 - \frac{3}{\sqrt{2}} \right) < 0.$$

This does not yet constitute a counte-rexample to (2) since the space is not asymptotically flat and do not possess horizons. In order to remedy these failures, we glue two such copies along the necks. The gluing procedure we use is an adaptation of the conformal perturbation method developed for the vacuum case in [4]. In fact in our setting, some of the technical difficulties arising from the generality of the construction in [4] are absent. However, while it is easy to show the existence of a two-component minimal surface in the resulting metric, we must also show that (2) is violated with R the area radius of the outermost horizon. This requires ruling out minimal surfaces outside the necks which we can accomplish by letting $m \to 0$ which is equivalent after rescaling to taking the two masses in the initial Majumdar-Papapetrou far apart.

Lastly we point out that this counter-example has little to do with the Cosmic Censorship conjecture. In fact, as pointed out by Jang [5], inequality (2) is equivalent to:

$$m - \sqrt{m^2 - Q^2} \leq R \leq m + \sqrt{m^2 - Q^2},$$

and only the upper bound would follow from Cosmic Censorship using Penrose's heuristic argument. Our counter-example violates the lower bound.

References

[1] H. BRAY, *Proof of the Riemannian Penrose conjecture using the positive mass theorem*, J. Differential Geom. 59 (2001), 177–267.

[2] G. W. GIBBONS, *The Isoperimetric and Bogomolny Inequalities for Black Holes*, in *Global Riemannian Geometry*, edited by T. J. WILLMORE AND N. HITCHIN, John Wiley & Sons, New York, 1984.

[3] G. HUISKEN AND T. ILMANEN, *The Inverse Mean Curvature Flow and the Riemannian Penrose Inequality*, J. Differential Geom. 59 (2001), 353–437.

[4] J. ISENBERG, R. MAZZEO AND D. POLLACK, *Gluing and Wormholes for the Einstein Constraint Equations*, Commun. Math. Phys. 231 (2002) 529–568.

[5] P. S. JANG, *Note on Cosmic Censorship*, Phys. Rev. D. 20 (1979) No. 4, 834–838.

[6] R. SCHOEN AND S. T. YAU, *On the proof of the positive mass conjecture in general relativity*, Comm. Math. Phys. 65 (1979) No. 1, 45–76.

[7] G. WEINSTEIN AND S. YAMADA, *On a Penrose inequality with charge*, Comm. Math. Phys. 257 (2005) No. 3, 703–723.

[8] E. WITTEN, *A new proof of the positive energy theorem*, Comm. Math. Phys. 80 (1981) No. 3, 381–402.

Numerical study of naked singularity

Ken-ichi Nakao[1], Yaunari Kurita[2] and Yoshiyuki Morisawa[3]

[1,3] *Department of Matematics and Physics, Osaka City University, Osaka 558-8585, Japan*
[2] *Yukawa Institute for Theoretical Physics, Kyoto University, Kyoto 606-8502, Japan*

Abstract

In this talk, we presented numerical examples of spacetime in which the cylindrically symmetric dust fluid collapses. A naked singularity is necessarily formed at its symmetry axis and we gave a prescription to deal with the naked singularity as a Cauchy problem. In the cylindrically symmetric system, there is a degree of freedom of gravitational radiation. We saw that the large amount of the gravitational radiation can be released from the naked singularity. As far as we are aware, this is the first example which represents the naked singularity formation accompanied by the non-linear gravitational emission developed from regular initial data.

1 Introduction

General relativity predicts the gravitational collapse of very massive objects and the formation of spacetime singularities which will be accompanied by the divergences of physical quantities like as the energy density, spacetime curvature and so on [1]. An important issue related to the attribute of the spacetime singularity is known as the cosmic censorship hypothesis [2]. Roughly speaking, this hypothesis states the impossibility of the formation of an observable singularity called the naked singularity in our universe. However, preceding studies revealed that there are candidates of counterexamples to this hypothesis [3]. These candidates imply a possibility that we observe physical processes at spacetime singularities in our universe other than the Big Bang singularity.

If we construct a naked-singular solution by solving Einstein equations as a Cauchy problem, we can not know the causal futures of the naked singularities, as long as we do not specify the boundary conditions at the naked singularities. Since the physical quantities including the Riemann tensor will blow up at the naked singularities, it seems to be impossible to treat those within the framework of general relativity. However, we should note that if a spacetime singularity is naked, there should be its causal future by definition. This means that there must be a boundary condition which guarantees the existence of the causal future of the naked singularity even in the framework of general relativity. Such a boundary condition might not be unique. If really so, the physical nature of the naked singularity itself depends on what boundary condition is imposed there. Unfortunately, at present, we do not know which is the physically reasonable boundary condition in such situations, since we have not yet known the complete theory which describes the physical processes at the spacetime singularities. Therefore, it will be very important in the research for the physics of spacetime singularities to construct naked-singular solutions and to investigate the relation between their features and the boundary conditions, although it is non-trivial technical issue how to find boundary conditions to guarantee the causal futures of the singularities.

In this talk, we consider the gravitational collapse of infinitely long cylindrical dust by numerically integrating Einstein equations as a Cauchy problem. In the present case, even if the spacetime singularity is formed, no trapped region appears, and thus the formed singularities will be naked [4, 5].

Here, we adopt the unit of $c = 1$. Greek indices mean the components with respect to the coordinate basis.

[1] E-mail:knakao@sci.osaka-cu.ac.jp
[2] E-mail:kurita@sci.osaka-cu.ac.jp
[3] E-mail:morisawa@sci.osaka-cuac.jp

2 Basic Equations for Cylindrical Dust System

The spacetime with whole cylinder symmetry [7] is defined by the following metric,

$$ds^2 = e^{2(\gamma-\psi)}\left(-dt^2+dr^2\right)+r^2\beta^2e^{-2\psi}d\varphi^2+e^{2\psi}dz^2, \tag{1}$$

where $0 \le r < +\infty$, $0 \le \varphi < 2\pi$ and $-\infty < z < +\infty$ constitute the cylindrical coordinate system, and γ, ψ and β are functions of t and r. The coordinate variables t, r and z are all normalized so as to be dimensionless.

We consider the dust fluid in this spacetime. The stress-energy tensor of dust is written as $T^{\mu\nu} = \rho u^\mu u^\nu$. By virtue of the assumed symmetry of the spacetime, the 4-velocity u^μ of each constituent particle of dust fluid is written in the form $u^\mu = u^t(1,v,0,0)$. Here we introduce the conserved rest mass density D defined by

$$D = r\beta e^{2(\gamma-\psi)}\rho u^t. \tag{2}$$

Then the equation of motion of matter $\nabla_\nu T^{\mu\nu} = 0$ leads

$$\dot{D}+(vD)' = 0, \tag{3}$$

$$\frac{dv}{dt} = \dot{v}+vv' = (1-v^2)\left\{v\left(\dot{\psi}-\dot{\gamma}\right)+\psi'-\gamma'\right\}, \tag{4}$$

where a dot is the time derivative while a dash means the radial derivative. It should be noted that the first equation represents the energy conservation and thus we have called D the conserved rest mass density, whereas Eq.(4) is the geodesic equation for the constituent particles of the dust fluid.

Einstein equations are given as

$$\gamma' = \left\{\beta^2+2r\beta\beta'+r^2(\beta'^2-\dot{\beta}^2)\right\}^{-1}\Big[r\beta(\beta+r\beta')\left(\dot{\psi}^2+\psi'^2\right)-2r^2\beta\dot{\beta}\dot{\psi}\psi'+2\beta\beta' + r\left(2\beta'^2+\beta\beta''-\dot{\beta}^2\right)+r^2\left(\beta'\beta''-\dot{\beta}\dot{\beta}'\right)+8\pi Ge^{2(\gamma-\psi)}Du^t\left(\beta+r\beta'+r\dot{\beta}v\right)\Big], \tag{5}$$

$$\dot{\gamma} = -\left\{\beta^2+2r\beta\beta'+r^2(\beta'^2-\dot{\beta}^2)\right\}^{-1}\Big[r^2\beta\dot{\beta}\left(\dot{\psi}^2+\psi'^2\right)-2r\beta(\beta+r\beta')\dot{\psi}\psi'-\beta\dot{\beta} + r\left(\dot{\beta}\beta'-\beta\dot{\beta}'\right)+r^2\left(\dot{\beta}\beta''-\beta'\dot{\beta}'\right)+8\pi Ge^{2(\gamma-\psi)}Du^t\left\{r\dot{\beta}+(\beta+r\beta')v\right\}\Big], \tag{6}$$

$$\ddot{\gamma}-\gamma'' = \psi'^2-\dot{\psi}^2, \tag{7}$$

$$\ddot{\beta}-\beta''-\frac{2}{r}\beta' = \frac{8\pi G}{r}e^{2(\gamma-\psi)}Du^t(1-v^2), \tag{8}$$

$$\ddot{\psi}+\frac{\dot{\beta}}{\beta}\dot{\psi}-\psi''-\frac{1}{r}\left(1+r\frac{\beta'}{\beta}\right)\psi' = \frac{4\pi G}{r\beta}e^{2(\gamma-\psi)}Du^t(1-v^2). \tag{9}$$

The first and second equations are the constraint whereas the remaining equations are the evolution equations for the metric variables γ, β and ψ, respectively.

3 Boundary condition

If the dust collapses to its symmetry axis, the naked singularity will form there. If the conserved density D is finite at the naked singularity, this naked singularity merely causes regular singular points of the differential equations (5)-(9) at $r = 0$. If really the case, from Eqs.(8) and (9), the boundary conditions on β and ψ at $r = 0$ should be

$$\beta' = -4\pi Ge^{\gamma-\psi}D\sqrt{1-v^2}, \tag{10}$$

$$\psi' = -\frac{4\pi G}{\beta}e^{\gamma-\psi}D\sqrt{1-v^2}, \tag{11}$$

whereas from Eq.(5), the boundary condition on γ at $r = 0$ should be

$$\gamma' = \frac{2}{\beta}\left(\beta' + \frac{4\pi G e^{\gamma-\psi} D}{\sqrt{1-v^2}}\right) = \frac{8\pi G e^{\gamma-\psi} D v^2}{\beta\sqrt{1-v^2}}, \tag{12}$$

where we have used $u^t = e^{-\gamma+\psi}/\sqrt{1-v^2}$ derived from the normalization $u^\mu u_\mu = -1$. These boundary conditions guarantee the finiteness of β, ψ and γ as long as D is finite. If $\dot{\gamma}$, γ', $\dot{\psi}$ and ψ' do not diverge, the right hand side of Eq.(4) is also finite. Therefore, if initial data is appropriately set, D and v remain finite even at the naked singularity. In reality, we do not find any divergent quantities in our numerical simulations shown below.

There is a freedom in what boundary conditions on the matter variables D and v are imposed at the naked singularity. Here we refer the Morgan's null dust solution [6]: the imploding cylindrical null dust is absorbed completely by the naked singularity. A similar boundary condition can be imposed on also in the case of the dust. More concretely speaking, we consider a fictitious region $r < 0$ and always assume $\dot{\gamma} = \gamma' = \dot{\psi} = \psi' = 0$ there. Then we solve Eqs.(3) and (4) for $r < 0$ as well as for the physical region $r \geq 0$. If we set the initial condition of $v \leq 0$, all of the collapsing dust will enter into the fictitious region $r < 0$ from the physical region $r \geq 0$.

4 Numerical Examples and Discussion

We consider the following initial density distribution and velocity field:

$$D = \frac{15\sigma}{32\pi w^5 l^5}\left[r - l(1-w)\right]^2\left[r - l(1+w)\right]^2 \quad \text{and} \quad v = -\sqrt{1-\exp\left(-\frac{\mu}{r}\right)}, \tag{13}$$

for $l(1-w) < r < l(1+w)$ and vanish elsewhere, where σ is the rest mass per unit Killing length along z-direction, l and $w < 1$ are positive parameters to control the location and thickness of the dust shell, respectively, and μ is the parameter to control the gradient of the velocity field v.

The initial data of metric variables, β, ψ and γ and their time derivatives is determined by the following manner. We set $\beta = 1$ and $\dot{\beta} = 0$. Then Eq.(5) determines γ whereas Eq.(6) gives directly the time derivative of γ. We are interested in the initial situation that the static gravitational field is realized in the vacuum region. Thus we set $\dot{\psi} = 0$ and further, in order to determine the initial data of ψ, we use Eq.(9) with $\ddot{\psi} = 0$,

$$\psi'' = -\frac{1}{r}\left(\psi' + 4\pi G e^{\gamma-\psi} D\sqrt{1-v^2}\right). \tag{14}$$

We numerically integrate Eqs.(5) and (14) simultaneously outward from $r = 0$ by imposing the boundary condition $\psi|_{r=0} = 0 = \psi'|_{r=0}$ and $\gamma|_{r=0} = 0$ since we assume the absence of singularity in the initial data.

The vacuum region of the initial data obtained by the above procedure agrees with the Levi-Civita solution which is the unique solution of vacuum static spacetime with whole cylinder symmetry: $\psi = -\kappa \ln r$, $\gamma = \kappa^2 \ln r + \lambda$ and $\beta = 1$, where κ, λ are constant numbers which characterize this solution. We assume the regular initial data and hence the positivity of the conserved rest mass density D implies the positivity of κ and λ in the outside vacuum region $r \geq l(1+w)$, while in the inside vacuum region $r \leq l(1-w)$, both κ and λ vanish and hence the flat space is realized.

C-energy $E(t,r)$ is the quasi-local energy per unit Killing length contained within the cylinder of coordinate radius r at the time t in the spacetime with whole cylinder symmetry [7]. Its definition is given by

$$E(t,r) = \frac{1}{8G}\left[1 + e^{-2\gamma}\left\{(r\dot{\beta})^2 - (r\beta)'^2\right\}\right]. \tag{15}$$

The total C-energy, $\lim_{r\to\infty} E$, of the initial data is obtained by using the metric of Levi-Civita spacetime. We find that the total C-energy is equal to $1/8G$ irrespective of the values of κ and λ if κ does not vanish. As shown by Hayward, $1/8G$ is the upper bound of the C-energy in the non-singular spacelike hypersurface, if the null energy condition is satisfied [5]. Therefore, the total C-energy of the present initial data takes the maximal value. Similar situations to the present case appear also in the case of Newtonian gravity. The Newtonian gravitational potential in a cylindrical system diverges logarithmically

and thus the gravitational binding energy of this system is always infinite regardless of the mass per unit length and its spatial distribution.

Now we can obtain numerical solutions which represent the formation processes of a naked singularity by the gravitational collapse of a cylindrically symmetric dust. We adopt the finite difference method and MacCormack scheme to solve the equations for the metric variables Eqs.(4)-(7). On the other hand, we adopt the method of Shapiro and Teukolsky to solve the dynamics of the dust fluid [8]; we follow the motion of constituent mass shells of dust fluid which move along timelike geodesics. For the integration of geodesic equations, we also adopt MacCormack scheme. Then we construct the conserved rest mass density D and the velocity field v from positions and velocities of the mass shells. We have assumed that all of the mass shells have an identical rest mass per unit Killing length along z-direction. Equations (5) and (6) are used for the check of accuracy. The relative errors estimated by the constraint equations are less than 10^{-3}. The numerically covered region is $0 \leq r \leq 30$, and the numbers of the spatial grid points and the mass shells are 3×10^3 and 10^3 in this numerical simulation, respectively.

All of the metric and matter variables are finite in the numerical simulations. However, when the dust reaches the symmetry axis $r = 0$, the rest mass density $\rho = e^{\psi - \gamma} D/r\beta$ blows up there. Since the Ricci scalar is equal to $8\pi G\rho$, it also diverges there. This means that the *s.p.* curvature singularity [1] forms by the collapse of the dust. Since β, ψ and γ themselves are everywhere finite and continuous, there is a causal future of this singularity and a Cauchy horizon associated with it exists. Therefore the naked singularity has formed in the spacetime constructed by our numerical simulation.

Our numerical simulation shows that γ everywhere approaches to the constant value $4G\sigma$ asymptotically for $10^{-5} \leq G\sigma \leq 3 \times 10^{-2}$ with the other parameters fixed. Therefore the C-energy becomes $(1 - e^{-8G\sigma})/8G$, irrespective of r, asymptotically. Since the initial value of the total C-energy is $1/8G$, we can consider that the energy $e^{-8G\sigma}/8G$ is released by the gravitational radiation. Thus the efficiency ε of gravitational emission, i.e., the ratio of the emitted energy to the initial total energy is given as $\varepsilon = e^{-8G\sigma}$. It is seen from this result that the efficiency ε is larger for lighter dust shell. In the zero-mass limit, the efficiency will be unity. But we should note that it is non-trivial how to relate the present results with the asymptotically flat cases, e.g., the situation studied by Shapiro and Teukolsky [8].

Acknowledgements

We are grateful to H. Ishihara and colleagues in the astrophysics and gravity group of Osaka City University for their useful and helpful discussion and criticism. KN would like to thank T. Harada for giving very useful information about the self-similar solution. This work is supported by the Grant-in-Aid for Scientific Research (No.16540264).

References

[1] S. W. Hawking and G. F. R. Ellis, *The large scale structure of space-time*, (Cambridge University Press, Cambridge, 1973).

[2] R. Penrose, Riv. Nuovo Cimento **1**, 252 (1969).

[3] T. Harada, H. Iguchi and K. Nakao, Prog. of Theor. Phys. **107**, 449 (2002); references are therein.

[4] K. S. Thorne, *in Magic Without Magic; John Archibald Wheeler*, edited by J. Klauder, (Frieman, San Francisco, 1972), p. 231.

[5] S. A. Hayward, Class. Quantum Grav. **17**, 1749 (2000).

[6] T. A. Morgan, Gen. Rel. Grav. **4**, 273 (1973).

[7] K. S. Thorne, Phys. Rev. **138**, B251 (1965).

[8] S. L. Shapiro and S. A. Teukolsky, Phys. Rev. Lett. **66** 994 (1991).

Angular momentum and conservation laws for dynamical black holes

Sean A. Hayward[1]

Institute for Gravitational Physics and Geometry, The Pennsylvania State University, University Park, PA 16802, U.S.A.

Abstract

Black holes can be practically located (e.g. in numerical simulations) by trapping horizons, hypersurfaces foliated by marginal surfaces, and one desires physically sound measures of their mass and angular momentum. A generically unique angular momentum can be obtained from the Komar integral by demanding that it satisfy a simple conservation law. With the irreducible (Hawking) mass as the measure of energy, the conservation laws of energy and angular momentum take a similar form, expressing the rate of change of mass and angular momentum of a black hole in terms of fluxes of energy and angular momentum, obtained from the matter energy tensor and an effective energy tensor for gravitational radiation. Adding charge conservation for generality, one can use Kerr-Newman formulas to define combined energy, surface gravity, angular speed and electric potential, and derive a dynamical version of the so-called "first law" for black holes. A generalization of the "zeroth law" to local equilibrium follows. Combined with an existing version of the "second law", all the key quantities and laws of the classical paradigm for black holes (in terms of Killing or event horizons) have now been formulated coherently in a general dynamical paradigm in terms of trapping horizons.

1 Komar integral and twist: $J[\psi]$, ω

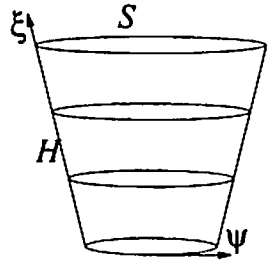

A 1-parameter family of topologically spherical spatial surfaces S
locally forms a foliated hypersurface H.
A generating vector $\xi^a = (\partial/\partial x)^a$ generates the constant-x surfaces S,
and can be taken to be normal, $h_{ab}\xi^b = 0$,
where h_{ab} is the induced metric of S.
The Komar integral is [Komar 1959]

$$J[\psi] = -\frac{1}{16\pi}\oint_S *\epsilon_{ab}\nabla^a\psi^b,$$

where ϵ_{ab} is the antisymmetric 2-form of the normal space
and $*1 = \sqrt{\det h}\, d\theta \wedge d\phi$ is the area form of S.
One can take null coordinates $x^\pm$ for the normal space,
labelling the outgoing and ingoing null hypersurfaces passing through each S.
Then $\epsilon_{ab} = e^{2\varphi}(dx^+_a dx^-_b - dx^-_a dx^+_b)$ in terms of a normalization function $e^{-2\varphi} = -g^{ab}dx^+_a dx^-_b$.
For a transverse vector ψ^a, $h^a_b\psi^b = \psi^a$, the Komar integral can be rewritten as

$$J[\psi] = \frac{1}{8\pi}\oint_S *\psi^a\omega_a$$

where $\omega_c = \frac{1}{2}e^{2\varphi}h^b_c(dx^+_a\nabla^a dx^-_b - dx^-_a\nabla^a dx^+_b) = \frac{1}{2}e^{2\varphi}h_{bc}[dx^+, dx^-]^b$ is the twist,
measuring the non-integrability of the normal space [Hayward 1993].
The twist is invariant under relabelling $x^\pm \to \tilde{x}^\pm(x^\pm)$ and therefore is an invariant of H
unless ξ^a becomes null, so the twist expression for $J[\psi]$ is also an invariant of H.
The gauge dependence of the Komar integral for a single S is fixed by H.

[1]E-mail:sean_a_hayward@yahoo.co.uk

2 Uniqueness: ψ

Assume that the axial vector ψ^a has vanishing transverse divergence, $D_a\psi^a = 0$,
where D_a is the covariant derivation of h_{ab}.
Then $J[\psi]$ can be defined equivalently in terms of other normal fundamental forms
differing by a gradient, $\omega_a \mapsto \omega_a + D_a\lambda$.
There are several such expressions, though they are gauge-dependent, fixing $\varphi = 0$
[Brown & York 1993, Ashtekar, Beetle & Lewandowski 2001, Ashtekar & Krishnan 2002, Booth & Fairhurst 2004].

To obtain a conservation law for angular momentum, expressing $L_\xi J[\psi]$ (Lie derivative),
it is natural to propagate ψ^a along ξ^a by $L_\xi\psi^a = 0$ [Gourgoulhon 2005].
There is a commutator identity $L_\xi(D_a\psi^a) - D_a(L_\xi\psi^a) = \psi^a D_a\theta_\xi$ for any normal vector ξ^a
and transverse vector ψ^a, where θ_ξ is the expansion along ξ^a, $*\theta_\xi = L_\xi(*1)$.
So $\psi^a D_a\theta_\xi = 0$.
This is automatic if $D_a\theta_\xi = 0$, as in spherical symmetry or along a null trapping horizon.
However, for generic H, one expects $D_a\theta_\xi \neq 0$ almost everywhere.
The hairy ball theorem states that a continuous vector field $(D^a\theta_\xi)$
must vanish somewhere on a sphere; however,
a generic situation is that the curves $\gamma \subset S$ of constant θ_ξ
form a smooth foliation of circles with two poles.

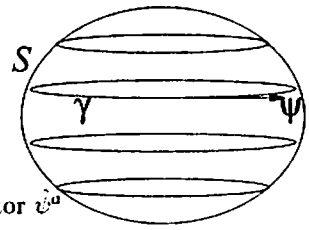

Assuming so, ψ^a must be tangent to γ.
Then one can find a unique ψ^a, up to sign, in terms of the unit tangent vector $\hat\psi^a$
and arc length ds along γ: $\psi^a = \hat\psi^a \oint_\gamma ds/2\pi$.
Then the angular momentum becomes unique up to sign, $J[\psi] = J$.
The sign is naturally fixed by $J > 0$ (if $J \neq 0$) and continuity of ψ^a.

For an axisymmetric space-time with axial Killing vector ψ^a, one has $D_a\psi^a = 0$.
Assuming that ξ^a respects the symmetry, $0 = L_\psi\xi^a = -L_\xi\psi^a$,
so the above construction, if unique, yields the correct ψ^a.
For example, consider a Kerr space-time in Boyer-Lindquist coordinates (t, r, θ, ϕ),
with S given by constant (t, r) and $\xi^a = (\partial/\partial r)^a$.
If $ma \neq 0$, $D_a\theta_\xi$ is a certain function of θ (and r),
non-zero except at the poles and equator (and isolated values of r),
so that a unique continuous ψ^a exists, $\psi^a = (\partial/\partial\phi)^a$.

3 Conservation: Θ

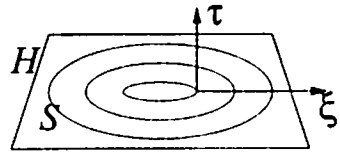

Introduce the normal vector τ^a dual to ξ^a:
$h_{ab}\tau^b = 0$, $g_{ab}\tau^a\xi^b = 0$, $g_{ab}\tau^a\tau^b = -g_{ab}\xi^a\xi^b$.
Its expansion θ_τ is given by $*\theta_\tau = L_\tau(*1)$.
There is a simple expression for the rate of change of angular momentum if $\psi^a D_a\theta_\tau = 0$,
which is generally inconsistent with the above constraint $\psi^a D_a\theta_\xi = 0$.
However, it is consistent:
(i) along a null H, $\tau^a = \xi^a$ [Damour 1978];
(ii) along a trapping horizon H, $|\theta_\tau| = |\theta_\xi|$ [Ashtekar & Krishnan, Booth & Fairhurst, Gourgoulhon];
(iii) along uniformly expanding flows, $D_a\theta_\xi = D_a\theta_\tau = 0$ [Hayward 1994].
The expression is

$$L_\xi J = -\oint_S * \left(T_{ia} - \frac{h^{jk} D_k \sigma_{aij}}{16\pi} \right) \psi^i \tau^a$$

where T_{ab} is the matter energy tensor, so that $T_{ia}\psi^i\tau^a$ is an angular momentum density,
and σ_{aij} is the shear form, the traceless part of the second fundamental form of S,
$\sigma_{\pm ij} = h_i^k h_j^l L_\pm h_{kl} - \frac{1}{2} h_{ij} h^{kl} L_\pm h_{kl}$, where $L_\pm$ are Lie derivatives along the null normals.

Then one can identify the transverse-normal block

$$\Theta_{i\pm} = -\frac{1}{16\pi} h^{jk} D_k \sigma_{\pm ij}$$

of an effective energy tensor Θ_{ab} for gravitational radiation.
The normal-normal block $(\Theta_{\pm\pm}, \Theta_{\pm\mp})$ occurs in the energy conservation law [Hayward 2004],
with energy densities $\Theta_{\pm\pm} = \|\sigma_\pm\|^2/32\pi$ of ingoing and outgoing gravitational radiation,
recovering the Bondi energy flux at null infinity
and the Isaacson energy density for high-frequency linearized gravitational waves.
It seems that gravitational radiation is encoded in null shear $\sigma_{\pm ij}$,
and that differential shear has angular momentum density $\Theta_{i\pm}\psi^i$.

Then conservation of angular momentum takes the same form

$$L_\xi J = -\oint_S *(T_{ab} + \Theta_{ab})\psi^a \tau^b$$

as conservation of energy [Hayward 2004]

$$L_\xi M = \oint_S *(T_{ab} + \Theta_{ab}) k^a \tau^b$$

for the Hawking mass M along a trapping horizon or a uniformly expanding flow,
where k^a is the normal dual of $\nabla^a R$, area $A = \oint_S *1$ defining R by $A = 4\pi R^2$.

4 Averagely conserved currents and charges: $j_{\{M,J,Q\}}$

For an electromagnetic field, charge Q and charge-current density j_Q are related by

$$[Q] = -\int_H *(j_Q^a \tau_a) \wedge dx = -\int_H \hat{*} j_Q^a \hat{\tau}_a$$

where the first expression holds for H of any signature and the second for spatial H,
$\hat{*}1$ being the proper volume element and $\hat{\tau}^a$ the unit normal vector.
The surface-integral form is

$$L_\xi Q = -\oint_S *j_Q^a \tau_a.$$

The above conservation laws can be written in the same form

$$L_\xi M = -\oint_S *j_M^a \tau_a, \quad L_\xi J = -\oint_S *j_J^a \tau_a$$

by defining

$$(j_M)^a = -(T^{ab} + \Theta^{ab}) k_b, \quad (j_J)^a = (T^{ab} + \Theta^{ab}) \psi_b.$$

The physical interpretation of the components is
j_M = (energy density, energy flux),
j_J = (angular momentum density, angular stress).
j_Q = (charge density, current density),
For spatial ξ, $\oint_S *(j_M, j_J, j_Q)^a \xi_a$ = (power, torque, current),
$-(j_M, j_J, j_Q)^a \tau_a$ = (energy density, angular momentum density, charge density).
Local charge conservation takes the form $\nabla_a j_Q^a = 0$.
For energy and angular momentum, one has only quasi-local conservation laws:

$$\oint_S *\nabla_a j_M^a = \oint_S *\nabla_a j_J^a = 0.$$

Then j_M and j_J are averagely conserved.

5 Laws of black-hole dynamics: E, (κ, Ω, Φ)

There are now three conserved quantities (M, J, Q), as for a Kerr-Newman black hole.
One can use the Kerr-Newman formula for the ADM energy to define an energy

$$E = \frac{\sqrt{((2M)^2 + Q^2)^2 + (2J)^2}}{4M}$$

for each marginal surface in a trapping horizon, where $R = 2M$.
Then surface gravity

$$\kappa = \frac{(2M)^4 - (2J)^2 - Q^4}{2(2M)^3\sqrt{((2M)^2 + Q^2)^2 + (2J)^2}},$$

angular speed

$$\Omega = \frac{J}{M\sqrt{((2M)^2 + Q^2)^2 + (2J)^2}}$$

and electric potential

$$\Phi = \frac{((2M)^2 + Q^2)Q}{2M\sqrt{((2M)^2 + Q^2)^2 + (2J)^2}}$$

can be defined by thermostatic-style formulas

$$\kappa = 8\pi\frac{\partial E}{\partial A} = \frac{1}{4M}\frac{\partial E}{\partial M}, \quad \Omega = \frac{\partial E}{\partial J}, \quad \Phi = \frac{\partial E}{\partial Q}.$$

There follows a dynamic version of the "first law of black-hole mechanics":

$$L_\xi E = \frac{\kappa}{8\pi} L_\xi A + \Omega L_\xi J + \Phi L_\xi Q,$$

really analogous to the Gibbs equation.
In energy-tensor form,

$$L_\xi E = \oint_S * \left((T_{ab} + \Theta_{ab})K^a \tau^b - \Phi j_Q^b \tau_b\right)$$

where $K^a = 4M\kappa k^a - \Omega\psi^a$ reduces to the stationary Killing vector on a Kerr-Newman black hole.

For $J \ll M^2$ and $Q \ll M$,

$$E \approx M + \tfrac{1}{2}I\Omega^2 + \tfrac{1}{2}Q^2/R$$

where $J = I\Omega$ defines the moment of inertia

$$I = M\sqrt{((2M)^2 + Q^2)^2 + (2J)^2} = ER^2.$$

Thus $E \geq M$ can be interpreted as a combined energy, including the irreducible mass M, rotational kinetic energy $\approx \frac{1}{2}I\Omega^2$ and electrostatic energy $\approx \frac{1}{2}Q^2/R$.
Energy $E - M$ can be extracted by Penrose-type processes, while $L_\xi M \geq 0$, assuming NEC, by the area law $L_\xi A \geq 0$ for black holes [Hayward 1994], cf. "second law".

Local equilibrium: $(j_M, j_J, j_Q)^a \tau_a = 0 \Rightarrow (M, J, Q)$ constant $\Rightarrow \kappa$ constant, cf. "zeroth law".

Acknowledgements. Thanks to Abhay Ashtekar, Ivan Booth and Eric Gourgoulhon for discussions and to the conference organizers for local support and hospitality. Research supported by NSF grants PHY-0090091, PHY-0354932 and the Eberly research funds of Penn State.

New dynamical solutions for the Einstein-scalar field system and their asymptotic behaviors

Makoto Yoshikawa[1],

[1] *Theoretical Astrophysics Group, Department of Physics, Kyoto University, Kyoto 606-8502, Japan*

Abstract

A new class of solutions for spherically symmetric Einstein-massless complex scalar field system is presented. The solutions are obtained by making a certain ansatz for the functional forms of metric components and the scalar field, which reduces the field equations into two sets of ordinary differential equations. Asymptotic behaviors of the solutions are investigated in the light of *similarity hypothesis*, which asserts that, under cirtain physical circumstances, spherically symmetric solutions will evolve to a self-similar form. We show that all physical solutions are asymptotically self-similar at the future or past asymptotic infinities, which supports the similarity hypothesis.

1 Introduction

Self-similar solutions in general relativity have been widely studied in many literatures. One reason why they are often studied is that they are relatively easily obtainable solutions. They are especially useful when the system is spherically symmetric, because the assumption of self-similarity simplifies the field equations to a set of ordinary differential equations (ODEs), which enables us to obtain inhomogeneous and dynamical solutions without solving partial differential equations.

Besides the mathematical convenience, it has been suggested recently that self-similar solutions also have some physical importance. Of particular importance is *the similarity hypothesis* proposed by B. J. Carr, which asserts that, in a variety of physical situations, solutions of the Einstein equations will evolve naturally to self-similar form even if the initial conditions are not self-similar (see, e.g., [1, 2]). Although there are many examples which support the hypothesis (see [1, 2] and references therein), it is still unclear on what condition the similarity hypothesis holds. In order to make it clear, we need to find solutions of the Einstein equations which are not self-similar, and then observe their asymptotic behaviors. However, it is not easy to obtain a non-self-similar solution except for when the system is highly symmetric. So testing the similarity hypothesis is difficult in general situations.

In this report, we consider the Einstein-massless complex scalar field system, and present a new class of solutions which contains not only self-similar solutions, but also many non-self-similar solutions. We also discuss asymptotic self-similarity of the solutions.

2 Formulation

We consider the Einstein-complex massless scalar field system in N (≥ 4) spacetime dimension. The action is given by

$$S = \int d^N x \sqrt{-g} \Big(R - 8\pi |\nabla \varphi|^2 \Big), \tag{1}$$

where φ is a complex scalar field. We take the scalar field to be complex because, with a real scalar field, the method introduced in this report gives very small number of solutions, so it is less attractive. The field equations are the Einstein equations $R_{ab} = 8\pi \mathrm{Re}[\partial_a \varphi^* \partial_b \varphi]$ and the wave equation for the scalar field, $\Box \varphi = 0$.

In order to solve the field equations, we make a metric ansatz

$$ds^2 = a^2(\eta)\{g(\zeta)(-d\eta^2 + d\zeta^2) + \rho(\zeta)^2 d\Omega_{N-2}^2\}. \tag{2}$$

[1] E-mail:makoto@tap.scphys.kyoto-u.ac.jp

where $d\Omega_{N-2}^2$ is the line element of an unit $(N-2)$-sphere, and an ansatz on the functional form of $\varphi(\eta,\zeta)$

$$\varphi(\eta,\zeta)=\sqrt{\frac{N-2}{8\pi}}\left(c_1\ln a(\eta)+c_2\int d\eta\{a(\eta)\}^{-(N-2)}+c_3\ln|g(\zeta)|+\text{const.}\right), \tag{3}$$

where c_1, c_2 and c_3 are complex constants. The metric form (2) is, in fact, a generalization of those for temporally or spatially self-similar spacetimes with spherical symmetry, because if we take $a(\eta)=e^{\eta}$, Eq. (2) becomes the general metric form for such spacetimes.

Under the ansatz Eqs. (2) and (3), the field equations can be separated out into two sets of ODEs: that for the ζ-independent variable, $a(\eta)$, and that for the η-independent variables, $g(\zeta)$ and $\rho(\zeta)$.

The equation for the $a(\eta)$ is given by

$$\frac{\ddot{a}}{a}+(N-3)\left(\frac{\dot{a}}{a}\right)^2+(N-2)\sigma=0, \tag{4}$$

where the overdot represents the derivative with respect to η, and σ is a separation constant normalized so that $\sigma=+1$ or 0 or -1. We can solve this equation analitically, and the solutions are classified into six types which are listed in Table 1. The value of σ is unique for each type of $a(\eta)$, which is also shown in the table. Note that type-III solutions are exactly self-similar. They are, in fact, the self-similar solutions in the *real* scalar field case because the phase of the scalar field φ is constant.

The equations for η-independent variables, $g(\zeta)$ and $\rho(\zeta)$, can be written in the form of a two-dimensional autonomous system,

$$\begin{aligned} &X'=-(N-2)(XY+\lambda\sigma),\\ &Y'=-X^2+2\lambda XY-Y^2-(1-\lambda^2)\sigma,\\ &\text{where}\qquad X\equiv\frac{1}{2\lambda}\frac{g'}{g},\qquad Y\equiv\frac{\rho'}{\rho}. \end{aligned} \tag{5}$$

together with a "constraint" equation given by

$$\mathcal{F}_C\equiv -X^2+2\lambda XY+(N-3)Y^2+(N-3+\lambda^2)\sigma=(N-3)\frac{g}{\rho^2}. \tag{6}$$

which do not contain second order derivatives of $g(\zeta)$ or $\rho(\zeta)$. Here, the prime represents the derivative with respect to ζ, and λ is another separation constant which is real-valued. The constraint equation is consistent with Eq. (5) in the sense that if $(g(\zeta),\rho(\zeta))$, a solution of Eq. (5), satisfies Eq. (6) initially, then it satisfies Eq. (6) for arbitrary ζ. This means what we have to do first is to solve Eq. (5), whereas Eq. (6) only constrains the integration constants that appear when we integrate X and Y to obtain g and ρ.

The field equations also give some relations between the constants in Eq. (3) (c_1, c_2 and c_3) and the separation constants (λ and σ), which are obtained in the process of deriving Eqs. (4)-(6). As the result, if we specify the type of $a(\eta)$, only λ remains to be a free parameter (although its domain is somewhat restricted), and c_1, c_2 and c_3 can be written in terms of λ. These results are summarized in Table 1.

To summarize, the procedure of obtaining a solution is as follows: (i) Choose the type of $a(\eta)$. At this point, the value of σ is determined. (ii) Choose a value of λ from the domain given in Table 1. (iii) Specify initial values (X_0,Y_0) and solve the autonomous system (5) (iv) Integrate the solution $(X(\zeta),Y(\zeta))$ to obtain $g(\zeta)$ and $\rho(\zeta)$. Here, integration constants are taken so that Eq. (6) is satisfied.

3 Phase spaces for the autonomous system

In this section, we focus on the autonomous system (5). Although it is difficult to solve Eq. (5) analytically, we can investigate qualitative behaviors of the solutions by analyzing the phase space structure. It will also help us when we study asymptotic behaviors (asymptotic self-similarity) of the solutions, which we will see in the next section.

type	$a(\eta)$	σ	domain of λ^2	c_1	c_2	c_3
I	1	0	–	–	–	–
II	$\eta^{1/(N-2)}$	0	$(0, N-1]$	$1/\sqrt{N-2}$	0	$\frac{\lambda+i\sqrt{N-1-\lambda^2}}{2\lambda\sqrt{N-1}}$
III	e^{η}	-1	$(0, +\infty)$	λ	0	$(2\lambda)^{-1}$
IV	$\{\cosh((N-2)\eta)\}^{1/(N-2)}$	-1	$[N-1, +\infty)$	λ	$i\sqrt{\lambda^2-N+1}$	$(2\lambda)^{-1}$
V	$\{\sinh((N-2)\eta)\}^{1/(N-2)}$	-1	$(0, N-1]$	λ	$i\sqrt{N-1-\lambda^2}$	$(2\lambda)^{-1}$
VI	$\{\sin((N-2)\eta)\}^{1/(N-2)}$	$+1$	$(0, N-1]$	λ	$i\sqrt{N-1-\lambda^2}$	$(2\lambda)^{-1}$

Table 1: Functional forms of $a(\eta)$.

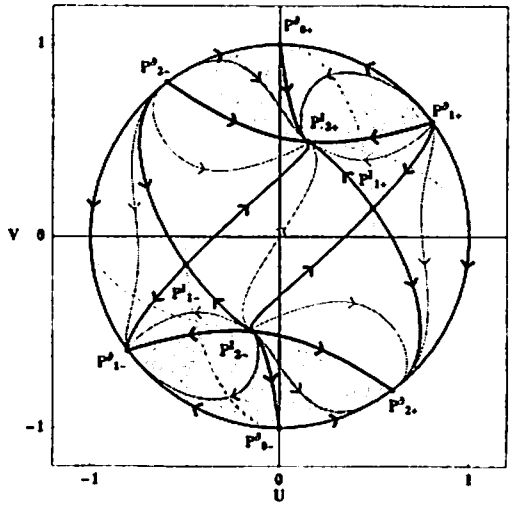

Figure 1: The global phase portrait for the autonomous system (5) with $N = 4$, $\lambda = 0.3$ and $\sigma = -1$. The purple lines are typical orbits and the red lines are separatrices. The metric coefficient g is positive in the dark gray regions, and is negative in the light gray regions. Orbits on black lines are meaningless because g becomes 0 on them.

In order to study the global structre of the phase space, we use a technic called the Poincaré sphere [3]. Namely, we change the variables (X, Y) to (U, V) defined by

$$U \equiv \frac{X}{\sqrt{8+X^2+Y^2}}, \qquad V \equiv \frac{Y}{\sqrt{8+X^2+Y^2}}. \tag{7}$$

With these variables, the original phase space, the (X, Y)-palne, is mapped onto a bounded region $U^2 + V^2 < 1$ on the (U, V)-plane, which allows us to look over the whole sphase space at a glance.

The phase portrait for the autonomous system with $N = 4$, $\lambda = 0.3$ and $\sigma = -1$ is shown in Fig. 1. The phase space structure changes as we move the values of N, λ and σ, so we obtain infinitly many phase portraits. However, it is proved that their topological structures can be classified into only seven patterns (for details, see [4]).

It follows from the constraint equation (6) that $g(\zeta)$ is positive in the region $\mathcal{F}_C > 0$, which are depicted as dark gray zones in Fig. 1, while $g(\zeta)$ is negative in the region $\mathcal{F}_C < 0$, which are depicted as light gray zones. Therefore, $\frac{\partial}{\partial\eta}$ is timelike (resp. spacelike) in dark (resp. light) gray zones. Orbits on the curves $\mathcal{F}_C = 0$, which are depicted as black lines, are forbidden because $g(\zeta)$ becomes 0 on them.

4 Asymptotic behaviors of the solutions

From the point of view of similarity hypothesis, it is important to study asymptotic behaviors of the solutions. This requires asymptotic behaviors of the functions which appear in the metric components, namely, $g(\zeta)$, $\rho(\zeta)$ and $a(\eta)$. We can easily obtain asymptotic behaviors of $a(\eta)$ because we have explicit functional forms which are listed in table 1.

In order to obtain asymptotic behaviors of the remaining functions, $g(\zeta)$ and $\rho(\zeta)$, we need asymptotic behaviors of $X(\zeta)$ and $Y(\zeta)$. Here, "asymptotic behaviors" of $X(\zeta)$ and $Y(\zeta)$ means behaviors of the corresponding orbit in the phase space near its start point and end point. We proved that the start point and the end point of every orbit are fixed points on the compactified phase space (as you see in fig. 1), so behaviors of an orbit near the start point and the end point can be studied by means of perturbative analysis around the fixed points. Therefore, asymptotic behaviors of $g(\zeta)$ and $\rho(\zeta)$ can be obtained from perturbative analysis of the autonomous system arond the fixed points. By this means, we obtained asymptotic forms of the metric near the boundaries of spacetime.

We next investigated asymptotic self-similarity of the solutions at the future or past asymptotic infinities by checking if the asymptotic forms of the metric are self-similar or not. We mainly focused on the solutions with regular Cauchy surfaces. The result is as follows.

Type-I, II The only solution with future or past asymptotic infinity and a regular Cauchy surface is a self-similar solution (Minkowski for type-I/flat FRW for type-II).

Type-III Every solution is exactly self-similar.

Type-IV, V Every solution with future (resp. past) asymptotic infinity and a regular Cauchy surface is asymptotically self-similar at the future (resp. past) asymptotic infinity.

Type-VI There is no solution with future or past asymptotic infinity.

5 Conclusion

We have obtained a class of solutions to spherically symmetric Einstein-massless complex scalar field system by making an ansatz for the functional forms of the metric components and the scalar field. With the ansatz, Einstein-scalar field equations have been separated out into two sets of ODEs, one of which can be solved analytically, and the other can be reduced to an autonomous system.

We have also analyzed asymptotic behaviors of the solutions in the light of similarity hypothesis. As the result, we have found that every solution which has a regular Cauchy surface and a future (resp. past) asymptotic infinity is asymptotically self-similar at the future (resp. past) infinity, which supports the similarity hypothesis.

References

[1] B. J. Carr & A. A. Coley, gr-qc/0508039.

[2] B. J. Carr & A. A. Coley, Class. Quant. Grav. **16**, R31-R71 (1999).

[3] L. Perko, *Differential Equations and Dynamical Systems*, Springer, New York, (1996).

[4] M. Yoshikawa, in preparation.

Time evolution of density perturbations in self-similar gravitational collapse of a perfect fluid

Eiji Mitsuda[1] and Akira Tomimatsu[2]

Department of Physics, Graduate School of Science, Nagoya University, Nagoya 464-8602, Japan

Abstract

We analytically study density perturbations during spherically symmetric self-similar gravitational collapse of a perfect fluid whose equation of state is $P = \alpha\rho$, where α is a constant lying in the range $0 < \alpha \leq 1$. We derive an autonomous perturbation equation available for all the self-similar background spacetime. Applying this equation to the flat Friedmann self-similar solutions, we investigate the stability of self-similar structure in the spatially homogeneous collapse.

1 Introduction

What kinds of solutions describe final stage of spherically symmetric gravitational collapse is one of the most important issue which has been addressed by many researchers in general relativity. In this context, there is a considerable hypothesis that the final stage is well approximated by spherically symmetric self-similar solutions (see recent review [1]). This hypothesis is called self-similarity hypothesis. As an important evidence to support it, there are numerical simulations of general non-self-similar collapse of a perfect fluid with the equation of state $P = \alpha\rho$ in the range $0 < \alpha \lesssim 0.036$ by Harada and Maeda[2]. However there exists no comprehensive proof of the self-similarity hypothesis. Stability analysis of spherically symmetric self-similar solutions in a wide parameter range will be an important step to prove the hypothesis.

Spherically symmetric self-similar solutions describing gravitational collapse of a perfect fluid have been widely studied, and it has been found that they admit naked singularity formation in a certain range of parameter values. Hence stability analysis of spherically symmetric self-similar solutions will provide an important implication to the cosmic censorship conjecture. In addition, to study time evolution of perturbation fields in background geometry involving a naked singularity is astrophysically interesting in terms of revealing some typical patterns observable as a precursor of naked singularity formation.

A notable spherically symmetric self-similar perfect fluid solution admitting naked singularity formation is a critical solution, which describes the collapse at the threshold of black hole formation. By definition, the critical solution is unstable against density perturbations. If density perturbations are generated during the critical collapse, they would form a small black hole or disperse to the spacial infinity, depending on their initial conditions, and a naked singularity would not be formed. To study how density perturbations evolve until black hole formation or dispersion during the critical collapse is an interesting problem to provide a deep insight into the critical phenomena of the gravitational collapse.

Motivated by the above, we consider density perturbations during spherically symmetric self-similar collapse of a perfect fluid. In spherically symmetric self-similar solutions, all dimensionless functions depend only on the one self-similar variable $z \equiv r/t$. By virtue of this symmetry, perturbations $\Psi(z,t)$ for the self-similar solutions can be expressed in separation of variables as $\Psi(z,t) = \psi(z,\omega)\exp(i\omega\log|t|)$. Hence perturbation analysis should be addressed via two steps, "frequency" ω-domain analysis and time-domain analysis after an integration of the function ψ with respect to the parameter ω.

In the frequency-domain analysis, the regularity conditions for the function ψ at the regular center and the sonic point before central singularity formation generate an eigenvalue problem for the parameter ω. Several works have been devoted to the frequency-domain analysis of density perturbations during spherically symmetric self-similar collapse of a perfect fluid with the equation of state $P = \alpha\rho$. Harada ana Maeda showed that no growth eigenmode is generated during the collapse described by the flat

[1]E-mail:emitsuda@gravity.phys.nagoya-u.ac.jp
[2]E-mail:atomi@gravity.phys.nagoya-u.ac.jp

Friedmann self-similar solution and the general relativistic version of the Larson-Penston self-similar solution for the range $0 < \alpha \leq 0.03$[2]. On the other hand, it was confirmed that there is one growth eigenmode in the critical collapse for the range $0 < \alpha \leq 1$[3, 4]. However, because all analyses were numerical, stability of many self-similar perfect fluid solutions lying in the other wide parameter range have been unknown.

Though there was not previous analysis of density perturbations in the time-domain analysis, we can learn an importance of the time-domain analysis from [5], in which electromagnetic perturbations during spherically symmetric self-similar collapse toward a naked singularity had been considered. It was found in this analysis that the contributions from high-frequency waves clarified by an integration with respect to the parameter ω as well as from eigenmodes of the self-similar system are important for energy flux of electromagnetic radiation just before naked singularity formation. In addition, the gravitational redshift and blueshift effect to affect the waves in the course of their propagation are clarified by the Green's function technique, and it was found that divergence of the energy flux of even an initially damped eigenmode is possible just before naked singularity formation. Consequently, various behaviors of the energy flux just before naked singularity formation were shown. The time domain analysis will also be important for density perturbations. It should be noted that an autonomous perturbation equation is necessary to the Green's function technique.

Our purpose is to develop analytical method to clarify time evolution of density perturbations during spherically symmetric self-similar collapse of a perfect fluid. In this paper we derive an autonomous wave equation for the density perturbations. This equation is available for any spherically symmetric self-similar perfect fluid solutions. As an application of this equation, we discuss the stability of the flat Friedmann self-similar solution.

2 Background spacetime

Let me begin with a brief review of spherically symmetric self-similar collapse of a perfect fluid. The line element of the background spacetime is given by

$$ds^2 = -e^{2\nu}dt^2 + e^{2\lambda}dr^2 + r^2S^2\left(d\theta^2 + \sin^2\theta d\varphi^2\right), \tag{1}$$

with the comoving coordinates t and r. As collapsing matter, we consider a perfect fluid with the equation of state $P = \alpha\rho$, where α is a constant lying in the range $0 < \alpha \leq 1$. In addition, we impose the self-similarity on the background spacetime, which means

$$\nu = \nu(z), \qquad \lambda = \lambda(z), \qquad S = S(z), \qquad 8\pi r^2\rho \equiv \eta = \eta(z), \tag{2}$$

where $z \equiv r/t$. In this spacetime, a singularity will appear at $t = r = 0$. In order to consider a model of the gravitational collapse, we require that the center $z = 0$ is regular before singularity formation (i.e., $t < 0$). In this paper we consider density perturbations in the epoch $t < 0$.

Here we introduce the function V defined as

$$V(z) = ze^{\lambda-\nu}, \tag{3}$$

which means the fluid velocity relative to the z =const surface. The Einstein equations of the self-similar system have a singularity at a point where $|V| = \sqrt{\alpha}$. We call this point sonic point and denote it by $z = z_s$. In this paper we focus on solutions regular at the sonic point.

In general spherically symmetric self-similar perfect fluid solutions can be described by three parameters including α. However the solutions considered as a background spacetime in this paper can be described by only two parameters because of the regular center condition. One is α and the other is D, where D is a constant associated with the central density defined as $D \equiv 4\pi\rho(t,0)t^2$. In addition, by requirement of the regularity condition at the sonic point to the solutions, the possible value of D is restricted. However the solutions still exist in a wide range of values of the parameter D for each α.

3 Density perturbations

We consider spherically symmetric density perturbations around the fixed self-similar solutions as

$$\eta(t,z) = \eta_0(z)\,(1+\delta\eta(t,z))\,. \tag{4}$$

Through the Einstein's equations, the metrics are also perturbed as

$$\nu(t,z) = \nu_0(z)\,(1+\delta\nu(t,z))\,, \qquad \lambda(t,z) = \lambda_0(z)\,(1+\delta\lambda(t,z))\,, \qquad S(t,z) = S_0(z)\,(1+\delta S(t,z))\,. \tag{5}$$

From Einstein equations linearized with respect to δ, we can obtain four partial differential equations for four unknown functions $\delta\eta$, $\delta\nu$, $\delta\lambda$ and δS. It is found from the two of these Einstein equations that the perturbation functions $\delta\nu$ and $\delta\lambda$ are written by undifferentiated $\delta\eta$ and δS. Hence we can obtain two second order partial differential equations in terms of only the functions $\delta\eta$ and δS. Here we introduce the Misner-Sharp mass function $m(t,z)$ and write

$$\frac{m}{2r} \equiv M(t,z) = M_0(z)\,(1+\delta M(t,z))\,. \tag{6}$$

Because the function m is written by the functions ν and λ and S, the function δM can be written by the functions $\delta\eta$ and δS. By adopting the functions δM and δS as variables instead of the functions $\delta\eta$ and δS, the two partial differential equations become first order. Here we introduce the function Ψ defined as

$$\Psi(t,z) = \delta S(t,z) + f(z)\delta M(t,z), \tag{7}$$

and rewrite the two first order partial differential equations to those in terms of Ψ and δM. We eliminate the first derivative term of the function δM from the two equations and vanish undifferentiated term of the function δM by appropriately determining the function f. Then we can obtain an autonomous wave equation written as

$$\Psi_{,uu} - \Psi_{,\zeta\zeta} + W(\zeta)\Psi_{,u} + F(\zeta)\Psi_{,\zeta} + U(\zeta)\Psi = 0\,, \tag{8}$$

where u and ζ are new coordinates related to old coordinates t and z by

$$u = \log(-t) + \int_{-\infty}^{z} \frac{V_0^2 d\bar{z}}{\bar{z}(V_0^2-\alpha)}, \qquad \zeta = \int_{-\infty}^{z} \frac{\sqrt{\alpha}V_0 d\bar{z}}{z(V_0^2-\alpha)}, \qquad V_0(z) = ze^{\lambda_0-\nu_0}, \tag{9}$$

and the functions W, F and U are written by the background self-similar metrics. Note that $\zeta = 0$ at the center $z = 0$ and $\zeta \to \infty$ as $z \to z_s$. Eq. (8) will be useful for the Green's function technique in the time-domain analysis.

In order to move on the frequency-domain analysis, we consider separation of variables $\Psi(u,\zeta) = \psi(\zeta,\omega)\exp(i\omega u)$. Then we obtain an ordinary differential equation written as

$$\psi_{,\zeta\zeta} - F\psi_{,\zeta} + \left(\omega^2 - i\omega W - U\right)\psi = 0\,. \tag{10}$$

This equation has two singularities at the center and the sonic point. As the boundary conditions, we require the regularity both at the center and at the sonic point to the solution of Eq. (10). Hence we must solve eigenvalue problem for the parameter ω. We denote the eigenfrequencies by ω_n and define the eigenmodes $\psi = \psi(\zeta,\omega_n)$ by $\psi_n(\zeta)$. The existence of the eigenmodes for the eigenfrequencies whose imaginary part is positive means that the background self-similar spacetime is unstable because then the wave functions $\Psi_n = \psi_n \exp(i\omega_n u)$ indefinitely increase as $t \to 0$.

Eq. (10) can be exactly solved for

$$\omega = \frac{1-\alpha}{1+\alpha}i, \tag{11}$$

and the solution satisfies the boundary conditions. However this eigenmode is unphysical because it is generated from the background self-similar solution by merely the coordinate transformation of t. We call this mode gauge mode and denote the eigenfrequency of Eq. (11) by ω_g. We must examine eigenmodes other than the gauge mode.

4 Stability of the flat Friedmann solution

In this section, using Eq. (10), we investigate stability of the flat Friedmann self-similar solution, which describes the monotonic collapse of a homogeneous perfect fluid. The flat Friedmann solution can be explicitly written as functions of z. For example the function V can be written as

$$V = V_c(-z)^q, \qquad q = \frac{1+3\alpha}{3(1+\alpha)}, \tag{12}$$

where V_c is a constant.

For convenience, we introduce a new variable x defined as $x = -V_0/\sqrt{\alpha}$. From Eqs. (9) and (12), we can find

$$\zeta = \frac{1}{2q}\log\frac{1+x}{1-x}. \tag{13}$$

Note that $x = 0$ at the center $z = 0$ and $x = 1$ at the sonic point $z = z_s$. In addition, we introduce a function ϕ defined as $\phi(\zeta,\omega) = \psi(\zeta,\omega)\exp(-i\omega\zeta)$. Then Eq. (10) can be rewritten as

$$q^2\left(1-x^2\right)^2\phi_{,xx} + q\left(1-x^2\right)(2i\omega - 2qx - F)\phi_{,x} - \{i\omega(F+W)+U\}\phi = 0. \tag{14}$$

The eigenmodes ϕ_n satisfy $\phi_n = 0$ at $x = 0$ and $\phi_n = \text{const} \neq 0$ at $x = 1$. Without loss of generality we can set $\phi_n(1) = 1$. We can find that the functions F and $F+W$ are always negative in the range $0 \leq x \leq 1$ for the range $0 < \alpha \leq 1$. In addition we can find that the function U is always positive in the range $0 \leq x \leq 1$ for the range $1/9 \leq \alpha \leq 1$.

For simplicity, hereafter we focus on eigenmodes for eigenfrequencies whose real part is zero. The gauge mode for Eq. (14) can be written as

$$\phi_g = \frac{4cx(1+x)^{-i\omega_g/q}}{3\{2(1-x)-3(1+\alpha)\}}, \tag{15}$$

where c is an arbitrary constant. Because this is a monotonic function, other physical eigenmodes must be non-monotonic. Here let us assume that the imaginary part of eigenfrequencies ω_n is positive. Then for the range $1/9 \leq \alpha \leq 1$, the value of $\phi_{n,xx}/\phi_n$ at the peak of ϕ_n (i.e., $\phi_{n,x} = 0$) is found to be necessarily negative from Eq. (14). However because of the boundary conditions $\phi_n(0) = 0$ and $\phi_n(1) = 1$, the value of $\phi_{n,xx}/\phi_n$ must be positive at least at one peak. This is a contradiction. Hence we can conclude that there is no growth eigenmode for eigenfrequency of pure imaginary at least for the range $1/9 \leq \alpha \leq 1$. We would like to emphasize that the same conclusion can be obtained for the background solutions in which $F + W < 0$ and $U > 0$.

Koike, Hara and Adachi showed that there is no growth eigenmode for eigenfrequency whose real part is nonzero in the critical solution[3]. If this is also true for the flat Friedmann solution, the flat Friedmann solution is stable at least for the range $1/9 \leq \alpha \leq 1$.

References

[1] B. J. Carr and A. A. Coley, qr-qc/0508039.

[2] T. Harada and H. Maeda, Phys. Rev. D **63**, 084022 (2001).

[3] T. Koike, T. Hara and S. Adachi, Phys. Rev. D **59**, 104008 (1999).

[4] D. W. Neilsen and M. W. Choptuik, Class. Quantum Grav. **17**, 761 (2000).

[5] E. Mitsuda, H. Yoshino and A. Tomimatsu, Phys. Rev. D **71**, 084033 (2005).

Signal-to-Noise Ratio of the CMB Angular Trispectrum Using the Full Radiative Transfer Functions

Noriyuki Kogo[1], Eiichiro Komatsu[2]

[1] *Department of Earth and Space Science, Graduate School of Science, Osaka University, Toyonaka 560-0043, Japan and*
Yukawa Institute for Theoretical Physics, Kyoto University, Kyoto 606-8502, Japan
[2] *Department of Astronomy, The University of Texas at Austin, 1 University Station, C1400, Austin, TX 78712, USA*

Abstract

We calculate the signal-to-noise ratio of the CMB angular trispectrum using the full radiative transfer functions without using any approximation such as the Sachs-Wolfe (SW) approximation. Compared with the SW approximation, the full-numerical result indicates steeper slope at high l. We also show that the signal-to-noise ratio of the trispectrum exceeds that of the bispectrum at $l \sim 10^5 |f_{\rm I}|^{-1}$, where $f_{\rm I}$ is the non-linearity parameter. Therefore, the trispectrum as well as the bispectrum may be useful to constrain the primordial non-Gaussianity for the future CMB experiments.

1 Introduction

Inflation scenario can nicely explain the origin of density fluctuations. Standard slow-roll single-field inflation model predicts Gaussian statistics of the primordial fluctuations. On the other hand, there are some models that generate large non-Gaussianity such as curvaton scenario. In this respect, non-Gaussianity of the primordial fluctuations plays a important role in testing and constraining inflation models. The primordial non-Gaussianity can be quantified by higher-order statistics of the CMB anisotropies. Non-Gaussian signatures in the CMB bispectrum (or three-point correlation function) have been studied actively [1, 2]. In contrast, because of its laboriousness, there have been rather a few studies about the trispectrum (or four-point correlation function) [3, 4]. In regard to forthcoming precise experimants of the CMB anisotropies such as the Planck mission [5], it is important to investigate observational implications for the trispectrum. Its signal-to-noise ratio was estimated by [4]. But, they used the Sachs-Wolfe (SW) approximation that is valid only on large scales ($l \ll 100$). In this poster, we present the results for the signal-to-noise ratio of the trispectrum calculated full-numerically including the transfer functions.

2 CMB Angular Trispectrum

Let us briefly review the formalism of the CMB angular trispectrum proposed in [3, 4]. We decompose the CMB temperature fluctuations into spherical harmonic components as

$$\frac{\delta T}{T}(\hat{\boldsymbol{n}}) = \sum_{lm} a_{lm} Y_{lm}(\hat{\boldsymbol{n}}). \tag{1}$$

Assuming the statistical isotropy, n-point correlation function must be rotational invariant. For $n = 4$, this implies

$$\langle a_{l_1 m_1} a_{l_2 m_2} a_{l_3 m_3} a_{l_4 m_4} \rangle = \sum_{LM} (-1)^M \begin{pmatrix} l_1 & l_2 & L \\ m_1 & m_2 & -M \end{pmatrix} \begin{pmatrix} l_3 & l_4 & L \\ m_3 & m_4 & M \end{pmatrix} T^{l_1 l_2}_{l_3 l_4}(L), \tag{2}$$

where $T^{l_1 l_2}_{l_3 l_4}(L)$ is the angular averaged trispectrum, L is the length of a diagonal that forms triangles with l_1 and l_2 and with l_3 and l_4. The matrix $\begin{pmatrix} l_1 & l_2 & l_3 \\ m_1 & m_2 & m_3 \end{pmatrix}$ is the Wigner 3-j symbol, where the triangle

[1] E-mail:kogo@yukawa.kyoto-u.ac.jp
[2] E-mail:komatsu@astro.as.utexas.edu

condition $|l_i - l_j| \leq l_k \leq l_i + l_j$ must be satisfied and the parity invariance requires $l_1 + l_2 + l_3 =$ even and $m_1 + m_2 + m_3 = 0$. These conditions determine the number of possible configurations. The trispectrum can be divided into two parts; the connected part and unconnected (or Gaussian) part as

$$T^{l_1 l_2}_{l_3 l_4}(L) = T^{l_1 l_2}_{c l_3 l_4}(L) + T_G{}^{l_1 l_2}_{l_3 l_4}(L). \tag{3}$$

The former contains non-Gaussian signatures while the latter is constructed by only the angular power spectrum $C_l \equiv \langle |a_{lm}|^2 \rangle$. From the permutation symmetry, the connected part of the trispectrum can be expressed as

$$\begin{aligned} T^{l_1 l_2}_{c l_3 l_4}(L) &= P^{l_1 l_2}_{l_3 l_4}(L) + (2L+1) \sum_{L'} \left[(-1)^{l_2 + l_3} \begin{Bmatrix} l_1 & l_2 & L \\ l_4 & l_3 & L' \end{Bmatrix} P^{l_1 l_3}_{l_2 l_4}(L) \right. \\ &\quad \left. + (-1)^{L+L'} \begin{Bmatrix} l_1 & l_2 & L \\ l_3 & l_4 & L' \end{Bmatrix} P^{l_1 l_4}_{l_3 l_2}(L) \right], \end{aligned} \tag{4}$$

where

$$P^{l_1 l_2}_{l_3 l_4}(L) = t^{l_1 l_2}_{l_3 l_4}(L) + (-1)^{L+l_1+l_2} t^{l_2 l_1}_{l_3 l_4}(L) + (-1)^{L+l_3+l_4} t^{l_1 l_2}_{l_4 l_3}(L) + (-1)^{2L+l_1+l_2+l_3+l_4} t^{l_2 l_1}_{l_4 l_3}(L), \tag{5}$$

the matrix is the Wigner 6-j symbol, and $t^{l_1 l_2}_{l_3 l_4}(L)$ is called the reduced trispectrum that contains all physical information of non-Gaussian sources. Here we consider non-Gaussianity from the primordial fluctuations. We parameterize the primordial curvature perturbation as

$$\Phi(x) = \Phi_L(x) + f_1 \left[\Phi^2_L(x) - \langle \Phi^2_L(x) \rangle \right] + f_2 \Phi^3_L(x), \tag{6}$$

where Φ_L is the linear Gaussian part and f_1 and f_2 are the non-linearity parameters. Suppose the adiabatic initial condition, the primordial fluctuations and CMB temperature fluctuations are related as

$$a_{lm} = 4\pi (-i)^l \int \frac{d^3k}{(2\pi)^3} \Phi(k) g_{Tl}(k) Y^*_{lm}(\hat{k}), \tag{7}$$

where $g_{Tl}(k)$ is the radiative transfer function that can be calculated by a numerical code such as the CMBFAST code [6]. Using this relation, we obtain the reduced trispectrum of the CMB anisotropies as

$$t^{l_1 l_2}_{l_3 l_4}(L) = \int r_1^2 dr_1 r_2^2 dr_2 F_L(r_1, r_2) \alpha_{l_1}(r_1) \beta_{l_2}(r_1) \alpha_{l_3}(r_2) \beta_{l_4}(r_2) h_{l_1 L l_2} h_{l_3 L l_4} \tag{8}$$

$$+ \int r^2 dr \beta_{l_2}(r) \beta_{l_4}(r) \left[\mu_{l_1}(r) \beta_{l_3}(r) + \beta_{l_1}(r) \mu_{l_3}(r) \right] h_{l_1 L l_2} h_{l_3 L l_4}, \tag{9}$$

where

$$F_L(r_1, r_2) = \frac{2}{\pi} \int K^2 dK P(K) j_L(K r_1) j_L(K r_2), \tag{10}$$

$$\alpha_l(r) = \frac{2}{\pi} \int k^2 dk (2 f_1) g_{Tl}(k) j_l(kr), \tag{11}$$

$$\beta_l(r) = \frac{2}{\pi} \int k^2 dk P(k) g_{Tl}(k) j_l(kr), \tag{12}$$

$$\mu_l(r) = \frac{2}{\pi} \int k^2 dk f_2 g_{Tl}(k) j_l(kr), \tag{13}$$

and

$$h_{l_1 L l_2} = \sqrt{\frac{(2l_1+1)(2l_2+1)(2L+1)}{4\pi}} \begin{pmatrix} l_1 & l_2 & L \\ 0 & 0 & 0 \end{pmatrix}. \tag{14}$$

We have defined the power spectrum of the primordial curvature perturbation as $P(k) \equiv (2\pi)^{-3} \langle |\Phi(k)|^2 \rangle$ and used $r = \eta_0 - \eta$, where η is the conformal time with η_0 being its present value. On large scales

($l \ll 100$), where the SW effect is dominant, the transfer function is approximately given by $g_{Tl}(k) \approx j_l(kr_*)/3$, where $r_* = \eta_0 - \eta_*$ and η_* is the conformal time at the recombination. This leads to a simple expression of the trispectrum as

$$t^{l_1 l_2}_{l_3 l_4}(L) \approx 9 C^{\rm SW}_{l_2} C^{\rm SW}_{l_4} \left[4 f_1^2 C^{\rm SW}_L + f_2 \left(C^{\rm SW}_{l_1} + C^{\rm SW}_{l_3} \right) \right] h_{l_1 L l_2} h_{l_3 L l_4}, \tag{15}$$

where

$$C^{\rm SW}_l = \frac{2}{9\pi} \int k^2 dk P_\Phi(k) j_l^2(kr_*) \equiv \frac{A}{l(l+1)}, \tag{16}$$

is the angular power spectrum in the SW regime and $A \approx 6 \times 10^{-10}$.

3 Estimation of Signal-to-Noise Ratio

The signal-to-noise ratio of the trispectrum is written as

$$\left(\frac{S}{N} \right)^2_{\rm tri} = \sum_{l_1 > l_2 > l_3 > l_4} \sum_L \frac{[T^{l_1 l_2}_{c\, l_3 l_4}(L)]^2}{(2L+1) \tilde{C}_{l_1} \tilde{C}_{l_2} \tilde{C}_{l_3} \tilde{C}_{l_4}}, \tag{17}$$

where $\tilde{C}_l \equiv C_l + N_l$ and N_l is the contribution from the detector noise. But, here we consider $N_l = 0$ case. At the beginning, let us estimate an order-of-magnitude of $(S/N)^2$. For simplicity, we take into account only the first terms in Eqs. (4) and (5) and only $L = 1$ modes because these turn out to be dominant. For $f_2 = 0$, in the SW approximation, we have

$$t^{l_1 l_2}_{l_3 l_4}(L=1) \approx 36 f_1^2 C^{\rm SW}_{L=1} C^{\rm SW}_{l_2} C^{\rm SW}_{l_4} h_{l_1,1,l_2} h_{l_3,1,l_4}. \tag{18}$$

Since $|l_1 - 1| \le l_2 \le l_1 + 1$ from the triangle condition and $l_1 > l_2$, $h_{l_1,1,l_2}$ is non-zero only if $l_1 - 1 = l_2$. To be more precise, we have

$$h^2_{l_1,1,l_2} = \frac{3}{4\pi}(2l_1+1)(2l_2+1) \begin{pmatrix} l_1 & l_2 & 1 \\ 0 & 0 & 0 \end{pmatrix}^2 = \frac{3 l_1}{4\pi} \delta_{l_1 - 1, l_2}. \tag{19}$$

Therefore, the signal-to-noise ratio can be estimated as

$$\left(\frac{S}{N} \right)^2_{\rm tri} \sim \sum_{l_1 > l_2 > l_3 > l_4} \frac{[t^{l_1 l_2}_{l_3 l_4}(L=1)]^2}{3 C^{\rm SW}_{l_1} C^{\rm SW}_{l_2} C^{\rm SW}_{l_3} C^{\rm SW}_{l_4}} \sim A^2 f_1^4 l^4_{\rm max}, \tag{20}$$

where $l_{\rm max}$ is the maximum multipole of the observation. Here we have analytically shown the dependence of $(S/N)^2$ on f_1 and $l_{\rm max}$ for the trispectrum. Note that the f_1-dependence as well as numerical result using the SW approximation have been already shown in [4]. To see the validity of the SW approximation and effects of acoustic oscillations in S/N of the trispectrum, we calculate it with full-radiative transfer functions by using the CMBFAST code. We set the normalozation as the height of the first acoustic peak of the WMAP data; $l(l+1)C_l/2\pi = (74.7 \mu{\rm K})^2$ at $l = 220$, and adopt the cosmological parameters as the concordance ΛCDM model with a scale-invariant primordial spectrum; $h = 0.72$, $\Omega_b = 0.047$, $\Omega_\Lambda = 0.71$, $\Omega_m = 0.29$, and $\tau = 0.17$. We compare the results of the full-numerical calculation with the SW approximation in Fig. 1. Since the full-numerical calculation is very time-consuming, our calculation is up to $l_{\rm max} = 100$. In the full-numerical calculation, because of the integrated SW effect, the denominator in Eq. (17) becomes larger at small l and this causes about a factor 2 smaller $(S/N)^2$ than that of the SW approximation at small l. As l is larger, however, we see $(S/N)^2$ of the full-numerical becomes steeper than that of the SW approximation. We also compare $(S/N)^2$ of the trispectrum with that of the bispectrum. As is shown above, for the trispectrum we have $(S/N)^2_{\rm tri} \propto f_1^4 l^4_{\rm max}$. On the other hand, for the bispectrum we have $(S/N)^2_{\rm bi} \propto f_1^2 l^2_{\rm max}$ as shown in [1]. It follows that the former becomes larger than the latter at $l_{\rm cross} \propto |f_1|^{-1}$. We show $(S/N)^2$ of the trispectrum and bispectrum for $f_1 = 100$ in Fig. 2. But, due to the limitation of the computational time, we extrapolate those by analytic functions at large l. As we see, the trispectrum crosses over the bispectrum at $l_{\rm cross} \approx 800$, from which we find $l_{\rm cross} \sim 10^5 |f_1|^{-1}$ in general.

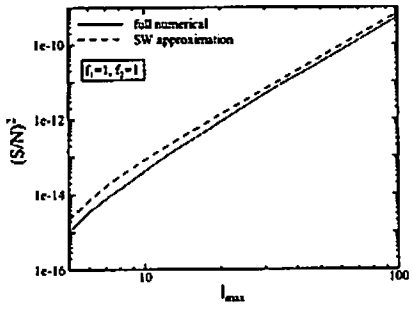

Figure 1: Comparison between the signal-to-noise ratios of the full-numerical calculation and the SW approximation.

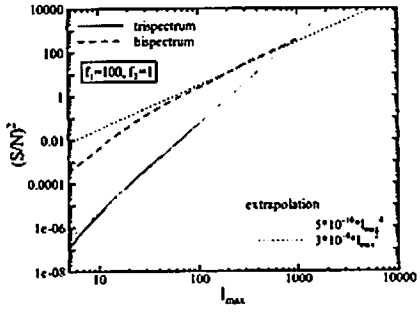

Figure 2: Comparison between the signal-to-noise ratios of the trispectrum and the bispectrum.

4 Conclusion

We have calculated the signal-to-noise ratio of the trispectrum with the transfer functions by using the CMBFAST code. We have found that the full-numerical result becomes steeper at high $l_{\rm max}$ than that for the SW approximation although it is not so significant up to $l_{\rm max} = 100$. We have also shown that the signal-to-noise ratio of the trispectrum exceeds that of the bispectrum at $l_{\rm cross} \sim 10^5 |f_1|^{-1}$. This implies that the trispectrum is as important as the bispectrum to investigate the primordial non-Gaussianity if f_1 is large enough. The combined analysis in which both the bispectrum and trispectrum are taken into account may be effective. In any case, an optimal method for the trispectrum analysis should be investigated to give observational constraints on the primordial non-Gaussianity by the next-generation experimants such as the Planck.

References

[1] E. Komatsu and D. N. Spergel, Phys. Rev. D **63**, 063002 (2001)

[2] E. Komatsu *et al.*, Astrophys. J. Suppl. **148**, 119 (2003)

[3] W. Hu, Phys. Rev. D **64**, 083005 (2001)

[4] T. Okamoto and W. Hu, Phys. Rev. D **66**, 063008 (2002)

[5] http://www.rssd.esa.int/index.php?project=PLANCK

[6] http://www.cmbfast.org/

Covariant boundary conditions for perturbation in compactified codimension-two braneworlds

Yuuiti Sendouda[a1], Shinji Mukohyama[a,b], Shunichiro Kinoshita[a], and Hiroyuki Yoshiguchi[a]

[a] *Department of Physics, The University of Tokyo, Tokyo 113-0033, Japan*
[b] *Research Center for the Early Universe, The University of Tokyo, Tokyo 113-0033, Japan*

Abstract

We show boundary conditions imposed on a brane in a codimension-two spacetime. For simplicity, we assume that the brane has only tension and the two-dimensional bulk is axisymmetric. The bulk can contain U(1) gauge field. The condition is formulated covariantly. As an application of the formalism, we show the stability of a low-energy model of warped flux compactification.

1 Introduction

Since the construction of four-dimensional de Sitter space in the framework of super string theory [1], the idea of so-called warped flux compactification has been gaining its importance in the context of modern cosmology. Recently the authors suggested a low-energy braneworld model which reflects some aspects of such an idea [2]. The model has two-dimensional bulk space. In order to investigate more properties of such spacetimes, e.g., their stability [3], we here formulate the covariant boundary condition for linear perturbation in codimension-two braneworlds [4].

2 Formulation

Let us consider a $(D+2)$-dimensional bulk spacetime $(\mathcal{M}, g)$ and a D-dimensional timelike brane $(\mathcal{B}, q)$ embedded in it. Generalization to many branes will be straightforward. Bulk coordinates are denoted by x^M where capital Latin indices run over all the dimensions $M, N = 0, \ldots, D+1$. Greek indices and small Latin indices are, respectively, of the brane and of the extra dimensions: $\mu, \nu = 0, \ldots, D-1$, $a, b = D, D+1$. We can in general take brane coordinates independent of bulk ones, so basically we indicate brane coordinates as y^μ rather than x^μ. The metrics of the bulk and the brane are denoted as g_{MN} and $q_{\mu\nu}$, respectively. The position of the brane is determined by embedding functions

$$x^M = Z^M(y), \tag{1}$$

by which the tangent vectors at each point on the brane are given as

$$e^M_\mu = \left.\frac{\partial Z^M}{\partial y^\mu}\right|_{x=Z} \tag{2}$$

and the metric induced on the brane is

$$q_{\mu\nu} = e^M_\mu e^N_\nu g_{MN}|_{x=Z}. \tag{3}$$

Two-dimensional bulk is now assumed to be axisymmetric with a spacelike Killing vector field φ^M satisfying $\nabla_M \varphi_N + \nabla_N \varphi_M = 0$, where ∇_M is the covariant derivative associated with g_{MN}. We define a unit vector n^M perpendicular to the brane by conditions below (signature is "almost positive" $-+\ldots+$)

$$n_M n^M|_{x=Z} = 1, n_M \varphi^M|_{x=Z} = n_M e^M_\mu|_{x=Z} = 0. \tag{4}$$

The signature of n^M is so taken that it directs inward to the bulk.

[1] E-mail:sendouda@utap.phys.s.u-tokyo.ac.jp

We consider background boundary condition imposed at the position of a brane with tension in the case that a brane is placed on the symmetry axis in the bulk. Then the boundary condition is given as the fact that the brane causes a deficit of the angle around it. To clarify, we utilize the length of the Killing vector

$$L \equiv \sqrt{g_{MN}\varphi^M\varphi^N}. \tag{5}$$

The boundary conditions are formulated through this L as follows. First of all, L should vanish at the brane because it is the symmetry axis from the bulk point of view. The other is required by the existence of the deficit angle. φ^M and n^M span coordinates in the neighborhood of the brane and we express them as $\varphi^M = \partial^M_\phi$ and $n_M = \partial^M_\rho$. We can generally set the position of the brane to be $\rho = 0$. Then the bulk metric is locally decomposed as

$$g_{MN}\mathrm{d}x^M\mathrm{d}x^N \simeq q_{\mu\nu}\mathrm{d}x^\mu\mathrm{d}x^\nu + \gamma_{ab}\mathrm{d}x^a\mathrm{d}x^b, \tag{6}$$

where two-dimensional bulk metric has a form

$$\gamma_{ab}\mathrm{d}x^a\mathrm{d}x^b = \mathrm{d}\rho^2 + L^2\mathrm{d}\phi^2. \tag{7}$$

Suppose the period of the original coordinate ϕ be $\phi \sim \phi + \Delta\phi$. We require the following condition should be satisfied under the limit $\rho \to 0+$

$$L^2 \simeq \rho^2\left(\frac{2\pi - \delta}{\Delta\phi}\right)^2 \tag{8}$$

where δ is the deficit angle induced by the tension of the brane σ. The relation between δ and σ is given with the fundamental mass scale of the bulk M_{D+2} as

$$\delta = \frac{\sigma}{M^D_{D+2}}. \tag{9}$$

In summary, the boundary conditions are given by

$$L|_{x=Z} = 0, \partial_\perp L|_{x=Z} = \frac{2\pi - \delta}{\Delta\phi}, \tag{10}$$

where $\partial_\perp \equiv n^M\partial_M$. Equivalent conditions are given in terms of squared length as

$$\mathcal{L}_0 \equiv L^2|_{x=Z} = 0, \tag{11}$$

$$\mathcal{L}_1 \equiv \partial_\perp L^2|_{x=Z} = 0, \tag{12}$$

$$\mathcal{L}_2 \equiv \partial^2_\perp L^2|_{x=Z} = 2\left(\frac{2\pi - \delta}{\Delta\phi}\right)^2. \tag{13}$$

U(1) gauge potential $A_M\mathrm{d}x^M$ may be present in the bulk. Without any charge or monopole associated to the brane, emanating flux $\int B_M n^M \mathrm{d}S \propto \oint A_M\varphi^M\mathrm{d}\ell \propto A_M\varphi^M$ must be zero, so the boundary condition is given by

$$\mathcal{A} \equiv A_M\varphi^M|_{x=Z} = 0. \tag{14}$$

Now we consider linearly perturbed geometry. Background geometry and the position of the brane are respectively perturbed as

$$g_{MN} = g^{(0)}_{MN} + \delta g_{MN}, \varphi^M = \varphi^{(0)M} + \delta\varphi^M, Z^M(y) = Z^{(0)M}(y) + \delta Z^M(y), \tag{15}$$

where background quantities are recognized by the indication of (0). Other linearly perturbed quantities are defined and calculated through above definitions and indices of perturbed tensors are raised or lowered by $g^{(0)}$. δZ^M generates an infinitesimal diffeomorphism which maps the brane from $x^M = Z^{(0)M}$ to $x^M = Z^M = Z^{(0)M} + \delta Z^M$. This causes perturbation for the quantities defined on the brane. The tangent vectors defined at $x = Z$ are described as $e^M_\mu = e^{(0)M}_\mu + \delta e^M_\mu$. The perturbation is

$$\delta e^M_\mu = \left.\frac{\partial\delta Z^M}{\partial y^\mu}\right|_{x=Z} = -\left.\mathcal{L}_{\delta Z}e^{(0)M}_\mu\right|_{x=Z} = -\left.\mathcal{L}_{\delta Z}e^{(0)M}_\mu\right|_{x=Z^{(0)}}, \tag{16}$$

where the value can be evaluated at $x = Z^{(0)}$ because the difference is of second order. It is understood that quantities defined in the tangent space of the brane are also perturbed with respect to position. Such quantities, with only brane indices, are viewed as scalars from the bulk point of view, so they are Taylor-expanded toward the direction of δZ^M. Thus the metric perturbation on the brane defined by $q_{\mu\nu} = q^{(0)}_{\mu\nu} + \delta q_{\mu\nu}$ is given as

$$\delta q_{\mu\nu} = \left[e^{(0)M}_{\mu} e^{(0)N}_{\nu} (\delta g_{MN} + \pounds_{\delta Z} g^{(0)}_{MN}) \right]_{x=Z^{(0)}}. \tag{17}$$

Next we calculate linear perturbation of the unit normal $n_M = n^{(0)}_M + \delta n_M$ using above perturbed quantities. Because the unitarity and orthogonality of vectors should be preserved, following conditions should hold at the brane position

$$\delta(n_M n^M|_{x=Z}) = \delta(n_M \varphi^M|_{x=Z}) = \delta(n_M e^M_{\mu}|_{x=Z}) = 0, \tag{18}$$

so δn_M is decomposed as

$$\delta n_M = \left[\frac{1}{2} \delta g_{PQ} n^{(0)P} n^{(0)Q} n^{(0)}_M - \frac{n^{(0)}_P \delta \varphi^P}{L^2_{(0)}} \varphi^{(0)}_M + \sum_{\mu=0}^{D-1} n^{(0)}_P (\pounds_{\delta Z} e^{(0)P}_{\mu}) q^{\mu\mu}_{(0)} e^{(0)}_{\mu M} \right]_{x=Z^{(0)}}, \tag{19}$$

where we utilized a relation $q^{\mu\nu}_{(0)} = (g^{(0)}_{QR} e^{(0)Q}_{\mu} e^{(0)R}_{\nu})^{-1}$. δn^M is given by $g^{(0)MN} \delta n_N$. Finally we consider perturbation of the boundary condition. In the bulk, the squared length of the Killing vector is perturbed as $L^2 = L^{(0)2} + \delta L^2$, where

$$\delta L^2 = 2\varphi^{(0)}_M \delta \varphi^M + \varphi^{(0)M} \varphi^{(0)N} \delta g_{MN}. \tag{20}$$

On the other hand, the normal derivative at the brane position is $\partial_\perp = \partial^{(0)}_\perp + \delta \partial_\perp$, where

$$\delta \partial_\perp = (\delta n^M - \delta g^{MN} n^{(0)}_N|_{x=Z^{(0)}}) \partial_M \tag{21}$$

with δn^M given above. In terms of these perturbations, the quantities required for boundary conditions are written down as

$$\delta \mathcal{L}_0 \equiv \delta(L^2|_{x=Z}) = [\delta L^2 + \pounds_{\delta Z} L^{(0)2}]_{x=Z^{(0)}} \tag{22}$$

$$\delta \mathcal{L}_1 \equiv \delta(\partial_\perp L^2|_{x=Z}) = [\delta \partial_\perp L^{(0)2} + \partial^{(0)}_\perp \delta L^2 + \pounds_{\delta Z} \partial^{(0)}_\perp L^{(0)2}]_{x=Z^{(0)}} \tag{23}$$

$$\delta \mathcal{L}_2 \equiv \delta(\partial^2_\perp L^2|_{x=Z}) = [\delta \partial_\perp \partial^{(0)}_\perp L^{(0)2} + \partial^{(0)}_\perp \delta \partial_\perp L^{(0)2} + \partial^{(0)2}_\perp \delta L^2 + \pounds_{\delta Z} \partial^{(0)2}_\perp L^{(0)2}]_{x=Z^{(0)}} \tag{24}$$

and

$$\delta \mathcal{A} \equiv \delta(A_M \varphi^M|_{x=Z}) = [\delta(A_M \varphi^M) + \pounds_{\delta Z} (A^{(0)}_M \varphi^{(0)M})]_{x=Z^{(0)}} \tag{25}$$

The boundary conditions on the perturbed geometry is given by

$$\delta \mathcal{L}_0 = \delta \mathcal{L}_1 = \delta \mathcal{L}_2 = \delta \mathcal{A} = 0. \tag{26}$$

3 Application

Now we apply the formalism developed in the previous section to a concrete example. We take a six-dimensional braneworld model in which two four-dimensional Minkowski brane are embedded, where the two-dimensional bulk is stabilized by a magnetic flux. The metric of the background spacetime is

$$g^{(0)}_{MN} \mathrm{d}x^M \mathrm{d}x^N = q^{(0)}_{\mu\nu} \mathrm{d}x^\mu \mathrm{d}x^\nu + \gamma^{(0)}_{ab} \mathrm{d}x^a \mathrm{d}x^b = \eta_{\mu\nu} \mathrm{d}x^\mu \mathrm{d}x^\nu + \frac{\mathrm{d}w^2}{f(w)} + f(w) \mathrm{d}\varphi^2 \tag{27}$$

where $f \equiv L^{(0)2} = 1 - w^2$ and the gauge potential is

$$A^{(0)}_M \mathrm{d}x^M = A_\varphi(w) \mathrm{d}\varphi = -w \mathrm{d}\varphi. \tag{28}$$

This is the low-energy "football"-shape limit of the model of warped flux compactification investigated in [3, 4]. Here all the physical scales are normalized to be unity for brevity.

Generally we can set the period of φ to match with the identical tension σ of the two branes placed at $w = \pm 1$, so the background boundary condition can be always satisfied. Linear perturbation for this spacetime is described by $\delta(g_{MN}\mathrm{d}x^M\mathrm{d}x^N) = \delta g_{MN}\mathrm{d}x^M\mathrm{d}x^N$, $\delta(A_M\mathrm{d}x^M) = \delta A_M\mathrm{d}x^M$, $\delta\varphi^M$, and $\delta Z_\pm^M$. Perturbations are expanded using the harmonics in Minkowski $Y \equiv \exp(ik_\mu x^\mu)$. In the following, components of δg and δA are denoted as h and a, respectively. Since the boundary condition is given through scalar quantities, those only couple with scalar perturbation. Thus we here show only the stability of scalar perturbation to clarify the utility of the boundary condition. Vector and tensor-type perturbation are discussed in [2, 3].

Scalar perturbation is given by

$$g_{MN}\mathrm{d}x^M\mathrm{d}x^N = (1+\Psi Y)\eta_{\mu\nu}\mathrm{d}x^\mu\mathrm{d}x^\nu + 2h_{(\mathrm{L})\varphi}V_{(\mathrm{L})\mu}\mathrm{d}x^\mu\mathrm{d}\varphi + [1+(\Phi_1+\Phi_2)Y]\frac{\mathrm{d}w^2}{1-w^2} + [1-(\Phi_1+3\Phi_2)Y](1-w^2)\mathrm{d}\varphi^2 \tag{29}$$

$$A_M\mathrm{d}x^M = a_w Y\mathrm{d}w + (-w+a_\varphi Y)\mathrm{d}\varphi \tag{30}$$

where we chose an analogue of the longitudinal gauge. From Einstein's and Maxwell's equations, four of six variables above are algebraically solved and the remaining field equations reduce to

$$(1-w^2)\Phi_1'' - 4w\Phi_1' - 2(\Phi_1+\Phi_2) + \mu^2\Phi_1 = 0, \tag{31}$$

$$(1-w^2)\Phi_2'' + \frac{\mu^2}{2}(\Phi_1+2\Phi_2) = 0, \tag{32}$$

where $\mu^2 = -\eta^{\mu\nu}k_\mu k_\nu$. The solution for this system is given by some linear combination of four Legendre functions $P_{\nu_\pm}$ and $Q_{\nu_\pm}$. By requiring the curvature scalars and vierbein components of the Weyl tensor to be regular on the boundaries $w = \pm 1$, regular combinations composed of above variables and their first derivatives are found. By the knowledge of the regular variables, we can drop terms which are regular combinations multiplied by vanishing quantities on the boundaries. Second order derivative of the metric component appears in the condition is removed by the equations of motion (31) and (32). After such reductions, the boundary conditions finally become

$$[\Phi_1 + 2\Phi_2]_{w=\pm 1} = 0. \tag{33}$$

Using it, the absence of zero mode with $\mu^2 = 0$ is easily shown by integrating eoms and imposing regularity. Kaluza-Klein mass spectrum is obtained from the lowest mode as

$$\mu^2 = 1, \frac{13-\sqrt{73}}{2}, 5, \frac{25-\sqrt{145}}{2}, \frac{13+\sqrt{73}}{2}, \frac{41-\sqrt{241}}{2}, \ldots \tag{34}$$

The above KK modes have positive μ^2 hence we conclude the spacetime is stable against linear scalar perturbation. Stability for tensor-type and vector-type perturbations are also shown in almost the same manner [3, 4].

References

[1] S. Kachru, R. Kallosh, A. Linde, and S.P. Trivedi, Phys. Rev. D **68** 046005 (2003).

[2] S. Mukohyama, Y. Sendouda, H. Yoshiguchi, S. Kinoshita, J. Cosmol. Astropart. Phys., 07 (2005) 013.

[3] H. Yoshiguchi, S. Mukohyama, Y. Sendouda, and S. Kinoshita, `hep-th/0512212`.

[4] Y. Sendouda, S. Mukohyama, S. Kinoshita, and H. Yoshiguchi, in preparation.

Effects of Gauss-Bonnet term on the final fate of gravitational collapse

Hideki Maeda[1]

Advanced Research Institute for Science and Engineering, Waseda University, Okubo 3-4-1, Shinjuku, Tokyo 169-8555, Japan

Abstract

We obtain a general spherically symmetric solution of a null dust fluid in $n(\geq 4)$-dimensions in Gauss-Bonnet gravity. This solution is a generalization of the n-dimensional Vaidya-(anti)de Sitter solution in general relativity. For $n = 4$, the Gauss-Bonnet term in the action does not contribute to the field equations, so that the solution coincides with the Vaidya-(anti)de Sitter solution. Using the solution for $n \geq 5$ with a specific form of the mass function, we present a model for a gravitational collapse in which a null dust fluid radially injects into an initially flat and empty region. It is found that a naked singularity is inevitably formed and its properties are quite different between $n = 5$ and $n \geq 6$. In the $n \geq 6$ case, a massless ingoing null naked singularity is formed, while in the $n = 5$ case, a massive timelike naked singularity is formed, which does not appear in the general relativistic case. The strength of the naked singularities is weaker than that in the general relativistic case. These naked singularities can be globally naked when the null dust fluid is turned off after a finite time and the field settles into the empty asymptotically flat spacetime. This paper is based on [1].

1 Model and solution

We begin with the following n-dimensional ($n \geq 5$) action:

$$S = \int d^n x \sqrt{-g} \left[\frac{1}{2\kappa_n^2} (R - 2\Lambda + \alpha L_{GB}) \right] + S_{\rm matter}, \tag{1}$$

where R and Λ are the n-dimensional Ricci scalar and the cosmological constant, respectively. κ_n is defined by $\kappa_n \equiv \sqrt{8\pi G_n}$, where G_n is the n-dimensional gravitational constant. The Gauss-Bonnet term L_{GB} is the combination of the Ricci scalar, Ricci tensor $R_{\mu\nu}$, and Riemann tensor $R^{\mu}{}_{\nu\rho\sigma}$ as

$$L_{GB} = R^2 - 4R_{\mu\nu}R^{\mu\nu} + R_{\mu\nu\rho\sigma}R^{\mu\nu\rho\sigma}. \tag{2}$$

In 4-dimensional spacetime, the Gauss-Bonnet term does not contribute to the field equations. α is the coupling constant of the Gauss-Bonnet term. This type of action is derived in the low-energy limit of heterotic superstring theory [2]. In that case, α is regarded as the inverse string tension and positive definite. Therefore, only the case where $\alpha \geq 0$ is considered in this paper. We consider a null dust fluid as a matter field, whose action is represented by $S_{\rm matter}$ in Eq. (1).

The gravitational equation of the action (1) is

$$G^{\mu}{}_{\nu} + \alpha H^{\mu}{}_{\nu} + \Lambda \delta^{\mu}{}_{\nu} = \kappa_n^2 T^{\mu}{}_{\nu}, \tag{3}$$

where

$$G_{\mu\nu} = R_{\mu\nu} - \frac{1}{2} g_{\mu\nu} R, \tag{4}$$

$$H_{\mu\nu} = 2\left[RR_{\mu\nu} - 2R_{\mu\alpha}R^{\alpha}{}_{\nu} - 2R^{\alpha\beta}R_{\mu\alpha\nu\beta} + R_{\mu}{}^{\alpha\beta\gamma}R_{\nu\alpha\beta\gamma} \right] - \frac{1}{2} g_{\mu\nu} L_{GB}. \tag{5}$$

[1] E-mail:hideki@gravity.phys.waseda.ac.jp

$H_{\mu\nu} \equiv 0$ holds for $n = 4$. The energy-momentum tensor of a null dust fluid is

$$T_{\mu\nu} = \rho l_\mu l_\nu, \tag{6}$$

where ρ is the non-zero energy density and l_μ is a null vector.

We obain the general spherically symmetric solution:

$$ds^2 = -f(v,r)dv^2 + 2dvdr + r^2 d\Omega^2_{n-2}, \tag{7}$$

$$f \equiv 1 + \frac{r^2}{2\tilde{\alpha}}\left\{1 \mp \sqrt{1 + 4\tilde{\alpha}\left[\frac{m(v)}{r^{n-1}} + \tilde{\Lambda}\right]}\right\}. \tag{8}$$

$$\rho = \frac{n-2}{2\kappa_n^2 r^{n-2}}\dot{m}, \tag{9}$$

$$l_\mu = -\partial_\mu v, \tag{10}$$

where $\tilde{\alpha} \equiv (n-3)(n-4)\alpha$ and $\tilde{\Lambda} \equiv 2/[(n-1)(n-2)]\Lambda$ and the dot denotes the derivative with respect to v. v is the advanced time coordinate and hence a curve $v = $ const denotes a radial ingoing null geodesic. $d\Omega^2_{n-2}$ is the line element of the $(n-2)$-dimensional unit sphere and $m(v)$ is an arbitrary function of v. In order for the energy density to be non-negative, $\dot{m} \geq 0$ must be satisfied.

In the general relativistic limit $\tilde{\alpha} \to 0$, the minus-branch solution is reduced to

$$f = 1 - \frac{m(v)}{r^{n-3}} - \tilde{\Lambda} r^2, \tag{11}$$

which is the n-dimensional Vaidya-(anti)de Sitter solution, while there is no such limit for the plus-branch solution. In the static case $\dot{m} = 0$, the solution (8) is reduced to the solution independently discovered by Boulware and Deser [3] and Wheeler [4].

2 Naked singularity formation

In this section, we study the gravitational collapse of a null dust fluid in Gauss-Bonnet gravity and compare it with that in general relativity by use of the solution obtained in the previous section. We consider the minus-branch solution for $n \geq 5$ in order to compare with the general relativistic case. For simplicity, we do not consider a cosmological constant, i.e., $\tilde{\Lambda} = 0$. We consider the situation in which a null dust fluid radially injects at $v = 0$ into an initially Minkowski region ($m(v) = 0$ for $v < 0$). The form of $m(v)$ is assumed to be

$$m = m_0 v^{n-3}. \tag{12}$$

where m_0 is a positive constant. In this case, the solution is reduced to the n-dimensional self-similar Vaidya solution in the general relativistic limit $\tilde{\alpha} \to 0$.

From Eq. (9), it is seen that there is a central singularity at $r = 0$ for $v > 0$. The point of $v = r = 0$ is more subtle but will be shown to be singular as well below. We will study the nature of the singularity.

We have

$$\frac{dr}{dv} = \frac{f}{2} \tag{13}$$

along a future-directed outgoing radial null geodesic, so that the region with $f < 0$ is the trapped region. A curve $f = 0$ represents the trapping horizon, i.e., the orbit of the apparent horizon, which is

$$m(v) = m_0 v^{n-3} = \tilde{\alpha} r^{n-5} + r^{n-3} \tag{14}$$

and shown to be spacelike for $v > 0$ and $r > 0$, i.e., it is a future outer trapping horizon, which is a local definition of black hole. From Eq. (14), only the point $v = r = 0$ may be a naked singularity in the case of $n \geq 6$, while the central singularity may be naked for $0 \leq v \leq v_{\rm AH}$ in the case of $n = 5$, where $v_{\rm AH}$ is defined by

$$m_0 v_{\rm AH}^2 = \tilde{\alpha}. \tag{15}$$

In order to determine whether or not the singularity is naked, we investigate the future-directed outgoing geodesics emanating from the singularity. It is shown that if a futre-directed radial null geodesic does not emanate from the singularity, then a future-directed causal (excluding radial null) geodesic does not also. So we consider here only the future-directed outgoing radial null geodesics. We found the asymptotic solution of Eq. (13)

$$v \simeq 2r \tag{16}$$

for $n \geq 6$, while

$$v \simeq v_0 + \frac{2}{1 - \sqrt{m_0 v_0^2/\tilde{\alpha}}} r \tag{17}$$

for $n = 5$, where $0 \leq v_0 < v_{\rm AH}$ is satisfied. Along these geodesics, the Kretschmann invariant $K \equiv R_{\mu\nu\rho\sigma}R^{\mu\nu\rho\sigma}$ diverges for $r \to 0$, so that they are actually singular null geodesics. We have now shown that at least a locally naked singularity is formed, and consequently the strong version of cosmic censorship hypothesis (CCH) is violated [5].

For $n \geq 6$, the naked singularity at $v = r = 0$ is massless and has the ingoing-null structure. In the case of $n = 5$, on the other hand, the singularity at $r = 0$ and $v = v_0$ with $0 \leq v_0 < v_{\rm AH}$ is massive and has the timelike structure. These naked singularities can be globally naked if we consider the situation in which the null dust fluid is turned off at a finite time $v = v_{\rm f} > 0$, whereupon the field settles into the Boulware-Deser-Wheeler spacetime with $m = m_0 v_{\rm f}^{n-3}$, which is asymptotically flat.

Next we consider the general relativistic case, i.e., the n-dimensional Vaidya solution. In this case, the trapping horizon is represented by $v = v_{\rm h} r$, where

$$v_{\rm h} \equiv \frac{1}{m_0^{1/(n-3)}}, \tag{18}$$

and hence only the point $v = r = 0$ may be naked. We find the exact power-law solution of the null geodesic equation (13):

$$v = v_1 r \tag{19}$$

for

$$m_0 \leq \frac{(n-3)^{n-3}}{2^{n-3}(n-2)^{n-2}}, \tag{20}$$

where v_1 satisfies

$$m_0 v_1^{n-2} - v_1 + 2 = 0. \tag{21}$$

Along these geodesics, the Kretschmann invariant diverges for $r \to 0$, so that they are actually singular null geodesics. The naked singularity at $r = v = 0$ is massless and has the ingoing-null structure. We can show that when Eq. (20) is satisfied, the singularity is always globally naked, i.e., the weak CCH is violated.

Next, we investigate the curvature strength of the naked singularity. We define

$$\psi \equiv R_{\mu\nu}k^\mu k^\nu, \tag{22}$$

where $k^\mu \equiv dx^\mu/d\lambda$ is the tangent vector of the future-directed outgoing radial null geodesic which emanates from the singularity and is parameterized by an affine parameter λ. We evaluate the strength of the naked singularity by the dependence of ψ on λ near the singularity.

After straightforward calculations, we show that

$$\lim_{\lambda \to 0} \psi \propto \frac{1}{\ln(\lambda + 1)} \tag{23}$$

for $n \geq 5$ in Gauss-Bonnet gravity, while

$$\psi \propto \frac{1}{\lambda^2}. \tag{24}$$

for $n \geq 5$ in general relativity, where $\lambda = 0$ corresponds to the singularity. Consequently, it is concluded by comparing Eq. (23) with Eq. (24) that the strength of the naked singularity in Gauss-Bonnet gravity is weaker than that in general relativity.

3 Discussion and conclusions

We have obtained an exact solution in Gauss-Bonnet gravity, which represents the spherically symmetric gravitational collapse of a null dust fluid in $n(\geq 5)$-dimensions. For $n \geq 5$, the solution is reduced to the n-dimensional Vaidya-(anti)de Sitter solution in the general relativistic limit. For $n = 4$, the Gauss-Bonnet term does not contribute to the field equations, so that the solution coincides with the Vaidya-(anti)de Sitter solution. Applying the solution to the situation in which a null dust fluid radially injects into an initially Minkowski region, we have investigated the effects of the Gauss-Bonnet term on the final fate of the gravitational collapse.

We have assumed that the mass function has the form of $m(v) = m_0 v^{n-3}$. Then, it has been found that there always exists a future-directed outgoing radial null geodesic emanating from the singularity in Gauss-Bonnet gravity, i.e., a naked singularity is inevitably formed. On the other hand, in the general relativistic case, there exists such a null geodesic only when m_0 takes a sufficiently small value. This result implies that the effects of the Gauss-Bonnet term on gravity worsen the situation from the viewpoint of CCH rather than prevent naked singularity formation.

Furthermore, the Gauss-Bonnet term drastically changes the nature of the singularity and the whole picture of gravitational collapse. The picture of the gravitational collapse for $n = 5$ is quite different from that for $n \geq 6$. For $n \geq 6$, as well as the general relativistic case for $n \geq 4$, a massless ingoing null naked singularity is formed. On the other hand, for the special case $n = 5$, a massive timelike naked singularity is formed. It is found from Eq. (14) that the formation of a massive timelike singularity in 5-dimensions is generic for the general mass function $m(v)$ which satisfies $m(0) = 0$ and $\dot{m} \geq 0$.

Here, we should mention the substantial work by Lake in 4-dimensional spherically symmetric spacetimes [6]. It has been shown under very generic situations that the massive singularities formed from regular initial data are censored [6]. In other words, if a naked singularity is formed from regular initial data, it is massless or with negative mass. This result was obtained without using the Einstein equations and may be extended into higher dimensions. One might think that this result is inconsistent with ours in Gauss-Bonnet gravity with $n = 5$. However, the discussion and results in [6] cannot apply directly to our system. In Lake's analysis, the Misner-Sharp mass is adopted to evaluate the mass of the singularity. On the other hand, we adopted $m(v)$, which is different from the higher-dimensional Misner-Sharp mass. $m(v)$ is shown to be preferable in Gauss-Bonnet gravity to evaluate the mass of the singularity [1].

Although naked singularities are inevitably formed in Gauss-Bonnet gravity, the Gauss-Bonnet term makes the strength of the naked singularity weaker than that in the general relativistic case. In association with this, there does exist a possible formulation of CCH, which asserts that the formation of weak naked singularities need not be ruled out [7]. In this sense, the Gauss-Bonnet term works well in the spirit of CCH.

References

[1] H. Maeda, gr-qc/0504028.

[2] D.J. Gross and J.H. Sloan, Nucl. Phys. **B291**, 41 (1987); M.C. Bento and O. Bertolami, Phys. Lett. **B368**, 198 (1996).

[3] D.G. Boulware and S. Deser, Phys. Rev. Lett. **55**, 2656 (1985).

[4] J.T. Wheeler, Nucl. Phys. **B268**, 737 (1986).

[5] R. Penrose, Riv. Nuovo Cim. 1, 252 (1969); R. Penrose, in *General Relativity, an Einstein Centenary Survey*, edited by S.W. Hawking and W. Israel (Cambridge University Press, Cambridge, England, 1979), p. 581.

[6] K. Lake, Phys. Rev. Lett. **68**, 3129 (1992).

[7] F.J. Tipler, C.J.S. Clarke, and G.F.R. Ellis, in *General Relativity and Gravitation*, edited by A. Held (Plenum, New York, 1980), vol. 2, p. 97.

Second order perturbation and energy loss by the KK modes in the RS model

Shunichiro Kinoshita[1], Hideaki Kudoh[2], Takahiro Tanaka[3]

[1,2] *Department of Physics, The University of Tokyo, Tokyo 113-0033, Japan*
[3] *Department of Physics, Graduate School of Science, Kyoto University, Kyoto 606-8502, Japan*

Abstract

In the braneworld, isolated dynamical systems will radiate gravitational waves into the bulk as well as on the brane, i.e., the Kaluza-Klein (KK) modes and the zero mode. The KK modes also take away the energy from matter sources on the brane, which leads to the extra energy loss. In order to know the energy loss of matter via the KK modes in the 5D Randall-Sundrum model, we consider the second order perturbation around the Minkowski brane. We then show that at the second order the energy conservation of the matter is satisfied taking account of the energy-momentum tensors of the massless graviton (the zero modes) and the KK massive graviton. We obtain the quadrupole formula of the energy loss rate via the KK modes, and show that this energy loss can be interpreted via the CFT picture.

1 Perturbation of the Minkowski brane

To investigate an asymptotically flat brane in the Randall-Sundrum model [1], we formulate a general perturbation scheme for the Minkowski brane. We take the five-dimensional Anti-de Sitter (AdS) metric as

$$ds^2 = g_{ab}dx^a dx^b = \frac{\ell^2}{z^2}[dz^2 + \gamma_{\mu\nu}dx^\mu dx^\nu], \tag{1}$$

where ℓ is the curvature radius of 5D AdS spacetime, and the brane is located at $z = \ell$. In this paper, we will adopt a coordinate system in which brane is always placed at $z = \ell$. The perturbations from exact AdS spacetime are given by $h_{\mu\nu} \equiv \gamma_{\mu\nu} - \eta_{\mu\nu}$. The contravariant components of the expanded metric are $\gamma^{\mu\nu} = \eta^{\mu\nu} - h^{\mu\nu} + h^\mu{}_\lambda h^{\nu\lambda} + \mathcal{O}(h^3)$. The indices are raised and lowered using $\eta^{\mu\nu}$. The Einstein equation in the bulk is

$$\mathcal{G}_{ab} \equiv {}^{(5)}G_{ab} + \Lambda\, g_{ab} = 0, \tag{2}$$

where the cosmological constant is $\Lambda = -6/\ell^2$, and we expand it around the background metric:

$$\mathcal{G}_{ab} = \mathcal{G}_{ab}[h] + \mathcal{G}_{ab}[h,h] + \cdots, \tag{3}$$

where $\mathcal{G}_{ab}[h]$ and $\mathcal{G}_{ab}[h,h]$ respectively denote linear terms and quadratic terms in $h_{\mu\nu}$. Higher order terms than cubic terms are omitted. Explicitly, the linear term is given by

$$\mathcal{G}_{\mu\nu}[h] = {}^{(4)}G_{\mu\nu}[h] - \frac{1}{2}\left(\frac{z}{\ell}\right)^3 \frac{\partial}{\partial z}\left[\left(\frac{\ell}{z}\right)^3 \frac{\partial}{\partial z}(h_{\mu\nu} - \eta_{\mu\nu}h)\right], \tag{4}$$

$$\mathcal{G}_{\mu z}[h] = \frac{1}{2}\frac{\partial}{\partial z}\partial^\nu(h_{\mu\nu} - \eta_{\mu\nu}h), \tag{5}$$

$$\mathcal{G}_{zz}[h] = -\frac{1}{2}\partial^\mu\partial^\nu(h_{\mu\nu} - \eta_{\mu\nu}h) - \frac{3}{2z}\frac{\partial}{\partial z}h. \tag{6}$$

Here ${}^{(4)}G_{\mu\nu}[h]$ is the linear term of four-dimensional Einstein tensor (well-known linearized Einstein tensor) defined by

$${}^{(4)}G_{\mu\nu}[h] \equiv -\frac{1}{2}\partial_\alpha\partial^\alpha\bar{h}_{\mu\nu} + \partial_{(\mu}\partial^\alpha\bar{h}_{\nu)\alpha} - \frac{1}{2}\eta_{\mu\nu}\partial^\alpha\partial^\beta\bar{h}_{\alpha\beta} \tag{7}$$

[1] E-mail:kinoshita@utap.phys.s.u-tokyo.ac.jp

where $\bar{h} \equiv h_{\mu\nu} - \frac{1}{2}\eta_{\mu\nu}h$. The quadratic terms are

$$\begin{aligned}
\mathcal{G}_{\mu\nu}[h,h] &= {}^{(4)}G_{\mu\nu}[h,h] - \frac{1}{4}\frac{\partial}{\partial z}h\frac{\partial}{\partial z}h_{\mu\nu} + \frac{1}{2}\frac{\partial}{\partial z}h_{\mu\alpha}\frac{\partial}{\partial z}h_{\nu}{}^{\alpha} + \frac{1}{8}\eta_{\mu\nu}\left[\frac{\partial}{\partial z}h\frac{\partial}{\partial z}h - 3\frac{\partial}{\partial z}h_{\alpha\beta}\frac{\partial}{\partial z}h^{\alpha\beta}\right] \\
&\quad + \frac{1}{2}\left\{h_{\mu\nu}\left[\frac{\partial^2}{\partial z^2} - \frac{3}{z}\frac{\partial}{\partial z}\right]h - \eta_{\mu\nu}h^{\alpha\beta}\left[\frac{\partial^2}{\partial z^2} - \frac{3}{z}\frac{\partial}{\partial z}\right]h_{\alpha\beta}\right\}, \qquad (8) \\
\mathcal{G}_{\mu z}[h,h] &= -\frac{1}{2}h^{\alpha\beta}\frac{\partial}{\partial z}\partial_\alpha h_{\beta\mu} + \frac{1}{2}h^{\alpha\beta}\frac{\partial}{\partial z}\partial_\mu h_{\alpha\beta} + \frac{1}{4}\partial_\mu h^{\alpha\beta}\frac{\partial}{\partial z}h_{\alpha\beta} - \frac{1}{2}\partial_\nu\left(h^{\nu\alpha} - \frac{1}{2}\eta^{\nu\alpha}h\right)\frac{\partial}{\partial z}h_{\alpha\mu}, \qquad (9) \\
\mathcal{G}_{zz}[h,h] &= -\frac{1}{2}{}^{(4)}R[h,h] + \frac{3}{2z}h^{\alpha\beta}\frac{\partial}{\partial z}h_{\alpha\beta} + \frac{1}{8}\left[\frac{\partial}{\partial z}h\frac{\partial}{\partial z}h - \frac{\partial}{\partial z}h^{\alpha\beta}\frac{\partial}{\partial z}h_{\alpha\beta}\right], \qquad (10)
\end{aligned}$$

where ${}^{(4)}G_{\mu\nu}[h,h]$ and ${}^{(4)}R[h,h]$ are the quadratic terms of four-dimensional Einstein tensor and Ricci scalar.

Expanding the metric perturbations as $h_{\mu\nu} = h^{(1)}_{\mu\nu} + h^{(2)}_{\mu\nu} + \cdots$, the Einstein equation up to the second order is given by $\mathcal{G}_{ab}[h^{(1)}] = 0$ and $\mathcal{G}_{ab}[h^{(2)}] = -\mathcal{G}_{ab}[h^{(1)}, h^{(1)}]$, where we omit higher order ones than third. Note that $h^{(i)}_{\mu\nu}$ represents i-th order of metric perturbation. Hereafter the superscripts in $h^{(i)}$ indicate the order of metric perturbations and we will drop the superscripts from such quantities when it is obvious. Obviously $\mathcal{G}_{ab}[h^{(1)}] = 0$ is the linearized 5D Einstein equation, and then the metric perturbation at each order is recursively determined, starting from $h^{(1)}_{\mu\nu}$. To solve the equations, it is crucially important to take into account the boundary condition at the brane. For the braneworld models, the boundary condition is given by the junction condition which involves energy-momentum tensor $T_{\mu\nu}$ of the matter fields on the brane, $K_{\mu\nu} - g_{\mu\nu}K - \frac{3}{\ell}g_{\mu\nu} = -\frac{\kappa}{2}T_{\mu\nu}$ $(z \to \ell + 0)$, where the 5D gravitational coupling constant is $\kappa \equiv 8\pi G_5$ $(G_5 = \ell G_4)$. Expanding the extrinsic curvature $K_{\mu\nu}$ in $h_{\mu\nu}$, the junction condition at each order are

$$\frac{\ell}{z}\frac{\partial}{\partial z}(h^{(1)}_{\mu\nu} - \eta_{\mu\nu}h^{(1)})\Big|_{z=\ell} = -\kappa T^{(1)}_{\mu\nu}, \qquad (11)$$

$$\frac{\ell}{z}\frac{\partial}{\partial z}(h^{(2)}_{\mu\nu} - \eta_{\mu\nu}h^{(2)})\Big|_{z=\ell} = -\kappa T^{(2)}_{\mu\nu} - \frac{\ell}{z}\left[\eta_{\mu\nu}h^{\alpha\beta}\frac{\partial}{\partial z}h_{\alpha\beta} - h_{\mu\nu}\frac{\partial}{\partial z}h\right]\Big|_{z=\ell}. \qquad (12)$$

2 Zero mode of second order perturbation

Let us consider the zero mode of the second order perturbations. To investigate the zero mode, we introduce the idea of zero mode extraction. We can split the metric perturbations into a zero mode and Kaluza-Klein modes $h_{\mu\nu} = h^{\rm zero}_{\mu\nu} + h^{\rm KK}_{\mu\nu}$.

The zero mode and the KK modes are characterized by their Green functions, in particular, the mode functions which depend on z. Since the mode functions satisfy the orthogonality relation, we can define zero mode extraction for a given metric perturbation by utilizing the orthogonality. The operator of zero mode extraction is

$$h^{\rm zero}_{\mu\nu} = \frac{2}{\ell}\int_\ell^\infty {\rm d}z\left(\frac{\ell}{z}\right)^3 h_{\mu\nu}(x,z). \qquad (13)$$

With respect to any order of metric perturbations we can perform the above operation and obtain the zero mode.

As an example, we first apply the zero mode extraction for the linear term of $\mathcal{G}_{\mu\nu}$,

$$\frac{2}{\ell}\int_\ell^\infty {\rm d}z\left(\frac{\ell}{z}\right)^3 \mathcal{G}_{\mu\nu}[h^{(i)}] = {}^{(4)}G_{\mu\nu}[h^{(i)}_{\rm zero}] + \frac{1}{\ell}\frac{\partial}{\partial z}(h^{(i)}_{\mu\nu} - \eta_{\mu\nu}h^{(i)})\Big|_{z=\ell}, \qquad (14)$$

This result holds true for any order of order metric perturbations $h^{(i)}_{\mu\nu}$. For the linear order perturbation, the linearized Einstein equation is given by $\mathcal{G}_{ab}[h^{(1)}] = 0$. Then, with the help of the junction condition (11), the zero mode extraction leads to ${}^{(4)}G_{\mu\nu}[h^{(1)}_{\rm zero}] = \frac{\kappa}{\ell}T^{(1)}_{\mu\nu}$. This is obviously the linearized 4D Einstein equation with the gravitational coupling constant $8\pi G_4 = \kappa/\ell$, so that our covariant approach of the zero mode extraction correctly recover the Einstein gravity at the linear order.

The zero mode extraction of the second order perturbations are also possible by the above method. We multiply the extraction operator to the second-order Einstein equation $\mathcal{G}_{ab}[h^{(2)}] = -\mathcal{G}_{ab}[h^{(1)}, h^{(1)}]$, and then the second order Einstein equation with the first order Einstein equation and the junction condition (12) becomes without any gauge fixing

$$ {}^{(4)}G_{\mu\nu}[h^{(2)}_{\rm zero}] = 8\pi G_4 T^{\rm eff}_{\mu\nu}[h^{(1)}, h^{(1)}]. \tag{15} $$

The source term is given by $T^{\rm eff}_{\mu\nu} = T^{\rm zero}_{\mu\nu} + T^{\rm KK}_{\mu\nu} - \bar{h}_{\mu\alpha}T^{(1)}{}_{\nu}{}^{\alpha} + T^{(2)}_{\mu\nu}$, where

$$ T^{\rm zero}_{\mu\nu} \equiv \frac{1}{32\pi G_4}\left[\bar{h}^{(0)}_{\alpha\beta,\mu}\bar{h}^{(0)\alpha\beta}_{,\nu} - \frac{1}{2}h^{(0)}_{,\mu}h^{(0)}_{,\nu} - \frac{1}{2}\eta_{\mu\nu}\left(\bar{h}^{(0)}_{\alpha\beta,\lambda}\bar{h}^{(0)\alpha\beta,\lambda} - \frac{1}{2}h^{(0)}_{,\lambda}h^{(0),\lambda}\right)\right], \tag{16} $$

and

$$ \begin{aligned} T^{\rm KK}_{\mu\nu} \equiv\ & \frac{\ell}{32\pi G_4}\int_0^\infty {\rm d}m\,|u_m(\ell)|^2\left[h^{(m)}_{\alpha\beta,\mu}h^{(m)\alpha\beta}{}_{,\nu} - h^{(m)}_{,\mu}h^{(m)}_{,\nu} - \frac{1}{2}\eta_{\mu\nu}\left(h^{(m)}_{\alpha\beta,\lambda}h^{(m)\alpha\beta,\lambda} - h^{(m)}_{,\lambda}h^{(m),\lambda}\right)\right. \\ & \left. -\frac{m^2}{2}\eta_{\mu\nu}\left(h^{(m)}_{\alpha\beta}h^{(m)\alpha\beta} - h^{(m)2}\right)\right]. \end{aligned} \tag{17} $$

$T^{\rm zero}_{\mu\nu}$ corresponds to the well-known energy-momentum tensor of massless 4D graviton $h^{(0)}_{\mu\nu}$, which can usually represent the gravitational energy in the 4D GR. On the other hand, $T^{\rm KK}_{\mu\nu}$ is the contribution from the KK modes, and we can think of the contribution as an energy-momentum tensor of the massive graviton $h^{(m)}_{\mu\nu}$ with mass m, which is given by summing up all massive Kaluza-Klein graviton. The remainder are local terms consisting of the energy-momentum tensor of the matter on the brane, i.e., $T^{(1)}_{\mu\nu}$ or $T^{(2)}_{\mu\nu}$, which will vanish outside matter distribution. We can easily find that all of above quantities can satisfy the local conservation law, $\partial^\mu T^{\rm eff}_{\mu\nu} = 0$. The result shows that the second-order zero mode is generated by the two types of mode coupling; zero-zero coupling and KK-KK coupling. The first type of mode coupling recovers the 4D Einstein gravity at this order. The latter mode coupling between the KK modes with the same mass gives the correction to the induced gravity on the brane at the far (vacuum) region. As we will see later we can interpret the correction as an energy radiated into the bulk. Note that mode couplings between different modes, i.e., the zero-KK coupling vanishes due to the orthogonality. As we will explicitly show in the following subsection, the order of the KK correction in the source term is $\mathcal{O}(\ell^2)$. This means the zero mode of the second order perturbation caused by the linear KK modes has the order $\mathcal{O}(\ell^2)$, as well as the linear order of KK modes which is also $\mathcal{O}(\ell^2)$.

3 Results

In General Relativity the energy loss of matter sources by radiating gravitational waves is calculated by utilizing the pseudo energy-momentum tensor of gravity. In the previous section we have derived the effective 4D Einstein equation for the second-order gravitational perturbations of the zero mode, the reduced Einstein equation (15) can be put into the form ${}^{(4)}G_{\mu\nu}[h^{(2)}_{\rm zero}] = 8\pi G_4\, T^{\rm eff}_{\mu\nu}$. The corresponding pseudo energy-momentum tensor of gravity in the present case will be described by the effective energy momentum tensor $T^{\rm eff}_{\mu\nu}$ due to gravitational backreaction. As we mentioned, the local conservation law $\partial^\mu T^{\rm eff}_{\mu\nu} = 0$ is satisfied and it represents the energy conservation for the matter on the brane, so that the energy loss rate of isolated matter sources is given by the surface integral of flux at infinity on the brane. This is given by

$$ \frac{{\rm d}E}{{\rm d}t} = -\oint_{S_\infty} T^{\rm eff}_{0i}{\rm d}S^i = \frac{2}{\kappa}\oint_{S_\infty}\left\{\int_\ell^\infty {\rm d}z\left(\frac{\ell}{z}\right)^3 \mathcal{G}_{0i}[h^{(1)}, h^{(1)}]\right\}{\rm d}S^i. \tag{18} $$

From the 5-dimensional point of view, $\mathcal{G}_{ab}[h^{(1)}, h^{(1)}]$ is regarded as the 5-dimensional gravitational (pseudo) energy-momentum tensor, and hence Eq. (18) means that matters on the brane lose their energy by gravitational-wave emission on the brane and *into* the bulk.

If we only consider zero mode contribution into the gravitational energy-momentum tensor neglecting all the KK modes, then Eq. (18) reproduces the well-known quadrupole formula for the energy loss according to the standard prescription, $\mathrm{d}E^{\mathrm{zero}}/\mathrm{d}t = -\frac{G_4}{5} \mathcal{I}_{ij}^{(3)} \mathcal{I}_{ij}^{(3)}$. Here the trace-free quadrupole moment $\mathcal{I}_{ij}$ of matter distribution is defined by $\mathcal{I}_{ij} = I_{ij} - \frac{1}{3}\delta_{ij} I$, where $I_{ij} = \int \mathrm{d}^3\mathbf{x}\, x_i x_j T_{00}$ is quadrupole moment and $I_{ij}^{(n)} \equiv \frac{\mathrm{d}^n}{\mathrm{d}t^n} I_{ij}$. As for the KK modes, all contributions from the KK modes can be expressed in terms of the quadrupole moment. The energy loss rate due to the KK modes becomes

$$\frac{\mathrm{d}E^{\mathrm{KK}}}{\mathrm{d}t} = -\frac{\ell^2 G}{1260}(67\, \mathcal{I}_{ij}^{(5)} \mathcal{I}_{ij}^{(5)} + \frac{10}{3}|I^{(5)}|^2). \tag{19}$$

Compared with the standard quadrupole formula for the zero mode, it is suppressed by $\ell^2\omega^2$ where ω is a typical frequency of matter sources. It is worthwhile to note that contrary to the 4D GR the matter sources on the brane can radiate the energy via the KK modes, even if their evolution is spherically symmetric on the brane. Furthermore, the energy loss rate is manifestly positive definite in round brackets, so the matter sources always lose their energy by exciting the KK modes.

We can interpret previous results in terms of 4D CFT. Considering the conformal field, inhomogeneous perturbations of external gravitational fields due to the time-dependent source yield the quantum particle creation [3]. A formula of the energy loss rate due to such particle creation is given by [2]

$$\frac{\mathrm{d}E}{\mathrm{d}t} = \frac{G^2}{18900\pi}(67\, \mathcal{I}_{ij}^{(5)} \mathcal{I}_{ij}^{(5)} + \frac{10}{3}|I^{(5)}|^2). \tag{20}$$

with respect to the conformal-coupled massless scalar fields. This result is the same as Eq.(19) up to the factor $\frac{G}{15\pi\ell^2}$. This indicates that in 5D classical picture the energy loss of matter sources by radiating the KK graviton to the bulk corresponds to that by quantum particle creation on the brane in 4D CFT picture [4].

References

[1] L. Randall and R. Sundrum, Phys. Rev. Lett. **83**, 3370 (1999) [arXiv:hep-ph/9905221]; L. Randall and R. Sundrum, Phys. Rev. Lett. **83**, 4690 (1999) [arXiv:hep-th/9906064].

[2] J. Garriga, D. Harari and E. Verdaguer, Nucl. Phys. B **339**, 560 (1990).

[3] J. A. Frieman, Phys. Rev. D **39**, 389 (1989).

[4] S. S. Gubser, Phys. Rev. D **63**, 084017 (2001) [arXiv:hep-th/9912001].

Detecting a gravitational-wave background with next-generation space interferometers

Hideaki Kudoh

Department of Physics, The University of Tokyo, Tokyo 113-0033, Japan

Abstract

Search for stochastic gravitational-wave backgrounds (GWBs) is one of the main targets for the future missions of gravitational-wave astronomy. We discuss and evaluate the prospects for direct measurement of isotropic and anisotropic components of (primordial) GWBs around the frequency 0.1 – 10 Hz. We consider several future space interferometer missions, like Big-Bang Observer (BBO), Deci-Hertz Interferometer Gravitational-wave Observer (DECIGO) and recently proposed Fabry-Perot type DECIGO. The astrophysical foregrounds that are expected at low frequency may be a big obstacle and significantly reduce the signal-to-noise ratio of GWBs. As a result, minimum detectable amplitude may reach $h^2\Omega_{gw} = 10^{-15} \sim 10^{-16}$, as long as foreground point sources are properly subtracted. Based on correlation analysis, we also discuss the sensitivity level required for detecting the dipole moment of GWB induced by the proper motion of our local system is closely examined.

1 Introduction

Several future missions of space-based interferometers have been proposed as follow-on missions of LISA. A main target of these missions is the primordial GWB produced during the inflationary epoch. While the conceptual designs of these projects differ from each other, it is commonly believed that the frequencies around $0.1 \lesssim f \lesssim 10$ Hz may be one of the best observational window filling the gap between the frequency covered by LISA and the ground-based detectors. We then wish to know the sensitivity of the next-generation space interferometers to the stochastic GWBs and to study the basic aspects of the signal processing strategy as well as the characteristics of each detector. To address these issues, the correlation analysis plays a key role since it is necessary to detect the stochastic signals in the presence of random noises.

As known well, not only the instrumental noises but also the stochastic signals themselves become a disturbance and prevent us from the detection of primordial GWBs. In this respect, the optimally filtered signal processing is suitable for the correlation analysis. In this paper, we discuss the sensitivity of the next-generation space interferometers and study the prospects for direct measurement of primordial GWBs. In addition, we also address the feasibility of direct measurement for anisotropic component of GWB. As for future space interferometers, we will consider DECIGO/BBO and recently proposed Fabry-Perot type space interferometer (FP-DECIGO) [1]. The details of optimal-filtered signal processing for isotropic and anisotropic GWB are discussed in our original paper [3].

2 Sensitivity of future space interferometers to stochastic GWBs

2.1 Interferometer design

Currently, practical interferometer design as well as precise orbital configurations for proposed future missions are still under debate and are not fixed. We assume that the future missions consists of four sets of detectors; two of which consist of three spacecrafts forming a triangular configuration, like LISA, and the remaining of which consists of six spacecrafts forming a star-like constellation. Each of the three detectors are located separately 120° ahead or behind on the orbit around the Sun. With this setup, we now consider the three possible cases summarized in Table 1. For comparison, we also list the instrumental parameters of LISA.

	L[m]	$S_{\text{shot noise}}$[m Hz$^{-1/2}$]	S_{accel}[m s^{-2} Hz$^{-1/2}$]	interferometric type
LISA	5×10^9	2×10^{-11}	3×10^{-15}	Doppler-tracking (DT)
TDI-DECIGO/BBO	5×10^7	1.2×10^{-16}	3.9×10^{-17}	DT
FP-DECIGO	1×10^6	2.2×10^{-18}	7.9×10^{-19}	Fabry-Perot with fineness $\mathcal{F} = 10$
Ultimate DECIGO	5×10^7	3×10^{-19}	3×10^{-19}	DT limited by quantum noise

Table 1: Instrumental parameters (arm length L, shot noise, acceleration noise) for next-generation space interferometers.

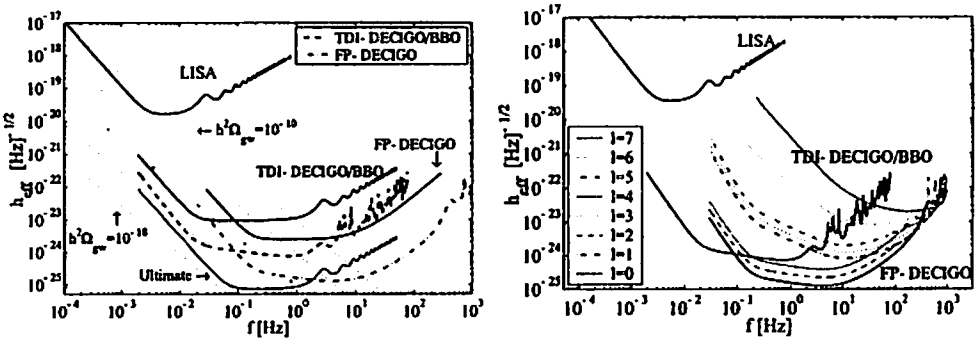

Figure 1: *Left.* Spectral amplitude sensitivity $h_{\rm eff}$ for several space-based interferometers. Solid curves show the sensitivity for self-correlation analysis for LISA, TDI-DECIGO/BBO, FP-DECIGO and ultimate DECIGO (Table 1). The dashed curves show the sensitivity for cross-correlation analysis, assuming the hexagonal spacecraft configuration. In these plots, we have taken $\overline{\rm SNR} = 5$, $\Delta f = f/10$, and $T_{\rm obs} = 1$ year. *Right.* Effective strain amplitude $h_{\rm eff}$ for FP-DECIGO. The interferometers are most sensitive to lower even multipoles of $\ell = 0, 2, 4$. Because of the hexagonal form, the detectors are also sensitive to lower odd multipoles $\ell = 1, 3, 5$. The sensitivity to higher multipoles $\ell \geq 6$ is very poor and this fact is especially evident in the low frequency band.

The original DECIGO (or BBO) is planning to use Doppler-tracking method as will be implemented in LISA. In such signal processing technique, the output signals sensitive to gravitational waves are constructed by time-delayed combination of laser pulses to cancel out laser frequency noises. This type of interferometry is known as time-delay interferometry (TDI). To distinguish the original DECIGO from FP-DECIGO, we call the original one TDI-DECIGO. FP-DECIGO may adopt the same technique as used in the ground detectors. The essential requirement is that the relative displacement between the spacecrafts to be constant during an observation. The third class of space interferometer discussed in this paper is the ultimate DECIGO. In Fig. 1, sensitivity curves are plotted.

2.2 Isotropic case

To see how the cross-correlation analysis improves the sensitivity to the GWB, let us first focus on the isotropic GWB and evaluate the sensitivity of each space interferometer. For this purpose, we take the weak-signal approximation. We introduce effective strain sensitivity:

$$h_{\rm eff}(f) = \overline{\rm SNR}^{1/2} \left\{ \frac{5}{2} \frac{N_I(f) N_J(f)}{|\gamma_{IJ}(f)|\, \Delta f\, T_{\rm obs}} \right\}^{1/4}, \tag{1}$$

where the quantity $\overline{\rm SNR}$ means the signal-to-noise of stochastic GWB over the frequency range $f \sim f + \Delta f$. Eq. (1) quantifies the strain amplitude of minimum detectable GWB for different frequency bin. Unlike the usual sense of the sensitivity curves, it depends on the observation time as well as the frequency interval.

While the effective strain sensitivity $h_{\rm eff}$ provides useful information on the frequency dependence of the detectable amplitude, for more precise estimate of the SNR, one must directly evaluate the expression,

integrating over the whole frequency bins. Assuming the flat spectrum, $\Omega_{\rm gw}(f) = \Omega_{\rm gw,0}\, f^0$, the resultant detectable values of $\Omega_{\rm gw}$ are

$$h^2\,\Omega_{\rm gw,0} = \begin{cases} 6.8\times10^{-18}\left(\dfrac{\rm SNR}{5}\right)\left(\dfrac{T_{\rm obs}}{1\,\rm year}\right)^{-1/2} & \text{(TDI-DECIGO/BBO)} \\ 1.1\times10^{-16}\left(\dfrac{\rm SNR}{5}\right)\left(\dfrac{T_{\rm obs}}{1\,\rm year}\right)^{-1/2} & \text{(FP-DECIGO)} \\ 4.2\times10^{-21}\left(\dfrac{\rm SNR}{5}\right)\left(\dfrac{T_{\rm obs}}{1\,\rm year}\right)^{-1/2} & \text{(ultimate DECIGO)} \end{cases} \tag{2}$$

As anticipated from the effective sensitivity curves, the minimum detectable value of $\Omega_{\rm gw}$ for TDI-DECIGO/BBO is an order of magnitude lower than that for FP-DECIGO. In this sense, the frequency band around $0.1 - 1$Hz covered by TDI-DECIGO/BBO may be the best observational window to probe the GWB of primordial origin.

The above discussion is, however, rather optimistic. In practice, one would not neglect several astrophysical foregrounds. For example, a cosmological population of white-dwarf binaries may produce a large signal at low-frequency band $f \lesssim 0.2$Hz, which would not be resolved individually. Hence, the cosmological white-dwarf binaries may act as a confusion noise and they prevent us from detecting the primordial GWB below the frequency $f_{\rm cut} = 0.2$ Hz. The effect of low-frequency cutoff is significant for TDI-DECIGO/BBO. The minimum detectable amplitude for $f_{\rm cut} \gtrsim 0.1$ Hz becomes 100 times worse. By contrast, as long as the cutoff frequency is below 0.1Hz, the minimum detectable amplitude of FP-DECIGO almost remains unchanged. With the cutoff frequency $f_{\rm cut} = 0.2$ Hz, the minimum amplitude $\Omega_{\rm gw,0}h^2$ is changed to

$$h^2\,\Omega^{\rm cutoff}_{\rm gw,0} = \begin{cases} 5.8\times10^{-15}\left(\dfrac{\rm SNR}{5}\right)\left(\dfrac{T_{\rm obs}}{1\,\rm year}\right)^{-1/2} & \text{(TDI-DECIGO)} \\ 4.8\times10^{-16}\left(\dfrac{\rm SNR}{5}\right)\left(\dfrac{T_{\rm obs}}{1\,\rm year}\right)^{-1/2} & \text{(FP-DECIGO)} \\ 1.2\times10^{-19}\left(\dfrac{\rm SNR}{5}\right)\left(\dfrac{T_{\rm obs}}{1\,\rm year}\right)^{-1/2} & \text{(ultimate DECIGO)} \end{cases} \tag{3}$$

2.3 Anisotropic case

GWBs may exhibit anisotropic components in the sky distribution. This seems quite natural because the GWB of astrophysical origin can trace the spatial distribution of luminous galaxies, which gives a strong clustering pattern on small angular scales. Further, the primordial GWB generated during the inflation may also give an anisotropic component, like the CMB. Here we briefly discuss the feasibility to detect dipole moment of GWB. Assuming that the CMB rest frame and the isotropic GWB rest frame are identical, we can estimate a possible anisotropy induced by our proper motion.

Assuming a flat spectrum of $\Omega_{\rm gw}$ in the observational band, our estimates of SNR to detect the dipole moment are

$$({\rm SNR})_1 = 5\left(\frac{T_{\rm obs}}{1\,\rm year}\right)^{1/2} \times \begin{cases} \dfrac{h^2\Omega_{\rm gw}}{1.2\times10^{-12}} & \text{(TDI-DECIGO/BBO)} \\ \dfrac{h^2\Omega_{\rm gw}}{2.0\times10^{-10}} & \text{(FP-DECIGO)} \\ \dfrac{h^2\Omega_{\rm gw}}{1.6\times10^{-16}} & \text{(Ultimate DECIGO)} \end{cases} \tag{4}$$

and

$$(\mathrm{SNR})_2 = 5\left(\frac{T_{\mathrm{obs}}}{1\,\mathrm{year}}\right)^{1/2} \times \begin{cases} \dfrac{h^2\Omega_{\mathrm{gw}}}{5.3\times10^{-12}} & \text{(TDI-DECIGO/BBO)} \\ \dfrac{h^2\Omega_{\mathrm{gw}}}{8.3\times10^{-10}} & \text{(FP-DECIGO)} \\ \dfrac{h^2\Omega_{\mathrm{gw}}}{6.7\times10^{-16}} & \text{(Ultimate DECIGO)} \end{cases} \tag{5}$$

It is thus challenging problem to test observationally whether the CMB rest frame and the GWB rest frame are identical. If the amplitude of isotopic GWB is larger than the values listed above, we could observe the induced dipole moment of GWB and tackle the problem. We note that at the frequency below 0.2 Hz, cosmological population of binaries constitutes the GWB with amplitude $\Omega_{\mathrm{gw}} \sim 10^{-11}$. Therefore, the induced dipole moment of the astrophysical foreground would be detectable.

3 Summary

We are currently in the early stage to make a conceptual design of next-generation space interferometers. The planned future missions will be dedicated to detect the stochastic GWB of cosmological origin. In this paper, we have discussed the detection of such GWB via correlation analysis and studied prospects for direct measurement of both isotropic and anisotropic components of GWBs by future missions. For this purpose, we have presented the general expressions for signal-to-noise ratio in Ref.[3].

Based on this formalism, we have demonstrated the feasibility of proposed future missions to detect the GWB produced during the inflation. The space interferometers, like TDI-DECIGO/BBO, which form a star-like configuration of spacecrafts will probe GWB of $h^2\Omega_{\mathrm{gw}} \lesssim 10^{-18}$, which is almost comparable to the sensitivities expected for future experiments of CMB polarization. However, there might possibly exist several astrophysical foregrounds in the observed frequency band, which act as a disturbance of detecting the primordial GWB. We have examined the effect of foreground sources by introducing the cutoff frequency and found that TDI-DECIGO/BBO is quite sensitive to the low-frequency cutoff, while the sensitivity of FP-DECIGO to the primordial GWB almost remains unchanged, resulting in the detection level $h^2\Omega_{\mathrm{gw}} \sim 10^{-16}$. Although there still remain some problems concerning the point-source subtraction, the result indicates that FP-DECIGO is a potentially suited design for detecting the primordial GWB.

In addition to the delectability of isotropic GWBs, we have investigated the directional sensitivity of next-generation space interferometer to the anisotropic GWB. As a demonstration, the dipole anisotropy induced by proper motion of local observer was considered. For cross-correlation signals extracted from the star-like spacecraft configuration, the interferometers are more sensitive to the even modes ($\ell = 0, 2, 4$) than the odd modes ($\ell = 1, 3, 5$) as anticipated from Ref. [2]. Accordingly, the detection of dipole anisotropy would be possible only when the isotropic component is $h^2\Omega_{\mathrm{gw}} \gtrsim 10^{-11}$. Hence, although very interesting, it would be hard to probe whether the CMB rest frame and a GWB rest frame are both identical or not.

References

[1] Seiji Kawamura et al. The japanese space gravitational wave antenna - decigo. *Amaldi 6 Conference, Japan*, 2005.

[2] Hideaki Kudoh and Atsushi Taruya. Probing anisotropies of gravitational-wave backgrounds with a space-based interferometer: Geometric properties of antenna patterns and their angular power. *Phys. Rev.*, D71:024025, 2005.

[3] Hideaki Kudoh, Atsushi Taruya, Takashi Hiramatsu, and Yoshiaki Himemoto. Detecting a gravitational-wave background with next- generation space interferometers. 2005.

Detecting a stochastic background of gravitational waves in presence of non-Gaussian Noise

Yoshiaki Himemoto[1], Atsushi Taruya[2], Hideaki Kudoh[3] and Takashi Hiramatsu[4]

[1,3,4] *Department of Physics, The University of Tokyo, Tokyo 113-0033, Japan*
[2] *Research Center for the Early Universe (RESCEU), School of Science, The University of Tokyo, Tokyo 113-0033, Japan*

Abstract

We discuss the detection of stochastic background of gravitational waves in presence of non-Gaussian noise. In this paper we apply two-component Gaussian noise as non-Gaussian noise model. Then using the generalized cross correlation (GCC) statistic that reduces to the standard cross correlation statistic (SCC) in which the probability distribution function of the detector noise behaves as Gaussian, we analytically and numerically show that the GCC performs better than the SCC in terms of the false alarm versus false dismissal curves and the minimum detectable gravitational signal amplitude.

1 Introduction

We expect that a stochastic background of gravitational waves exists in our universe. A stochastic background of gravitational waves can be produced by cosmological and astrophysical events [1]. Especially if we could detect a stochastic background of cosmological origin, we may observe the very early universe directly. Therefore it is very important and interesting to develop the detection methods for a stochastic background of gravitational waves.

Generally gravitational wave detectors have to search for very weak signal in detector noise. In such a situation we have no practical way to discriminate between detector noise and a stochastic background of gravitational waves using a single gravitational detector. Then in order to search for a stochastic background we use the cross-correlation statistic of the outputs at the different detector [2].

Most of the data analysis of a stochastic background of gravitational waves have been studied under the assumption that the detector noise is Gaussian. However the almost gravitational wave detectors do not have the pure Gaussian noise. In Ref.[3] the standard cross-correlation (SCC) method has been extended to deal with the more realistic detector noise efficiently. This modified statistic is called by the generalized cross-correlation statistic (GCC). In this paper considering the output data including the non-Gaussian noise, we analytically and numerically discuss the performance and the validity of GCC compared to SCC.

2 Optimal Detection Statistics in presence of non-Gaussian Noise

In a single detector, we can not extract a stochastic background of gravitational waves from the observational data including detector noise. Therefore we consider two gravitational wave detectors to use the cross-correlation analysis and to search for a common signal between their detectors. We denote the output of each detector by s_i^k, with

$$s_i^k = h_i^k + n_i^k, \tag{1}$$

where $i = 1, 2$ labels the detector, and $k = 1, ..., N$ is time index. Here h_i^k is a gravitational signal and n_i^k is the detector noise. $N \times 2$ output matrix S is made up of these outputs. Considering that the

[1] E-mail:himemoto@utap.phys.s.u-tokyo.ac.jp
[2] E-mail:ataruya@phys.s.u-tokyo.ac.jp
[3] E-mail:kudoh@utap.phys.s.u-tokyo.ac.jp
[4] E-mail:hiramatsu@utap.phys.s.u-tokyo.ac.jp

gravitational signals originating from a stochastic background are very weak, we assume that the signal amplitude $|h_i^k| \equiv \epsilon$ is very small in this paper.

To judge whether a gravitational signal is detected or not, one uses a detection statistic $\Lambda = \Lambda(\mathcal{S})$. When Λ exceeds a threshold Λ_*, one says that a signal is detected and not detected otherwise. Λ, which is made up random variables $\mathcal{S}$, is also a random variable, so that we unfortunately have the two types of the error related to the detection criterion Λ_*. One is the probability that we fail to detect a signal which in fact is present, we call it the false dismissal probability $P_{\rm FD}(\Lambda_*)$. Another is the probability that we assert to have detected a signal which in fact is absent, we call it the false alarm probability $P_{\rm FA}(\Lambda_*)$. We intuitively recognize that the optimal detection statistic should be determined by minimizing these error probability. Neyman and Pearson showed that the likelihood ratio is the optimal decision statistic which minimizes $P_{\rm FD}$ for any $P_{\rm FA}$. The likelihood ratio is defined by

$$\Lambda = \frac{p(\mathcal{S}|\epsilon)}{p(\mathcal{S}|0)}. \tag{2}$$

Here $p(\mathcal{S}|\epsilon)$ is the probability distribution function (PDF) of the observational data $\mathcal{S}$ with ϵ. As mentioned above, setting that ϵ is much smaller than the detector noise amplitude, Λ is expanded respect to ϵ around $\epsilon = 0$ as

$$\Lambda = 1 + \epsilon\Lambda^{(1)} + \epsilon^2\Lambda^{(2)} + O(\epsilon^3). \tag{3}$$

If $\Lambda^{(1)}$ becomes zero, then $\Lambda^{(2)}$ is the optimal decision statistic. This statistics are called ***locally optimal statistics*** in [3].

Under some assumptions, we consider the locally optimal statistics for the stochastic background of gravitational waves. For simplicity, we assume that the two detectors are coincident and co-aligned. Furthermore we assume that the statistical noise distribution behaves as white and stationary. According to (3), the locally optimal statistic related to cross correlated statistic is given by

$$\Lambda_{\rm GCC} \equiv \frac{1}{N}\sum_{k=1}^{N} f_1'(s_1^k)\, f_2'(s_2^k). \tag{4}$$

Here we introduced an arbitrary function $f_i(n_i^k)$ to express non -Gaussian distribution. If we set that $f_i = x^2/2 + \log(2\pi)/2$, Eq.(4) reduces to the standard cross-correlation statistic (**SCC**):

$$\Lambda_{\rm SCC} \equiv \frac{1}{N}\sum_{k=1}^{N} s_1^k s_2^k. \tag{5}$$

Hence we call Eq.(4) the generalized cross-correlation statistic (**GCC**).

3 Performance Comparison between GCC and SCC

In this section we compare the performances of GCC and SCC for Gaussian signal in presence of non-Gaussian noise. Here we apply the two-component Gaussian noise model given by

$$p_{n,i}(x) \;=\; e^{-f_i(x)} = \frac{(1-P_i)}{\sqrt{2\pi}\sigma_i} e^{-x^2/2\sigma_i^2} + \frac{P_i}{\sqrt{2\pi}\bar{\sigma}_i} e^{-x^2/2\bar{\sigma}_i^2}, \tag{6}$$

to non-Gaussian noise [3]. where $0 < \sigma_i < \bar{\sigma}_i$. P_i is the probability which deviates from the main Gaussian noise characterized by the variance σ_1. We call it the tail rate. On the other hands, we assume that the gravitational signal is given by Gaussian with zero mean and the signal amplitude ϵ.

Our main purpose is the comparison of the performance of GCC and SCC by using the probability of false dismissal (PFD:$P_{\rm FD}$) versus the probability of false alarm (PFA:$P_{\rm FA}$) curves. If we could calculate the mean and variance for any detection statistic, using the central limit theorem in the large N limit, we can obtain the PFA-PFD relation given by

$$P_{\rm FD}(P_{FA}, \Lambda) = 1 - \frac{1}{2}{\rm erfc}\left[\left\{\sqrt{2}{\rm erfc}^{-1}[2P_{\rm FA}] - \rho + \frac{\langle\Lambda^{(0)}\rangle}{\Delta\Lambda^{(0)}}\right\}\frac{\Delta\rho}{\sqrt{2}}\right], \tag{7}$$

where ρ and $\Delta\rho$ are given by

$$\rho = \frac{\langle \Lambda^{(1)} \rangle}{\Delta\Lambda^{(0)}} \quad , \quad \Delta\rho = \frac{\Delta\Lambda^{(0)}}{\Delta\Lambda^{(1)}}. \tag{8}$$

The superscript (0) and (1) means that signal is absent and present respectively. We find that ρ means effectively the signal to noise ratio. Therefore the larger ρ is, the smaller $P_{\rm FD}$ is for any $P_{\rm FA}$.

4 Results

In order to evaluate the PFA-PFD curve analytically, we have to obtain the concrete form of the mean and variance for the detection statistic. However it is very difficult to estimate the mean and variance for GCC (4) in the two-component Gaussian model (6) without an approximation. Considering the behaviour that $f_i'(x) \approx x/\sigma_i^2$ for $|x|$ small compared to σ_i and $f_i'(x) \approx x/\bar{\sigma}_i^2$ for large $|x|$, we can approximately obtain the analytical PFA-PFD curve by using the *two-step* approximation that means introducing the critical value that ends x/σ_i^2 and starts $x/\bar{\sigma}_i^2$ as the decision statistic. Figure.1 shows some analytic PFA-PFD

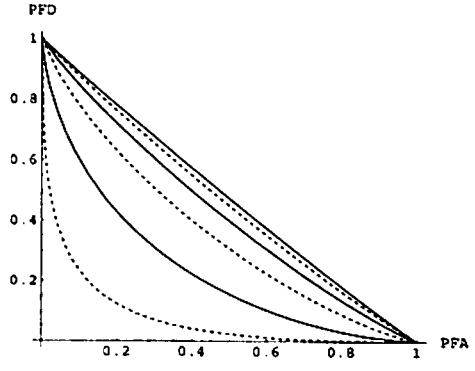

Figure 1: Sample analytic PFA-PFD curves with various signal amplitude for $\Lambda_{\rm GCC}$(dashed) and $\Lambda_{\rm SCC}$(solid) given by Eq.(7) with two-step approximation.

curves with various signal amplitude. We can confirm that the GCC of the dashed curves performs better than the SCC for each signal amplitude. Here for simplicity we assumed $\sigma_1 = \sigma_2$, $\bar{\sigma}_1 = \bar{\sigma}_2$ and $P_1 = P_2$ for the reminder of this paper.

Next we numerically investigate the performance of the GCC compared to the SCC for the various parameters P_i and $\bar{\sigma}_i/\sigma_i \equiv \Sigma$ related to the non-Gaussian character.

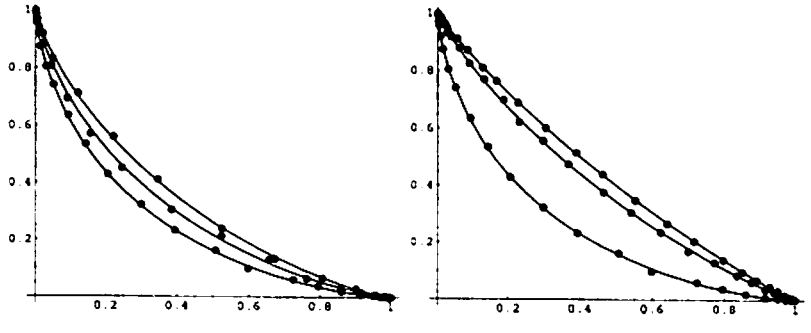

Figure 2: Simulation results and analytic PFA-PFD curves with various tail rate for GCC (left) and SCC (right).

In Figure.2 we investigated the dependence of the tail rate P_1 of PFA-PFD curves. for fixed $\bar{\sigma}_1/\sigma_1 = 4$, $\epsilon = 0.1$ and $N = 10000$. The dots in this figure are the numerical results of PFA-PFD curves. The lines are the analytical curves given by Eq.(7) with two-step approximation. As expected we find that SCC performs the worse than GCC as the tail rate P_1 becomes large.

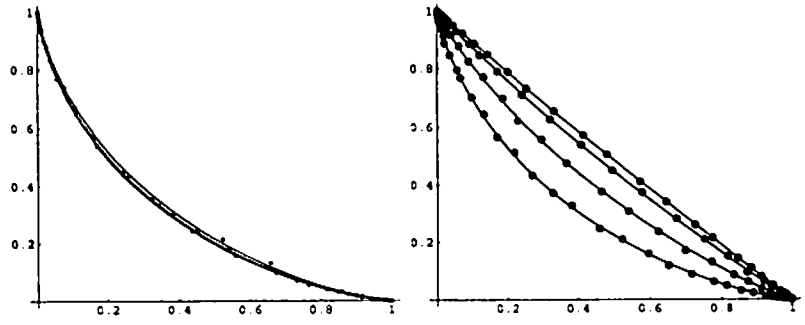

Figure 3: Analytic PFA-PFD curves and simulation results with various tail variance for GCC and SCC.

In Figure.3 we investigated the dependence of the variance ratio of PFA-PFD curves. The figure shows that GCC is insensitive to the variance ratio. Therefore we find that GCC performs much better than SCC as the tail variance becomes large.

Lastly we discuss the comparison between GCC and SCC in terms of the minimum signal amplitude $\epsilon_{\rm det}$. $\epsilon_{\rm det}$ is determined by choosing thresholds $P_{\rm FA}$ and $P_{\rm FD}$. Figure.4 shows the numerically found the $\epsilon_{\rm det}$ that satisfies $P_{\rm FA} = P_{\rm FD} = 0.1$ for the various tail variance. The lower plots are the $\epsilon_{\rm det}$ for GCC.

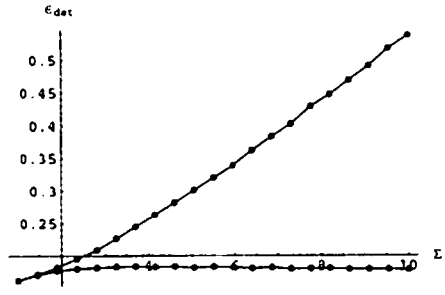

Figure 4: Minimum detectable signal amplitude with the various tail rate for GCC(lower) and SCC(upper). Σ means the variance ratio: $\bar{\sigma}_1/\sigma_1$.

The horizontal axis of Figure.4 means the variance ratio. This Figure shows that the minimum detectable signal amplitude for GCC is insensitive to the value of the variance ratio. This result is equivalent to Figure.3.

To summarize, using the analytical and numerical approach for PFA-PFD relation, we confirmed that GCC performs better than SCC in presence of non-Gaussian noise. We believe that this strategy is useful for the future plan of the search for a stochastic background of gravitational wave.

References

[1] M. Maggiore Phys. Rept. **331**, 283 (2000)

[2] B. Allen and J.D. Romano Phys. Rev. D **59**, 102001 (1999)

[3] B. Allen, J.D.E. Creighton, E.E. Flanagan and J.D. Romano Phys. Rev. D **65**, 122002 (2002)

Gravitational Self-force for Low Multipole Modes
— Monopole and dipole contributions —

Hiroyuki Nakano[1], Norichika Sago[2], Wataru Hikida[3], Misao Sasaki[4]

[1] *Department of Mathematics and Physics, Graduate School of Science, Osaka City University, Osaka 558-8585, Japan*
[2] *Department of Earth and Space Science, Graduate School of Science, Osaka University, Osaka 560-0043, Japan*
[3,4] *Yukawa Institute for Theoretical Physics, Kyoto University,Kyoto 606-8502, Japan*

Abstract

We discuss the gravitational self-force on a particle in the Schwarzschild spacetime. When we consider a point particle, the full self-force diverges at the location of the particle. Therefore, we need some regularization.

1 Introduction

The observation of gravitational waves is absolutely a new window to observe our universe. We also expect that the observation of gravitational waves provides a direct experimental test of general relativity. LISA will detect the gravitational waves from a solar-mass compact object orbiting a supermassive black hole.

For the above binary system, we use the black hole perturbation (BHP) approach, where the compact object is approximated by a point particle orbiting a Kerr black hole, and evaluate the correction to the equation of motion of a particle on the background geometry, i.e., the reaction force acting locally on the orbit. By this force, the orbit deviates from the geodesic, because the spacetime is perturbed by the particle. We can interpret this deviation as the effect of the self-force of the particle on itself. Since it is essential to take account of this deviation to predict the orbital evolution, we have to derive the equation of motion that includes the self-force. The gravitational self-force is, however, not easily obtainable.

The full metric perturbation diverges at the location of the particle, hence so does the self-force. The full metric perturbation can be formally divided into two parts under the Lorenz (L) gauge; the direct part that comes from the perturbation propagating along the light cone of the background spacetime directly from the point particle, and the tail part that arises from the curvature scattering of the perturbation, which exists within the light cone. The (regularized) MiSaTaQuWa self-force is given by the tail part of the metric perturbation which is regular at the location of the particle [1, 2].

Recently, this is reformulated in a more elaborated way by Detweiler and Whiting [3]. They found a slight but important modification, and the full metric perturbation in the L gauge is now decomposed as

$$h^{\rm full,L}_{\mu\nu} = h^{\rm S,L}_{\mu\nu} + h^{\rm R,L}_{\mu\nu}\,, \tag{1}$$

where the S part, $h^{\rm S,L}_{\mu\nu}$, satisfies the same linearized Einstein equations with source under the Lorenz gauge condition as the full metric perturbation, $h^{\rm full,L}_{\mu\nu}$, $\bar{h}^{\rm S,L}_{\mu\nu;\alpha}{}^{;\alpha} + 2R_\mu{}^\alpha{}_\nu{}^\beta \bar{h}^{\rm S,L}_{\alpha\beta} = -16\pi T_{\mu\nu}$, where $\bar{h}_{\alpha\beta} = h_{\alpha\beta} - \frac{1}{2} g_{\alpha\beta} h_\mu{}^\mu$. The new tail part, called the R part, $h^{\rm R,L}_{\mu\nu}$, is then a homogeneous solution. And, they showed that the regularized self-force is given by the R part of the metric perturbation. Namely, we have

$$\frac{d^2 z^\alpha}{d\tau^2} + \Gamma^\alpha_{\mu\nu} \frac{dz^\mu}{d\tau}\frac{dz^\nu}{d\tau} = \frac{1}{\mu} F^\alpha[h^{\rm R,L}]\,, \tag{2}$$

where $z^\alpha(\tau)$ is an orbit of the particle parametrized by the background proper time, and $F_\alpha[h] = -\mu(\delta_\alpha{}^\beta + u_\alpha u^\beta)(\bar{h}_{\beta\gamma;\delta} - g_{\beta\gamma}\bar{h}^\epsilon{}_{\epsilon;\delta}/2 - \bar{h}_{\gamma\delta;\beta}/2 + g_{\gamma\delta}\bar{h}^\epsilon{}_{\epsilon;\beta}/4)u^\gamma u^\delta$, where $u^\alpha = dz^\alpha/d\tau$.

[1] E-mail:denden@sci.osaka-cu.ac.jp
[2] E-mail:sago@vega.ess.sci.osaka-u.ac.jp
[3] E-mail:hikida@yukawa.kyoto-u.ac.jp
[4] E-mail:misao@yukawa.kyoto-u.ac.jp

Since the R part is a solution of the Einstein equations, it is perfectly legitimate to consider a gauge transformation of it to another gauge. Therefore we can define the R part in an arbitrary gauge by a gauge transformation of this part from the L gauge. We thus have an unambiguous definition of the self-force in an arbitrary gauge. Here, we consider the self-force in the Regge-Wheeler (RW) gauge, in which we can obtain the full metric perturbation on the Schwarzschild spacetime [4, 5].

2 Regular gauge transformation to the Regge-Wheeler gauge

In this paper, we consider the Schwarzschild background and use the usual Schwarzschild coordinates,

$$ds^2 = -\left(1-\frac{2M}{r}\right)dt^2+\left(1-\frac{2M}{r}\right)^{-1}dr^2+r^2\left(d\theta^2+\sin^2\theta d\phi^2\right), \tag{3}$$

In this background spacetime, the full metric perturbation of a black hole geometry can be calculated by the Regge-Wheeler-Zerilli formalism in the RW gauge [4, 5]. So, we want to derive the regularized gravitational self-force under the RW gauge, and consider the regularization analytically because to subtract the singular pieces is very delicate problem.

Here, we consider the gauge transformation of the R part of the metric perturbation from the L gauge to the RW gauge [6], $x^{\rm L}_\mu \to x^{\rm RW}_\mu = x^{\rm L}_\mu + \xi^{\rm L\to RW}_\mu[h^{\rm R,L}_{\alpha\beta}]$, where $\xi^{\rm L\to RW}_\mu$ is the generator of the gauge transformation. Using this gauge transformation, the self-force in the RW gauge is given by

$$F^{\rm RW}_\alpha(\tau) = \lim_{x\to z(\tau)} F_\alpha\left[h^{\rm R,RW}\right] = \lim_{x\to z(\tau)}\left(F_\alpha\left[h^{\rm full,RW}\right](x) - F_\alpha\left[h^{\rm S,L} - 2\nabla\xi^{\rm L\to RW}\left[h^{\rm S,L}\right]\right](x)\right). \tag{4}$$

So, if we obtain the gauge transformation for the S part, the regularized self-force can be derived.

3 Regularization under the Regge-Wheeler gauge

First, we focus on the S part of the self-force under the L gauge. When the S part is expanded in terms of the spherical harmonics, the S force is known to take the form called as the standard form;

$$\lim_{x\to z_0} F^S_{\alpha\ell} = A_\alpha L + B_\alpha + D_{\alpha\ell}, \tag{5}$$

where $F^S_{\alpha\ell}$ is the ℓ-mode of the S force, $L=\ell+1/2$, and A_α and B_α are independent of L. When summed over ℓ, the A-term gives rise to a quadratic divergence and the B-term diverges linearly, and

$$D_{\alpha\ell} = \frac{d_\alpha}{L^2-1} + \frac{e_\alpha}{(L^2-1)(L^2-4)} + \frac{f_{\alpha\ell}}{(L^2-1)(L^2-4)(L^2-9)} + \cdots. \tag{6}$$

Then the summation of D^μ_ℓ over ℓ (from $\ell=0$ to ∞) vanishes. So, when the S force has the standard form, we may know only the A and B-terms.

Next, we consider the S force under the RW gauge. We found that the standard form recovers under the RW gauge [7]. It is possible to use the same regularization procedure as that of the L gauge;

$$\begin{aligned} F^\mu_{\rm R,RW} &= \sum_{\ell\geq 2}\left(F^\mu_{\rm full,RW}\Big|_\ell - F^\mu_{\rm S,RW}\Big|_\ell\right) = \sum_{\ell\geq 2}\left(F^\mu_{\rm full,RW}\Big|_\ell - A^\mu_{\rm RW}L - B^\mu_{\rm RW} - D^\mu_{\ell,\rm RW}\right) \\ &= \sum_{\ell\geq 2}\left(F^\mu_{\rm full,RW}\Big|_\ell - A^\mu_{\rm RW}L - B^\mu_{\rm RW}\right) + \sum_{\ell=0,1}\left(F^\mu_{\rm full,RW}\Big|_\ell - A^\mu_{\rm RW}L - B^\mu_{\rm RW}\right). \end{aligned} \tag{7}$$

Here, it is noted that, the $A^\mu_{\rm RW}$, $B^\mu_{\rm RW}$ and $D^\mu_{\ell,\rm RW}$ defined for the $\ell\geq 2$ modes can not be used for the $\ell=0$ and 1 modes. This is because there are some tensor harmonics that do not exist for $\ell=0$ and/or $\ell=1$. The S force for the $\ell\geq 2$ modes is derived from the full force by using the new analytic regularization [8] and the $\ell=0$ and 1 modes are discussed separately (See Ref. [9]).

Here, we show the regularized self-force for $\ell\geq 2$ modes in the case of circular orbit.

$$F^t_{\rm R,RW}(\ell\geq 2) = -\frac{32\,\mu^2\,M^3}{5\,r_0^5},\ F^r_{\rm R,RW}(\ell\geq 2) = -\frac{3\,\mu^2\,M}{4\,r_0^3}\left(1-\frac{97\,M}{16\,r_0}+\frac{(164\,\pi^2-739)\,M^2}{192\,r_0^2}\right). \tag{8}$$

This calculation can be done for general orbits.

4 Low multipole modes

4.1 $\ell = 0$ and 1 odd modes

The calculation of the $\ell = 0$ and 1 odd parity modes are straightforward. In order to fix the gauge completely, we choose the L gauge (which satisfies the "RW" gauge) with the retarded boundary condition for the full metric perturbation [9, 10]. Here, we show only the result of the R force.

$$F^r_{\rm R,L}|_{\ell=0} = \frac{\mu^2}{r_0^2}\left(-\frac{9}{8}\frac{M}{r_0} - \frac{707}{128}\frac{M^2}{r_0^2} - \frac{30905}{1536}\frac{M^3}{r_0^3}\right), \tag{9}$$

$$F^r_{\rm R,L}|_{\ell=1,\,\rm odd} = \frac{\mu^2}{r_0^2}\left(\frac{3}{8}\frac{M^2}{r_0^2} + \frac{123}{64}\frac{M^3}{r_0^3}\right). \tag{10}$$

4.2 $\ell = 1$ even mode

For the $\ell = 1$ even parity mode, it is also necessary to solve the perturbation equations in the L gauge with the retarded boundary condition. But, because the perturbation equations is complicated, coupled hyperbolic equations in the L gauge, we need the numerical calculation. Here, we give up fixing the gauge unambiguously, but solve the perturbation equations in the "RW" gauge, imposing a gauge condition by hand. This is the same procedure as our previous work [9].

Zerilli has chosen $K = 0$ and $h_0^{(e)} = h_1^{(e)} = 0$ (Zerilli (Z) gauge, which satisfy the RW gauge condition), where H_0, H_1, H_2, $h_0^{(e)}$, $h_1^{(e)}$, K and G are the coefficients of the even tensor harmonics. Please see [5]. The full metric perturbation in the Z gauge are given by

$$H^{\rm full,Z}_{21m}(t,r) \sim O(r^{-2}),\ H^{\rm full,Z}_{11m}(t,r) \sim O(r^{-1}),\ H^{\rm full,Z}_{01m}(t,r) \sim O(r^{1}), \tag{11}$$

where $m = \pm 1$ and we have shown only the asymptotic behavior at $r \to \infty$. The regularized self-force is

$$F^r_{\rm R,RW}|_{\ell=1,\,\rm even} = \frac{\mu^2}{r_0^2}\left(-1 - \frac{21}{8}\frac{M}{r_0} - \frac{739}{128}\frac{M^2}{r_0^2} - \frac{9723}{512}\frac{M^3}{r_0^3}\right). \tag{12}$$

The Newtonian term in the above result is not same as usual derivation. This is because the metric perturbation does not satisfy an asymptotic-flat (AF) gauge condition.

Next, in order to understand this regularized self-force, we discuss a pure gauge transformation. Here, the AF gauge condition, i.e., $h_0^{(e)} = 0$ and $H_0 = H_2$ is considered as an appropriate gauge for the full metric perturbation. The asymptotic behavior of the full metric perturbation is obtained as

$$\begin{aligned} &H^{\rm full,AF}_{01m}(t,r) = H^{\rm full,AF}_{21m}(t,r) \sim O(r^{-3}),\ H^{\rm full,AF}_{11m}(t,r) \sim O(r^{-2}),\ K^{\rm full,AF}_{1m}(t,r) \sim O(r^{-3}), \\ &h^{(e)\rm full,AF}_{01m}(t,r) = 0,\ h^{(e)\rm full,AF}_{11m}(t,r) \sim O(r^{-2}), \end{aligned} \tag{13}$$

where $m = \pm 1$. And, the regularized self-force for $\ell = 1$ even parity mode becomes

$$F^r_{\rm R,AF}|_{\ell=1,\,\rm even} = \frac{\mu^2}{{r_0}^2}\left(2 - \frac{9}{8}\frac{M}{r_0} - \frac{4243}{128}\frac{M^2}{{r_0}^2} + \frac{20325}{512}\frac{M^3}{{r_0}^3}\right). \tag{14}$$

The Newtonian force recovers and this r is the radius from the center of mass of the system.

5 Discussion

We consider the consistency check with the standard post-Newtonian (SPN) method. Here, we focus on the perturbed energy and angular frequency, which are physically observable in the SPN and derived from the conservative part of the self-force in the BHP. First, we can obtain the perturbed energy and angular momentum as

$$E = \frac{1-2M/r}{\sqrt{1-3M/r}}\left(1 - \frac{r}{2}\left(1-\frac{2M}{r}\right)^{-1}F^r\right),\ L = \sqrt{\frac{Mr}{1-3M/r}}\left(1 - \frac{r^2}{2M}F^r\right), \tag{15}$$

for circular orbit. And, the angular frequency is defined by

$$\omega = \frac{d\phi}{dt} = \frac{L/r^2}{(1-2M/r)^{-1}E} = \sqrt{\frac{M}{r^3}}\left(1 - \frac{r^2(1-3M/r)}{2M(1-2M/r)}F^r\right). \tag{16}$$

For the gauge transformation, $x^\mu \to \tilde{x}^\mu = x^\mu + \xi^\mu$; $\xi^\mu \sim R(r)e^{-im(\sqrt{M/r^3}\,t-\phi)}$, which does not contribute the dissipative force, this frequency changes as

$$\tilde{\omega} = \sqrt{\frac{M}{r^3}}\left(1 - \frac{r^2(1-3M/r)}{2M(1-2M/r)}F^r + \frac{3}{2r}\xi^r\right). \tag{17}$$

Anyway, by using the above E and ω, let's compare with those of the SPN for the Newtonian order. We use the self-force (14) in the BHP, which is obtained from the $\ell = 1$ even mode under the AF gauge. Then, the perturbed energy and angular frequency are

$$E = \mu\left(1 - \frac{1}{2}\frac{M}{r} - \frac{\mu}{r}\right), \omega^2 = \frac{M-2\mu}{r^3}. \tag{18}$$

In the following, we ignore the rest mass energy. On the other hand, in the SPN [11],

$$E_{\rm PN} = -\frac{\mu_{\rm PN}M_{\rm PN}}{2r'}, \omega^2_{\rm PN} = \frac{M_{\rm PN}}{r'^3}, \tag{19}$$

where $M_{\rm PN} = m_1 + m_2$, $\mu_{\rm PN} = m_1m_2/(m_1+m_2)$ and r' are the total mass, reduced mass and distance between two particles with mass m_1 and m_2, respectively. When, we assume $\omega = \omega_{\rm PN}$, and consider r as the radius from the center of mass, i.e., $r' = (1+\mu/M)r$ or $\xi^r = (\mu/M)r$ as the gauge difference, we must define the mass as

$$M_{\rm PN} = M + \mu, \mu_{\rm PN} = \mu\left(1 + \frac{2\mu}{M}\right). \tag{20}$$

But, we can not obtain the consistent result for the higher PN order. This discrepancy may be solved by the second order calculation in the BHP.

Acknowledgements

We would like to thank S. Mukohyama, K. Nakamura and H. Tagoshi for useful discussions. HN is supported by the JSPS Research Fellowships for Young Scientists, No. 5919.

References

[1] Y. Mino, M. Sasaki and T. Tanaka, Phys. Rev. D **55**, 3457 (1997).

[2] T. C. Quinn and R. M. Wald, Phys. Rev. D **56**, 3381 (1997); Phys. Rev. D **60**, 064009 (1999).

[3] S. Detweiler and B. F. Whiting, Phys. Rev. D **67**, 024025 (2003).

[4] T. Regge and J. A. Wheeler Phys. Rev. **108**, 1063 (1957).

[5] F. J. Zerilli, Phys. Rev. D **2**, 2141 (1970).

[6] This idea was originally due to Y. Mino (private communication).

[7] H. Nakano, N. Sago, W. Hikida, M. Sasaki and H. Tagoshi, in preparation.

[8] W. Hikida, S. Jhingan, H. Nakano, N. Sago, M. Sasaki and T. Tanaka, Prog. Theor. Phys. **111** (2004) 821.

[9] H. Nakano, N. Sago and M. Sasaki, Phys. Rev. D **68**, 124003 (2003).

[10] S. Detweiler and E. Poisson, Phys. Rev. D **69**, 084019 (2004).

[11] L. Blanchet, Living Rev. Rel. **5**, 3 (2002).

The Accelerating Universe and Spin-interacting Fields in Einstein-Cartan Theory

Tomoki Watanabe[1]

Advanced Research Institute for Science and Engineering, Waseda University, Tokyo 169-8555, Japan

Abstract

We present a cosmological model in which the inflationary expansion of the universe can be caused by a spin-interaction between two Dirac fields, which naturally arises in the Einstein-Cartan theory. We have found that, although a single Dirac field cannot be a source of the acceleration, its interaction with another Dirac field can provide negative pressure at the classical level. The acceleration condition is explicitly established, and the spectral index as well as its scale-dependence are also discussed.

1 Introduction

Nowadays, it has widely been believed that inflation is caused by a slow-rolling inflaton (spin-0 boson) which naturally predicts $n_s = 1+O(\epsilon)$ being in excellent agreement with recent observations[1]. However, it remains a task to identify the inflaton with a certain particle in promissing particle-physics models theoritically and experimentally. Then a question arises: could other fields drive inflation?

In this paper we show Dirac fields can be a source of inflation within the Einstein-Cartan theory, and try to prove compatibility of the model with the observations by calculating the power spectrum of density fluctuations of the Dirac fields and its scale-dependence.

2 Einstein-Cartan theory

Among natural extentions of General Relativity is the Einstein-Cartan theory[2, 3], in which the background spacetime is described by the Riemann-Cartan geometry characterized by curvature and torsion, where $\nabla_\rho g_{\mu\nu} = 0$ is assumed. The two field equations in this theory relate the curvature to energy-momentum as well as the torsion to spin:

$$G_\mu{}^a \equiv R_\mu{}^a - \frac{1}{2}e_\mu{}^a R = 8\pi G\, T_\mu{}^a, \tag{1}$$

$$C^\mu{}_{ab} + 2e^\mu{}_{[a}C^\nu{}_{b]\nu} = -8\pi G i \frac{\partial \mathcal{L}_{\rm m}}{\partial D_\mu \phi^A}(S_{ab})^A{}_B \phi^B \equiv -16\pi G S^\mu{}_{ab}, \tag{2}$$

where $C^\rho{}_{\mu\nu} \equiv 2\Gamma^\rho_{[\mu\nu]}$ is the torsion tensor, D_μ is the Lorentz covariant derivative with the Lorentz generator S_{ab}, $e^\mu{}_a$ is a tetrad having both world indices μ and Lorentz indices a.

The Eq.(2) states that the torsion is equivalent to the spin density $S^\mu{}_{ab}$. Therefore, by substituting the spin for torsion in Eq.(1), one obtains the combined equation:

$$\tilde{G}_{\mu\nu} = 8\pi G\left(\tilde{T}_{(\mu\nu)} + T^{(\rm spin)}_{\mu\nu}\right),$$

where $\tilde{G}_{\mu\nu}$ is the Einstein tensor composed of the Riemann curvature and then $T^{(\rm spin)}_{\mu\nu}$ gains a position as the "spin correction" to the usual energy-momentum tensor $\tilde{T}_{(\mu\nu)}$. The explicit form of this tensor is, including the coupling of matter to torsion $T^{(\rm t)}_{\mu\nu}$, given by

$$\begin{aligned} T^{(\rm spin)}_{\mu\nu} &= T^{(\rm t)}_{(\mu\nu)} + 2(\nabla_\rho - 8\pi G S^\sigma{}_{\rho\sigma})S_{(\mu\nu)}{}^\rho \\ &-8\pi G\Big[4S^{(\rho\sigma)}{}_\mu S_{(\rho\sigma)\nu} - S_\mu{}^{\rho\sigma}S_{\nu\rho\sigma} - 2S^\rho{}_{\mu\rho}S^\sigma{}_{\nu\sigma} - \frac{g_{\mu\nu}}{2}\left(4S^{(\rho\sigma)\lambda}S_{(\rho\sigma)\lambda} - S^{\rho\sigma\lambda}S_{\rho\sigma\lambda} - 2S^{\sigma\rho}{}_\sigma S^\lambda{}_{\rho\lambda}\right)\Big]. \end{aligned} \tag{3}$$

[1] E-mail:tomoki@gravity.phys.waseda.ac.jp

3 Cosmological model

3.1 Background solution

What we are interested in is the cosmological meanings of the spin correction. As a sorce of the spin, we introduce two classical Dirac fields whose Lagrangians are given by

$$\mathcal{L}_\psi = \frac{i}{2}\left[\bar{\psi}\gamma^\mu D_\mu\psi - (\overline{D_\mu\psi})\gamma^\mu\psi\right] - m_1\bar{\psi}\psi, \quad \mathcal{L}_\Psi = \frac{i}{2}\left[\bar{\Psi}\gamma^\mu D_\mu\Psi - (\overline{D_\mu\Psi})\gamma^\mu\Psi\right] - m_2\bar{\Psi}\Psi,$$

into the flat Friedmann universe, where the "FRW tetrad" is simply chosen to $(e_\mu{}^a) = \mathrm{diag}\,(1, a\delta_i{}^{\hat{m}})$.

Assuming $\partial_i\psi = 0$ for consistency with the homogeneous and isotropic spacetime, we obtain the equation of motion (e.g. for ψ)

$$\dot{\psi} + \frac{3}{2}H\psi + im_1\gamma^{\hat{0}}\psi + 3i\pi G\left[(\phi^{\hat{0}} + \Phi^{\hat{0}})\gamma_5 + (\phi^{\hat{m}} + \Phi^{\hat{m}})\gamma_{\hat{0}}\gamma_{\hat{m}}\gamma_5\right]\psi = 0, \tag{4}$$

where $\phi^a \equiv \bar{\psi}\gamma_5\gamma^a\psi$ and $\Phi^a \equiv \bar{\Psi}\gamma_5\gamma^a\Psi$. The self-interaction in Eq.(4) comes from the coupling of the Dirac fields to torsion through the covariant derivative. It should be noted that, for the Dirac field, the spin correction (3) to the energy-momentum takes the diagonal form:

$$T_{\mu\nu}^{(\mathrm{spin})} = \frac{3\pi G}{2}(\phi_a + \Phi_a)(\phi^a + \Phi^a)g_{\mu\nu},$$

which leads to the total energy denstiy and the total pressure including the spin as follows:

$$\rho_{\mathrm{tot}} = m_1\bar{\psi}\psi + m_2\bar{\Psi}\Psi - \frac{3\pi G}{2}(\phi_a + \Phi_a)(\phi^a + \Phi^a), \quad p_{\mathrm{tot}} = -\frac{3\pi G}{2}(\phi_a + \Phi_a)(\phi^a + \Phi^a).$$

Also note that pressure of a single field is inevitably positive because of $\phi_a\phi^a < 0$, which is guaranteed by the Fierz identity. However in the two-field model, if the cross term $\phi_a\Phi^a$ is positive and dominant, then negative pressure can be generated. In what follows, we concentrate our consideration on such solutions.

Now the evolution equations for $a(t)$ are given by

$$\begin{aligned} H^2 &= \frac{8\pi G}{3}\left[m_1\bar{\psi}\psi + m_2\bar{\Psi}\Psi - \frac{3\pi G}{2}(\phi^a + \Phi^a)^2\right], \\ \frac{\ddot{a}}{a} &= -\frac{4\pi G}{3}\left[m_1\bar{\psi}\psi + m_2\bar{\Psi}\Psi - 6\pi G(\phi^a + \Phi^a)^2\right]. \end{aligned}$$

From these equations we find the condition for the acceleration of the universe:

$$1 < 2\cdot\frac{m_1\bar{\psi}\psi + m_2\bar{\Psi}\Psi}{3\pi G(\phi^a + \Phi^a)^2} \equiv F(t) < 4,$$

which demands that the spin-interaction should be comparable to the energy density. Such a situation can be realized on a high energy scale because of the factor G, i.e. the term acceleration here means inflation in the early universe. Moreover the expansion at the situation is just the de Sitter expansion, since, in the energy conservation

$$\frac{d}{dt}\rho_{\mathrm{tot}} = -3H\left[m_1\bar{\psi}\psi + m_2\bar{\Psi}\Psi - 3\pi G(\phi^a + \Phi^a)^2\right],$$

the right-hand side approximately vanishes and therefore ρ_{tot} becomes constant. We show an example of the inflationary solutions in Figs.1 and 2.

3.2 Perturbations

A next task is to examine the consistency of our model with the observations of the spectrum of CMB temperature fluctuations. Although a proper analysis for this purpose should be based on gauge-invariant

perturbation theories where both spacetime and matter fields are perturbed, we will not consider the metric perturbations but only the perturbed field $\delta\psi$ for simplicity[4].

The plane-wave expansion of $\delta\psi$ is given by

$$\delta\psi = \int \frac{d^3k}{(2\pi)^{3/2}} \sum_s \left[u_s(t,k) a_s(k) e^{ik\cdot x} + v_s(t,k) b_s^\dagger(k) e^{-ik\cdot x} \right], \tag{5}$$

where the anticommutation relations $\{a_s(k), a_{s'}^\dagger(k')\} = \{b_s(k), b_{s'}^\dagger(k')\} = \delta_{ss'}\delta^3(k-k')$ are imposed. On the other hand, we employ a characteristic variable for the density perturbation:

$$\zeta \equiv \frac{\delta\rho}{\rho + p},$$

which is defined analogously to the gauge-invariant Bardeen variable $\zeta_B = -\varphi - H\delta\rho/\dot{\rho}$. Then using the Fierz transformation, we have the power spectrum of ζ on comoving scales $1/k$ in terms of Eq.(5):

$$\mathcal{P}(k) = \frac{k^3}{4\pi^2(\rho+p)^2} \sum_s \left[(m_1^2 - \{3\pi G(\phi_a + \Phi_a)\}^2) \bar{\psi}\psi \bar{v}_s v_s \right],$$

where the Fourier component v_s obeys the perturbed equation of motion:

$$\delta\dot{\psi}_k(t) + \frac{3}{2}H(t)\delta\psi_k(t) + im_1\gamma^0\delta\psi_k(t) - i\gamma^0\gamma^{\hat{m}}\frac{k_{\hat{m}}}{a}\delta\psi_k(t) + \text{ spin term } = 0. \tag{6}$$

The general solution of Eq.(6) can be expressed through a factorized form $\delta\psi_k = A(k,t)\delta\psi_{\text{free}}$, where the dynamics of $A(k,t)$ is governed by the interaction term in Eq.(6) and can be solved numerically, whereas $\delta\psi_{\text{free}}$ is the analytic solution without the interaction; during inflation we have

$$\delta\psi_{\text{free}} = a^{-\frac{3}{2}}\sqrt{-k\eta}\frac{e^{-\frac{\pi m_1}{2H}}}{2}\left[\begin{pmatrix} H_\nu^{(1)}(-k\eta)C_1(k) \\ e^{-\frac{\pi m_1}{H}} H_{\nu^*}^{(1)}(-k\eta)\frac{k\cdot\sigma}{k}C_1(k) \end{pmatrix} + \begin{pmatrix} H_\nu^{(2)}(-k\eta)\frac{k\cdot\sigma}{k}C_2(k) \\ -e^{\frac{\pi m_1}{H}} H_{\nu^*}^{(2)}(-k\eta)C_2(k) \end{pmatrix} \right],$$

where η is conformal time, $H_\nu^{(1,2)}$ are the Hankel function with $\nu = 1/2 - im_1/H$ and the constant spinors $C_{1,2}$ are determined according to choice of vacuum states.

We take a standard manner in which the constants are chosen in order that $v_{\text{free}} \propto e^{ik\eta}$ as $\eta \to -\infty$:

$$v_s(\eta,k) = -A(k,t)a^{-\frac{3}{2}}\sqrt{-\pi k\eta}\frac{e^{-\frac{\pi m_1}{2H}}}{2}\begin{pmatrix} H_\nu^{(2)}(-k\eta)\frac{k\cdot\sigma}{k}\omega^s \\ e^{\frac{\pi m_1}{H}} H_{\nu^*}^{(2)}(-k\eta)\omega^s \end{pmatrix}.$$

Thus in the limit $-k\eta \ll 1$ we find

$$\mathcal{P}(k) = -\frac{a^{-3}k^3}{2\pi^3(\rho+p)^2}\left[A(k)^2(m_1^2 - \{3\pi G(\phi_a+\Phi_a)\}^2)\bar{\psi}\psi|\Gamma(\nu)|^2 \sinh\frac{\pi m_1}{H} \right],$$

which leads to the scale-dependent spectral index:

$$n_s(k) = 4 + 2k\frac{A'(k)}{A(k)}.$$

It is worth mentioning that the spectral index without the spin-interaction turns out to be $n_s = 4$[4], which is in strong disagreement with the observations. However, the presence of torsion can solve this problem; we can expect that the extra contribution $kA'(k)/A(k)$ due to the spin reduces the value of n_s to the observed one. We show the numerical plot of $kA'(k)/A(k)$ in Fig.3, which exhibits that $n_s = O(1)$ is reproduced on small k.

4 Summary

We have shown that the spin-interaction, which is peculiar to the Einstein-Cartan theory, between two Dirac fields can drive inflation of the universe and found that the model predicts the scale-dependent spectral index. Our conclusion suggests that, in construction of realistic cosmological models, one might have to consider comprehensive effects of a rich diversity of matter fields on geometry; the wide variety is just what particle-physics or promissing theories beyond it offer.

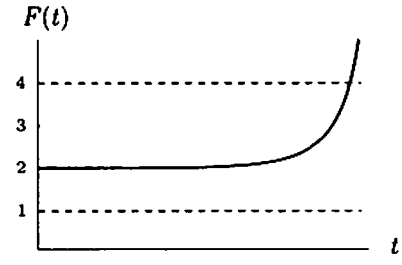

Figure 1: The plot of $F(t)$, the function giving the condition for inflation. Inflation ends at $F(t) = 4$. The masses chosen here are $m_1 \sim m_2 \sim 10^9$GeV. ($m_1 \gg m_2$ is also possible.) The initial values of ψ and Ψ have been chosen to satisfy $\rho_{\rm tot}(t_{\rm in}) \sim (10^{15}{\rm GeV})^4$.

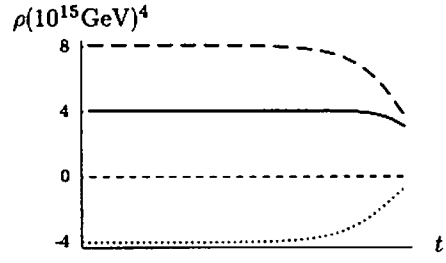

Figure 2: The evolution of the energy density. The solid line represents $\rho_{\rm tot}$, the dashed line and dotted line denote $m_1\bar{\psi}\psi + m_2\bar{\Psi}\Psi$ and $-3\pi G(\phi_a + \Phi_a)^2/2$ respectively. While $F(t) \sim 2$, $\rho_{\rm tot}$ is nearly constant i.e. $H \sim$ const.

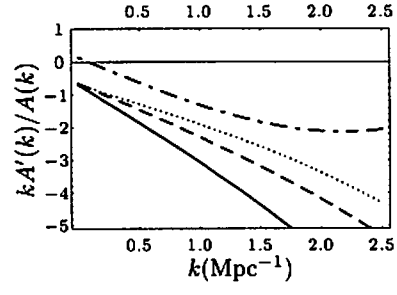

Figure 3: The scale-dependence of $kA'(k)/A(k)$. The dash-dotted, dotted, solid and dashed line are plotted for $m_1 \sim 10^{11}$GeV, 10^{10}GeV, 10^9GeV, and 10^8GeV respectively. Typically on small k, n_s is suppressed and can then take the value $O(1)$.

References

[1] M. Tegmark et.al, Phys. Rev. **D69**, 103501 (2004);U. Seljak et.al, Phys. Rev. **D71**, 103515 (2005).

[2] F. W. Hehl, P. von der Heyde and G. D. Kerlick, Rev. Mod. Phys. **48**, 393 (1976).

[3] D. Puetzfeld, New Astron. Rev. **49**, 59 (2005), and references therein.

[4] C. Armendariz-Picon and P. B. Greene, Gen. Rel. Grav. **35**, 1637 (2003).

Solitonic solutions of five dimensional vacuum Einstein equations generated by the inverse scattering method

Shinya Tomizawa[1], Yoshiyuki Morisawa[2] and Yukinori Yasui[3]

Department of Mathematics and Physics, Graduate School of Science, Osaka City University, 3-3-138 Sugimoto, Sumiyoshi, Osaka 152-8551, Japan

Abstract

We study stationary and axially symmetric two solitonic solutions of five dimensional vacuum Einstein equations by using the inverse scattering method developed by Belinski and Zakharov. In this generation of the solutions, we use five dimensional Minkowski spacetime as a seed. It is shown that if we restrict ourselves to the case of one angular momentum component, the generated solution coincides with a black ring solution with a rotating two sphere which was found by Mishima and Iguchi recently.

1 Introduction

Recently, higher dimensional black holes have much attention since the possibility of higher dimensional black hole production in a linear collider is predicted in TeV gravity [2]. However, it has not been clear what black holes will be formed through the collisions of protons in the linear collider. Though at first glance it seems that we cannot expect to obtain a complete description of real black holes due to the complexity of Einstein equations, essentially their nonlinearity, the uniqueness theorem of higher dimensional black holes would let us know the answer, at least, some information on the final states. However, it is unlikely that in a higher dimensional stationary black hole spacetime there exists the uniqueness theorem in the sense of one in a four dimensional black hole spacetime, which means that the set of the parameters of mass, angular momentum and charge fails to determine a higher dimensional black hole uniquely. In fact, after the discovery of Myers-Perry solution whose horizon is topologically S^3 [3], Emparan and Reall found a five dimensional rotating black ring solution with the horizon homeomorphic to $S^1 \times S^2$ [4]. It has been found that there is a range within which these two solutions have the same mass and angular momentum. This implies the absence of the original uniqueness theorem like that of four dimensional black holes. If one restricts the topology of a horizon to S^3, it has been shown that the only asymptotically flat black hole solution is Myers-Perry solution [5]. In this view, what kind of black hole solutions there can exist in five or higher dimensional spacetimes is an interesting problem, and in order to find such black hole solutions admitted as possible, we have to develop generating-techniques of solutions of higher dimensional Einstein equations.

In four dimensional Einstein gravity, systematic generation-techniques of stationary and axisymmetric solutions have been developed by a lot of authors [6]. Recently, Mishima and Iguchi [7] applied one of these techniques, Castejon-Amenedo-Manko's method [8], to five dimensional vacuum spacetimes and derived the asymptotically flat black ring solution which rotates in the azimuthal direction of two sphere. This solution is generated from five dimensional Minkowski spacetime as a seed. The expression of this solution as a C-metric coordinate was studied by Figueras [9]. As a solitonic generation-technique in four dimensional Einstein gravity, Belinski and Zakharov developed the inverse scattering method [10]. They generated Kerr-NUT solutions as simple two solitonic solutions on the Minkowski background. This technique is also used for the generations of multi-black hole solutions [6]. We would expect that the application of this method to more than four dimensions might lead to the generation of a lot of physical solutions. In fact, Myers-Perry solution with two angular momentum components was reproduced by using this technique [11].

[1]E-mail:tomizawa@sci.osaka-cu.ac.jp
[2]E-mail:morisawa@sci.osaka-cu.ac.jp
[3]E-mail:yasui@sci.osaka-cu.ac.jp

We apply the inverse scattering method established by Belinski et al. to five dimensional stationary and axisymmetric spacetimes, which means that there are a timelike Killing vector field and two axial Killing vector fields. We choose five dimensional Minkowski spacetime as a seed. Mishima-Iguchi's method gives solutions with only one angular momentum. On the other hand, in general, this inverse scattering method generates solutions with two angular momentum components. However, such a solution generated from Minkowski seed is not regular. Therefore, we focus on the case with a single angular momentum and show that it coincides with a black ring solution with a rotating two sphere which was derived by Mishima and Iguchi [7].

2 Five dimensinal two-solitonic solutions

As mentioned in the introduction, we are interested in two solitonic solutions in five dimensional vacuum spacetimes as the simplest case. Two soliton solutions are expressed in the form

$$g_{ab}^{(\mathrm{phys})} = \rho^{-\frac{4}{3}}(\mu_1\mu_2)^{\frac{2}{3}} g_{ab}^{(\mathrm{unphys})}, \tag{1}$$

where $g_{ab}^{(\mathrm{unphys})}$ is a three dimensional unphysical metric which takes the form of

$$g^{(\mathrm{unphys})} = g_0 - \sum_{k,l=1}^{2} \mu_k^{-1}\mu_l^{-1}\Pi^{kl} m_{0e}^{(l)} m_{0f}^{(k)} (g_0)_{ca}(g_0)_{db}[\psi_0^{-1}(\mu_l,\rho,z)]^{ec}[\psi_0^{-1}(\mu_k,\rho,z)]^{fd}. \tag{2}$$

For simplicity of notation, we hereafter put $m_{01}^{(1)} = a$, $m_{01}^{(2)} = b$, $m_{02}^{(1)} = c$, $m_{02}^{(2)} = d$, $m_{03}^{(1)} = e$, $m_{03}^{(2)} = f$. The two poles are given by

$$\begin{aligned} \mu_1 &= w_1 - z \pm \sqrt{(w_1 - z)^2 + \rho^2}, \\ \mu_2 &= w_2 - z \pm \sqrt{(w_2 - z)^2 + \rho^2}. \end{aligned} \tag{3}$$

Through the below, we put $w_1 = -w_2 = -\sigma$ and choose both of signs as $+$:

$$\mu_1 = -\sigma - z + \sqrt{(\sigma + z)^2 + \rho^2}. \tag{4}$$

$$\mu_2 = +\sigma - z + \sqrt{(\sigma - z)^2 + \rho^2}. \tag{5}$$

3 solutions generated from Minkowski seed

In four dimensional stationary and axisymmetric spacetimes, the solution generated from flat background as a seed is most interesting, since it was shown that a double soliton on a Minkowski background gives a Kerr solution, which is one of physically most important black hole solutions [10]. Therefore, we can expect that in five dimensions, this inverse scattering method might also give us interesting and important black holes with asymptotic flatness, and great insight into higher dimensional black holes. In this section, we focus on the simplest case, i.e. a two solitonic solution on five dimensional flat background spacetime. As a seed solution g_0, we choose Minkowski spacetime whose metric is given by [12]

$$ds^2 = -dt^2 + \lambda_1 d\phi^2 + \lambda_2 d\psi^2 + \frac{1}{2\sqrt{\rho^2 + (z + \kappa\sigma)^2}}(d\rho^2 + dz^2), \tag{6}$$

where

$$\lambda_1 = \sqrt{\rho^2 + (z + \kappa\sigma)^2} - (z + \kappa\sigma), \quad \lambda_2 = \sqrt{\rho^2 + (z + \kappa\sigma)^2} + (z + \kappa\sigma). \tag{7}$$

The generating matrix ψ_0 for the static seed g_0 is diagonal, i.e. $\psi_0(\lambda,\rho,z) = \mathrm{diag}(\psi_1(\lambda,\rho,z), \psi_2(\lambda,\rho,z)$ Its components are given by

$$\psi_1(\lambda,\rho,z) = -1,$$
$$\psi_2(\lambda,\rho,z) = \lambda_1 - \lambda = \sqrt{\rho^2+(z+\kappa\sigma)^2} - z - \kappa\sigma - \lambda,$$
$$\psi_3(\lambda,\rho,z) = \lambda_2 + \lambda = \sqrt{\rho^2+(z+\kappa\sigma)^2} + z + \kappa\sigma + \lambda \tag{8}$$

with $\psi_0(\lambda=0,\rho,z) = g_0$. Substituting the equations (8), (4) and (5) into the equation (2), we obtain the unphysical metric with eight parameters $\{\sigma,\kappa,a,b,c,d,e,f\}$.

3.1 Single angular momentum case

As mentioned in the previous section, we focus on a solution with a single angular momentum; this is the case where the three dimensional metric g is block-diagonalized. Choosing the parameters as $e=f=0$, we study a physical metric which is generated with four dimensional normalization. The solution can be written in the following form:

$$g_{11}^{(\mathrm{phys})} = -\frac{G_{11}}{\mu_1\mu_2\Sigma}, \quad g_{12}^{(\mathrm{phys})} = -\lambda_1\frac{(\rho^2+\mu_1\mu_2)G_{12}}{\mu_1\mu_2\Sigma}, \quad g_{22}^{(\mathrm{phys})} = -\lambda_1\frac{G_{22}}{\mu_1\mu_2\Sigma}, \tag{9}$$

$$g_{33}^{(\mathrm{phys})} = \lambda_2, \quad g_{23}^{(\mathrm{phys})} = g_{13}^{(\mathrm{phys})} = 0, \tag{10}$$

where μ_1, μ_2, λ_1 and λ_2 are given by the equations (4), (5) and (7). The functions G_{11}, G_{12}, G_{22} and Σ are defined as

$$\begin{aligned} G_{11} &= -a^2b^2(\lambda_1-\mu_1)^2(\lambda_1-\mu_2)^2(\mu_1-\mu_2)^2\rho^4 + a^2d^2\lambda_1\mu_2^2(\rho^2+\mu_1\mu_2)^2(\lambda_1-\mu_1)^2 \\ &+ b^2c^2\lambda_1\mu_1^2(\rho^2+\mu_1\mu_2)^2(\lambda_1-\mu_2)^2 - c^2d^2\lambda_1^2\mu_1^2\mu_2^2(\mu_1-\mu_2)^2 \\ &- 2abcd\lambda_1(\lambda_1-\mu_1)(\lambda_1-\mu_2)(\rho^2+\mu_1^2)(\rho^2+\mu_2^2)\mu_1\mu_2, \end{aligned} \tag{11}$$

$$\begin{aligned} G_{22} &= a^2b^2\mu_1^2\mu_2^2(\mu_1-\mu_2)^2(\lambda_1-\mu_1)^2(\lambda_1-\mu_2)^2 + c^2d^2\lambda_1^2(\mu_1-\mu_2)^2\rho^4 \\ &- a^2d^2\lambda_1\mu_1^2(\lambda_1-\mu_1)^2(\rho^2+\mu_1\mu_2)^2 - b^2c^2\lambda_1\mu_2^2(\lambda_1-\mu_2)^2(\rho^2+\mu_1\mu_2)^2 \\ &+ 2abcd\lambda_1\mu_1\mu_2(\lambda_1-\mu_2)(\lambda_1-\mu_1)(\rho^2+\mu_1^2)(\rho^2+\mu_2^2), \end{aligned} \tag{12}$$

$$\begin{aligned} G_{12} &= ab^2c\mu_2(\mu_1-\mu_2)(\lambda_1-\mu_2)^2(\lambda_1-\mu_1)(\rho^2+\mu_1^2) + acd^2\lambda_1\mu_2(\mu_2-\mu_1)(\lambda_1-\mu_1)(\rho^2+\mu_1^2) \\ &+ a^2bd\mu_1(\mu_2-\mu_1)(\lambda_1-\mu_1)^2(\lambda_1-\mu_2)(\rho^2+\mu_2^2) + bc^2d\mu_1\lambda_1(\lambda_1-\mu_2)(\rho^2+\mu_2^2)(\mu_1-\mu_2), \end{aligned} \tag{13}$$

$$\begin{aligned} \Sigma &= a^2b^2(\lambda_1-\mu_1)^2(\lambda_1-\mu_2)^2(\mu_1-\mu_2)^2\rho^2 + c^2d^2\lambda_1^2(\mu_1-\mu_2)^2\rho^2 \\ &+ a^2d^2\lambda_1(\lambda_1-\mu_1)^2(\rho^2+\mu_1\mu_2)^2 + c^2b^2\lambda_1(\lambda_1-\mu_2)^2(\rho^2+\mu_1\mu_2)^2 \\ &- 2abcd\lambda_1(\lambda_1-\mu_1)(\lambda_1-\mu_2)(\rho^2+\mu_1^2)(\rho^2+\mu_2^2). \end{aligned} \tag{14}$$

In order to see relation between the generated solution and the solution obtained by Mishima and Iguchi, let us consider the coordinate transformation of the physical metric such that

$$t \to t' = t - \omega\phi, \quad \phi \to \phi' = \phi, \tag{15}$$

where ω is an arbitrary constant and $x^1 = t, x^2 = \phi, x^3 = \psi$. We should note that the transformed metric also satisfies the supplementary condition $\det g = -\rho^2$. Under this transformation, the physical metric components become

$$g_{tt} \to g_{t't'} = g_{tt}, \tag{16}$$
$$g_{t\phi} \to g_{t'\phi'} = g_{t\phi} + \omega g_{tt}, \tag{17}$$
$$g_{\phi\phi} \to g_{\phi'\phi'} = g_{\phi\phi} + 2\omega g_{t\phi} + \omega^2 g_{tt}. \tag{18}$$

If we choose the parameters such that

$$ab = \beta, \tag{19}$$
$$bc = \sigma^{\frac{1}{2}}(\kappa - 1), \tag{20}$$
$$ad = -\sigma^{\frac{1}{2}}\alpha\beta(\kappa + 1), \tag{21}$$
$$cd = -\sigma\alpha(\kappa^2 - 1), \tag{22}$$
$$\omega = C_1, \tag{23}$$

and use the spherical polar coordinate (x, y) defined as $\rho = \sigma\sqrt{(x^2-1)(1-y^2)}$, $z = \sigma xy$, then we can make sure that the transformed metric with components (16), (17) and (18) coincide with the metric of a black ring solution with a rotating two sphere obtained by Mishima and Iguchi [7]. In order to show this coincidence, it is sufficient to calculate only two components g_{tt} and $g_{t\phi}$ due to the supplementary condition $\det g = -\rho^2$ and the fact that the metric function f is determined by three dimensional metric g.

4 Summary and discussion

We studied two solitonic solutions of vacuum Einstein equations from five dimensional Minkowski spacetime using the inverse scattering method. The solution with one angular momentum includes six parameters $\{a, b, c, d, \sigma, \kappa\}$, however, physical parameters are only four since the only ratios of a/c and b/d appear in the metric components (9) i.e. the transformations of parameters which leave these ratios invariant are isometries. As a result, we reproduced a black ring solution with a rotating two sphere which was obtained by Mishima and Iguchi. However, we could not obtain a black ring solution which was found by Emparan and Reall from Minkowski spacetime with this inverse scattering method.

References

[1] Shinya Tomizawa, Yoshiyuki Morisawa, Yukinori Yasui, arXive:hep-th/0512252.

[2] T. Banks and W. Fischler, arXiv:hep-th/9906038; S. B. Giddings and S. D. Thomas, Phys. Rev. D **65**, 056010 (2002); S. Dimopoulos and G. Landsberg, Phys. Rev. Lett. **87**, 161602 (2001).

[3] R. C. Myers and M. J. Perry, Annals Phys. **172**, 304 (1986).

[4] R. Emparan and H. S. Reall, Phys. Rev. Lett. **88**, 101101 (2002).

[5] Y. Morisawa and D. Ida, Phys. Rev. D **69**, 124005 (2004).

[6] H. Stephani, D. Kramer, M. MacCallum, C. Hoenselaers and E. Herlt, *Exact solutions of Einstein's Field Equations, 2nd ed.* (Cambridge University Press, Cambridge, 2003).

[7] T. Mishima and H. Iguchi, arXiv:hep-th/0504018.

[8] J. Castejon-Amenedo and V. S. Manko, Phys. Rev. D **41**, 2018 (1990).

[9] Pau Figueras, JHEP 0507, 039 (2005).

[10] V. A. Belinskii and V. E. Zakharov, Sov. Phys. JETP **50**, 1 (1979); V. A. Belinskii and V. E. Zakharov, Sov. Phys. JETP **48**, 985 (1978).

[11] A. A. Pomeransky, arXiv:hep-th/0507250.

[12] T. Harmark, Phys. Rev. D **70**, 124002 (2004).

Skyrme Branes

Noriko Shiiki[1], Jose J. Blanco-Pillado[2], Nobuyuki Sawado[3]

[1,3]*Department of Physics, Tokyo University of Science, Noda, Chiba 278-8510, Japan*
[2]*Center for Cosmology and Particle Physics, Department of Physics, New York University, 4 Washington Place, New York, NY 10003*

Abstract

In this paper we consider static regular flat brane solutions in seven dimensional spacetime using the Skyrme model as a brane source. The solutions realize a flat extra space far from the skyrmion core and are considered as a regular solution in the Dvali-Gabadadze-Porrati (DGP) theory with three dimensional infinite-volume extra space.

1 Introduction

Theories with extradimensions have been expected to solve the hierarchy problem. The phenomenological model was originally proposed in [1] where extra dimensions are compact with a finite volume. It was later shown that the extra dimensions can be non-compact but have a finite volume by warping the geometry [2]. The finite volume makes possible to obtain a nomalizable zero-mode graviton in the spectrum of fluctuations about the background. The extra dimensions are directly manifested only at short distances. Above a certain distance, 4D Newtonian gravity is reproduced.

On the other hand, there are also theories with infinite extra space. Since the volume is infinite, the zero-mode is not any longer normalizable. Nevertheless it was shown that the correct Newtonian limit can be recovered at intermediate distances by exchanging a metastable resonance mode [3]. In [4, 5], the theory with asymptotically flat infinite-volume extra space was studied. If an induced 4D Ricci scalar is included on the brane, the correct 4D potential can be recovered at short distances. Due to the feature of extra dimensions showing up at large scales, this model has a possibility to solve the problem of the cosmological constant and supersymmetry breaking. The problem in such an asymptotically flat background, however, is the presence of two kinds of codimension singularities; one is a horizon singularity and the other is a core singularity. Especially for codimension greater than 2 cases, these singularities are more severe. Thus, smoothing out procedures are somehow required. The horizon singularity can be removed by letting a brane inflate [6]. For the core singularity, one possible smoothing technique is to introduce higher curvature term which softens the graviton propagator [7, 8]. Alternatively, in [10], the author indicated that an adequate choice of core model should smooth out the singularity. In this paper we follow the latter step and construct static regular 3-brane solutions with asymptotically flat spacetime using the Skyrme model as a brane source.

2 The Skyrme Brane Model

The $D = 7$ Einstein-Skyrme system is defined by the action

$$S_{ES} = \int d^7x\sqrt{-g}\left[\frac{1}{2\kappa^2}R + \mathcal{L}_S\right] \tag{1}$$

where $\kappa^2 = 1/M_7^5$ and M_7 is the $D = 7$ Planck mass.

The Skyrme Lagrangian $\mathcal{L}_S$ is given by [9]

$$\mathcal{L}_S = \frac{F_0^2}{4}\mathrm{tr}(U^\dagger\partial_A U U^\dagger\partial^A U) + \frac{1}{32e^2}\mathrm{tr}[U^\dagger\partial_A U, U^\dagger\partial_B U]^2 . \tag{2}$$

[1]E-mail:norikoshiiki@mail.goo.ne.jp
[2]E-mail:blanco-pillado@physics.nyu.edu
[3]E-mail:sawado@ph.noda.tus.ac.jp

where A runs $1, 2, \cdots, 7$, F_0 and e are free parameters, and U is a chiral $SU(2)$ matrix. In the 4D Skyrme model as a nucleon model, U is related to pions and F_0 corresponds to the pion decay constant. In our model, however, U is unrelated to pions and F_0, e have the dimension of $M^{5/2}$, $M^{-3/2}$ respectively.

Since we are interested in solitonic solutions, the Skyrme field should fall off at a finite distance in the extra direction and hence the metric are expected to take a similar asymptotic form as the solution of the vacuum Einstein equations derived by Gregory in Ref. [10],

$$ds^2_\infty = \left(1 - \frac{c_1}{r}\right)^{1/\sqrt{10}} \eta_{\mu\nu} dx^\mu dx^\nu + \left(1 - \frac{c_1}{r}\right)^{-2\sqrt{2/5}} dr^2 + r^2 \left(1 - \frac{c_2}{r}\right)^{1-2\sqrt{2/5}} d\Omega^2 . \tag{3}$$

where c_1 and c_2 are constants. Thus, we impose the metric ansatz as

$$ds^2 = A^2(r)\eta_{\mu\nu} dx^\mu dx^\nu + \frac{1}{A^8(r)} dr^2 + C^2(r) d\Omega^2 . \tag{4}$$

where $\eta_{\mu\nu} = (-1, +1, +1, +1)$ and

$$A = \left(1 - \frac{m_1(r)}{r}\right)^{\frac{1}{\sqrt{40}}}, \qquad C = r\left(1 - \frac{m_2(r)}{r}\right)^{\frac{1-2\sqrt{\frac{2}{5}}}{2}} . \tag{5}$$

For the chiral field, we impose the hedgehog ansatz as

$$U = \cos f(r) + i \frac{r^a}{r} \tau^a \sin f(r) . \tag{6}$$

where τ^a is the Pauli matrix with $a = 1, 2, 3$. Using the ansatz (4) and (6), one can write the Skyrme energy as

$$E = 2\pi \frac{F_0}{e} \int \left[A^8 u (f')^2 + v\right] d^4x\, dx \tag{7}$$

where we have introduced the dimensionless coordinate $x = eF_0 r$ and the prime denotes differentiation with respect to x. $u = \hat{C}^2 + 2\sin^2 f$ and $v = \sin^2 f(2 + \sin^2 f/\hat{C}^2)$ with $\hat{C} = eF_0 C$. Correspondingly, we define the dimensionless metric fields as $\hat{m}_i = m_i/eF_0$ for $i = 1, 2$.

According to the variational principle, the field equation for skyrmions is derived as

$$f'' = -\frac{1}{u}\left[2\left(4\frac{A'}{A}u + \hat{C}\hat{C}'\right) f' + (f')^2 \sin 2f - \frac{\sin 2f}{A^8}\left(1 + \frac{\sin^2 f}{\hat{C}^2}\right)\right] . \tag{8}$$

In terms of the functions $\hat{m}_1$ and $\hat{m}_2$, the metric field equations can be written as

$$\begin{aligned} \hat{m}_1'' &= -\sqrt{40} x \Delta_1 \left[-\left(\frac{1}{5} - \frac{1}{\sqrt{40}}\right) \frac{1}{\Delta_1^2} \left(\frac{\hat{m}_1}{x^2} - \frac{\hat{m}_1'}{x}\right)^2 - \frac{1}{\sqrt{40}} \left(1 - 2\sqrt{\frac{2}{5}}\right) \frac{1}{\Delta_1 \Delta_2} \left(\frac{\hat{m}_1}{x^2} - \frac{\hat{m}_1'}{x}\right) \right. \\ &\quad \left. \times \left(\frac{\hat{m}_2}{x^2} - \frac{\hat{m}_2'}{x}\right) + \frac{\alpha^2}{5} \frac{\sin^2 f}{x^2 \Delta_2^{1-2\sqrt{\frac{2}{5}}}} \left(2f'^2 + \frac{\sin^2 f}{x^2 \Delta_1^{2\sqrt{\frac{2}{5}}} \Delta_2^{1-\sqrt{\frac{2}{5}}}}\right) \right] \end{aligned} \tag{9}$$

$$\begin{aligned} \hat{m}_2'' &= -\frac{2}{1 - 2\sqrt{\frac{2}{5}}} x \Delta_2 \left[\frac{3}{20} \frac{1}{\Delta_1^2} \left(\frac{\hat{m}_1}{x^2} - \frac{\hat{m}_1'}{x}\right)^2 - \frac{3}{20} \frac{1}{\Delta_2^2} \left(\frac{\hat{m}_2}{x^2} - \frac{\hat{m}_2'}{x}\right)^2 - \frac{\alpha^2}{10} \left\{ \left(5 + \frac{16 \sin^2 f}{x^2 \Delta_2^{1-2\sqrt{\frac{2}{5}}}}\right) \right. \right. \\ &\quad \left. \left. \times f'^2 + 3 \frac{\sin^4 f}{x^4 \Delta_1^{2\sqrt{\frac{2}{5}}} \Delta_2^{2-4\sqrt{\frac{2}{5}}}} \right\} \right] \end{aligned} \tag{10}$$

where we have defined $\alpha^2 = \kappa^2 F_0^2$ and $\Delta_i = 1 - \hat{m}_i(x)/x$ for $i = 1, 2$. These coupled equations are solved numerically with appropriate boundary conditions discussed below.

Since solutions are regular at the origin, we have the boundary conditions

$$\hat{m}_1 = 0\,, \quad \hat{m}_2 = 0\,, \quad \text{as } x \to 0\,. \tag{11}$$

A skyrmion solution with winding number one in the extra space should satisfy $f(0) = \pi$ and $f(\infty) = 0$. Thus, we can expand the functions around the origin as

$$f(x) = \pi + f_1 x + O(x^2) \tag{12}$$
$$\hat{m}_1(x) = ax + O(x^2) \tag{13}$$
$$\hat{m}_2(x) = bx + O(x^2) \tag{14}$$

where f_1, a and b are shooting parameters determined by the boundary conditions at $x \to \infty$. We seek solutions which behave like the metric (3) as $x \to \infty$, *i.e.*

$$f \to 0\,, \quad \hat{m}_1 \to c_1\,, \quad \hat{m}_2 \to c_2\,, \quad \text{as } x \to \infty\,. \tag{15}$$

with constant values, c_1 and c_2.

3 Numerical Results

In Figs. 1-3, we present brane solutions obtained by solving the equations (8-10) numerically under the boundary conditions (12-15). The numerical method we employed is a shooting method with the shooting parameters f_1, a and b. Integration of the differential equations is based on the fourth-order Runge-Kutta method with a grid size 0.05.

Fig. 1 shows the Skyrme profile function $f(x)$ for $\alpha^2 = 0.005, 0.010, 0.015$. As the value of the coupling constant increases, the skyrmion gets slightly smaller in size. The same behavior has been observed in gravitational skyrmions in the 4D Einstein-Skyrme system [11]. The 4D gravitational skyrmions also exhibit two branches of solutions: one is stable and the other is unstable. We were, however, not able to find the second branch in this model. Fig. 2, 3 show the metric function $\hat{m}_1(x)$ and $\hat{m}_2(x)$ respectively. Both functions converge to a constant value, which means that our solution recovers the asymptotic metric (3). It is observed that c_1 and c_2 take larger values as α increases. Since the c_1 is interpreted as the ADM mass, the Skyrme brane energy increases for a distant observer from the brane core as α increases.

References

[1] N. Arkani-Hamed, S. Dimopoulos, D. Dvali, Phys. Lett. B429 (1998) 263; Phys. Rev. D59 (1999) 0860.

[2] L. Randall, R. Sundrum, Phys. Rev. Lett. 83 (1999) 3370; Phys. Rev. Lett. 83 (1999) 4690.

[3] R. Gregory, V. A. Rubakov, S. M. Sibiryakov, Phys. Rev. Lett. 84 (2000) 5928.

[4] G. Dvali and G. Gabadadze, M. Porrati, Phys. Lett. B485 (2000) 208.

[5] G. Dvali and G. Gabadadze, Phys. Rev. D63 (2001) 065007.

[6] G. Dvali, G. Gabadadze and M. Shifman, Phys. Rev. D67 (2003) 044020.

[7] O. Corradini, A. Iglesias, Z. Kakushadze, P. Langfelder, Mod. Phys. Lett. A17 (2002) 795.

[8] G. Dvali, G. Gabadadze, X. Hou, E. Sefusatti, Phys. Rev. D67 (2003) 044019.

[9] T. H. R. Skyrme, Proc. Roy. Soc. A260 (1961) 127.

[10] R. Gregory, Nucl. Phys. B467 (1996) 159.

[11] P. Bizon and T. Chmaj, Phys. Lett. B297 (1992) 55.

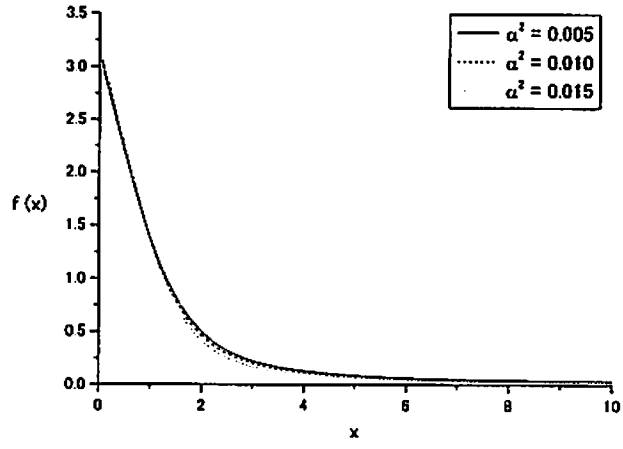

Figure 1: Skyrme profile function f as a function of x with $\alpha^2 = 0.005, 0.010, 0.015$.

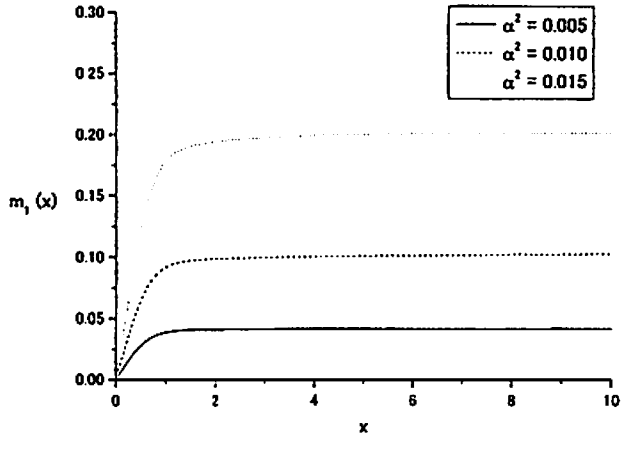

Figure 2: $\hat{m}_1$ as a function of x with $\alpha^2 = 0.005, 0.010, 0.015$.

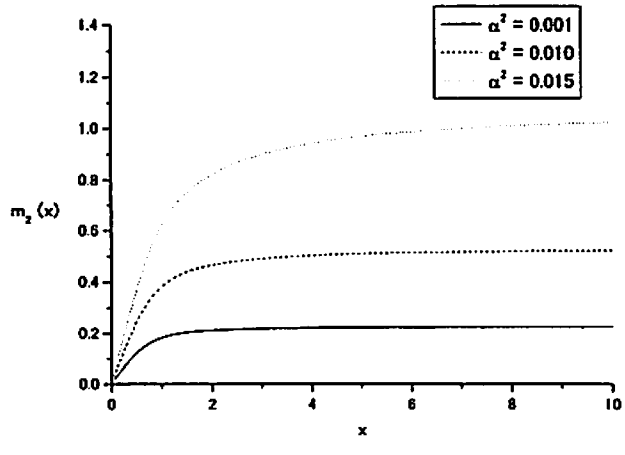

Figure 3: $\hat{m}_2$ as a function of x with $\alpha^2 = 0.005, 0.010, 0.015$.

Induced metric on classical brane fluctuation

Konosuke Sawa[1]

Department of Physics, Tokyo University of Science,
1-3 Kagurazaka, Shinjyuku-ku, Tokyo 162-0861, Japan

Abstract

We can consider that the existence of brane gives rise to the spontaneous breaking of bulk isometry. It produces the Nambu-Goldstone (NG) mode which is responsible for brane fluctuation. When this mode is regarded as classical field, it contributes to background metric. We investigate a possibility that the NG mode exhibits other configurations in the brane.

1 Introduction

The braneworld scenario suggests that the SM particles are confined to the world volume of a 3-brane, while only gravity propagates freely in bulk spacetime [1, 2]. This concept is based on a string-inspired expectation that the 3-brane might arise as a topological defect in a field theoretic model. We can consider that the dynamical degrees of freedom described by the Nanmbu-Goldstone (NG) mode are due to the breaking of the continuous isometries in bulk space-time. The most important aspect of this theory is that the metric and the vierbein are replaced by the induced metric and the induced vierbein, respectively. In general, although the Kaluza-Klein (KK) theory assumes periodic limits such as a torus structure in extra dimensions, the braneworld scenarios need not possess these limits since the configuration of the extra dimensions is determined by gravity, position of the branes, cosmological constant, etc. Therefore, we can argue higher dimensional gravity apart from the usual KK-theory. This effect would be applicable to various higher dimensional models in particle and cosmological physics.

2 Brane fluctuation

The NG mode produces a new coupling with matter. This interaction is very similar to gravitational interactions since the NG mode couples to the all the matter fields with the same strength. The NG mode physics was discussed in [3, 4, 5, 6, 8, 9, 10, 11].

We consider the bulk space-time $M_4 \times B$ with $(4+n)$-dimensions, where M_4 is a 4-dimensional Minkowski space-time and B is a given n-dimensional manifold. Under the gauge fixing condition $x^\mu = \delta^\mu{}_m Y^m(x)$, the induced metric is as follows:

$$g_{\mu\nu} = \eta_{\mu\nu} + \gamma_{mn}\partial_\mu Y^m \partial_\nu Y^n. \tag{1}$$

For simplicity, we suppose that the off-diagonal components of the vielbein are zero, as shown below:

$$E^A_M(X) = \begin{pmatrix} \delta^\alpha_\mu & 0 \\ 0 & E^a_m \end{pmatrix}. \tag{2}$$

In order to obtain the induced vierbein on the brane, we use the following definition [3]:

$$e^\alpha_\mu \equiv R^\alpha_A E^A_M(X)\partial_\mu Y^M. \tag{3}$$

Thus, the induced vierbein obtains the following expression up to the second order:

$$e^\alpha_\mu = \delta^\alpha_\mu + \frac{1}{2}\gamma_{mn}\partial^\alpha Y^m \partial_\mu Y^n + \cdots. \tag{4}$$

[1]E-mail: sa1203704@rs.kagu.tus.ac.jp

where the ellipsis represents the terms of derivative of the Y^m. The expansion of $\sqrt{-g}$ of induced metric (1) becomes

$$\begin{aligned}\sqrt{-g} &= 1-\frac{1}{2}\partial^\alpha Y^m\partial_\alpha Y^m+\frac{1}{8}\partial^\alpha Y^m\partial_\alpha Y^m\partial^\beta Y^n\partial_\beta Y^n \\ &\quad -\frac{1}{4}\partial^\alpha Y^m\partial^\beta Y^m\partial_\alpha Y^n\partial_\beta Y^n+\cdots. \end{aligned} \tag{5}$$

The ellipsis represents the higher dimension terms of $\partial_\mu Y^m$ in pairs. When using the above expansion and the following canonical normalization for Y^m:

$$\partial_\mu Y^m\partial^\mu Y^m \to \frac{1}{f^4}\partial_\mu Y^m\partial^\mu Y^m, \tag{6}$$

the minimal brane action

$$S_{brane} = \int d^4x\sqrt{-g}\Big[-f^4+\mathcal{L}_4(g_{\mu\nu})\Big] \tag{7}$$

is transformed into

$$\begin{aligned}S_{brane} &= \int d^4x\Big[-f^4+\mathcal{L}_4(\eta_{\mu\nu})+\frac{1}{2}\partial_\mu Y^m\partial^\mu Y^m+\frac{1}{2}\partial_\mu Y^m\partial_\nu Y^m T^{\mu\nu}_{matter} \\ &\quad -\frac{1}{8f^4}\partial_\mu Y^m\partial^\mu Y^m\partial_\nu Y^n\partial^\nu Y^n+\frac{1}{4f^4}\partial_\mu Y^m\partial_\nu Y^m\partial^\mu Y^n\partial^\nu Y^n+\cdots\Big], \end{aligned} \tag{8}$$

where $T^{\mu\nu}_{matter}$ is the conserved energy-momentum tensor of matter fields evaluated in the 4-dimensional Minkowski space-time. These interaction terms are expressed in terms of the same coupling $1/f^4$. In previous papers [12, 13], we have investigated the brane-stretching effect which is a static solution of the NG-mode, up to the second order of the derivative expansion. The static brane fluctuation allows Y^m to acquire $\mathbf{x}=x^i(i=1,2,3)$ dependence. Therefore, we can parametrize Y^m as follows:

$$Y^m(\mathbf{x}) = Y_0^m + M_f\bar{e}_i^m E x^i, \tag{9}$$

where Y_0^m is a constant, $\bar{e}_i^m$ are three basis vectors, and E is the energy scale of the physical process. The x^i dependence is characterized by the dimensionless coordinate Ex^i based on dimensional analysis. Using this solution, the induced metric can be expressed as

$$g_{\mu\nu} = \begin{pmatrix} 1 & 0 \\ 0 & \eta_{ij}\left(1+\frac{E^2M_f^2}{f^4}\right)\end{pmatrix}. \tag{10}$$

This indicates that the spatial part of brane is stretched and its magnitude depneds on the energy scale E. This configuration maintains the general covariance for fermion in the background metric. By substituting (9) into the spin connection

$$\omega_\mu^{\alpha\beta} = \frac{1}{2}e^{\alpha\nu}(\partial_\mu e_\nu^\beta-\partial_\nu e_\mu^\beta) \tag{11}$$

via induced vierbein (4), we can directly obtain the following expression:

$$\omega_\mu^{\alpha\beta} = -\frac{1}{2}\partial_\mu\left[\partial^\beta Y^m\partial^\alpha Y^m\right] \tag{12}$$

$$= 0. \tag{13}$$

The vanishing of the spin connection denotes that the equation of motion of a fermion is consistent with the laws of special relativity. Therefore, solution (9) supports Lorentz symmetry.

3 Virial theorem

In this section, in order to investigate a static background solution, we apply the virial theorem [14] to the D-dimensional static NG-mode except for the matter coupling. In general, although it is difficult that we obtain an analytic solutions of non-linear systems, this theorem examines the existence of stable non-trivial solutions. A static solution $Y_s^m = Y_s^m(\mathbf{x})$ for the Y^m equation of motion obeys

$$\partial_\mu\Big[\partial^\mu Y_s^m - \frac{1}{2f^4}\partial^\mu Y_s^m \partial_\nu Y_s^n \partial^\nu Y_s^n + \frac{1}{f^4}\partial^\mu Y_s^n \partial_\nu Y_s^m \partial^\nu Y_s^n + \cdots\Big] = 0. \tag{14}$$

This equation satisfies the extremum condition $\delta W = 0$ for the static energy functional expressed as

$$W[Y_s] = W_1[Y_s] + W_2[Y_s], \tag{15}$$

$$W_1[Y_s] = \int d^D x\Big[\frac{1}{2}\partial^i Y_s^m \partial^i Y_s^m\Big], \tag{16}$$

$$W_2[Y_s] = \int d^D x\Big[\frac{1}{8f^4}\partial^i Y_s^m \partial^i Y_s^m \partial^j Y_s^n \partial^j Y_s^n - \frac{1}{4f^4}\partial^i Y_s^m \partial^j Y_s^m \partial^i Y_s^n \partial^j Y_s^n\Big], \tag{17}$$

When we introduce a scaling parameter λ as

$$Y_\lambda^m(\mathbf{x}) = Y_s^m(\lambda\mathbf{x}), \tag{18}$$

we obtain

$$W[Y_\lambda] = W_1[Y_\lambda] + W_2[Y_\lambda] \tag{19}$$

$$= \int d^D x\Big[\frac{1}{2}\partial_i Y_\lambda^m \partial^i Y_\lambda^m + \frac{1}{8f^4}\partial_i Y_\lambda^m \partial^i Y_\lambda^m \partial_j Y_\lambda^n \partial^j Y_\lambda^n \tag{20}$$

$$-\frac{1}{4f^4}\partial_i Y_\lambda^m \partial_j Y_\lambda^m \partial^i Y_\lambda^n \partial^j Y_\lambda^n\Big]$$

$$= \int d^D x \frac{1}{\lambda^D}\Big[\frac{\lambda^2}{2}\partial_i Y_s^m \partial^i Y_s^m + \frac{\lambda^4}{8f^4}\partial_i Y_s^m \partial^i Y_s^m \partial_j Y_s^n \partial^j Y_s^n \tag{21}$$

$$-\frac{\lambda^4}{4f^4}\partial_i Y_s^m \partial_j Y_s^m \partial^i Y_s^n \partial^j Y_s^n\Big]$$

$$= \lambda^{2-D} W_1[Y_s] + \lambda^{4-D} W_2[Y_s]. \tag{22}$$

Since the configuration of Y_s^m is a local minimum of the static energy functional (15), we require

$$\Big[\frac{d}{d\lambda}W[Y_\lambda]\Big]_{\lambda=1} = 0, \tag{23}$$

$$\Big[\frac{d^2}{d\lambda^2}W[Y_\lambda]\Big]_{\lambda=1} \geq 0, \tag{24}$$

i.e.,

$$(2-D)W_2[Y_s] + (4-D)W_2[Y_s] = 0, \tag{25}$$

$$(2-D)(1-D)W_1[Y_s] + (4-D)(3-D)W_2[Y_s] \geq 0. \tag{26}$$

This leads to the conclusion that when W_1 and W_2 are non-negative, some static solutions may exist in $D = 3$. It is obvious that solution (9) satisfies these condition:

$$W_1[Y_s] = \int d^3x \partial^i Y^m \partial^i Y^m = 3\int d^3x M_f^2 E^2 > 0, \tag{27}$$

$$W_2[Y_s] = \int d^3x \partial^i Y^m \partial^j Y^m \partial^i Y^n \partial^j Y^n = \frac{3}{8f^4}\int d^3x M_f^4 E^4 > 0. \tag{28}$$

The integrals in Eqs. (27) and (28) result in a divergence, which implies that solution (9) represents a non-localized configuration over all space. When the NG-mode action involves self-interactions of higher

order derivatives, it can realize stability in its non-trivial state (refer to [15, 16] where such states have been studied under suitable assumptions).

Although we have focused on the negative tension brane, we discuss fluctuation on the positive tension brane. In this case, NG-mode physics gives rise to a kinetic term with an opposite sign; this implies an instability of the brane. Hence, while taking into account a positive tension brane, we should consider the case when it is located on an orbifold fixed point as observed in the Randall-Sundrum models [17, 18]. In a non-rigid negative tension brane, NG-mode physics play an important role. The virial theorem suggests that other static solutions exist. This class of scalar field configurations should be restricted by condition (13) for maintaining the general covariance of fermions in the flat brane. Otherwise, it would relate with Lorentz violation.

References

[1] N. Arkani-Hamed, S. Dimopoulos and G. R. Dvali, Phys. Lett. B **429**, (1998) 263.

[2] I. Antoniadis, N. Arkani-Hamed, S. Dimopoulos and G. R. Dvali, Phys. Lett. B **436**, (1998) 257.

[3] R. Sundrum, Phys. Rev. D **59**, (1999) 085009.

[4] M. Bando, T. Kugo, T. Noguchi and K. Yoshioka, Phys. Rev. Lett. **83**, (1999) 3601.

[5] J. Hisano and N. Okada, Phys. Rev. D **61**, (2000) 106003.

[6] T. Kugo and K. Yoshioka, Nucl. Phys. B **594**, (2001) 301.

[7] G. R. Dvali, I. I. Kogan and M. A. Shifman, Phys. Rev. D **62**, (2000) 106001.

[8] A. Dobado and A. L. Maroto, Nucl. Phys. B **592**, (2001) 203.

[9] H. Murayama and J. D. Wells, Phys. Rev. D **65**, (2002) 056011.

[10] J. Alcaraz, J. A. R. Cembranos, A. Dobado and A. L. Maroto, Phys. Rev. D **67**, (2003) 075010.

[11] K. Akama, Lect. Notes Phys. **176**, (1982) 267.

[12] K. Sawa, arXiv:hep-ph/0506190; Accepted in PRD.

[13] K. Sawa, arXiv:hep-ph/0509132.

[14] G. H. Derrick, J. Math. Phys. **5**, 1252 (1964).

[15] J. A. R. Cembranos, A. Dobado and A. L. Maroto, Phys. Rev. D **65**, 026005 (2002)

[16] J. A. R. Cembranos, A. Dobado and A. L. Maroto, arXiv:hep-ph/0107155.

[17] L. Randall and R. Sundrum, Phys. Rev. Lett. **83**, 3370 (1999).

[18] L. Randall and R. Sundrum, Phys. Rev. Lett. **83**, 4690 (1999).

Effects of Lovelock terms on the final fate of gravitational collapse

Masato Nozawa[1], Hideki Maeda[2]

[1] *Department of Physics, Waseda University, 3-4-1 Okubo, Shinjuku-ku, Tokyo 169-8555, Japan*
[2] *Advanced Research Institute for Science and Engineering, Waseda University, Shinjuku, Tokyo 169-8555, Japan*

Abstract

We find an exact solution in dimensionally continued gravity in arbitrary dimensions which describes the gravitational collapse of a null dust fluid. Considering the situation that a null dust fluid injects into the initially anti-de Sitter spacetime, we show that a naked singularity can be formed. In even dimensions, a massless ingoing null naked singularity emerges. In odd dimensions, meanwhile, a massive timelike naked singularity forms. These naked singularities can be globally naked if the ingoing null dust fluid is switched off at a finite time; the resulting spacetime is static and asymptotically anti-de Sitter spacetime. The curvature strength of the massive timelike naked singularity in odd dimensions is independent of the spacetime dimensions or the power of the mass function. This is a characteristic feature in Lovelock gravity.

1 Introduction

It has been shown that spacetimes necessarily have a singularity under physically reasonable conditions [1]. Gravitational collapse is one of the presumable scenarios that singularities are formed. In order for spacetimes not to be pathological, Penrose made a celebrated proposal, the *cosmic censorship hypothesis* (CCH) [2, 3], that is, singularities which are formed in a physically reasonable gravitational collapse should not be seen by distant observers. Although there is a long history of research on the final fate of the gravitational collapse, we are far from having achieved consensus on the validity of the CCH, which is one of the most important open problems in general relativity.

Lately it has been of great importance to consider higher-dimensional spacetimes. There exists a natural extension of general relativity in higher dimensions, Lovelock gravity [4]. Higher-order curvature terms come into effect where gravity becomes very strong. One of the present authors has discussed the gravitational collapse of a null dust fluid in Gauss-Bonnet gravity [5]. The purpose of the present work is to analyze how higher-order Lovelock terms modify the final fate of gravitational collapse in comparison to the Gauss-Bonnet or general relativistic cases.

Bañados, Teitelboim and Zanelli have proposed a method which simplifies the analysis in Lovelock gravity [6]. An exact solution in the theory of gravity, called dimensionally continued gravity (DC gravity), representing a static vacuum solution, has been found [6, 7], which is a higher-dimensional generalization of BTZ solution [9]. We extend our investigations on the gravitational collapse of a null dust fluid in Gauss-Bonnet gravity [5] into DC gravity in order to see the effects of higher-order Lovelock terms on the final fate of gravitational collapse. A detailed analysis is reported in [8].

2 Null Dust Solution in DC gravity

Lovelock gravity is a natural extension of general relativity in $D(\geq 3)$-dimensional spacetimes, whose action is given by $I = \int \mathcal{L}_D + I_m$ with

$$\int \mathcal{L}_D \equiv \kappa \sum_{p=0}^{[(D-1)/2]} \alpha_p I_p, \quad I_p \equiv \int_{\mathcal{M}} \epsilon_{a_1 \cdots a_D} \mathcal{R}^{a_1 a_2} \wedge \cdots \wedge \mathcal{R}^{a_{2p-1} a_{2p}} \wedge e^{a_{2p+1}} \wedge \cdots \wedge e^{a_D}, \tag{1}$$

[1] E-mail:nozawa@gravity.phys.waseda.ac.jp
[2] E-mail:hideki@gravity.phys.waseda.ac.jp

The $[(D+1)/2]$ real constants α_p in the action have dimensions $[\text{length}]^{-(D-2p)}$. The special combinations of Lovelock coefficients in DC gravity are given by [6]

$$\alpha_p = \begin{cases} \dfrac{1}{D-2p}\begin{pmatrix} n-1 \\ p \end{pmatrix} l^{-D+2p}, & \text{for } D = 2n-1, \\ \begin{pmatrix} n \\ p \end{pmatrix} l^{-D+2p}, & \text{for } D = 2n, \end{cases} \tag{2}$$

where $n \equiv [(D+1)/2]$. We find an exact solution of DC gravity in D-dimensional spacetimes representing a radially ingoing null dust fluid:

$$ds^2 = -f(v,r)dv^2 + 2dvdr + r^2 d\Sigma^2_{k,D-2} \tag{3}$$

with

$$f(v,r) = \begin{cases} k - (2M(v)/r)^{1/(n-1)} + l^{-2}r^2, & \text{for } D = 2n, \\ k - M(v)^{1/(n-1)} + l^{-2}r^2, & \text{for } D = 2n-1. \end{cases} \tag{4}$$

From the field equations, the energy density of the null dust fluid is given by

$$\rho(v,r) = \frac{1}{\Omega_{D-2} r^{D-2}} \dot{M} \tag{5}$$

both in odd and even dimensions. $\dot{M} \geq 0$ is required due to the weak energy condition. We shall call the solution (3) DC-Vaidya solution. When $M = \text{const.}$, Eq. (3) describes a static solution, which we shall call DC-BTZ solution.

3 Naked Singularity Formations

We consider the situation in which a null dust fluid radially falls into the initial AdS spacetime ($M(v) = 0$) at $v = 0$ in even dimensions at first. We set $M(v) = M_0 v^q$ for simplicity, where $M_0 (> 0)$ and $q (\geq 1)$. Then a central singularity appears at $r = 0$ for $v > 0$ both in odd and even dimensions.

We first consider the even dimensional case. We find the radial null geodesics emanating from the singularity with asymptotic form $v \simeq K_1 r$. Along these null geodesics, the energy density for the null dust fluid (5) and the Kretschmann scalar $I_1 = R_{\mu\nu\rho\sigma}R^{\mu\nu\rho\sigma}$ diverge as $r \to 0$ for $1 \leq q < D-1$. Thus, the spacetime represents the formation of a naked singularity.

In order to see whether the singularity is globally naked, we consider the situation in which the null dust fluid is switched off at $v = v_f > 0$. If $v_f \simeq 0$, the singularity can be globally naked. The Penrose diagram of the gravitational collapse is drawn in Fig. 1 (1) for the globally naked singularity formation.

Next we examine the odd dimensional case. We choose the mass function as the power-law form. The singularity $r = 0$ might be naked for $0 \leq v \leq v_{AH}$, where $v_{AH} \equiv M_0^{-q}$. We find null geodesics from the singularity with the asymptotic form $v \simeq v_0 + K_2 r$ for $0 \leq v_0 < v_{AH}$. Along the radial null geodesics from the singularity $v = r = 0$, the Kretschmann scalar diverges for $D \geq 5$. In the meanwhile, it is finite for $D = 3$. However, the energy density of the null dust fluid (5) diverges along the null geodesics for $D \geq 3$. On the other hand, the radial null geodesics from the singularity $r = 0$, $0 < v < v_{AH}$ are singular null geodesics for any $q (\geq 1)$. Along them, the Kretschmann scalar and the energy density of the null dust fluid diverge for $D \geq 5$ and $D \geq 3$, respectively.

In the case of $0 < v_f < v_{AH}$, the singularity is timelike and a Penrose diagram of the gravitational collapse is shown in Fig. 1 (2). In the case of $v_f \geq v_{AH}$, the singularity is timelike for $0 < v < v_{AH}$. For $0 < v_f \leq v_{AH}$, the singularity is always globally naked. In the case of $v_f > v_{AH}$, the singularity can be globally naked if $v_f \simeq v_{AH}$. The possible Penrose diagrams are depicted in Fig. 1 (3) or (4) for $v_f > v_{AH}$ and in Fig. 1 (5) or (6) for $v_f = v_{AH}$.

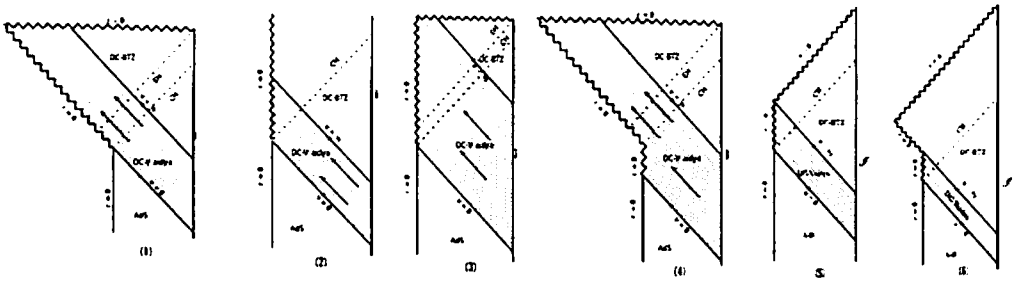

Figure 1: Possible Penrose diagrams

4 Strength of naked singularities

In this section, we investigate the strength of naked singularities along the radial null geodesics. We calculate

$$\psi \equiv R_{\mu\nu}k^\mu k^\nu = -\frac{2(D-2)\dot{f}}{rf^2}(k^r)^2, \tag{6}$$

where $k^\mu = dx^\mu/d\lambda$. In four dimensions, the strong curvature condition and the limiting focusing condition are satisfied along an affinely parametrized geodesic if $\lim_{\lambda\to 0}\lambda^2\psi > 0$ and $\lim_{\lambda\to 0}\lambda\psi > 0$, respectively [10, 11]. W obtain

$$\lim_{\lambda\to 0}\lambda^2\psi = \frac{s_1(D-2)}{(1+s_1)^2} > 0 \qquad \text{for } q=1,\ D=2n \tag{7}$$

$$\lim_{\lambda\to 0}\lambda^{2(1-(q-1)/(D-2))}\psi = s_2(D-2) > 0, \qquad \text{for } q>1,\ D=2n \tag{8}$$

We next consider the odd dimensional case. For the singularity $r=0$ and $0<v<v_{AH}$, we find

$$\lim_{\lambda\to 0}\lambda\psi = s_3(D-2). \tag{9}$$

For the singularity $v=r=0$ in odd dimensions, we obtain

$$\lim_{\lambda\to 0}\lambda^{2(1-q/(D-1))}\psi = s_4(D-2). \tag{10}$$

It is emphasized that the strength depends both on the spacetime dimensions and the power of the mass function, except for the singularity $r=0$ and $0<v<v_{AH}$ in odd dimensions.

5 Conclusions and Discussions

We analyzed the $D(\geq 3)$-dimensional gravitational collapse of a null dust fluid in DC gravity. We supposed that (i) the power-law mass function $M(v) = M_0 v^q$, where $M_0 > 0$ and $q \geq 1$, and (ii) the null geodesics obey a power law near the singularity.

We found that globally naked singularities can be formed in DC gravity. Furthermore, the final states of the gravitational collapse differ substantially depending on whether the spacetime dimensions are odd or even. A massless ingoing null naked singularity can appear in the even-dimensional case for $1 \leq q < D-1$. In the odd-dimensional case, on the other hand, a massive timelike naked singularity is formed for any $q(\geq 1)$. These naked singularities can be globally naked. As a result, the formation of a naked singularity cannot be avoided in DC gravity, nor in general relativity. In DC gravity, massive timelike singularities appear in odd dimensions. The formation of a massive timelike singularity in odd dimensions is considered to be a characteristic feature in Lovelock gravity.

We also investigated the strength of naked singularities. The strength of the naked singularity at $v=r=0$ depends on D and q both in odd and even dimensions. In contrast, around the massive timelike singularity at $r=0$ and $0<v<v_{AH}$ in odd dimensions, ψ diverges as λ^{-1}, independent of D or q. Massive timelike singularities diverging as λ^{-1} might be salient features in Lovelock gravity.

References

[1] S. W. Hawking and G. F. R. Ellis, *The large scale structure of space-time* (Cambridge University Press, 1973)

[2] R. Penrose, *Riv. Nuovo Cim.* 1, 252 (1969)

[3] R. Penrose, in *General Relativity, an Einstein Centenary Survey*, edited by S.W. Hawking and W. Israel (Cambridge University Press, Cambridge, England, 1979), p. 581.

[4] A. Lovelock, J. Math. Phys. 12 498 (1971)

[5] H. Maeda, gr-qc/0504028

[6] M. Bañados, C. Teitelboim and J. Zanelli, Phys. Rev. D. 49 975 (1994)

[7] R-G. Cai and K. Soh, Phys Rev. D. 59 044013 (1999)

[8] M. Nozawa and H. Maeda, gr-qc/0510070

[9] M. Bañados, C. Teitelboim and J. Zanelli, Phys. Rev. Lett. 69 1849 (1992)

[10] C. J. S. Clarke and K. Królak, J. Geom. Phys. 2 127 (1985)

[11] K. Królak, J. Math. Phys. 28 138 (1987)

Wronskian Formulation for the Spectrum of Curvature Perturbations

Shuichiro Yokoyama[1], Takahiro Tanaka[2], Misao Sasaki[3], Ewan. D. Stewart[4]

[1,2] *Department of Physics, Kyoto University, Kyoto 606-8502, Japan*
[3] *Yukawa Institute for Theoretical Physics, Kyoto University, Kyoto 606-8502, Japan*
[4] *Department of Physics, KAIST, Daejeon 305-701, Republic of Korea*

Abstract

We reformulate the evaluation of the initial spectrum of curvature perturbations generated during multi-scalar inflation. We point out that we can easily and systematically construct a unified formulation by using the fact that the Wronskian is constant.

1 Introduction

In the inflationary universe, curvature perturbations, which seed the structure formation of the universe, are generated from vacuum fluctuations of the scalar field. One can test various models of inflation, by comparing the theoretical prediction for the spectrum of curvature perturbations with observations.

In making realistic models of inflation based on supersymmetry and supergravity theories, it seems more natural to consider models composed of multi-component scalar field, in which the slow-roll conditions are also possibly violated. In order to identify necessary conditions for viable models of inflation among various proposed possibilities, any simple and sufficiently accurate formula for the spectrum is useful, especially if the formula is applicable to a wide class of models.

For multi-component inflation, evaluating the curvature perturbations is a more difficult issue in comparison with single-component inflation [3, 4, 5]. Generally, in the case of a D-component field, the evolution equations for the perturbations are D coupled second order differential equations. It is a heavy task to solve the full set of equations. However, in the estimation of the spectrum, what we need is only the final value of the curvature perturbation $\mathcal{R}_c(\eta_f)$. Here, η is a conformal time given by $\eta = \int dt/a$, and η_f is taken sufficiently late after the convergence of the background trajectories. So, if we can identify the part of perturbations that contributes to $\mathcal{R}_c(\eta_f)$, we may solve only that part to obtain its value without solving the full set of perturbation equations. The δN formalism [5] was based on this idea. This formulation was developed based on the fact that the perturbation of $e-$folding number stays roughly constant in the flat slicing on super-horizon scales. In a new δN formalism [6] which we have developed, we derived a perturbation equation for a single projected component of scalar field corresponding to the perturbation of $e-$folding number. The derivation of the new δN formalism is rather intuitive in this sense, which helps its physical meaning rather transparent. As a drawback, however, the derivation of the formula is not so simple. Moreover, in this formula, we have neglected the super-horizon contributions pointed out in Ref. [1].

Here we propose alternative slightly different framework to evaluate the evolution of perturbations of a multi-component scalar field. The method we will discuss in this paper takes full advantage of the fact that the Wronskian stays constant.

2 Use of Wronskian

We consider a D-component scalar field, ϕ^α $(\alpha = 1, 2, \cdots, D)$. The evolution equations for the scalar field perturbations on flat slicing, $\delta\phi^\alpha_F$, are represented as an equation which formally takes the form of

$$\left[\partial_\eta^2 + Q(\eta) + k^2\right]\varphi^\alpha = P^\alpha_\beta(\eta)\varphi^\beta, \tag{1}$$

[1] E-mail:shu@tap.scphys.kyoto-u.ac.jp

where $\varphi^\alpha \equiv a\delta\phi^\alpha_F$, and P^α_β symmetric with respect to the indices α and β. The Wronskian

$$W(\boldsymbol{n}, \boldsymbol{\varphi}) \equiv \boldsymbol{n}' \cdot \boldsymbol{\varphi} - \boldsymbol{n} \cdot \boldsymbol{\varphi}', \tag{2}$$

introduced in a usual manner is constant if $\boldsymbol{n}$ and $\boldsymbol{\varphi}$ are solutions of Eq. (1). Here we used vector notation $\boldsymbol{n}$ and $\boldsymbol{\varphi}$ to represent n^α and φ^α for brevity and $\boldsymbol{n} \cdot \boldsymbol{\varphi} \equiv \delta_{\alpha\beta} n^\alpha \varphi^\beta$.

In the general multi-component models, the background trajectories in the phase space of the multi-component scalar field well converge to a single one after which the background universe undergoes a universal evolution and the only remaining modes of scalar-type perturbations are adiabatic ones. It is known that at this stage $\mathcal{R}_c$ becomes constant in time on super-horizon scales [5]. In such cases we may use the constancy of δN on super-horizon scales. The δN formalism [5] is a very useful tool to evaluate the evolution of perturbations for multi-component inflation models. It tells us that the final value of the curvature perturbation, $\mathcal{R}_c(\eta_f)$ is given by $\delta\mathcal{N}(\eta_f, \eta_i)$, the perturbation in the e-folding number between the initial flat hypersurface at $\eta = \eta_i$ during inflation and the final comoving hypersurface at $\eta = \eta_f$. Then we have

$$\mathcal{R}_c(\eta_f) \approx -\delta N(\eta_i) = W(\boldsymbol{n}, \boldsymbol{\varphi})\big|_{\eta_i}, \tag{3}$$

with the boundary conditions at $\eta = \eta_i$ for $\boldsymbol{n}$;

$$n^{\alpha\prime} = \delta^{\alpha\beta}\left(-\frac{1}{a}\frac{\partial N}{\partial\phi^\beta} + \frac{\mathcal{H}}{a}\frac{\partial N}{\partial\phi^{\beta\prime}}\right), \qquad n^\alpha = \delta^{\alpha\beta}\frac{1}{a}\frac{\partial N}{\partial\phi^{\beta\prime}}. \tag{4}$$

Since the Wronskian is constant, it can be evaluated at any time. Therefore, once $\boldsymbol{n}$ is solved backward in time until the wavelength of the mode is well inside the horizon scale, we do not have to evolve $\boldsymbol{\varphi}$ at all in the forward direction. This will be advantageous in the case of multi-component field. In order to solve $\boldsymbol{\varphi}$ in the forward direction, we need to solve all $2D$ independent modes, where D is the number of species. In contrast, to evolve $\boldsymbol{n}$ backward in time, we only need to solve a single mode. Hence, the advantage of solving $\boldsymbol{n}$ instead of $\boldsymbol{\varphi}$ becomes prominent as the number of species increases. An extreme example is the models with extra-dimensions [7]. Since D is infinite in the brane world models, solving for all $\boldsymbol{\varphi}$ is impossible and numerical integration is necessary.

3 Extended general slow-roll formula

Even if we use the Wronskian method, we still need to solve $\boldsymbol{n}$ backward for each k^2. However, we can avoid solving $\boldsymbol{n}$ for each value of k^2 in the long wavelength limit. In this limit, we can find solution for $\boldsymbol{n}$ in the series expansion with respect to k^2. Of course, this approximation does not hold when the wavelength becomes shorter than the horizon scale. For the evolution before the horizon crossing, one may use the slow-roll approximation or the more general formula called general slow-roll developed by Stewart[2]. By using these approximations , we can evaluate the evolution of mode function to a large extent analytically.

However, in the original slow-roll or general slow-roll formula [2, 6], one assume no contribution on the super-horizon scales i.e., in these formulae, we cannot take into account super-horizon effects which is pointed out in Ref. [1].

Then, in order to take in super-horizon effects, one may naturally think of matching two approximation at an appropriate time $\eta = \eta_*$ where the mode is already well outside the horizon scale but the slow-roll or the general slow-roll conditions are still maintained. However, the matching does not seem to be so trivial since the solutions in the long wavelength approximation look quite different from those in the slow-roll or the general slow-roll approximation.

As an application of the Wronskian method, we consider this matching problem. The goal of this section is to obtain an improved general slow-roll formula. Since the Wronskian W is constant in time, it is allowed to be evaluated at $\eta = \eta_*$. If we know both $\boldsymbol{\varphi}$ and $\boldsymbol{n}$ at $\eta = \eta_*$, what we have to do is simply to compute $W(\boldsymbol{n}, \boldsymbol{\varphi})$ there. Then we can avoid the messy computation for explicitly matching solutions obtained in the two different approximation schemes term by term. To obtain $\boldsymbol{\varphi}$ and $\boldsymbol{n}$ at $\eta = \eta_*$, we evolve $\boldsymbol{\varphi}$ in the forward time direction by using the general slow-roll approximation, while $\boldsymbol{n}$ in the backward direction by using the long wavelength approximation.

3.1 Evaluation of Wronskian

Here we mean that $max(P^{\alpha}_{\beta})$ is small by "the general slow-roll condition" as a simple generalization to the multi-component case. We write the solution solved in the forward direction in an expansion with respect to $\boldsymbol{P}$, which is $P^{\alpha}_{\beta}(\eta)$ in matrix notation, as

$$\varphi = \Delta\varphi_{(0)} + \Delta\varphi_{(1)} + \cdots, \tag{5}$$

where $\Delta\varphi_{(p)}$ is the correction of $O(\boldsymbol{P}^p)$. We also introduce variables $\varphi_{(p)} \equiv \sum_{j=0}^{p} \Delta\varphi_{(j)}$.

Using the Green's function method, to the first order in $\boldsymbol{P}$ and to the q-th order in k^2, we have

$$\begin{aligned}
\mathcal{R}^{(q)}_{(1)} &\equiv W(\boldsymbol{n}^{(q)}, \varphi_{(1)})|_{\eta_*} = \boldsymbol{n}^{(q)'} \cdot \varphi_{(1)} - \boldsymbol{n}^{(q)} \cdot \varphi_{(1)}{}' \\
&= W(\boldsymbol{n}^{(q)}, \varphi_{(0)})|_{\eta_*} + \Pi\Big[W(\boldsymbol{n}^{(q)}, u_0)|_{\eta_*} \int_{-\infty}^{\eta_*} d\eta' u_0^*(\eta')\boldsymbol{P}(\eta')\varphi_{(0)}(\eta') \\
&\qquad - W(\boldsymbol{n}^{(q)}, u_0^*)|_{\eta_*} \int_{-\infty}^{\eta_*} d\eta' u_0(\eta')\boldsymbol{P}(\eta')\varphi_{(0)}(\eta')\Big],
\end{aligned} \tag{6}$$

where $\Pi = W(u_0, u_0^*)^{-1}$, and $u_0(\eta)$ is a solution of $(\partial_\eta^2 + Q(\eta) + k^2)u_0 = 0$. Here $f^{(q)}$ means the truncation of the function f at $O(k^{2q})$.

Considering to compare our formula with the standard slow-rll formula, it is worthwhile to obtain a formula in which the leading term is evaluated not at η_* but at η_k. The above formula, Eq. (6), still contains an ambiguous choice of the matching time η_*. Although the expression is rather independent of the choice of η_*, we cannot simply replace it with η_k, which is the time of the horizon crossing since the long wavelength approximation is not valid at $\eta = \eta_k$.

Thus to the first order in $\boldsymbol{P}$ and to the q-th order in k^2, the power spectrum, that is, expectation value of $|\mathcal{R}|^2$ will be evaluated as

$$\begin{aligned}
\mathcal{P}_{\mathcal{R}} \sim \langle|\mathcal{R}|^2\rangle^{(q)}_{(1)} &= \Bigg[|\Phi|^2 + 4i\Pi \int_{-\infty}^{\eta_*} d\eta' \Big\{ \mathrm{Im}\,[\tilde{u}_0^*(\eta')\Phi] \cdot \boldsymbol{P}(\eta')\mathrm{Re}\,[\tilde{u}_0^*(\eta')\Phi] \\
&\qquad - \theta(\eta' - \eta_k)\mathrm{Im}\,[u_0^*(\eta')\Phi] \cdot \boldsymbol{P}(\eta')\mathrm{Re}\,[u_0^*(\eta')\Phi] \Big\}\Bigg]^{(q)} + \mathcal{O}(\boldsymbol{P}^2),
\end{aligned} \tag{7}$$

where $\Phi \equiv [W(n, u_0)]_{\eta_k}$, and we should remind that Π is a pure imaginary number. Here the function with tilde $\tilde{f}$ means that we keep the original form of the function f without expanding it in powers of k^2, namely, $\tilde{f}^{(q)} = f$. This expression still contains η_* but the integrand takes the form of $f - \theta(\eta - \eta_k)f^{(q)}$. Therefore all the terms up to $O(k^{2q})$ cancel, and hence the integrand shows improved fall off at $\eta \to 0$. As a result, even if fall off of $\boldsymbol{P}$ in the limit $\eta \to 0$ is not very fast, we may be allowed to set η_* to 0. In this sense, the independence from the choice of η_* is more manifest in Eq. (7).

3.2 Extension to the higher order in general slow-roll expansion

The extension to the higher order in $\boldsymbol{P}$ is rather straightforward in our formulation.

$\mathcal{R}$ including higher order corrections up to $O(\boldsymbol{P}^p, k^{2q})$ is given by

$$\mathcal{R}^{(q)}_{(p)} = \sum_{j=0}^{p} \Delta\mathcal{R}^{(q)}_{(j)}, \tag{8}$$

with

$$\begin{aligned}
&\Delta\mathcal{R}^{(q)}_{(0)} \equiv \left[W(\boldsymbol{n}, \varphi_{(0)})\right]^{(q)}_{\eta_k}, \qquad \Delta\mathcal{R}^{(q)}_{(1)} \equiv \hat{\mathcal{R}}[\varphi_{(0)}]^{(q)}, \qquad \Delta\mathcal{R}^{(q)}_{(2)} \equiv \hat{\mathcal{R}}\left[\Delta\hat{\varphi}[\varphi_{(0)}]\right]^{(q)}, \\
&\Delta\mathcal{R}^{(q)}_{(3)} \equiv \hat{\mathcal{R}}\left[\Delta\hat{\varphi}[\Delta\hat{\varphi}[\varphi_{(0)}]]\right]^{(q)}, \qquad \cdots,
\end{aligned} \tag{9}$$

where

$$\hat{\mathcal{R}}[\varphi] \equiv \Pi\Big\{ W(\boldsymbol{n}, u_0) \int_{-\infty}^{\eta_*} d\eta' \boldsymbol{P}(\eta') \left[\tilde{u}_0^*(\eta')\tilde{\varphi}(\eta') - \theta(\eta' - \eta_k) u_0^*(\eta')\varphi(\eta')\right] - W(\boldsymbol{n}, u_0^*) \int_{-\infty}^{\eta_*} d\eta' \boldsymbol{P}(\eta') \left[\tilde{u}_0(\eta')\tilde{\varphi}(\eta') - \theta(\eta' - \eta_k) u_0(\eta')\varphi(\eta')\right] \Big\}_{\eta_k},$$

$$\Delta\hat{\varphi}[\varphi](\eta) \equiv \Pi\Big\{ u_0(\eta) \int_{-\infty}^{\eta_*} d\eta' \boldsymbol{P}(\eta') \left[\tilde{u}_0^*(\eta')\tilde{\varphi}(\eta') - \theta(\eta' - \eta) u_0^*(\eta')\varphi(\eta')\right] - u_0^*(\eta) \int_{-\infty}^{\eta_*} d\eta' \boldsymbol{P}(\eta') \left[\tilde{u}_0(\eta')\tilde{\varphi}(\eta') - \theta(\eta' - \eta) u_0(\eta')\varphi(\eta')\right] \Big\}. \tag{10}$$

4 Summary

We have proposed a new formulation for systematic derivation of formulas for the spectrum of the curvature perturbations from multi-component inflation. First we discussed the advantage of using the fact that the Wronskian W is constant in time. Using this fact, the problem of evaluating the curvature perturbation at the end of inflation can be easily shown to be equivalent to solving a single "decaying" mode backward in time.

As an example to show the efficiency of this new approach, we have shown a quick derivation of an improved general slow-roll formula, whose original form was obtained in Ref. [2]. The improvement that was done here is to take into account the merit of the long-wavelength approximation for the late time evolution after the horizon crossing pointed out in Ref. [1]. In Ref. [2] or [6], we assumed the extra assumption that we neglect the super-horizon effects. while here we can take into account the super-horizon effects using the long wavelength approximation for the evolution on super-horizon scales. The matching of two approximations has been easily performed by using the constancy of the Wronskian. We also extended the general slow-roll formula to multi component case, though the way of extension presented here may not be completely satisfactory. A different way of extension which avoids some of limitations of our present approach will be discussed in our future publication.

References

[1] S. M. Leach, M. Sasaki, D. Wands and A. R. Liddle, Phys. Rev. D **64**, 023512 (2001).

[2] E. D. Stewart, Phys. Rev. D **65**, 103508 (2002),
J. Choe, J. O. Gong and E. D. Stewart, JCAP **0407**, 012 (2004).

[3] K. A. Malik and D. Wands, Phys. Rev. D **59**, 123501 (1999).
C. Gordon, D. Wands, B. A. Bassett and R. Maartens, Phys. Rev. D **63**, 023506 (2001).

[4] T. T. Nakamura and E. D. Stewart, Phys. Lett. B **381**, 413 (1996).

[5] M. Sasaki and E. D. Stewart, Prog. Theor. Phys. **95**, 71 (1996).
M. Sasaki and T. Tanaka, Prog. Theor. Phys. **99**, 763 (1998).

[6] H. C. Lee, M. Sasaki, E. D. Stewart, T. Tanaka and S. Yokoyama, JCAP **0510**, 004 (2005)

[7] D. S. Gorbunov, V. A. Rubakov and S. M. Sibiryakov, JHEP **0110**, 015 (2001).
T. Kobayashi and T. Tanaka, arXiv:hep-th/0511186.

Thermodynamics of Kaluza-Klein black holes

Yasunari Kurita[1], Hideki Ishihara[2]

[1] *Yukawa Institute for Theoretical Physics, Kyoto University, Kyoto 606-8502, Japan*
[2] *Department of Physics, Osaka City University, Osaka 558-8585, Japan*

Abstract

We investigate thermodynamics of 5-dimensional black hole with a compact extra-dimension. Using Euclidean formulation, we obtain thermodynamic quantities for the black hole solution and find a non-trivial work term.

1 Introduction

Recently, Ishihara and Matsuno studied spacetime structure of charged static black holes in five-dimensional Einstein-Maxwell theory[1]. The black hole has one or two horizons in the shape of squashed S^3. At the spatial infinity, the spacetime looks like a twisted S^1 bundle over four-dimensional flat spacetime. The size of S^1 is asymptotically constant. Then, we call the black holes Kaluza-Klein black holes.

Black hole is thermodynamic object because it radiates Hawking radiation[2]. This property does not depend on details of spacetime geometry but only on the existence of horizon. Thus, it is natural to think that black hole obeys thermodynamic law even when the spacetime is deformed or squashed, like Kaluza-Klein black holes here.

The Kaluza-Klein black holes solution has three parameters which characterize mass, electric charge and squashing of the spacetime. Thus, it is natural to consider that thermodynamic quantities include some thermodynamic variables representing the squashing. In this paper, we consider vacuum solutions for simplicity and find thermodynamic quantities including non-trivial work term representing squashing spacetime by using Euclidean formulation for black hole thermodynamics.

The paper is organized as follows: in the next section, we give a brief description for the Kaluza-Klein black holes and some properties of the spacetime. In section 3, we discuss its thermodynamic quantities and obtain a work term corresponding to squashing the spacetime. Finally, section 4 is devoted to summary and discussion.

2 The solution

In this section, we give a brief description of the black hole solution we consider here. It is a five-dimensional vacuum solution of Einstein gravity, whose metric is

$$
\begin{aligned}
ds^2 &= -f(r)dt^2 + \frac{k(r)^2}{f(r)}dr^2 + \frac{r^2}{4}\left[k(r)d\Omega_{S^2}^2 + \chi^2\right], \qquad (1)\\
& f(r) = 1 - \frac{r_g^2}{r^2}, \quad k(r) = \frac{(r_\infty^2 - r_g^2)r_\infty^2}{(r_\infty^2 - r^2)^2},\\
& d\Omega_{S^2}^2 = d\theta^2 + \sin\theta^2 d\phi^2, \quad \chi = d\psi + \cos\theta d\phi.
\end{aligned}
$$

The black hole horizon is at $r = r_g$, whose topology is S^3. The solution is parametrized by r_g and r_∞.

A time slice of the spacetime is foliated by three-dimensional surfaces $r = R$, say Σ_R. Each surface Σ_R has the shape of squashed S^3. Usually, three sphere S^3 can be thought of as twisted S^1 fiber over S^2 base space, and the aspect ratio of the size of S^2 base space to S^1 fiber is unity. The surface Σ_R also has such a geometrical structure. However, the aspect ratio of S^2 base space to S^1 fiber is not unity but the function $k(R)$. If one consider the limit $r_\infty \to \infty$, then $k(r) \to 1$, and thus the surface Σ_R becomes S^3 and the spacetime becomes the 5-dimensional Schwarzschild spacetime.

[1] E-mail:kurita@yukawa.kyoto-u.ac.jp
[2] E-mail:ishihara@sci.osaka-cu.ac.jp

The apparent singularity at $r = r_\infty$ is spatial infinity, where the volume of the surface Σ_R diverges because the function $k(r)$ takes the value of zero. The spacetime asymptotes to a twisted S^1 fiber bundle over four-dimensional Minkowski spacetime. To see this, let us change coordinate as follows:

$$\rho := \rho_0 \frac{r^2}{r_\infty^2 - r^2}, \quad \rho_0 := \frac{z\, r_\infty}{2}, \quad z := \sqrt{f(r_\infty)}. \tag{2}$$

Then, in the limit $\rho \to \infty$ ($r \to r_\infty$), the metric approaches

$$ds^2 = -dT^2 + d\rho^2 + \rho^2 d\Omega_{S^2}^2 + \frac{r_\infty^2}{4}\chi^2, \quad T := zt. \tag{3}$$

From the above metric, we can see that the parameter r_∞ represents the size of S^1 at spatial infinity.

As is other black hole spacetimes, this black hole has no horizon limit; $r_g \to 0$. Then, the solution reduces to the Gross-Perry-Sorkin monopole solution[3][4]. It is a 5-dimensional vacuum solution of Einstein gravity while, in four-dimensional point of view, it looks like a monopole solution in the sense of Kaluza-Klein theory. We call this solution as GPS monopole spacetime.

3 Thermodynamic quantities

In this section, we apply Euclidean formulation to obtain thermodynamic quantities of the black hole. Euclidean formulation gives some statistical mechanical basis for black hole thermodynamics and is based on semi-classical approximation of Euclidean path integral for metric field;

$$Z = \int \mathcal{D}g \exp\left(-\hat{I}[g]\right) \approx \exp[-I], \tag{4}$$

where integral is taken for the field having Euclidean time periodicity $\tau \sim \tau + \beta$ and β is thought of as the inverse of temperature. $\hat{I}$ is a Euclidean action for the system and I is the classical action of the solution. This is the partition function of the system at temperature β^{-1}, and free energy is given as

$$G = -\frac{1}{\beta}\log Z \approx \frac{I}{\beta}. \tag{5}$$

We can obtain thermodynamic quantities from free energy by using thermodynamic relation.

The Euclidean action of 5-dimensional Einstein gravity is

$$I = -\frac{1}{16\pi G}\int_M R\sqrt{g}d^5x - \frac{1}{8\pi G}\int_{\partial M} K\sqrt{h}d^4x, \tag{6}$$

where the second term is so-called Gibbons-Hawking term [5]. Here, we consider a vacuum solution and thus, its Ricci scalar equals zero, then only the second term contribute to the classical action. We set the boundary ∂M at $r = R$ and we take the limit $R \to r_\infty$ after evaluation. The classical action for the Kaluza-Klein black hole is

$$I = -\frac{\pi\Delta\tau}{4G}\left[\frac{1}{r_\infty - R}\frac{(r_\infty^2 + R^2)(R^2 - r_g^2)}{r_\infty} + \frac{(r_\infty^2 + R^2)(R^2 - r_g^2)}{(r_\infty + R)r_\infty} + R^2\right], \tag{7}$$

where $\Delta\tau$ is the period of Euclidean time determined by the regularity at the horizon as follows:

$$\Delta\tau = 2\pi r_g \frac{r_\infty^2}{r_\infty^2 - r_g^2}. \tag{8}$$

We can see that the classical action I diverges in the limit $R \to r_\infty$. Thus, in order to obtain physical free energy, some regularization is needed[3].

[3]Such a regularization is almost always necesssary. However, as far as we know, the only exceptional case is lower-dimensioanl brane world black holes. For details, see Kudoh and Kurita [6].

Now, we take GPS monopole solution as a background spacetime and regularize the classical action by the background subtraction method. The action of GPS monopole solution having the same temperature and squashing at the boundary is

$$I_{GPS} = -\frac{\pi\Delta\tau}{4G}\sqrt{f(R)}\left[R^2 + 2\frac{(2\sqrt{f_\infty}-1)r_\infty^2 + R^2}{r_\infty^2 - R^2}\right] \tag{9}$$

Then the classical Euclidean action of Kaluza-Klein Black hole on the GPS monopole background is

$$I - I_{GPS} = \frac{\pi^2}{2G}\frac{1-z}{z^2}r_g r_\infty^2 + \mathcal{O}(r_\infty - R) \tag{10}$$

This remains finite in the limit $R \to r_\infty$ and the classical action is regularized.

We can easily calculate Hawking temperature of the black hole as

$$T = \beta^{-1} = \frac{z}{2\pi r_g}, \tag{11}$$

which can be obtained both from surface gravity and from regularity of Euclidean section at the horizon. The free energy of the Kaluza-Klein black hole on the GPS background can be calculated as

$$G = \frac{I - I_{GPS}}{\beta} = \frac{\pi}{4G}\frac{1-z}{z}r_\infty^2 \tag{12}$$

Here we assume that entropy is given by Beckenstein-Hawking formula, and we take Komar mass as the thermodynamic mass as follows:

$$S = \frac{A}{4G} = \frac{\pi^2}{2G}\frac{r_g^3}{z}, \quad M = \frac{3\pi}{8G}\frac{r_g}{z}. \tag{13}$$

Using these quantities, we can evaluate the following quantity:

$$G - M + TS = \frac{\pi}{8G}r_\infty^2\frac{(1-z)^2}{z} \neq 0, \tag{14}$$

which means that there is some unknown term. In ideal gas system, the above non-zero value should be $-PV$ where P is pressure and V is volume of the system. The unknown term can be interpreted as a work term concerning squashing the spacetime.

We set unknown variables as X and Y. These variables can be determined up to constant by the following thermodynamic relations:

$$XY = \frac{\pi}{8G}r_\infty^2\frac{(1-z)^2}{z}, \quad \left(\frac{\partial G}{\partial \beta}\right)_X = \frac{S}{\beta^2}, \quad \left(\frac{\partial G}{\partial X}\right)_\beta = Y. \tag{15}$$

After a brief calculation, we obtain the thermodynamic quantities as

$$X = Cr_\infty^2, \quad Y = \frac{1}{8\pi C}\frac{(1-z)^2}{z}, \tag{16}$$

where C is a constant. Note that the quantity X depends only on the parameter r_∞ which represent the size of extra-dimension and squashing of the spacetime.

4 Summary and Discussion

In this paper, we investigate thermodynamic quantities of Kaluza-Klein black holes whose metric is given by eq. (1). In the frame work of Euclidean formulation, we obtain new thermodynamic quantities corresponding to squashing of the spacetime.

In order to obtain some property of thermodynamic variables X and Y, 5-dimensional Schwarzschild limit ($r_\infty \to \infty$) may be helpful. In this limit, these variables behave as $X \to \infty$, $Y \to 0$ and $XY \to 0$.

The variable X depends only on r_∞, and we may interpret X as volume and Y as pressure in analogy with the work term in ideal gas system. If it is true, the spherically symmetric limit is something like infinite volume and zero pressure limit.

The free energy is monotonically increasing function of X and takes the maximum value in the Schwarzschild limit $X \to \infty$. However we can not say that 5-dimensional Schwarzschild black hole is thermodynamically unstable for two reasons. Firstly, the free energy evaluated in this paper is relative quantity of Kaluza-Klein black holes to GPS monopole background, and it is not definite value determined only by the black hole. The second reason is that the heat capacity of the black holes is negative as is the case of Schwarzschild black hole, and they are thermodynamically unstable in a heat bath. In canonical ensemble, GPS monopole spacetime will be only a stable state in these solutions.

In isolated system, the direction of thermodynamic change of state is usually determined by the direction of increasing entropy. In this case, Beckenstein-Hawking entropy takes its minimum value at 5-dimensional Schwarzschild case. This means, even in isolated system, 5-dimensional Schwarzschild is the most unstable state. Of cause, in order to make a 5-dimensional Schwarzschild black hole to a Kaluza-Klein one, asymptotic structure has to be deformed and infinite energy will be needed. Thus, such a thermodynamic instability should not be considered seriously.

There is an open question. How can we determine the constant C in the thermodynamic variables X and Y? The situation is similar to the case of determination of black hole temperature and entropy. In that case, Hawking radiation determined the coefficient of surface gravity, and entropy was determined as horizon area over $4G$. Also in this case, in order to determine the coefficient C, another input such as Hawking radiation is wanted. This is an interesting subject for future study.

5 Acknowledgments

YK thanks to the Yukawa memorial foundation for its support.

References

[1] H. Ishihara and K. Matsuno, hep-th/0510094

[2] S. W. Hawking, Commun. Math. Phys. **43**, 199 (1975) [Erratum-ibid. **46**, 206 (1976)].

[3] D. J. Gross and M. J. Perry, Nucl. Phys. B **226**, 29 (1983)

[4] R. Sorkin, Phys. Rev. Lett. **51**, 87 (1983)

[5] G. W. Gibbons and S. W. Hawking, Phys. Rev. D **15**, 2752 (1977).

[6] H. Kudoh and Y. Kurita, Phys. Rev. D **70**, 084029 (2004) [arXiv:gr-qc/0406107].

Second order gauge invariant perturbation theory and cosmological perturbations

Kouji Nakamura[1]

Department of Astronomical Science, the Graduate University for Advanced Studies, Osawa, Mitaka, Tokyo 181-8588, Japan.

Abstract

The general framework of the second order gauge invariant perturbation theory in the papers [K. Nakamura, Prog. Theor. Phys. **110** (2003), 723; *ibid* **113** (2005), 481.] is reviewed through the application to the cosmological perturbation theory. We define the complete set of the gauge invariant variables of the second order cosmological perturbations in the Friedmann-Robertson-Walker universe filled with perfect fluid. We also discuss the second order Einstein equations of cosmological perturbations in terms of these gauge invariant variables without any gauge fixing.

The general relativistic cosmological *linear* perturbation theory is has been developed to a high degree of sophistication during the last 25 years[1]. The motivation of this development is to clarify the relation between the scenarios of the early Universe and cosmological data such as the cosmic microwave background anisotropies.

With the increase of precision of the CMB data, the study of relativistic cosmological perturbations beyond linear order is becoming a topical subject, especially to study primordial non-Gaussianity[2]. Since the general framework of the *second order* gauge invariant perturbation theory on the generic background spacetime is recently developed[3] by the present author, it is interesting to apply this general framework to cosmological perturbations.

In this article, we briefly review this general formulation through the application to cosmological perturbation theory. We define the complete set of the gauge invariant variables of the second order cosmological perturbations in the Friedmann-Robertson-Walker universe filled with perfect fluid. We also discuss the second order Einstein equations of cosmological perturbations in terms of these gauge invariant variables without any gauge fixing.

In any perturbation theories, we always keep in mind two spacetimes $\mathcal{M}$ and $\mathcal{M}_0$. $\mathcal{M}$ is the physical spacetime which we want to describe by the perturbative analyses, and $\mathcal{M}_0$ is the background spacetime which is prepared for the analyses of perturbations by us. As pointed out by Stewart et al.[4], the "*gauge choice*" in perturbation theories is a point identification map $\mathcal{X}$ between these two spacetimes $\mathcal{M}_0$ and $\mathcal{M}$. This point identification is implicitly done through the equation $Q(\text{“}p\text{”}) = Q_0(p) + \delta Q(p)$ which is always written in the perturbation theory. It is important to note that this gauge choice $\mathcal{X} : \mathcal{M}_0 \to \mathcal{M}$ is not unique when we impose general covariance on the theory. Rather, we should regard that there is the degree of freedom corresponding to the choice of the map $\mathcal{X}$. The "*gauge transformation*" is simply regarded as the change $\mathcal{X} \to \mathcal{Y}$ of the gauge choice. Any physical variable Q on the physical spacetime $\mathcal{M}$ are pulled back into the background spacetime $\mathcal{M}_0$ by each gauge choice $\mathcal{X}$ and $\mathcal{Y}$ and the pulled back variables are transformed by $\Phi^* := \left(\mathcal{X}^{-1} \circ \mathcal{Y}\right)^*$ if we change the gauge choice from $\mathcal{X}$ to $\mathcal{Y}$. This is the gauge transformation of the perturbed variables.

Following to this basic understanding of the *gauge* in perturbation theory, the general form of the Taylor expansion and the gauge transformation rules of higher order perturbations are developed by Bruni et al.[5]. According to their development, when we change the gauge choice from $\mathcal{X}$ to $\mathcal{Y}$, the first and the second order perturbations are transformed as

$$ {}^{(1)}_{\mathcal{Y}}Q - {}^{(1)}_{\mathcal{X}}Q = \pounds_{\xi_{(1)}} Q_0, \quad {}^{(2)}_{\mathcal{Y}}Q - {}^{(2)}_{\mathcal{X}}Q = 2\pounds_{\xi_{(1)}} {}^{(1)}_{\mathcal{X}}Q + \left\{ \pounds_{\xi_{(2)}} + \pounds^2_{\xi_{(1)}} \right\} Q_0, \tag{1} $$

respectively. In these transformation rules, the field Q on the physical spacetime $\mathcal{M}$ is pulled-back to the background spacetime $\mathcal{M}_0$ as $\mathcal{X}^*Q$ and $\mathcal{Y}^*Q$ by two different gauge choices $\mathcal{X}$ and $\mathcal{Y}$, respectively, $\mathcal{X}^*Q$

[1] E-mail:kouchan@th.nao.ac.jp

and $\mathcal{Y}^*Q$ are expanded so that $\mathcal{X}^*Q = \sum_{k=0}^{\infty} \frac{\lambda^k}{k!} {}^{(k)}_{\mathcal{X}}Q$, $\mathcal{Y}^*Q = \sum_{k=0}^{\infty} \frac{\lambda^k}{k!} {}^{(k)}_{\mathcal{Y}}Q$, and λ is the infinitesimal parameter for the perturbation. $\xi_{(1)}$ and $\xi_{(2)}$ are generators associated with the gauge transformation $\Phi := \mathcal{X}^{-1} \circ \mathcal{Y}$. The arbitrariness of the gauge choice $\mathcal{X}$ or $\mathcal{Y}$ is given as the arbitrariness of the generators $\xi_{(1)}$ and $\xi_{(2)}$. These gauge transformation rules are easily extended to the case of the higher order and *multi*-parameter perturbations[3, 5].

Inspecting the above gauge transformation rules, we can define the gauge invariant variables for perturbations of the metric and the other matter fields[3]. The starting point of the general argument of the construction of gauge invariant variables is the following assumption : Suppose that we have already known the procedure to find a vector field ${}^{(1)}_{\mathcal{X}}X_a$ associated with the linear order metric perturbation ${}^{(1)}_{\mathcal{X}}h_{ab}$ which satisfies the properties

$$ {}^{(1)}_{\mathcal{Y}}X^a - {}^{(1)}_{\mathcal{X}}X^a = \xi^a_{(1)}, \quad {}^{(1)}_{\mathcal{X}}h_{ab} =: {}^{(1)}_{\mathcal{X}}\mathcal{H}_{ab} + \pounds_{{}^{(1)}_{\mathcal{X}}X} g_{ab}, \tag{2} $$

where g_{ab} is the metric on $\mathcal{M}_0$ and the metric $\bar{g}_{ab}$ on $\mathcal{M}$ is expanded in the form $\mathcal{X}^*\bar{g}_{ab} = \sum_{k=0}^{\infty} \frac{\lambda^k}{k!} {}^{(k)}_{\mathcal{X}}h_{ab}$, and ${}^{(0)}_{\mathcal{X}}h_{ab} = g_{ab}$. The first property in Eq.(2) is the gauge transformation rule of the vector field ${}^{(1)}_{\mathcal{X}}X^a$ under the gauge transformation $\Phi := \mathcal{X}^{-1} \circ \mathcal{Y}$, and the second property is regarded as the definition of the gauge invariant variable ${}^{(1)}_{\mathcal{X}}\mathcal{H}_{ab}$ of the liner order metric perturbation. Actually, from the gauge transformation rules (1) and (2), we can easily see that ${}^{(1)}_{\mathcal{X}}\mathcal{H}_{ab}$ is the gauge invariant part of the metric perturbation, i.e., ${}^{(1)}_{\mathcal{Y}}\mathcal{H}_{ab} - {}^{(1)}_{\mathcal{X}}\mathcal{H}_{ab} = 0$, and the vector field ${}^{(1)}_{\mathcal{X}}X^a$ is the gauge variant part of the metric perturbation. In the paper[3], it is shown that we can always find the gauge invariant variables for higher order metric perturbations and the perturbations of arbitrary matter fields other then metric.

This assumption is valid in the case of the cosmological perturbations. In this case, the metric on $\mathcal{M}_0$ is given by

$$ g_{ab} = a^2(\eta)\left((d\eta)_a(d\eta)_b + \gamma_{ij}(dx^i)_a(dx^i)_b\right), \tag{3} $$

where γ_{ij} is the metric on the maximally symmetric 3-space. The linear order metric perturbation on this background spacetime is decompose in the standard manner :

$$ \begin{aligned} &{}^{(1)}_{\mathcal{X}}h_{ab} =: h_{\eta\eta}(d\eta)_a(d\eta)_b + 2h_{\eta i}(d\eta)_{(a}(dx^i)_{b)} + h_{ij}(dx^i)_a(dx^i)_b, \\ &h_{\eta i} =: D_i h_{(VL)} + h_{(V)i}, \quad h_{ij} =: a^2 h_{(L)}\gamma_{ij} + a^2 h_{(T)ij}, \quad D^i h_{(V)i} = \gamma^{ij} h_{(T)ij} = 0, \\ &h_{(T)ij} =: \left(D_iD_j - \frac{1}{3}\gamma_{ij}\Delta\right) h_{(TL)} + 2D_{(i}h_{(TV)j)} + h_{(TT)ij}, \quad D_i h_{(TV)i} = 0 = D^i h_{(TT)ij}, \end{aligned} \tag{4} $$

where D_i is the covariant derivative associated with the metric γ_{ij}. Through this decomposition, we can easily find the above gauge variant part ${}^{(1)}X_a$ of the metric perturbation is given by

$$ {}^{(1)}X_a = \left(h_{(VL)} - \frac{1}{2}a^2\partial_\eta h_{(TL)}\right)(d\eta)_a + a^2\left(h_{(TV)} + \frac{1}{2}D_i h_{(TL)}\right)(dx^i)_a, \tag{5} $$

and the gauge invariant part of the metric perturbation takes the form

$$ \mathcal{H}_{ab} = a^2\left(-2\Phi(d\eta)_a(d\eta)_b + 2\nu_i(d\eta)_{(a}(dx^i)_{b)} + (-2\Psi\gamma_{ij} + \chi_{ij})(dx^i)_a(dx^j)_b\right), \tag{6} $$

where $D^i\nu_i = \gamma^{ij}\chi_{ij} = 0 = D^i\chi_{ij}$. Hence, we do know the procedure to find gauge invariant variables for the linear order metric perturbation.

According to the general procedure in the paper [3], we easily find the gauge invariant variables for the second order metric perturbation using the above procedure of the linear order. We show the general procedure in [3] in the case of cosmological perturbations. The gauge transformation rule of the second order metric perturbation is given by the second equation in Eqs.(1). Inspecting this gauge transformation rule, we define the variable

$$ {}^{(2)}\hat{H}_{ab} := {}^{(2)}h_{ab} - 2\pounds_{{}^{(1)}X}{}^{(1)}h_{ab} + \pounds^2_{{}^{(1)}X} g_{ab} \tag{7} $$

by using the liner order metric perturbations ${}^{(1)}X$ and ${}^{(1)}h_{ab}$. From the gauge transformation rule (1) and (2), we easily see that the variable ${}^{(2)}\hat{H}_{ab}$ is transformed as

$$ {}^{(2)}_{\mathcal{Y}}\hat{H}_{ab} - {}^{(2)}_{\mathcal{X}}\hat{H}_{ab} = \pounds_{\sigma_{(2)}} g_{ab}, \quad \sigma^a_{(2)} = \xi^a_{(2)} + \left[\xi_{(1)}, X\right]^a. \tag{8} $$

This transformation rule is same as that of the linear perturbation of the metric. Hence, using the above procedure of the decomposition of the linear order metric perturbation into the gauge invariant and variant parts, we can find tensor fields ${}^{(2)}_{\chi}\tilde{H}_{ab}$ so that

$$ {}^{(2)}_{\chi}\tilde{H}_{ab} =: {}^{(2)}_{\chi}\mathcal{H}_{ab} + \pounds_{(2)X} g_{ab}, \quad {}^{(2)}_{\mathcal{Y}}\mathcal{H}_{ab} - {}^{(2)}_{\chi}\mathcal{H}_{ab} = 0, \quad {}^{(2)}_{\mathcal{Y}}X_a - {}^{(2)}_{\chi}X_a = \sigma_{(2)a}, \tag{9} $$

i.e., ${}^{(2)}\mathcal{H}_{ab}$ is the gauge invariant part of the second order metric perturbation. As in the case of the first order metric perturbation, the components of the gauge invariant variable ${}^{(2)}\mathcal{H}_{ab}$ are given by

$$ {}^{(2)}\mathcal{H}_{ab} = a^2 \left(-2 \overset{(2)}{\Phi} (d\eta)_a (d\eta)_b + 2 \overset{(2)}{\nu_i} (d\eta)_{(a} (dx^i)_{b)} + \left(-2 \overset{(2)}{\Psi} \gamma_{ij} + \overset{(2)}{\chi_{ij}} \right) (dx^i)_a (dx^j)_b, \right) \tag{10} $$

where $D^i \overset{(2)}{\nu_i} = \gamma^{ij} \overset{(2)}{\chi_{ij}} = 0 = D^i \overset{(2)}{\chi_{ij}}$.

As showed in the paper [3], we also define the gauge invariant variables for the first and the second order pertrubation of an arbitrary matter field Q using the above vector field ${}^{(1)}X_a$ and ${}^{(2)}X_a$ as follows :

$$ {}^{(1)}Q := {}^{(1)}Q - \pounds_{(1)X} Q_0, \quad {}^{(2)}Q := {}^{(2)}Q - 2\pounds_{(1)X} Q_1 - \left\{ \pounds_{(2)X} - \pounds^2_{(1)X} \right\} Q_0. \tag{11} $$

We consider the perfect fluid as the matter field whose energy momentum tensor is given by

$$ \bar{T}_a{}^b = (\bar{\epsilon} + \bar{p})\, \bar{u}_a \bar{g}^{bc} \bar{u}_c + \bar{p} \delta_a{}^b. \tag{12} $$

We expand the fluid component $\bar{\epsilon}$, $\bar{p}$, $\bar{u}_a$ and the above energy momentum tensor so that

$$ \bar{\epsilon} = \sum_{k=0}^{\infty} \frac{\lambda^k}{k!} \overset{(k)}{\epsilon}{}_{,}, \quad \bar{p} = \sum_{k=0}^{\infty} \frac{\lambda^k}{k!} \overset{(k)}{p}{}_{,}, \quad \bar{u}_a = \sum_{k=0}^{\infty} \frac{\lambda^k}{k!} \overset{(k)}{(u_a)}, \quad \bar{T}_a{}^b = \sum_{k=0}^{\infty} \frac{\lambda^k}{k!} \overset{(k)}{(T_a{}^b)}. \tag{13} $$

Applying the general definitions (11) of the gauge invariant variables, gauge invariant variables of the first and the second order pertubation of the energy density $\bar{\epsilon}$ and the pressure $\bar{p}$, and the four velocity $\bar{u}_a$ are given by as follows:

$$ \begin{aligned} &\overset{(1)}{\mathcal{E}} := \overset{(1)}{\epsilon} - \pounds_{(1)X}\epsilon, \quad \overset{(1)}{\mathcal{P}} := \overset{(1)}{p} - \pounds_{(1)X} p, \quad \overset{(1)}{\mathcal{U}_a} := \overset{(1)}{(u_a)} - \pounds_{(1)X} u_a, \\ &\overset{(2)}{\mathcal{E}} := \overset{(2)}{\epsilon} - 2\pounds_{(1)X} \overset{(1)}{\epsilon} - \left(\pounds_{(2)X} - \pounds^2_{(1)X} \right) \epsilon, \quad \overset{(2)}{\mathcal{P}} := \overset{(2)}{p} - 2\pounds_{(1)X} \overset{(1)}{p} - \left(\pounds_{(2)X} - \pounds^2_{(1)X} \right) p, \\ &\overset{(2)}{\mathcal{U}_a} := \overset{(2)}{(u_a)} - 2\pounds_{(1)X} \overset{(1)}{(u_a)} - \left(\pounds_{(2)X} - \pounds^2_{(1)X} \right) u_a. \end{aligned} \tag{14} $$

Substituting these definitions of gauge invariant variables into the expansion of Eq.(12), we obtain

$$ {}^{(1)}(T_a{}^b) = (\rho + p) \left(\overset{(1)}{\mathcal{U}_a}\, u^b - \mathcal{H}^{bc} u_c u_b + g^{bc} \overset{(1)}{\mathcal{U}_c}\, u_a \right) + \left(\overset{(1)}{\mathcal{E}} + \overset{(1)}{\mathcal{P}} \right) u_a u^b + \overset{(1)}{\mathcal{P}}\, \delta_a{}^b + \pounds_{(1)X} T_a{}^b, \tag{15} $$

$$ =: {}^{(1)}\mathcal{T}_a{}^b + \pounds_{(1)X} T_a{}^b, \tag{16} $$

$$ \begin{aligned} {}^{(2)}(T_a{}^b) = {} & \left(\overset{(2)}{\mathcal{E}} + \overset{(2)}{\mathcal{P}} \right) u_a u^b + 2 \left(\overset{(1)}{\mathcal{E}} + \overset{(1)}{\mathcal{P}} \right) u_a \left(\overset{(1)}{\mathcal{U}^b} - \mathcal{H}^{bc} u_c \right) \\ & + (\epsilon + p)\, u_a \left(g^{bc} \overset{(2)}{\mathcal{U}_c} - 2\mathcal{H}^{bc} \overset{(1)}{\mathcal{U}_c} + 2\mathcal{H}^{bc} \mathcal{H}_{cd} u^d - g^{bc} {}^{(2)}\mathcal{H}_{cd} u^d \right) + 2 \left(\overset{(1)}{\mathcal{E}} + \overset{(1)}{\mathcal{P}} \right) \overset{(1)}{\mathcal{U}_a}\, u^b \\ & + 2(\epsilon + p) \overset{(1)}{\mathcal{U}_a} \left(g^{bc} \overset{(1)}{\mathcal{U}_c} - \mathcal{H}^{bc} u_c \right) + (\epsilon + p) \overset{(2)}{\mathcal{U}_a}\, u^b + \overset{(2)}{\mathcal{P}}\, \delta_a{}^b \\ & + 2\pounds_X {}^{(1)}(T_a{}^b) + \left\{ \pounds_Y - \pounds^2_X \right\} T_a{}^b \end{aligned} \tag{17} $$

$$ =: {}^{(2)}\mathcal{T}_a{}^b + 2\pounds_X {}^{(1)}(T_a{}^b) + \left\{ \pounds_Y - \pounds^2_X \right\} T_a{}^b. \tag{18} $$

Note that these expression of each order perturbative energy momentum tensor have the same form as the definition of gauge invariant variables for an arbitrary matter field. We also note that these expression of the perturbative energy momentum tensor is valid even if the background spacetime is changed.

As shown in the paper [3], the first and the second order perturbative Einstein tensor are given in the form

$$ {}^{(1)}G_a{}^b = {}^{(1)}\mathcal{G}_a{}^b\left[{}^{(1)}\mathcal{H}\right] + \pounds_{(1)X}G_a{}^b, \tag{19} $$

$$ {}^{(2)}G_a{}^b = {}^{(1)}\mathcal{G}_a{}^b\left[{}^{(2)}\mathcal{H}\right] + {}^{(2)}\mathcal{G}_a{}^b\left[{}^{(1)}\mathcal{H}, {}^{(1)}\mathcal{H}\right] + 2\pounds_{(1)X}{}^{(1)}G_a{}^b + \left\{\pounds_{(2)X} - \pounds^2_{(1)X}\right\}G_a{}^b, \tag{20} $$

where ${}^{(1)}\mathcal{G}_a{}^b[*]$ and ${}^{(2)}\mathcal{G}_a{}^b[*,*]$ are gauge invariant parts of the perturbative Einstein tensor and the explicit definitions of these are given in the paper [3]. Imposing the perturbative Einstein equation order by order, ${}^{(i)}G_a{}^b = 8\pi G^{(i)}T_a{}^b$, $(i = 0, 1, 2)$, The Einstein equations of each order are necessarily given in the gauge invariant form:

$$ {}^{(1)}\mathcal{G}_a{}^b\left[{}^{(1)}\mathcal{H}\right] = 8\pi G^{(1)}T_a{}^b, \tag{21} $$

$$ {}^{(1)}\mathcal{G}_a{}^b\left[{}^{(2)}\mathcal{H}\right] + {}^{(2)}\mathcal{G}_a{}^b\left[{}^{(1)}\mathcal{H}, {}^{(1)}\mathcal{H}\right] = 8\pi G^{(2)}T_a{}^b. \tag{22} $$

We can also derive the explicit form of the components of these perturbative Einstein equations from these equations.

In this article, we have shown the second order cosmological perturbation theory along the general framework developed in the papers [3]. We have verified the framework in these papers is applicable to cosmological perturbations. In the poster presentation of this conference, we also showed the explicit form of the second order Einstein equations in terms of gauge invariant variables. The Einstein equations derived here will be useful when we discuss the non-Gaussianity in CMB due to the nonlinear effects. To accumplish this, we will have to discuss the generation of the seed of the non-Gaussianity in the fluctuation, evolution of the second order perturbation, and the final temperature fluctuation in CMB which is observed today. Though these are discussed in some references[2] using gauge fixing method, we will reconsider these issue using within second order gauge invariant formulation of cosmological perturbations. This will be the future work.

References

[1] J. M. Bardeen, Phys. Rev. D**22** (1980), 1882; H. Kodama and M. Sasaki, Prog. Theor. Phys. Suppl. No.78 (1984), 1; V. F. Mukhanov, H. A. Feildman, and R. H. Brandenberger, Phys. Rep. **215** (1992), 203;

[2] V. Acquaviva, N. Bartolo, S. Matarrese and A. Riotto, Nucl. Phys. B **667** (2003), 119 ; K. A. Malik, D. Wands, Class. Quantum Grav. **21** (2004), L65; N. Bartolo, S. Matarrese and A. Riotto, Phys. Rev. Lett. **93** (2004), 231301 ; N. Bartolo, E. Komatsu, S. Matarrese and A. Riotto, Phys. Rep. **402** (2004), 103 ; N. Bartolo, S. Matarrese and A. Riotto, Phys. Rev. D **69** (2004), 043503 ; N. Bartolo, S. Matarrese and A. Riotto, JHEP **0404** (2004), 006; K. Tomita, Phys. Rev. D **71** (2005), 083504 ; K. Tomita, Phys. Rev. D **72** (2005), 043526 ; K. Tomita, Phys. Rev. D **72** (2005), 103506.

[3] K. Nakamura, Prog. Theor. Phys. **110**, (2003), 723; K. Nakamura, Prog. Theor. Phys. **113**, (2005), 481; K. Nakamura, "General framework of higher order gauge invariant perturbation theory," in *Proceedings of the thirteenth workshop on general relativity and gravitation in Japan* [arXiv:gr-qc/0402032].

[4] J. M. Stewart and M. Walker, Proc. R. Soc. London A **341** (1974), 49; J. M. Stewart, Class. Quantum Grav. **7** (1990), 1169; J. M. Stewart, *Advanced General Relativity* (Cambridge University Press, Cambridge, 1991).

[5] M. Bruni, S. Matarrese, S. Mollerach and S. Sonego, Class. Quantum Grav. **14** (1997), 2585; M. Bruni and S. Sonego, *ibid* **16** (1999), L29. M. Bruni, L. Gualtieri, and C.F. Sopuerta, *ibid* **20** (2003), 535; C.F. Sopuerta, M. Bruni, L. Gualtieri, Phys. Rev. D**70** (2004), 064002.

HIGH-ENERGY EFFECTIVE THEORY FOR A BULK BRANE

[1]Claudia de Rham [2]Shunsuke Fujii [2,3,4]Tetsuya Shiromizu [2]Hirotaka Yoshino

[1]*DAMTP, University of Cambridge, Wilberforce Road, Cambridge CB3 0WA, UK*
[2]*Theoretical Astrophysics Group, Department of Physics, Tokyo Institute of Technology, Tokyo 152-8551, Japan*
[3]*Department of Physics, The University of Tokyo, Tokyo 113-0033, Japan*
[4]*Advanced Research Institute for Science and Engineering, Waseda University, Tokyo 169-8555, Japan*

Abstract

We derive an effective theory describing the physics of a bulk brane in the context of the RS1 model. This theory goes beyond the usual low-energy effective theory in that it describes the regime where the bulk brane has a large velocity and the radion can change rapidly. We achieve this by concentrating on the region where the distance between the orbifold planes is small in comparison to the AdS length scale. Consequently our effective theory will describe the physics shortly before a bulk/boundary or boundary/boundary brane collision. We study the cosmological solutions and find that at large velocities, the bulk brane decouples from the matter on the boundary branes, a result which remains true for cosmological perturbations

1 Introduction

The study of brane collisions has recently gained a special interest as it may provide a new scenario for the creation of the hot big-bang Universe [1,2]. Motivated by heterotic M-theory and the Randall-Sundrum (RS) model [3], the collision between two orbifold branes has been explored, leading to a five-dimensional singularity [4]. When the boundary branes are close, an effective theory can be derived for this scenario and is hence valid just before or just after the collision [1,5?8]. In this paper, we extend this analysis to the case where a brane is present in the bulk. This regime is of interest as it allows us to study a bulk/orbifold brane collision in a situation where the fivedimensional geometry remains regular similarly as in the first Ekpyrotic scenario [1]. What is particularly interesting about the effective theory we will develop, is that it is capable of describing the regime where the branes have large velocities, something which the usual low-energy effective theory cannot do. Although similar work has been derived for close boundary branes, [6?8] it relied strongly on the presence of a Z2 orbifold symmetry which is generically broken for bulk branes. This work will hence give us a general formalism for the derivation of an effective theory on a generic non Z2-brane. Such branes are interesting to study as they represent more realistic candidates for cosmology and at high-energies, their behavior is expected to be strongly modified [9]. In order to get some insight on the brane geometry one should in principal solve the full higher-dimensional theory exactly before being able to infer the geometry on the brane. Unfortunately, this is only possible in very limited cases, and for more general situations, one should in practice either rely on numerical simulation or work in some specific regime where effective theories may be derived. This is the approach which is generally undertaken in order to derive a low-energy effective theory. Assuming a lowenergy regime, it is possible to express the geometry on the brane as the lowest order of a gradient expansion [1,10? 12]. In this paper, we use a similar method, but choose instead to work in a close-brane regime, where we only consider terms of leading order in the distance between the branes. This method allow us to highlight the presence of eeasymmetricff terms on the bulk brane (generic to the absence of Z2-symmetry) which are negligible at lowenergies and are usually discarded. As far as we are aware, this is the first effective-theory that models these terms in a covariant way beyond the low-energy limit. The rest of this paper is organized as follows. In Sec. II, we consider three branes and derive the effective theory on the asymmetric bulk brane. In that theory, two scalar dynamical degrees of freedom are present, namely, the distance between the bulk brane and each of the boundary branes. We point out the low-energy limit of this theory, and check its consistency with previous results. In particular, we show that the theory on

the bulk brane is a standard scalar-tensor theory of gravity coupled with two scalar fields. In Sec. III, we apply our effective theory to cosmology and compare our result with solutions from the fivedimensional theory. We show that for large velocities, the matter on the orbifold branes do not affect the bulk brane. As a specific example, we present the derivation of tensor perturbations. As expected, at large velocities the perturbations on the bulk brane decouple from the stress energy on the boundary branes. Finally, we summarize our study and present some possible extensions as future works in Sec. IV.

In this paper, an effective theory describing the gravitational behavior of a bulk brane has been derived. The absence of any reflection symmetry across a generic bulk brane makes its behavior especially interesting to study. In the eelightff-brane limit, i.e. when the five-dimensional geometry is almost unaffected by the presence of the brane, the asymmetry on the brane itself is important and affects its own behavior. In this work, we have developed a fourdimensional effective theory capable of describing this eeasymmetryff in a covariant way. For that, we have considered a close-brane approximation, where we assumed the bulk brane to be close to both orbifold branes. Using this approximation, we obtained a resulting theory of gravity coupled in a nontrivial way with two scalar fields representing the distance between the bulk brane and each of the orbifold branes. This four-dimensional theory can be tested in several limits, such as at low-energy, when a reflection symmetry is imposed by hand and for cosmology. In all these regimes, predictions from the close-brane theory agree perfectly with the expected results. The case of cosmology is of special interest, at high-velocity the DE RHAM, FUJII, SHIROMIZU, AND YOSHINO PHYSICAL REVIEW D 72, 123522 (2005) 123522-8 bulk geometry is not sensitive to the matter present on the orbifold branes, and this result remains valid for tensor perturbations. In the limit where the AdS length scale is the same on both side of the brane, ie. the bulk is not perturbed by the brane, we show that the Hubble parameter couples linearly to the energy density on the bulk brane. This is an interesting result, which might strongly affect the gravitational behavior on such a brane. This effective theory could as well be derived on the orbifold branes in the presence of such a brane in the bulk. We may point out that the asymmetric tensor we derived on the bulk brane depends on the bulk brane metric. It will hence be necessary to find its expression in terms of the orbifold brane metric before being able to derive an effective theory for these orbifold branes. This is left for a future study. A straightforward extension of this model, would be the scenario where the bulk brane is close to only one of the orbifold branes, and the radion representing the distance with the other orbifold brane is moving slowly. One side of the theory would hence be modeled by the low-energy effective theory while the close-brane theory would be a good description for the other side. Such a model would be of interest if one considers the collision of the bulk brane with one of the orbifold branes. Such a process might produce a phase transition which could have some interesting consequences from a cosmological point of view. This is also left for a future study.

References

[1] J. Khoury, B. A. Ovrut, P. J. Steinhardt and N. Turok, Phys. Rev. **D64**, 123522(2001).

[2] U. Gen, A. Ishibashi and T. Tanaka Phys. Rev. **D66**, 023519(2002); J. J. Blanco-Pillado, M. Bucher, S. Ghassemi and F. Glanois, Phys. Rev. **D69**, 103515(2004).

[3] L. Randall and R. Sundrum, Phys. Rev. Lett. **83**, 3370 (1999).

[4] J. Khoury, B. A. Ovrut, N. Seiberg, P. J. Steinhardt and N. Turok, Phys. Rev. D **65**, 086007 (2002) [arXiv:hep-th/0108187].

[5] A. Neronov, JHEP **0111**, 007(2001); D. Langlois, K. Maeda and D. Wands, Phys. Rev. Lett. **88**, 181301(2002); S. Kanno, M. Sasaki and J. Soda, Prog. Theor. Phys. **109**, 357(2003).

[6] T. Shiromizu, K. Koyama and K. Takahashi, Phys. Rev. **D67**, 104011(2003).

[7] C. de Rham and S. Webster, Phys. Rev. **D71**, 124025(2005).

[8] C. de Rham and S. Webster, Phys. Rev. **D72**, 64013(2005).

[9] A. C. Davis, S. C. Davis, W. B. Perkins and I. R. Vernon, Phys. Lett. **B504**, 254(2001); B. Carter and J. P. Uzan, Nucl. Phys. **B606**, 45(2001); K. Takahashi and T. Shiromizu, Phys. Rev. **D70**, 103507(2004); L. A. Gergely, E. Leeper and R. Maartens. Phys. Rev. **D70**, 104025(2004); I. R. Vernon and D. Jennings, JCAP **0507**, 011(2005).

[10] T. Wiseman, Class. Quant. Grav. **19**, 3083(2002); S. Kanno and J. Soda, Phys. Rev. **D66**, 043526(2002); ibid, 083506,(2002); T. Shiromizu and K. Koyama, Phys. Rev. **D67**, 084022(2003); C. de Rham, Phys. Rev. **D71**, 024015(2005).

[11] L. Cotta-Ramusino, "Low energy effective theory for brane world models", MPhill. thesis, University of Portsmouth(2004).

[12] J. Garriga, O. Pujolas and T. Tanaka, Nucl. Phys. **B655**, 127(2003); P. Brax, C. van de Bruck, A. C. Davis and C. S. Rhodes, Phys. Rev. **D67**, 023512(2003); G. A. Palma and A. C. Davis, Phys. Rev. **D70**, 106003(2004); S. L. Webster and A. C. Davis, hep-th/0410042; S. Kanno and J. Soda, Phys.Rev. **D71**, 044031(2005).

[13] T. Shiromizu, K. Maeda and M. Sasaki, Phys. Rev. **D62**, 024012(2000).

Can we create a universe in the laboratory?

Nobuyuki Sakai[a,b,1], Ken-ichi Nakao[c,2], Hideki Ishihara[c,3], and Makoto Kobayashi[b]

[a] *Department of Education, Yamagata University, Yamagata 990-8560, Japan*
[b] *Department of Physics, Yamagata University, Yamagata 990-8560, Japan*
[c] *Department of Physics, Osaka City University, Osaka 558-8585, Japan*

Abstract

To explore the possibility that an inflationary universe can be created out of a stable particle in the laboratory, we consider the classical and quantum dynamics of a magnetic monopole in the thin-shell approximation. Classically there are three types of solutions: stable, collapsing and inflating monopoles. We argue that the transition from a stable monopole to an inflating one could occur either by collision with a domain wall or by quantum tunneling.

1 Introduction

If a false-vacuum bubble is larger than the de Sitter horizon, the bubble expands and becomes a new inflationary universe [1]. Farhi and Guth [2] discussed whether such a large false-vacuum bubble is created without an initial singularity, applying the Penrose theorem. The theorem states that, if (a) there exists a noncompact Cauchy surface, (b) $\mathcal{R}_{\mu\nu}k^\mu k^\nu \geq 0$ for all null vector k^μ, and (c) there exists an anti-trapped surface, then there exists an initial singularity. As a consequence of the Einstein equations $\mathcal{R}_{\mu\nu} = 8\pi G T_{\mu\nu}$, condition (b) is rewritten as $T_{\mu\nu}k^\mu k^\nu \geq 0$. Because any standard theory of matter, including a canonical scalar field, obeys this energy condition, we may conclude that it is impossible to create a universe in the laboratory. However, because the above argument is based on the classical field theory, a quantum process could make it possible to produce a large false-vacuum bubble without an initial singularity. Actually, Farhi *et al.* [3] and Fischler *et al.* [4] considered a quantum decay from a small bubble without an initial singularity to a large bubble which becomes an inflationary universe, and calculated its probability.

As Guendelman and Portnoy [5] pointed out, however, there is a problem in the model. Because the effective potential which governs the shell trajectories has no local minimum, there is no stable solution. Even if we success to make a small false-vacuum bubble, the bubble collapses the moment it is created; there is little chance for a quantum decay to happen during its lifetime. To solve this problem, Guendelman and Portnoy proposed a new model. They assumed a $(2+1)$-dimensional gauge field localized on the surface of a false-vacuum bubble. Due to the gauge field, there exists a static and stable classical configuration, which eventually decays into an inflationary universe.

In this paper we consider the possibility that an stable magnetic monopole evolves into an inflationary universe. In the Einstein-Yang-Mills-Higgs system there are stable solutions as well as inflating and collapsing solutions [6]. We therefore expect the scenario that a stable monopole eventually evolves into an inflationary universe. Although magnetic monopoles have never been detected, unified theories of elementary particles predict their existence. Furthermore, monopole inflation, which is free from the fine-tuning problem of initial conditions and the graceful exit problem, is still viable. Therefore, the monopole model is more realistic and motivated than the previous models.

[1] Electronic address: nsakai@e.yamagata-u.ac.jp
[2] Electronic address: knakao@sci.osaka-cu.ac.jp
[3] Electronic address: ishihara@sci.osaka-cu.ac.jp

2 Classical dynamics

We adopt the thin-shell model of Arrega *et al.* [7], except for the form of the surface density. We assume that the inside is de Sitter spacetime and the outiside is Reissner-Nordström:

$$ds^2 = -A_+ dt_+^2 + \frac{dr_+^2}{A_+} + r_+^2(d\theta_+^2 + \sin^2\theta_+ d\varphi_+^2), \quad A_+(r_+) \equiv 1 - \frac{2GM}{r_+} + \frac{Q^2}{r_+^2}. \tag{1}$$

$$ds^2 = -A_- dt_-^2 + \frac{dr_-^2}{A_-} + r_-^2(d\theta_-^2 + \sin^2\theta_- d\varphi_-^2), \quad A_-(r_-) \equiv 1 - H^2 r_-^2, \tag{2}$$

The boundary $R = r_+ = r_-$ is supposed to be a timelike hypersurface. Because the dominant energy on the shell is not only gradient energy of the Higgs field but also that of the gauge field, the surface density takes the form,

$$\sigma(\tau) = \sigma_0 + \frac{\sigma_1}{R(\tau)^2}, \tag{3}$$

where σ_0 and σ_0 are constant, and τ is the proper time of the shell.

The junction condition is given by

$$\beta^+ - \beta^- = -4\pi G R\left(\sigma_0 + \frac{\sigma_1}{R^2}\right), \quad \beta^\pm \equiv \frac{\partial r_\pm}{\partial n} = \epsilon^\pm \sqrt{\left(\frac{dR}{d\tau}\right)^2 + A_\pm(R)}, \quad \epsilon^\pm = +1 \text{ or } -1, \tag{4}$$

where n is the normal coordinate of the shell. Following Arreaga *et al.* [7], we introduce dimensionless

$$\tilde{R} \equiv HR, \quad \tilde{\tau} \equiv H\tau, \quad m \equiv HM, \quad q \equiv HQ, \quad s_0 \equiv \frac{4\pi G\sigma_0}{H}, \quad s_1 \equiv 4\pi G H \sigma_1, \tag{5}$$

to rewrite Eq.(4) as

$$\left(\frac{d\tilde{R}}{d\tilde{\tau}}\right)^2 + U(\tilde{R}) = -1, \quad U(\tilde{R}) \equiv -\left(\frac{1-s_0^2}{2}\tilde{R} - \frac{s_0 s_1}{\tilde{R}} - \frac{m}{\tilde{R}^2} + \frac{q^2 - s_1^2}{2\tilde{R}^3}\right)^2 \left(s_0 + \frac{s_1}{\tilde{R}^2}\right)^{-2} - \tilde{R}^2. \tag{6}$$

To understand the global spacetime structure, it is necessary to know the positions of horizons and the signs of $\beta = \partial r/\partial n$ in terms of $\tilde{R}$. De Sitter horizons $\tilde{R}_D$, the black-hole outer horizon $\tilde{R}_{(+)}$ and the inner horizon $\tilde{R}_{(-)}$ are characterized by

$$\tilde{R}_D = 1, \quad \tilde{R}_{(\pm)} = m \pm \sqrt{m^2 - q^2}, \tag{7}$$

respectively. To clarify the sings of $\beta^\pm$, using (4), we reexpress them as

$$\beta^\pm = \left(\frac{\mp s_0^2 - 1}{2}\tilde{R} + \frac{m}{\tilde{R}^2} - \frac{q^2}{2\tilde{R}^3}\right)\left(s_0 + \frac{s_1}{\tilde{R}}\right)^{-1}. \tag{8}$$

Here we show some of the solutions and discuss whether stable monopoles can evolve into inflating monopoles without an initial singularity. Figure 1 shows a stable oscillating monopole in a horizonless spacetime (type A) with $m = 0.58$, $q = 0.6$, $s_0 = 0.6$ and $s_1 = 0.1$. In the same potential there is another expanding solutions for large $\tilde{R}$ (type A').

If we increase m, the feature of solutions changes drastically. Figure 2 shows an inflating monopole (type B) with $m = 0.64$, $q = 0.6$, $s_0 = 0.6$ and $s_1 = 0.1$. We expect that type A monopoles can evolve into type B by adding mass. Specifically, we consider the model that an spherical domain wall surrounding the monopole eventually collides with it. Possible trajectories before and after the collision is shown in Fig. 3. This could be a classical process that an inflationary universe is created in the laboratory. What about an initial singularity? Because we only suppose a classical process, the singularity theorem applies. Because there is no noncompact Cauchy surface, however, the theorem does not mean the existence of an initial singularity.

In the intermediate case between A and B solutions, there are stable oscillating solutions with black-hole horizons. Figure 4 shows the case of $m = 0.61$, $q = 0.6$, $s_0 = 0.6$ and $s_1 = 0.1$. In this case there are two types of classical solutions: a stable oscillating monopole (type C) and an inflating monopole (type C'). Quantum tunneling from C to C' is the subject of the next section.

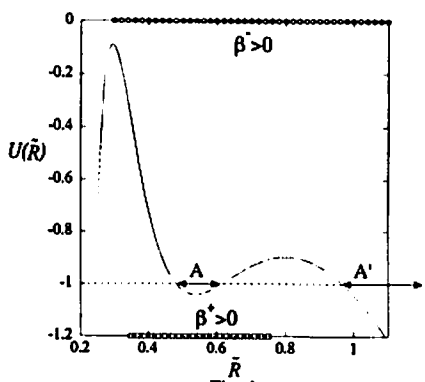

Fig. 1

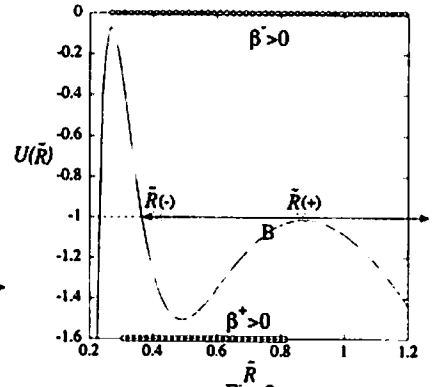

Fig. 2

3 Quantum tunneling

Following Farhi *et al.* [3] and Ansoldi *et al.* [8], we execute canonical quantization of the system described by (4) and take the lowest order the WKB expansion. In the classically forbidden region we assume that there is a solution $R(\tau_E)$ to the classical equation of motion, where τ_E is the Euclidean time defined as $\tau_E \equiv i\tau$. The ratio of amplitudes of the wave function Ψ at R_i and R_f is given by

$$\frac{\Psi(R_f)}{\Psi(R_i)} \approx e^{-B}, \quad B = \frac{1}{GH^2}\int_{\tilde{\tau}_E^i}^{\tilde{\tau}_E^f} d\tilde{\tau}_E \tilde{R}\frac{d\tilde{R}}{d\tilde{\tau}_E}\left[\tan^{-1}\left(\frac{d\tilde{R}/d\tilde{\tau}_E}{\beta}\right)\right]^{\pm}, \tag{9}$$

We calculate the decay rate from a stable monopole C to inflating one C'. Some of the results are shown in Fig. 5. (a) $m = 0.6$, $s_0 = 0.6$ and $s_1 = 0.1$; (b) $m = 0.4$, $s_0 = 0.6$ and $s_1 = 0.1$; (c) $m = 0.6$, $s_0 = 0.3$ and $s_1 = 0.1$; (d) $m = 0.6$, $s_0 = 0.6$ and $s_1 = 0.2$. The factor $1/GH^2$ is given by $\sim (m_{Pl}/\eta)^4$, where η is the VEV of the Higgs field. Therefore, if η^4 is not much smaller than the Planck density, B is not much larger than unity and the probalitiy e^{-B} is considerable. Because of complexity of the effective potential U defined in (6), it is not easy to understand how B depends on s, m and q. Some cusps appear in Fig. 5 because of catastrophic change of the potential barrier.

4 Summary and Discussions

To explore the possibility that an inflationary universe can be created out of a stable particle in the laboratory, we have considered the classical and quantum dynamics of a magnetic monopole in the thin-shell approximation.

First, we have found a classical solution that a stable monopole evolves into an inflationary universe with an initial singurality. This solution does not contradict with the Penrose theorem, because of nonexistence of a noncompact Cauchy surface. However, we should discuss instability of the inner horizon in the solution. Poisson and Israel [9] argued that, if radial perturbations are given, the gravitational mass inside the Cauchy horizon increases infinitely, which leads the appearance of a spacelike singularity near the Cauchy horizon. If this phenomenon happens in the present model, classical solutions beyond the Cauchy horizon may break down. According to Dafermos [10], however, the spacetime could be extendible beyond such singularity as a C^0 metric. Therefore, a physical consequence of our classical solutions is still unclear.

We have also analyzed a quantum decay from a stable monopole to an inflating one. We have adopted the canonical quantization to evaluate the probability amplitude to lowest order in WKB approximation.

A problem of this model and other related models is the difficulty of detecting an inflationary universe because it is surrounded by an event horizon, which eventually disappears by Hawking radiation. Recently, Hawking [11] argued that information is preserved in black hole formation and evaporation,

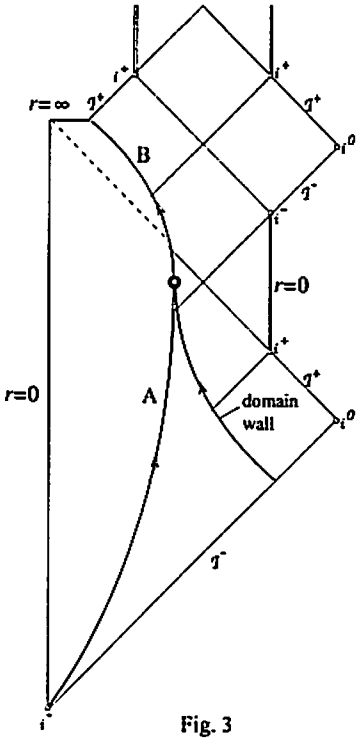

Fig. 3

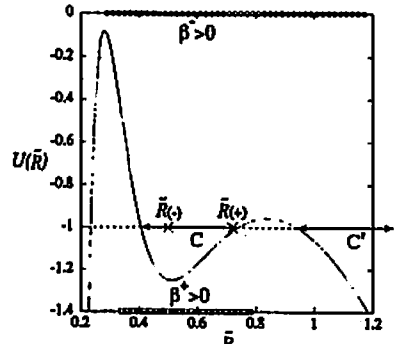

Fig. 4

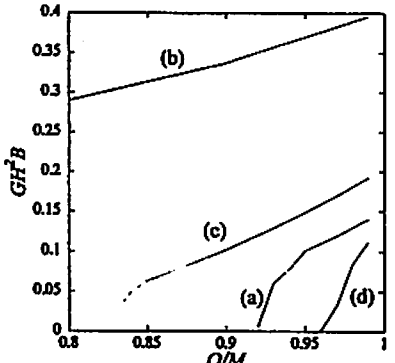

Fig. 5

and information could get out of a black hole by radiation. Although this conjecture is uncertain at the moment, we expect that it will be a clue to detect a universe in the laboratory.

We thank M. Dafermos, H. Kodama, R. Myers, and M. Sasaki for useful discussions. The substantial part of this work was done while NS stayed at Department of Physics, Osaka City University. NS thanks his colleagues there for their hospitality. This work was supported in part by MEXT Grant-in-Aid for Young Scientists (B) No. 15740132 and that for Scientific Research (C) No. 16540264.

References

[1] K. Sato, M. Sasaki, H. Kodama, and K. Maeda, Prog. Theor. Phys. **65**, 1443 (1981); S. K. Blau, E. Guendelman, and A. Guth, Phys. Rev. D **35**.

[2] E. Farhi and A. H. Guth, Phys. Lett. B **183**, 149 (1987).

[3] E. Farhi, A. H. Guth, and J. Guven, Nucl. Phys. **B339**, 417 (1990).

[4] W. Fischler, D. Morgan, and J. Polchinski, Phys. Rev. D **41**, 2638 (1990); **42**, 4042 (1990).

[5] E. I. Guendelman and J. Portnoy, Class. Quantum Grav. **16**, 3315 (1999).

[6] N. Sakai, Phys. Rev. D **54** 1548 (1996); N. Sakai, K. Nakao, and T. Harada, *ibid.* **61**, 127302 (2000).

[7] G. Arreaga, I. Cho, and J. Guven, Phys. Rev. D **62**, 043520 (2000).

[8] S. Ansoldi, A. Aurilia, R. Balbinot, and E. Spallucci, Class. Quantum Grav. **14**, 2727 (1997).

[9] E. Poisson and W. Israel, Phys. Rev. D **41**, 1796 (1990).

[10] M. Dafermos, arXiv: gr-qc/0401121.

[11] S. W. Hawking, arXiv: hep-th/0507171.

A new canonical formalism of $f(R)$-type gravity in terms of Lie derivatives

Y. Ezawa[1], H. Iwasaki[2], Y. Ohkuwa[3], S. Watanabe[4], N. Yamada[5] and T. Yano[6]

[1,2,4,5] *Department of Physics, Ehime University, Matsuyama, 790-8577, Japan*
[3] *Section of Mathematical Science, Faculty of Medicine, University of Miyazaki, Kiyotake, Miyazaki, 889-1692, Japan*
[6] *Department of Electrical Engineering, Ehime University, Matsuyama, 790-8577, Japan*

Abstract

We propose a new canonical formalism of $f(R)$-type gravity that resolves the problem in the formalism of Buchbinder and Lyakhovich(BL). The new coordinates corresponding to the time derivatives of the metric are taken to be its Lie derivatives which is the same as in BL. The momenta canonically conjugate to them and Hamiltonian density are defined similarly to the formalism of Ostrogradski. It is shown that our method resolves the problem of BL.

1 Introduction

Recently $f(R)$-type higher-curvature gravity is applied to cosmology to explain, e.g. inflation at the early stage of the universe or expansion of the present universe which seems to be in the stage of an accelerating expansion.[1, 2] In this work we address the problem of the canonical formalism of $f(R)$-type higher- curvature gravity and propose a consistent formalism[3]. The higher-curvature gravity is a theory with higher order time derivatives. Standard procedure for the canonical formalism of higher order time derivatives has been given by Ostrogradski[4]. In the usual method of canonical formalism of gravity in terms of ADM variables, this method however is not applicable directly. The reason is that the curvatures depend on the time derivatives of the lapse function and the shift vector so that they obey field equations, which leads to the breaking of general covariance.

This problem was resolved by the method of Buchbinder and Lyakhovich(BL)[5, 6] in which the new generalized coordinates corresponding to the time derivatives of the metric was chosen to be the extrinsic curvature that is the Lie derivatives of the three metric. The time derivatives of the lapse function and the shift vector are absorbed in the time derivatives of the extrinsic curvature.

However, in this method of BL, a change of the original generalized coordinates induces a change of Hamiltonian. For example, in the case of FRW spacetime, the Hamiltonian is different whether we use the scale factor or its logarithm as the generalised coordinate. If the Hamiltonian represents the energy of the system, this is physically unreasonable.

We propose a new canonical formalism which resolves this problem. We combine the advantageous points of both the methods of Ostrogradski and BL. We choose the extrinsic curvature as the new generalized coordinate as in BL. And we define the momenta canonically conjugate to them and Hamiltonian similarly to Ostrogradski's method. The resulting Hamiltonian is shown in fact invariant under the transformation of the original generalized coordinates which do not change the 3-dimensional metric of the hypersurface of constant time.

In section 2, we explain how the Hamiltonian changes under the transformation of the original generalized coordinate in the method of BL. Section 3 is devoted to a new canonical formalism for a higher-curvature gravity of $f(R)$-type. In section 4 we demonstrate the invariance of the Hamiltonian under the transformations of the generalized coordinates, the three metric. Summary is given in section 5.

[1] E-mail:ezawa@sci.ehime-u.ac.jp
[2] E-mail:hirofumi@phys.sci.ehime-u.ac.jp
[3] E-mail:ohkuwa@med.miyazaki-u.ac.jp
[4] E-mail:shizuka@phys.sci.ehime-u.ac.jp
[5] E-mail:naohito@phys.sci.ehime-u.ac.jp
[6] E-mail:yanota@eng.ehime-u.ac.jp

2 A problem in the method of Buchbinder and Lyakhovich

In this section we show that in the method of BL how the Hamiltonian changes under the transfornation of the generalized coordinates by using a simple model. Let us consider a system described by a Lagrangian $L = L(q^i, \dot{q}^i, \ddot{q}^i)$ where i runs from 1 to N. The new generalized coordinates are defined as $Q^i \equiv \dot{q}^i$. In the method of BL, the Lagrangian is modified using the Lagrange multiplier method so that the above definition of Q^i is derived from variational principle. Denoting the modified Lagrangian as L^*, we have $L^* \equiv L + p_i(\dot{q}^i - Q^i)$, $L = L(q^i, Q^i, \dot{Q}^i)$. The multipliers p_i are the momenta canonically conjugate to q^i. The canonical formalism is obtained by the Legendre transformation starting from L^*. Momenta P^i canonically conjugate to Q_i are given by $P^i \equiv \frac{\partial L^*}{\partial \dot{Q}_i} = \frac{\partial L}{\partial \dot{Q}_i}$. Then the Hamiltonian H^* is given as $H^* \equiv p_i\dot{q}^i + P_i\dot{Q}^i - L^* = p_iQ^i + P_i\dot{Q}^i - L$. Now we make transformations of the generalized coordinates:

$$q^i \to \phi^i = f^i(q^j), \quad \text{or} \quad q^i = g^i(\phi^j). \tag{2.1}$$

Momenta conjugate to ϕ^i are denoted as π_i, new generalized coordinates as Φ^i and momenta canonically conjugate to Φ^i as Π_i. These variables are not uniquely related to old variables. First, since Q^i and Φ^i are related, respectedly, to $\dot{q}^i$ and $\dot{\phi}^i$ through the variational principle, relations between Q^i and Φ^i are not fixed a priori. The solutions obtained through variational principle are, however, $Q^i = \dot{q}^i$ and $\Phi = \dot{\phi}$, it is natural to assume the transformation of Q^i to be the same as $\dot{q}^i$. Differentiating q^i, we have $\dot{q}^i = \frac{\partial q^i}{\partial \phi^j}\dot{\phi}^j$, which lead to the transformations, $Q^i = \frac{\partial q^i}{\partial \phi^j}\Phi^j$. Secondly, the momenta p_i are Lagrange multipliers, so that their transformations are also not fixed a priori. We fix their transformations by requiring that the modified Lagrangians are the same: $L^*(q^i, Q^i, \dot{Q}^i) = \bar{L}^*(\phi^i, \Phi^i, \dot{\Phi}^i) = \bar{L}(\phi^i, \Phi^i, \dot{\Phi}^i) + \pi_i(\dot{\phi}^i - \Phi^i)$. Then we have $p_i(\dot{q}^i - Q^i) = \pi_i(\dot{\phi}^i - \Phi^i)$. Using the above equations, we have $\pi_i = \frac{\partial q^j}{\partial \phi^i}p_j$. The Hamiltonian, obtained by the Legendre transformation of the modified Lagrangian $\bar{L}^*$, is expressed as $\bar{H}^* \equiv \pi_i\dot{\phi}^i + \Pi_i\dot{\Phi}^i - \bar{L}^* = \pi_i\Phi^i + \Pi_i\dot{\Phi}^i - \bar{L}$. Since $L = \bar{L}$, the change of the Hamiltonian is $\Delta H^* = \bar{H}^* - H^* = \Pi_i\dot{\Phi}^i - P_i\dot{Q}^i$. Now $\Pi_i \equiv \frac{\partial \bar{L}}{\partial \dot{\Phi}^i} = \frac{\partial L}{\partial \dot{\phi}^i} = P_j\frac{\partial q^j}{\partial \phi^i}$ and $\dot{\Phi}^i = \frac{\partial^2 f^i}{\partial q^j \partial q^k}\dot{q}^kQ^j + \frac{\partial f^i}{\partial q^j}\dot{Q}^j$. Using these equations , we have

$$\Delta H^* = \frac{\partial^2 f^i}{\partial q^k \partial q^j}Q^kQ^j\Pi_i \neq 0. \tag{2.2}$$

Thus the Hamiltonian is not invariant under the transformation of the original generalized coordinates and reasonable transformation of other canonical variables. If the Hamiltonian represents the energy of the system, which is often the case, this noninvariance is physically unreasonable. The difference depends on the variables characteristic to higher derivative theory. We note that if the variables transform to make the Hamiltonian invariant, the Lagrangian is changed. In application of $f(R)$-type gravity to homogeneous and isotropic cosmology, Hamiltonian density $\mathcal{H}$ in terms of the scale factor a is different from the Hamiltonian density $\bar{\mathcal{H}}$ in terms of $\ln a \equiv \phi$. In order to resolve this problem, we propose a new canonical formalism which can be interpreted to be the generalization of the Ostrogradski's method.

3 A new canonical formalism in terms of Lie derivatives

Following Ostrogradski, let us consider a system described by a Lagrangian containing the n-th time derivatives of the generalized coordinates q^i $(i = 1, \ldots, N)$, $L = L(q^i, \dot{q}^i, \ldots, q^{i(n)})$. Take the following variation of the action $\delta S \equiv \int_{t_1+\delta t_1}^{t_2+\delta t_2} L(q^i + \delta q^i, \ldots, q^{i(n)} + \delta q^{i(n)})dt - \int_{t_1}^{t_2} L(q^i, \ldots, q^{i(n)})dt$ where $\delta q^i \equiv (q+\delta q)^i(t+\delta t) - q^i(t)$ are decomposed as the sum of the variations of the function $(q+\delta q)^i(t+\delta t) - q^i(t+\delta t)$, which we denote by $\delta^* q^i$, and those due to the change of the time, $q^i(t+\delta t) - q^i(t) \approx \dot{q}^i\delta t$: $\delta q^i = \delta^* q^i + \dot{q}^i\delta t$, where the second terms are assumed to contribute only near the end points. Then the above variation is written, retaining only the first order terms in small quantities, as $\delta S = \int_{t_1+\delta t_1}^{t_1} L(q^1, \ldots, q^{i(n)})dt + \int_{t_2}^{t_2+\delta t_2} L(q^1, \ldots, q^{i(n)})dt + \delta^* \int_{t_1}^{t_2} Ldt$. Using the approximation $\int_{t_k}^{t_k+\delta t_k} L(q^1, \ldots, q^{i(n)})dt = L\left(q^1(t_k), \ldots, q^{i(n)}(t_k)\right)\delta t_k$, $(k = 1, 2)$, we can rewrite the first two terms in δS as $[L\delta t]_{t_1}^{t_2} \equiv \delta S_1$. Rearranging the sum in the third term of δS, we have $\delta S_2 \equiv \delta^* \int_{t_1}^{t_2} Ldt = [\delta F]_{t_1}^{t_2} + \delta^* S_2$ where $\delta F = \sum_{i=1}^{N}\left[\sum_{s=0}^{n-1}\left\{\sum_{r=s+1}^{n}(-1)^{r-s-1}D^{r-s-1}\left(\frac{\partial L}{\partial (D^r q^i)}\right)\right\}\delta^* q^{i(s)}\right]$ and

$\delta^* S_2 = \sum_{i=1}^N \int_{t_1}^{t_2} \sum_{s=0}^n (-1)^s D^s \left(\frac{\partial L}{\partial (D^s q^i)} \right) \delta^* q^i dt$, where D represents the time derivative, i.e. $D \equiv \frac{d}{dt}$. Thus we have $\delta S = [L\delta t + \delta F]_{t_1}^{t_2} + \delta^* S_2$. $\delta^* S_2$ vanishes if we require the variational principle. The new generalized coordinates are taken as $q_s^i \equiv D^s q^i$ and the momenta canonically conjugate to these cordinetes are defined by the coefficients of the variations of these coordinates δq_s^i in δF : $p_i^s \equiv \sum_{r=s+1}^n \left[(-1)^{r-s-1} D^{r-s-1} \left(\frac{\partial L}{\partial D^r q^i} \right) \right]$. The Hamiltonian is defined as $(-1)\times$ the coefficient of δt in $L\delta t + \delta F$, that is $H = \sum_{i=1}^N \sum_{s=0}^{n-1} p_i^s D q_s^i - L$. Note that for $s = n-1$, $p_i^{n-1} = \frac{\partial L}{\partial \dot{q}_{n-1}^i}$. Thus the Ostrogradski transformation is a generalization of the Legendre transformation. It is noted that the highest order derivatives need not be the same for all i.

In this work we investigate the higher-curvature gravity of $f(R)$-type in which the Lagrangian density is given by a function of the scalar curvature

$$\mathcal{L} = \sqrt{-g} f(R) \tag{3.1}$$

where $g \equiv \det g_{\mu\nu}$. The action is given as usual: $S = \int_{t_1}^{t_2} L dt$, $L = \int \mathcal{L} d^3x$. We adopt as the generalized coordinates the ADM variables $N(\mathbf{x}, t)$, $N^i(\mathbf{x}, t)$ and $h_{ij}(\mathbf{x}, t)$ with respect to a hypersurface $t = constant(\Sigma_t)$. In terms of these variables, the scalar curvature is expressed as follows $R = 2N^{-1} h^{ij} \partial_0 K_{ij} - U - 2N^{-1} \Delta N - 2N^{-1} (N^k \partial_k K + 2N^{i;j} K_{ij})$. Here K_{ij} is the extrinsic curvature of Σ_t and given by $K_{ij} = \frac{1}{2N} (\partial_0 h_{ij} - N_{i;j} - N_{j;i})$, and $U \equiv 3K_{ij} K^{ij} - K^2 - \tilde{R}$, where $K \equiv h^{ij} K_{ij}$ and $\tilde{R}$ is the scalar curvature of Σ_t. The determinant g is expressed as $-N^2 h$ with $h \equiv \det h_{ij}$.

In this case δF takes the following form $\int d^3x \Big[\frac{\partial \mathcal{L}}{\partial (\partial_0 h_{ij})} \delta^* h_{ij} - \partial_0 \left(\frac{\partial \mathcal{L}}{\partial (\partial_0^2 h_{ij})} \right) \delta^* h_{ij} + \frac{\partial \mathcal{L}}{\partial (\partial_0 \partial_k h_{ij})} \delta^* \partial_k h_{ij} + \frac{\partial \mathcal{L}}{\partial (\partial_0^2 h_{ij})} \delta^* \partial_0 h_{ij} + \frac{\partial \mathcal{L}}{\partial (\partial_0 N)} \delta^* N + \frac{\partial \mathcal{L}}{\partial (\partial_0 \partial_k N^i)} \delta^* \partial_k N^i + \frac{\partial L}{\partial (\partial_0 N^i)} \delta^* N^i \Big]$. From this expression, it appears that N and N^i, which represent the choice of the coordinate system, have the momenta canonically conjugate to them. In that case, they are allowed to be only the solutions of dynamical equations and the general covariance is broken. However, the time derivatives, $\partial_0^2 h_{ij}$, $\partial_0 N$, $\partial_0 N^i$ and $\partial_0 \partial_k N^i$ are involved only through $\partial_0 K_{ij}$. It is also noted that time derivatives $\partial_0 h_{ij}$ and $\partial_0 \partial_k h_{ij}$ are involved through $\partial_0 K_{ij}$, K_{ij} and $\partial_k K_{ij}$. Thus δF reduces to the integration of

$$\begin{aligned} \frac{\partial \mathcal{L}}{\partial (\partial_0 K_{ij})} \delta^* K_{ij} + \Bigg[& \frac{\partial \mathcal{L}}{\partial (\partial_0 h_{ij})} - \partial_0 \left(\frac{\partial \mathcal{L}}{\partial (\partial_0^2 h_{ij})} \right) - \partial_k \left(\frac{\partial \mathcal{L}}{\partial (\partial_0 \partial_k h_{ij})} \right) \\ & - \frac{\partial \mathcal{L}}{\partial (\partial_0 K_{kl})} \frac{\partial K_{kl}}{\partial h_{ij}} + \partial_m \left(\frac{\partial \mathcal{L}}{\partial (\partial_0 K_{kl})} \frac{\partial K_{kl}}{\partial (\partial_m h_{ij})} \right) \Bigg] \delta^* h_{ij} \end{aligned} \tag{3.2}$$

where we use the relations, e.g. $\frac{\partial (\partial_0 K_{kl})}{\partial (\partial_0 N)} = \frac{\partial K_{kl}}{\partial N}$. From this expression, if we adopt K_{ij} as the new generalized coordinate, instead of $\partial_0 h_{ij}$, time derivatives of N and N^i are absorbed in that of K_{ij} and the restriction on N and N^i disappears. So K_{ij} is taken as the new generalized coordinate as in the method of BL and is denoted as Q_{ij}. The momenta canonically conjugate to h_{ij} and Q_{ij}, p^{ij} and Π^{ij} respectively, are taken as the coefficients of $\delta^* h_{ij}$ and $\delta^* Q_{ij}$ in (3.2), according to Ostrogradski: $p^{ij} = \frac{\partial \mathcal{L}}{\partial (\partial_0 h_{ij})} - \partial_0 \left(\frac{\partial \mathcal{L}}{\partial (\partial_0^2 h_{ij})} \right) - \partial_k \left(\frac{\partial \mathcal{L}}{\partial (\partial_0 \partial_k h_{ij})} \right) - \frac{\partial \mathcal{L}}{\partial (\partial_0 K_{kl})} \frac{\partial K_{kl}}{\partial h_{ij}} + \partial_m \left(\frac{\partial \mathcal{L}}{\partial (\partial_0 K_{kl})} \frac{\partial K_{kl}}{\partial (\partial_m h_{ij})} \right)$ and $\Pi^{ij} = \frac{\partial \mathcal{L}}{\partial (\partial_0 Q_{ij})}$. Hamiltonian H is defined as the coefficient of $(-1) \times \delta t$ in $L\delta t + \delta F$ after using $\delta q^i = \delta^* q^i + \dot{q}^i \delta t$. Then Hamiltonian density is given by

$$\mathcal{H} = p^{ij} \partial_0 h_{ij} + \Pi^{ij} \partial_0 Q_{ij} - \mathcal{L}. \tag{3.3}$$

It is noted that K_{ij} is half the Lie derivative of h_{ij} along the normal to the hypersurface Σ_t. The momenta p^{ij}, Π^{ij} are rewritten explicitely in terms of the Lie derivatives as follows

$$\begin{cases} p^{ij} = -\sqrt{h} \left[f'(R) Q^{ij} + h^{ij} f''(R) \mathcal{L}_n R + N^{-2} \partial_k N N^k f'(R) h^{ij} \right] \\ \Pi^{ij} = 2\sqrt{h} f'(R) h^{ij} \end{cases} \tag{3.4}$$

where the scalar curvature is expressed as $R = 2h^{ij} \mathcal{L}_n Q_{ij} + Q^2 - 3Q_{ij} Q^{ij} + \tilde{R} - 2\Delta(\ln N)$. It is seen from (3.4) that Π^{ij} has only the trace part and is written $\Pi^{ij} = \frac{1}{d} \Pi h^{ij}$ with $\Pi = 2d\sqrt{h} f'(R)$ where

d is the dimension of space. Converting this relation, we obtain the scalar curvature expressed as $R = f'^{-1}(\Pi/2d\sqrt{h}) \equiv \psi(\Pi/2d\sqrt{h})$.

4 Invariance of the Hamiltonian

Let us consider the following transformation of the generalized coordinates

$$h_{ij} \to \phi_{ij} = F_{ij}(h_{kl}) \quad \text{or} \quad h_{ij} = G_{ij}(\phi_{kl}). \tag{4.1}$$

Under this transformation, three dimensional space is unchanged so that the new generalized coordinate $Q_{ij} = \mathcal{L}_n h_{ij}/2$ is unchanged and so is the momentum canonically conjugate to it $\Pi^{ij} = \partial\mathcal{L}/\partial(\partial_0 Q_{ij})$. These are expressed in terms of the transformed quantities as $Q_{ij} = \frac{1}{2}\mathcal{L}_n G_{ij}(\phi_{kl}), \Pi^{ij} = 2\sqrt{h}f'(\psi)G^{ij}(\phi_{kl})$. Then using these equations, (3.4), and the relation $\delta h_{ij} = \frac{\partial G_{ij}}{\partial \phi_{kl}}\delta\phi_{kl}$, we can show that the first term of δF, (3.2), takes the following form $-\sqrt{h}\left\{f'(\psi)Q^{ij} + G^{ij}f''(\psi)\mathcal{L}_n\psi + N^{-2}\partial_k N N^k f'(\psi)G^{ij}\right\}\frac{\partial G_{ij}}{\partial\phi_{kl}}\delta^*\phi_{kl} + 2\sqrt{h}f'(\psi)G^{ij}\delta^* Q_{ij}$. The momentum p_ϕ^{ij} canonically conjugate to ϕ_{ij} is defined as the coefficient of $\delta^*\phi_{ij}$: $p_\phi^{ij} = -\sqrt{h}\left\{f'(\psi)Q^{kl} + G^{kl}f''(\psi)\mathcal{L}_n\psi + N^{-2}\partial_k N N^k f'(\psi)G^{ij}\right\}\frac{\partial G_{kl}}{\partial\phi_{ij}}$. From (3.4) and this expression of p_ϕ^{ij}, we have the relation, $p^{ij} = \frac{\partial F_{kl}}{\partial h_{ij}}p_\phi^{kl}$. Transformed Hamiltonian density $\mathcal{H}_\phi$ is defined as $\mathcal{H}_\phi \equiv p_\phi^{ij}\dot{\phi}_{ij} + \Pi^{ij}\dot{Q}_{ij} - \mathcal{L}$. The change of the Hamiltonian density is given by $\Delta\mathcal{H} \equiv \mathcal{H}_\phi - \mathcal{H} = p_\phi^{ij}\dot{\phi}_{ij} - p^{ij}\dot{h}_{ij}$. Using (4.1) and the above relation of p^{ij} and p_ϕ^{kl}, we can show that $\Delta\mathcal{H}$ vanishes:

$$\Delta\mathcal{H} = 0. \tag{4.2}$$

This result should be necessary if the Hamiltonian has something to do with the energy.

Application to the FRW spacetime, in which the transformation is from the scale factor $a(t)$ to its function $G(a)$, e.g., $\ln a(t)$, is straightforward.

5 Summary

The formalism of BL is an improved formalism of Ostrogradski, but we showed in the method of BL that a change of the original generalized coordinates induces a change of the Hamiltonian. We proposed a new canonical formalism of $f(R)$-type higher-curvature gravity by combining those of Ostrodradski and BL using the Lie derivatives instead of the time derivatives. The Hamiltonian is shown to be invariant under the transformation of generelized coordinates preserving the hypersurface Σ_t, contrary to the case of the BL method. In fact, the transformation properties in higher-curvature gravity have not been addressed so far.

References

[1] S. Nojiri and S. D. Odintsov, *Phys. Rev. D.* **68** (2003), 123512 : *hep-th/0307288*

[2] S. M. Carroll, V. Duvvuri, M. Trodden and M. S. Turner, *Phys. Rev. D.* **70** (2004), 043528: *astro-ph/0306438*; S. M. Carroll, A. De Felice, V. Duvvuri, D. A. Easson, M. Trodden and M. S. Turner, *astro-ph/0410031*; S. Nojiri and S. D. Odintsov, *Phys. Lett.* **B576** (2003), 5: *hep-th/0307071*; X. Meng and P. Wang, *Class. Quantum Grav.* **20** (2003), 4949 : *astro-ph/0307354*; E. Flanagan, *Phys. Rev. Lett.* **92** (2004), 071101: *astro-ph/0308111*

[3] Y. Ezawa, H. Iwasaki,Y. Ohkuwa, S. Watanabe, N. Yamada and T. Yano, gr-qc/0507060 and see the references cited herein.

[4] M. Ostrogradski, *Mem. Acad. Sci. St. Petersberg* **VI 4** (1850), 385

[5] I. L. Buchbinder and S. L. Lyakhovich, *Class. Quantum Grav* **4** (1987), 1487
I. L. Buchbinder, I. Yu Karataeva and S. L. Lyakhovich, *Class. Quantum Grav.* **8** (1991), 1113

[6] Y. Ezawa, M. Kajihara, M. Kiminami, J. Soda and T. Yano, *Class. Quantum Grav.* **16** (1999), 1873

Non-Gaussianity of one-point distribution functions in the Universe

Takayuki Tatekawa[1], Shuntaro Mizuno[2]

[1]*Department of Physics, Ochanomizu University, Tokyo 112-8610, Japan*
[2]*Department of Physics, Waseda University, Tokyo 169-8555, Japan*

Abstract

We study the one-point probability distribution functions (PDFs) of the density fluctuation in a cosmological fluid. Within the perturbative approach to the structure formation scenario, the effect of "pressure" in the fluid has recently been an area of research interest. Here we analyze the effect of "pressure" for Lagrangian linear perturbation PDFs. Then we consider the dependence of the dark energy models. According to recent observations, the existence of the dark energy has been considered. Even though we have obtained the constraint of the equation of the state for the dark energy ($p = w\rho$) as $-1 \leq w \leq -0.78$ by combining WMAP data with other astronomical data, in order to pin down w, it is necessary to present other independent observational tools. For this purpose, we consider the w dependence of the non-Gaussianity of the density distribution generated by the nonlinear dynamics. In order to subtract the non-Gaussianity, we follow the semi-analytic approach based on the Lagrangian linear perturbation theory which provide accurate value for the quasi-nonlinear region.

1 Background

According to recent observations for type Ia Supernovae [1], the expansion of the Universe is accelerating. Combining measurements of Cosmic Microwave Background Radiation [2] and recent galaxy redshift survey [3], the Universe is almost flat and we are forced to recognize the existence of a cosmological constant, or a kind of dark energy whose value is almost the same order of magnitude as the present density of the Universe [4]. From the viewpoint of particle physics, however, it is quite difficult to explain such a tiny value by 14 orders of magnitude smaller than the electroweak scale. The failure of theoretical explanation for the present value of the cosmological constant is known as the so-called the " cosmological constant problem" [5].

Here we briefly introduce the evolution equations for the background including the information of the dark energy. Assuming the homogeneous and isotropic Universe, the cosmic expansion law is described by the Friedmann equations and the energy conservation equation.

$$H^2 = \frac{8\pi G}{3}\rho - \frac{\mathcal{K}}{a^2}, \tag{1}$$

$$\frac{\ddot{a}}{a} = -\frac{4\pi G}{3}(\rho + 3p), \tag{2}$$

$$\dot{\rho} + 3H(\rho + p) = 0, \tag{3}$$

where a is a scale factor of the Universe, $H = \dot{a}/a$ is its Hubble parameter, $\mathcal{K}$ is a curvature constant, and p and ρ are the total pressure and total energy of matter fields.

As for matter fields, since we are interested in the stage much later than the radiation-matter equality, we consider the matter fluid and the dark energy, i.e., $\rho = \rho_m + \rho_{DE}$, where ρ_m and ρ_{DE} are the energy densities of the matter fluid and the dark energy, respectively.

In order to obtain the evolution of the energy densities for each components, we must specify the properties of the dark energy which are strongly dependent on the dark energy models.

[1]E-mail:tatekawa@cosmos.phys.ocha.ac.jp
[2]E-mail:shuntaro@gravity.phys.waseda.ac.jp

Even though there are some dark energy models in which the dark energy couples explicitly to the ordinal matter [6], the dark energy interacts with ordinal matter by only gravitationally in many models. We consider this case in which the energy conservation of the each component holds independently. For these situations, since the pressure of the matter is negligible, the energy density of the matter evolves as usual

$$\rho_m \propto a^{-3}. \tag{4}$$

As for the evolution of the dark energy, we can use the fact that it is possible to model the dark energy as fluid in many dark energy models [5]. For this case, the dynamical properties of the dark energy are determined through its effective equation of state w:

$$p_{DE} = w(\rho_{DE})\rho_{DE}, \tag{5}$$

where, in general, w is an analytic function of the energy density, or equivalently, the scale factor. However, since it is technically difficult to specify the time dependence of w by observations in near future, we concentrate on the case for constant w, in which case the dark energy density evolves as

$$\rho_{DE} \propto a^{-3(w+1)}. \tag{6}$$

Assuming flat spacetime ($\mathcal{K} = 0$), and using Eqs. (4) and (6), we can rewrite the constraint Eq. (1) as

$$H^2 = H_0^2 \left[\Omega_{m0} a^{-3} + \Omega_{DE0} a^{-3(w+1)}\right], \tag{7}$$

where we have defined the density parameters for the matter and the dark energy:

$$\Omega_{(m,\ DE)} \equiv \frac{8\pi G}{3H^2}\rho_{(m,\ DE)}. \tag{8}$$

and the subscripts 0 denote the corresponding quantities are evaluated at present.

Under this constraint, we solve the Friedmann equation (Eq. (2)).

2 Perturbation

Here we briefly introduce the evolution equation for cosmological fluid. In the comoving coordinates, the basic equations for cosmological fluid are described as

$$\frac{\partial \delta}{\partial t} + \frac{1}{a}\nabla_x \cdot \{\mathbf{v}(1+\delta)\} = 0, \tag{9}$$

$$\frac{\partial \mathbf{v}}{\partial t} + \frac{1}{a}(\mathbf{v}\cdot\nabla_x)\mathbf{v} + \frac{\dot{a}}{a}\mathbf{v} = \frac{1}{a}\tilde{\mathbf{g}} - \frac{1}{a\rho}\nabla_x P, \tag{10}$$

$$\nabla_x \times \tilde{\mathbf{g}} = 0, \tag{11}$$

$$\nabla_x \cdot \tilde{\mathbf{g}} = -4\pi G \rho_b a \delta, \tag{12}$$

$$\delta \equiv \frac{\rho - \rho_b}{\rho_b}. \tag{13}$$

In the Lagrangian perturbation theory [7], the displacement from homogeneous distribution is considered.

$$\mathbf{x} = \mathbf{q} + \mathbf{s}(\mathbf{q}, t), \tag{14}$$

where $\mathbf{x}$ and $\mathbf{q}$ are the comoving Eulerian coordinates and the Lagrangian coordinates, respectively. $\mathbf{s}$ is the displacement vector that is regarded as a perturbative quantity. To solve the perturbative equations, we decompose the Lagrangian perturbation to the longitudinal and the transverse modes:

$$\mathbf{s} = \nabla S + \mathbf{s}^T, \tag{15}$$

$$\nabla \cdot \mathbf{s}^T = 0, \tag{16}$$

where ∇ means the Lagrangian spacial derivative. Hereafter we consider only the longitudinal mode.

Using the Lagrangian displacement, we obtain the first-order perturbative equation.

$$\nabla^2\left(\ddot{S}^{(1)}+2\frac{\dot{a}}{a}\dot{S}^{(1)}-4\pi G\rho_b S^{(1)}-\frac{\kappa\gamma\rho_b^{\gamma-1}}{a^2}\nabla^2 S^{(1)}\right)=0. \tag{17}$$

The first-order solutions for the longitudinal mode depend on spacial scale. Therefore the solutions are described with a Lagrangian wavenumber K. For simplicity, in this paper, we discuss only perturbative solutions in the Einstein-de Sitter Universe model [8].

$$\widehat{S}^{(1)}(\mathrm{K},t) = C^+(\mathrm{K})D^+(\mathrm{K},t)+C^-(\mathrm{K})D^-(\mathrm{K},t), \tag{18}$$

$$D^{\pm}(\mathrm{K},t) = \begin{cases} t^{-1/6}\mathcal{J}_{\pm 5/(8-6\gamma)}(A|\mathrm{K}|t^{-\gamma+4/3}) & \text{for } \gamma\neq\frac{4}{3}, \\ t^{-1/6\pm\sqrt{25/36-B|\mathrm{K}|^2}} & \text{for } \gamma=\frac{4}{3}, \end{cases} \tag{19}$$

$$A\equiv\frac{3\sqrt{\kappa\gamma}(6\pi G)^{(1-\gamma)/2}}{|4-3\gamma|},\quad B\equiv\frac{4}{3}\kappa(6\pi G)^{-1/3},$$

where $\mathcal{J}$ means Bessel function. $C^{\pm}(\mathrm{K})$ is given by the initial condition.

In this model, the behavior of the solutions strongly depends on the relation between the scale of fluctuation and the Jeans scale. Here we define the comoving Jeans wavenumber as

$$K_J\equiv\left(\frac{4\pi Ga^2}{\kappa\gamma\rho_b^{\gamma-2}}\right)^{1/2}. \tag{20}$$

It depends on the ratio between the comoving Jeans wavenumbers and the wavenumber of the fluctuation whether the fluctuation grows. When we ignore the pressure term, we obtain the solutions of ZA.

$$S^{(1)}=t^{2/3}S_+(\mathrm{q})+t^{-1}S_-(\mathrm{q}). \tag{21}$$

$S_{\pm}(\mathrm{q})$ is given by the initial condition.

3 Non-Gaussianity of the one-point probability distribution

In order to analyze the statistics, we introduce the one-point probability distribution function (PDF). For example, here we show the one-point PDF of the density fluctuation field $P(\delta)$ (PDF of the density perturbation) which denotes the probability to obtain the value δ. If δ is a random Gaussian field, the PDF of the density perturbation is determined as

$$P(\delta)=\frac{1}{(2\pi\sigma^2)^{1/2}}e^{-\delta^2/2\sigma^2},$$

where $\sigma\equiv\left\langle(\delta-\langle\delta\rangle)^2\right\rangle$ and $\langle\ \rangle$ denotes the spacial average.

If the PDF deviates from Gaussian distribution, in order to specify it, it is necessary to introduce the following higher order statistical quantities [9, 10, 11]:

$$\text{skewness} \ : \ \gamma=\left\langle\left(\frac{\delta-\langle\delta\rangle}{\sigma}\right)^3\right\rangle,$$

$$\text{kurtosis} \ : \ \eta=\left\langle\left(\frac{\delta-\langle\delta\rangle}{\sigma}\right)^4\right\rangle-3,$$

which mean the display asymmetry and non-Gaussian degree of "peakiness", respectively.

For initial condition, we consider the Gaussian density field generated by COSMICS [12] and we set the value of the density fluctuation and the peculiar velocity to be those obtained by the Lagrangian linear perturbation with the time evolution of the background to be $a\propto t^{2/3}$.

First we analyse the one-point PDFs of the peculiar velocity and the density fluctuation in both the dust model and the EJN model [13]. Because the pressure reflects a nonlinear effect of the motion of the fluid. the pressure model would include nonlinear effects. However, we found that the PDFs of the peculiar velocity remain Gaussian, even if we consider the pressure. For the PDFs of the density fluctuation, the occurrence of non-Gaussianity depends on the "equation of state" for the fluid.

Then we consider the w dependence of the non-Gaussianity of the density distribution [14]. In the quasi-nonlinear region, i.e. high-z region, we showed the difference of the non-Gausianity between several cases of w with Lagrangian linear perturbation. For the highly non-linear region, we estimate the difference by combining with this perturbative approach and N-body simulation executed for our previous paper. From this, we can expect the difference is enhanced more in low-z region, which suggests that the non-Gaussianity of the density distribution potentially play important role for existing the information of the dark energy. Therefore we would propose that we can take a limit for w with the non-Gaussianity of the density fluctuation from future galaxy survey projects.

References

[1] S. Perlmutter *et al.*, Astrophys. J. **517**, 565 (1999); A. G. Riess, Astron. J. **116**, 1009 (1998).

[2] C. L. Bennett *et al.*, Astrophys. J. Supp. **148**, 1 (2003).

[3] M. Tegmark *et al.*, Astrophys. J. **606**, 702 (2004).

[4] D. N. Spergel *et al.*, Astrophys. J. Supp. **148**, 175 (2003).

[5] S. Weinberg, Rev. Mod. Phys. **61**, 1 (1989); V. Sahni and A. A. Starobinsky, Int. J. Mod. Phys. D **9**, 373 (2000).

[6] J. A. Frieman, C. T. Hill, and R. Watkins, Phys.Rev. **D46** 1226 (1992); L. Amendola, Phys. Rev. **D62**, 043511 (2000); J. Khoury and A. Weltman, Phys. Rev. Lett. **93**, 171104 (2004).

[7] Ya. B. Zel'dovich, Astron. Astrophys. **5**, 84 (1970); V. Sahni and P. Coles, Phys. Rep. **262**, 1 (1995); T. Tatekawa, astro-ph/0412025.

[8] M. Morita and T. Tatekawa, Mon. Not. R. Astron. Soc. **328**, 815 (2001); T. Tatekawa, M. Suda, K. Maeda, M. Morita, and H. Anzai, Phys. Rev. **D66**, 064014 (2002).

[9] L. Kofman, E. Bertschinger, J. M. Gelb, A. Nusser and A. Dekel, Astrophys. J. **420**, 44 (1994).

[10] P. J. E. Peebles, *The Large-Scale Structure of the Universe* (Princeton: Princeton University Press, 1980) p 151

[11] J. Peacock, *Cosmological Physics* (Cambridge: Cambridge University Press, 1999)

[12] C. P. Ma and E. Bertschinger, Astrophys. J. **455**, 7 (1995).

[13] T. Tatekawa, JCAP **04**, 018 (2005).

[14] T. Tatekawa and S. Mizuno, astro-ph/0511688.

Non-BPS D9-branes in the Early Universe

Kenji Hotta[1]

[1] *High Energy Accelerator Research Organization (KEK), Tsukuba, Ibaraki, 305-0801, Japan*

Abstract

We have shown that non-BPS D9-branes become stable near the Hagedorn temperature based on boundary string field theory in our previous work. This implies that there is a possibility that non-BPS D9-branes exist in the early universe. We study the time evolution of the universe in the presence of non-BPS D9-branes based on boundary string field theory. We obtain some classical solutions for dilaton gravity.

1 Introduction

Non-BPS D-branes and D-brane–anti-D-brane pairs are unstable systems in superstring theory. The spectrum of open strings on these unstable branes contains a tachyon field T. We have pointed out that the spacetime-filling branes such as non-BPS D9-branes and D9-$\overline{\text{D9}}$ pairs become stable near the Hagedorn temperature based on boundary string field theory (BSFT) [1]. The aim of article is to apply these works to cosmology. We will investigate the time evolution of the universe in the presence of non-BPS D9-branes. We must consider gravity coupled to non-BPS D9-branes in order to analyze a time evolution of the universe. Since we have computed the finite temperature effective potential based on BSFT, it is natural to deal with the tachyon field at low temperature based on BSFT. The time dependent background at zero temperature has been discussed by Sugimoto and Terashima based on BSFT [2]. It would be interesting to generalize their calculation to the finite temperature case. We try to construct the following scenario for the early universe: The universe expands near the Hagedorn temperature and the open string gas on the non-BPS D9-branes dominates the total energy of the system at first. The temperature decreases as the universe expands. Then $T = 0$ becomes the local maximum of the potential and the non-BPS D9-branes become unstable at low temperature. Finally, the tachyon rolls down the potential and the non-BPS D9-branes disappear. This article is based on our paper [3].

2 Action

The low energy effective action for tree level closed strings is described by type IIA supergravity. We shall focus on 10-dimensional metric $g_{\mu\nu}$ and dilaton ϕ. The action is given by[2]

$$S_{dil} = -\frac{1}{2\kappa^2}\int d^{10}x\sqrt{-g}\, e^{-2\phi}\left(\mathcal{R} + 4\nabla_\mu\phi\nabla^\mu\phi\right). \tag{1}$$

We must also consider the action for non-BPS D9-branes. We only deal with the high temperature case and the zero temperature case. First, let us describe the high temperature case. In the case that the universe is sufficiently hot and the non-BPS D9-branes are stable, $T = 0$ is the potential minimum [1]. In this case it is sufficient to deal with the action for open string gas [1]. The action is represented as

$$S_{gas} = \int d^{10}x\sqrt{-g}\; F(\beta\sqrt{g_{00}}), \tag{2}$$

where F is the free energy of open string gas. The energy-momentum tensor can be represented in a perfect fluid form such as $T_\mu{}^\nu = diag(-\rho, p, \cdots, p)$. The equation of state is approximated as

$$p \simeq 0. \tag{3}$$

[1] E-mail:khotta@post.kek.jp

[2] We have also investigated the constant dilaton case [3]

Secondly, we describe the zero temperature case. Since we have computed the finite temperature effective potential for non-BPS D-branes based on BSFT, it is consistent to argue the zero temperature case based on BSFT. We shall focus on tachyon T, metric $g_{\mu\nu}$ and dilaton ϕ. Then the action is given by

$$S_{dilT} = \mu \int d^{10}x\sqrt{-g}\, e^{-\phi} e^{-\alpha T^2} \mathcal{F}\left(\lambda \nabla_\mu T \nabla^\mu T\right), \qquad \mathcal{F}(z) = \frac{\sqrt{\pi}\,\Gamma(z+1)}{\Gamma\left(z+\frac{1}{2}\right)}, \tag{4}$$

where α, λ and μ are constants. Here we include the factor $e^{-\phi}$ as a contribution of dilaton since this action is derived from the tree level (disk) amplitude of open strings.

3 Open String Gas Case

Let us first consider the high temperature case. The action we consider is the sum of (1) and (2). We assume that the universe is spatially homogeneous and isotropic, and that the metric is given by the spatially flat Robertson-Walker one. The equation of motion is calculated as

$$\begin{aligned} 9(\dot{H}+H^2) - 2\ddot{\phi} + \kappa^2 e^{2\phi}\rho &= 0, & (5)\\ \dot{H} + 9H^2 - 2H\dot{\phi} - \kappa^2 e^{2\phi} p &= 0, & (6)\\ 9(\dot{H}+5H^2) + 2\dot{\phi}^2 - 2\ddot{\phi} - 18H\dot{\phi} &= 0. & (7) \end{aligned}$$

By using the equation of state (3), we can show that the total energy is a constant $E \equiv \rho a^9 \simeq E_0$. In this case we can obtain the general solution. The expansion solution is given by

$$a(t) = a_0 \left(\frac{t-b_2}{t+b_1}\right)^{\frac{1}{3}}, \qquad \phi(t) = \ln \frac{2{a_0}^9 \mid t-b_2 \mid}{\kappa^2 E_0 (t+b_1)^2}, \tag{8}$$

where a_0, b_1 and b_2 are constants. This solution is defined in the region $t < -b_1$ or $t > b_2$. We display the time evolution of the scale factor $a(t)$ and the coupling $g_s(t) = e^{\phi(t)}$ in Figure 1. For $t < -b_1$, the universe evolves from the infinite past in the accelerated expansion phase. It should be noted that there is no initial singularity. The scale factor diverges at $t = -b_1$. However, the temperature decreases as the scale factor increases, and $T = 0$ becomes the local maximum of the potential. Then the tachyon starts to roll down the potential. For $t \geq b_2$, on the other hand, the universe evolves in the decelerated expansion phase at first. We cannot avoid the initial singularity in this case. We must consider the α' correction near the curvature singularity. The scale factor asymptotically approaches to a constant. If ${E_0}/{{a_0}^9}$ is smaller than the string scale, we can show that the temperature becomes much lower than the Hagedorn temperature and the tachyon rolls down the potential [3].

4 Rolling Tachyon Case

Let us next consider the zero temperature case. The action we consider is the sum of (1) and (4). The equations of motion is calculated as[3]

$$\begin{aligned} 18(\dot{H}+H^2) - 4\ddot{\phi} + \mu\kappa^2 e^{\phi-\alpha T^2}\left\{4\lambda\dot{T}^2\mathcal{F}'(-\lambda\dot{T}^2) + \mathcal{F}(-\lambda\dot{T}^2)\right\} &= 0, & (9)\\ 2(\dot{H}+9H^2) - 4H\dot{\phi} + \mu\kappa^2 e^{\phi-\alpha T^2}\mathcal{F}(-\lambda\dot{T}^2) &= 0, & (10)\\ 18(\dot{H}+5H^2) + 4\dot{\phi}^2 - 4\ddot{\phi} - 36H\dot{\phi} - \mu\kappa^2 e^{\phi-\alpha T^2}\mathcal{F}(-\lambda\dot{T}^2) &= 0, & (11)\\ 2\lambda^2\dot{T}^2\ddot{T}\mathcal{F}''(-\lambda\dot{T}^2) - \lambda\left(\ddot{T} + 9H\dot{T} - 2\alpha T\dot{T}^2 - \dot{\phi}\dot{T}\right)\mathcal{F}'(-\lambda\dot{T}^2) + \alpha T\mathcal{F}(-\lambda\dot{T}^2) &= 0. & (12) \end{aligned}$$

In order to obtain the reasonable initial condition for numerical calculation, we derive the exact solution in the $T = 0$ case. By using the parameter τ, the solution is represented as

$$a = |c_1\tau + c_2|^{\frac{2}{9}} \exp\left[-\frac{2}{9}(\tau^2 + c_3\tau + c_4)\right], \qquad \phi = \frac{2}{3}\left\{\ln|c_1\tau + c_2| - 2(\tau^2 + c_3\tau + c_4)\right\}, \tag{13}$$

$$\frac{d\tau}{dt} = \frac{3\mu^{\frac{1}{2}}\kappa}{4}|c_1\tau + c_2|^{\frac{1}{3}} \exp\left[-\frac{2}{3}(\tau^2 + c_3\tau + c_4)\right], \tag{14}$$

[3]The independent equations are only three equations under the condition $\dot{\phi} \neq 0$.

where $c_1 \sim c_4$ are integration constants with $c_1 c_3 = 2c_2$. Since the right hand side of (14) is positive in $\tau < -c_2/c_1$ and $\tau > -c_2/c_1$, t is a monotone increasing function of τ in both regions. For $\tau \leq -c_2/c_1$, the universe evolves in the accelerated expansion phase at first and turns to be in the decelerated expansion phase, then contracts towards a singularity, while for $\tau \geq -c_2/c_1$ the universe evolves in the decelerated expansion phase at first and turns to be in the contraction phase as is depicted in Figure 2.

Let us now turn to the numerical calculation. We first consider the initial condition close to the decelerated expansion phase for $\tau \geq -c_2/c_1$ in the $T = 0$ case. It is expected that the decelerated expansion solution in the high temperature case is smoothly connected to this phase. If we take a large c_1, the transition to the contraction phase occurs before the tachyon rolls down the potential. We must set c_1 to a small value in order to keep the decelerated expansion phase. The tachyon asymptotically approaches to

$$T \to \frac{t}{\sqrt{\lambda}} + \text{const.} \tag{15}$$

as $t \to \infty$. This comes from the divergence of $\mathcal{F}(z)$ and its derivative at $z = -1$. We can derive (15) from $-\lambda \dot{T}^2 = -1$. Sugimoto and Terashima have shown that the ratio p/ρ for the tachyon field vanishes at $z = -1$ [2]. Thus, tachyon matter is produced, and the equation of state becomes $p = 0$.

Secondly, let us consider the initial condition close to the decelerated expansion phase for $\tau \leq -c_2/c_1$ in the $T = 0$ case. It is expected that the accelerated expansion solution in the high temperature case is smoothly connected to the accelerated expansion phase for $\tau \leq -c_2/c_1$ in the $T = 0$ case. The results are very sensitive to the initial condition. If we set the tachyon $T = 0.01$ and its derivative $\dot{T} = 0$ at $\tau = -1.17$ the universe evolves from deceleration to acceleration, while if we set them at $\tau = -1.16$ the universe evolves from expansion to contraction as is depicted in Figure 3. The scale factor diverges or vanishes within finite time, and the curvature diverges in both cases. We must deal with the α' corrections in these cases. We can see from Figure 3 that the tachyon asymptotically approaches to (15) as $t \to \infty$ in both cases. Thus, the tachyon matter is produced also in these cases.

5 Conclusion and Discussion

We have investigated the time evolution of the universe in the presence of non-BPS D9-branes by using dilaton gravity. We obtain two types of cosmological scenario. First, the universe evolves in the decelerated expansion phase at high temperature, and this phase is kept even at low temperature. Secondly, the universe evolves from the infinite past in the accelerated expansion phase, and the universe evolves in the accelerated expansion phase or in the accelerated contraction phase at last.

We have only considered the very simple case that the tachyon rolls down homogeneously. In general, we must deal with the inhomogeneous case. If the tachyon condensates in a topologically non-trivial configuration, lower dimensional branes form as topological defects. All the lower-dimensional D-branes in type II string theory are realized as topological defects through tachyon condensation from non-BPS D9-branes and D9-$\overline{\text{D9}}$ pairs. Thus, if there exist non-BPS D9-branes in the early universe, various kinds of branes may form through tachyon condensation. It would be interesting to examine the possibility that our Brane World forms as a topological defect in a cosmological context. In this sense, our work is a first step towards 'Brane World Formation Scenario'.

References

[1] K. Hotta, "Brane-Antibrane Systems at Finite Temperature and Phase Transition near the Hagedorn Temperature," JHEP **0212** (2002) 072, hep-th/0212063; "Finite Temperature Systems of Brane-Antibrane on a Torus," JHEP **0309** (2003) 002, hep-th/0303236; "Finite Temperature Systems of Brane-Antibrane Pairs and Non-BPS D-branes," Prog. Theor. Phys. **112** (2004) 653, hep-th/0403078.

[2] S. Sugimoto and S. Terashima, "Tachyon Matter in Boundary String Field Theory," JHEP **0207** (2002) 025, hep-th/0205085.

[3] K. Hotta, "Non-BPS D9-branes in the Early Universe," hep-th/0601133.

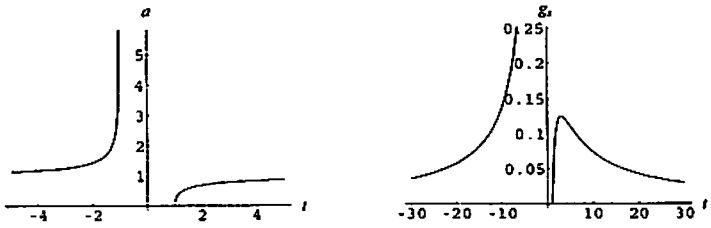

Figure 1: The time evolution of the scale factor $a(t)$ (left) and the string coupling $g_s(t)$ (right) in the case of dilaton gravity coupled to open string gas. We have set $a_0 = b_1 = b_2 = 1$.

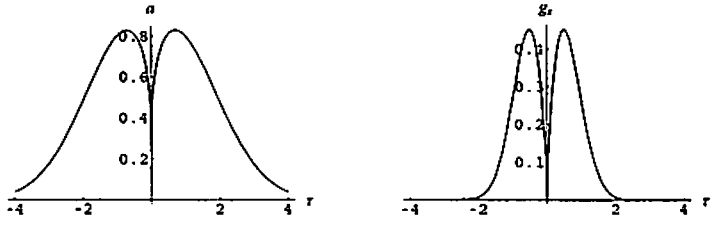

Figure 2: The time evolution of the scale factor $a(t)$ (left) and the string coupling $g_s(t)$ (right) in the $T = 0$ case. We have set $c_1 = 1, \quad c_2 = c_3 = c_4 = 0$.

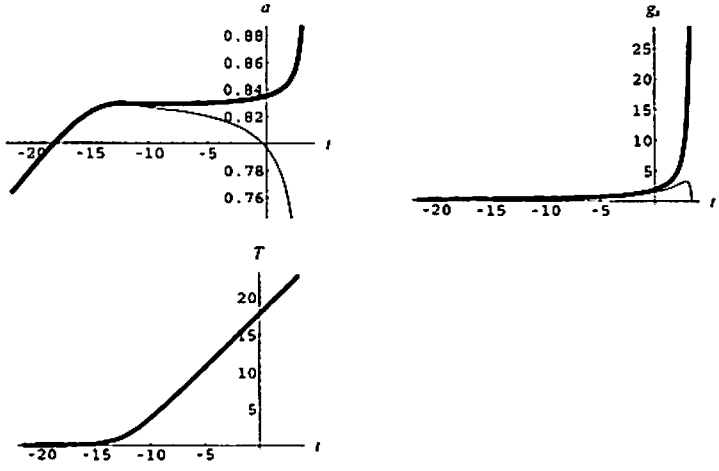

Figure 3: The time evolution of the scale factor $a(t)$ (left), the string coupling $g_s(t)$ (right) and the tachyon $T(t)$ (below) for the initial parameter $\tau = -1.17$ (thick line) and $\tau = -1.16$ (thin line). We have set $c_1 = 1, \quad c_2 = c_3 = c_4 = 0$. The initial condition for the tachyon is $T = 0.01$ and $\dot{T} = 0$.

Black Hole Evaporation in Vaidya Spacetime

Shintaro Sawayama[1]

[1] *Theoretical Astrophysics Group, Department of Physics, Tokyo Institute of Technology, Tokyo 152-8551, Japan*

Abstract

We consider how the black holes mass decreases by the Hawking radiation as the back re-action in the Vaidya spacetime. And we can obtain the analytical equation how the black holes mass decreases using the dynamical horizon equation considered by Ashtekar and Krishnan. The back re-action problem in the black hole universe can be solved to use the technique of the dynamical horizon.

1 Introduction

How the mass of black holes decreases by the Hawking effect [1] is long standing problem. Because to take into account of the Hawking radiation, we should solve the field equation, which is fourth order differential equation and it is not easy to fined analytical equation. There are many works concerning this problem, which comes from the string theories [2][3][4] or the apparent horizons[5][6] or numerical simulations[7][8]. Old work was given by Page that is $M \sim M^{-2}$[9]. Recently, Ashtekar and Krishnan defined the dynamical horizon and they derived the equation that tells us how black hole radius changes from the Einstein equation[10][11]. Using the dynamical horizon equation, we can treat the back re-action problem and we can obtain the analytical equation how black holes mass decreases.

In section 2, dynamical horizon is reviewed. In section 3, the location of the dynamical horizon in the Vaidya spacetime is identified. And then in section 4, the dynamical horizon equation is written down in the case of Vaidya matter with the Hawking effect being taken into account. Section 5 is devoted to conclusion and discussions. This paper is shorted and modified version of my previous paper [12].

2 Dynamical Horizon

Ashtekar and Krishnan considered dynamical horizon, and derived a new equation that dictates how the dynamical horizon radius changes. Apparent horizon is a time slice of the dynamical horizon. The definition of dynamical horizon is,

Definition (modified version). A smooth, three-dimensional, spacelike or **timelike** submanifold H in a space-time is said to be a *dynamical horizon* if it is foliated by preferred family of 2-spheres such that, on each leaf S, the expansion $\Theta_{(l)}$ of a null normal l^a vanishes and the expansion $\Theta_{(n)}$ of the other null normal n^a is strictly negative.

The requirement that one of the null expansions is zero comes from the intuition that black hole does not emit even light. And the requirement that other null expansion is strictly negative comes from that null matter goes in black holes inwards.

In this definition, we can recapitulate the important formula which gives a change of the dynamical horizon radius by the matter flow, using 3+1 and 2+1 decompositions and also the Gauss-Bonet theorem, we can obtain

$$(\frac{R_2}{2G} - \frac{R_1}{2G}) = \int_{\Delta H} \tilde{T}_{ab}\hat{\tau}^a\xi^b_{(R)}d^3V + \frac{1}{16\pi G}\int_{\Delta H}(|\sigma|^2 + 2|\zeta|^2)d^3V. \quad (1)$$

Here $\tilde{T}_{ab}$ means it contains cosmological constant, however we does not use cosmological constant in this paper. This is the dynamical horizon equation that tells how the horizon radius changes by the matter

[1] E-mail:shintaro@phys.titech.ac.jp

flow, shear and expansion. In the spherically symmetric case that we shall consider in what follows the second term of the right hand side vanishes. Although in the case of quantum field theory in curved space time, the dominant energy condition does not hold[13][14], we can use the dynamical horizon equation because it is valid even when the black hole radius decreases. And the dynamical horizon equation is a consequence of the Einstein equation. We use the dynamical horizon equation in place of the Einstein equation.

3 Vaidya Spacetime

The Vaidya metric is of the form

$$ds^2 = -Fdv^2 + 2Gdvdr + r^2 d\Omega^2, \tag{2}$$

where F and G are functions of v and r, and v is the null coordinate and r is the area radius, and M is the mass defined by $M = \frac{r}{2}(1 - \frac{F}{G^2})$, a function of v and r. This metric is spherically symmetric. By substituting the Vaidya metric (2) into the Einstein equation so that we can identify the energy-momentum tensor T_{ab} as

$$8\pi T_{vv} := \frac{2}{r^2}(FM_{,r} + GM_{,v}) \tag{3}$$

$$8\pi T_{vr} := -\frac{2G}{r^2}M_{,r} \tag{4}$$

$$8\pi T_{rr} := \frac{2G_{,r}}{rG}. \tag{5}$$

We do not need to check that the solution of the dynamical horizon equation satisfies the Einstein equation. Because we would like to consider the Schwarzschild like metric, we set $v = t + r^*$, where r^* is tortoise coordinate with dynamics

$$r^* = r + 2M(v)\ln\left(\frac{r}{2M(v)} - 1\right). \tag{6}$$

For later convenience, we write $a = \partial r/\partial r^*|_v$. There are two null vectors,

$$l^a = \begin{pmatrix} l^t \\ l^{r_*} \\ l^\theta \\ l^\phi \end{pmatrix} = \begin{pmatrix} -a^{-1} \\ a^{-1} \\ 0 \\ 0 \end{pmatrix}, \quad \text{and} \quad n^a = \begin{pmatrix} n^t \\ n^{r_*} \\ n^\theta \\ n^\phi \end{pmatrix} = \begin{pmatrix} -a^{-1} \\ -\frac{F}{F-2Ga}a^{-1} \\ 0 \\ 0 \end{pmatrix}. \tag{7}$$

Here we multiply a^{-1} so that $l^a = v^a$. From now on we put,

$$F = \left(1 - \frac{2M(v)}{r}\right) \tag{8}$$

$$G = 1, \tag{9}$$

in a similar form to the Schwarzschild metric, assuming that $M(v)$ is a function of v only. For a constant M, the metric coincides with the Schwarzschild metric. We calculate the expansions $\Theta_{(l)}$ and $\Theta_{(n)}$ of the two null vectors l^a, n^a, because the definition of the dynamical horizon requires one of the null expansions to be zero and the other to be minus. The result is, [2]

$$\Theta_{(l)} = \frac{1}{r}(2F - a) \tag{10}$$

$$\Theta_{(n)} = \frac{1}{ar}\left(\frac{-2F^2 + aF - 2a^2}{-F + 2a}\right). \tag{11}$$

From $\Theta_{(l)} = 0$ we obtain,

$$r_D = 2M + 2Me^{-v/2M}. \tag{12}$$

Note that this dynamical horizon radius is outside of the $r = 2M$, that is anothor solution.

[2] This result is different from Ashtekar and Krishnan, because of the definition of r^*. There is another difinition of r^*, that is $r^* = \int F^{-1}dr$.

4 Dynamical Horizon Equation with Hawking Radiation

At first we calculate the dynamical horizon equation only of the Vaidya matter. Calculating the stress-energy tensor $T_{\hat{t}\hat{l}}$ as,

$$T_{\hat{t}\hat{l}} = -\frac{1}{4\pi r^2}\frac{5}{2}M_{,v}F^{-1}. \tag{13}$$

For the dynamical horizon integration (1), we obtained

$$\int_{r_1}^{r_2} 4\pi r_D^2 T_{\hat{t}\hat{l}} dr_D = \frac{5}{2}\int_{M_1}^{M_2}(1+e^{-v/2M})dM. \tag{14}$$

In the above calculation, we treat $M_{,v}$ and F^{-1} with r_D fixed, because these functions are used only in the integration. Inserting equation (14) to the dynamical horizon equation (1), we obtain

$$\frac{1}{2}(2M+2Me^{-v/2M})\Big|_{M_1}^{M_2} = \int_{M_1}^{M_2}\frac{5}{2}(1+e^{-v/2M})dM. \tag{15}$$

Taking the limit $M_2 \to M_1 = M$, we obtain

$$-\frac{3}{2}(1+e^{-v/2M}) + \frac{v}{2M}e^{-v/2M} = 0. \tag{16}$$

This equation is the dynamical horizon equation in the case that only the Vaidya matter is present. There is no solution of this equation, except the trivial one ($F = 0$ or $r = 2M$), so

$$r_D = 2M(v). \tag{17}$$

Here $M(v)$ is the arbitrary function only of the v, which represent the Vaidya black hole spacetime.

Next, we take into account the Hawking radiation. To solve this problem, we use two ideas that is to use the dynamical horizon equation, and to use the Vaidya metric. The reason to use the dynamical horizon equation comes from the fact that we need only information of matter near horizon, without solving the full Einstein equation with back reaction being the fourth order differential equations, for a massless scalar field. For the matter on the dynamical horizon, we use the result of Candelas [15], which assumes that spacetime is almost static and is valid near the horizon, $r \sim 2M$.

$$T_{\hat{t}\hat{l}} = \frac{1}{2M^4 c\pi^2(1-2M/r)^2}, \tag{18}$$

where $c = 61440$. This matter energy is negative near the event horizon. In the dynamical horizon equation, if black hole absorbs negative energy, black hole radius decreases. This is one of the motivations to use the negative energy tensor. Calculating the integration on the right hand side of (1) for this matter,

$$b\int \frac{r_D^2}{M^4(1-2M/r_D)^2}dr_D = b\int_{R_1}^{R_2}\frac{4(1+e^{-v/2M})^4}{M^2}e^{-v/M}\left(2(1+e^{-v/2M}) + \frac{v}{M}e^{-v/2M}\right)dM. \tag{19}$$

Here b is a constant, that is $b = 1/30720\pi$. If we also take account of the contribution of the Vaidya matter, and inserting this into the integration to the dynamical horizon equation (1), we obtain

$$\frac{1}{2}(2M+2Me^{-v/2M})\Big|_{M_1}^{M_2} = b\int_{M_1}^{M_2}\frac{2^2(1+e^{-v/2M})^4}{M^2}e^{-v/M}\left(2(1+e^{-v/2M}) + \frac{v}{M}e^{-v/2M}\right)dM + \int_{M_1}^{M_2}\frac{5}{2}(1+e^{-v/2M})dM. \tag{20}$$

Taking the limit $M_2 \to M_1 = M$, we finally get

$$M^2 = \frac{8b(1+e^{-v/2M})^4 e^{v/M}}{-\frac{3}{2}(1+e^{-v/2M}) + \frac{v}{2M}e^{-v/2M}}\left((1+e^{-v/2M}) + \frac{v}{2M}e^{-v/2M}\right). \tag{21}$$

This is the main result of the present work that describes how the mass of black hole decreases. This equation is the transcendental equation, so usually it cannot be solved analytically. However, with the right hand side depending only on $-v/2M$, we can easily treat Eq.(21) numerically.

5 Conclusion and Discussions

We have derived an equation which describes how the black hole mass changes taking into account of the Hawking radiation, in the special Vaidya spacetime which becomes the Schwarzschild spacetime in the static case. From the analysis of the transcendental equation (21), we have shown that the black hole mass eventually vanishes and the spacetime becomes the Minkowski spacetime independent of the initial black hole mass size.

The dynamical horizon method in this paper can take into account of the back reaction of the Hawking radiation without solving the field equation which contains the fourth order differentials.

In the limit of the black hole mass going to zero, the derivative of the mass becomes small in proportion to the null coordinate ($v = t+r^*$). On the other hand as the black hole mass becomes large, the derivative behaves the minus of the inverse of the logarithm of the mass. Our result, which is different from Page's result, comes from the fact that in the large mass limit, the black hole radius behaves like quadratic of the black hole mass. This probably comes from when large mass limit that the approximation $r \to 2M$ is broken.

We would like to compare the present work to the preceding works. Sorkin and Piran or Hamade and Stewart used a massless scalar field instead of the Hawking radiation as the back reaction directly. The conclusion of their paper is that black hole starts with the small mass and it evaporates or increases. However, it is shown in the present work that even if the black hole starts with a large mass it always vanishes.

Although we have treated the black hole evaporation semi-classically, we hope this work will give an intuition to quantization of black holes.

References

[1] S.W.Hawking *Commun. Math. Phys.* **43** 199 (1975)

[2] C.M.Harris and P.Kanti *JHEP* 0310 014 hep-ph/0309054 (2003)

[3] J.G.Russo hep-th/0501132

[4] T.Tanaka *Prog.Theor.Phys.Suppl* **148** 307 (2003)

[5] P.Anninos et. al. *Phys. Rev. Lett.* **74** 630 (1995)

[6] S.A.Hayward gr-qc/0506126 gr-qc/0404077 gr-qc/0408008

[7] E.Sorkin and T.Piran *Phys. Rev.* **D 63** 124024 (2001)

[8] R.S.Hamade and J.M.Stewart *Class. Quantum Grav.* **13** 497 (1996)

[9] D.N.Page *Phys. Rev.* **D 13** 198 (1976)

[10] A.Ashtekar, B.Krishnan *Phys. Rev. Lett* **89** 261101 (2002)

[11] A.Ashtekar, B.Krishnan gr-qc/0407042 (2005)

[12] S.Sawayama gr-qc/0509048 (2005)

[13] L.H.Ford gr-qc/9707062 (1997)

[14] N.D.Birrell and P.C.W.Davies *Quantum fields in curved space* Cambridge University Press (1982)

[15] P.Candelas *Phys. Rev.* **D 21** 2185 (1980)

Can thick braneworlds be self-consistent?

Masato Minamitsuji[1], Wade Naylor[2], Misao Sasaki[3]

[1] *Department of Earth and Space Science, Graduate School of Science, Osaka University, Toyonaka 560-0043, Japan*
[2] *Department of Physics, Ritsumeikan University, Kusatsu, Shiga 525-8577, Japan*
[3] *Yukawa Institute for Theoretical Physics, Kyoto University, Kyoto 606-8502, Japan*

Abstract

We discuss the backreaction of a massless, minimally coupled, quantized scalar field on a thick, two-dimensional de Sitter (dS) brane. We show that a finite brane thickness *naturally* regularizes the backreaction on the brane. The quantum backreaction exhibits a quadratic divergence in the thin wall limit. We also give a *theoretical* bound on the brane thickness, in terms of the *brane* self-consistency of the quantum corrected Einstein equation, namely the requirement that the size of the backreaction should be smaller than that of the background stress-energy at the center of the brane. Finally, we discuss the *brane* self-consistency for the case of a four-dimensional dS brane.

1 Introduction

Recent progress in string theory suggests that our universe is, in reality, a four-dimensional submanifold, *brane*, embedded into a higher-dimensional spacetime, *bulk*. The model which was proposed by Randall and Sundrum (RS) succeeds in the localization of gravity around the brane due to the warping of the extra-dimension [1] and have given phenomenological grounds from various aspects of higher-dimensional theories of gravity, see e.g., Ref. [2].

In RS braneworlds, occasionally, fields which exist in the bulk affect the dynamics of the brane. These bulk fields are naturally set into the bulk as a result of a dimensional reduction of some higher-dimensional gravitational theory. Then, the problem we pose is whether or not the self-consistency of the quantum corrected Einstein equations can be kept on the brane: The quantum backreaction of any bulk fields, especially for the higher-dimensional, Kaluza-Klein (KK) modes, should be much smaller than the background stress-energy, such that the original features of the classical model are not changed. However, it is well-known that for thin branes surface divergences of KK modes remain on the brane even after UV regularization, which prevents one from evaluating any quantities exactly on the brane, e.g., see Ref. [3] and references therein.

To overcome this pathology, in Ref. [4] we proposed a new regularization scheme by a finite brane thickness and demonstrated this for a thick dS brane model discussed in Ref. [5]. In this presentation, based on Ref. [6], we shall demonstrate that, similarly, a finite thickness also regularizes the quantum backreaction. We give a *theoretical* bound on the thickness in terms of *brane* self-consistency and comment on the realistic case of a four-dimensional brane.

2 Set-up

The action of the system is given by

$$S = \frac{1}{2}\int d^{d+1}x\sqrt{-g}\Big({}^{(d+1)}R - (\partial\phi)^2 - 2V_0\big(\cos\big[\frac{\phi}{\phi_0}\big]\big)^{2(1-\sigma)} - (\partial\chi)^2\Big), \tag{1}$$

where the bulk field ϕ, which is assumed to be static ($\phi = \phi(z)$), supports the thick brane configuration and $\chi(x^\mu, z)$ is a test quantized scalar field propagating on the background produced by the scalar field

[1] E-mail:masato@vega.ess.sci.osaka-u.ac.jp
[2] E-mail:naylor@se.ritsumei.ac.jp
[3] E-mail:misao@yukawa.kyoto-u.ac.jp

ϕ. Note that $-\infty < z < \infty$ represents the coordinate of the extra-dimension and we choose the center of the domain wall to be at $z = 0$. We work with units such that the $(d+1)$-dimensional gravitational constant $\kappa_{d+1}^2 = M_{d+1}^{-(d-1)}$ is set to unity, where M_{d+1} is the $(d+1)$-dimensional Planck mass. Here, we are assuming that the field χ is a massless, minimally coupled scalar field, which is formally equivalent to tensor metric perturbations [4]. The thick dS brane solution is given by

$$ds^2 = b^2(z)\left(dz^2 + \gamma_{\mu\nu}dx^\mu dx^\nu\right); \quad b(z) = \left(\cosh\left(\frac{Hz}{\sigma}\right)\right)^{-\sigma},$$
$$\phi(z) = \sqrt{(d-1)\sigma(1-\sigma)}\sin^{-1}\left(\tanh\left(\frac{Hz}{\sigma}\right)\right), \quad H^2 = \frac{2\sigma V_0}{(d-1)[1+(d-1)\sigma]}; \qquad (2)$$

$\gamma_{\mu\nu}$ is the d-dimensional dS metric [5] with $\gamma_{\mu\nu}dx^\mu dx^\nu = -dt^2 + H^{-2}\cosh^2(Ht)d\varphi^2$ for $d = 2$, where $-\infty < t < +\infty$ and $0 \le \varphi < 2\pi$. The brane thickness is parameterized by σ (the physical thickness is σ/H), which is restricted to $0 < \sigma < 1$.

3 Backreaction of a quantized bulk scalar field

We shall discuss the quantum backreaction of the scalar field χ on such a thick-brane background, specifically at $z = 0$. By varying the χ-field part of the action, in Eq. (1), with respect to the bulk metric we obtain the stress-energy tensor for the χ-field; $T_{ab} := \chi_{;a}\chi_{;b} - (1/2)g_{ab}g^{cd}\chi_{;c}\chi_{;d}$.

Furthermore, for simplicity we shall consider the three-dimensional ($d = 2$) case. The method is then based on a dimensional reduction of the higher dimensional canonically quantized fields, see [7]. For a given vacuum, we can calculate the vacuum expectation value of the stress-energy tensor. Hereafter, we work in the Euclideanized space $\gamma^{E}_{\mu\nu}dx^\mu dx^\nu = H^{-2}(d\theta^2 + \sin^2\theta d\varphi^2)$, where the substitution $\theta \to \pi/2 - iHt$ Wick rotates back to the Lorentzian frame. Choosing the Euclidean vacuum corresponds to a dS invariant vacuum in the original Lorentzian frame. The Hamiltonian density for the field χ in this frame is classically defined by $\rho(z, x^i) := -b^2(z)T^\theta{}_\theta(z, x^i)$.

In general, for one non-trivial extra dimension we can have untwisted, $f^+(-z) = f^+(z)$, and twisted field configurations, $f^-(-z) = -f^-(z)$. Note that the untwisted and twisted solutions are equivalent to the mode degeneracy (for one non-trivial dimension). As we shall see, the total Hamiltonian density is given by a combination of untwisted and twisted fields, i.e., $\rho = \rho^{(+)} + \rho^{(-)}$. This quantity diverges when all the modes are naively summed up and we need to employ some kind of regularization scheme. To this end, after a dimensional reduction, we shall employ the point-splitting method in conjunction with zeta function regularization [4, 7], both for untwisted and twisted modes:

$$\zeta^{\pm}(z, x^i, z', x^{i'}; s) := \frac{2\mu^{2(s-1)}H}{b^{1/2}(z)b^{1/2}(z')H^{2(s-1)}}\sum_n f_n^{\pm}(z)f_n^{\pm}(z')\sum_{j,m}\frac{Y_{jm}(x^i)Y^*_{jm}(x^{i'})}{\left[q_n^2 + (j+\frac{1}{2})^2\right]^s}, \qquad (3)$$

where $f_n^+(z)$ and $f_n^-(z)$ correspond to normalized untwisted and twisted field configurations respectively. The solutions $f_n^{\pm}(z)$ are written in terms of associated Legendre functions and $Y_{jm}(x^i)$ are the usual spherical harmonics defined on the two-sphere, S^2. The parameter s is initially assumed to be complex with $\mathrm{Re}(s) > (d+1)/2$ in $(d+1)$-dimensions. After analytic continuation to $s \to 1$, we obtain the (ultra-violet) regularized results.

Given that we are interested only in the dependence of the backreaction on the bulk coordinate z we integrate out over the trivial dimensions, in this case over S^2:

$$\rho(z) := \int d\Omega_2 \lim_{s\to 1}\lim_{X'\to X}\frac{1}{2}\left(H^2\partial_\varphi\partial_{\varphi'} + \partial_z\partial_{z'}\right)\zeta(z, x^i, z', x^{i'}; s) \qquad (4)$$

where $d\Omega_2$ is the volume element of S^2. Note that because of the spherical symmetry transverse to the brane we may focus on the the equatorial plane $\theta = \pi/2$ and remove the dependence on θ. Hence, we obtain the angle-integrated Hamiltonian density

$$\rho^{\pm}(z) = 2H\lim_{s\to 1}\sum_{n,j}\frac{j+\frac{1}{2}}{\left[q_n^2 + (j+\frac{1}{2})^2\right]^s}\left[\frac{H^2}{2}j(j+1)f_n^{\pm 2}(z) + \left(f_n^{\pm\prime}(z) - \frac{b'(z)}{2b(z)}f_n^{\pm}(z)\right)^2\right].$$

We are primarily interested in the backreaction on the brane at $z = 0$, given that this is supposed to be where our world is localized. In this case the contribution from the untwisted and twisted parts can be expressed simply as

$$\rho^+(0) = H \lim_{s\to 1} \sum_{n,j} H^2 f_n^{+\,2}(0) \frac{j(j+1)(j+\frac{1}{2})}{[q_n^2 + (j+\frac{1}{2})^2]^s}\,, \quad \rho^-(0) = 2H \lim_{s\to 1} \sum_{n,j} f_n^{-\,\prime 2}(0) \frac{j+\frac{1}{2}}{[q_n^2 + (j+\frac{1}{2})^2]^s} \tag{5}$$

respectively. The total backreaction is given by the sum of each: $\rho(0) = \rho^+(0) + \rho^-(0)$.

We can also derive similar expressions for the pressures normal and parallel to the brane; $T^z{}_z(z, x^i)$ and $T^\varphi{}_\varphi(z, x^i)$, respectively. Like for the Hamiltonian density they are given by a combination of untwisted and twisted fields. In the Euclidean frame these pressures are defined by $p_z(z, x^i) := b^2(z) T^z{}_z(z, x^i)$ and $p_\varphi(z, x^i) := b^2(z) T^\varphi{}_\varphi(z, x^i)$. Then, as for the case of the Hamiltonian density, the angle-integrated total pressure normal to the brane $p_z(z) = \int d\Omega_2 p_z(z, x^i)$ becomes $p_z(0) = -\rho^+(0) + \rho^-(0)$ on the brane. The angle-integrated pressure parallel to the brane ($p_\varphi(z) = \int d\Omega_2 p_\varphi(z, x^i)$) has the same amplitude with opposite sign, i.e., $p_\varphi(z) = -p_z(z)$. Thus, and hereafter, we may concentrate only on $p_z(0)$. It is also worth mentioning that the angle-integrated trace of the stress-energy tensor in the Euclidean frame has the same amplitude of the Hamiltonian density with the opposite sign; $b^2(z) T^a{}_a(z) = \int d\Omega_2 b^2(z) T^a{}_a(z, x^i) = -\rho(z)$.

Here, we omit explanation about the detailed regularization scheme, see Ref. [4, 6]. Essentially, we convert the mode sums over $\{n\}$ into an integral along the contour as depicted in Fig. 4 of Ref. [4] by employing the residue theorem. For the twisted configuration there is no bound state and hence, we need not worry about how the contour approaches the imaginary axis.

4 Self-consistency condition on the brane

In the thin wall limit, $\sigma \to 0$, the leading order behavior can easily be obtained

$$\rho(0) \to -\frac{3H^3}{2\sigma^2} I\,, \quad p_z(0) \to -\frac{H^3}{2\sigma^2} I\,, \tag{6}$$

respectively. Here $I := \frac{1}{4}\int_0^\infty dx [x^2 \left(\psi(\frac{x}{2}) - 2\psi(\frac{x+1}{2}) + \psi(\frac{x}{2}+1)\right) + 1] \approx 0.213139$. Thus, in the thin wall limit both the total Hamiltonian density and pressure exhibit quadratic divergences.

We now come to discuss the *brane* self-consistency of the quantum corrected Einstein equations: The stress-energy of the backreaction should not become larger than the background stress-energy on the brane. In Figs. 1 the Hamiltonian density, $\rho(0)$, is compared with respect to their (angle-integrated) classical counterparts:

$$4\pi \left(-\frac{1}{2}(\phi'(z))^2 - b^2(z) V(\phi(z)) \right) \delta^\alpha{}_\beta = -\frac{4\pi H^2}{\sigma \cosh^2\left(\frac{Hz}{\sigma}\right)} \delta^\alpha{}_\beta \overset{z=0}{\to} -\frac{4\pi H^2}{\sigma} \delta^\alpha{}_\beta\,, \tag{7}$$

for the special case $H = 1 = M_3$. Note, that in Fig. 1 the Hamiltonian density is multiplied by a power of σ, in order to easily distinguish between the two, and the three-dimensional Planck mass $M_3 := \kappa_3^{-2}$ is set to unity.

The quantum backreaction scales as H^3/σ^2, whereas the background stress-energy scales as $H^2 M_3/\sigma$. Thus, the ratio of the backreaction to the background energy density scales as $O(H/M_3\sigma)$. From Fig. 1, for the special case $H = M_3$, we can infer that for brane thicknesses with $\sigma \gtrsim 0.3$ the quantum backreaction is at least an order of magnitude smaller than the classical value. We also have a quite similar result for the case of bulk pressure on the brane $p_z(0)$, see Ref. [6]. Thus, taking these facts into consideration, we obtain a plausible theoretical bound on the brane thickness, $\sigma \gtrsim 0.3\,(H/M_3)$. Of course, this bound is only valid on the brane not in the whole bulk. In this sense it might not be a sufficient condition, but just a necessary one. However, we are mainly interested in the behavior of the quantum backreaction at $z = 0$, where the backreaction is expected to be largest and our world exists by assumption. Thus, it may be considered as a stringent bound on the brane thickness.

For the more realistic case : $d = 4$, it is not hard to convince ourselves that in the thin wall limit, $\sigma \to 0$, the quantum backreaction exhibits a quartic divergence proportional to H^5/σ^4 for $d = 4$, whereas

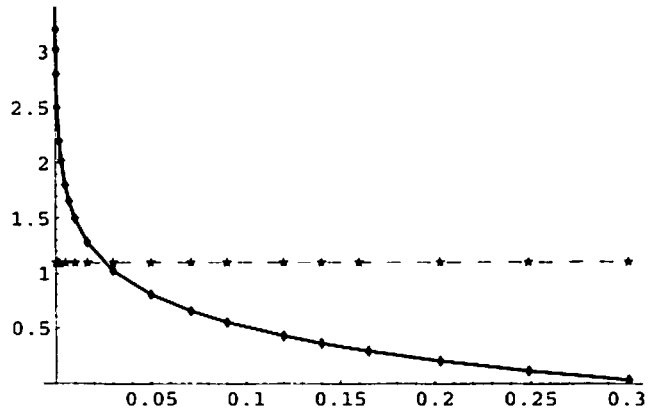

Figure 1: The backreaction of the Hamiltonian density (thick curve) and the background energy density (dashed curve), multiplied by a power of the brane thickness, σ, are shown as a function of σ for the case of $H = 1 (= M_3)$. Note, the scale of the vertical axis is set to $\log_{10}$.

the background stress-energy scales as $H^2 {M_5}^3/\sigma$. Thus, the ratio of the quantum backreaction to the background stress-energy will be of order $O(H^3/(\sigma M_5)^3)$. Therefore, the brane should satisfy $\sigma \gtrsim H/M_5$ in order to have *brane* self-consistency. Actually, this bound depends on the ratio between the energy scale for brane inflation, H, and M_5. Hence, in order for the bound to be consistent with the assumption $0 < \sigma < 1$ we should require $H \lesssim M_5$. This condition can also be regarded as a bound on the energy scale for brane inflation.

We might ask whether or not this bound on the brane thickness is consistent within the framework of the background model. The thick brane model we have investigated has an asymptotically flat bulk, which can be regarded as the high-energy limit ($H\ell \to \infty$) of an asymptotically Anti de Sitter (AdS) bulk, where ℓ is curvature radius of AdS spacetime. Quite clearly $\sigma \ll H\ell$ and thus, combining this inequality with the previous theoretical bound, $\sigma \gtrsim H/M_5$, we find that $H/M_5 \ll H\ell$ for *brane* self-consistency. Note that in the RS II set-up the four-dimensional Planck scale on the brane effectively becomes ${M_{\rm pl}}^2 = {M_5}^3 \ell (\approx 10^{19}{\rm GeV})$, which is determined at low energies ($H\ell \ll 1$) [1, 2]. Then, *brane* self-consistency, $H/M_5 \ll H\ell$, is equivalent to the condition $M_{\rm pl} \gg M_5$, which seems to be quite a natural one. Indeed, it is not difficult to construct a model with $M_5 \ll M_{\rm pl}$; just as long as the scale is larger than 10^9 GeV, derived from constraints on the size of any extra-dimensions, $\ell \lesssim 0.1$mm, which is determined from experimental tests of Newton's law on short distance scales. Thus, we conclude that thick braneworlds, even if they are extremely thin, can be *brane* self-consistent.

References

[1] L. Randall and R. Sundrum, Phys. Rev. Lett. **83**, 4690 (1999) [arXiv:hep-th/9906064].

[2] R. Maartens, Living Rev. Rel. **7**, 7 (2004) [arXiv:gr-qc/0312059].

[3] A. Knapman and D. J. Toms, Phys. Rev. D **69**, 044023 (2004) [arXiv:hep-th/0309176].

[4] M. Minamitsuji, W. Naylor and M. Sasaki, arXiv:hep-th/0508093, to appear in Nucl. Phys. B.

[5] A. z. Wang, Phys. Rev. D **66**, 024024 (2002) [arXiv:hep-th/0201051].

[6] M. Minamitsuji, W. Naylor and M. Sasaki, arXiv:hep-th/0510117, to appear in Phys. Lett. B.

[7] W. Naylor and M. Sasaki, Prog. Theor. Phys. **113**, 535 (2005) [arXiv:hep-th/0411155].

Non-Gaussianity from Multi-field Stochastic Inflation [1]

Takeshi Hattori[2], Kazuhiro Yamamoto

Theoretical Astrophysics Group, Department of Physics,
Hiroshima University, Hiroshima 739-8526, Japan

Abstract

We have investigated the statistical nature of the multi-field inflation with the stochastic approach, in which the evolution of the scalar fields is described by the Langevin equations. To solve the corresponding Fokker-Planck equation analytically, we adopt the technique of the scaling approximation. We have improved the previous investigation [Amendola, 1993] requiring the probability function to have the symmetry in exchanging the field parameters. We have investigated the non-Gaussian nature of the probability function by decomposing the fields into the adiabatic and the isocurvature components. We find that the non-Gaussianity of the isocurvature component can be large compared with that of the adiabatic component. The adiabatic and isocurvature components may be correlated at nonlinear order in the skewness and kurtosis even if uncorrelated at linear level. To check the results, we perform numerical simulation of the distribution function by solving the Langevin equation repeatedly.

1 Formulation

We consider the chaotic inflation model with the two scalar fields ϕ and χ with the Lagrangian density

$$\mathcal{L} = \frac{1}{2}\nabla^\mu\phi\nabla_\mu\phi - V_1(\phi) + \frac{1}{2}\nabla^\mu\chi\nabla_\mu\chi - V_2(\chi), \tag{1}$$

where V_1 and V_2 are the potential,

$$V_1(\phi) = \frac{\lambda_1}{2n}\sigma^4\left(\frac{\phi}{\sigma}\right)^{2n}, \quad V_2(\chi) = \frac{\lambda_2}{2n}\sigma^4\left(\frac{\chi}{\sigma}\right)^{2n}. \tag{2}$$

Here λ is the non-dimensional coupling constants, n is the parameter, and we introduced $\sigma^{-2} = 8\pi G$. During the slow-roll regime, neglecting the kinetic terms, the Friedman equation gives

$$H^2 = \frac{V_1(\phi) + V_2(\chi)}{3\sigma^2} \tag{3}$$

where H is the Hubble parameter.

In the stochastic inflation, the field dynamics coarse-grained over the horizon size is described by the Langevin equation. For the two-field inflation, we have

$$\dot{\phi} = \frac{-V_{1,\phi}}{3H} + \frac{H^{3/2}}{\sigma^{1/2}}\eta_\phi, \quad \dot{\chi} = \frac{-V_{2,\chi}}{3H} + \frac{H^{3/2}}{\sigma^{1/2}}\eta_\chi, \tag{4}$$

where η describes the stochastic noise, which has the nature of the Morkovian Gaussian noise with zero mean and the correlation

$$\langle\eta_i(t)\rangle = 0, \quad \langle\eta_i(t)\eta_j(t')\rangle = \delta_{ij}\frac{\sigma}{4\pi^2}\delta(t-t'). \tag{5}$$

Note that, even if the field potentials consist of independent function of ϕ and χ, the dynamics is coupled to each other because the Hubble parameter H depends on the both fields.

[1] Part of this work is based on the ref. JCAP 0507 (2005) 005

[2] E-mail:tkc@hiroshima-u.ac.jp

For the convenience, we introduce the parameter θ by

$$\cos\theta = \frac{\dot{\phi}_{cl}}{\sqrt{\dot{\phi}_{cl}^2 + \dot{\chi}_{cl}^2}} = (1 + L^{1/(1-n)})^{-1/2}, \quad \sin\theta = \frac{\dot{\chi}_{cl}}{\sqrt{\dot{\phi}_{cl}^2 + \dot{\chi}_{cl}^2}} = (L^{1/(n-1)} + 1)^{-1/2}, \tag{6}$$

where ϕ_{cl} and χ_{cl} are the background solution for the Langevin equation without the noise term, and they satisfy $\phi_{cl} = L^{1/2(n-1)}\chi_{cl}$ with $L = \lambda_2/\lambda_1$.

Our formulation relies on rewriting the Langevin equation in term of the variables r and Θ, instead of ϕ and χ. We define the variables r and Θ by

$$r = \phi\cos\theta + \chi\sin\theta, \quad \Theta = \frac{-1}{2(n-1)}\left[\frac{1}{\lambda_1}\left(\frac{\phi}{\sigma}\right)^{2(1-n)} - \frac{1}{\lambda_2}\left(\frac{\chi}{\sigma}\right)^{2(1-n)}\right]. \tag{7}$$

From the Langevin equation for ϕ and χ, we write

$$\dot{r} = \frac{-\tilde{\lambda}\sigma^3}{3H}\left(\frac{r}{\sigma}\right)^{2n-1} + \frac{H^{3/2}}{\sigma^{1/2}}(\cos\theta\eta_\phi + \sin\theta\eta_\chi), \quad \dot{\Theta} = \left(\frac{\eta_\phi}{V_{1,\phi}} - \frac{\eta_\chi}{V_{2,\chi}}\right)H^{3/2}\sigma^{3/2}. \tag{8}$$

where we defined $\tilde{\lambda} \equiv (\lambda_1^{1/(1-n)} + \lambda_2^{1/(1-n)})^{1-n}$. It is clear that r is the variable parallel to the classical trajectory. On the other hand Θ can be regarded to represent the component perpendicular to the classical trajectory. In the latter discussion, we may regard r and Θ as the variables parallel with the component that contributes to the adiabatic and isocurvature perturbation.

Instead of solving the Langevin equation, we solve the corresponding Fokker-Planck equation, which describes the evolution of the probability function $P(\phi, \chi)$. To find the solution analytically, we adopt the scaling approximation. To find the scaling solution, two transformation on the variable is performed to yield a Langevin equation with drift term vanished.

$$(1)\ r \to z = \int_r^\infty \frac{dr'}{H^{3/2}(r')/\sigma^{1/2}}, \quad (2)\ z \to \xi = F^{-1}[e^{\Lambda t}F(z)]. \tag{9}$$

Now the Langevin equation for ξ is

$$\dot{\xi} = \left(\frac{\xi}{z}\right)^{(n+2)/(3n-2)}(\cos\theta\eta_\phi + \sin\theta\eta_\chi). \tag{10}$$

Also, the Langevin equation for Θ has no drift term initially.

We follow the standard choice of the initial condition for the probability distribution, the delta-function distribution. Furthermore, assuming the limit of small diffusion, we adopt the Gaussian form of the probability function

$$P_{sc}(\phi, \chi) = \frac{1}{2\pi\sqrt{v_{11}v_{22}}}\exp\left[-\frac{(\xi(\phi,\chi) - \xi_*)^2}{2v_{11}} - \frac{\Theta(\phi,\chi)^2}{2v_{22}}\right]|J(\phi,\chi)|, \tag{11}$$

where $J(\phi, \chi)$ is the Jacobian of the transformation,

$$v_{11} = \frac{1}{16\pi^2}\sqrt{\frac{3}{2n\tilde{\lambda}}}\left(\frac{r_*}{\sigma}\right)^{2-n}\left[1 - \left(\frac{r_{cl}}{r_*}\right)^4\right] \qquad (n \geq 2) \tag{12}$$

$$v_{22} = \begin{cases} \dfrac{\tilde{\lambda}}{192\pi^2}\left(\dfrac{1}{\lambda_1^2\cos^6\theta} + \dfrac{1}{\lambda_2^2\sin^6\theta}\right)\left[-\ln\left(\dfrac{r_{cl}}{r_*}\right)\right] & (n = 2) \\ \dfrac{\tilde{\lambda}}{96\pi^2n^2(n-2)}\left(\dfrac{1}{\lambda_1^2\cos^{2(2n-1)}\theta} + \dfrac{1}{\lambda_2^2\sin^{2(2n-1)}\theta}\right)\left[\left(\dfrac{r_{cl}}{\sigma}\right)^{2(2-n)} - \left(\dfrac{r_*}{\sigma}\right)^{2(2-n)}\right] & (n > 2) \end{cases} \tag{13}$$

where r_* is the initial value of the classical solution, and we used the classical solution $r_{cl}(t)$.

2 Non-Gaussian behaviour

To focuse on the non-Gaussian statistical nature, we introduce the variable Δr and Δs as the component that contributes to the adiabatic and isocurvature perturbations,

$$\begin{pmatrix} \Delta r \\ \Delta s \end{pmatrix} = \begin{pmatrix} \cos\theta & \sin\theta \\ -\sin\theta & \cos\theta \end{pmatrix} \begin{pmatrix} \phi - \phi_{cl} \\ \chi - \chi_{cl} \end{pmatrix}. \tag{14}$$

And we rewrite the probability distribution function in terms of Δr and Δs.

Here let us introduce the variable $\mathcal{N}$ from the relation between the classical solution and the e-folding number N,

$$\left(\frac{r_{cl}(t)}{r_*}\right)^2 = \frac{n+6N}{n+6N_*} \equiv \mathcal{N} \leq 1 \quad (n \geq 2), \tag{15}$$

where the e-folding number from a time t to the final time of the inflation t_f, $N(t) = \int_t^{t_f} H(t')dt'$.

The part of the probability function written by ξ provides us with information about the adiabatic component, which can be expanded as follows, by setting $r = r_{cl} + \Delta r$,

$$\begin{aligned} \exp\left[-\frac{(\xi-\xi_*)^2}{2v_{11}}\right] &= \exp\left[-R_n\left\{\left(\frac{\Delta r}{r_{cl}}\right)^2 - \left(n-1+\frac{n+2}{2}\mathcal{N}^{2-n}\right)\left(\frac{\Delta r}{r_{cl}}\right)^3 \right.\right. \\ &\quad + \left(\frac{(n-1)(7n-3)}{12} + \frac{3(n-1)(n+2)}{4}\mathcal{N}^{2-n} \right. \\ &\quad \left.\left. \left. + \frac{(n+2)(30-n)}{48}\mathcal{N}^{2(2-n)}\right)\left(\frac{\Delta r}{r_{cl}}\right)^4 \cdots\right\}\right] \quad (n \geq 2), \end{aligned} \tag{16}$$

where we defined

$$R_n = \frac{96\pi^2}{\bar{\lambda}}\left(\frac{3}{2n}\right)^n n^2(\mathcal{N}^{-2}-1)^{-1}(n+6N)^{-n}. \tag{17}$$

On the other hand, the part of the probability function of Θ is expanded as

$$\begin{aligned} \exp\left[-\frac{\Theta^2}{2v_{22}}\right] &= \exp\left[-S_n\left\{\left(\frac{\Delta s}{r_{cl}}\right)^2 + (2n-1)\Gamma_n\left(\frac{\Delta s}{r_{cl}}\right)^3 \right.\right. \\ &\quad -2(2n-1)\left(\frac{\Delta r}{r_{cl}}\right)\left(\frac{\Delta s}{r_{cl}}\right)^2 + \frac{2n-1}{12}((14n-3)\Gamma_n{}^2+8n)\left(\frac{\Delta s}{r_{cl}}\right)^4 \\ &\quad \left.\left. -(2n-1)(4n-1)\Gamma_n\left(\frac{\Delta r}{r_{cl}}\right)\left(\frac{\Delta s}{r_{cl}}\right)^3 + (2n-1)(4n-1)\left(\frac{\Delta r}{r_{cl}}\right)^2\left(\frac{\Delta s}{r_{cl}}\right)^2 \cdots\right\}\right] \end{aligned} \tag{18}$$

where we defined $\Gamma_n \equiv \tan\theta - \cot\theta = (1/L)^{1/2(n-1)} - L^{1/2(n-1)}$ and

$$S_n = \frac{96\pi^2}{\bar{\lambda}} \times \begin{cases} \dfrac{9}{32}(1+3N)^{-2}(-\ln\mathcal{N})^{-1} & (n=2) \\ \dfrac{(n-2)n^2}{2}\left(\dfrac{3}{2n}\right)^n (n+6N)^{-n}(1-\mathcal{N}^{n-2})^{-1} & (n>2) \end{cases}. \tag{19}$$

To investigate the deviation of the probability distribution function from the Gaussian statistics quantitatively, we define the local skewness

$$\mathcal{T} \equiv \frac{P_{sc}(+\Delta r, +\Delta s)}{P_{sc}(-\Delta r, -\Delta s)}. \tag{20}$$

This represents the asymmetry of the probability function. In the limit of the Gaussian statistics, approaches to zero. From our probability function, we have the expression of the leading order

$$\mathcal{T}-1 \approx 2\left[\left(n-1+\frac{n+2}{2}\mathcal{N}^{(2-n)/2}\right)R_n\left(\frac{\Delta r}{r_{cl}}\right)^3-(2n-1)\Gamma_n S_n\left(\frac{\Delta s}{r_{cl}}\right)^3\right.$$
$$\left.+2(2n-1)S_n\left(\frac{\Delta r}{r_{cl}}\right)\left(\frac{\Delta s}{r_{cl}}\right)^2\right] \qquad (n\geq 2). \qquad (21)$$

We have investigated the non-Gaussian nature of the probability function by decomposing the fields into the adiabatic and the isocurvature components (Figure 1).

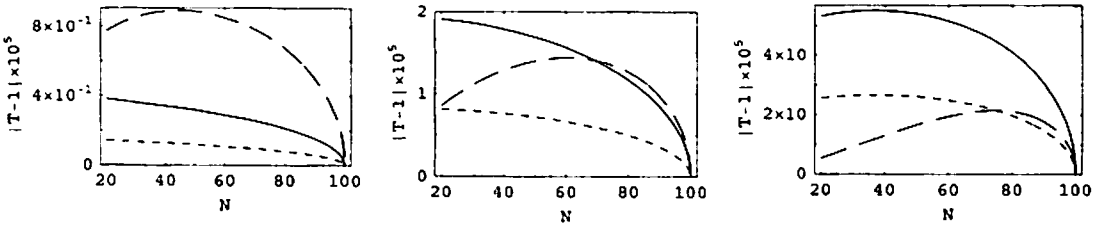

Figure 1: The skewness of Δr and Δs as function of N for $n = 1.5, 2, 3$ (left to right). The dotted (dashed) curve plots Δr (Δs) for the model with the parameters $\lambda_1 = 10^{-12}$ and $\lambda_2 = 10^{-13}$, while the solid curve plots Δr with $\lambda_1 = \lambda_2 = 10^{-2}$. Here we adopted $N_* = 100$.

We have found the followings: (1) The amplitude of the skewness is determined by the combination of the coupling constant λ_1, λ_2 and n. The amplitude of the skewness of the adiabatic component is determined by the combination of the coupling constant $\tilde{\lambda}$ and n, while that of the isocurvature component depends on $\tilde{\lambda}$, n and the ratio of the coupling constant Γ_n. Then the skewness of the isocurvature component can be large compared with that of the adiabatic one due to the factor Γ_n. (2) The similar feature can be seen in the kurtosis of the adiabatic and isocurvature components. (3) The adiabatic and isocurvature components may have correlation at the nonlinear order in the skewness and kurtosis, even if there is no correlation at the linear order. To test the analytic result, we are going to perform a numerical simulation that solve the Langevin equation repeatedly to obtain the distribution and the skewness. This is a preliminary result, however, the agreement is good for the adiabatic component, while the agreement is not so good for the isocurvature component. Further investigation will be needed for definite conclusion.

References

[1] Amendola L, Gordon C, Wands D and Sasaki M 2002 Phys. Rev. Lett. **88**, 211302

[2] Starobinsky A A 1986 *Field Theory, Quantum Gravity and Strings* ed H J de Vega and N Sanches (Springer Lecture Notes in Physics) 246

[3] Nakao K, Nambu Y and Sasaki M 1998 Prog. Theor. Phys. **80** 1041

[4] Matarrese S, Ortolan A and Lucchin F 1989 Phys. Rev. D **40** 290

[5] Amendola L 1993 Class. Quantum Grav. **10** 1267